The Late Aptian-Albian Transgression in the Agadir-Essaouira Basin, Morocco

Walid Hassanein

Communauté
UNIVERSITÉ Grenoble Alpes

THÈSE

Pour obtenir le grade de

DOCTEUR DE LA COMMUNAUTE UNIVERSITE GRENOBLE ALPES

préparée dans le cadre d'une cotutelle entre la *Communauté d'Université Grenoble Alpes* et l'*Université du Caire*

Spécialité : **Terre Solide**

Présentée par

« Walid HASSANEIN»

Thèse dirigée par **« Prof. Fabienne Giraud»** et **« Prof. Etienne Jaillard»**
codirigée par **« Prof. Mohamad Aly»**

préparée au sein du **Laboratoire ISTerre (Institut des Sciences de la Terre** - **UMR 5275)**

dans **l'École Doctorale TUE**

La Transgression Aptienne-Albienne Dans Le Bassin d'Agadir-Essaouira, MAROC

Thèse soutenue publiquement le **« 4 octobre 2016 »**,
devant le jury composé de :

Prof. Emanuela MATTIOLI
Professeur - Université Claude Bernard Lyon 1, (Examinateur)
Prof. Philippe RAZIN
Professeur - Institut Polytechnique Bordeaux (Rapporteur)
Prof. Abdel Aziz TANTAWY
Professeur - ASWAN University, EGYPT (Rapporteur)
Dr. Mohamed HAMMED
Chercheur - Cairo University, Giza, Egypt (Examinateur)
Prof. Fabienne GIRAUD
Professeur assistant - Université de Grenoble 1 (Directeur de these)
Prof. Etienne JAILLARD
Professeur - Université de Grenoble 1 (Co- directeur de these)
Prof. Mohamad ALY
Professeur - Cairo University, Giza, Egypt (Co- directeur de these)

THE APTIAN-ALBIAN TRANSGRESSION IN THE AGADIR-ESSAOUIRA BASIN, WESTERN MOROCCO

Dissertation for the doctorate degree

of the Université Grenoble-Alpes
FRANCE

Prepared at the Institut des Sciences de la Terre (ISTerre)

Submitted by

Walid Hassanein

Grenoble, 2016

Supervising Committee:

Dr. Fabienne Giraud
Prof. of Micropaleontology and Sedimentology, ISTerre, Grenoble University.

Dr. Etienne Jaillard
Prof. of Sedimentology and Tectonics, ISTerre, Grenoble University.

Dr. Mohamad Aly
Prof. of Paleontology and Stratigraphy, Geology Department, Faculty of Science, Cairo University.

Approval Sheet Submission

THE APTIAN-ALBIAN TRANSGRESSION IN THE AGADIR-ESSAOUIRA BASIN, WESTERN MOROCCO

Dissertation for the doctorate degree
of the Université de Grenoble-Alpes
FRANCE

Submitted by

Walid Hassanein

Defense committee:

Prof. Emanuela MATTIOLI	**Examiner**
Prof. Philippe RAZIN	**Reporter**
Prof. Abdel Aziz TANTAWY	**Reporter**
Dr. Mohamed HAMMED	**Examiner**
Prof. Fabienne GIRAUD	**Director of the thesis**
Prof. Etienne JAILLARD	**Co-director of the thesis**
Prof. Mohamad ALY	**Co-director of the thesis**

Grenoble, 2016

NOTE

Besides the work carried out in this thesis, the candidate Walid Hassanein, has pursued post graduate studies, in Cairo University for the partial fulfillment of Ph.D. Degree in the following topics:

1. Micropaleontology
2. Advanced Paleoecology
3. Advanced Stratigraphy (1)
4. Advanced Stratigraphy (2)
5. Advanced Structural Geology
6. Basin Mapping
7. Advanced Seismic, Structural and Stratigraphic interpretation and 3D Modeling
8. Basin Analysis for Oil and Gas

He passed successfully an examination in the above mentioned topics, in June 2011.

ACKNOWLEDGEMENTS

First and above all, I would like to express my great thanks to my God, for helping me to accomplish this work.

I am really grateful to my committee members; I wish to express my sincere gratitude and appreciation to my supervisors **Prof. Fabienne Giraud, Prof. Etienne Jaillard, Prof. Mohamad Aly**, and **Dr. Mohamed Hammed** for their supervision, assistance, patience, field guidance and encouragement. They supervised this study and helped to direct the research toward success by numerous discussions and informative reviews of reports and manuscripts. They also gave me plenty of freedom to make and guide my own ideas.

Special thanks to my supervisors, Prof. **Fabienne Giraud** and Prof. **Etienne Jaillard** for many things 1) giving me the opportunity to join their group Tectonic Relief and Basins (TRB) in ISTerre, 2) to work on Moroccan sections when the working on Egyptian sections from north Sinai became impossible during the time of revolution, 3) for receiving me at Grenoble and ISTerre for the first time and booking my residence, 4) for their support in the lab, affording me what I need for research, 5) helping me to stay more time in Grenoble, 6) in solving all difficulties during my stay in France, 7) continuous encouraging, and for guiding my way through my PhD with such a great enthusiasm. Many thanks Fabienne and Etienne for giving me your support, and letting me develop my own ideas with complete freedom.

Many thanks to our Moroccan colleagues; **Prof. Khadija El Hariri**, **Prof. Yamina Bourgeoini**, **Prof. Mohssine Ettachfini** from Cadi Ayyad University-Marrakech, and **Prof. Moussa Masrour**, **Prof. Lhoussaine Bouchaou**, **Prof. Mohamed Aoutem**, from Ibn Zohr University-Agadir for accepting me as a member of PHC-Toubkal Programme, and to their assistance in the field work. Especial thanks to **Prof. Moussa Masrour** for his good reception, welcoming and hosting in Agadir city.

This work would not have been possible without the most patient help and support during the constructive discussion during the preparation of the thesis.

This work has been supported by grants from the **Institut Français d'Egypte**, the Institut de Recherche pour le Dévelopment (**IRD**), the **Rhône-Alpes Region** (France), and the **Labex OSUG@2020** (Observatoire des Sciences de l'Univers de Grenoble), during my stays in France, in 2011, between 2012 and 2014 and in 2016 for the Ph.D's defence, and from Cairo University during my stays in Egypt. The financial support for research work was possible thanks to the following projects**: PHC-IMHOTEP,** 2010-2011 (between Université Joseph Fourier (UJF) and Cairo University); **STDF-IRD,** 2011-2013 (between Science & Technology Development Fund in Egypt and Institut de Recherche pour le Développement in France); **PHC-VOLUBILIS-TOUBKAL,** 2013-2015 (between UJF, Ibn Zohr and Cadi Ayad Universities, Maroc).

Special thanks to staff members and postgraduates from ISTerre, **Prof. Anne-Marie Boullier, Prof. Anne Replumaz, Prof. Matthias Bernet, Prof. Stéphane Guillot, Prof. Philippe Cardin, Baptiste Dazas, Romain Lafay, Mélanie Noury, Hélène Delavault, Piero Poli, Anthony Pimbert, Karim Malamoud, Alaa Hamze, Christelle Salameh, Isandra Fortuna, Alexis Grandhomme, Rachel Abrahami, Nancy Salloum, Latifa El Yacoby, Afaf Hamdouni, Rachid Rashidovic, Ahmed Dawelbeit**. They made my staying in France, very special memories. Thank you for your help, guidance, advice, friendship, laughter and for allowing me to be part of the department family.

I am grateful to the administration and technical staff in ISTerre, Grenoble; to **Christine Bigot** (Doctorate School), **Abderrahman Salhi, Rodolphe Pinon, Hafid Bouchafa and Kamil Adoum** for their assistance and advice during my stay in France.

Special thanks are also to all colleagues of the Geology Department, particularly to the head of the geology department **Prof. Mohamed Hemdan** for his continuous advice and encourage, **Prof. Mohamad Gamil, Prof. Mohamed Darwish, Prof. Abdel Moneim El-Araby** and **Prof. Niazy El Barkooky** for advice, valuable assistance,

suggestions and discussions and to **Mr. Said Zidan, Mr. Raid Badr** and **Mr. Mohamed Saleh**, for their help in the Sinai field trip.

I must thank my mother, my wife Samar and our Children Jana, Nour and Yara, for their unconditional love and support now and ever. They were an important source for the successful accomplishment of the study.

Abstract

The Aptian-Early Albian interval of the southern Tethyan margin is poorly understood since sedimentary successions are frequently incomplete and dating is difficult. The Essaouira-Agadir Basin (EAB), Morocco, presents numerous, very good and accessible outcrops of the Early Cretaceous series. The aim of this work is to (1) establish an integrated stratigraphic framework of the Aptian-Albian series based on (a) high-resolution ammonites and calcareous nannofossil biostratigraphy, (b) identification of sedimentary discontinuities and (c) carbon isotope stratigraphy; (2) reconstruct the paleoenvironmental evolution during this interval through both sedimentary facies evolution and qualitative and quantitative nannofossil analyses, and (3) propose a functioning model for the sedimentation on the mixed, carbonate/clastic ramp of the EAB.

In the EAB, the **Late Barremian** is defined by the *sarasini* ammonite zone and the NC5 nannofossil zone. The **Barremian/Aptian boundary** is defined by ammonites. The **Early Aptian** is defined by the *deshayesi* to *furcata* ammonite zones, and is bounded by a first minimum $\delta^{13}C$ value at the base and a first maximum value at the Early/Late Aptian Boundary. The **Late Aptian** interval, is defined by four ammonite zones (*martini*, *melchioris*, *nolani* and *jacobi*), two discontinuity surfaces, four maximum and minimum $\delta^{13}C$ values, and by the upper part of the NC6, the NC7 and the lowermost part of the NC8 nannofossil zones. The **Aptian/Albian boundary** is placed within the discontinuity D4 (base of the *Leymeriella tardefurcata* ammonite zone), supported by the First Occurrence (FO) of the *Prediscosphaera columnata* and *Hayesites albiensis* nannofossil taxa, and by decreasing $\delta^{13}C$ values. **Early Albian** times are represented by the *tardefurcata* and *mammillatum* ammonite zones, the FO of *Hayesites albiensis*, and by minimum $\delta^{13}C$ values.

The facies and depositional environments of the Aptian-Early Albian rocks are identified based on their lithology, sedimentary structures, fossil content and microfacies. These allowed to identify (1) four types of key surfaces related subaerial or submarine erosion, (2) four sedimentary carbonated facies in the Aptian corresponding to outer to inner ramp depositional environments, and (3) four Early Albian sedimentary facies, represented by sandstones and shales, of basin to middle ramp depositional setting. These facies reflect deposition in adjacent and gradational paleoenvironments. The Aptian-Early Albian stratigraphic interval of the EAB, has been subdivided into two major cycles, floored by two major erosional surfaces. The latest Barremian-Aptian cycle is underlined by a major karstified-erosional surface and consists of four third-order depositional sequences. The Early Albian cycle, overlies a major submarine erosional surface, and also contains four depositional sequences. In each cycle, the vertical changes in facies indicates a deepening upward trend related to sea level rise.

The carbonate production in the EAB is higher in the Aptian than during the Early Albian, due to warm conditions, slow rise of sea level, shallow depth of the basin, and little detrital influx. The nannofossil total absolute abundance decreases from the Aptian to the Early Albian, due to increasing sedimentation rate, associated with rapid subsidence. The nutrient input, fertility and calcareous nannofossil primary productivity is higher in the Early Albian with respect to the Aptian, and are mainly controlled by rising sea level and upwelling currents. The Latest Aptian-Early Albian period is characterized by a high abundance of cold taxa, and the migration of cosmopolitan biota from Boreal realm into the Tethyan realm, which may reflect the occurrence of a glacial climatic event.

Résumé

L'intervalle Aptien-Albien inférieur de la marge sud-téthysienne est mal connu en raison de successions souvent incomplètes et de difficultés à les dater. Le Bassin d'Essaouira-Agadir (BEA), au Maroc, présente de nombreuses coupes, bien exposées et accessibles du Crétacé inférieur. Le but de ce travail est de (1) établir un cadre stratigraphique intégré de la série apto-albienne, basé sur (a) la biostratigraphy haute résolution des ammonites et des nannofossiles calcaires, (b) l'identification des discontinuités sédimentaires et (c) la stratigraphy isotopique du carbone; (2) reconstituer l'évolution paléoenvironnementale pendant cet intervalle, par l'étude des facies sédimentaires et l'analyse qualitative et quantitative des nannofossiles, et (3) proposer un modèle de fonctionnement de la plateforme-rampe mixte, carbonate-clastique, du BEA.

Dans le BEA, le **Barrémien supérieur** est défini par la zone d'ammonites à *sarasini* et par la zone de nannofossiles NC5. La **limite Barrémien-Aptien** est définie par les ammonites. L'**Aptien inférieur** est déterminé par les zones d'ammonites à *desahayesi* jusqu'à *furcata*, et est limité par un premier minimum de $\delta^{13}C$ à la base, et par un premier maximum à la limite Aptien inférieur-moyen. L'**Aptien supérieur** est défini par quatre zones d'ammonites (*martini*, *melchioris*, *nolani* et *jacobi*), deux surfaces de discontinuité, quatre maxima et minima de $\delta^{13}C$, et comprend la partie supérieure de NC6, NC7 et la base de NC8. La **limite Aptien-Albien** est placée dans la discontinuité D4 (base de la zone d'ammonites à *Leymeriella tardefurcata*), en accord avec la première occurrence (FO) des nannofossiles *Prediscosphaera columnata* et *Hayesites albiensis*, et par une diminution des valeurs de $\delta^{13}C$. L'**Albien inférieur** est daté par les zones d'ammonites à *tardefurcata* et *mammillatum*, par la FO du nannofossile *Hayesites albiensis*, et par des valeurs minimales de $\delta^{13}C$.

Les faciès et environnements de dépôt des sédiments aptien à Albien inférieur ont été déterminés par leur lithologie, les figures sédimentaires, leur contenu faunique et les microfaciès. Ils ont permis d'identifier (1) quatre types de surface liées à des érosions subaériennes ou sous-marines, (2) quatre faciès sédimentaires carbonatés dans l'Aptien, correspondant à des environnements de rampe interne à distale, et (3) quatre faciès sédimentaires argilo-gréseux dans l'Albien inférieur, représentant des dépôts de rampe médiane à hémipélagiques. Ces faciès reflètent des milieux adjacents et passant de l'un à l'autre. L'intervalle Aptien-Albien inférieur du BEA a été subdivisé en deux cycles, soulignés par deux surfaces d'érosion majeures. Le cycle Barrémien terminal-Aptien est souligné par une surface karstifiée et erosive et comprend quatre séquences de dépôt de troisème ordre. Le cycle Albien surmonte une surface majeure d'érosion sous-marine, et contient au moins quatre sequences de dépôt. Dasns chaque cycle, l'évolution vertical des faciès indique un approfondissement ds milieux de depot liée à une hausse eustatique.

Dans le BEA, production carbonatée est plus élevée à l'Aptien qu'à l'Albien inférieur, en raison d'un climat chaud, une lente montée du niveau de la mer, un milieu de dépôt peu profond et de faibles apports détritiques. L'abondance totale absolue des nannofossiles décroît entre l'Aptien et l'Albien inférieur, en raison d'un taux de sedimentation plus élevé associé à une subsidence plus rapide. L'apport en nutriments, la fertilité et la production primaire sont plus élevés à l'Albien inférieur qu'à l'Aptien, et sont principalement contrôlés par la montée du niceau de la mer et les courants d'upwellings. La transition Aptien terminal-Albien inférieur est marquée par l'abondance de taxons d'eau froide et par la migration de faunes cosmopolitaines du domaine boréal vers le domaine téthysien, qui pourrait traduire un événement climatique froid, voire glaciaire.

TABLE OF CONTENTS

CHAPTER ONE

INTRODUCTION

CHAPTER ONE
INTRODUCTION

1.1. AIM OF THE STUDY

In North Africa, the Aptian-Albian interval is known for a long time as to be marked by (1) a widespread marine transgression, (2) tectonic events, materialised by syn-sedimentary deformations, local emergences, clastic deposits and rapid facies variations (Guiraud et al., 2005), (3) a rich endemic ammonite fauna (e.g. Pervinquière, 1907; Douvillé, 1916; Moret and Mahmoud, 1953; Dubourdieu, 1956; Latil, 2011; Robert in Peybernes et al., 2013) and 4) deposition of black shales, related to high productivity model, associated with upwelling current, in Tunisia such as: OAE1a (Heldt et al, 2008; Elkhazri et al., 2009, 2013; Godet et al., 2014), and OAE1b (Fadhel et al., 2011, 2014).

.

The Late Aptian-Early Albian transgression is still poorly understood, because of the thick, monotonous and poorly fossiliferous shaly succession that represent most of the Albian stage.

The main goals of this present work are as follows:

❖ to establish an integrated stratigraphic framework of the Aptian-Albian sediments in the Essaouira-Agadir Basin based on (1) a high-resolution biostratigraphy (ammonites and calcareous nannofossil biozonations), (2) identification of sedimentary discontinuities and depositional sequences, and (3) chemo-stratigraphy, based on stable carbon isotopes.

❖ to reconstruct paleoenvironmental conditions during the Aptian-Early Albian interval for the Essaouira-Agadir Basin through both qualitative and quantitative nannofossil analyses and sedimentary facies evolution.

❖ to propose a functioning model for the sedimentation on the mixed, carbonate/clastic ramp of the Essaouira-Agadir Basin.

1.2. PREAMBLE

1.2.1. Tectonism during Aptian-Albian times

The Mid Cretaceous Aptian-Albian interval (100.5-126.3 Ma; Gradstein et al., 2012**)** is associated with major plate tectonic movements, landmass rearrangement, and tectonic evolution of the proto-Atlantic (Wagner and Pletsch, 1999; Poulsen et al., 2003), and is marked by the ongoing break-up of Pangea and Gondwana, with the rift-to-drift transition between South America and Africa associated with the development of both south Atlantic Ocean (rifting began in the south during Early Cretaceous (≈ 133 Ma) (e.g. Rabinowitz and LaBrecque 1979; Emery and Uchupi 1984; Uchupi, 1989; Binks and Fairhead, 1992; Guiraud and Maurin, 1992; Bodin et al.,2010; Moulin et al., 2010; Kochhann et al., 2013, 2014; Frizon de Lamotte et al., 2015; Granot and Dyment, 2015; Fig.1.1) and western Mediterranean Sea opening in Early Jurassic (Biju-Duval et al., 1977; Guiraud et al., 2005; Frizon de Lamotte et al., 2015; Hosseinpour et al., 2016; Müller et al., 2016; Fig.1.1). This resulted in sea-floor spreading, along the slow-spreading Mid-Atlantic ridge (2 to 3 cm/y in total), leading to an Atlantic Ocean wide enough to allow significant mixing of waters across the equator in Late Albian, since 100 Ma (Pletsch et al., 2001; Ford and Golonka, 2003; Browning and Watkins, 2008; Torsvik et al. 2009; Pérez-Díaz and Eagles, 2014).

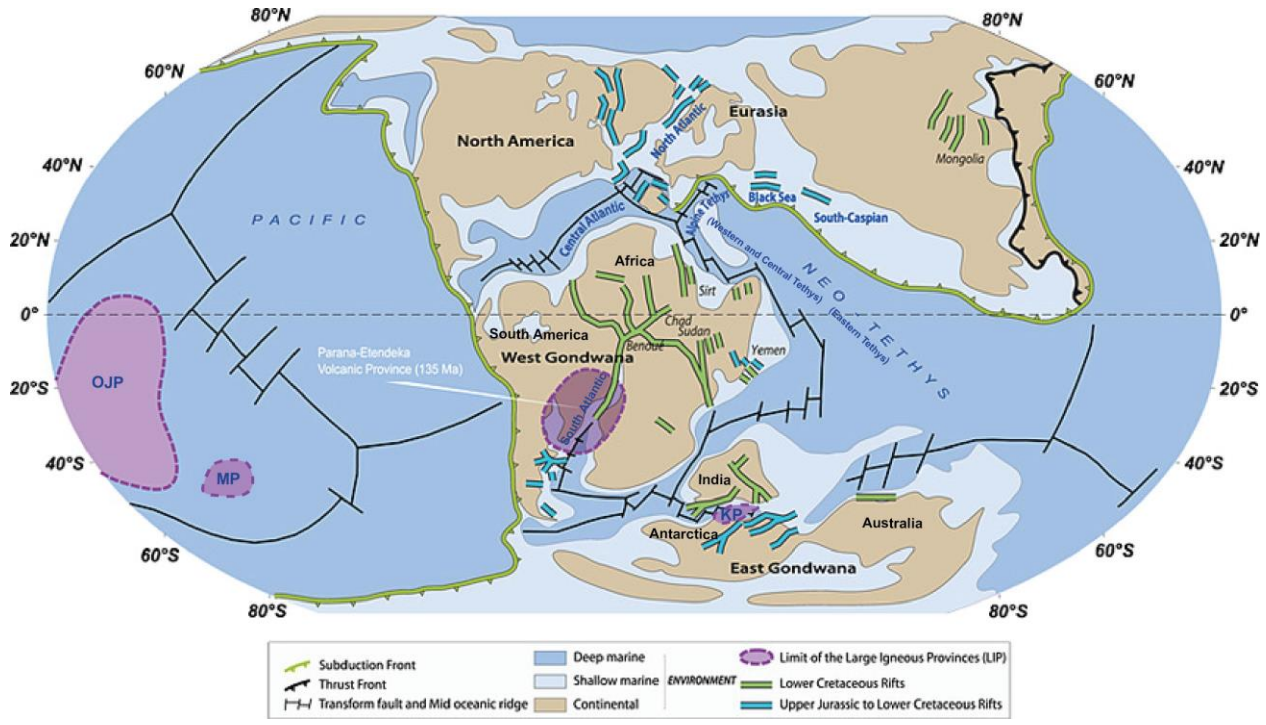

Figure 1.1: Sketch map showing the Earth at 120 Ma (Aptian), modified after Frizon de Lamotte et al. (2015). The map shows the main Jurassic and Lower Cretaceous rift systems and the Aptian-Albian igneous provinces; OJP: Ontong Java Plateau; MP: Manihiki Plateau in mid-Pacific Ocean, and KP: Kerguelen Plateau, in Indian Ocean. The background of the map is from Plate tectonic maps and continental drift animations by C. R. Scotese, PALEOMAP Project (www.scotese.com).

1.2.2. Climatic conditions during Aptian-Albian times

The paleoclimate of the Aptian-Albian time is strongly influenced by the paleogeography of the three large continents (Fig. 1.2A, B; the climatic belts are after Chumakov et al., 1995; Voigt, 1996): (1) North America-Eurasia in the northern hemisphere with a predominantly humid climate; (2) South America-Antarctica-India-Madagascar-Australia, with both arid and humid climatic conditions, and (3) Africa in the southern hemisphere with both arid and humid climatic conditions.

The Aptian-Albian period, is generally considered as a greenhouse period, with high atmospheric CO_2 concentrations and high global mean temperatures. This is shown by stretched boundaries of the reef line, vast forests in Polar Regions, and the absence of expanded ice sheets at the poles (Francis and Frakes, 1993; Simo et al., 1993; Harland et al., 2007; Hay, 2008).

Substantial evidence for this warmth includes upper ocean isotopic paleotemperatures of 22-28°C at southern high latitude sites (Huber et al., 1995), bathyal temperatures reaching 20°C in the subtropical North Atlantic (Norris and Wilson, 1998; Fassell and Bralower, 1999; Huber et al., 1999), and a large champsosaurid reptile that was intolerant of freezing conditions discovered at 78°N (Tarduno et al., 1998). These data suggest that globally averaged surface temperatures in the mid Cretaceous were more than 10ºC higher than today.

However, successive episodes (<1 my-5 my) of warming and cooling (Price, 2003; Pucéat et al., 2003; Weissert and Erba, 2004; Takashima et al., 2007; Wagner et al., 2008; Ando et al., 2008) are recorded during this time interval (e.g. Takashima et al., 2006; Erba et al., 2015). Warming, greenhouse conditions prevailed during deposition of the Aptian-Early Albian organic-rich sediments. The climatic conditions during the Early Aptian OAE 1a changed after the onset of the OAE1a, from cool to very warm (e.g., Bralower et al., 1993; Menegatti et al., 1998; Larson and Erba, 1999; Ando et al., 2008; Keller et al., 2011). The climate during OAE 1b was characterized by extremely warm conditions that are well-documented in the Blake Nose and the Mazagan Plateau sediments (Erbacher et al., 2001; Herrle, 2002; Wagner et al., 2008). Recently McAnena et al. (2013) have documented on the basis of TEX86 data, a ≈2 my long interval of relatively cool conditions (≈28–29 °C) in the late Aptian in the Proto-North Atlantic followed by a warming (up to ≈31 °C) close to the Aptian/Albian Boundary linked to the OAE 1b.Tropical and temperate belts extended much farther toward the poles (Hallam, 1975, 1984; Barron, 1983). The latest Aptian/Early Albian interval was interrupted by cold snaps episodes (Bown, in Kennedy et al., 2000; Jeremiah, 2001; Herrle and Mutterlose, 2003; Mutterlose et al., 2003; Rückheim et al., 2006b; Heimhofer et al., 2008; Mutterlose et al., 2009, McAnena et al., 2013; Peybernes et al., 2013; Millán et al., 2014; Bottini et al., 2015).

Climatic variations follow changes in volcanic activity, rates of oceanic crust production (Larson, 1991a, b; Seton et al., 2009) and release of methane (Jenkyns, 2003, 2010). Volcanic activity and methane release, led to high atmospheric pCO_2, perhaps up to 10 times the present pCO_2 level (Berner et al., 1983; Barron and Washington, 1985, Beerling and Royer, 2002; Jenkyns, 2010; Bottini et al., 2014; Erba et al., 2015), elevated average temperatures (Sellwood et al., 1994; Barron et al., 1995).

The Late Aptian and/or Early Albian cooling episode

It is supported by the following evidences.

1. Ice rafted dropstones and glendonites have been observed in Upper Aptian sediments from Arctic Canada, Australia (Kemper, 1987; Frakes et al, 1995), Spain (Rodríguez-López et al., 2016), and glendonite beds have been found in the upper Aptian to lower Albian deposits, in the High Arctic of Canada (Sverdrup Basin, Kemper, 1987; Herrle et al., 2015).

2. Stable oxygen isotope analyzed on a) benthic foraminifera at DSDP site 511 (Fassell and Bralower, 1999), b) planktonic foraminifera, at ODP site 1049 on the Blake Nose Plateau (Huber et al., 2003), and c) on belemnite shells (Ditchfield et al., 1994; Pirrie et al., 1995, 2004) sampled in Antarctica, Australia and Argentina show "cool" conditions during the Early Albian both in the shelf seas and ocean around the Gondwana margin.

3. Abundance of high-latitude fossil plant (Francis and Poole, 2002), pollens (Heimhofer et al., 2008), calcareous nannofossils (Mutterlose et al., 2009) taxa support the existence of a cooling event at Aptian-Albian transition. Moreover, extinction of the rudist bivalves in the Late Aptian would result from a cooling of seawater, in the Arabian platform (e.g. Strohmenger et al., 2010; Maurer et al., 2013), Qatar (Raven et al., 2010) and Iran (Mansouri-Daneshvar et al., 2015).

The higher relative abundance of cold-water taxa in the Tethyan realm during the Late Aptian-Early Albian with respect to the Early Aptian indicates migration of cosmopolitan biota from high-latitude sites close to the poles of both hemispheres into the Tethyan realm (Heimhofer et al., 2008). Where, the Equatorial Atlantic Seaway between Africa and South America came into existence only in the Late Aptian-Albian allowing for an exchange of biota (Mutterlose et al., 2009).

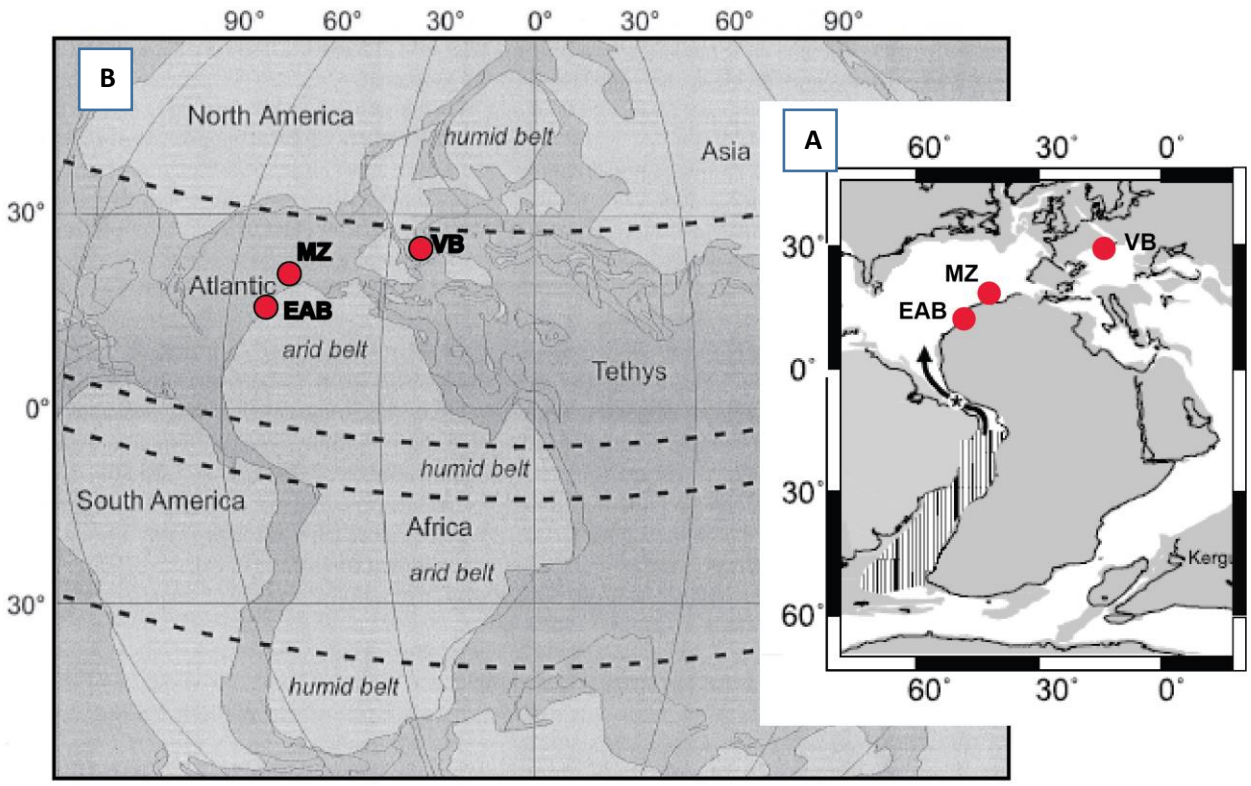

Figure 1.2: A) Paleogeography of the mid-Cretaceous (modified after Browning and Watakins, 2008), the arrow indicates a shallow to intermediate connection through the central Atlantic seaway (denoted by the black star) based on studies from Arthur and Natland (1979) and Moullade et al. (1993). B) Showing the high sea-level stand shorelines (after Herrle, 2002). Light grey areas indicate land. Humid and arid belts after Chumakov et al. (1995) and Voigt (1996). Red circles indicate the study area of Essaouira-Agadir Basin (EAB) and areas mentioned in the text Mazagan Plateau (MZ), NW Africa and Vocontian Basin (VB), in Southeast France (the Aptian/Albian type locality).

1.2.3. Paleoceanography during Aptian-Albian times

The sea level was fluctuate between 100 and 200 m higher than today during the Aptian-Albian interval (Haq et al., 1987, 2014). The total land area flooded was more than 40 percent greater than at present, resulting in the expansion of continental shelf environments and intra-continental seaways (Hays and Pitmann, 1973). The oceanic circulation pattern in the Mid-Cretaceous was also fundamentally different than that observed in the present ocean. The northern and southern continents were separated by the large eastern Tethys and the narrow western Tethys (western Mediterranean Sea) and Central Atlantic Ocean (Fig.1.1). The Tethyan and Atlantic oceans provided a circumglobal oceanic connection, enhancing the development of the upwelling currents along the southern margin of the Tethyan Ocean, and thus increasing fertility and primary productivity (Hay et al., 1999; Trabucho-Alexandre et al., 2011, Fig. 1.3) in the EAB. Oxygen

isotope data from benthic foraminifera indicate that deep oceans were significantly warmer than at present (Erbacher et al., 2001; Huber et al., 2002, 2011). These observations have been taken as evidence that deep water formation occurred at low-latitudes within the Tethyan Ocean (Brass et al., 1982). This conclusion is supported by general oceanic circulation simulations (Barron and Peterson, 1990).The Mid-Cretaceous warm and saline bottom water probably formed in the subtropics-tropics as a result of a greater atmospheric content of CO_2 and CH_4, reinforced by water vapor content and meridional heat transported as heat of vaporization of H_2O (Hay, 2008). North (1985), Baudin (1995) and Leckie et al. (2002) have suggested that the low-latitude position of the western Tethys and Atlantic Ocean favored the development of anoxic conditions. Therefore, development of anoxic conditions in Aptian-Albian interval were controlled by warming conditions.

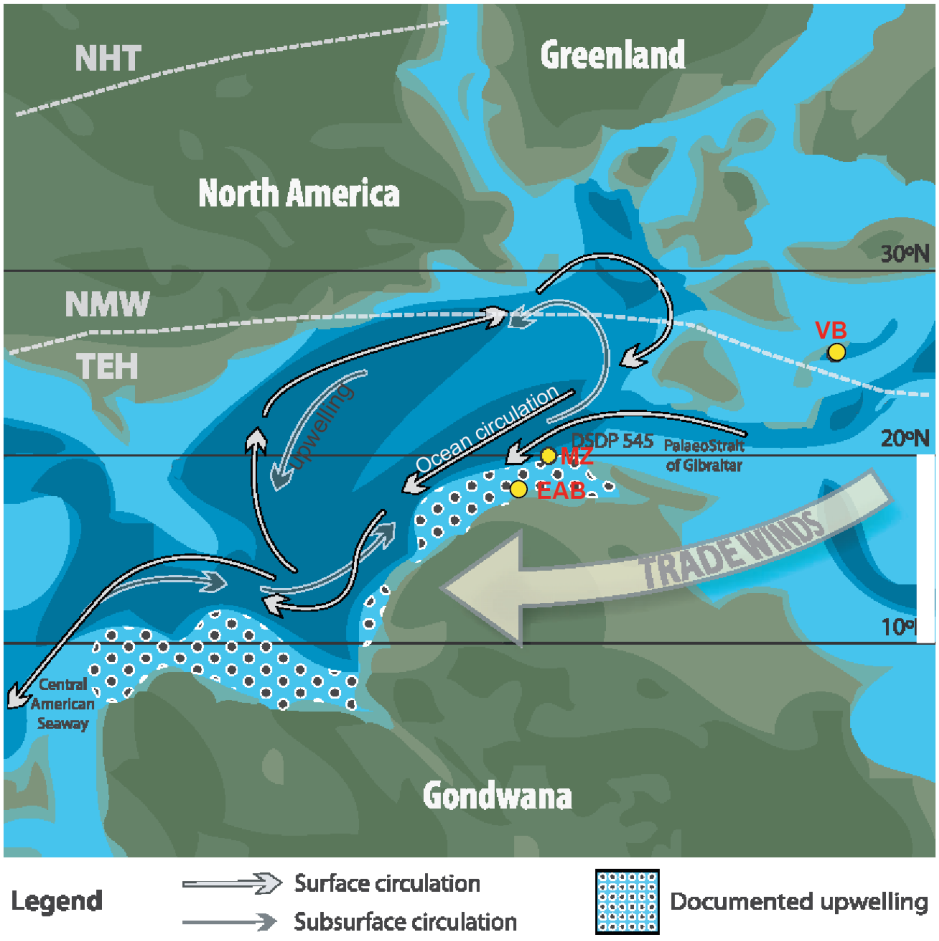

Figure 1.3: Paleogeographical map of the Aptian/Albian North Atlantic region. Map based on paleogeographical reconstructions by R. Blakey. Modified after Trabucho-Alexander et al. (2011). Yellow circles indicate the study area of Essaouira-Agadir Basin (EAB) and areas mentioned in the text Mazagan Plateau (MZ), NW Africa and Vocontian Basin (VB), in Southeast France (the Aptian/Albian type locality). Aspects of oceanic and atmospheric circulation are also shown. Climate zonation for the Aptian/Albian (dashed lines) is based on Chumakov et al. (1995): TEH, tropical–equatorial hot arid belt; NMW, northern mid-latitude warm humid belt; NHT, northern high-latitude temperate humid belt.

1.2.4. Volcanism during Aptian-Albian times

Large Igneous Provinces (LIPs) were constructed during voluminous magmatic events that took place over geologic time intervals between ≈1 and 10 my (Keller, 2008). These events are thought to be associated with massive thermal anomalies in the mantle known as "superplumes" (Larson, 1991). The volume of crust produced by LIPs in the mid-Cretaceous was almost three times greater than in prior and subsequent time periods (Larson, 1991). In particular two prominent LIPs were formed during this interval (Fig. 1.1, 1.4). The Ontong Java Plateau (OJP) and Manihiki Plateau (MP) in the Pacific formed ~123 to 117 Ma in the Early Aptian (Courtillot and Renne 2003), and the Kerguelen Plateau (KP) and Rajmahal trap (RT) in the Indian Ocean was erupted in the late Aptian and early Albian from 109 to 118 Ma (Courtillot and Renne 2003).

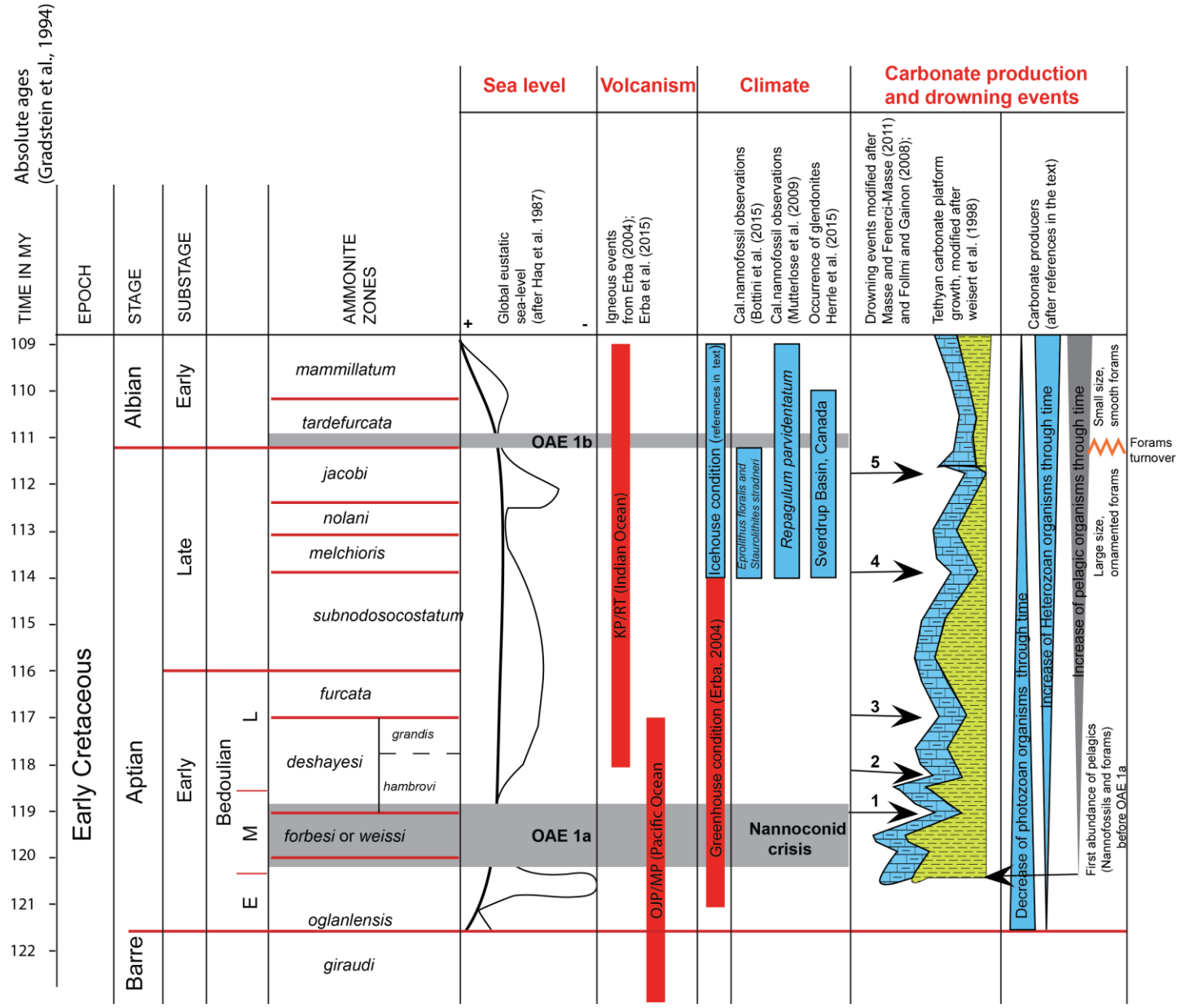

Figure 1.4: Aptian/Albian biostratigraphy, Oceanic Anoxic Events, eustatic sea level, igneous events, climate conditions, carbonate producers and drowning events, and the evolution of the pelagic planktonic community. OAE1a placed in the interval starting from *forbesi* to lower *deshayesi* ammonite zones, according to Erba (1996); Mutterlose (1998); Mutterlose and Böckel (1998). OAE1b occurred during the *tardefurcata* ammonite Zone, according to Herrle and Mutterlose (2003), Herrle et al. (2004). Abbreviations; OJP: Ontong Java Plateau; MP: Manihiki Plateau; KP: Kerguelen Plateau; RT: Rajmahal trap. The drowning events are shown by numbers from 1 to 5.

1.2.5. Oceanic Anoxic Events (OAEs) during Aptian- Albian times

The Aptian to Albian sections in the Tethys, Atlantic and Pacific sites (Arthur et al., 1990; Bralower et al., 1993; Leckie et al., 2002; Ando et al., 2008), as well as in low and high latitudes (Herrle, 2002; Herrle at al., 2004, 2010, 2015; Mutterlose et al., 2014), reveal a great number of black shales, some of which appear to be synchronous in different basins and have therefore been identified as Oceanic Anoxic Events (OAEs), e.g. the OAE 1a (Selli event, ≈120 Ma) of Early Aptian age (e.g. Schlanger and Jenkyns, 1976; Arthur et al., 1990; Bralower et al., 1994) and the OAE 1b (Paquier event, ≈111 Ma) of Early Albian age (e.g. Bréheret, 1988; Bralower et al., 1993; Erbacher et al., 1999, Herrle, 2002). The early Aptian (Selli event, OAE 1a, first identified in the Umbria-Marche Basin, Italy; Coccioni et al., 1987) and early Albian OAE (Paquier event, OAE 1b, first recognized in the Vocontian Trough of southeast France (Bréhéret, 1985) have the most extensive geological record (Arthur et al., 1990). Computing the exact durations of OAEs based on cyclostratigraphy, the duration of the early Aptian OAE 1a is comprised between 1 and 1.3 Ma (Li et al., 2008; Malinverno et al., 2010), whereas its of the early Albian OAE 1b is ~ 45 Ka; as reported from Wagner et al. (2008).

There are three hypotheses for formation of the mid-Cretaceous OAEs: (1) the stagnant ocean (the density driven stratification) model of the upper water column, enhanced preservation of organic matter; Schlanger and Jenkyns, 1976; Bralower and Thierstein, 1984; Premoli Silva et al., 1989a, 1989b; Tribovillard and Gorin, 1991; Erba, 1992; Erbacher et al., 1996, 2001; Takashima et al., 2006), equivalent to Preservation model of Galeotti et al. (2003), and/or (2) Oxygen Minimum (High productivity) model, in which the elevated primary productivity is attributed to upwelling currents; Arthur et al., 1987, 1990; Weissert and Lini, 1991; Calvert and Pederson, 1992; Bralower et al., 1994; Erba, 1994, 2004; Leckie et al., 2002; Galeotti et al., 2003; Snow et al., 2005; Takashima et al., 2006 ; Fig. 1.5), and (3) an abrupt warming, induced by rapid influx of CO_2 into the atmosphere from volcanogenic and/or methanogenic sources (Bailey et al., 2003; Forster et al., 2007; Ando et al., 2008; Jenkyns, 2010).

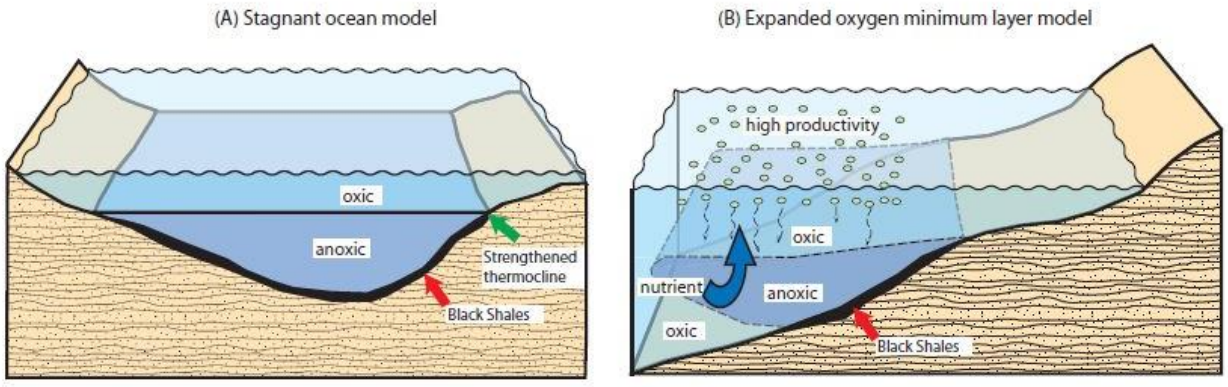

Figure 1.5: Representative models for productivity and black shale deposition: (A) The stagnant ocean model, and (B) The oxygen-minimum layer model (after Takashima et al., 2006).

OAE1a is generally interpreted as due to accelerated burial of organic matter during episodes of enhanced productivity (Weissert, 1989; Arthur et al., 1990; Weissert and Lini, 1991; Erba, 1994; Erbacher et al., 1996; Weissert et al., 1998; Jenkyns, 1999, 2003, 2010; Larson and Erba, 1999; Leckie et al., 2002; Aguado et al., 2014).

OAE1b The deposition of organic-rich sediments of OAE 1b was a consequence of the enhanced productivity favored by upwelling or by river nutrient input (Hofmann et al., 2008; Fadhel et al., 2011; Trabucho-**A**lexandre et al., 2011), during a warm and humid climate (Hu et al., 2014). OAE1b resulted from monsoonally driven reduction bottom water ventilation as in the Vocontian Basin in southeast France (~1.5%; Herrle, 2002; Herrle et al., 2003; Herrle et al., 2004), and Mazagan Plateau in the eastern Central Atlantic (~1.2%; Herrle, 2002; Herrle et al., 2004).

Volcanism, associated with the emplacement of the Ontong Java Plateau (OJP), is thought to be the main triggering mechanism for global anoxia as well as for imposed greenhouse conditions and ocean acidification during OAE 1a (e.g. Larson, 1991; Erba, 1994; Bralower et al., 1994; Larson and Erba, 1999; Jones and Jenkyns, 2001; Leckie et al., 2002; Jenkyns, 2003; Méhay et al., 2009; Tejada et al., 2009; Erba et al., 2010; Bottini et al., 2012). Simulation for OAE1b volcanogenic CO2 emission as trigger for OAE1b did not provide realistic results consistent with the geological record and climate context (Wagner et al., 2008). In addition, CO_2 outgassing during volcanism may have increased global temperatures and altered deep water circulation patterns

leading to increased anoxia in warm deep waters (e.g., Arthur et al., 1985; Keller et al., 2011; Bottini et al., 2015; Erba et al., 2015).

The relationship between LIP formation and OAEs derived from radiometric estimates is less straight forward (Keller, 2008). Radiometrically dated basalts from the second phase of OJP and Manihiki Plateau ≈ 121 Ma, while the Selli black shale (OAE1a) and associated isotopic ratio anomalies occurred at ≈ 120 Ma, with ≈ 1 my later. Basalts from the Kerguelen Plateau suggest major volcanic activity, beginning at ≈ 109-119 Ma, which possibly continued at decreased rates and contributed to OAE1b (≈111 Ma) and elevated paleotemperatures in the Albian. It is still unclear to what extent the volcanism might have caused the biotic and carbon-cycle perturbations (Keller, 2008, Fig. 1.6).

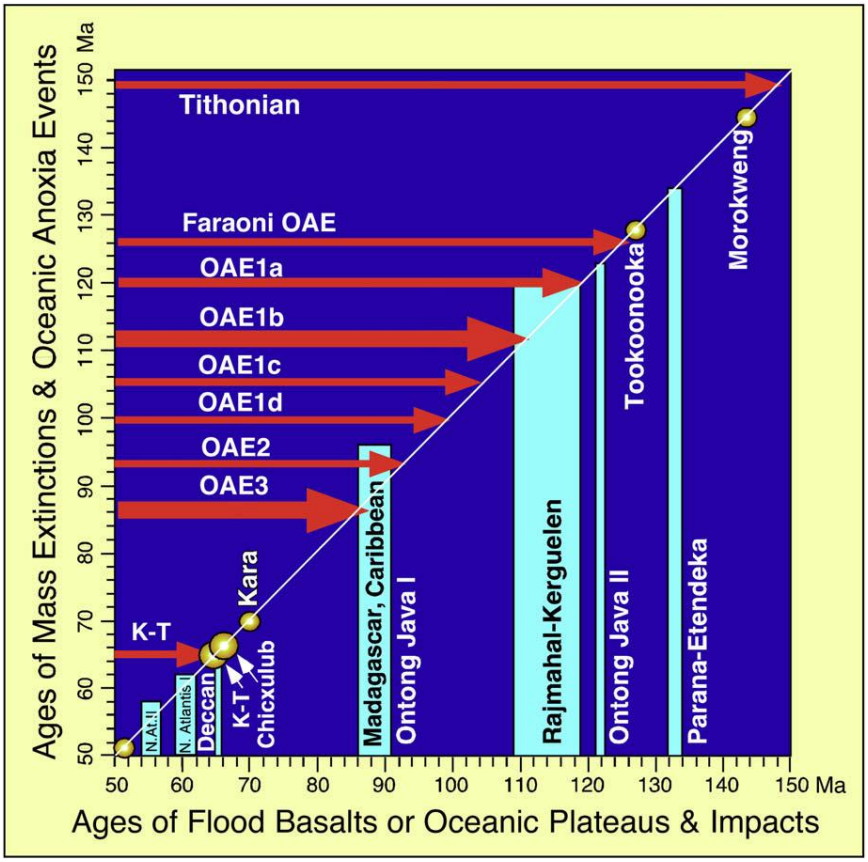

Figure 1.6: A plot of Cretaceous volcanism and impacts versus extinction intensity and oceanic anoxic events (OAEs) reveals a good correlation for the K-T boundary and potential correlation between LIPs and OAE1a, 1b and OAE3, though precise age control is lacking. LIPs may contribute to OAEs, but apparently are not the primary cause; there is no correlation with impact other than at the K-T boundary. After Keller (2008).

1.2.6. Carbonate platforms during Aptian-Albian times

The sea-level during the Aptian-Albian interval fluctuates between 100 and 200 m higher than today and large areas of the continental shelves were flooded, providing vast space for shallow-water carbonate platform development in the subtropical-tropical realm (e.g., Atlantic, Tethys and Pacific margins; Haq et al., 1987; Simo et al., 1993; Ziegler et al., 2003; Fig. 1.7).

The Aptian and/or Albian carbonate platform occur along the northern Tethys margin from Portugal (Rey, 1972), Spain (e.g. Fernandez-Mendiola and Garcia-Mondejar, 1989; Vilas et al., 1995; Rosales, 1999; Castro et al., 2008; Fernandez-Mendiola et al., 2015), France (e.g. Peybernès, 1976; Masse, 1976; Arnaud-Vanneau and Arnaud, 1990; Hunt and Tucker, 1993; Pictet et al., 2015), Switzerland (e.g. Schwizer, 1984; Funk et al., 1993; Föllmi et al., 2007; Godet et al., 2010), Italy (e.g. D'Argenio et al., 1987; Graziano, 2000; Raspini, 1998, 2012; Ruberti et al. 2013; Graziano and Raspini, 2015); Croatia (e.g. Velic et al., 1987; Velic, 2007), Hungary (e.g. Peybernès, 1979; Császár, 2002; Császár et al., 2013), Bulgaria (e.g. Nikolov, 1969; Peybernès et al., 1979), Romania (e.g. Neagu, 1986; Bucur, 1988), Greece (Carras, 1995), Turkey (Yilmaz and Altiner, 2007; Masse et al., 2009), and Iran (e.g. Van Buchem et al., 2010a,b; Mansouri-Daneshvar et al., 2015).

Along the southern Tethys margin from Morocco (e.g. Butt et al., 1984; Witam, 1998), Algeria (Vila, 1980; Bracene et al., 2003), Tunisia (e.g. Heldt et al., 2008; Chihaoui et al., 2010; Fadhel et al., 2011; Hfaiedh et al., 2013), Egypt and Israel (Bachmann et al., 2010), Syria (Mouty and Saint-Marc, 1982), Lebanon (Saint-Marc, 1970), from Arabian peninsula (Immenhauser et al., 2004), and Oman (Pittet et al., 2002; Grèselle and Pittet, 2005; Van Buchem et al., 2010a,b). In addition to, the Aptian-Albian carbonate platform successions are recognized in boreal areas such as England, northwestern France, northwestern Germany, Canada, and in southern temperate areas such as South Africa and Madagascar (Ouwehand 1987), and from Mexico (e.g. Bralower et al., 1999; Lehmann et al., 1999; Barragan-Manzo and Diaz-Otero, 2004) and Venezuela (Arnaud et al., 2000; Dot et al., 2015).

The Aptian-Albian carbonate platforms are characterized by carbonate facies composed of limestones, argillaceous limestone, marls intercalated with detritus-rich sediments, consisting of fine grained sandstone, siltstone and shale, associated with glauconitic and phosphatic sediments.

These Aptian-Albian lithofacies are marked by both temporal and spatial change in fossil content. The Early Aptian deposits present common Photozoan communities, including green algae, corals and rudists, which appear to be the main contributors to the formation of the neritic carbonate (Kiessling et al., 1999; Pictet et al., 2015). Communities changed upward, during the Late Aptian and Early Albian with dominant heterozoan organisms, including brachiopods, bivalves and echinoids (Föllomi and Gainon, 2008; this study).

Carbonate platforms are highly sensitive ecological systems, which typically show rapid and characteristic response modes to environmental and climatic changes acting both on a regional and global scale (Huck et al., 2013), most carbonate precipitating organisms require specific ecological conditions (Philip, 2003; Ruberti et al., 2013).

In the mid-Cretaceous, the greenhouse climate was characterized by warm oceans, high concentrations of CO_2 in the atmosphere and high global sea levels; these conditions led to widespread deposition of shallow water carbonates but also to the deposition of organic-rich facies in basinal environments (Skelton, 2003). Within this context, shallow- and deep-water carbonate successions may have recorded global-scale stratigraphic events (Masse, 1989; Arthur et al., 1990). Increased geodynamic activity and massive injection of carbon dioxide in the ocean-atmosphere system accelerated the water cycle and increased weathering rates, thus threatening carbonate precipitating organisms (e.g. Larson and Erba, 1999; Jahren, 2002; Hu et al., 2005; Coffin et al., 2006; Najarro et al., 2011; Hong and Lee, 2012; Hu et al., 2012; Huang et al., 2012). High nutrient transfer from continents to oceans (Weissert and Erba, 2004; Wortmann et al., 2004) and an increase of dissolved $Ca^{2}+$ and $HCO-_{3}$ (Kump et al., 2000) led to the blooming of mesotrophic and eutrophic biota on carbonate platforms (Bachmann and Hirsch, 2006; Burla et al., 2008), including the microbial colonization of wide-spread shallow water environments (Whalen et al., 2002; Wortmann et al., 2004). In addition, deep-sea igneous activity influenced the chemical composition of seawater, and the concomitant low Mg/Ca ratio and high concentration of Ca favored the development of low-Mg calcite secreting organisms (e.g. Stanley, 2006).

The carbonate platform evolution during the Aptian was punctuated by a series of biotic and environmental changes (e.g. Weissert et al., 1998; Takashima et al., 2007; Föllmi and Gainon, 2008; Föllmi, 2008, 2012; Huck et al., 2010, 2012; Masse and Fenerci-Masse, 2011; Huck et al., 2010; Donnadieu et al., 2011; Graziano, 2013; Pictet et al., 2015) that resulted in drowning events,

i.e. its submergence below the euphotic zone (Weissert et al., 1998; Skelton, 2003). Platform drowning occurs if its upward growth rate fails to keep pace with rates of subsidence or sea level rise, due to unfavorable conditions for primary carbonate producers, such as: 1) rapid subsidence, 2) rise of sea level, and 3) nutrification of shallow marine environments, either by increased coastal runoff and/or by upwelling (Weissert et al., 1998; Föllmi et al., 2006; Huck et al., 2012). Furthermore, highly elevated atmospheric CO_2 levels could have supported ocean acidification, reduced calcification potential of some shallow water calcifiers, leading to calcification crisis, which additionally destabilized shallow marine ecosystems (Herrle and Mutterlose, 2003; Wissler et al., 2003, Weissert and Erba, 2004; Millán et al., 2011; Graziano et al., 2013; Erba et al., 2015).

On the northern Tethyan margin, Masse and Fenerci-Masse (2011) and Pictet et al. (2015) have defined three Early Aptian age (Bedoulian) drowning events in carbonates platform of SE France. Föllmi and Gainon (2008) defined two additional drowning events in the Late Aptian carbonate platform in Switzerland. The five drowning events are recognized based on sedimentological and stratigraphical evidence, and their timing, referred to ammonite zones and subzones. The drowning events could be dated as follows: (1) Middle Bedoulian (*weissi-deshayesi* transition), (2) Mid late Bedoulian (*hambrovi* subzone), (3) Late Bedoulian (*grandis-furcata* transition), (4) Early Late Aptian (*subnodosocostatum* and *melchioris* zones), and (5) latest Aptian (*jacobi* zone). The phases of renewed platform-carbonate production intervening between the drowning phases were all in a heterozoan mode (Föllmi and Gainon, 2008). Some authors suggested that one of the Early Aptian drowning event recorded on the carbonate platforms of the subtropical realm, most notably in the northern Tethys margin during the Early Aptian was coincident with the OAE 1a (Fig. 1.4; e.g. Masse, 1989; Weissert et al., 1998; Larson and Erba, 1999; Skelton, 2003b; Wissler et al., 2003; Weissert and Erba, 2004; Föllmi et al., 2006; Burla et al., 2008; Föllmi, 2008, 2012; Masse et al., 2009; Huck et al., 2010, 2011; Jenkyns, 2010), However, it is not recorded in the shallow paleoenvironments of the southern Tethyan margin (Oman, Immenhauser et al., 2005; Egypt, Thielemann, 2006; Tunisia, Heldt et al., 2008). Focusing on the Tunisian carbonate platform, Heldt et al. (2010) show that no widespread platform drowning is recorded at this time, possibly due to non-eutrophication of this platform located within the broad arid climate belt of Chumakov et al. (1995).

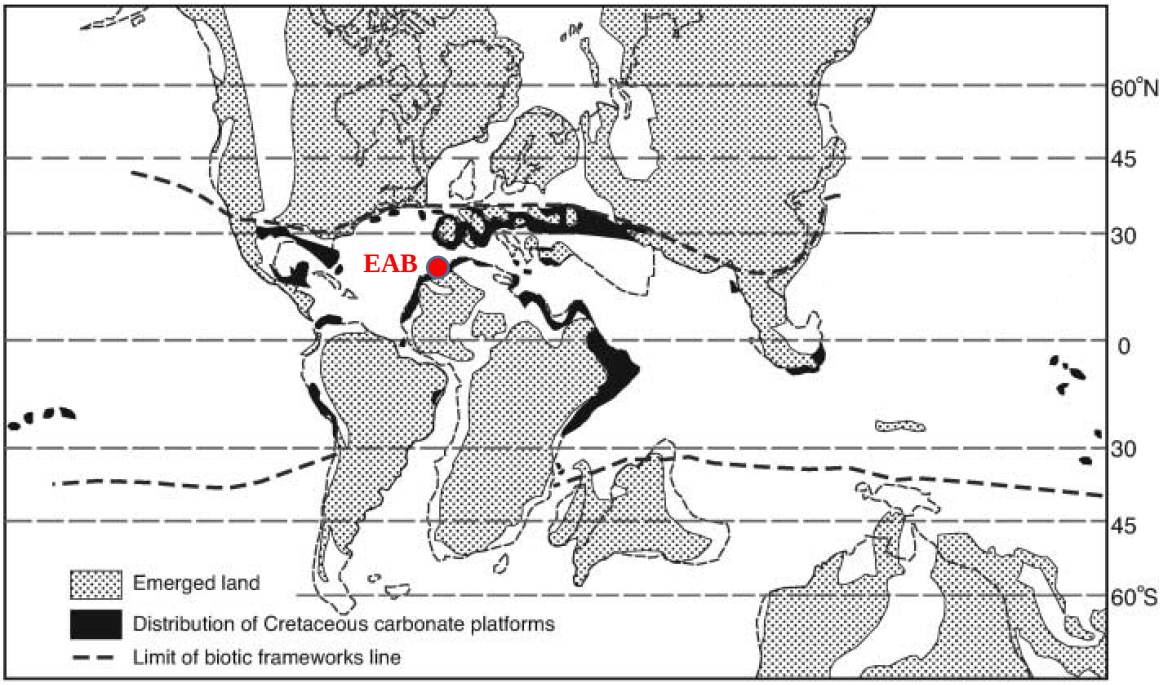

Figure 1.7: Distribution of Cretaceous carbonate platforms. After Simo et al. (1993).

The deep marine carbonate producers were mainly calcareous nannofossils and planktonic foraminifers (hedbergellids, rarely globigerinelloidids; Heldt et al., 2008).

1.2.7. Carbon and Oxygen isotope during Aptian-Early Albian times

The carbon and oxygen isotope records for the Aptian- Early Albian time is a useful tool to establish stratigraphic correlations in a basin or between distinct basins, and to provide informations about paleo-environments. The Aptian-Early Albian carbon isotope record (inorganic and organic) appears better suited for long-distance short-term correlation of different marine and terrestrial environments than biostratigraphy, because of the synchroneity of carbon isotope signals in a range of sediment types (Herrle et al., 2004).

The base of Early Aptian OAE1a is characterized by a sharp negative $\delta^{13}C$ excursions and a subsequent positive excursion have been observed worldwide (Menegatti et al., 1998; Jenkyns and Wilson, 1999; Jenkyns, 2003; Wissler et al., 2003; Föllmi et al., 2006; Huck et al., 2011; Millán

et al., 2011; Najarro et al., 2011; Yamamoto et al., 2013; Bottini et al., 2014; Bottini et al., 2015), which would be associated with a CO_2 pulse triggered by volcanism (Weissert and Erba, 2004; Yamamoto et al., 2013; Bottini et al., 2014, Erba et al., 2015) and/or a sudden burst of clathrates (Méhay et al., 2009). The negative $\delta^{13}C$ excursions in marine organic carbon and carbonate, found in all successions analyzed at high resolution, suggest that isotopically light carbon $\delta^{13}C$ was supplied in pulses to the ocean–atmosphere system (Menegatti et al., 1998; Jenkyns, 2003; Kemp et al., 2005). The OAE 1a is followed by a positive carbon isotope excursion extends into the late Aptian (e.g. Weissert, 1989; Weissert and Lini, 1991; Jenkyns, 1995; Menegatti et al., 1998; Bralower et al., 1999; Erba et al., 1999; Bellanca et al., 2002; Price, 2003; van Breugel et al., 2007; Ando et al., 2002, 2008; Heldt et al., 2008; Méhay et al., 2009; Malkoč et al., 2010; Mahanipour et al., 2011; Millán et al., 2009; Stein et al., 2011; Bottini et al., 2012; Hu et al., 2012; Elkhazri et al., 2013; Lorenzen et al., 2013).

In the Early Albian, at the base of OAE 1b, the carbon isotope records are marked by a sharp negative $\delta^{13}C$ shift recognized in different areas (Bralower et al., 1999; Herrle et al., 2004; Lucina et al., 2004; Wagner et al., 2007; Alexandre et al., 2011; Petrizzo et al., 2012, 2013; Sabatino et al., 2015; Li et al., 2016). The decrease of early Albian carbon isotope values took place earlier (estimated as 1–3 kyr) in terrestrially derived leaf wax than in marine carbonate (Wagner et al., 2008), thus suggesting that the isotopic signal propagated downward relatively slowly from the atmosphere into marine waters (Jenkyns, 2010).

The oxygen isotope records have been used for the reconstruction of temperature and productivity changes in Cretaceous marine environments (e.g., Menegatti et al., 1998; Stoll and Schrag, 2000; Erbacher et al., 2001).

High-resolution oxygen isotope data, display a prominent negative anomaly of $\approx -2‰$ crossing the OAE 1a interval for a DSDP Site in the mid-Pacific Mountains and in northwest Germany, suggesting a pulse of rapid warming of ~8°C immediately before and during OAE 1a, followed by a cooling trend (Ando et al., 2008; Kuhnt et al., 2011; Mutterlose et al., 2014).

In Southeastern France, the oxygen isotope values increase below the Niveau Paquier, then abrupt decrease with a negative oxygen isotope shift at the base of OAE 1b. This decrease continued within the Niveau Paquier in OAE 1b (Herrle, 2002), suggesting as much as 8°C

warming during OAE 1b (Herrle et al., 2003b). The OAE 1b is followed by a continuous increase of oxygen isotope values to the top of the Early Albian succession (Herrle, 2002). This negative oxygen isotope shift at the base of OAE1b followed by cooling event is recognized from Atlantic deep-sea drilling cores, in Blake Nose Plateaus (Erbacher et al., 2001), and in the Vocontian Basin and Mazagan Plateau (Herrle, 2002). The negative oxygen isotope shift at the base of OAE1b reflects an increase of surface water temperatures coeval with the onset of OAE 1b event. The negative oxygen isotope shift at the base of OAE 1b and beginning of OAE 1b in the Vocontian Basin and Mazagan Plateau has been explained by a monsoonally driven reduction in deep water formation and reduced deep water ventilation rates (Herrle, 2002). The negative oxygen isotope shift at Blake Nose at the base of OAE 1b would be due to a well-mixed, well ventilated, upper water column characterized by high-salinity and low-temperature surface waters, which underwent both a moderate temperature increase and a decrease in salinity leading to the initiation of OAE1b (Erbacher et al., 2001).

1.2.8. Calcareous nannofossils during Aptian-Early Albian times

Calcareous nannofossils are an important component of marine phytoplankton during the Cretaceous (Mutterlose et al., 2005). Calcareous nannofossils became homogenized and cosmopolitan during Aptian time, related to rising of sea-level (Mutterlose, 1992a, 1992b; Keupp and Mutterlose, 1994; Mutterlose and Böckel, 1998). Calcareous nannofossils are useful for biostratigraphic schemes, allowing detailed zonations and global correlation for marine Cretaceous sediments (Mutterlose et al., 2005). Many authors have proposed the first occurrence (FO) of *Prediscosphaera columnata* as a stratigraphic marker approximately indicating the Aptian/Albian Boundary (e.g., Thierstein, 1971; Bralower et al., 1995; Bown et al., 1998). The changes in morphology of calcareous nannofossil species are controlled by temperature changes and nutrient availability, or are controlled by local/regional factors (Mattioli and Pittet, 2002; Tremolada and Erba, 2002). They were the most important carbonate contributors to pelagic sediments in the earliest Cretaceous (Bornemann et al., 2003; Erba, 2004; Mutterlose et al., 2005). The Oceanic Anoxic Events 1a characterized by a strong decrease in abundance of the rock-forming big calcareous nannofossils (nannoconids) in pelagic successions; named “nannoconid crisis” (Erba,

1994; Erba and Tremolada, 2004; Erba et al., 2010). The reduced biocalcification rates in surface waters either related to CO_2-driven ocean acidification (Wissler et al., 2003; Weissert and Erba, 2004; Erba and Tremolada, 2004) or to highly elevated trophic levels (Coccioni et al., 1992; Erba, 2004).

Calcareous nannofossils are useful indicators for paleoceanographic and paleoclimatic changes with different species being sensitive to climatic changes and variations in nutrient contents (Mutterlose, 1992a; Erba et al., 1992; Street and Bown, 2000; Mutterlose et al., 2005). Variations in calcareous nannofossil assemblages (decline of Tethyan taxa and expansion of high latitude taxa) from both low and high palaeolatitudes during the Late Aptian - Early Albian suggest a global cooling (Herrle and Mutterlose, 2003; Mutterlose et al., 2009).

Leckie et al. (2002) documented the evolutionary patterns of calcareous plankton (planktic foraminifera and calcareous nannoplankton) during the mid-Cretaceous. When combined with the radiolarian record through the same interval (Erbacher et al., 1996), there is compelling evidence that the highest rates of evolutionary turnover, i.e., speciation plus extinction, occur at or near the major Oceanic Anoxic Events. The association of plankton turnover and carbon isotopic excursions with each of the major OAEs suggests widespread changes in the ocean-climate system. The episodes of accelerated evolutionary activity in the plankton have been attributed to changing upper water column structure, increased delivery of nutrients including dissolved iron, greater oceanic productivity, and carbonate dissolution (Erba, 1994; Erbacher et al., 1996; Leckie et al., 2002).

Leckie et al. (2002) concluded that plankton evolution was tectonically-forced, particularly by increased submarine volcanism and hydrothermal activity, due to tectonic influences on global climate, ocean chemistry, nutrient availability, ocean circulation, and water column structure. One of the most significant turnover points in the evolutionary history of planktonic foraminifera occurs just across the Aptian/Albian Boundary associated with the OAE 1b (Fig. 1.4; e.g., Erbacher et al., 1999, 2001; Premoli Silva and Sliter, 1999; Barker et al., 2001; Holbourn and Kuhnt, 2001; Kuypers et al., 2001, 2002; Herrle, 2002, 2003; Leckie et al., 2002; Herrle et al., 2003, 2004; Friedrich et al., 2005; Wagner et al., 2007; Hofmann et al., 2008; Huber and Leckie, 2011; Petrizzo et al., 2012) with a change from large-sized and heavily ornamented species in the Late Aptian, to small-sized globigeriniform specimens in the Early Albian (Bréhéret et al., 1986; Leckie, 1989; Premoli Silva and Sliter, 1999; Kennedy et al., 2000; Leckie et al., 2002).

1.3. LOCATION OF THE STUDY AREA AND STUDIED SECTIONS

The study area is located in the Western High Atlas (WHA), in western Morocco (Fig. 1.8). It is bounded by the following coordinates: longitudes between 9º 55\ and 9º 20\ W and latitudes between 30º 30\ and 31º 05\ N. The present work was achieved based on studying four sections for nannofossil and geochemical analysis, and nine sections for sedimentology and sequence stratigraphic analysis. All sections are located between the Agadir and Essaouira cities. These sections are: Tinfoul, Alma, Anzate, Addar, Tamri, Tissakatine east, Tissakatine Center, Taounarine and Ida w Shayq (Fig. 1.8), among which Tinfoul, Anzate, Tissakatine Center and Ida w Shayq were studied for nannofossils.

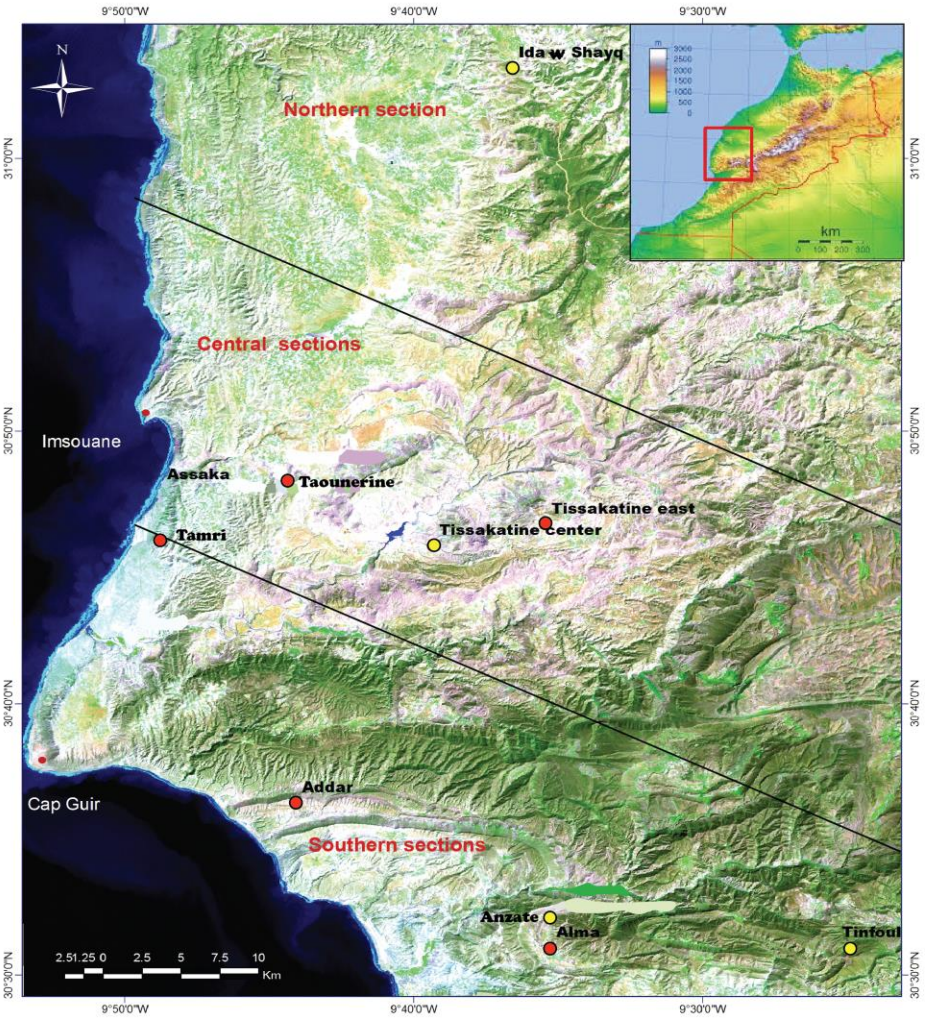

Figure 1.8: Location map of the study area and studied sections. The studied sections are: Tinfoul (Tf); Alma (Alm); Anzate (Anz); Addar (Add); Tamri (Ta); Tissakatine east (TKe); Tissakatine Center (TKC); Taounerine (To); and Ida w Shayq (Ida). All sections studied for sedimentology, sections indicated by yellow circles are investigated for nannofossil and geochemistry.

1.4. PHYSIOGRAPHY AND TECTONIC UNITS OF MOROCCO AND MAZAGAN PLATEAU

The Atlas chains of Morocco consist of two branches, the ENE-trending High Atlas, with summits of 4000 m (highest peak south of Marrakech), and the NE-trending Middle Atlas, which reaches 3000 m (Fig.1.9). These chains are fold-thrust belts formed during the Cenozoic by inversion of Triassic–Jurassic transtensional troughs in the interior of the African plate (e.g. Mattauer et al., 1977; Warme, 1988; Giese and Jacobshagen, 1992; Frizon de Lamotte et al., 2000; Pique´ et al., 2002; Arboleya et al., 2004).

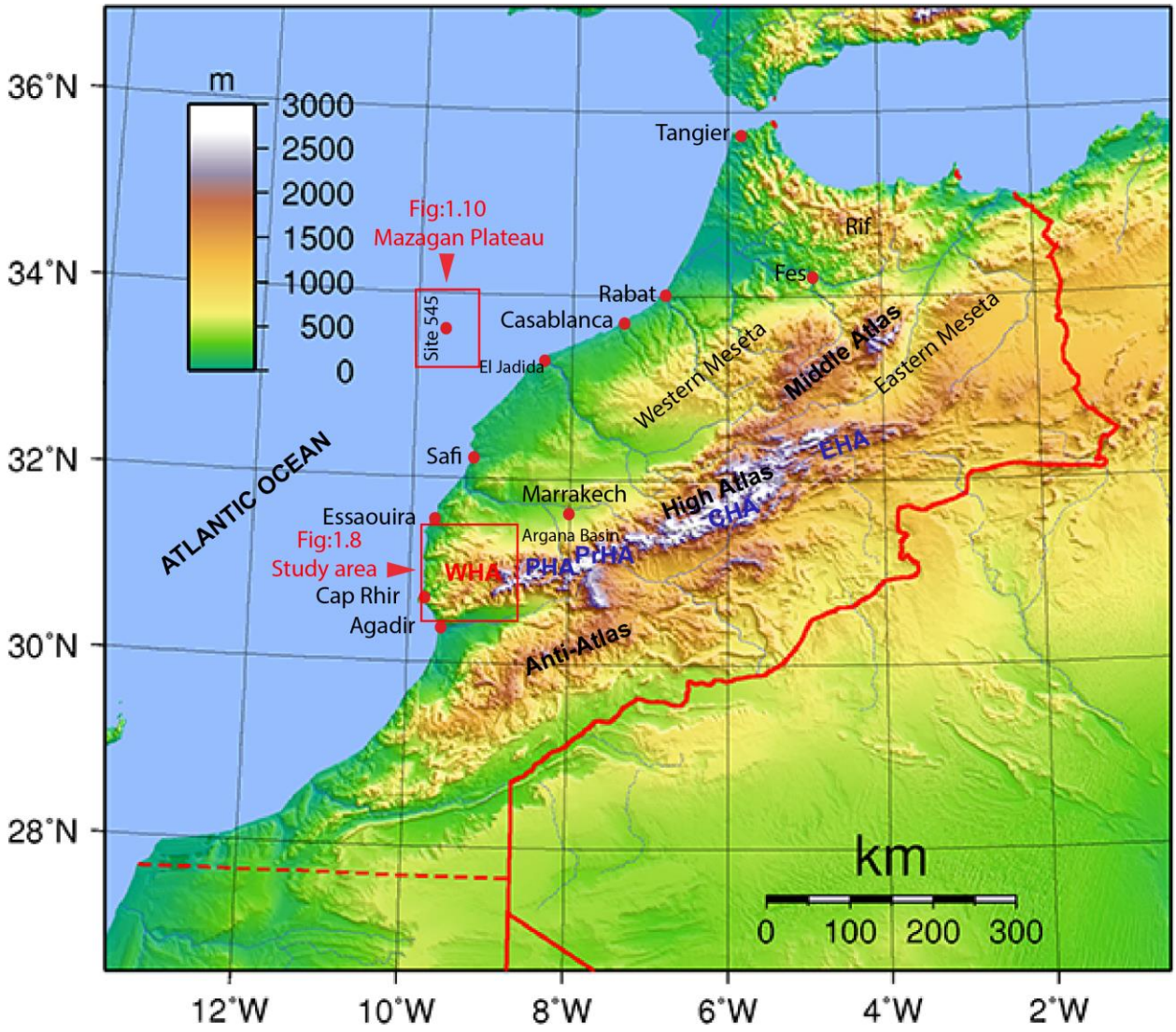

Figure 1.9: Showing the topographic and tectonic units of Morocco, the tectonic setting of the study area and the Mazagan Plateau (the closest locality being investigated for our study).

The plateaus and chains bordering or included within the Atlas belts (such as Rif, Meseta and Anti-Atlas mountains; Fig.1.9), have a high elevation, with altitudes between 1000 and 2000 m. These young mountains were uplifted during the Cenozoic and resulted from the Alpine cycle (Frizon de Lamotte et al., 2008).

The High Atlas is about 800 km long and 40 to 100 km wide, and comprises four parts, which are, from west to east: the Western High Atlas (WHA); the Paleozoic High Atlas (PHA), a horst of Paleozoic terranes intruded by Carboniferous granites and thinly covered by Mesozoic strata; the Precambrian High Atlas (PrHA), a horst of slightly deformed Infra-Cambrian and Precambrian rocks with very thin Mesozoic strata; and the Central and Eastern High Atlas (CHA, EHA; Schaer, 1987).

SEDIMENTARY-TECTONIC HISTORY OF HIGH ATLAS

The tectonic and stratigraphic evolution the Western High Atlas (WHA) was related to the development of the Atlantic margin of northwest Africa, while the rest of the High Atlas was partly to mostly controlled by the evolution of the Tethys Ocean. From the Atlantic coast of Morocco it extends eastward for about 50 to 70 km to the Argana Basin, where the Triassic is up to 5 km thick and comprises essentially detrital and locally conglomeratic facies with evaporitic sequences appearing in the west. Mesozoic strata in the Western High Atlas thicken to the west and consist of Jurassic and Cretaceous calcareous, marly, sandy and locally evaporitic facies, whereas continental strata are predominant in the east. The Western High Atlas was only affected by differential subsidence. Bouatmani et al. (2007) studied the subsidence history of the Western High Atlas in the Essaouira-Agadir Basin and defined 3 main episodes: (i) a fast initial subsidence during the late Triassic – Early Liassic was followed by a slow thermo-tectonic stage from late Liassic to Callovian times; (ii) a new fast tectonic stage during Oxfordian to Berriasian times, was followed by a slower subsidence in Valanginian to Aptian times; (iii) finally, a rapid subsidence occurred in Albian to Cenomanian times, and was followed by a slower or even inverse subsidence during the Late Cretaceous and Tertiary.

The Central and Eastern High Atlas, also known as the Calcareous High Atlas because of thick Mesozoic carbonates, extend as a deep rift trough all the way to the Algerian border. Its

stratigraphic and structural evolution, summarized by Stets and Wurster (1982) and Warme (1988), show the following major phases. Continental rifting in the Late Triassic created the Atlas rift, in which broad alluvial fans prograded towards the center of the grabens (Lorenz, 1988; Manspeizer, 1982; Mattis, 1977) and deposited brick-red fluvial sandstones, conglomerates and mudstones, intercalated with evaporitic horizons (dolomite, gypsum and halite), and with tholeiitic dolerites at the top of the Triassic sequence. While the supply of terrigenous clastics continued during the Jurassic, marine invasions coming from the Tethys along the Atlas gulf, flooded the Moroccan Meseta. In addition to, transgression proceeded eastward from the nascent Atlantic Ocean to the west. From the Early to Middle Jurassic major carbonate build-ups including shallow marine limestones and reefs were established on shoals formed by faulted blocks, whereas gravity-generated limestones and olistostromes accumulated in adjacent deeps (Warme, 1988). Emergence during the Late Jurassic to Early Cretaceous led to the deposition of fluvial, lacustrine and continental red beds (Laville and Pique, 1992). Middle Cretaceous subsidence in the Atlas rift and global sea-level rise caused a major transgression, which extended over adjacent platform areas. During the following regression, fluvial and deltaic fans prograded into the Atlas gulf from east and west. Subsidence ended after the Turonian and, from latest Cretaceous onwards, the Atlas rift began to rise. Border faults were inverted into thrust faults, along which slices of Mesozoic strata were thrust onto the adjacent platforms. The trough fill, now uplifted, was eroded into new alluvial fan systems which filled marginal foredeeps. Structures in the Central High Atlas are ENE-trending asymmetrical folds with tight or faulted anticlines and flat bottomed synclines (Ellero et al., 2012), while in the western part of the Central High Atlas, folding was caused by basement faulting (Schaer, 1988).

THE MAZAGAN PLATEAU

The Mazagan (El Jadida) Plateau and Escarpment constitute the seaward extension of the Moroccan Meseta (Ruellan et al., 1984), located about 200 km southwest of Casablanca in the Central Atlantic and offer an excellent example of a starved continental margin bordering the oldest part of the Atlantic Ocean (Hinz et al., 1984). Detailed morphological features of the Mazagan Plateau and Escarpment is given in Auzende et al. (1984). We present here only the main morphological units (Fig. 1.10).

The shelf and plateau show a gentle slope towards the northwest from the shore down to about 1300 m water depth in the southern part and 1750 m in the northern part. To the South, the Mazagan Plateau segment is an offshore extension of the Moroccan Meseta (Jansa et al., 1984). The crescent shape Escarpment that borders the Plateau is a major feature. It is constituted by a succession of narrow steps formed by vertical cliffs. In the southern part, its depth ranges from 1200 to 2300 m, and in the northern part from 2000 to 3800 m. At the foot of the escarpment there is a large apron marking the transition between the escarpment and the Seine Abyssal plain. This apron is cut by numerous small canyons running towards the west (Fig. 1.10). The sedimentary sequence consists of Jurassic to Early Cretaceous shelf carbonates overlain by Late Cretaceous to Cenozoic hemipelagic and clastic sediments. Site 545 was drilled at the foot of the steep Mazagan Escarpment at a depth of 3150 m. It records a virtually complete succession of hemipelagic sediments of early Late Aptian to Middle Cenomanian age (Leckie. 1984; Fig. 1.10). During the Aptian/Albian, DSDP Site 545 was located at a palaeolatitude of about 20"N (Fig. 1.2) and the palaeo-water depth was in the range from 200 to 1500 m (e.g. Hofmann et al., 2008). The site was located within the easterly trade wind belt and the adjacent African continent was located within the tropical arid belt as indicated by the occurrence of detrital palygorskite in marine sediments and by the occurrence of evaporate deposits along the West African coastal region (Pletsch et al., 1996).

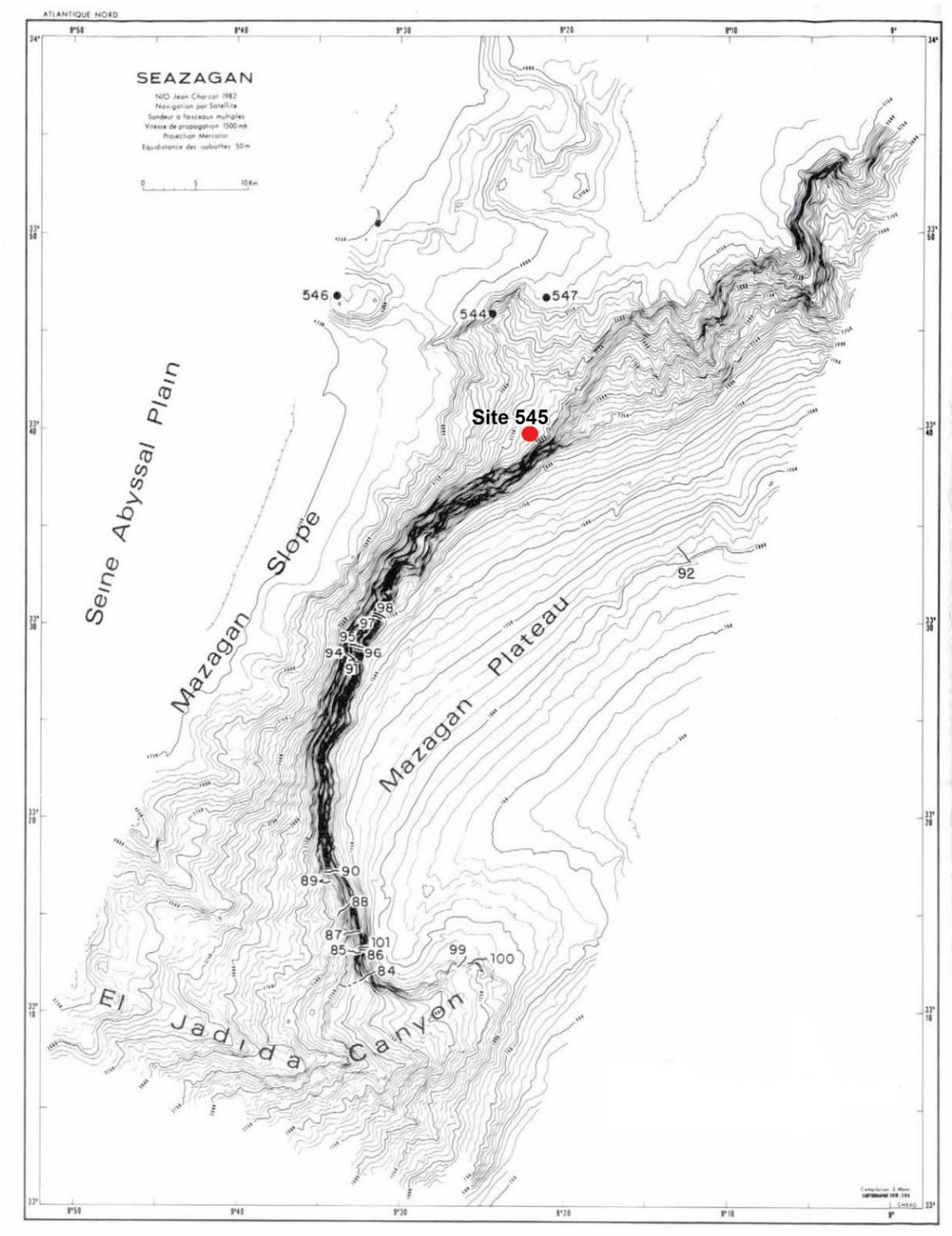

Figure 1.10: Seabeam bathymetric map of Mazagan Plateau with locations of DSDP sites Leg 79 (after Ruellan et al., 1985). Site 545 marked by red circle.

CHAPTER TWO

PREVIOUS WORK

CHAPTER TWO

PREVIOUS WORK

2.1. GEOLOGICAL SETTING

The Essaouira-Agadir Basin (EAB) is part of the African passive margin of the Central Atlantic Ocean (Stets and Wurster, 1982; Coward and Ries, 2003; Zühlke et al., 2004; Hafid et al., 2008). Atlantic rifting started in the Late Permian-Triassic, and culminated with the initiation of oceanic crust accretion in the early Middle Jurassic (Hafid, 2000; Le Roy and Piqué, 2001; Gouiza, 2011). Following the appearance of the oceanic crust, the passive margin entered the post-rift stage characterized by thermal subsidence during Middle Jurassic to Early Cretaceous (Gouiza, 2011), combined with well-recorded eustatic transgressions (Le Roy et al., 1998). Passive margin evolution ended in the Late Cretaceous with the onset of compressional deformations, which culminated in the Late Eocene-Pliocene, with the Atlasic orogeny (Frizon de la Motte et al., 2000, 2008). The folded sedimentary pile of the EAB is presently included in the Western High Atlas Chain (Fig. 2. 1). In the study area, three East-West folds can be distinguished: (1) a central, gentle synclinorium dipping westward, (2) a northern Amsiten anticline, and (3) a southern Cap Rhir-Anklout anticline (Fig. 2. 1). These E-W folds define three areas in the EAB: the southern (Agadir), central (Tamanar), and northern (Essaouira) areas (Fig. 2. 1).

In subsurface, the EAB is composed of various Triassic faulted half-grabens, 10 km wide and 20-50 km long. These grabens are limited by N20°E trending faults, with a dip to the west (Le Roy and Piqué, 2001). The Syn-rifting stage (Late Permian-Triassic to early Middle Jurassic) gave way to the deposition of thick clastic red bed deposits of Late Permian-Triassic age, overlain by a thick series of shales and evaporites intercalated with tholeiitic basaltic flows dated as Early Jurassic (Medina, 1994, 1995; Hafid et al., 2000; Davison, 2005). The post-rifting stage (Middle Jurassic to Early Cretaceous) coincides with the onset of low thermal subsidence of the margin (Medina, 1994; Bouatmani et al., 2007) and with the development of a widespread, shallow marine carbonate platform, and deeper marine carbonates to the West (Zühlke et al., 2004; Davison, 2005; Hafid et al., 2008).

The Cretaceous transgression followed a sharp regression of latest Jurassic age (Zühlke et al., 2004). A first transgressive-regressive cycle began with Berriasian shelf limestones and reached a maximum with Valanginian-Lower Hauterivian open marine marls (Rey et al., 1988; Masrour et al., 2004). The overlying, Late Hauterivian fluvial sandstones and siltstones are shallowing upward deposits, which are overlain by inner shelf limestones or fluvial to shallow marine sandstones of Late Hauterivian-Barremian age (Canérot et al., 1986; Witam, 1998). A second cycle began with Early Aptian shelf limestones grading upwards into open marine shales of Late Aptian to Albian age, which are in turn overlain by shallow marine marls and limestones, or even sandstones of latest Albian age (Butt, 1982; Essafraoui et al., 2010). Late Cretaceous times are then characterized by two additional transgressive-regressive cycles; one of Cenomanian-Turonian age, marked by a regional discontinuity at the Cenomanian/Turonian Boundary (Ettachfini et al., 2005; Jati et al., 2010), and another of Senonian age, which is represented by an important regression due to compressional tectonic event of Campanian age, followed by a transgression during the Maastrichtian (Algouti et al., 1999). Salt tectonic and diapir activity began in the Jurassic and occurred repeatedly during the Cretaceous, mainly controlling facies distribution in the distal, offshore part of the basin (Tari et al., 2000; Mehdi et al., 2004; Zühlke et al., 2004).

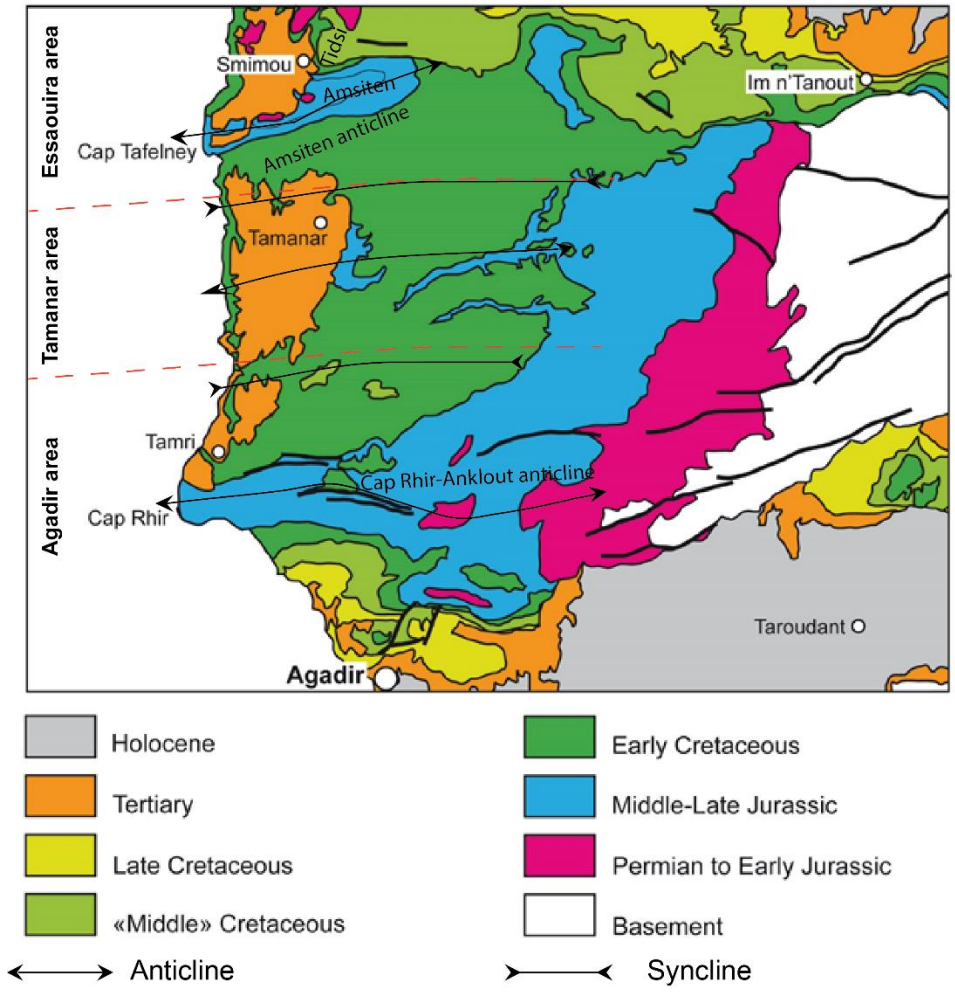

Figure 2.1: Geological map of the Essaouira-Agadir Basin modified after Saadi (1982).

2.2. LITHOSTRATIGRAPHY OF THE APTIAN-ALBIAN ROCKS IN EAB

The Aptian-Albian lithostratigrapy in EAB is compiled from the studies of the following workers: Choubert and Faure-Muret (1962), Ambroggi (1963), Duffaut et al. (1966), Wiedmann et al. (1978), Butt (1981, 1982), But et al (1984), Jansa and Wiedmann, (1982), Wiedman et al. (1982), Behrens et al. (1978, 1982), Canérot et al. (1986), Rey et al. (1988), Andreu (1989, 1991, 1992a, b), Tajeddine et al. (1993), Witam et al. (1993), Bourgeoini (1994), Witam (1998), Nouidar and Chellai, (2001), Bourgeoini et al. (2002), and Zühlke et al. (2004).

2.2.1. Upper Bouzergoun Formation (Upper Barremian-Lower Aptian)

Author: Duffaud et al. (1966**)**.

Type section: North Tamri.

Thickness: It varies from 5 m (jbel Mradma) to 18 m (Oued T'Iit).

Synonyms: Tazought Fm. (defined by Rey et al., 1986b; located in the Northeastern part of EAB).

Description: Thin bedded, rippled sandstones, purplish-blue or green clays, are intercalated by thin carbonate beds with algal laminations, yellow crystalline dolomites and bivalve-bearing limestones with large oblique stratification.

Faunal content: it is rich in microfossils (e.g. *Chofatella decipiens* and ostracods; Witam, 1998), and macrofossils (brachiopods, bivalves, echinoids, rare ammonites, gastropods, annelids and bryozoans). The microfauna comprises *Blowiella duboisi*, *Blowiella gottisi*, *Lilliputianella similis*, *Hedbergella infracretacea*, *Praehedbergella sigali, Globigerinelloides cepedei, Lenticulina nodosa*, *Lenticulina secans, Choffatella decipiens, Gavelinella barremiana* Bettenstaedt, as well as the ostracods *Cytherella* gr. *parallela, Cytherella ovata*, *Protocythere derooi*, *Cythereis (Rehacythereis) btaterensis* and *Rehacythereis punctatafoveolata* (Bourgeoini et al., 2002).

Age: Duffaud (1966) assigned the Upper Bouzergoun Fm to the Early Aptian (Bedoulian) and Bettar (1988), based on palynology, assigned it to the Upper Barremian-Lower Bedoulian.

Depositional environments: Shallow shelf (Rey et al., 1988) to paralic deposits (Butt, 1982; Witam et al. 1993; Nouidar and Chellai, 2001).

Stratigraphic boundaries: underlain and overlain by hard surface (Witam, 1998; Bourgeoini et al., 2002).

2.2.2. Tamzergout Formation (Middle Aptian)

Author: Duffaud et al. (1966)

Type section: East of Tadhart village.

Thickness: 6 m (jbel Mradma) to 15 m (Oued Tlit, Jbel Talbourine)

Synonyms: Tadhart Formation, defined by Rey et al. (1986a).

Description: The Tamzergout Fm is mainly made of wavy-bedded marly limestones alternating with sandy yellow marls and nodular marly limestones.

Faunal content: It is rich in microfossils (Globigerinids, Rotaliporoids and Lagenids; Witam, 1998), and macrofossils (brachiopods, bivalves, echinoids, ammonites, belemnites, gastropods, annelids; Witam, 1998). The microfossil fauna is mainly composed of *Blowiella duboisi/Blowiella gottisi, Blowiella blowi, Gorbachickella hoterivica*, *Lilliputianella bizonae*, *Schackoina cabri*, *Hedbergella gorbachikae*, *Globigerinelloides ferreolensis*, G. *algerianus*, *Hedbergella* aff. *trochoidea* Gandolfi, *Blefuscuiana* cf. *aptica*, *Biglobigerinelloides barri*, *Lenticulina (Planomalina) complanata*, *Dorothia oxycona*, *Epistomina chapmani* and *Ammobaculites subcretaceous*. The ostracods are represented by the genera *Dordoniella, Schuleridea, Paracypris, Bairdia* and *Eocytheropteran* (see Bourgeoini et al., 2002).

Age: "Middle" Aptian (Gargasian), *Subnodosocostatum*, *Melchioris* and *Nolani* ammonite zones (Canerot et al., 1986; Witam, 1998).

Depositional environments: Inner shelf depositional environment (Butt, 1982; Witam, 1998).

Stratigraphic boundaries: The Tamzergout Fm is underlain by a hard surface capping the littoral clastic sediments of the Bouzergoun Fm, and is overlain by perforated, hard surface covering yellow silty limestone facies (Rey et al., 1988; Witam, 1998, Bourgeoini et al., 2002).

Remarks: Witam (1998) reported that there is no lithological differences between the Tamzergout and Tadhart fms, so that they could not be differentiated in the field. So, he suggested that the Tadhart Fm should be replaced by the Tamzergout Fm.

2.2.3. The Lemgo Formation (Late Aptian)

Author: Duffaud et al. (1966)

Type section: Jbel Lemgo ridge, east of Imi N'Tanout.

Thickness: 16.5 m thick.

Synonyms: Equivalent to the lower Qued Tidsi Fm defined by Rey et al. (1986a) in the western part of EAB.

Description: It consists of alternated beds of green/yellow sandy marls and sandy dolomites

Faunal content: The Lemgo Fm is rich in microfossils (Globigerinids, Rotaliporoids and Lagenids; Witam, 1998), and macrofossils (brachiopods, bivalves, echinoids, ammonites,

belemnites, gastropods; Witam, 1998). The microfossils chiefly consist of *Favusella washitensis*, *Ticinella bejaouensis*, *Pleurostomella subnodosa*, *Epistomina spinulifera* and *Valvuleneria* affl. *Parva* (Bourgeoini et al., 2002).

Age: Late Aptian (Clansayesian; *Jacobi* ammonite Zone, Canerot et al. 1986; Rey et al. 1986a; Rey et al.1988; Witam, 1998), confirmed by *Ticinella bejaouensis* planktonic foraminiferal Zone of Clansayesian age (Andreu, 1992; Tajeddine et al., 1993; Bourgeoini, 1994; Bourgeoini et al., 2002).

Depositional environments: The Lemgo Fm has been deposited in a deep water**,** outer shelf depositional environment (Butt, 1982; Butt et al., 1984; Witam, 1998).

Stratigraphic boundaries: It is underlain by a hard perforated, ferruginous surface and is overlain by a hard oxidized, perforated surface (Witam, 1998; Bourgeoini et al., 2002).

2.2.4. Oued Tidsi Formation (Early Albian)

Author: Duffaud et al. (1966**)**.

Type section: Oued Tlit in Oued Tidsi valley, 5 km to the north of Smimou.

Thickness: At the type locality in the western part of the basin (Oued Tlit), it reaches a thickness of 230 m; in the eastern part, it reaches 38 m at Imi N'Tanout.

Synonyms: Lemgo Fm in the eastern part of EAB is equivalent to lower Oued Tidzi Fm.

Description: The Oued Tidsi Fm consists of green/yellow shales and marls rich in ammonites, globigerinids, rotalids, lagenids, intercalated with sandy dolomites; it is marked by small size pyritized ammonite (Rey et al. 1986a).

Faunal content: It contains rare planktonic foraminifera and diverse benthic foraminifera (But et al. 1982; 1984). Typical planktonic foraminifera are *Ticinella bejaouaensis, Favusella washitensis, Ticinella primula, Hedbergella amabilis* and *H. planispira.* Typical benthic foraminifera are *Valvulineria gracillima* and *Epistomina spinulifera.* Nodosariids are abundant with a high frequency of lenticulinids, but agglutinated foraminifers such as *Textularia, Dorothia, Reophax* and *Haplophragmoides* are rare (see But et al. 1984).

Age: In the western and central parts of EAB, the Oued Tidzi Fm is assigned to the Clansayesian to Albian interval. In the eastern part of EAB (lmi N'Tanout and Amizmiz), it is ascribed to the Early Albian (Andreu, 1991; Bourgeoini, 1994), marked by *Beudanticeras*

dupinianum and *Leymeriella* cf. *tardefurcata* beds of Wiedmann et al. (1978) and Rey et al. (1986a), and characterized by the *Hedbergella planispira* and *Ticinella primula* planktonic foraminiferal Zones (Bourgeoini et al., 2002).

Depositional environments: The Oued Tidsi Fm was deposited in deep open marine, outer shelf environment to basin margin setting (Butt, 1982; Canerot et al., 1986; Zühlke et al., 2004).

Stratigraphic boundaries: It is bounded at the base and top by two regional, hard oxidized surfaces. The lower surface separates the yellow limestone beds of the Lemgo Fm from the green marls of the Oued Tidsi Fm; the upper boundary separates the Oued Tidsi Fm from the sandy dolomite beds of the Kechoula Fm (Zühlke et al., 2004).

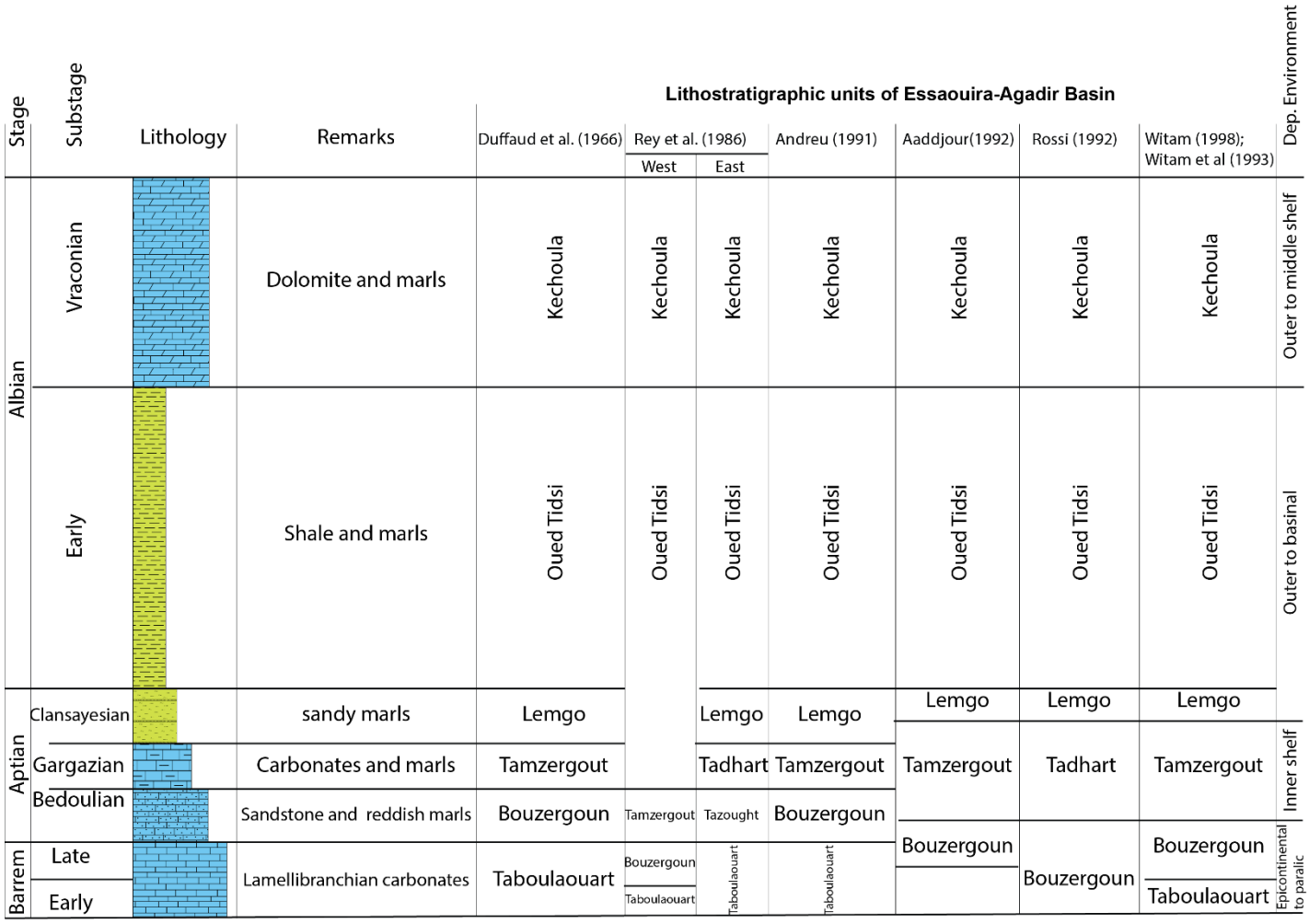

Figure 2.2: Showing the Aptian-Albian stratigraphic units defined by Duffaud et al. (1966) and its equivalents in the EAB.

2.3. BIOSTRATIGRAPHY

2.3.1. Ammonite

Ammonites from the Aptian and Albian deposits of the EAB have been first reported respectively by Lemoine (1905) and Brives (1905), Gentil (1905), Kilian and Gentil (1906, 1907), and later, Roch (1930), listed some faunas and proposed stratigraphic interpretations. Ambroggi (1963) published the first regional synthesis, which remains until today the reference for the understanding of the Jurassic and Cretaceous stratigraphy of the basin. Robert *in* Peybernes et al. (2013) established an Aptian-Early Albian ammonite biostratigraphic framework for the EAB, from a detailed analysis of the ammonite species identified in five Aptian-Albian sections located along an E-W transect. From the reference section of Addar, Robert correlated the established ammonite biozones of EAB with the Standard Mediterranean Zonation proposed by IUGS Lower Cretaceous Ammonite Working Group ("Kilian Group"; Reboulet et al., 2011). Part of the ammonite biozone succession observed in the EAB was well-correlated with the four Late Aptian standard zones (*Epicheloniceras martini*, *Parahoplites melchioris*, *Acanthohoplites nolani* and *Hypacanthoplites jacobi*) and with the first two zones of the Early Albian (*Leymeriella tardefurcata* Zone and *Douvilleiceras mammillatum* Superzone). The uppermost Early Aptian standard zones (*Deshayesites deshayesi* and *Dufrenoyia furcata*) have also been identified but with less confidence because of condensed sedimentation and temporal hiatuses (Robert *in* Peybernes et al., 2013). The so-defined ammonite zones are assemblage or interval zones. Robert (*in* Peybernes et al., 2013) identified the Aptian/Albian boundary in EAB between the *Hypacanthoplites jacobi* Zone and the *Leymeriella tardefurcata* Zone. In the present study, we will also use the last occurrence of *Hypacanthoplites jacobi* and/or the first occurrence of a marker species of the *Leymeriella tardefurcata* zone to locate the Aptian/Albian Boundary.

STAGES		Reboulet et al. (2009; 2011; 2014) "The Standard Mediterranean Zonation" ZONES	Robert in Peybernes et al. (2013) in EAB ZONES
ALBIAN	Middle	*Euhoplites lautus* / *Euhoplites loricatus* / *Hoplites dentatus*	Not studied
	Lower	*Douvilleiceras mammillatum*	*Douvilleiceras mammillatum*
		Leymeriella tardefurcata	*Leymeriella tardefurcata*
APTIAN	Upper	*Hypacanthoplites jacobi*	*Hypacanthoplites jacobi*
		Acanthohoplites nolani	*Acanthohoplites nolani*
		Parahoplites melchioris	*Parahoplites melchioris*
		Epicheloniceras martini	*Epicheloniceras martini*
	Lower	*Dufrenoyia furcata*	*Dufrenoyia furcata*
		Deshayesites deshayesi	*Deshayesites deshayesi*
		Deshayesites weissi /forbesi	*Deshayesites weissi*
		Deshayesites oglanlensis	*Deshayesites oglanlensis*
BARRE	Upper	*Imerites giraudi*	

Table 2.1: Ammonite standard zonation of the Aptian-Early Albian stages of Mediterranean province compared with its counterpart in the Essaouira-Agadir Basin, as studied by Robert (*in* Peybernés et al., 2013).

2.3.2. Planktonic foraminifera

Bourgeoini et al. (2002) identified seven planktonic foraminiferal zones in the Aptian-Early Albian succession of the EAB (Fig. 2.3). They replaced the standard foraminiferal Zone of *Hedbergella trochoidea* by the *H. gorbachikae* Zone. The upper Late Aptian-Early Albian foraminiferal zones defined by Bourgeoini et al. (2002) in the EAB can be correlated with their counterparts in the Tethyan domain defined by Leckie (2002; Fig. 2.3). Leckie (1984) studied the Late Aptian-Early Albian planktonic foraminifera of the DSDP Site 545, located off Central Morocco (Mazagan Plateau, Central Atlantic), and recognized the following Late Aptian zones: *Globigerinelloides ferreolensis*, *G. algerianus*, *Hedbergella trochoida*, and *Ticinella roberti*

(corresponding to the *Ticinella bejaouensis Zone*, Bralower et al., 1993; 1997), and the Early Albian *Hedbergella planispira* zones (Fig. 2.3).

The Aptian/Albian boundary interval (AABI) in the EAB is difficult to recognize with foraminifera. Bourgeoini et al. (2002) could not recognize the Aptian/Albian Boundary precisely, because some planktonic foraminiferal zonal boundaries remained uncertain, poor foraminiferal preservation is frequent, and microfossils are quite scarce in some intervals leading species identification difficult. Then, Bourgeoini et al. (2002) reported that the Aptian/Albian Boundary in EAB is recognized based on the first occurrence of a marker of the *Leymeriella tardefurcata* ammonite zone. At DSDP Site 545, Bralower et al. (1993) placed the Aptian/Albian Boundary at the last occurrence of *T. bejaouensis*. Moreover, the identification for the Aptian/Albian Boundary based on the LO of *T. bejaouensis* is not accepted by many others (e.g. Caron, 1985; Hart et al., 1996; Kennedy et al., 2000; Leckie et al., 2002). Consequently, the Aptian/Albian Boundary at Site 545 remains a matter of debate.

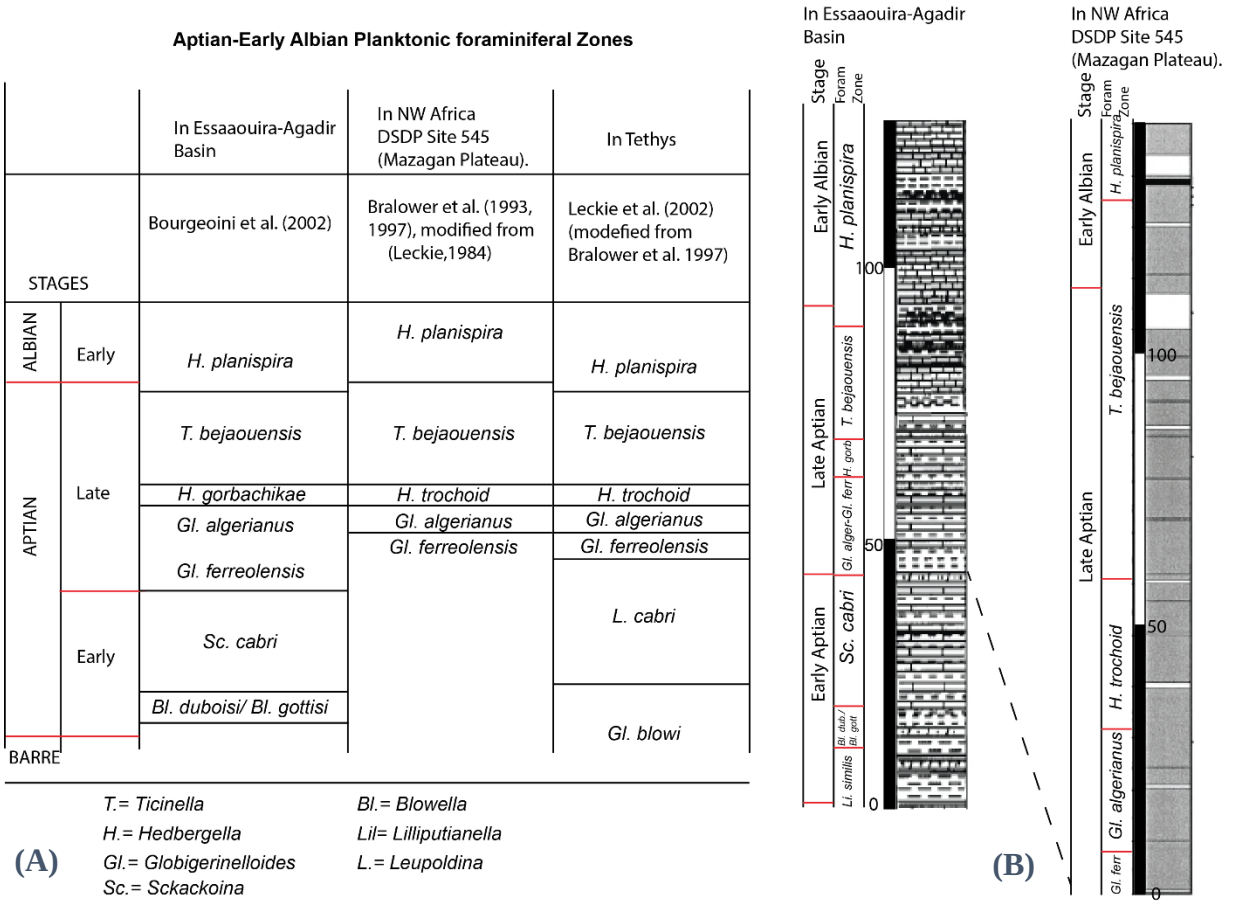

Figure 2.3: A) Planktic foraminiferal biostratigraphy of the Aptian to Early Albian of the EAB by Bourgeoini et al. (2002); DSDP Site 545 (Mazagan Plateau) after Leckie (1984), with modifications by Bralower (1992), Bralower et al. (1993, 1997), and Herrle (2002); in the Tethys Ocean from Leckie et al. (2002), modified from Bralower et al. (1997); B) Showing the planktonic foraminiferal zonation differences between the studied composite section in the EAB by Bourgeoini et al. (2002) and the Mazagan Plateau section studied by Herrle (2002) and Herrle et al. (2004).

2.3.3. Calcareous nannofossils

The Aptian-Albian nannofossil biostratigraphy of the EAB has not been done before this present work and only a paleoenvironmental study is available for this basin (Peybernès et al., 2013). The Late Aptian-Early Albian interval of DSDP Site 545 (Mazagan Plateau, NW Africa; Fig. 2.4) was initially studied by Wiegand (1984), then modified by Bralower et al. (1993; 1997), and three nannofossil Subzones NC7C, NC8A and NC8B have been recognized. Recently, Herrle (2002) recognized two nannofossil zones: (1) the *R. angustus* Zone (NC7) of Late Aptian age, subdivided into NC7B and NC7C, and (2) the *P. columnata* Zone of Late Aptian-Early Albian age, subdivided into NC8A (Late Aptian) and NC8B (latest Aptian-Early Albian). The

Aptian/Albian Boundary at Site 545 is not defined based on nannofossil (Bralower et al., 1993; Herrle, 2002; Fig. 2.4).

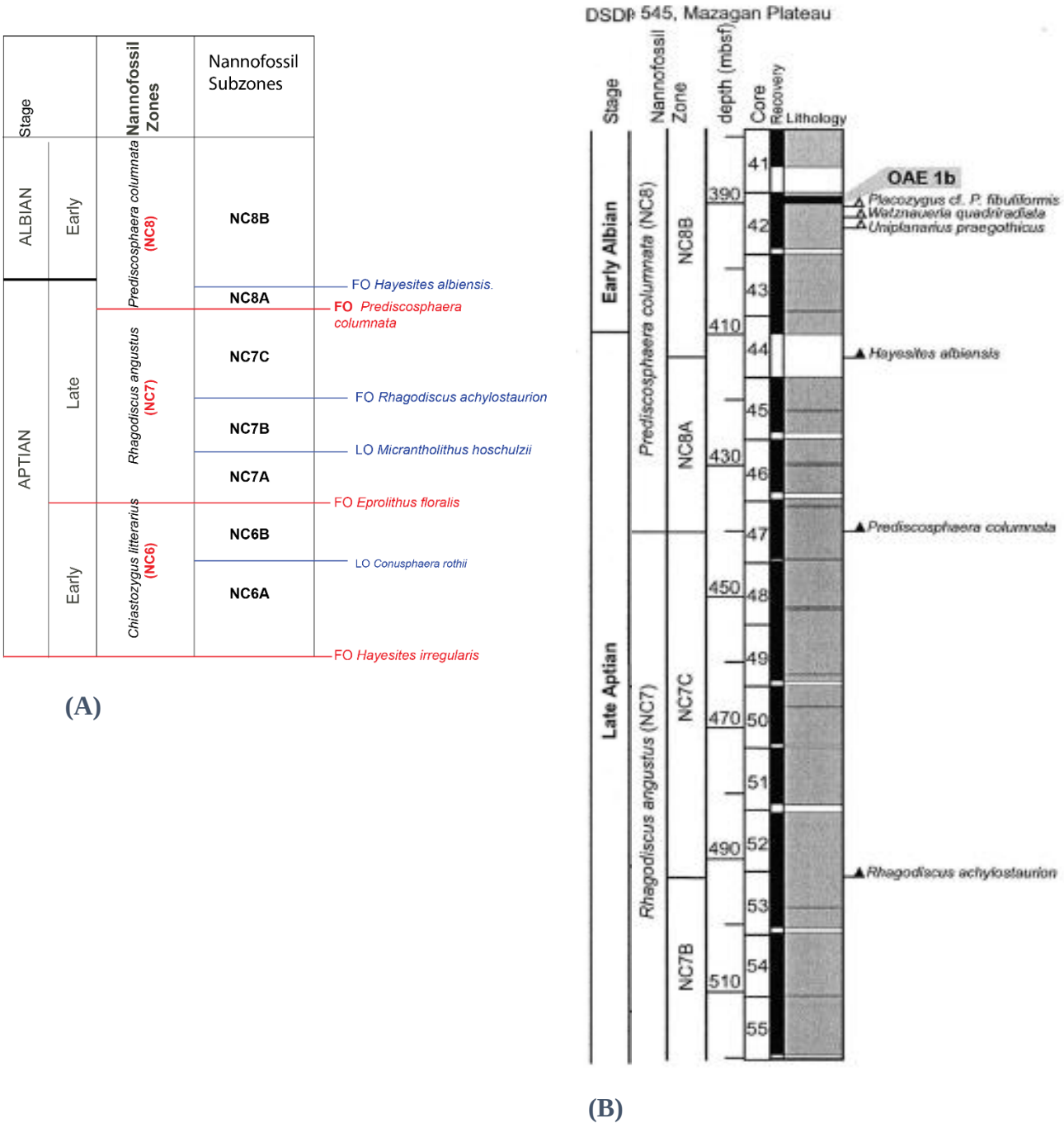

Figure 2.4: (A) Standard nannofossil biozones by Bralower et al. (1995) showing the relationship between nannofossil zones and the position of the Aptian/Albian boundary, zone and subzone markers are shown on the right. (B) Calcareous nannofossil biostratigraphy of the Aptian to Early Albian of DSDP Site 545 (Mazagan Plateau) after Wiegand (1984) with modifications by Bralower et al. (1993, 1997), and Herrle (2002).

2.4. STABLE ISOTOPE

The Aptian-Albian carbon isotope stratigraphy of the EAB has not been documented before this work. Herrle (2002) and Herrle et al. (2004) present a carbon isotope record of the Mazagan Plateau (DSDP Site 545; Fig. 2.5) and proposed correlations with the high-resolution and detailed carbon isotope stratigraphy established in the Vocontian Basin (SE France) for the Aptian-Albian interval.

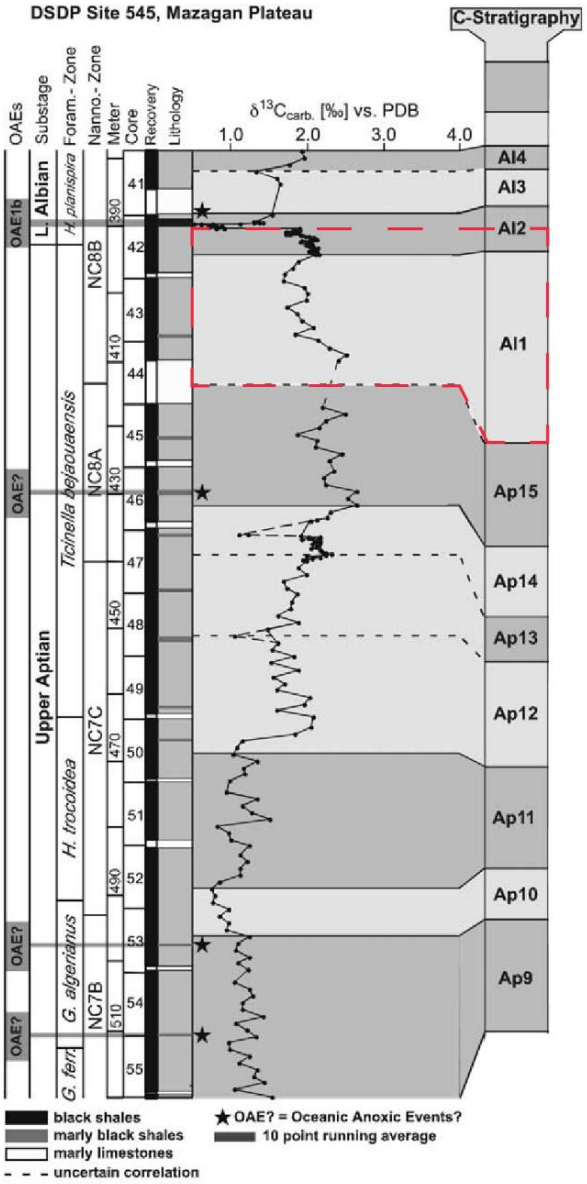

Figure 2.5: Carbon isotope stratigraphy for the Aptian to Lower Albian of the Mazagan Plateau with regional and supra-regional key beds plotted against biostratigraphy by Herrle (2002) and Herrle et al. (2004). Biostratigraphy of the Mazagan Plateau after Leckie (1984), Wiegand (1984), and Bralower et al. (1993; 1997). "The break point between the end of the uppermost Aptian positive carbon isotope and the onset of the pronounced negative shift of $\delta^{13}C$ values, which can be recognized in the terrestrial records, carbonate platforms, and in hemipelagic and pelagic environments, is proposed as an alternative criterion to determine the Aptian/Albian boundary " (red dashed interval) (Herrle et al., 2004).

2.4.1. Carbon isotope

Herrle (2002) and Herrle et al. (2004) introduced a new terminology to describe both long- and short-term of $\delta^{13}C$ fluctuations, and defined 11 units in the Late Aptian-Early Albian interval in the Mazagan Plateau (Shown in Fig. 2.5; summarized in Table 2.2), with the prefix "Ap" for the Aptian stage and "Al" for the Albian stage. The Late Aptian is composed of 7 units (Ap9 to Ap15) and the Early Albian comprises 4 units (Al1 to Al4). Herrle (2002) and Herrle et al. (2004) combined the carbon isotope changes with the nannofossil biostratigraphic record as shown in Table (2.2):

Table 2.2
Definition of the boundaries of the carbon isotope stratigraphic units Ap8 to Al4 and their nannofossil biostratigraphic positions

Stages	Units	Carbon isotope stratigraphy	Nannobiostratigraphy
Early Albian	Al3/Al4	transition from low to high $\delta^{13}C$ values	middle part of NC8B
	Al2/Al3	transition from high to decreasing $\delta^{13}C$ values	middle part of NC8B
	Al1/Al2	transition from low to increasing $\delta^{13}C$ values	lower part of NC8B
Late Aptian	Ap15/Al1	end of the second positive carbon isotope excursion	lowermost part of NC8B
	Ap14/Ap15	transition from low to high $\delta^{13}C$ values	uppermost part of NC7b/NC7C
	Ap13/Ap14	transition from high to low $\delta^{13}C$ values	upper part of NC7b/NC7C
	Ap12/Ap13	transition from low to increasing $\delta^{13}C$ values	upper part of NC7b/NC7C
	Ap11/Ap12	onset of the second Aptian positive carbon isotope excursion	middle part of NC7b/NC7C
	Ap10/Ap11	transition from decreasing $\delta^{13}C$ to an interval without a general change in $\delta^{13}C$ values	lower part of NC7b/NC7C
	Ap9/Ap10	transition to decreasing $\delta^{13}C$ values	lower part of NC7b/NC7C
	Ap8/Ap9	transition from decreasing $\delta^{13}C$ values to an interval	lowermost part of NC7b/NC7C

In Summary: The Aptian/Albian Boundary could be recognized from the carbon isotope stratigraphy, through a slight decrease of the $\delta^{13}C$ values at the top of Ap15, followed by a continuous decrease of $\delta^{13}C$ values in unit Al1 reaching up to 1.5‰ (Fig. 2.5).

2.4.2. Oxygen isotope

The Aptian-Albian oxygen isotope of the EAB has not been studied before the present work. Herrle (2002) studied the $\delta^{18}O$ record from bulk rock samples of the Mazagan Plateau (DSDP Site 545; Fig. 2.6). The interval between the base of the succession to the upper two third of NC7B calcareous nannofossil Subzone is characterized by slightly decreasing $\delta^{18}O$ values, followed by increasing values in the lower part of the NC7C calcareous nannofossil Subzone. The interval corresponding to the upper part of the NC7C calcareous nannofossil Subzone is characterized by increasing values of $\delta^{18}O$. Several shifts to more negative $\delta^{18}O$ values can be recognized from the upper part of the NC7C to the lower part of the NC8B calcareous nannofossil subzones. In the upper part of the NC8B calcareous nannofossil Subzone, the $\delta^{18}O$ record shows a decreasing trend, with the most negative values within the black shale, reflecting warmer conditions, followed by increasing values until the top of the succession, indicate cooler conditions during Early Albian (Fig. 2.6). The $\delta^{18}O$ values are interpreted to eflect predominantly a primary signal.

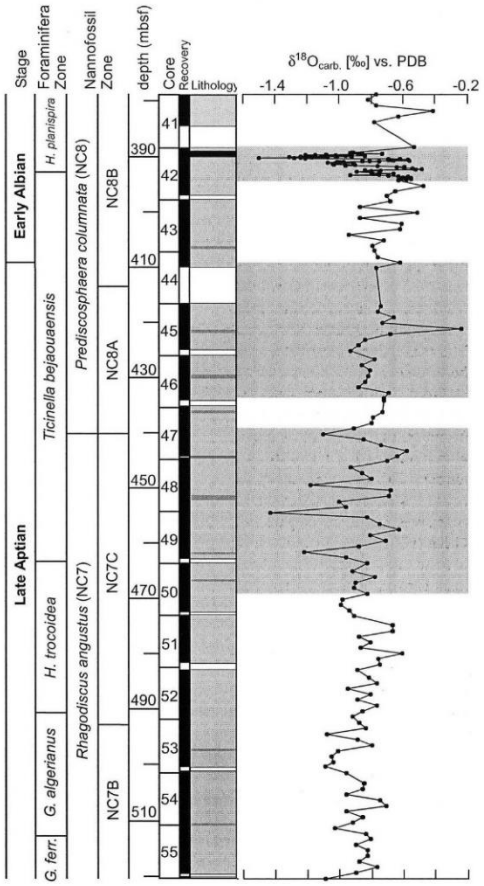

Figure 2.6: $\delta^{18}O$ values of the Aptian to Early Albian interval from the Mazagan Plateau (DSDP Site 545) by Herrle (2002).

2.5. THE APTIAN/ALBIAN BOUNDARY

2.5.1. The biostratigraphic markers across the Aptian/Albian Boundary (AAB)

At the conclusion of the meeting of the Working Group on the Albian Stage (Brussels, 1995; Hart et al., 1996), several biomarkers were identified to define the base of the Albian Stage. These were : (1) the first appearance of the ammonite *Leymeriella schrammeni*, as shown in artificial exposures at Vöhrum, west of Hannover, Germany (Owen, 1979; Hart et al., 1996), and based on the studies of Col de Pré-Guittard section (Drôme, France; Kennedy et al., 2000; Herrle and Mutterlose, 2003; Kennedy et al., 2014) , (2) the first occurrence of the ammonite *Leymeriella tardefurcata*, (3) the first occurrence of the calcareous nannofossil species *Prediscosphaera columnata*, (4) the last occurrence of the ammonite *Hypacanthoplites jacobi*. Recently, Petrizzo et al. (2012, 2013) and Kennedy et al. (2014) re-visited the Pré-Guittard section and proposed a new definition for the base of the Albian Stage with the first occurrence of the planktic foraminifera *Microhedbergella renilaevis*, within the Niveau Kilian, in the lowermost part of NC8 nannofossil Zone, and beneath the globally recognizable OAE 1b.

At Vöhrum, the definition of the base of the Albian Stage has been rejected, as *Leymeriella schrammeni* can only be recognized over a limited area, and no more widely recognized secondary markers have been documented (Kennedy et al., 2000).

At the Col de Pré-Guittard section, the Aptian-Albian Boundary (AAB) is difficult to identify, since there is a hiatus close to the boundary in the section (Kennedy et al., 2000), in spite of a well-developed sequence (Kennedy et al., 2014). Because of its limited distribution, the first occurrence of *Leymeriella tardefurcata* is difficult to identify outside southeastern France and the European province (Owen, 2002; Premoli Silva, 2010). Planktonic foraminifera are not helpful either, since only small *Hedbergella* are common because of a distinctive crisis during the AAB interval. The disappearance of the genus *Ticinella* and the last occurrence of *Ticinella bejaouensis* at critical intervals across the AAB (Hart et al., 1996), makes it difficult to use the LO of *Ticinella bejaouensis* as a suitable bioevent, as have been used by many workers (leckie, 1984; Bralower et al. 1993).

DSDP Site 511 (southern South Atlantic) is the most complete and best preserved of the studied AABI in deep-sea sections. There, Huber and Leckie (2011a) defined a major planktic foraminiferal species turnover accompanied by a dramatic reduction in shell size, a fundamental change in shell architecture, and a sharp drop in the abundance of planktic relative to benthic

species occurring across the Aptian/Albian boundary interval (AABI). They defined one very small, smooth-surfaced, thin walled species of *Microhedbergella*: *Microhedbergella miniglobularis*. The latter species have also been identified just above the Kilian black shale level in the Vocontian Basin (southeast France; Huber and Leckie, 2011).

In central Italy, Premoli Silva (1989a) placed the AAB within the late *Ticinella bejaouaensis* foraminiferal Zone, whereas Leckie et al. (2002), in a synthesis, located it at the base of the *Hedbergella planispira* foraminiferal Zone (Fig. 2.3).

The calcareous nannofossils biostratigraphic signal has been also recently challenged. The important index species *Prediscosphaera columnata* (circular) first occurs in the Pré-Guittard section about 3 m above the top of the Paquier level, while in the Tartonne section (Vocontian Basin, SE France), it can be found more than 11 m below the base of the Paquier level. This would imply diachroneity of the Paquier level between the two studied sections. Bown (*in* Kennedy et al., 2000) mentions that the circular form is difficult to determine. The earlier occurrence of *Prediscosphaera* forms known from the uppermost Aptian of north Germany are taxonomically less strictly defined (nearly round, subcircular) and thus difficult to use. In spite of this, *Prediscosphaera columnata* is a globally distributed planktonic species and should remain a candidate at least as a secondary marker event close to the Aptian/Albian Boundary. However, strict morphological definition needs to be specified in order to obtain stratigraphic consistency (in Kennedy et al., 2014).

In summary: the ammonite marker species (*Leymeriella schrammeni* and *Leymeriella tardefurcata*) are of limited known distribution. The foraminiferal marker species used to define the AAB differ from a worker to another: LO of the *T. bejaouensis* (Bralower et al., 1993); late *Ticinella bejaouaensis* foraminiferal Zone (Permoli Silva, 1989a); base of *Hedbergella planispira* foraminiferal Zone (Leckie et al., 2002); within the *Ticinella* bejaouaensis Zone (Kennedy et al., 2000; Herrle and Mutterlose, 2003); FO of the *Microhedbergella renilaevis* (Petrizzo et al., 2012; Kennedy et al., 2014). Moreover, the foraminiferal marker species disappear in critical intervals around the AAB. The FO of the nannofossil marker species *P. columnata* seems to be diachroneous and its morphological definition should be specified (Bown, *in* Kennedy et al., 2000, 2014). Consequently, the identification of AAB depending on the biostratigraphy is still a controversial issue.

2.5.2. The Carbon isotope signals a cross the Aptian/Albian Boundary

The Aptian/Albian Boundary is characterized by a minimum value of a negative excursion of approximately 1‰ in $\delta^{13}C$ records, which can be traced in many Tethyan and Atlantic settings (Bralower et al., 1999; Herrle, 2002; Herrle et al., 2004; Lucina et al., 2004; Wagner et al., 2007; Trabucho-Alexandre et al., 2011; Petrizzo et al., 2012, 2013).

2.5.3. The Aptian/Albian Boundary in EAB and Mazagan Plateau

The Aptian/Albian Boundary is poorly documented in the EAB and identified until this work only with ammonites, and placed between the *Hypacanthoplites jacobi* Zone and the *Leymeriella tardefurcata* Zone (Robert *in* Peybernes et al., 2013). In the Mazagan Plateau the Aptian/Albian Boundary is identified by the last occurrence of *Ticinella bejaouensis* (Bralower et al., 1993) and by the decrease in the $\delta^{13}C$ values (Herrel, 2002; Herrle et al., 2004).

2.6. SEQUENCE STRATIGRAPHY

Witam (1998) studied the sedimentology and sequence stratigraphy of the Barremian-Aptian succession in the EAB, and recognized seven third order sequences. Each sequence was defined by its lower and upper sequence boundary (SB), transgressive and maximum flooding surfaces (TS, MFS), Lowstand Systems Tract (LST), Transgressive Systems Tract (TST) and Highstand Systems Tract (HST).

Sequence Ba-Ap1 (Upper Barremian-lowermost Aptian). This sequence corresponds to the Upper Bouzergoun Fm, and exhibits clastic facies. The Lower SB would correspond to a ravinement surface; the LST is represented by valley fill deposits; the TST would be made of two parasequences of alternated red sandstone and calcareous sandstone, the MFS being difficult to identify; and the HST corresponds to shallow marine red sandstone and sandy limestone.

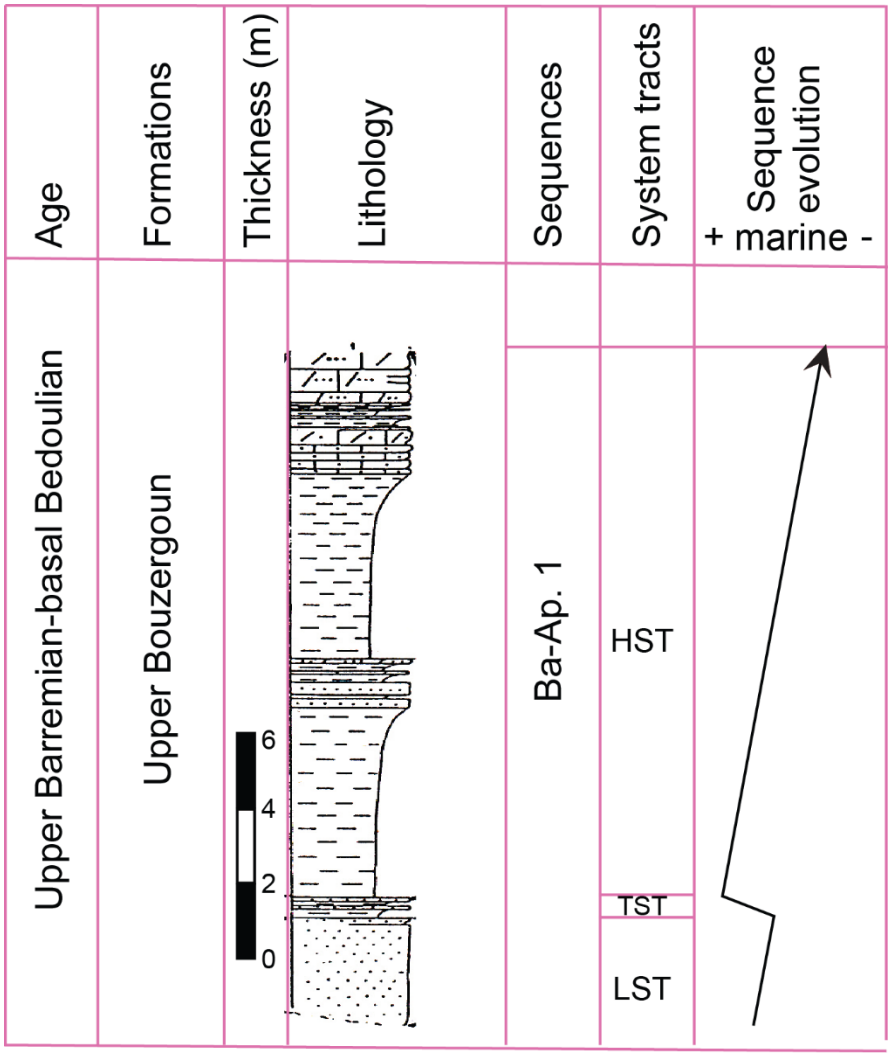

Figure 2.7: Ba-Ap. 1 Sequence at Tamzergout section, EAB by Witam (1998).

Sequence Ap. 2 (Lower Aptian-Middle Aptian; *weissi*, *deshayesi* and *furcata* ammonite zones). It corresponds to the Upper Bouzergoun and basal Tamzergout fms. The Lower SB is a perforated and slightly hard surface; the LST (uppermost part of the Bouzergoun Fm) would be made of sandy, bivalve-rich limestone; the TST corresponds to two beds of bioclastic limestone rich in bivalves; the MFS would be represented by an undulated, slightly hard, oxidized surface rich in fossils and serpulids; and the HST (Tamzergout Fm) is made of green marl rich in planktonic and benthonic foraminifera, and ostracods, intercalated with thin beds of limestone rich in ammonite, belemnites, brachiopods, bivalves and gastropods.

Sequence Ap. 3 (Middle Aptian-lower Upper Aptian; *subnodosocostatum*, *melchioris* and *nolani* ammonite zones). It mostly corresponds to Tamzergout Fm (except the basal and

uppermost parts). The Lower SB was unidentified in the field, and is probably represented by an erosional, ravinment surface; the LST (lower part of Tamzergout Fm), would correspond to a thin bed of sandy, bivalve-rich limestone; the TST is made of many parasequences of sandy foraminiferal marl and bioclastic limestone, rich in ammonites and belemnites; the MFS has been placed at the base of a thin bed of nodular limestone rich in microfossils; and the HST, would be a thickening upward succession of parasequences indicating a shallowing upward trend. The parasequences are made of sandy marl rich in foraminifera and ostracods, and thin beds of bioclastic limestone rich in ammonites, belemnites, brachiopods, bivalves and gastropods. The facies become more clastic toward the North.

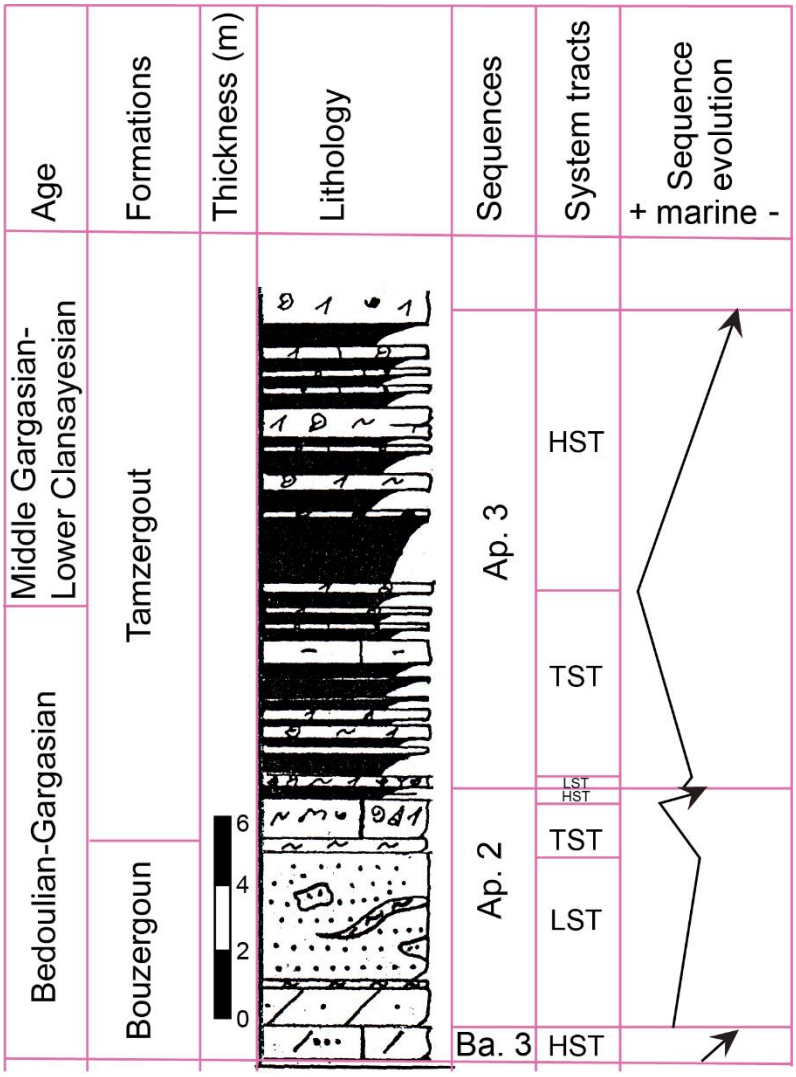

Figure 2.8: Ap. 2 and Ap. 3 Sequences at Tamzergout section, EAB by Witam (1998).

Sequence Ap. 4 (latest Aptian, *Hypacanthoplites jacobi* ammonite Zone and *Ticinella bejaouensis* planktonic foraminiferal Zone). It mostly corresponds to the uppermost part of the Tamzergout Fm, and to the Lemgo Fm in the Agadir area. The Lower SB is poorly defined. The LST (uppermost part of Tamzergout Fm), is made of an alternation of white marl and bioclastic limestone, both rich in foraminifera (hedbergellids, globigerinellids and lenticulinids), indicating an open marine environment; the TST (Lemgo Fm), is a parasequence of yellow marl with foraminifera and ostracods, and bioclastic limestone beds containing bivalves, brachiopods, serpulids and ammonites; the MFS, hardly identifiable, would be a hard oxidized surface at the top of a bioclastic limestone bed; and the HST (Lemgo Fm), would correspond to a thickening upward succession of parasequences made of yellow marl rich in foraminifera and ostracods, and thin beds of bioclastic limestone rich by bivalves, ammonite and serpulids. Upward the limestone beds are replaced by shallow marine, cross bedded sandy limestone.

Nouidar and Chellai (2002) studied the Late Barremian succession in the Southern part of the EAB. They interpret these sediments as a stacked series deposited by wave-dominated deltas, which presents thickening and coarsening-upward parasequences, formed during fifth or fourth-order regression, and building a third-order highstand systems tract. Vertical facies evolution in the parasequences reflects flooding, followed by shoaling. They evolve from offshore transition facies, to lower shoreface/lower delta front hummocky bedforms, and to upper shoreface/upper delta front cross-bedded sandstones. The Late Barremian wave-dominated deltas prograded towards the WSW over Early Barremian offshore deposits, forming a third order sea level cycle. Then, maximum sea-level fall led to the development of an unconformity interpreted as a sequence boundary. The subsequent Early Aptian relative sea-level rise contributed to the development of an extensive, transgressive surface, emphasized by a conglomerate lag.

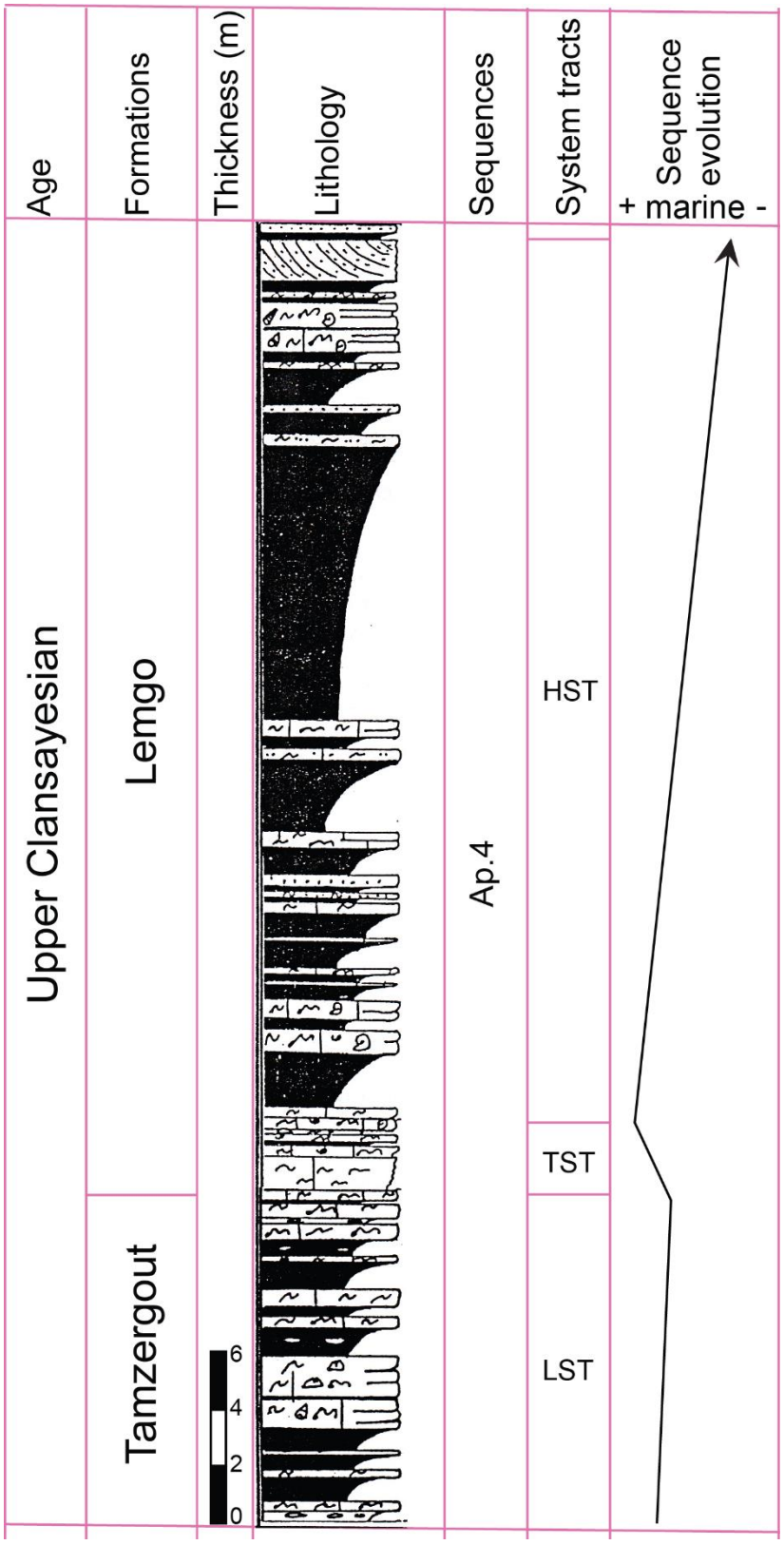

Figure 2.9: Ap. 4 Sequence at Imi N' Tanout section, EAB, by Witam (1998).

2.7. PALEOENVIRONMENTS

A paleoenvironmental study integrating a multidisciplinary approach (sedimentology and micropaleontology) has already been done by Peybernès et al. (2013) for three Late Aptian-Early Albian sections located along an East-West transect in the southern part of the EAB. Results obtained in this preliminary study have been compared with those obtained from both the Mazagan Plateau and the Vocontian Basin by Herrle (2002, 2003), Herrle and Mutterlose (2003), and Herrle et al., 2003a, 2003b, 2010). The major results and interpretations of this study are: (1) a decrease in both the calcium carbonate content and *Nannoconus* abundances at the Aptian-Albian transition, probably due to a cooling and/or enhanced terrigenous input and associated nutrients in the marine realm; (2) the nannofossil fluxes in the EAB were two times lower than in the upwelling influenced Mazagan Plateau area and eight times lower than in the Vocontian Basin; (3) the nannofossil primary productivity seems to be lower in the southern Tethyan margin (both EAB and Mazagan Plateau) than in the northern margin (Vocontian Basin) for the Early Albian.

In the Mazagan Plateau, Herrle (2002) used calcareous nannofossil assemblages to reconstruct the paleoenvironmental changes during earliest Albian times across the OAE 1b. The following interpretations have been proposed : (1) Nutrient index fluctuations corresponding to the astronomical precession signal have been identified and are less expressed in the Mazagan Plateau than in the Vocontian Basin; (2) temperature index variations have also been recognized and were dominated by the eccentricity signal, in the range of 25°N - 30°N of the subtropical belt, representing a supraregional climate signal; (3) fertility changes in the surface waters are superimposed on longer-term temperature cycles corresponding to the eccentricity signal, and acted over most of the Tethyan and Atlantic oceans; (4) deposition of the OAE 1b black shale in both the Tethyan and Atlantic oceans was linked to supraregional climatic and oceanographic changes; (5) surface water fertility changes reflected regional variability of the prevailing wind systems; on the Mazagan Plateau, the surface water fertility was controlled by the southwestward trade wind system, and was highest during cold intervals, when subtropical/tropical pressure gradients were slightly increased.

CHAPTER THREE

INTEGRATED STRATIGRAPHY IN THE EAB

CHAPTER THREE
INTEGRATED STRATIGRAPHY IN THE EAB

3.1 . APTIAN-EARLY ALBIAN LITHOSTRATIGRAPHY OF EAB

The Aptian-Early Albian lithostratigraphy of the Essaouira-Agadir Basin (EAB), is first described by Duffaud et al (1966) and subdivided into four lithostratigraphic units based on lithology and dominant colors (Fig. 2.2). Three Aptian and one Albian formations named Bouzergoun (sandstone and reddish marl), Tamzergout (limestone and marl), Lemgo (sandy marl) and Oued Tidzi (shale and marl) respectively.

Detailed stratigraphic analysis of the Aptian-Early Albian rock units has been performed on four sections in the EAB. Field description, sampling and microfacies analysis have been made to help interpreting their depositional environment(s). This includes the following:

Four sections have been logged bed-by-bed and described for their litho-and microfacies macrofaunal and calcareous nannofossil contents. These sections are: Ida w Shayq, Tissakatine Center, Anzate and Tinfoul (Figs. 3.1: 3.4).

The Aptian-Early Albian deposits in the studied sections are different from section to another (Figs. 3.1: 3.4). Ida w Shayq and Anzate sections can be divided into two parts separated by sedimentary discontinuities (D): a lower part of marly limestones separated by marls (below D3; Tamzergout Fm) and an upper part with green/grey shales intercalated with marly sandstones (above D3, Oued Tidzi Fm). Tissakatine Center section also presents two parts: a lower part of marly limestones containing very few and fine grained detrital quartz (below D5, Tamzergout Fm) and an upper of marls intercalated with sandstones (above D5, Oued Tidzi Fm). Tinfoul section is mostly characterized by green shales intercalated with sandstones (Oued Tidzi Fm).

The lithostratigraphic units defined by Duffaud et al (1966) have not been completely recognized in the studied sections. Moreover, the recognized units are not time equivalent in the different sections (Fig. 3.1: 3.4). Consequently, the lithostratigraphic units are diachronic, and the same lithostratigraphic unit is not correlatable in the different sections. Then, both ammonite

and nannofossil biostratigraphy, and carbon isotope stratigraphy have been made to construct a stratigraphic framework allowing correlations between the different studied sections.

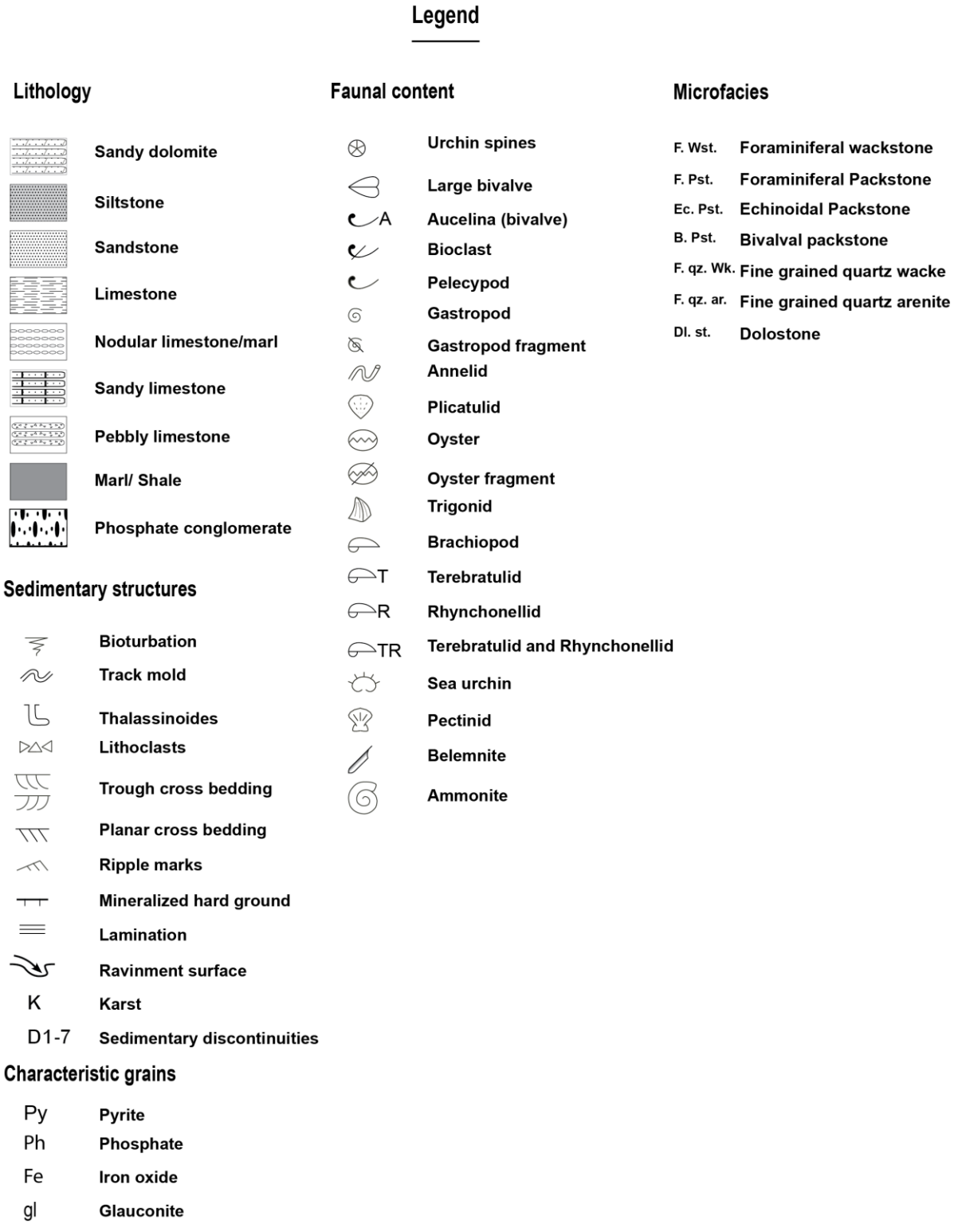

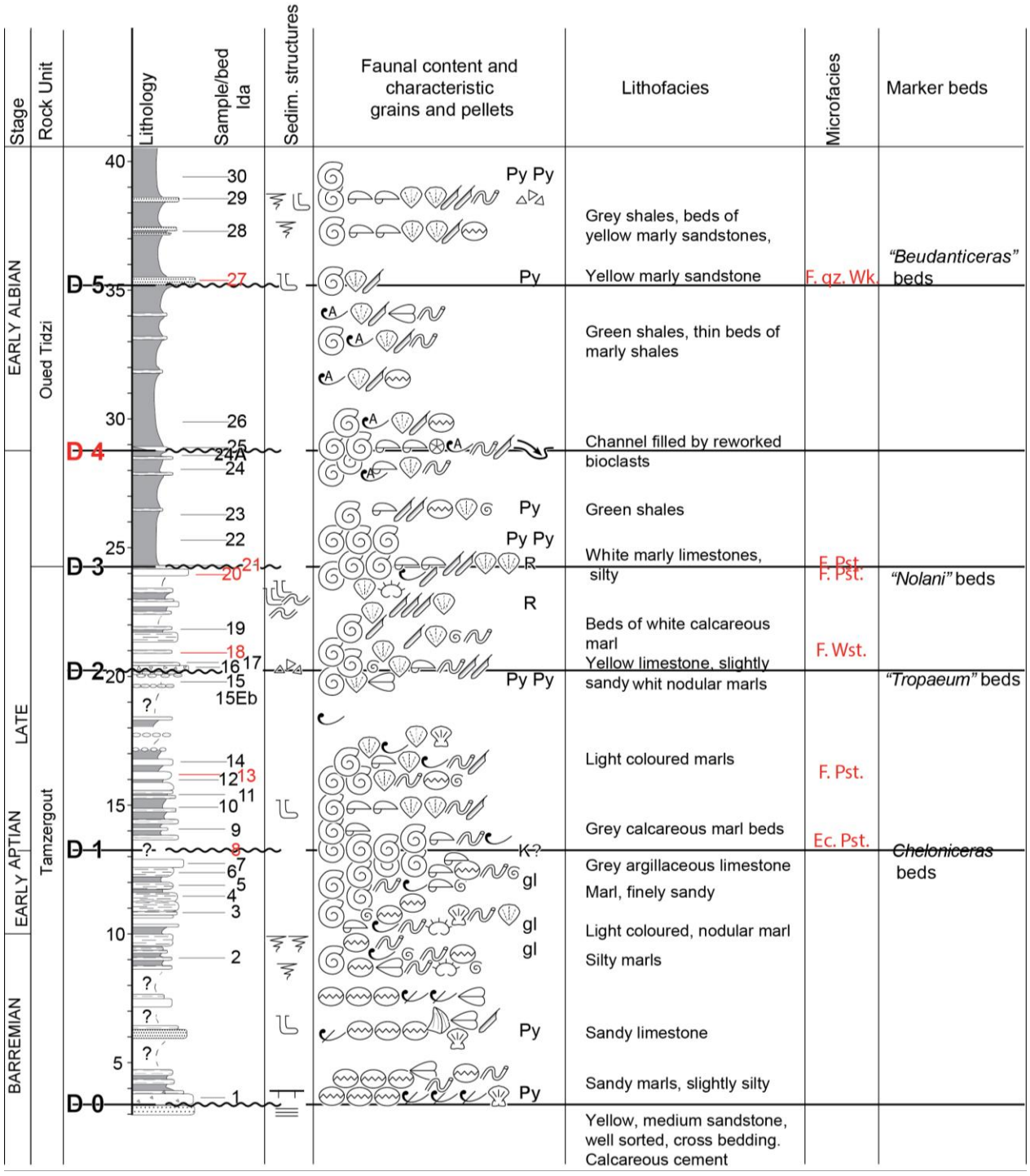

Figure 3.1: Stratigraphic succession of the Ida w Shayq section showing the lithostratigraphic rock units and marker beds

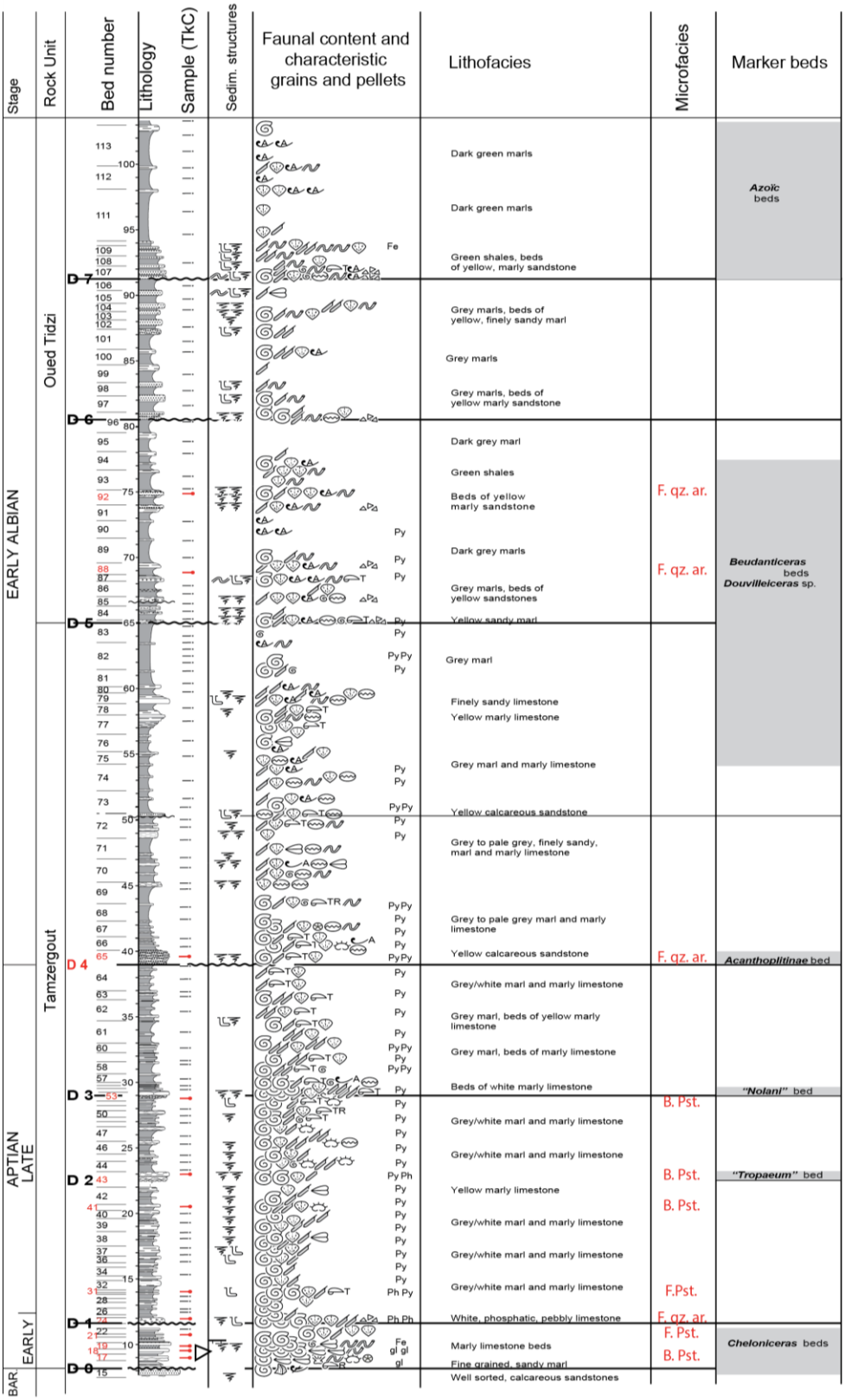

Figure 3.2: Stratigraphic succession of the Tissakatine Center section showing the lithostratigraphic rock units and marker beds

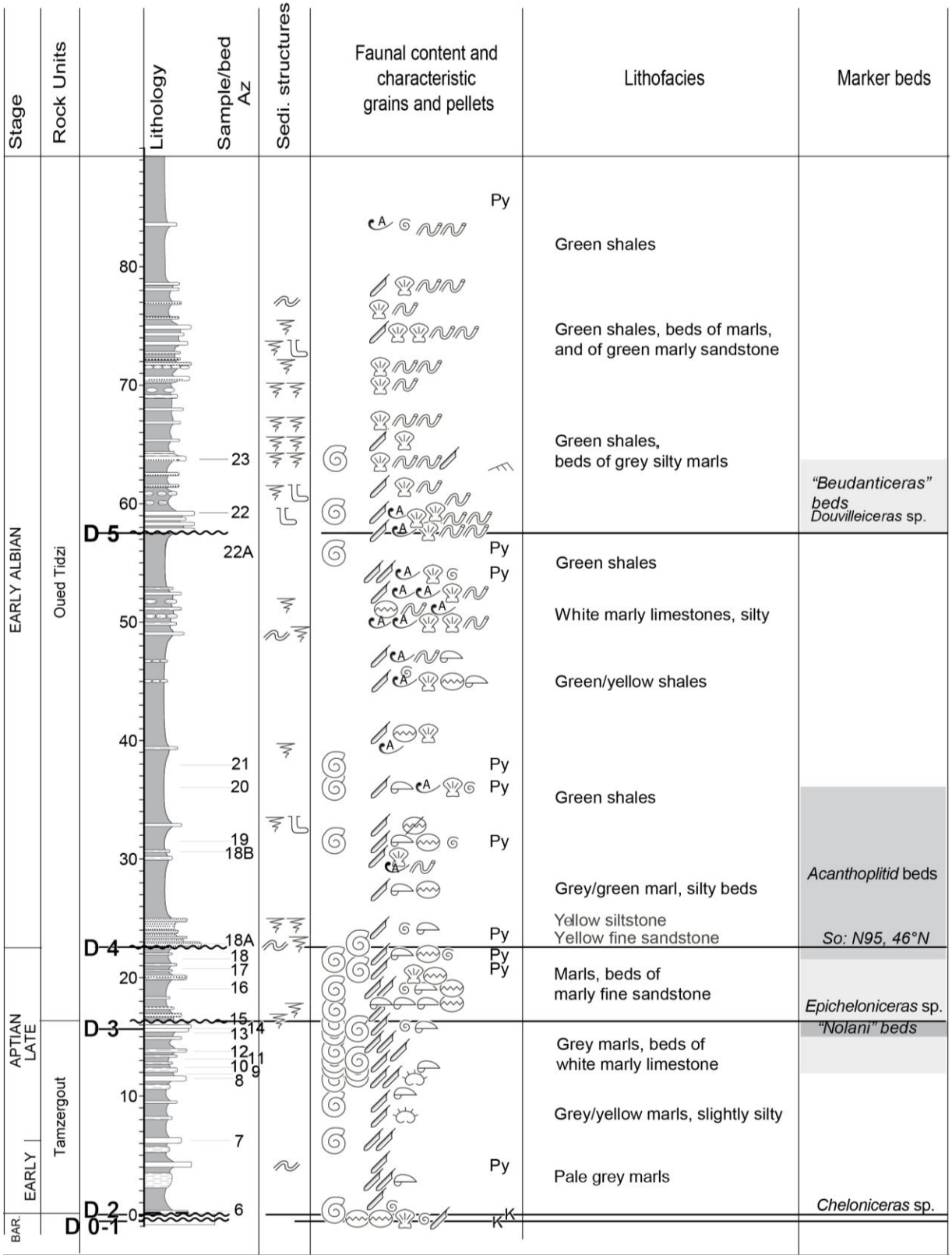

Figure 3.3: Stratigraphic succession of the Anzate showing the lithostratigraphic rock units and marker beds

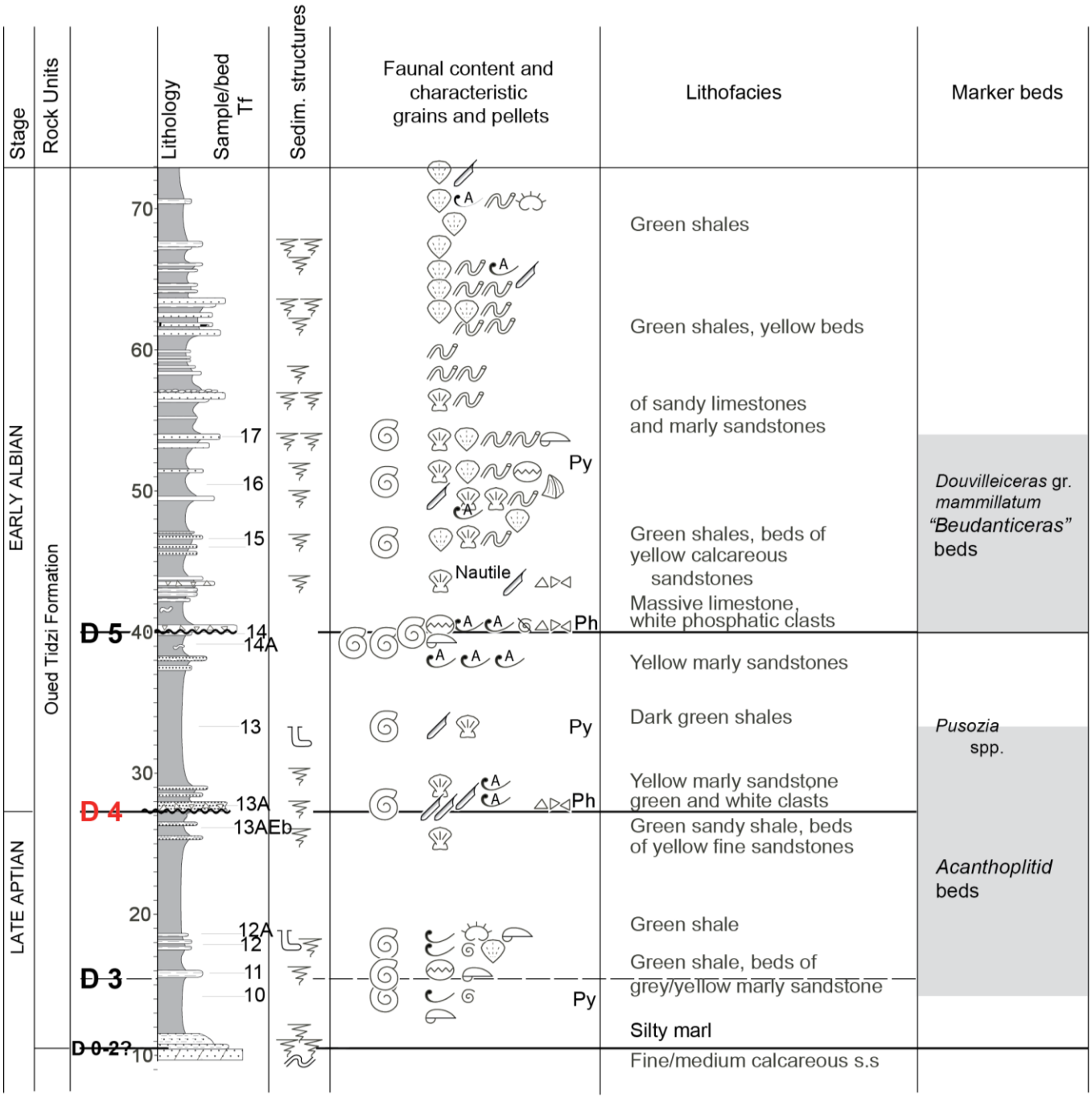

Figure 3.4: Stratigraphic succession of the Tinfoul showing the lithostratigraphic rock units and marker beds

3.2. AMMONITE BIOSTRATIGRAPHY (done by Robert E., Lyon University)

3.2.1. Material and methodology

3.2.1.1. Ammonites

The sampling of ammonites was carried out in 98 levels collected in 4 sections: Ida w Shayq, Tissakatine Center, Anzate and Tinfoul. This material is part of an important biostratigraphic regional study, based on the analysis of more than 1500 specimens collected in numerous levels on 12 sections of the EAB from 2008 till 2013.

Collected ammonites were compared with historical South Moroccan collections (Gentil, Kilian, Roch, Breistroffer), and other Mediterranean Aptian/Albian specimens from the Mediterranean provinces of French universities and museum's collections.

Identification of ammonites at species-level is difficult, either because some of these are preserved as small pyritized molds, or because the rest of them, preserved as internal calcareous molds, are fragmented, crushed and incomplete. Consequently, important characteristics, such as inner stages or the strength of ribs and tubercles cannot be well recognized. Finally, those modes of conservation make difficult to compare the south Moroccan assemblages with its counterparts in Mediterranean provinces, in term of ontogenetic and phylogenetic analysis.

The material is stored and referenced in the paleontological collection of the Observatoire des Sciences de l'Univers de Grenoble (OSUG).

3.2.1.2. Zonal boundaries

From a strictly biostratigraphical point of view, the zones are assemblages or interval zones (Peybernes et al., 2013). Their bases are defined either by the first occurrence datum (FOD) of the index species or of a diagnostic ammonite faunas.

However, if we expand our analysis to the regional stratigraphical context, several arguments led us to reconsider this approach: a. bases of *Leymeriella tardefurcata* and *Douvilleiceras mammillatum* zones almost overcome important sedimentary discontinuities, respectively D4 and D5; b. more generally, numerous temporal hiatuses occur in the whole series. In consequence, bases of biozones are frequently difficult to define. This is particularly the case for the Aptian/Albian Boundary in many basins as it has been shown in several recent papers (from Hart et al., 1996 to Peybernes et al., 2013). At least for the uppermost Aptian and

lowermost Albian, we consider that the bases of the biozones can be contained within the discontinuities.

3.2.2. Results

A first revision of the regional biostratigraphic framework was proposed by Robert in Peybernes et al. (2013). Analysis of the distribution of the ammonites in numerous sections allowed us to establish detailed faunal assemblages. A regional zonation will be proposed in a forthcoming publication. Meanwhile, the ammonite assemblages can be compared with those of the north and south tethyan margins due to the presence of tethyan and cosmopolitan taxa. Consequently, the Standard Zonation (Reboulet et al., 2014) is used to date the EAB sections.

The Early Aptian – basal Late Aptian interval is identified with difficulties in the EAB because of condensed sedimentation and temporal hiatuses. In contrast, we were able to characterize the Late Aptian and Earliest Albian standard zones. Several new species and genus have been recognized in the ammonite fauna of the EAB. However, as our discussion is of stratigraphical order, their systematic description is not presented here.

3.2.2.1. Ida w Shayq (IDA) Section

Ammonites collected at the base of the Ida w Shayq section (*Kutatissites* sp. and *Pseudocrioceras* sp. in level Ida-2) (Fig. 3.5) indicate the uppermost Barremian *Martelites sarasini* Zone (Ropolo et al., 1999). The Barremian/Aptian Boundary is not precisely characterized; this is also the case of the overlying *Paradeshayesites oglanlensis* and *Deshayesites weissi* zones.

First representatives of both genera *Cheloniceras* and *Ancyloceras*, at level Ida-3, indicate the *Deshayesites deshayesi* Zone (*Cheloniceras cornuelianum*, *C. quadratum* and *Ancyloceras* sp.). The *Dufrenoyia furcata* Zone is recognized by the appearance of *Cheloniceras meyendorfi* (Casey, 1961, 1962; Dutour, 2005), which occurs in level Ida-6. Both Ida-6 and Ida-8 levels, contain similar associations (*Cheloniceras cornuelianum*, *C. meyendorfi*, *Ancyloceras* gr. *matheronianum*, *A. mantelli*); they might date a transitional interval between the *D. deshayesi* and *D. furcata* zones. Therefore, it is named *D. deshayesi /D. furcata* Zone. The first co-occurrence of *Australiceras* sp. and *Epicheloniceras* sp. at level Ida-14 allows to recognize the *Epicheloniceras martini* Zone. The base of the *Parahoplites melchioris* Zone is not

characterized; the index species is absent and other ammonites attributable to this zone are very scarce. As a consequence, the exact position of the lower boundary is uncertain (Fig. 3.5). Its lower limit is placed at the first appearance of the genus *Nolaniceras* (level Ida-19; Robert, pers. comm.). The first *Nolaniceras nolani* are found in level Ida-21, allowing the identification of the *N. nolani* Zone. The overlying *Hypacanthoplites jacobi* Zone starts, at level Ida-22 defined with the presence of *Hypacanthoplites clavatus*, *H. elegans* and *Pseudorbulites convergens*, among others. More generally, the *H. jacobi* Zone is characterized by the presence of representatives of *Pseudorbulites* sp. (Ida 22 to 24), *Eogaudryceras (Eotetragonites)* cf. *gardneri* (Ida-23) and *Phyllopachyceras baborense* (Ida-24) (Murphy, 1967; Joly and Delamette, 2008).

The *Douvilleiceras* genus characterizes the Early Albian substage, and the first occurrence of *D. leightonense* is recognized at level Ida-24A. The *Leymeriella tardefurcata* Zone is characterized by the presence of *Puzosia quenstedti* (Ida-25), *Neosilesites palmensis* (Ida-25) and representatives of the genera *Melleguericeras* sp. (Ida-27 to 29) or *Parabrancoceras* sp. (Ida-29) (Kennedy et al., 2000; Latil, 2011). The base of this zone occurs within the sedimentary discontinuity D4, as is the case in all the studied sections. The overlying *Douvilleiceras mammillatum* Zone has not been characterized.

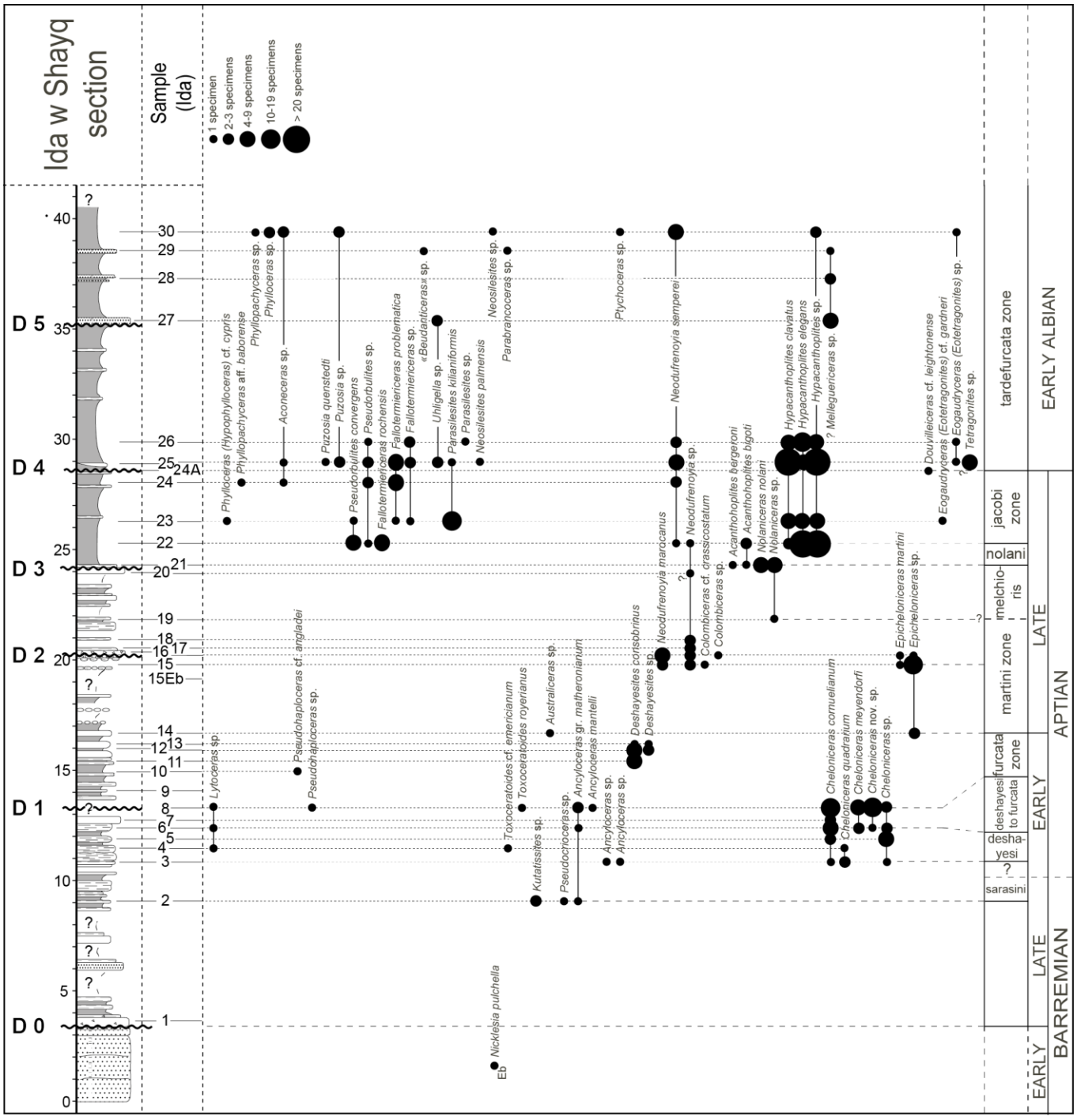

Figure 3.5: Lithological sequences, ammonite occurrences and biostratigraphic interpretation of the Ida w Shayq section.

3.2.2.2. Tissakatine Center (TKC) Section

The presence of *Deshayesites* cf. *grandis* and representatives of the genus *Cheloniceras* allowed to ascribe levels TKC-18 to TKC-20 to the *Deshayesites deshayesi* Zone (Fig. 3.6).

Ammonites of the next characteristic level, TKC-24, have been collected within the discontinuity D1. They comprise characteristic species of both *Dufrenoyia furcata* and *Epicheloniceras martini* zones (Dutour, 2005, Moreno Bedmar et al., 2010a, Peybernès et al., 2013): *Pseudohaploceras angladei*, *Toxoceratoides emericianum*, *Colombiceras* cf. *crassicostatum*, *Epicheloniceras martini*, *E. debile* and *Vectisites caprotinus*, among others. This suggests that the Early/ Late Aptian boundary could be included within the discontinuity D1.

As for the whole EAB basin, the base of the *Parahoplites melchioris* Zone is not characterized. Its lower limit is placed at the first occurrence of the genus *Nolaniceras* (Robert, pers. comm.).

The "Nolaniceras beds" roughly coincide with the *Nolaniceras nolani* Zone with the first occurrence of the index species at level TKC-52, associated with others representatives of both genera *Nolaniceras* and *Acanthohoplites*.

The overlying *Hypacanthoplites Jacobi* Zone is defined by the appearance of *Hypacanthoplites* cf. *paucicostatus* and *Ptychoceras* sp. at level TKC-59. The zone is particularly marked by the presence of *Hypacanthopites elegans* (TKC-60 and 61), *Pseudorbulites* sp. (TKC-61), *Epicheloniceras clansayense* (TKC-62 and 63) and *Diadochoceras* cf. *caucasicus* (TKC-64), among others (Casey, 1965; Robert et al., 2001; Dutour, 2005).

Douvilleiceras leightonense, marker of the Early Albian, appears at level TKC-65. But, as in the Tinfoul and Anzate sections, the base of the *Leymeriella tardefurcata* Zone occurs within the discontinuity D4. More generally, the *L. tardefurcata* Zone is assumed by the presence of *Hypacanthoplites* cf. *roberti* (TKC-65), *Phylloceras (Hypophylloceras) cypris* (TKC-66), *Eogaudryceras (Eotetragonites)* cf. *gardneri* (TKC-73), *Tetragonites rectangularis* (TKC-73), *Pusozia* sp. (TKC-73 and 74) and *Oxytropidoceras (Oxytropidoceras)* sp. (TKC-76) (Murphy, 1967; Joly, 2000; Kennedy et al., 2000; Latil, 2011).

The first appearance of *"Beudanticeras" revoili* marks the base of the *Douvilleiceras mammillatum* Zone (Fig. 3.7) at level TKC-82. It should be noted that, unlike the others sections,

base of the zone would lie under the discontinuity D5, as supported by the presence of *"Beudanticeras" africana* and *Uhligella rebouli* in the level TKC-92.

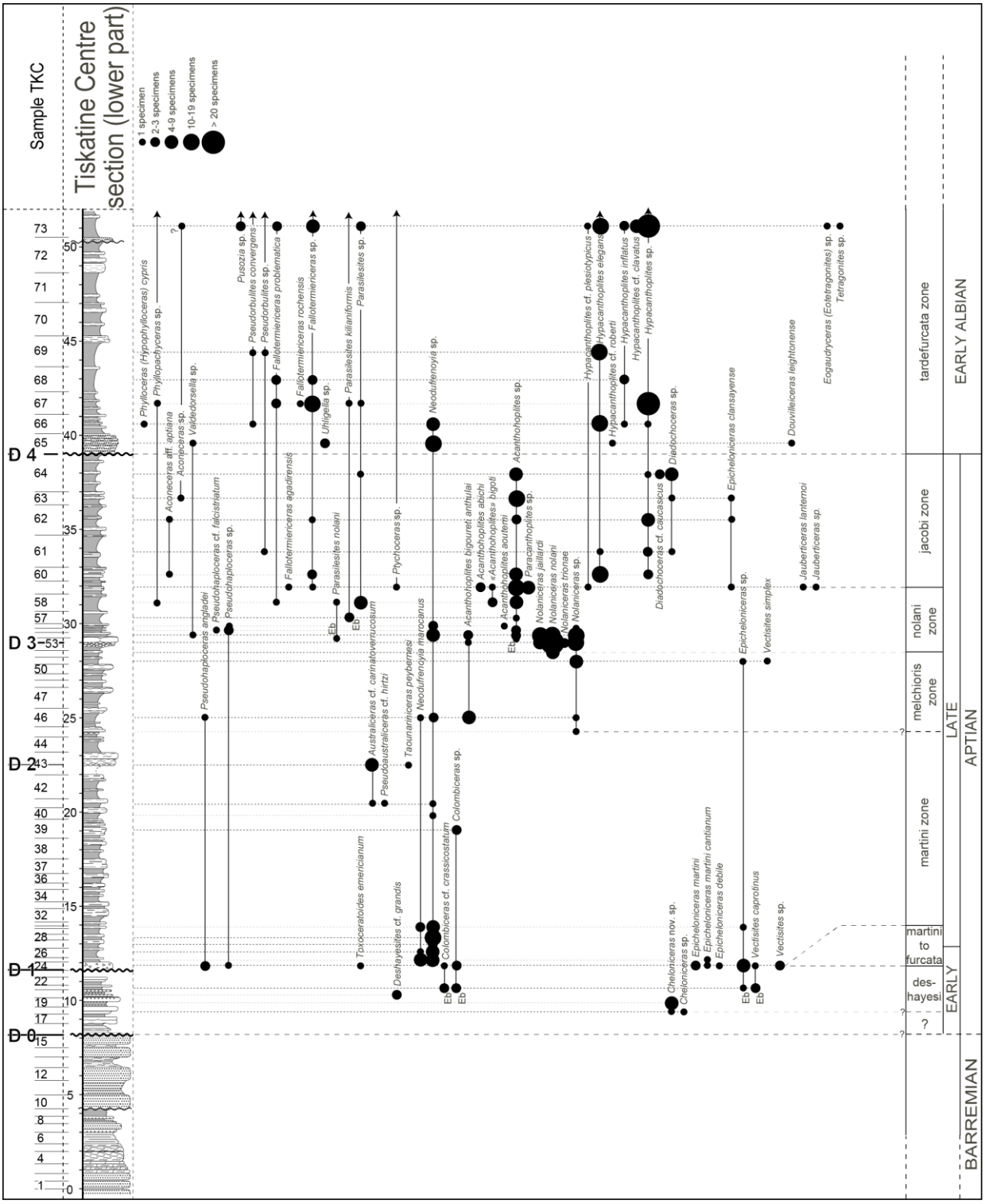

Figure 3.6: Lithological sequence, ammonite occurrences and biostratigraphic interpretation of the lower part of the Tissakatine Centre section.

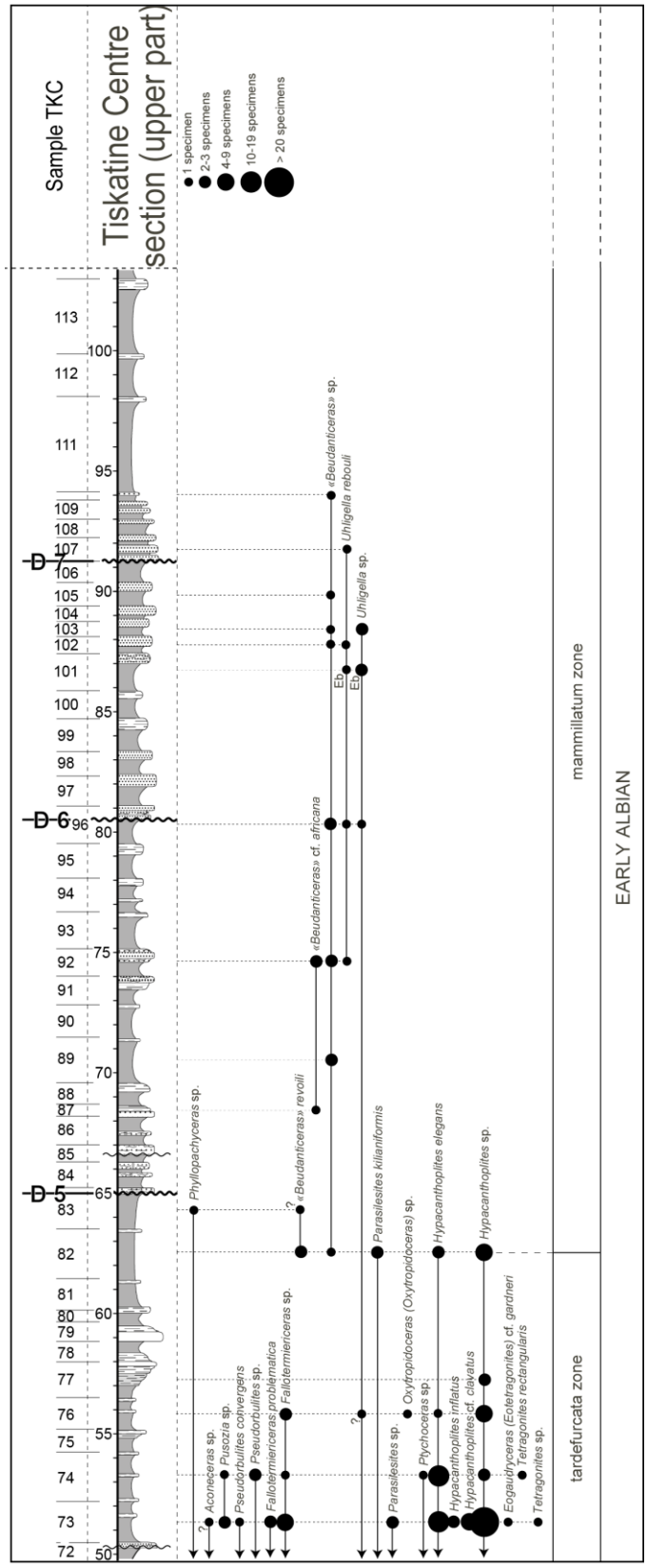

Figure 3.7: Lithological sequence, ammonite occurrences and biostratigraphic interpretation of the upper part of Tissakatine Centre section.

3.2.2.3. Anzate (ANZ) Section

The Anzate section illustrates a biostratigraphic interval, from the early Late Aptian *Epicheloniceras martini* Zone to the Early Albian *D. mammillatum* Zone. The interval selected for the study of calcareous nannofossils is however restricted to its upper, Early Albian part (Fig. 3.8).

The *L. tardefurcata* Zone is confirmed by the presence of *Parengonoceras* cf. *bassei* in level ANZ-18B, *Hypacanthoplites* gr. *elegans* in bed ANZ-20, *Pusozia quenstedti*, *Pusozia* sp. and *Eogaudryceras (Eotetragonites) plurisulcatus* in levels ANZ-21 and ANZ-22A (Bréhéret et al., 1986; Latil and Aly, 2012).

The co-occurrence of *Douvilleiceras* sp. and *"Beudanticeras" revoili* in bed ANZ-22, associated with *Uhligella* cf. *rebouli* in level ANZ-23, would indicate the presence of the *D. mammillatum* Zone for the uppermost part of the section (see discussion above).

Lower limits of both the *L. tardefurcata* and *D. mammillatum* zones are placed within the discontinuities D4 and D5, respectively.

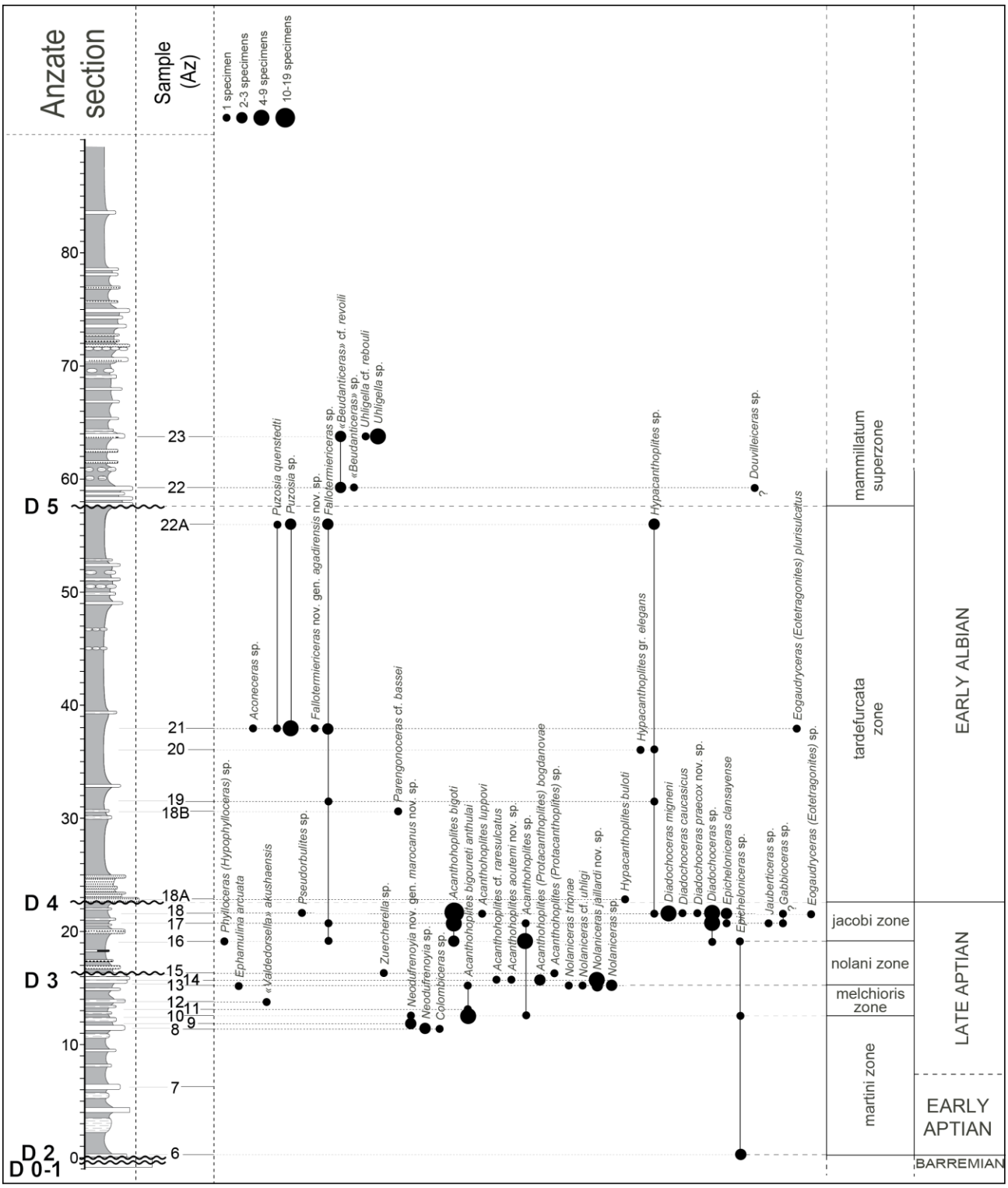

Figure 3.8: Lithological sequence, ammonite occurrences and biostratigraphic interpretation of the Anzate section.

3.2.2.4. Tinfoul (TF) Section

Resting on the Barremian massive limestones, the lowermost part of the section did not yield ammonites. More generally, ammonites are scarce and poorly preserved due to sandy facies (Fig. 3.9).

The presence of *Fallotermiericeras* sp. and representatives of the genus *Acanthohoplites* dates the level TF-10 of the *Nolaniceras nolani* Zone. The co-occurrence of *Acanthohoplites bigoureti anthulai* and *Hypacanthoplites nolaniformis* in level TF-11 allows to ascribe this level from the *Nolaniceras nolani* and/or *Hypacanthoplites jacobi* zones. The presence of *Hypcanthoplites paucicostatus* in the level TF-13B/C allows to assign it to the *Hypacanthoplites jacobi* Zone.

The genera *Hypacanthoplites* (species *elegans*) and *Fallotermiericeras* (species *rochensis*) characterizing the earliest Albian *Leymeriella tardefurcata* Zone have been recognized until level TF-13. *Pusozia quenstedti* and *Pusozia* sp., makers of Early and Middle Albian., appear in this same level TF-13 (Bréhéret et al., 1986; Robert et al., 2001; Latil, 2011; Peybernes et al., 2013). Considering the regional stratigraphic context (see discussion hereunder), the base of the *L. tardefurcata* Zone, and therefore the Aptian/Albian Boundary, is placed within the discontinuity D4.

The uppermost part of the Tinfoul section is dated from the Early Albian *Douvilleiceras mammillatum* Zone with the apparition of the species *Douvilleiceras mammillatum aequinodum* in level TF-16. The co-occurrence of "*Beudanticeras*", here dominated by the species *B. revoili*, another marker of the *D. mammillatum* Zone, is observed on the whole EAB Basin (cf. "*Beudanticeras*" beds horizon of the literature) but also in Tunisia (Latil, 2011). On the basis of the regional stratigraphic context, we placed the base of the *D. mammillatum* Zone within the discontinuity D5.

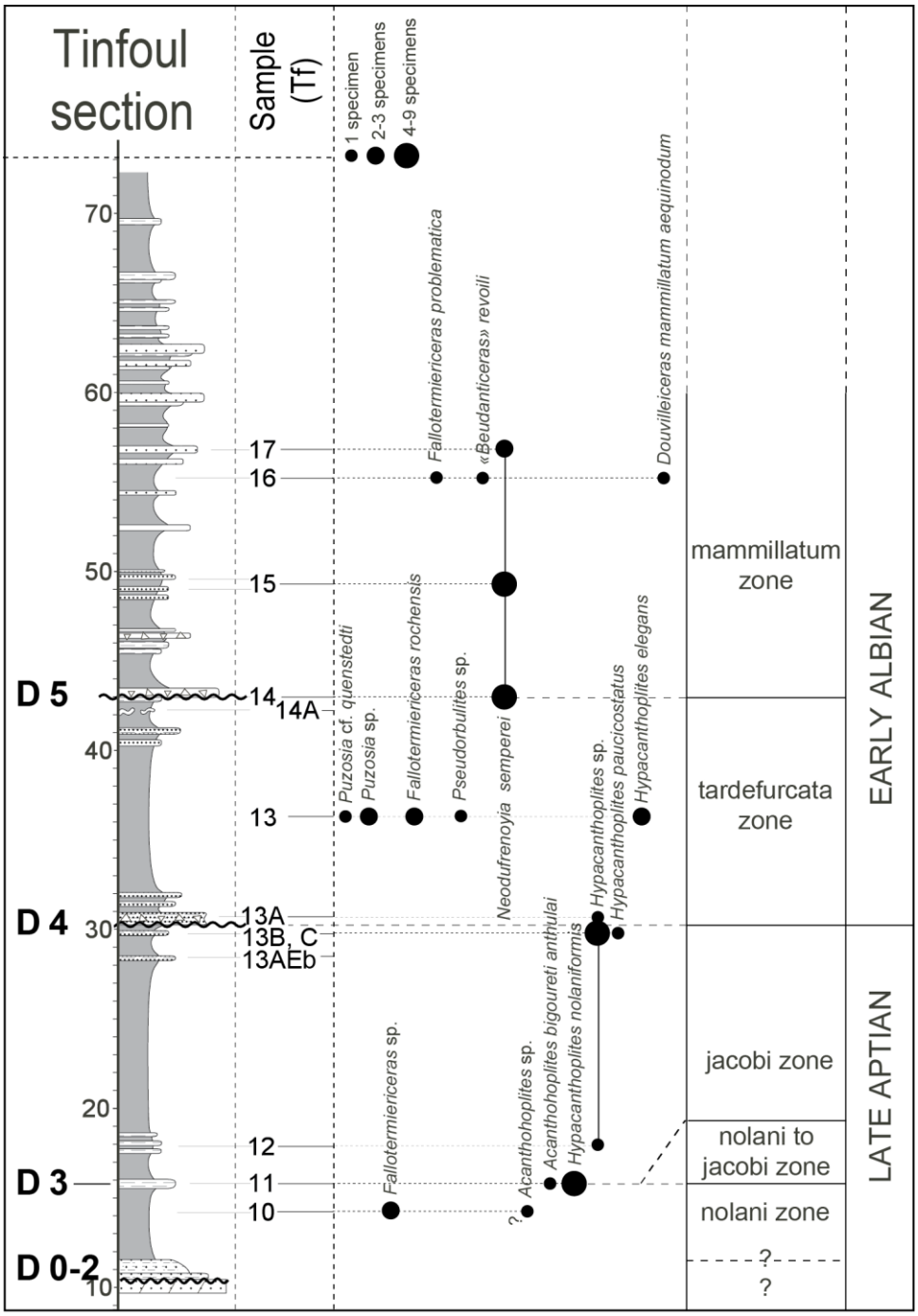

Figure 3.9: Lithological sequence, ammonite occurrences and biostratigraphic interpretation of the Tinfoul section.

3.3. CALCAREOUS NANNOFOSSIL BIOSTRATIGRAPHY

3.3.1. Material and methodology

One hundred and thirty nine samples were investigated for calcareous nannofossil studies in the four sections. They were selected from different lithologies, from calcareous clay to limestone. Smear slides were prepared using the random settling technique of Geisen et al. (1999), a method adapted from Beaufort (1991), which allows calculating absolute abundances. Nannofossils were observed using light polarizing microscope, at 1560 X magnification. In the richest samples, 500 specimens were generally counted in a variable number of fields of view. In the poorest samples, 150 to 300 specimens were counted following different longitudinal transverses. The observation of marker species has been achieved by counting from 5 to 7 and 6 to 13 subsequent longitudinal transverses (200 fields of view), in the richest and poorest samples respectively. All nannofossils with at least more than half of the specimen preserved have been counted. The taxonomic frameworks of Perch-Nielsen (1985) and Burnett et al. (in Bown, 1998) were followed. Countings are given in Appendix (1 to 4).

3.3.2. Biostratigraphy

The nannofossil zones and subzones applied to the investigated sections are the NC zones of Bralower et al. (1993, 1995) modified from Roth (1978). This zonation scheme has been selected because of its applicability to low-latitude Tethyan continental margins (Bralower et al., 1993). In addition, numerous bioevents can be recognized within the zones. These bioevents are considered less important biostratigraphically because they are either potentially less accurately determinable or not recognizable in each section. We also used the late Aptian "*Nannoconus truittii* acme" described by Mutterlose (1989, 1991), characterized by high abundances of *N. truittii*, and observed in the Tethyan and Boreal realms (Mutterlose, 1989; Erba, 1994; Herrle and Mutterlose, 2003); it occurs in the *martini* ammonite Zone. The "*Nannoconus truittii* acme" is recognized in two studied sections of the EAB (Ida w Shayq and Tissakatine Center).

3.3.2.1. Ida w Shayq (IDA) Section

In the Ida w Shayq section, we identified four nannofossil zones (Fig. 3.10). The *Watznaueria oblonga* Zone (NC5) of Barremian age, the *Chiastozygus litterarius* Zone (NC6) of Early to "middle" Aptian age, the *Rhagodiscus angustus* Zone (NC7) of Late Aptian age, and the *Prediscosphaera columnata* Zone (NC8) of Late Aptian-Early Albian age. Zone NC6 is subdivided into the NC6A (lower) and NC6B (upper) subzones. Both NC7 and NC8 zones are subdivided into three subzones, called respectively A, B and C.

3.3.2.1.1. *Watznaueria Oblonga* (NC5), Late Barremian

The NC5 Zone is defined as the interval from the LO of *Cruciellipsis cuvillieri* to the FO of *Hayesites irregularis.* The LO of *Cruciellipsis cuvillieri* has not been recognized. Therefore, the base of NC5 Zone is not defined. However, the top of NC5 Zone is defined by the FO of *Hayesites irregularis* at level 9.3 m, in sample IDA 4 (Fig. 3.10). Consequently, the base of the Ida w Shayq succession is included within the NC5 Zone.

The FO of *Hayesites irregularis* is recognized in the middle part of the *Martelites sarasini* ammonite Zone of Late Barremian age (Fig. 3.10).

3.3.2.1.2. *Chiastozygus litterarius* Zone (NC6), Early to early Late Aptian

The NC6 Zone is defined as the interval from the FO of *Hayesites irregularis* to the FO of *Eprolithus floralis* and is subdivided into NC6A and NC6B Subzones:

3.3.2.1.2.1. Subzone NC6A

Subzone NC6A is defined as the interval from the FO of *Hayesites irregularis* to the LO of *Conusphaera rothii.* The LO of *Conusphaera rothii* is observed at level 15.3 m, in sample IDA 9 (Fig. 3.10). Therefore, the base and top of the NC6A Subzone are recognized, and the NC6A Subzone spans the lower part of the Ida w Shayq section.

The LO of *Conusphaera rothii* is observed in the middle part of the *furcata* ammonite Zone of Early Aptian age (Fig. 3.10).

3.3.2.1.2.2. Subzone NC6B

Subzone NC6B is defined as the interval from the LO of *Conusphaera rothii* to the FO of *Eprolithus floralis*. FO of *Eprolithus floralis* is generally dated to the top of the Early Aptian,

below the Early/Late Aptian Boundary (Luciani et al., 2006). The FO of *Eprolithus floralis* is documented at 20.5 m, in sample IDA 16 (Fig. 3.10). The FO of *Eprolithus floralis* occurs in the upper part of the *martini* ammonite Zone of early Late Aptian age in this section, which is later with respect to its FO generally observed. This could be due to the poor preservation of nannofossils recognized in the lower part of Ida w Shayq section, characterized by limestone beds, which are generally not suitable for a good nannofossil preservation (Roth and Thierstein, 1972). Therefore, the base and top of NC6B are observed and the NC6B Subzone is well defined. Consequently, the lower part of the Ida w Shayq section corresponds to the *Chiastozygus litterarius* Zone. However, the presence of *Nannoconus vocontiensis/wassalli*, *Nannoconus circularis*, *Nannoconus truittii*, *Rhagodiscus gallagheri*, small forms of *Assipetra infracretacea* and *Rucinolithus terebrodentarius* (Fig. 3.10) is rather characteristic of latest Early Aptian assemblages (Deres and Achéritéguy, 1980; Erba et al., 1995; Tremolada and Erba, 2002).

3.3.2.1.3. *Rhagodiscus angustus* Zone (NC7), Late Aptian

Zone NC7 is defined as the interval from the FO of *Eprolithus floralis* to the FO of *Prediscosphaera columnata* (Fig. 3.10). The FO of *E. floralis* is close to the Early Aptian/Late Aptian Boundary (Bralower et al., 1993, 1995). In addition, the FO of *Orastrum perspicuum* is recognized within the nannofossil Subzone NC7B, and the *Nannoconus truitti* acme is defined within the nannofossil Subzone NC7B/C in the Vocontian Basin (SE France; Herrle and Mutterlose, 2003).

3.3.2.1.3.1. Subzone NC7A, Late Aptian

The NC7A Subzone, is defined as the interval from the FO of *E. floralis* to the LO of *Micrantholithus* spp. (Roth, 1978; Bralower et al., 1995). The LO of *Micrantholithus hoschulzii* occurs at 22.85 m, in sample IDA19. Therefore, the base and top of the NC7A are recognized, and the NC7A Subzone corresponds to the middle part of Ida w Shayq section (Fig. 3.10).

The LO of *Micrantholithus hoschulzii* is recognized in the lower part of the *melchioris* ammonite Zone of middle Late Aptian age (Fig. 3.10). The FO of *Orastrum perspicuum* is observed in sample IDA16 (Fig. 3.10), and then within the Subzone NC7A, which is earlier than previously reported by Herrle and Mutterlose (2003) in the Vocontian Basin.

3.3.2.1.3.2. Subzone NC7B, Late Aptian

The NC7B Subzone is defined as the interval from the LO of *Micrantholithus* spp. to the FO of *Rhagodiscus achlyostaurion.* In the Ida w Shayq section, the FO of *R. achlyostaurion* is defined at level 24.4 m, in sample IDA 21. Therefore, the base and top of the NC7B Subzone are recognized in the Ida w Shayq section (Fig. 3.10).

The FO of *Rhagodiscus achlyostaurion* is recognized at the base of the *nolani* ammonite Zone of Late Aptian age (Fig. 3.10). The *Nannoconus truitti* acme is defined in the interval between IDA17 and IDA21, within the nannofossil subzones NC7A and NC7B, which is earlier than previously illustrated by Herrle and Mutterlose (2003) in the Vocontian Basin. While, it is located younger in the upper part of *martini* and *melchioris* ammonite zones in Ida w Shayq section (Morocco) with respect to *martini* Zone in Vocontian Basin; Herrle and Mutterlose (2003).

3.3.2.1.3.3. Subzone NC7C, Late Aptian

The NC7C Subzone, is defined as the interval between the FO of *Rhagodiscus achlyostaurion* and the FO of *Prediscosphaera columnata.* In the Ida w Shayq section, the FO of *P. columnata* is recognized at level 26.55 m, in sample IDA 22. Therefore, the base and top of the NC7C Subzone are recognized (Fig. 3.10).

The FO of *Prediscosphaera columnata* is recorded in the middle part of the *jacobi* ammonite Zone of latest Aptian age (Fig. 3.10).

3.3.2.1.4. *Prediscosphaera columnata* Zone (NC8), Latest Aptian-Early Albian

The NC8 Zone represents the interval between the FO of *Prediscosphaera columnata* and the FO of *Axopodorhabdus albianus.*

3.3.2.1.4.1. Subzone NC8A, Latest Aptian-Early Albian

The NC8A Subzone, lower part of the NC8 Zone, is defined as the interval from the FO of *Prediscosphaera columnata* to the FO of *Hayesites albiensis*.

Transitional forms of both *P. columnata* and *H. albiensis*, have been recognized in Tethyan and/or Boreal sections and have been considered as stratigraphic markers (Bown, in Kennedy et al., 2000, 2014; Mutterlose et al., 2003); they are presented and discussed below:

Most authors proposed the FO of *P. columnata* to be a stratigraphic marker, approximately indicating the Aptian/Albian Boundary (e.g., Thierstein, 1971; Bralower et al., 1995; Bown et al., 1998).

The genus *Prediscosphaera* in the Late Aptian-Early Albian interval is composed of two species: (1) an elliptical form with an axial cross which is called *P. spinosa*; it appears first (Barrier, 1977; Perch-Nielsen, 1979; Mutterlose, 1996), and is reported from the Late Aptian (Barrier, 1977; Perch-Nielsen, 1979); it is followed by (2) a subcircular to circular, small sized form, with an axial cross, which is called *P. columnata* (Bown in Kennedy et al., 2000, 2014; Mutterlose et al, 2003). The FO of *P. columnata* is reported within the Lower Albian in the upper part of the *Leymeriella tardefurcata* Zone by Thierstein (1973), above the Aptian/Albian Boundary in North Sea and the Mediterranean sea according to Perch-Nielsen (1979) and in northwest Germany based on Mutterlose et al. (2003), in the uppermost Aptian of the Vocontian Basin (Bréhéret et al., 1986; Delamette et al., 1986), and in the lower part of the *jacobi* ammonite Zone of latest Aptian age in Vocontian Basin (Kennedy et al., 2000, 2014)**.** These differences can be due to different taxonomic definitions for *P. columnata* according to the different authors.

Bown (in Kennedy et al., 2000; and in Petrizzo et al., 2012) in a study dedicated to the Vocontian Basin, recognized for *Prediscosphaera columnata*, three transitional forms from sub-circular in the Late Aptian to near-circular in the latest Aptian and circular in the Early Albian. Recently, Bown (in Kennedy et al., 2014) investigated closely spaced samples from the Vocontian Basin, and precised that the circular form of *P. columnata* occurred in the latest Aptian, within the *jacobi* ammonite Zone and just below the Kilian level. Bown (in Kennedy et al., 2000, 2014) considered the lowest occurrence of the sub-circular form of the *P. columnata* as the base of the Subzone NC8A. In North Germany, the sub-circular forms of *P. columnata* occurred in latest Aptian layers (Mutterlose et al., 2003). The specimens of *P. columnata* encountered in the Essaouira-Agadir Basin, also present sub-circular to circular forms, ranging in size from 3 to 5 µm. However, no time-related morphological evolution was noticed either in Ida w Shayq than in the other sections (Tissakatine Center and Tinfoul). In the Ida w Shayq

section, the earliest, latest Aptian occurrence of the *P. columnata* is the circular form. Therefore, *P. columnata* does not present any gradual evolution in morphology through time (Figs. 3.10-3.13). The morphological evolution of *P. columnata* through time, from sub-circular, near circular to circular forms described by Bown (in Kennedy et al., 2000) is not recognized in the EAB.

Regarding the species *Hayesites*, two species with close morphologies can be recognized. *H. irregularis*, described by Roth and Thierstein (1972) as a form comprising 9 to 11 imbricate elements of variable size, and *H. albiensis* defined by Perch-Nielsen (1985) as an Early Albian species showing a star shape with 6-8 rays. In the Vocontian Basin, Bown (in Kennedy et al., 2000) observed a transitional form between *H. irregularis* and *H. albiensis* with regular 6-7 short rays. In all the studied Moroccan sections, *H. irregularis* has been recognized more or less all along the successions, even in the Early Albian (see Appendix 1-4, in supplementary data), whereas the transitional form described by Bown, has not been observed. *H. albiensis* recognized sporadically in this study is characterized by a large size of ~ 5-6 µm, with 6 to 8 rays in the Ida w Shayq, Tissakatine Center and Anzate sections. In Tinfoul, *H. albiensis* has been recognized in a poorly preserved sample (IDA 16), with less than six rays, about 3 rays being counted. Therefore, it is defined as *H.* cf *albiensis*.

At Ida w Shayq, the FO of *P. columnata* is observed in sample 22 (at 26.55 m) below D4 **(**Fig. 3.10**)**. *P. columnata* has been identified in eight levels (in samples 22 (26.6m), 23 (27.9m), 24 (28.7m), 25 (29.05m), 28 (33m), 30 (35m), 32 (36.85m) and 35 (38.9m); Fig. 3.10); in two of these levels, two specimens were identified, while only one specimen was identified in the six other levels. *H. albiensis* has been only identified in sample IDA 25 (29.05 m) just above D4 (Fig. 3.10); it is observed at the base of the *tardefurcata* ammonite Zone of Early Albian age. The NC8A is then very reduced in the Ida w Shayq section (Fig. 3.10)

3.3.2.1.4.2. Subzone NC8B, Early Albian

Subzone NC8B is defined as the interval between the FO of *Hayesites albiensis* and the FO of *Tranolithus orionatus*. The FO of *T. orionatus* has not been observed in the Ida w Shayq section. The upper part of the Ida w Shayq section is marked by the FO of *Placozygus* cf.

fibuliformis, characterizing the NC8B Subzone (Herrle, 2002; Herrle and Mutterlose, 2003). Consequently, the top of this section is included in the Subzone NC8B (Fig. 3.10).

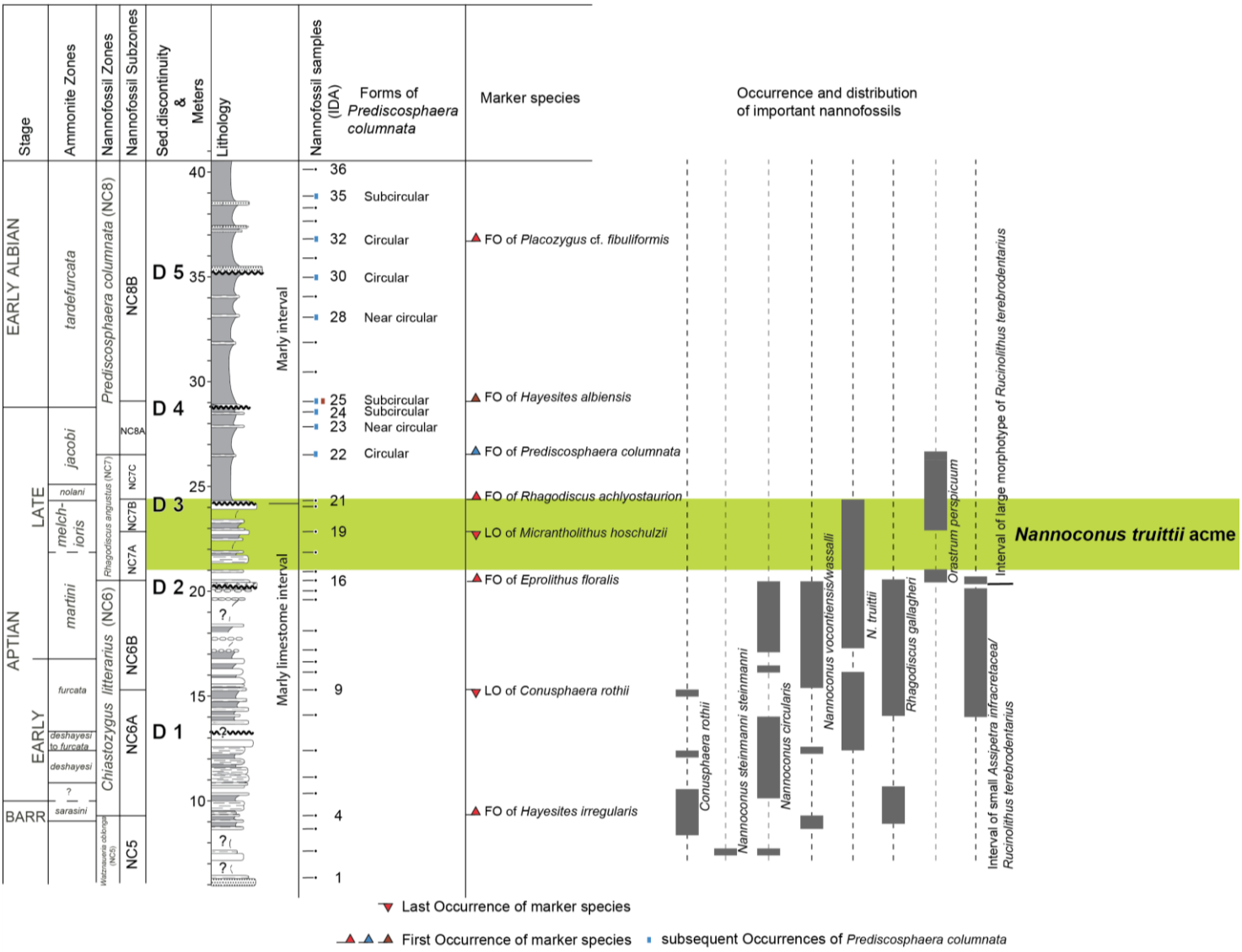

Figure 3.10: Biostratigraphy of the Aptian to Early Albian of the Ida w Shayq section. Arrows in red, blue and brown colors indicate first and last occurrences of calcareous nannofossil marker species.

3.3.2.2. Tissakatine Center (TKC) Section

In the Tissakatine Center section, we identified the same four nannofossil zones as Ida w Shayq section, namely the *Watznaueria oblonga* Zone (NC5) of Barremian age, the *Chiastozygus litterarius* Zone (NC6) of Early Aptian age, the *Rhagodiscus angustus* Zone (NC7) of Late Aptian age, and the *Prediscosphaera columnata* Zone (NC8) of Latest Aptian-Early Albian Age. The base of the Tissakatine Center section is characterized by small spacing between the FOs of *Hayesites irregularis*, *Eprolithus floralis*, and LO of *Braarudosphaera hockwoldensis*, which contrasts with the considerable spacing between the FOs of *R. achlyostaurion*, *P. columnata* and *H. albiensis* in the upper part of the succession. The close occurrence of these FOs and LO in about 2.5 m in addition to the presence of sedimentary discontinuity (D1) within the Early Aptian interval suggests a condensed succession and/or a major sedimentary gap in Early Aptian times. The Early Aptian is marked elsewhere by the OAE 1a. The presence of a hiatus (D1) could include the time interval corresponding to the globally distributed OAE 1a.

The FO of *Hayesites irregularis* is observed in the middle part of the poorly defined *deshayesi* ammonite Zone of Early Aptian age (Figs. 3.11). Based on ammonite data, the age of NC5 extends to the earliest Aptian as in Bralower (1999) and the Barremian/Aptian Boundary is not well recognized with ammonites. In the TKC section, the Barremian/Aptian Boundary may be placed at the FO of *Hayesites irregularis.* The FO of *Eprolithus floralis* is observed in the lower part of the *martini/furcata* ammonite zones of latest Early Aptian-earliest Late Aptian age (Fig. 3.11). The LO of *Micrantholithus hoschulzii* is observed in the upper part of the *martini/furcata* zones of Early Aptian-Late Aptian age (Fig. 3.11). The FO of *Rhagodiscus achlyostaurion* is observed in the upper part of the *martini* ammonite Zone of early Late Aptian (Fig. 3.11). The FO of *Prediscosphaera columnata* is observed in the upper part of the *jacobi* Zone of Late Aptian age (Fig. 3.11). The FO of *H. albiensis* is observed in the basal part of *tardefurcata* Zone at Tissakatine Center section (Fig. 3.11).

3.3.2.2.1. *Watznaueria oblonga* (NC5), Late Barremian

The LO of *Cruciellipsis cuvillieri* has not been recognized. Therefore, the base of NC5 Zone could not be defined. The top of NC5 Zone is defined by the FO of *Hayesites irregularis* at

10.8 m (sample TKC 21; Fig. 3.11). Consequently, the base of the Tissakatine Center section is included in the NC5 Zone.

3.3.2.2.2. *Chiastozygus litterarius* Zone (NC6), Early Aptian

3.3.2.2.2.1. Subzones NC6A-B

The FO of *Hayesites irregularis* has been observed at 10.8 m (sample TKC 21; Fig. 3.11), whereas *Conusphaera rothii* has not been recognized in the Tissakatine Center section.

The FO of *Eprolithus floralis* is documented at 12.6 m, in sample TKC 26 (Fig. 3.11). The absence of the LO of *C. rothii* does not allow the NC6A/NC6B boundary to be defined. Therefore, both NC6A and NC6B subzones cannot be distinguished in Tissakatine Center. Consequently, the lower part of the Tissakatine Center section corresponds to the *Chiastozygus litterarius* Zone.

3.3.2.2.3. *Rhagodiscus angustus* Zone (NC7), Late Aptian

3.3.2.2.3.1. Subzone NC7A, Late Aptian

The LO of *Micrantholithus hoschulzii* is observed at level 13.7 m (sample TKC 29). Therefore, the base and top of NC7A Subzone are defined. Consequently, the NC7A Subzone is defined in the lower part of Tissakatine Center section (Fig. 3.11).

3.3.2.2.3.2. Subzone NC7B, Late Aptian

The FO of *Rhagodiscus achlyostaurion* is documented at level 22 m, in sample TKC 43. Therefore, the base and top of NC7B Subzone, and therefore, the NC7B Subzone are defined in Tissakatine Center (Fig. 3.11).

3.3.2.2.3.3. Subzone NC7C, Late Aptian

The FO of *Prediscosphaera columnata* is observed at level 36.6 m, in sample TKC 63a. Consequently, both the base and top of the NC7C Subzone were recognized in the Tissakatine Center section (Fig. 3.11). The *Nannoconus truitti* acme is defined in the interval between TKC42 and TKC44, within the nannofossil subzones NC7B and NC7C, as in the Vocontian Basin (Herrle and Mutterlose, 2003).

3.3.2.1.4. *Prediscosphaera columnata* Zone (NC8), Latest Aptian- Early Albian

3.3.2.2.4.1. Subzone NC8A, Latest Aptian-Early Albian

The lower boundary of the NC8A Subzone, defined as the FO of *P. columnata*, is observed below D4 at Tissakatine Center. The upper boundary of NC8A Subzone, the FO of *H. albiensis* is observed just above D4 at level 40.35 m, in sample TKC 66a **(**Fig. 3.11**)**. Therefore, the NC8A Subzone is well defined in the Tissakatine Center section. *H. albiensis* has been identified with only one specimen in two levels of the Tissakatine Center section (Fig. 3.11).

3.3.2.2.4.2. Subzone NC8B, Latest Aptian-Early Albian

The FO of *Tranolithus orionatus*, which defines the top of this subzone, has not been observed in the Tissakatine Center section. The FO of *Placozygus* cf. *fibuliformis*, which occurs in the NC8B Subzone (Herrle, 2002; Herrle and Mutterlose, 2003), is recognized at level 60.5 m, below D5, in sample TKC 81. Consequently, the top of the Tissakatine Center section belongs to the Subzone NC8B (Fig. 3.11).

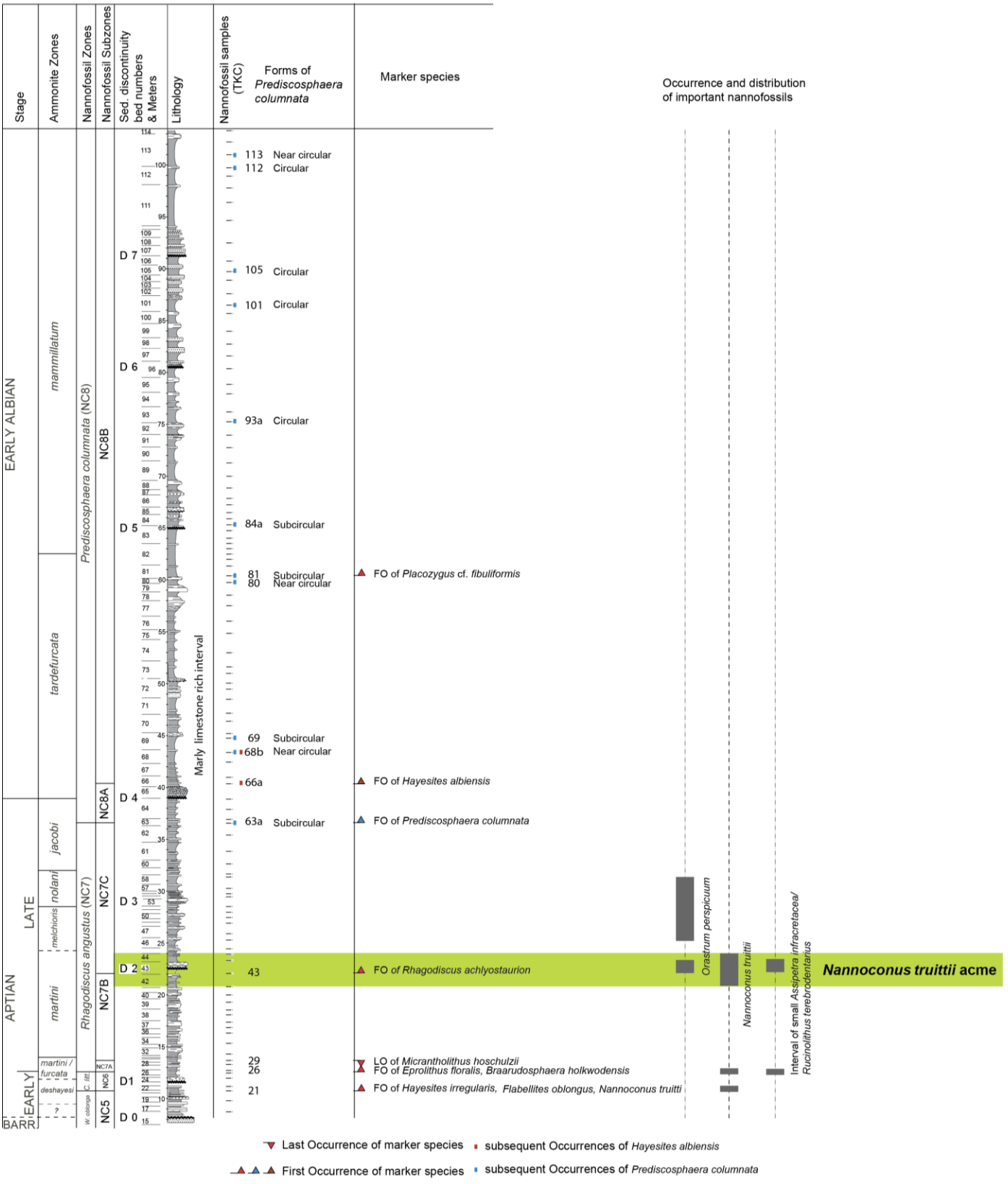

Figure 3.11: Biostratigraphy of the Aptian to Early Albian of the Tissakatine Center section. Arrows in red, blue and brown colors indicate first and last occurrences of calcareous nannofossil marker species.

3.3.2.3. Anzate (ANZ) Section

The studied succession at Anzate encompasses the NC7C/NC8A and NC8B nannofossil subzones, of Late Aptian-Early Albian age.

3.3.2.3.1. Subzones NC7C/NC8A, Late Aptian-Early Albian

Rhagodiscus achlyostaurion being present from the base to the top of the succession (see Appendix 3, in supplementary data), the FO of *R. achlyostaurion* cannot be observed, and the base of the NC7C cannot be recognized.

A concomittant first occurrence of *P. columnata* and *H. albiensis* is observed (sample ANZ 4, Fig. 3.12). There, *P. columnata* has been identified with only one specimen in three levels (samples ANZ 4, 16 and 21). The coeval FO of *P. columnata* and *H. albiensis* in Anzate does not allow the NC7C/NC8A boundary to be defined, and the NC7C and NC8A subzones are undistinguishable. The FO of *H. albiensis* is observed at the middle part of the *tardefurcata* ammonite Zone (sample ANZ 4; Fig. 3.12).

3.3.2.3.2. Subzone NC8B, Early Albian

The FO of *T. orionatus* has not been observed in the Anzate section. Consequently, the top of the Anzate succession is included in the Subzone NC8B (Fig. 3.12).

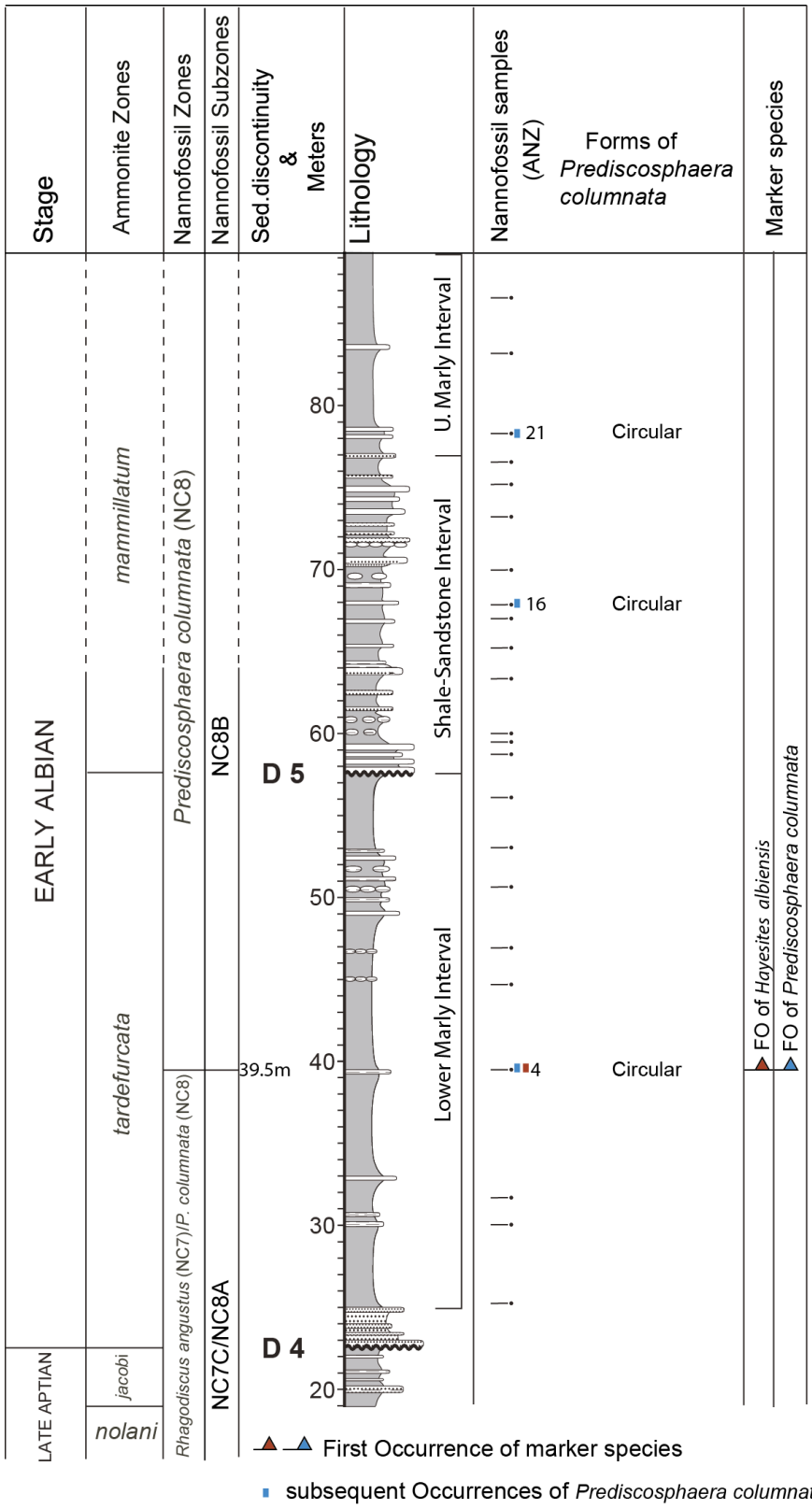

Figure 3.12: Biostratigraphy of the Late Aptian to Early Albian of the Anzate section. Arrows in brown and blue colors indicate first occurrences of calcareous nannofossil marker species.

3.3.2.4. Tinfoul (TF) Section

Three nannofossil subzones of Late Aptian-Early Albian age are recognized in the Tinfoul section.

3.3.2.4.1. Subzone NC7C, Late Aptian

Rhagodiscus achlyostaurion is present from the base to the top of the succession (see Appendix 4, in supplementary data). Therefore, the base of NC7C, defined by the FO of *R. achlyostaurion*, has not been recognized. The FO of *P. columnata* is observed at level 28 m, sample TF7, thus defining the top of the NC7C Subzone. The FO of *P. columnata* is observed in the upper part of the *jacobi* ammonite Zone, and *P. columnata* is observed in six levels in Tinfoul (Fig. 3.13).

3.3.2.4.2. Subzone NC8A, Latest Aptian-Early Albian

The lower boundary of the NC8A Subzone, i.e. the FO of *P. columnata*, is observed below D4 in Tinfoul. The upper boundary of the NC8A Subzone, is defined by the FO of *H.* cf *albiensis*. The 6 to 8 rays of typical *H. albiensis* are not recognized at Tinfoul. In the poorly preserved sample TF 16, only three rays in the *H. albiensis* have been seen, the other rays being probably dissolved. *H. albiensis* determined in the Tinfoul section is not a typical form, and has been, therefore, called *H.* cf. *albiensis.* The FO of *H.* cf. *albiensis* is observed above D5 at level 49.5 m, in the lower part of the *mammillatum* ammonite Zone (sample TF16; Fig. 3.13). Therefore, the NC8A Subzone is defined at Tinfoul even if *H.* cf. *albiensis* is observed in only three levels (Fig. 3.13).

3.3.2.4.3. Subzone NC8B, Early Albian

The FO of *Tranolithus orionatus*, which defines the top of this subzone, has not been observed in the Tinfoul section. Consequently, the top of the Tinfoul succession belongs to the NC8B Subzone.

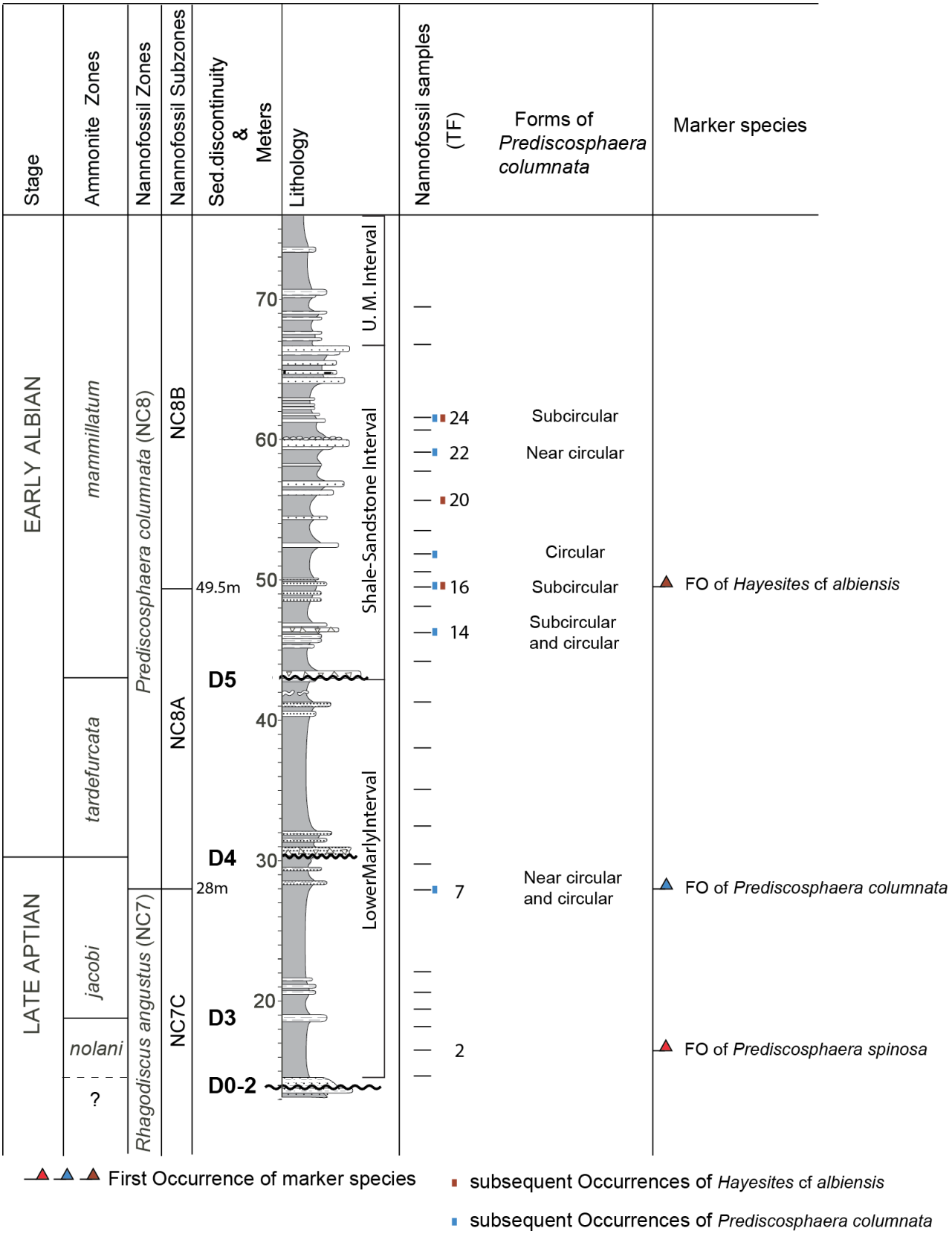

Figure 3.13: Biostratigraphy of the Aptian to Early Albian of the Tinfoul section. Arrows in red, blue and brown colors indicate first occurrences of calcareous nannofossil marker species.

3.3.3. Aptian-Early Albian nannofossil biostratigraphy in the Essaouira-Agadir Basin

The Barremian/Aptian Boundary is defined by the FO of *Hayesites irregularis* (Leckie et al., 2002; Masse, 2003; Bown, 2005). In the EAB, the FO of *H. irregularis* is recognized in both Ida w Shayq and Tissakatine Center sections (Figs. 3.10-3.11). In Ida w Shayq, the FO of *H. irregularis* is recognized in the *sarasini* ammonite Zone of Late Barremian age. In Tissakatine Center section the FO of *H. irregularis* is observed younger, in the *deshayesi* ammonite Zone of Early Aptian age. In the EAB the discrepancy between Ida w Shayq and Tissakatine sections, could reflect prevelance of preservational process. The lowest part of the Tissakatine section characterized by important siliciclastic deposits, is not suitable for the preservation of delicate specimens such as *Hayesites*, which presents rays possibly destroyed by siliciclastic input leading the recoginition of this genus difficult. In both other Tethyan basins and boreal realms, the FO of *H. irregularis* is recorded within the Early Aptian. *H. irregularis* first occurred in *tuarkyricus* (*oglanlensis*) ammonite Zone of earliest Aptian age, in the La Bedoule-Cassis Basin in SE France (e.g. Masse, 2003), in the Kopet Dagh Basin, NE Iran (Mahanipour et al., 2011), in the *weissi* ammonite Zone, in Prebetic Domain of the Betic Cordillera, SE Spain (Aguado et al. 1999). Moreover, in boreal realm *H. irregularis* first occurred in *fissicostatus* and *forbesi* ammonite zones of earliest Aptian age (Bown et al., 1998). The *fissicostatus* and *forbesi* ammonite zones of boreal realm are equivalent to *tuarkyricus* (*oglanlensis*) and *weissi* ammonite zones in Tethyan realm, respectively. The earlier occurrence of *H. irregularis* in Late Barremian in the EAB, in addition to the low latitude and the warm water affinity of this taxon (Bown, 2005), could explain the earlier occurrence for this taxon in the EAB.

Chiastozygus litterarius nannofossil Zone (NC6) is defined by the FO of *Hayesites irregularis* and the FO of *Eprolithus floralis*. In the EAB, the FO of *E. floralis* is recognized in the lower part of *martini* ammonite Zone at Ida w Shayq, and in lower part of *furcata/martini* ammonite zones at Tissakatine Center. While, in other Tethyan basins the FO of *E. floralis* is observed earlier, in the *furcata* ammonite Zone, in Prebetic Domain, SE Spain (Aguado et al., 1999), in the *deshayesi* ammonite Zone, in Umbria-Marche Basin, C Italy (Erba et al., 1996), in the La Bedoule-Cassis Basin in SE France (Masse, 2003), in the Kopet Dagh Basin, NE Iran (Mahanipour et al., 2011). Moreover, the FO of *E. floralis* can define the Early/Late Aptian Boundary, in Gargano Promontory area, Southern Italy (Luciani et al., 2006); in Cismon and

Apennines areas, Northern Italy (Bralower et al., 1993), and in many Sites of DSDP and ODP, studied by Bralower et al. (1993) such as in; DSDP Site 402 (Bay of Biscay), DSDP Site 364 (Angola Basin), Site DSDP 511 (Falkland Plateau), Site DSDP 463 (Mid-Pacific Mountains) and in Site ODP 641 (Galicia Bank).

Discrepancies in the FO of *E. floralis* recognized both in the different sections of the EAB and between the EAB and the other basins could be due to both scarcity and poor preservation of nannofossils in the EAB, leading the Early/Late Aptian Boundary difficult to be defined based on nannofossils in this basin. Second hypothesis: *E. floralis* is interpreted as a high latitude taxon (Roth and Krumbach, 1986); a migration from north to south could explain a later occurrence in the southern part of Tethys with respect to the northern part.

Rhagodiscus angustus nannofossil Zone (NC7) is defined by the FO of *E. floralis* and the FO of *Prediscosphaera columnata*. In EAB, the FO of *P. columnata* is observed in the Late Aptian, within the *jacobi* ammonite Zone in Ida w Shayq, Tissakatine Center and Tinfoul sections. In Anzate section the FO of *P. columnata* is recorded younger in *tardefurcata* ammonite Zone of Early Albian age, and coeval with the FO of *Hayesites albiensis.* In the Vocontian Basin, (SE France; Herrle, 2002; Herrle and Mutterlose, 2003), the FO of *P. columnata* is also recorded in the *jacobi* ammonite Zone.

The Aptian/Albian Boundary is expected close to the FO of *Prediscosphaera columnata* (e.g., Thierstein, 1971; Bralower et al., 1995; Hart et al., 1996; Bown et al., 1998; Bown in Kennedy et al., 2000; Mutterlose et al., 2003). Consequently, the Aptian/Albian Boundary in the EAB, could be expected close to the FO of *P. columnata*. The FO of *P. columnata* within the Latest Aptian *jacobi* ammonite Zone, support the proximity of AAB (Figs. 3.10-3.14).

In the EAB, the *Prediscosphaera columnata* nannofossil Zone (NC8) is represented both by NC8A and NC8B subzones. The base and top of the NC8A Subzone is defined by the FO of *P. columnata* and the FO of *Hayesites albiensis* respectively. In Ida w Shayq and Tissakatine Center sections, the FO of *H. albiensis* is recorded in the lowermost part of *tardefurcata* ammonite Zone, in middle *tardefurcata* ammonite Zone in Anzate section and in lowermost part of *mammillatum* ammonite Zone in Tinfoul section. While, in Vocontian Basin (SE France), the FO of *H. albiensis* is recognized earlier in upper *jacobi* ammonite Zone (Herrle, 2002; Herrle

and Mutterlose, 2003). The base and top of the NC8B Subzone is defined by the FO of *H. albiensis* and the FO of *Tranolithus orionatus* respectively. The FO of *T. orionatus* is not recorded in the EAB. Younger ages given by most of Late Aptian-Early Albian nannofossil marker species in the EAB with respect to the Vocontian Basin could be due to prevalence of poorly-preserved nannofossils in this basin as it has been already recognized in the Tethyan carbonate platform sediments (e.g. Bralower et al., 1989; Bown, 2005).

The integration between nannofossil and ammonite zonations have been done for the first time in the EAB for the Late Aptian-Early Albian time interval. Younger ages for FO of the nannofossil marker species with respect to those observed in the hemipelagic sections of the Tethyan northern margin, could be due to the generally poor preservation of nannofossil assemblages observed in the different sections of the EAB.

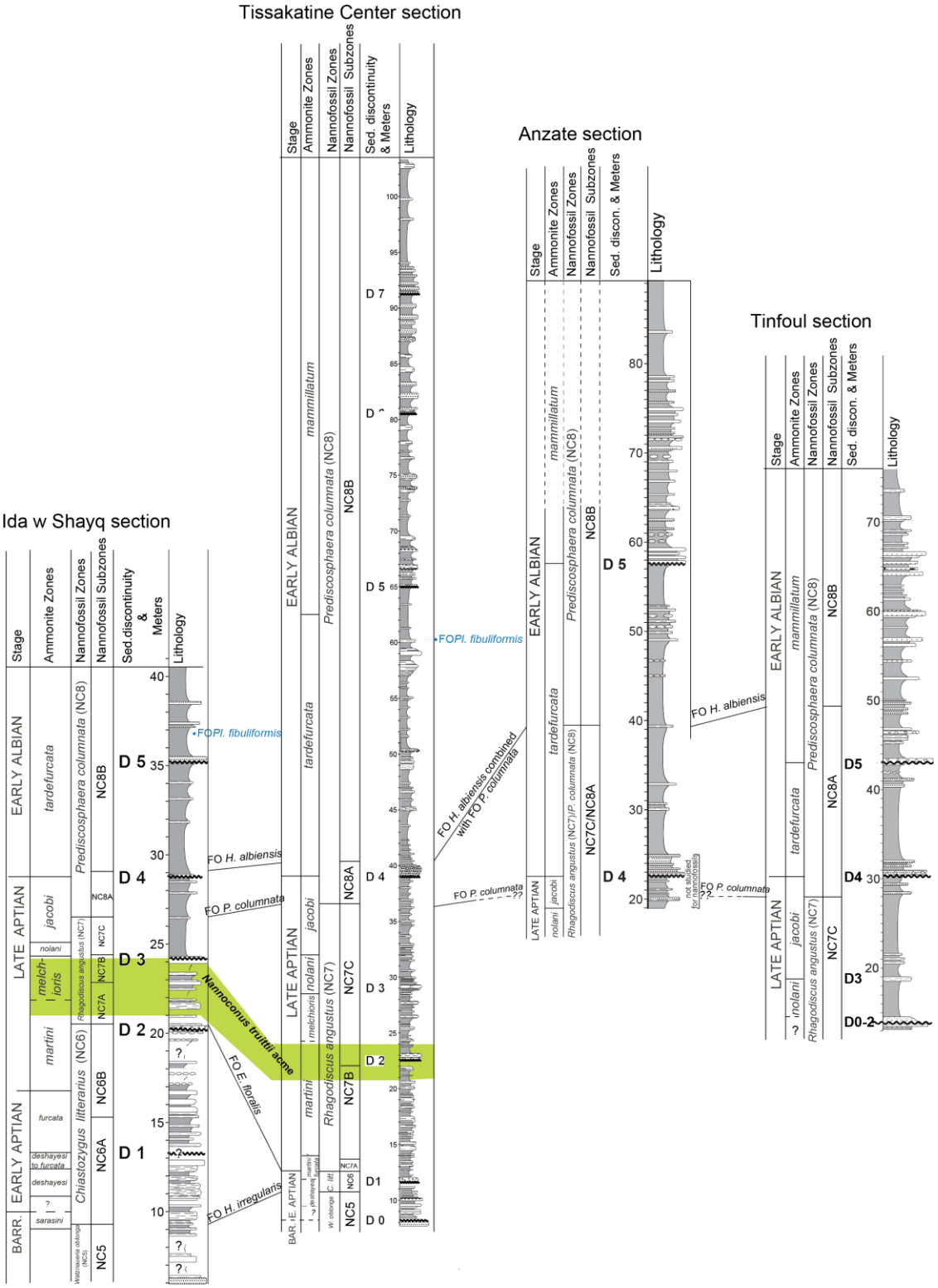

Figure 3.14: Integration between the nannofossil and ammonite biostratigraphy of the Aptian to Early Albian in the studied sections of EAB. The FO of *P. columnata* is recognized in *jacobi* ammonite Zone in all studied sections, except in Anzate section, in which the FO of *P. columnata* is recorded younger in *tardefurcata* ammonite Zone. In Anzate section, the *jacobi* ammonite Zone is not sampled for nannofossil study. With sampling and future study for Anzate section, the FO of *P. columnata* is expected earlier in *jacobi* ammonite Zone, around the dashed lines, below D4.

3.4. SEDIMENTOLOGY OF DISCONTINUITIES IN the EAB

Six main discontinuities have been recognized, named D0, D1, D2, D3, D4 and D5. They are correlatable in all studied sections thus defining at least five main sedimentary sequences (Figs. 3.1; 3.4). These discontinuities are considered as time-lines, and correlation tools between sections of the studied area, and, if acknowledged as eustasy-related, as correlation tools worldwide. That is why we write about the sedimentology of discontinuities in a chapter devoted to integrated stratigraphy.

3.4.1. The zero discontinuity (D0, Late Barremian to earliest Aptian)

The D0 is marked by an abrupt change in lithology, since it separates calcareous sandstones of late Barremian and sandy marl beds of Early Aptian age. It is defined as an erosional surface marked by reworked fragments of pelecypod, oyster, trigonid, brachiopod and accumulation of ammonites in the sections of Ida w Shayq and Tissakatine Center. In Ida w Shayq this discontinuity is overlain by *Kutatissites* sp. (Late Barremian-Early Aptian) and *Pseudocrioceras* sp., this latter genus being of latest Barremian age. It is, therefore, probably of latest Barremian age. However, in Anzate, it is a karstified surface, amalgamated with D1, and in Tinfoul, D0 may be amalgamated with D1 and D2.

3.4.2. The first discontinuity (D1; Early Aptian)

It is usually located at the top of the massive calcareous sandstones of Late Barremian age. It is marked, according to the sites, by an erosional surface marked by bioturbation, accumulation of phosphatic ammonites, bio- and litho-clasts (Tissakatine Center, Ida w Shayq), or by a karstified surface (Anzate, Ida w Shayq, Tinfoul sections). It is probably amalgamated with D2 in the Tinfoul section. This unconformity, located near the top of the *Cheloniceras* beds (Ida w Shayq and Tissakatine Center sections), is of Early Aptian age, close to the boundary between the *Deshayesites deshayesi* and *Dufrenoyia furcata* zones (Fig. 3.5).

3.4.3. The second discontinuity (D2; late Early Aptian to early Late Aptian age)

This discontinuity is either amalgamated with the first one in Tinfoul, or located 1 m, or less, above the first one in Anzate. It consists of, either an erosional surface marked by an

accumulation of reworked lith-and bio-clastic fragments (Ida w Shayq and Tissakatine Center sections), or a karstified surface (Anzate and Tinfoul). In Ida w Shayq, Tissakatine Center and Anzate, the ammonites associated with D2 indicate that it is located close to the boundary between the *Dufrenoyia furcata* and *Epicheloniceras martini* zones (transition from Early to Late Aptian; Figs. 3.5, 3.6, 3.8, 3.9).

3.4.4. A third discontinuity (D3; Late Aptian)

D3 seems to be located near the top of the "Nolani Beds". It is marked by an erosional surface overlain by reworked clasts (Ida w Shayq and Anzate) or by a condensed, bioturbated surface marked by ammonite accumulations (Tissakatine Center). It has not been clearly observed as yet in the Tinfoul section. Since it lies within the lower part of the *Nolaniceras nolani* Zone, it is of Late Aptian age; Figs. 3.5, 3.6, 3.8, 3.9).

3.4.5. The fourth discontinuity (D4; Aptian/Albian Boundary)

The fourth discontinuity is marked by a very constant layer of reddish to yellow sandstones, which contains commonly green phosphatic, reworked clasts and fossil fragments (Ida w Shayq, Tissakatine Center, Anzate and Tinfoul). Because no evidences of subaerial exposure have been found, it probably corresponds to a submarine hiatus. Species of *Epicheloniceras* (Late Aptian) have been found 1 to 2.5 m below D4 in Ida w Shayq, Anzate and Tissakatine Center, while specimens of *Douvilleiceras* were collected on the proper surface in Ida w Shayq, and 0.5 m above D4 in Tissakatine Center. The underlying sequence is, therefore, of latest Aptian age (*Hypacanthoplites jacobi* Zone), and the overlying sequence is of earliest Albian age (*Leymeriella tardefurcata* Zone). This surface is thought to mark the Aptian/Albian Boundary in the EAB, and the time span of the submarine hiatus probably contains the Aptian/Albian Boundary time slice (Figs. 3.5, 3.6, 3.8, 3.9).

3.4.6. The fifth discontinuity (D5; Early Albian)

This discontinuity commonly coincides with the base of the "Beudanticeras Beds". It is marked by a constant bed of yellow sandstones, which reworks white phosphatic clasts, ammonite fragments, and shaly flat pebbles, thus documenting a sedimentary hiatus and a period of submarine erosion. In the Anzate section, species of *Hypacanthoplites* were found 1.5 m

below D5, while *Douvilleiceras* sp. is present 2 m above it (Fig. 3.8). Since *Hypacanthoplites* disappear at the top of the *tardefurcata* Zone (Latil, 2011), the age of D5 is considered close to the boundary between the t*ardefurcata* and *mammillatum* zones. This interpretation is supported by the occurrence of *Beudanticeras revoili* 2.5 m below D5 in Tissakatine Center (Fig. 3.7), and by the presence of *Douvilleiceras mammillatum aequinodum* 12 m above D5 in Tinfoul (Fig. 3.9).

The overlying marly series contains several beds of sandstones with erosional base, which probably represent additional discontinuities (D6 and D7; in Tissakatine Center section). Since no ammonites of Middle Albian age have been found, they seem to be located within the *Douvilleiceras mammillatum* Superzone of Early Albian Age.

In summary, these unconformity surfaces are widely distributed and defined almost in all studied sections. The unconformity surfaces could be considered as sequence boundaries enclosing five sedimentary sequences. The subaerially exposed, karstified unconformity surfaces (D0, D1, and D2) can be classified as type one sequence boundary (SB0, SB1, SB2). The submarine, erosional unconformity surfaces emphasized by yellowish sandstone beds (D3, D4, D5 in addition to D6 and D7 in the Tissakatine Center section) are classified as type two sequence boundaries (SB3, SB4, SB5 in addition to SB6 and SB7 at Tissakatine Center).

3.5. ISOTOPE RECORDS AND CHEMOSTRATIGRAPHY

3.5.1. Methodology

Carbon and oxygen isotope analysis have been performed on the same 139 samples studied for calcareous nannofossils at the stable isotope laboratories of the Institute of Earth Sciences of the University of Lausanne, using a Thermo Fisher Scientific Gas Bench II carbonate preparation device connected to a Delta Plus XL isotope ratio mass spectrometer (IRMS; Révész et al., 2001). The CO_2 extraction was done at 70°C. The stable carbon and oxygen isotope ratios are reported in the delta (δ) notation as $\delta^{13}C$ and $\delta^{18}O$. Values in mil (‰) express the variations relative to the Vienna Pee Dee belemnite standard (VPDB), where $\delta = (R_{sample} - R_{standard})/R_{standard} \times 1000$ and $R = \delta^{13}C/^{12}C$ or $^{18}O/^{16}O$. The standardization of the $\delta^{13}C$ and $\delta^{18}O$ values relative to the international VPDB scale was done by calibration of the reference gases

and working standards with IAEA standards. Analytical uncertainty (1σ), monitored by replicate analyses of the international calcite standard NBS-19 and the laboratory standard Carrara Marble is no greater than ±0.05‰ for $\delta^{13}C$ and ±0.1‰ for $\delta^{18}O$.

3.5.2. Results

3.5.2.1. Ida w Shayq section

The $\delta^{13}C$ record varies between -1.2 and 0.9‰ (Fig. 3.15). Values firstly increase in the Early Aptian, reaching a maximum, with positive values around 0.9‰ above D2 in the Late Aptian. From the latest Aptian to the Early Albian, the $\delta^{13}C$ slightly decreases with negative values and reaches a minimum value at D4. From D4 to the top of the succession, only small variations are recorded.

The $\delta^{18}O$ record varies between -4.5 and -0.7‰ (Fig. 3.15). These values firstly increase in the Early Aptian, reaching a maximum around -0.7% before D2 in the Late Aptian. Then they decrease until a minimum value around -4.5% below D3. Above D3, the oxygen isotope values slightly decrease and remain relatively constant up to the top of the studied succession. The $\delta^{18}O$ are lower in the Early Albian with respect to the Aptian.

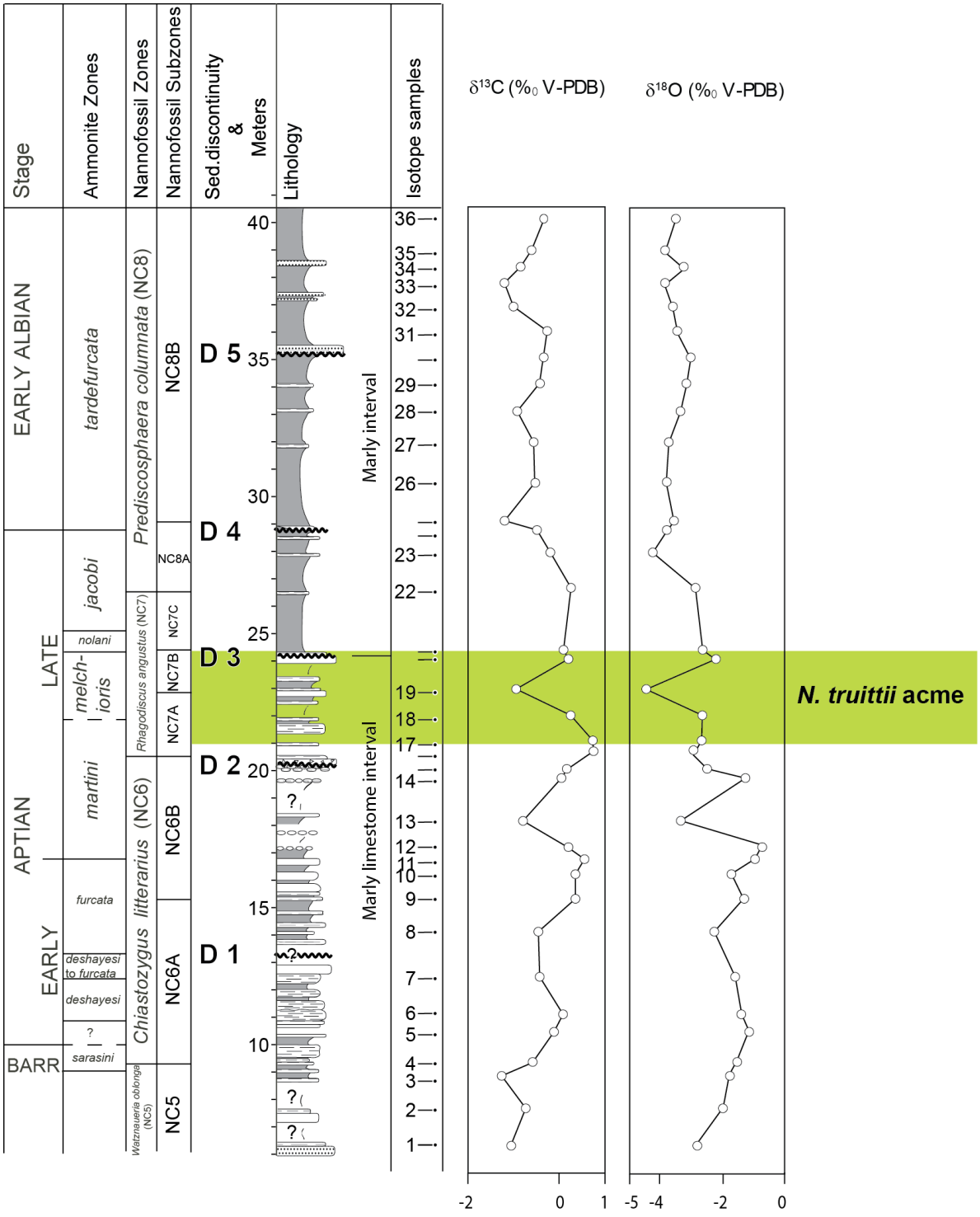

Figure 3.15: Biostratigraphy and stratigraphic changes in carbon and oxygen isotope of the Ida w Shayq section during Aptian to Early Albian times

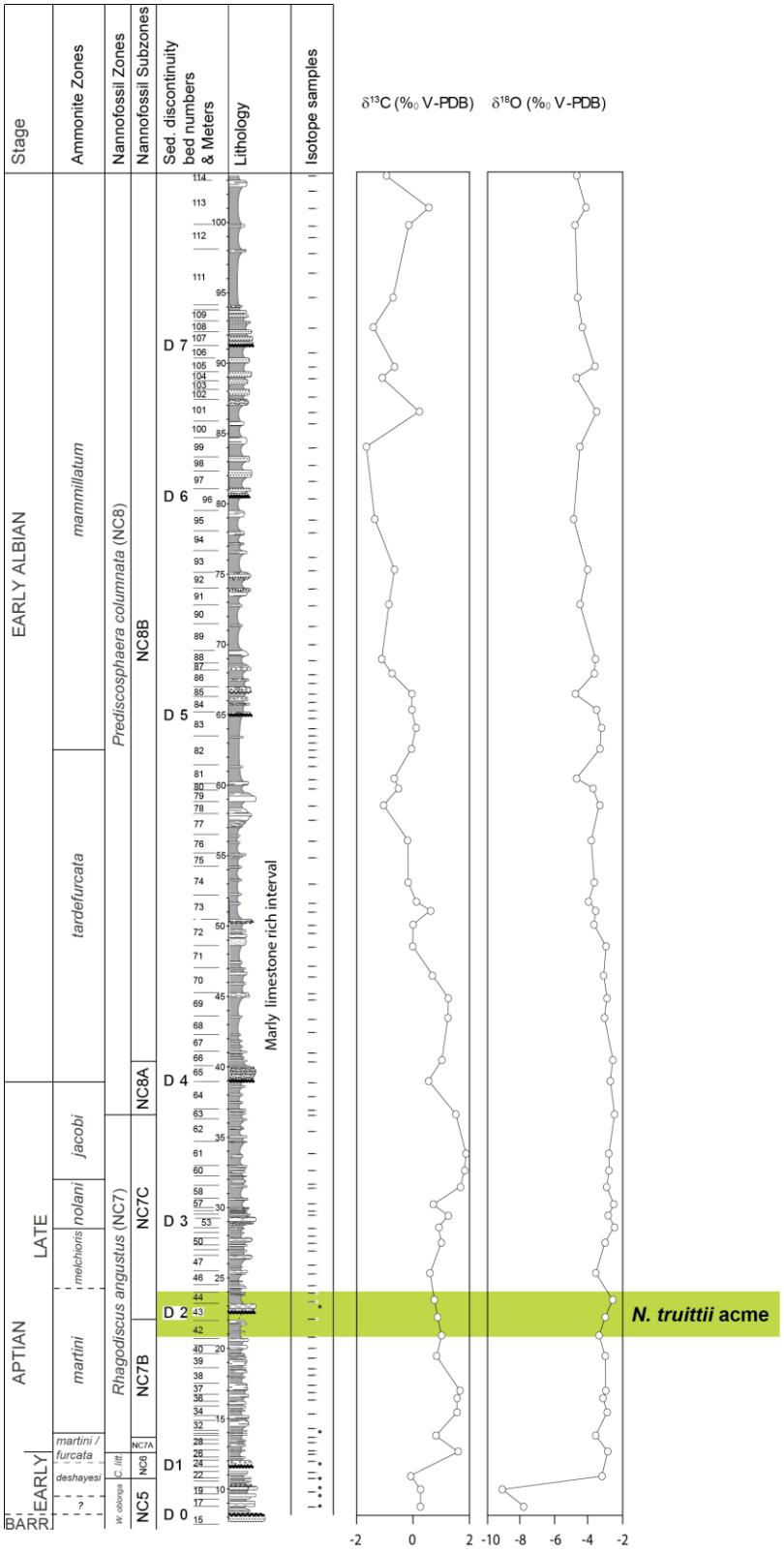

Figure 3.16: Biostratigraphy and stratigraphic changes in carbon and oxygen isotope of the Tissakatine Center section during Aptian to Early Albian times

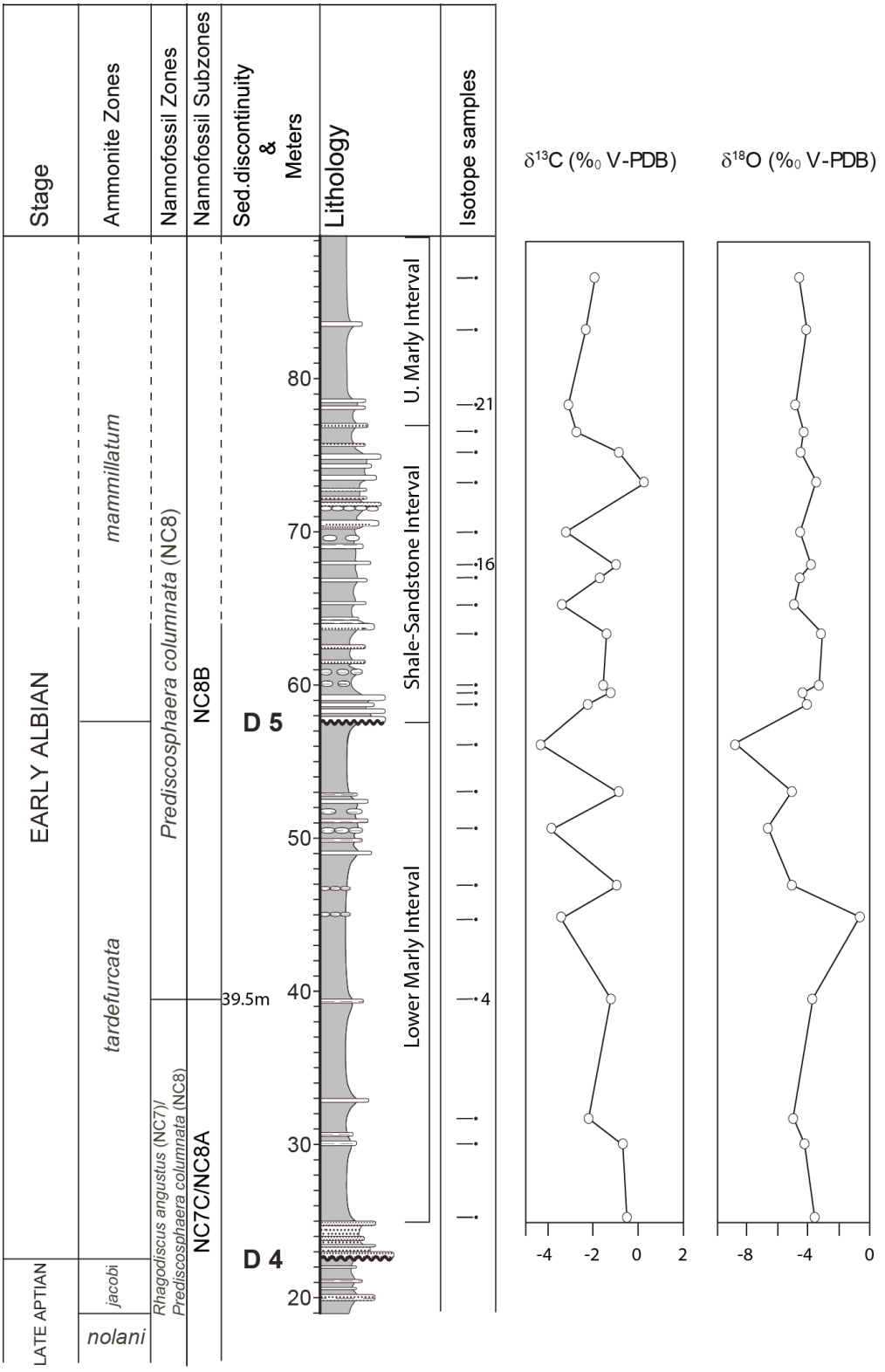

Figure 3.17: Biostratigraphy and stratigraphic changes in carbon and oxygen isotope of the Anzate section during the Aptian to Early Albian time

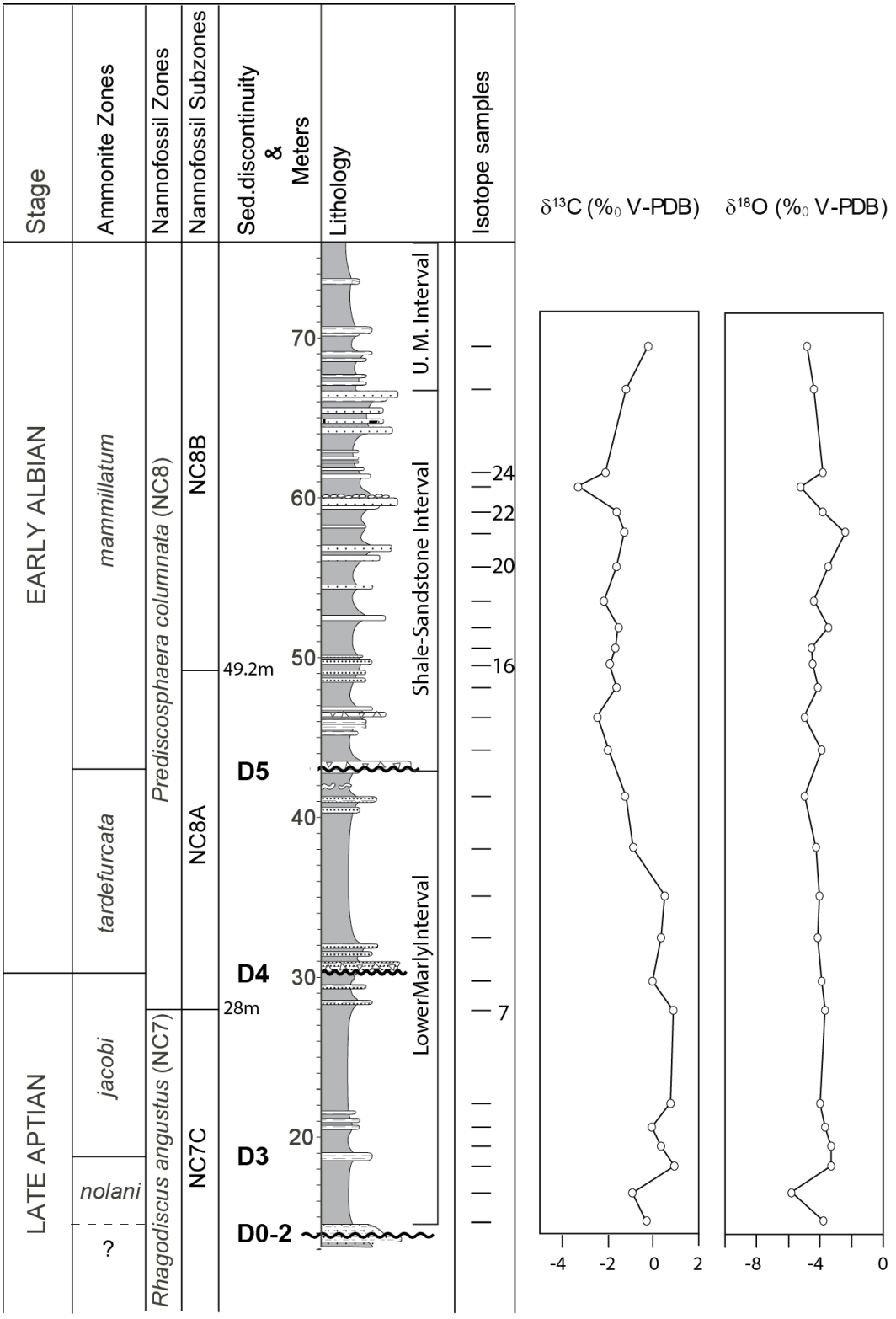

Figure 3.18: Biostratigraphy and stratigraphic changes in carbon and oxygen isotope of the Tinfoul section during the Aptian to Early Albian time

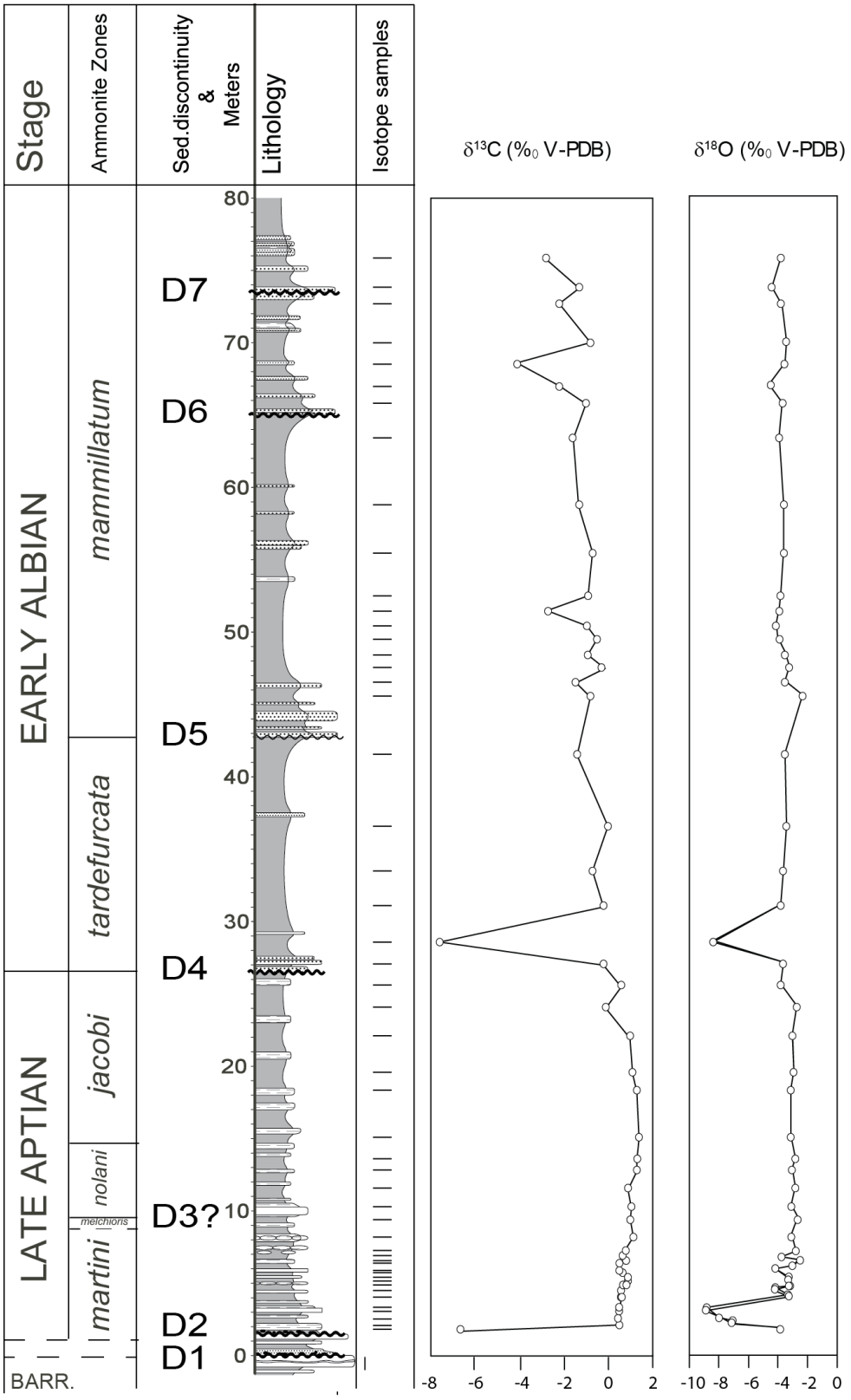

Figure 3.19: Biostratigraphy and stratigraphic changes in carbon and oxygen isotope of the Addar section during the Aptian to Early Albian time (the ammonite biostratigraphy collected from Peybernes et al., 2013)

3.5.2.2. Tissakatine Center section

The $\delta^{13}C$ record varies between -1.6 and 1.8 ‰ (Fig. 3.16). From the base, the $\delta^{13}C$ values increase reaching a maximum value before D4. Then, they decrease upward reaching a minimum value above D6. Then, the $\delta^{13}C$ values increase in the upper part of the succession. The $\delta^{13}C$ values are higher in the Late Aptian with respect to the Early Albian.

The $\delta^{18}O$ record varies between -9.1 and -2.5 ‰ (Fig. 3.16). After a sharp increase at the base of the section, the oxygen isotope values remain relatively constant until D4; then, they slightly decrease until D5 and remain constant in the upper part of the section. Highest values are recorded in the Late Aptian-earliest Albian time interval.

3.5.2.3. Anzate section

The $\delta^{13}C$ record varies between -4.6 and 0.2‰ (Fig. 3.17). The values decrease from the base of the studied succession toward the sedimentary discontinuity D5. Above D5, the $\delta^{13}C$ record slightly increases reaching a maximum, with a positive value at 73 meters. Then, values firstly decrease then increase in the uppermost part of the studied interval.

The $\delta^{18}O$ record varies between -9 and -0.9‰ (Fig. 3.17). The values firstly increase in the earliest Albian. Then values decrease until a minimum below the sedimentary discontinuity D5. Above D5, the oxygen isotope values slightly increase and stay relatively constant up to the top of the studied succession.

3.5.2.4. Tinfoul section

The $\delta^{13}C$ values vary between -3.3 and 0.9‰ (Fig. 3.18). After a slight increase recorded at the base of the section, they present a plateau in the Late Aptian. Then, the values decrease reaching -2‰ just above D5. Values slightly increase to form a second plateau in the middle part of the *mammillatum* ammonite Superzone. Then, the $\delta^{13}C$ records a minimum value and

increases at the top of the section. As for the Ida w Shayq and Tissakatine Center sections, $\delta^{13}C$ values are higher in the Late Aptian with respect to the Early Albian.

The $\delta^{18}O$ record varies between -5.8 and -2.4‰ (Fig. 3.18). The lowest value is recorded at the base of the succession. Values decrease from the Late Aptian up to the earliest Albian, just below D5. Above D5, values increase. Then values decrease and stay low in the rest of the succession.

3.5.2.5. Addar section

Addar section is the reference section of EAB. So, we correlate this section with the four sections studied in this work, based on ammonite and isotope stratigraphy. The ammonite biostratigraphy for Addar section has been done (see Peybernes et al., 2013). We don't have nannofossil biostratigraphy for this section since the work of Peybernes et al. (2013) only concerns the paleoenvironment. The stable isotope analysis was recently made for Addar section, and being included in this study for correlation with the other studied sections in EAB.

At Addar, the $\delta^{13}C$ values vary between -7.6 and 1.4‰ (Fig. 3.19). After a slight increase recorded at the base of the section, they present a plateau in the Late Aptian. Then, the values decrease reaching a minimum of -7.6‰ just above D4. In the Early Albian, the values slightly increase to form a second plateau, dissected by two very short decrease and increase around meters 51 and 68.5 respectively. $\delta^{13}C$ values are higher in the Late Aptian with respect to the Early Albian.

The $\delta^{18}O$ record varies between -8.9 and -2.3 ‰ (Fig. 3.19). After a sharp decrease reaching a minimum, followed by a rapid increase at the base of the section, the oxygen isotope values remain relatively constant until below D4; then, they slightly decrease just above D4. Then values increase reaching the highest value above D5, followed by a slight decrease until above D6, before a small recovery at the top of the succession.

3.5.3. Interpretation

3.5.3.1. The diagenetic hypothesis

The Aptian-Albian Moroccan sections studied belong to a shallow marine carbonate ramp (see sedimentology part in section 4. A). Shallow-marine carbonate sections generally present a complex geochemical record because the sediments are commonly first exposed to meteoric waters before reaching mineralogical stability (Allan and Matthews, 1982). Sections can also in a secondary stage, be exposed to a burial diagenesis.

Diagenetic features could be detected from both petrography and geochemistry (Marshall, 1992; Moore, 2001). Cement type can be diagnostic of a particular diagenetic environment. However, identical cement types may be formed in different diagenetic environments. Equant drusy spar cement may precipitate in near-surface meteoric environments and under deep burial conditions (Flügel, 2004).

Most of the Aptian-Albian studied sections are fine-grained shales and marls with few carbonate and sandstone interbeds. The cementation in the shale and marl beds is difficult to identify using transmitted light microscopy. In the carbonate and sandstone beds, the cementation shows a drusy mosaic spar cement filling the intergranular pore spaces, and reaching about 20% of the total rock components (Fig. 3.20A). This indicates cementation under influence of meteoric waters for the Aptian-Albian sediments. Presence of coarse-crystalline dolomite rhombs, representing about 25% of the total rock (Fig. 3.20B) reflects the occurrence of dolomitization processes after cementation during early late diagenetic stage, in the mixing zone with meteoric waters. Because, it is well recognized very close to karstified surfaces, influenced by meteoric water (see sedimentology part in section 4. A), resulted from the change of the depositional suite during short-term relative global sea-level fall (El Araby, 1999) or as a result of karstification during a relative sea-level fall (Moss and Tucker, 1996). There is a minor diagenetic effect in the studied sections, which increases in the carbonate-rich intervals with respect to the shale-rich ones.

The oxygen and carbon isotopic compositions of meteoric cements depend on the isotopic composition of the meteoric waters invading the sediment (Colombié et al. 2011). The meteoric diagenesis leads to a decrease of the $\delta^{18}O$ and $\delta^{13}C$ contents of carbonates (Colombié et al. 2011; Godet et al., 2016).

The range of carbon and oxygen isotope values of the five studied sections are presented in Table 3.1, with data recovered from other basins, for the same interval. Among the sections representing other basins than EAB, two belong to carbonate platform, the others correspond to hemi-pelagic to pelagic environments. Both $\delta^{18}O$ and $\delta^{13}C$ values are lower in EAB with respect to other sections, even the carbonate platform sections. The meteoric diagenesis could be effective in EAB.

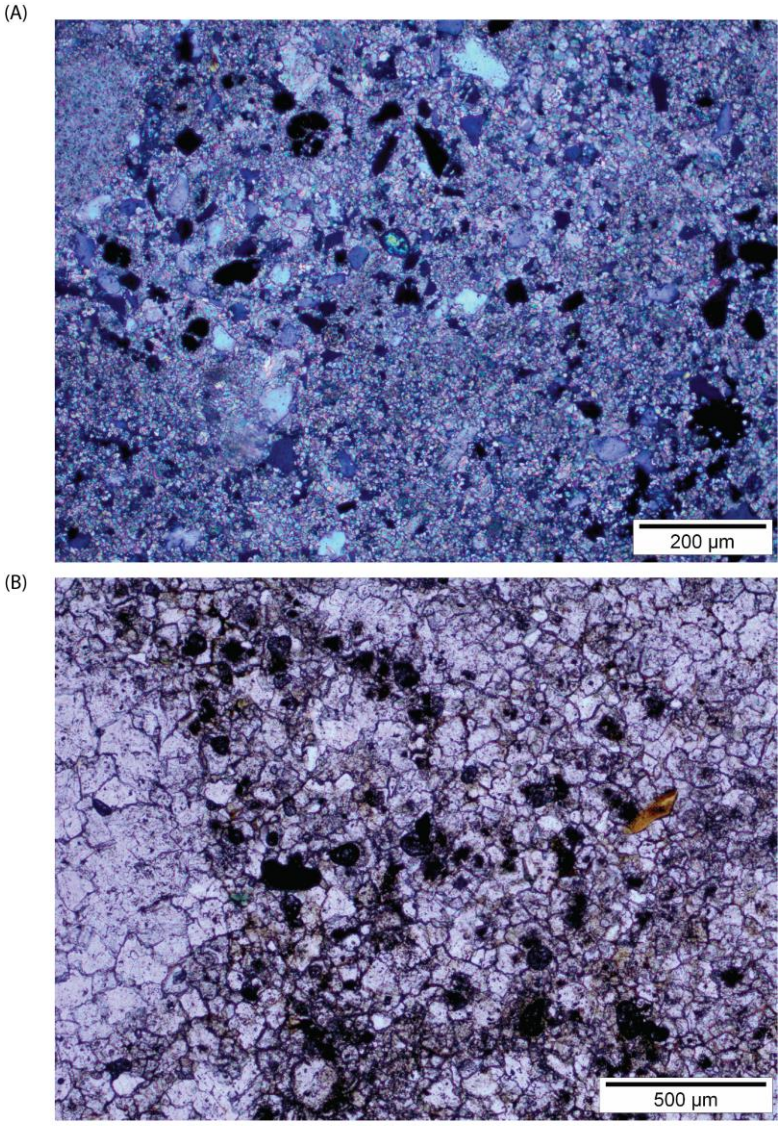

Figure 3.20:
(A) Thin section photomicrograph of blocky mosaic fine crystals of calcite cement vary in size fills the intergranular pore spaces, interval between D1 and D2, unit Ida 13, Ida w Shayq section, Crossed Nichols (XPL).
B) Thin section photomicrograph of coarse, zoned, rhombic, dolomite crystals replacing all components of the sediments, interval between D0 and D1, unit Tkc 17, Tissakatine Center section, Plane Polarized Light (PPL).

Table 3.1: The range of carbon and oxygen isotope values of the five studied sections in the EAB, with data recovered from other basins

Environment	Section Name	Locality	$\delta^{13}C$ values varies between	Uppermost Aptian $\delta^{13}C$ +ve excursion (progressive fall)	Early-Albian $\delta^{13}C$ +ve excursion (less prominent)	$\delta^{18}O$ values varies between	Author(s)
Platform carbonate	Ida w Shayq	SW Morocco	-1.2 and 0.9‰	-1 and 0.5	-1.2 and -0.2‰	-1.2 and 0.9‰	This study
	Tissakatine Center	SW Morocco	-1.6 and 1.8‰	0.5 and 1.8	-1.6 and 1.2‰	-9.1 and -2.5‰	
	Anzate	SW Morocco	-4.6 and 0.2	-0.7 and -0.6	0.2 at 73 m	-9 and -0.9	
	Tinfoul	SW Morocco	-3.3 and 0.9	0 and 0.9	-3.3 and -0.2%	-5.8 and -2.4	
	Addar	SW Morocco	-7.6 and 1.4	-7.6 and 1	-4.4 and 0	-8.9 and -2.3	
	Coppa della Nuvola	Gargano Promontory, S. Italy	-10 and 5	Relatively (~ +1.8) (C10)	-3 (C11)	-4.5 and 0	Luciani et al (2004)
	Serra Sbregavitelli	Southern Apennines, S. Italy	2 and 4.8	3 and 4.8	2 and 3.5	……	D'Argenio et al (2004)

	Resolution Guyot	ODP, Site 866, Mid-Pacific	1 and 5.5	3.5 and 5.5	1 and 3.5	-1 to -3	Jenkyns (1995)
	Mount Kanala	Greece	1 and 3.5	1 and 3.5 (NJ)	~ 1.2 and 2.7 (NP)	…….	Grőtsch et al (1998)
Hemipelagic- pelagic	Mazagan Plateau	NW Africa, Central Atlantic	0.5 and 2.7	2 to 2.5	0.5 to 2	-1.5 and -0.2	Herrle (2002), Herrle et al (2004)
	Cole De Pre-Guittard	Vocotian Basin, SE France	0.5 and 4	2 and 4 (~3)	1 and 2.5 (NP)	-2 and -3	Kennedy et al (2000)
	Composite section	Vocotian Basin, SE France	0.9 and 4.8	2.5 to 3.5 Ap12-Ap15 spans ~2.9Ma	1 to 2.5 AL2 spans ~ 0.3Ma	-4.5 and -2.5	Herrle (2002), Herrle et al (2004)
	Peregrina Canyon	Sierra Madre, NE Mexico	2 and 4	3.5 and 4.5	3 and 4	…….	Bralower et al (1999)

Carbon and oxygen isotopes measured in carbonates may be altered by the addition of isotopically light cement during burial diagenesis (Kennedy et al, 2000). The impact of higher temperatures related to burial diagenesis is stronger on oxygen isotope composition of the bulk carbonate than on the carbon isotope composition (Weissert, 1989). A strong positive correlation between oxygen and carbon isotope values can then be observed (Jenkyns and Clayton, 1986; Marshall, 1992; Jenkyns, 1996). Therefore, the $\delta^{18}O$ values could be more influenced by burial diagenesis than carbon isotopes. Daoudi et al. (2010) have shown with clay minerals analysis that, in the Agadir area of the Essaouira-Agadir Basin, the Mid-Albian interval has been buried up to 1800 meters, indicating that this part has been subject to deep burial. The correlations between $\delta^{18}O$ and $\delta^{13}C$ for the different sections are presented in Figure (3.21). For the Tissakatine Center, Ida w Shayq and Anzate sections, the correlation coefficient of Pearson is statistically significant ($p < 0.05$) showing a positive correlation between $\delta^{18}O$ and $\delta^{13}C$ (Fig. 3.21A-C). For Tinfoul, the positive correlation is not statistically significant (Fig. 3.21 D). These results suggest that the stable isotope compositions for three sections were certainly altered by burial diagenesis.

The $\delta^{18}O$ values widely fluctuated in all the studied sections (Figs. 3.15-3.19). Both low $\delta^{18}O$ values and large fluctuations in the $\delta^{18}O$ record indicate unequal fractionation and addition of variable amounts of isotopically light cement (Jenkyns and Clayton, 1986; Weissert and Breheret, 1991; Korte et al. 2009).

In conclusion, both meteoric and/or burial diagenesis were in part responsible for the low $\delta^{18}O$ and $\delta^{13}C$ values recorded in the Aptian-Albian of the EAB, with respect to the other basins. Then, the use of $\delta^{18}O$ for paleoenvironment reconstructions will be not considered in this study. For the $\delta^{13}C$ record, even if the absolute values from the EAB are lower with respect to the other sections, general trends can be recognized (Figs. 3.15-3.19) and will be used to establish a carbon isotope stratigraphy.

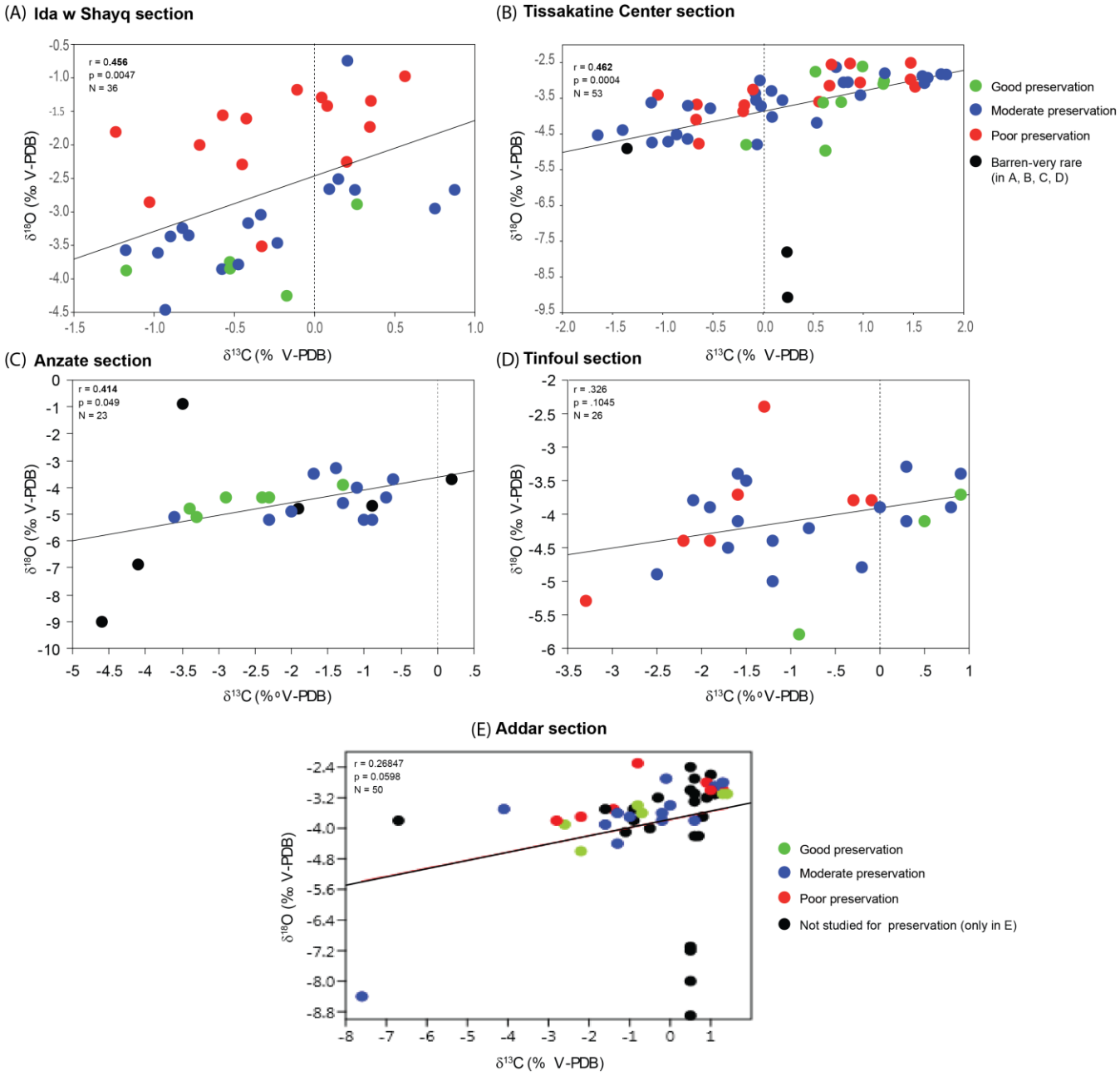

Figure 3.21: Bivariate plots showing a weak positive correlation between carbon and oxygen isotopes for the Ida w Shayq (A), Tissakatine Center (B), Anzate (C). Tinfoul (D) and Addar (E) sections. Abbreviations: r, coefficient of correlation; p, probability; N, number of measurements.

3.5.3.2. Carbon isotope stratigraphy

The carbon isotope records of the four studied sections have been compared, and calibrated with the reference section of Addar, for which ammonite biostratigraphy is well-defined (Fig. 3.22).

The $\delta^{13}C$ resolution sampling of the different EAB sections is too large to define segments as those previously described **either** by Menegatti et al (1998) and Bralower et al. (1999), for the Late Barremian–Early Aptian interval (segments C1–C8), after extending the codification of Menegatti et al. (1998) through the rest of the Aptian-Early Albian Stages (C1–C13) **or** defined by Herrle et al. (2004), for a high resolution chemostratigraphic units and extended by Bottini et al. (2015). Presence of sedimentary gaps in the EAB sections can also explain the difficulty to define isotope segments (see section 5.1, in chapter of discussion).

However, in the EAB, nine reference points can be defined in the $\delta^{13}C$ record, named A, B, C, D, E, F, G, H and I, representing maximum and minimum values during the Aptian-Early Albian interval.

A (black star, Fig. 3.22) is a first minimum carbon isotope value in Early Aptian, recorded in both Ida w Shayq and Tissakatine Center sections, which seems to correlate with the earlier minimum values, in segments C1 to C3 of Bralower et al. (1999).

B (red star, Fig. 3.22) is a first maximum around the Early/Late Aptian Boundary, also recorded in both Ida w Shayq and Tissakatine Center sections, which correlates fairly well with values in C4 of Bralower et al. (1999).

C (dark blue star, Fig. 3.22) is a second maximum in the *martini* ammonite Zone of early Late Aptian age, recorded in Ida w Shayq, Tissakatine Center and Addar sections, C=C6 of Bralower el al. (1999).

D (pale blue star, Fig. 3.22) is a second minimum in the *melchioris* ammonite Zone of Late Aptian age, observed in Ida w Shayq, Tissakatine Center and Addar sections, D= minimum between C8 and C9 of Bralower el al. (1999).

E (green star, Fig. 3.22) a third maximum carbon isotope value, in the *jacobi* ammonite Zone, of latest Aptian age, recorded in Ida w Shayq, Tissakatine Center and Addar sections, E=C10 of Bralower el al. (1999).

F (violet star, Fig. 3.22) is a third minimum defined at the top of the *jacobi* ammonite Zone,

below Aptian/Albian Boundary, in all sections except Anzate, in which the Aptian stage has not been studied for isotope stratigraphy. F=min.before C12 of Bralower el al. (1999).

G (orange star, Fig. 3.22) is a fourth minimum within the *tardefurcata* ammonite Zone, in Early Albian, well defined in all sections, G=min. before C15 of Bralower el al. (1999).

H (yellow star, Fig. 3.22) is a fifth minimum in the *mammillatum* ammonite Superzone, in Early Albian, recorded in all sections.

I (white star, Fig. 3.22) is a sixth minimum also recorded in the *mammillatum* ammonite Superzone, recorded in all sections except Ida w Shayq, in which the *mammillatum* Superzone is very reduced and could be incomplete.

These two latter minimum values (H, I) being losely defined because of poor data, and no possibilities of correlations with the cited works.

In conclusion; the carbon isotope stratigraphy in EAB, defined by nine minimum and maximum values is correlated with ammonite biostratigraphy**;** the Aptian/Albian Boundary is characterized by a negative shift with decreasing for the carbon isotope values as recorded in many Pacific, Atlantic and Tethyan settings.

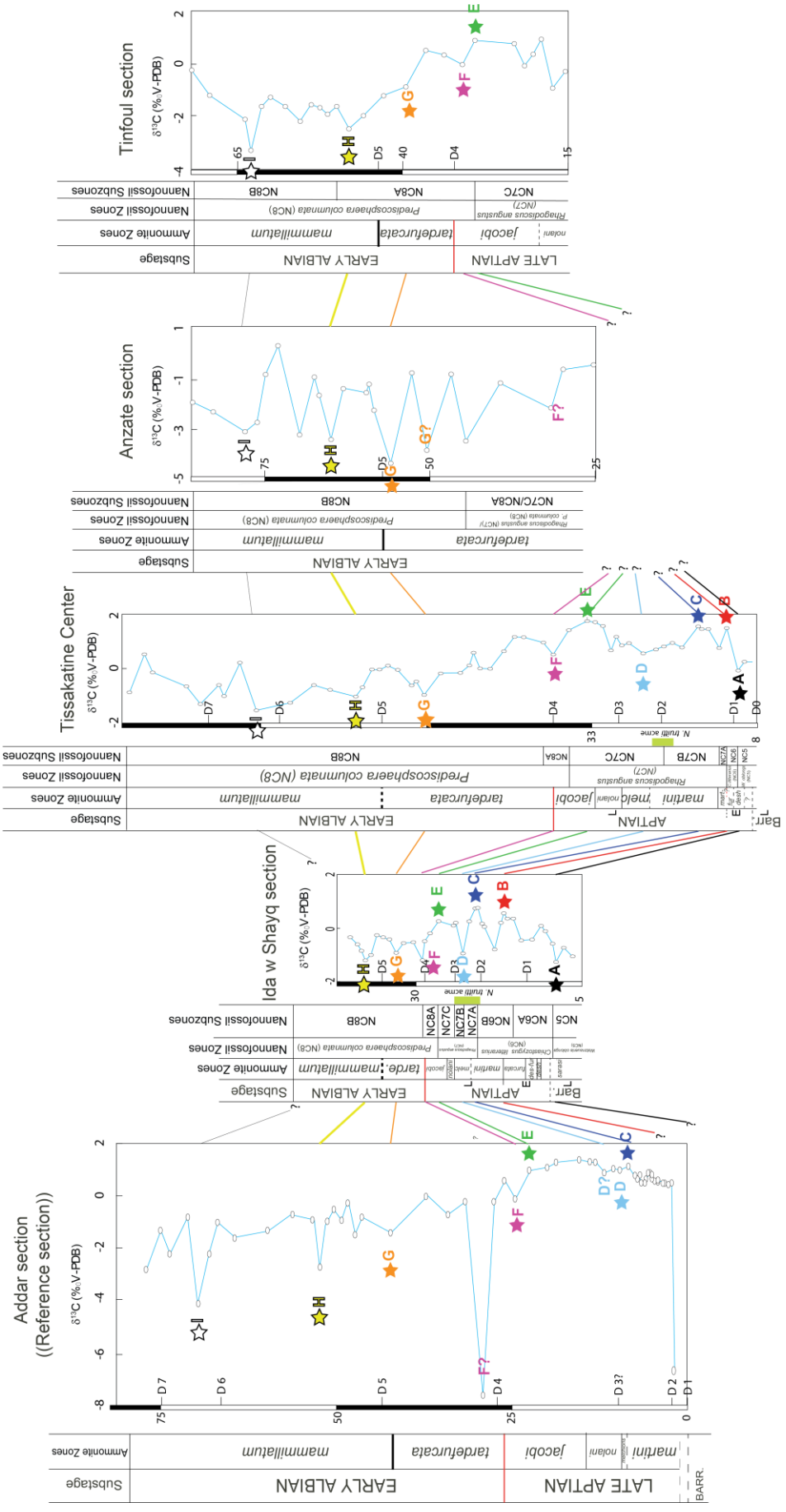

Figure 3.22: Carbon isotope correlation of the Aptian-Early Albian interval of the studied sections compared with the reference section of Addar, based on definition of nine carbon isotope maximum and minimum values (A,B,C,D,E,F,G,H,I), integrated with the ammonite and nannofossil zones, and correlated to chemostratigraphic units of Bralower et al. (1999), A=C3; B=C4; C=C6; D=minimum between C8 and C9; E=C10; F=min. before C12; G=Min. before C15. In all sections, the boundary between the *tardefurcata* and *mammillatum* ammonite zones is included within D5, along which, the highest parts of the *tardefurcata* and the lowest parts of the *mammillatum* zones are relatively eroded and missed during development of this sedimentary discontinuity (D5).

3.6. INTEGRATED BIO- AND CHEMOSTRATIGRAPHY IN THE EAB

The development of integrated stratigraphic schemes that combine both ammonite and calcareous nannofossil biostratigraphy with chemostratigraphic data and reliable sedimentary discontinuities aims to constrain as much as possible the age of the studied deposits in EAB.

Integrated stratigraphy of the studied sections in the Essaouira-Agadir Basin (EAB) was never done before this study. This work provides an excellent opportunity to calibrate the nannofossil record to that of ammonite as well as carbon isotope stratigraphy, resulted in a coherent scheme for the latest Barremian-Early Albian interval (Figs. 3.22 and 3.23).

The Late Barremian age, is only recognized at the base of Ida w Shayq section (Fig. 3.22). It is defined by the *sarasini* ammonite Zone, NC5 nannofossil Zone.

The Barremian/Aptian Boundary is defined by ammonites; at Ida w Shayq, where several species of *Cheloniceras* (Early Aptian) occur two meters above *Kutatissites* sp. and *Pseudocrioceras* sp. of latest Barremian age. At Tissakatine Center, the Barremian/Aptian Boundary is relatively placed one meter below the FO of *Cheloniceras* sp. at 9.5 meters.

The Early Aptian age is recognized in both Ida w Shayq and Tissakatine Center sections, around sedimentary discontinuity (D1), and defined by *deshayesi* to *furcata* ammonite zones.

Therefore, in EAB, the Early Aptian age is constrained by ammonites and C-isotope stratigraphy, where it is bounded by the first minmum value at the base (A) and the first maximum value (B) at the Early/Late Aptian Boundary (Fig. 3.20).

The Late Aptian interval in EAB, is documented in all studied sections based on ammonites. It is defined by four ammonite zones (*martini*, *melchioris*, *nolani* and *jacobi*) in Ida w Shayq, Tissakatine Center and Anzate sections (Figs. 3.5, 3.6, 3.8), whereas only two zones are recognized (*nolani* and *jacobi*) in Tinfoul section (Fig. 3.9). It is marked by two discontinuity surfaces (D2 and D3), in both Ida w Shayq and Tissakatine Center sections; D2 occurs within the *martini* ammonite Zone, and D3 lies at the base of the *nolani* ammonite Zone (Figs. 3.20, 3.22). The Late Aptian maximum and minimum $\delta^{13}C$ values (C, D, E, F), are recorded in Ida w Shayq, Tissakatine Center and Addar sections. In both Tinfoul and Anzate sections, the

sampling was restricted to the upper part of the successions. Therefore, the Late Aptian is only represented by a maximum and a minimum values (E and F) respectively, at Tinfoul, and not sampled in Anzate section**.** The minimum (D) value is correlatable to segments C8-C9 recognized in the Vocontian Basin (Herrle et al., 2004). The minimum (E) and maximum (F) values could correspond to values observed in segments C10 and C11 recognized in both Vocontian Basin, SE France (Herrle et al., 2004), and Mexican sections (Bralower et al., 1999). The Late Aptian part of the successions are studied for nannofossils only in Ida w Shayq, Tissakatine Center and Tinfoul sections. The FO of *P. columnata* is recognized in the upper part of the *jacobi* ammonite Zone of latest Aptian age in the studied sections with respect to lower part of the *jacobi* ammonite Zone in Vocontian Basin (Herrle, 2002; Herrle and Mutterlose, 2003; Kennedy et al., 2014) and in North Atlantic (Trabucho-Alexandre et al., 2011). Luciani et al. (2006) have shown that the FO of *P. columnata* occurred in latest Aptian within *Ticinella primula* planktonic foraminiferal Zone in Ischitella section (S Italy). Thierstein (1973) recognized the FO of *P. columnata* within the Early Albian in the upper part of the *Leymeriella tardefurcata* ammonite Zone in the Col de Palluel section (Vocontian Basin, SE France). Still for the Vocontian Basin, Bréhéret (1997) recorded the FO of *P. columnata* "just below horizon Delits Calcaire (DC2, uppermost Aptian)**.** Whereas Kennedy et al. (2000, 2014) found *P. columnata* 3 m above the Niveau Jacobi in the Pré-Guittard section. Based on the FO of *P. columnata* 2.5 m above it, the Livello black shale in Italy is synchronous with the Niveau Jacob in the Vocontian Basin as interpreted by Erba, (1988), Erba et al. (1989) and Bréhéret (1997). The FO of *P. columnata* (marking the base of NC8A) in the Upper Aptian is occured earlier in both Ida w Shayq and Tissakatine Center sections with respect to Tinfoul section. The younger occurrence of *P. columnata* in Tinfoul section, could be attributed to the poor preservation of nannofossil due to increase of siliciclastic thin beds, intervening this interval, in such as proximal section. Therefore, the Late Aptian in EAB is characterized by the upper part of *Chiastozygus litterarius* (NC6; but only the base of the Late Aptian), *Rhagodiscus angustus* (NC7) and lowest part of the *Prediscosphaera columnata* (NC8) nannofossil zones in Ida w Shayq section, by *Rhagodiscus angustus* (NC7) and lowest part of *Prediscosphaera columnata* (NC8) nannofossil zones in Tissakatine Center section**,** and by *Rhagodiscus angustus* (NC7C) nannofossil Subzone and lowest part of *Prediscosphaera columnata* (NC8) nannofossil Zone in Tinfoul section (Fig. 3.22). These results are comparable with what it is recognized in other

Tethyan basins, where the Late Aptian sediments correspond to the great part of *Rhagodiscus angustus* (NC7) and to lower part of *P. columnata* NC8 nannofossil zones (base of NC8B nannofossil Subzone) (e.g. Bralower et al., 1999; Herrle and Mutterlose, 2003; Herrle et al., 2004). The *N. truittii* acme is a globally observed bioevent characteristic for the Late Aptian age. It has been recognized in both Ida w Shayq and Tissakatine Center sections. In Ida w Shayq section, the *N. truittii* acme lies in the upper part of the *martini* and *melchioris* ammonite zones, corresponding to NC7A, NC7B nannofossil Subzones, as it has been documented in other basins by Erba, (2004) and Coccioni et al (2006). Whereas in Tissakatine Center section it lies in upper part of the *martini* ammonite Zone and NC7B, NC7C nannofossil subzones, such as in Vocontian Basin (e.g Herrle and Mutterlose, 2003). Therefore, the Late Aptian nannofossil zones in EAB, are comparable its counterparts in other basins. The Late Aptian rocks in EAB, are well dated both by ammonite and nannofossil biostratigraphy and carbon isotope stratigraphy.

The Aptian/Albian Boundary (AAB); In this study, we have followed Kennedy et al. (2000) and placed the Aptian/Albian Boundary between the *Hypacanthoplites jacobi* Zone and the *Leymeriella tardefurcata* Zone. In EAB, the AAB is determined by recognition the base of the *Leymeriella tardefurcata* ammonite Zone which is marked by the presence of *Puzosia quenstedti* and *Neosilesites palmensis* in Ida w Shayq, and by the presence of *Hypacanthoplites* cf. *roberti* at Tissakatine Center, where these ammonite markers are not recognized in Tinfoul and Anzate sections. In all studied sections, the base of the *L. tardefurcata* Zone, and therefore the Aptian/Albian Boundary, is placed within the discontinuity D4; 28.8m at Ida w Shayq; 39m at the Tissakatine Center; 22.5 at Anzate and 30.3m at Tinfoul section (Figs. 3.5-3.9). The AAB identification is also supported by the FO of both *Prediscosphaera columnata* and *Hayesites albiensis* nannofossil taxa around D4 (Figs. 3.10-3.14). The AAB is also marked by decreasing of carbon isotope values in all studied sections (Figs. 3.15-3.19),

The Early Albian age, is represented by the *tardefurcata* ammonite Zone in Ida w Shayq section (Figs. 3.14, 3.20), and by the *tardefurcata* and *mammillatum* ammonite zones in Tissakatine Center, Anzate and Tinfoul sections as what has been observed in Vocontian Basin (SE France; e.g. Herrle and Mutterlose, 2003; Herrle et al., 2004). The FO of *Hayesites albiensis*

is recognized at the base of the *tardefurcata* ammonite Zone in Ida w Shayq and Tissakatine Center sections, in lower part of the *tardefurcata* ammonite Zone at Anzate and in lower part of the *mammillatum* ammonite Zone at Tinfoul. Herrle (2002) and Herrle and Mutterlose (2003) have recognized the FO of *Hayesites albiensis* earlier in the upper part of the *jacobi* ammonite Zone, below the Niveau Paquier black shale, in the Vocontian Basin (SE France). Still in the Vocontian Basin, Bralower et al. (1993) recognized the FO of *H. albiensis* 0.5 m below the Niveau Paquier black shale. The younger ages given by nannofossils in EAB, particularly in Anzate and Tinfoul section, with respect to the Vocontian Basin (northern Tethyan margin) could be related to the poor preservation of nannofossil due to the silicoclastic nature of Albian sediments.

The *tardefurcata* ammonite Zone is marked by the fourth minimum values (G=min. before C15) in all studied sections, in EAB. The *mammillatum* ammonite Superzone is characterized by the fifth and sixth $\delta^{13}C$ minimum values (H and I), recorded in all sections except Ida w Shayq, where, only H value is recorded. The $\delta^{13}C$ minimum values (G, H, I) are recorded in the NC8B, mostly in all sections, except H minimum value, which lies in NC8A at Tinfoul.

During the Early Albian, the ammonite as well as the nannofossil biostratigraphy are correlatable and consistent with the C- isotope curves. Therefore, the Early Albian rocks in EAB, could be recognized based on ammonite, nannofossil and carbon isotope records.

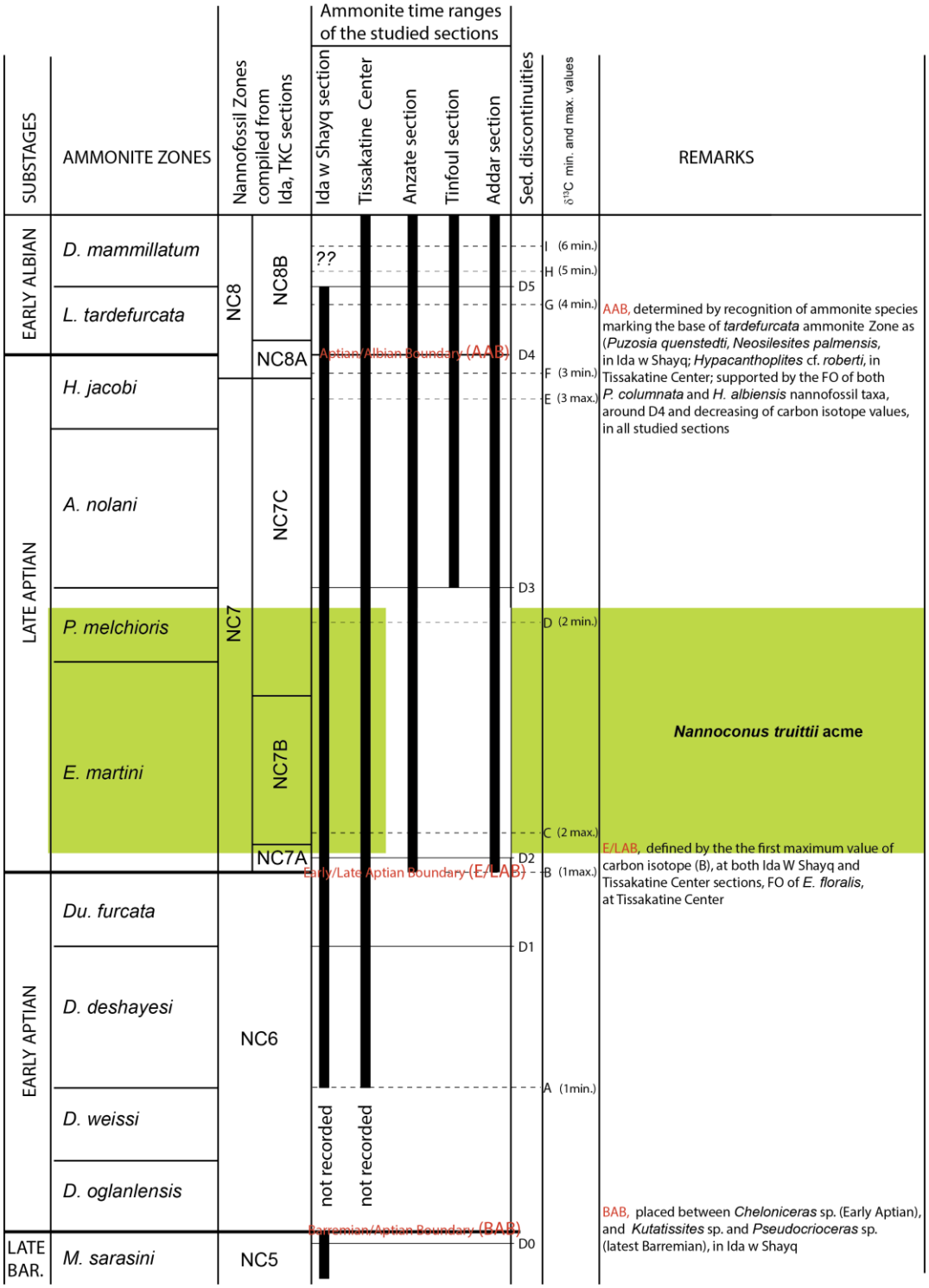

Figure 3.23: Summary of the ammonite, nannofossil biostratigraphy, integrated with the carbon isotope maximum and minimum values as well as, the sedimentary discontinuities during the Aptian-Early Albian time in EAB. Abbreviations: *M, Martelites; D, Deshayesites ; Du, Dufrenoyia; E, Epicheloniceras; P, Parahoplites; A, Acanthohoplites; H, Hypacanthoplites; L, Leymeriella; D, Douvilleiceras;*min., minimum; max., maximum; BAB, Barremian/Aptian Boundary; E/LAB, Early/Late Aptian Boundary; AAB, Aptian/Albian Boundary; Ida, Ida w Shayq; TKC, Tissakatine Center. Note: In Anzate and Addar sections, the ammonites have been studied for the whole sections and that for nannofossils, only the latest Aptian-Early Albian have been studied in Anzate section. The *N. truittii* acme (green interval) is recorded only in Ida w Shayq and Tissakatine Center sections.

CHAPTER FOUR

4. PALEOENVIRONMENTAL EVOLUTION IN THE EAB

PART (A): SEDIMENTARY FACIES AND DEPOSITIONAL ENVIRONMENTS

CHAPTER FOUR

PALEOENVIRONMENTAL EVOLUTION IN THE EAB

4. A. SEDIMENTARY FACIES AND DEPOSITIONAL ENVIRONMENTS

4. A.1. Introduction

Analysis and interpretation of cyclic sedimentation on continental margins and their controlling factors are among the most important topics in sedimentology and stratigraphy (Bachmann and Willems, 1996). Depositional systems are controlled by many interrelated and interacting factors including sea level change, subsidence, climate, and sediment production and input (Hillgartner, 1998). These parameters vary through space and time in amplitudes and frequencies. They are important in controlling the nature and volume of sediment, and how much of the sediment can potentially be preserved (Strasser et al., 1999). In a first step, I suppose a constant rate of subsidence for the whole area, assuming that tectonic processes were negligible during Aptian-Albian times.

Previous studies of Lower Cretaceous strata in the Essaouira-Agadir area dealt mainly with general lithostratigraphic relationships (Choubert and Faure-Muret, 1962; Ambroggi, 1963; Duffaud et al., 1966), biostratigraphy (Ambroggi, 1963; Wiedmann et al., 1982; Rey et al., 1988; Witam et al., 1993), or palaeogeography (Butt, 1982). According to some of these works, deposition of the Aptian-Albian sediments occurred in shallow shelf to marginal marine environments (Butt, 1982; Canérot, et al., 1986). However no previous studies of the Aptian-Albian succession have dealt with the interpretation of depositional environments by using an integrated sedimentologic, and high-resolution stratigraphic approach. The aims of this study are: (1) to identify sequence bounding discontinuities and their significance; (2) to characterize the sedimentary facies making up the Aptian-Albian deposits and to interpret them in terms of depositional processes and environments; (3) to interpret the evolution of sedimentary facies in terms of relative sea-level changes and sequence stratigraphy; and (4) to interpret the facies distribution in terms of paleogeographical evolution and of behavior and functioning of the platform.

The study area is located within the Essaouira-Agadir Basin (EAB, Fig. 1.8). Eleven sedimentary sections were measured in the field, two of them being incomplete. Nine sedimentary sections, mainly representing the Aptian-Albian time interval in the

EAB and well distributed in the basin, are selected to present the facies variations and evolution in the EAB (Figs. 4.1-4.12).

These sections can be grouped with (Fig. 1.8.) in (1) a southern, ESE—WNW transect, which includes the Tinfoul (Tf), Alma (Alm), Anzate (Anz), Addar (Add) and Tamri (Ta) sections (Figs. 4.1-4.6); 2) a central, ESE—WNW transect comprising the Tissakatine east (TKe), Tissakatine Center (TKC), Taounerine (To) sections (Figs. 4.7-4.10); and 3) a northern section (Ida w Shayq; Ida; Figs. 4.11,12).

In all studied sections, the Aptian-Albian succession overlies massive calcareous sandstones grossly of upper Barremian age (Witam, 1998; Company et al., 2008; Al Yacoubi, in progress) and can be divided, at a first order, into a lower unit, chiefly made of grey to white marls and limestones, a middle unit comprising grey-green shales and yellow calcareous sandstones, and a thick upper unit made of monotonous shaly marls interbedded with scarce sandstone or limestone beds. According to their ammonite content, the lower unit is mainly of Aptian age, the middle unit spent most of the Early Albian substage, and the upper unit seems to be mostly of Middle (?) and Upper Albian age. The upper unit, mostly shaly and unfossiliferous, has not been studied in the present work.

Because the lower and middle units illustrate distinct shelf types, carbonate ramp and mixed, clastic-carbonate ramps, respectively, their facies and environments will be described and studied separately. The facies and depositional environments of the Aptian-Early Albian rocks are identified based on their lithology, biogenic sedimentary structures, fossil content and microfacies, when possible. As a matter of fact, the dominantly marly nature of the succession did not allow to make numerous thin sections, and microscopic observations are, therefore, rather scarce. In the Aptian-Albian succession, we identified (1) four depositional surfaces (S1, S2, S3 and S4), (2) four major sedimentary facies in the Aptian (F1, F2, F3, F4) and (3) four Early Albian sedimentary facies (F I, F II, F III, F IV). These facies reflect deposition in adjacent and gradational paleoenvironments.

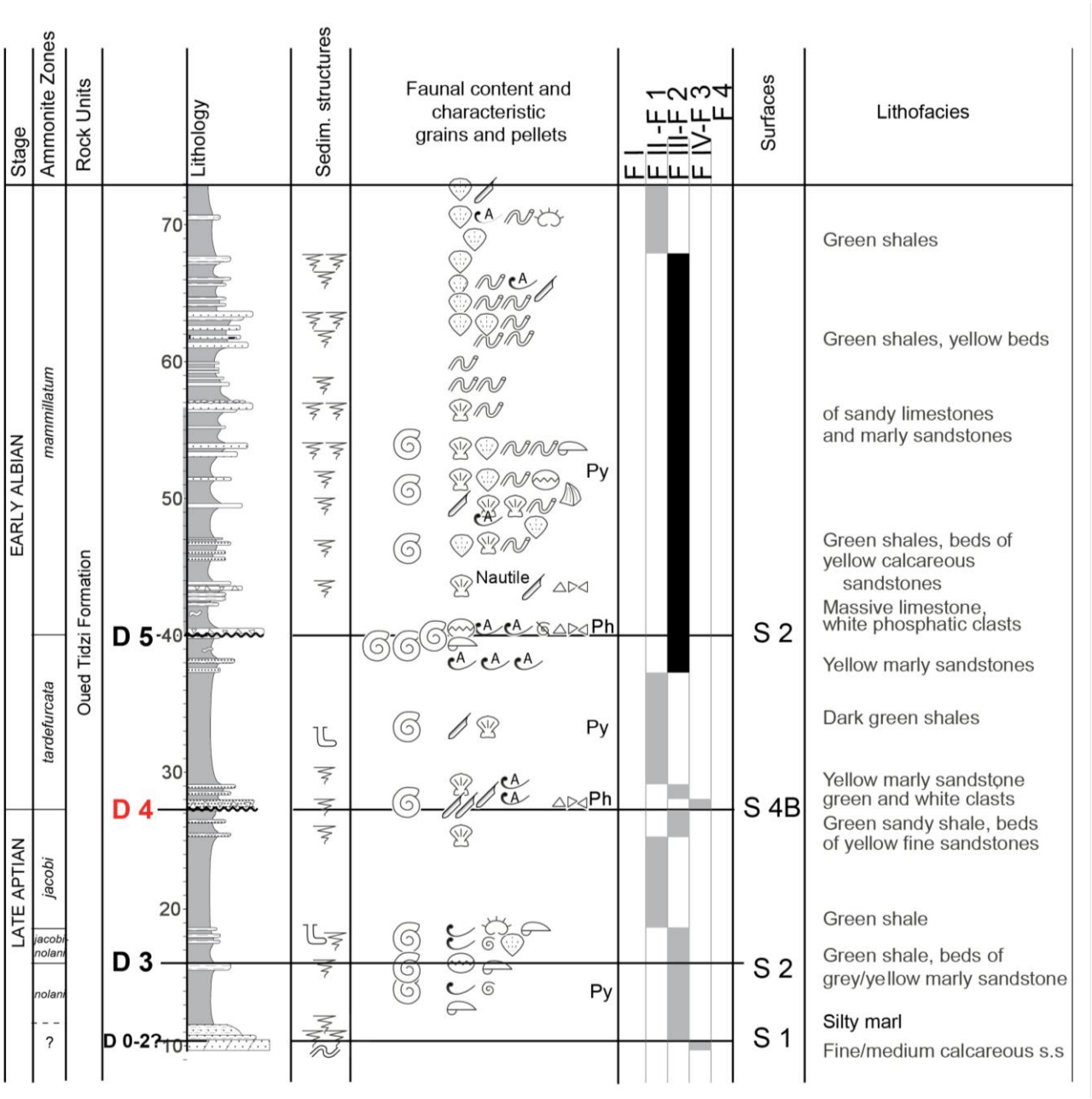

Figure 4. 1: Stratigraphic succession of Tinfoul section showing the biostratigraphical and sedimentological aspects. Gray bar: normal (oxic) facies; Black bar: dysoxic sediments.

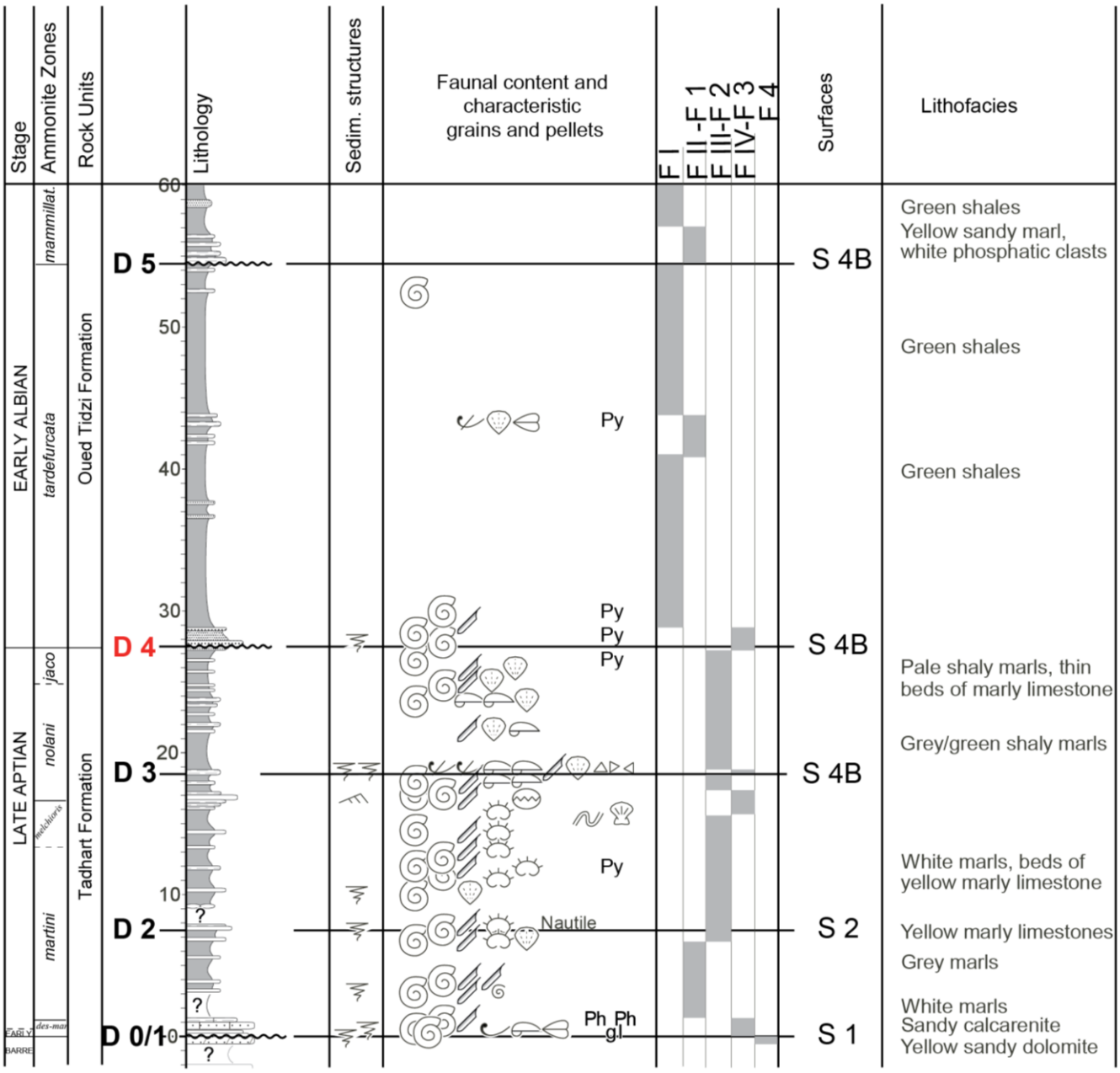

Figure 4.2: Stratigraphic succession of Alma section showing the biostratigraphical and sedimentological aspects.

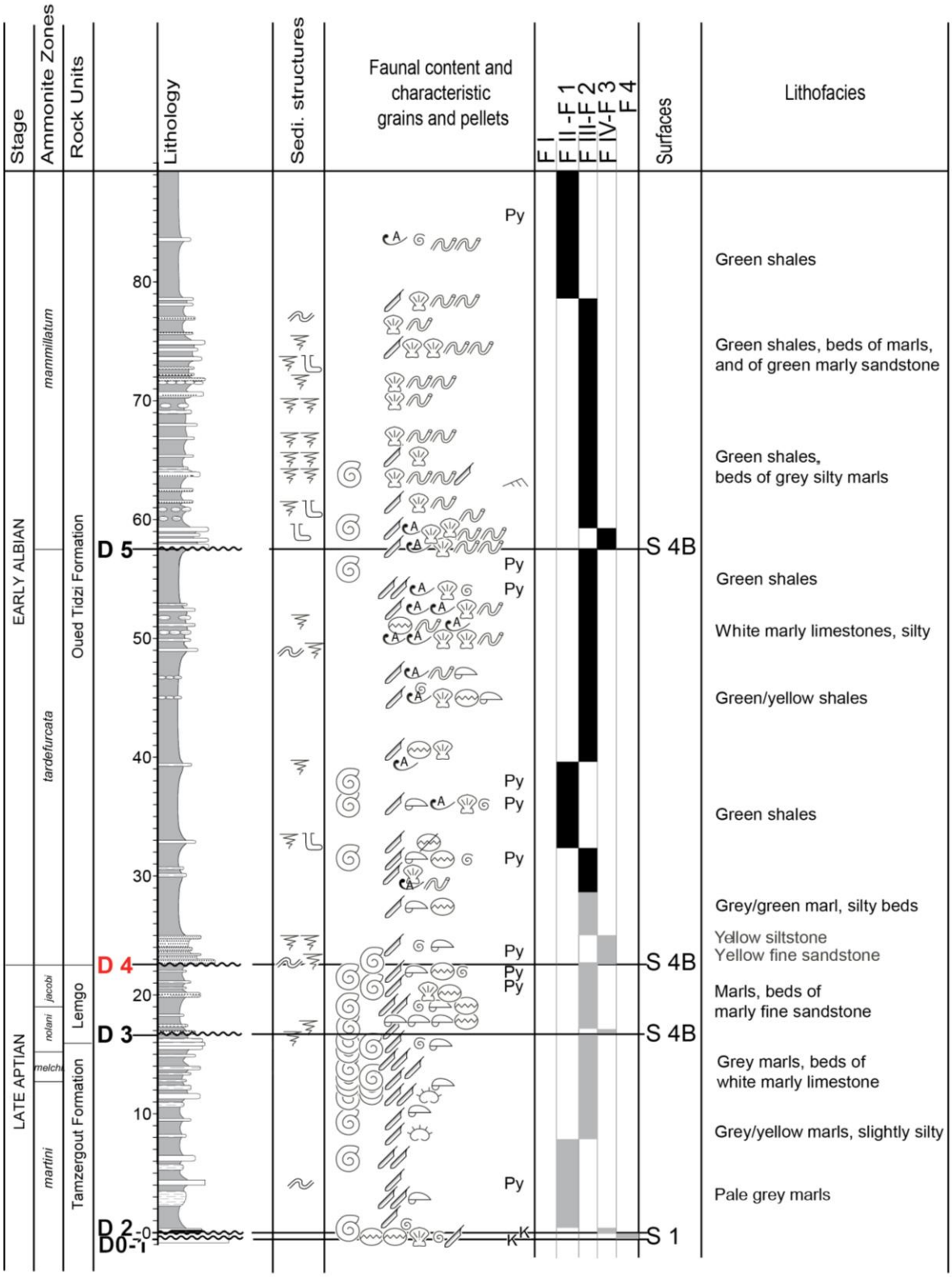

Figure 4.3: Stratigraphic succession of Anzate section showing the biostratigraphical and sedimentological aspects.

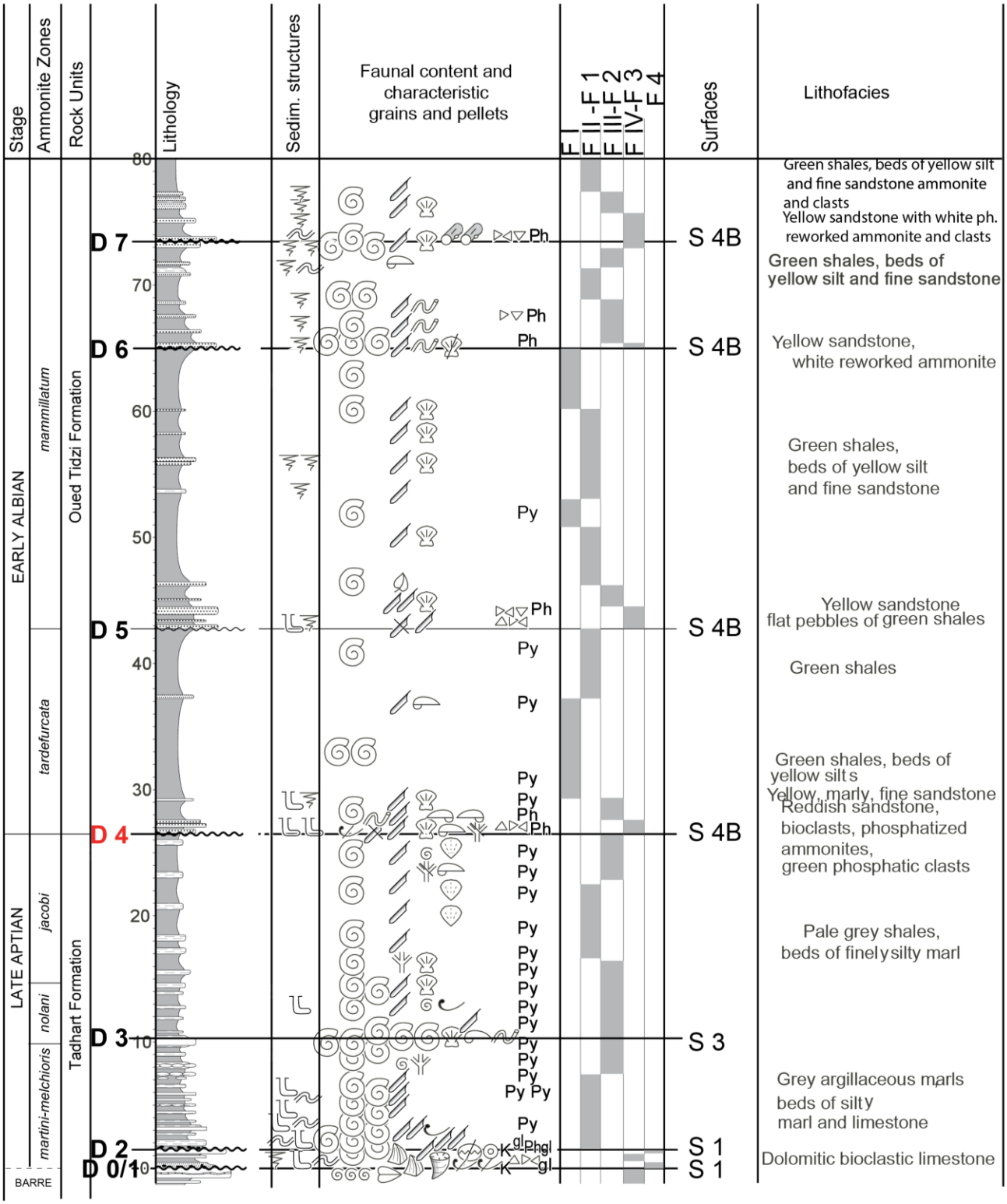

Figure 4.4: Stratigraphic succession of Addar section showing the biostratigraphical and sedimentological aspects

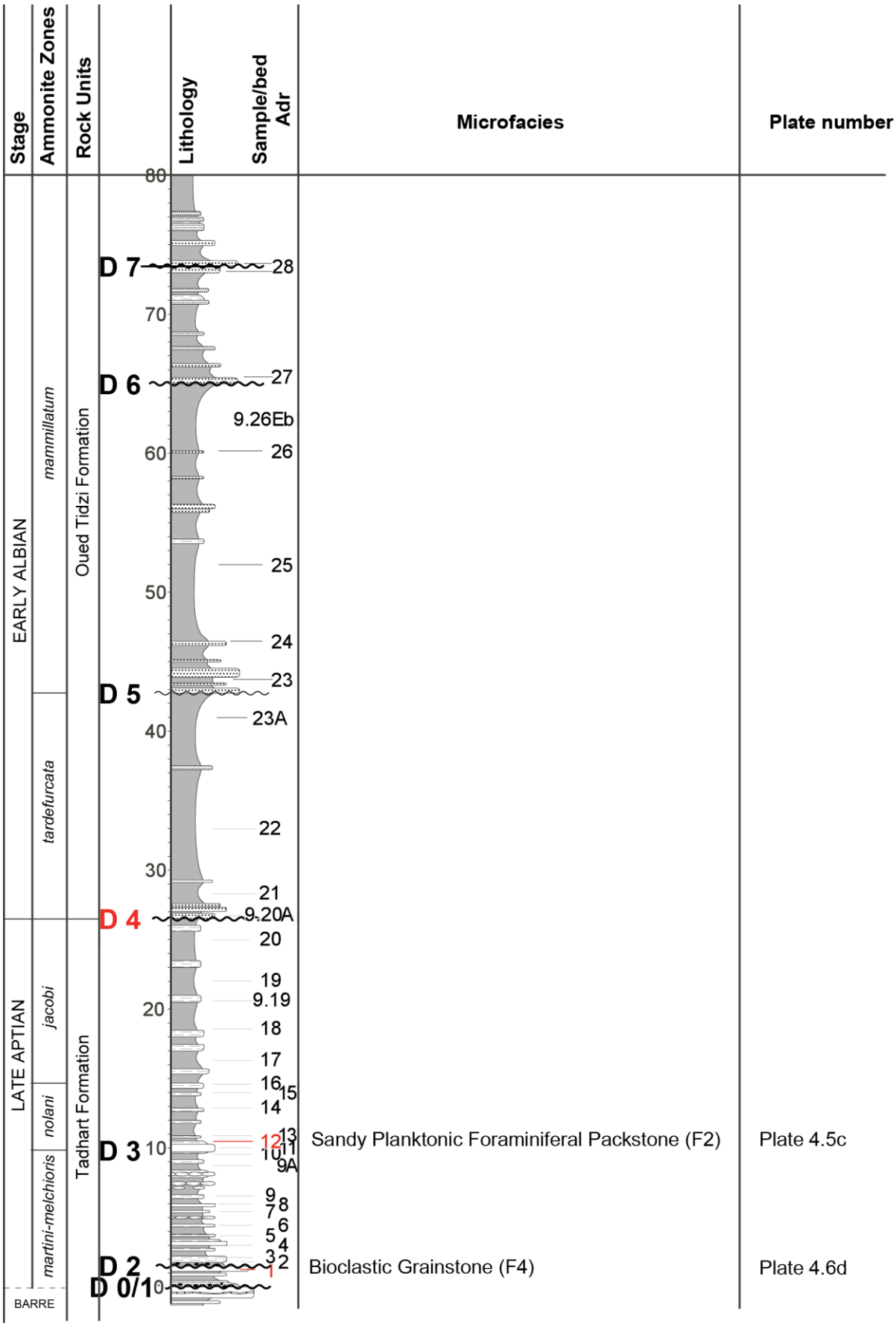

Figure 4.5: **Stratigraphic succession of Addar section showing the studied samples for microfacies: nu, number**

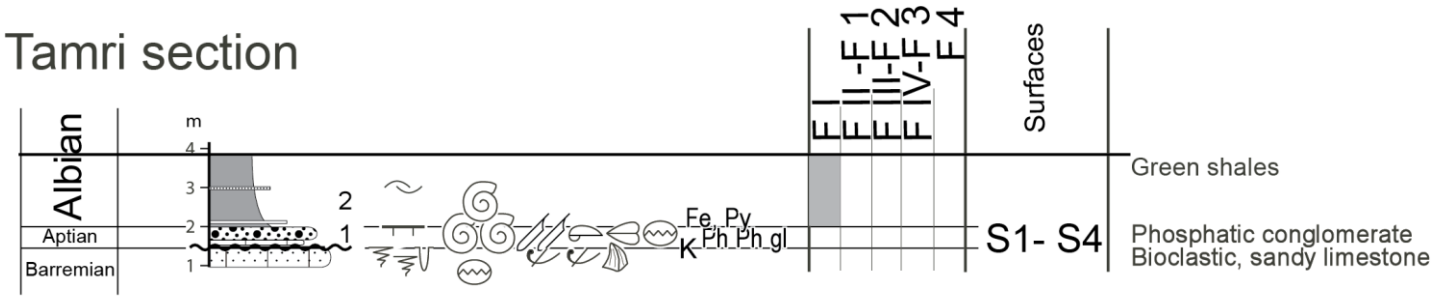

Figure 4.6: Stratigraphic succession of Tamri section showing the sedimentological aspects.

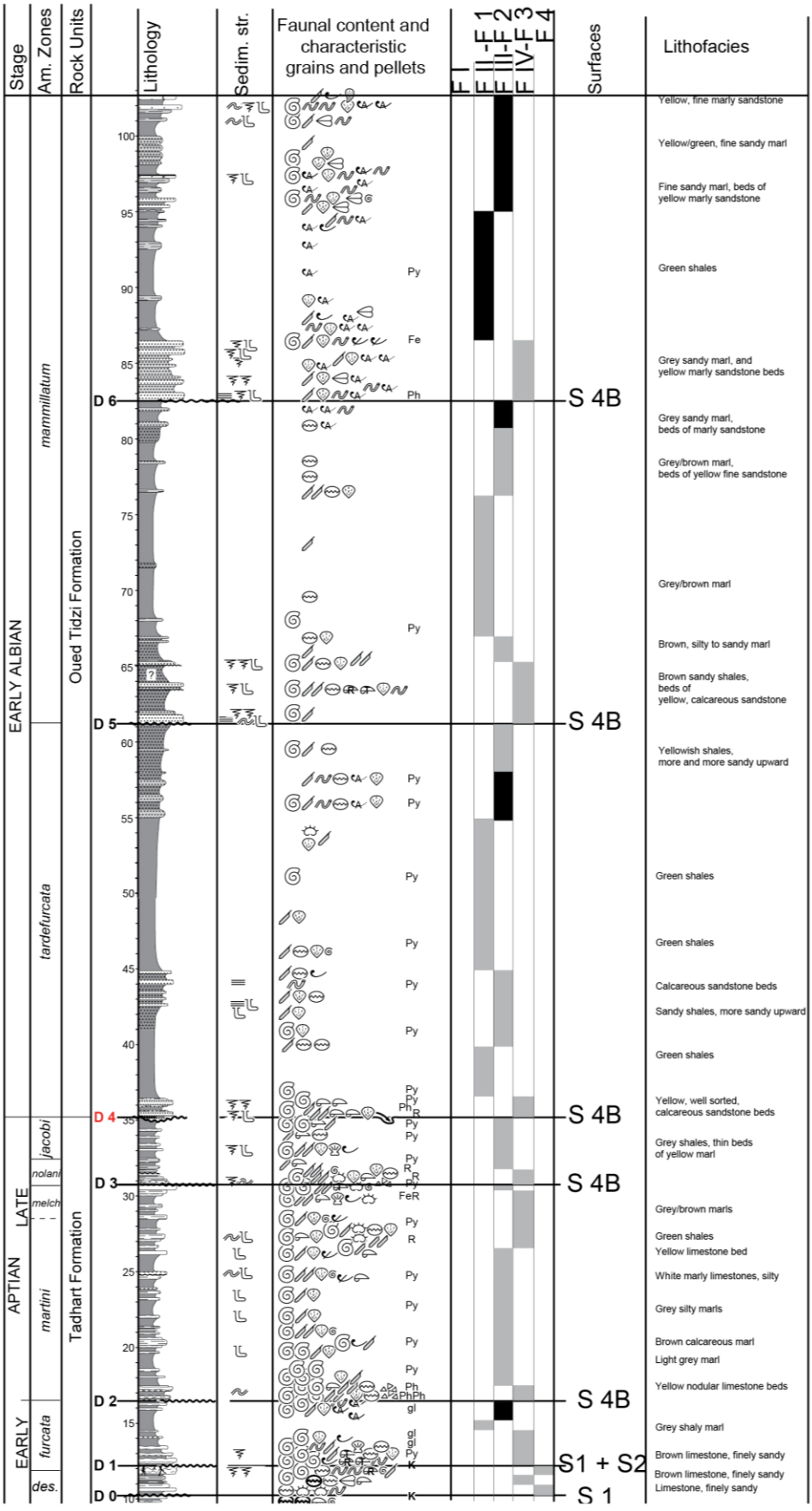

Figure 4.7: Stratigraphic succession of Tissakatine east, showing the biostratigraphical and sedimentological aspects.

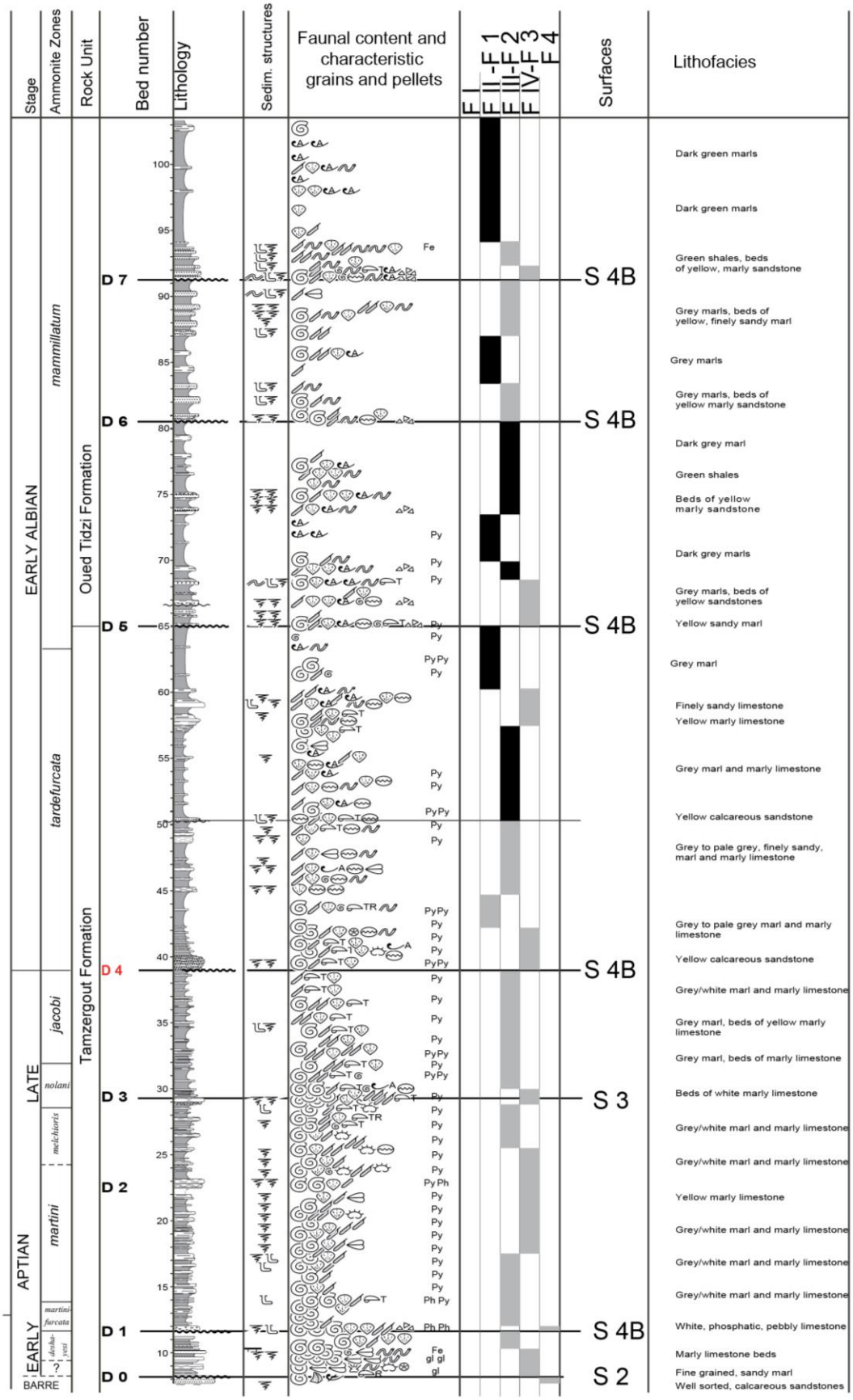

Figure 4.8: Stratigraphic succession of Tissakatine Center, showing the biostratigraphical and sedimentological aspects.

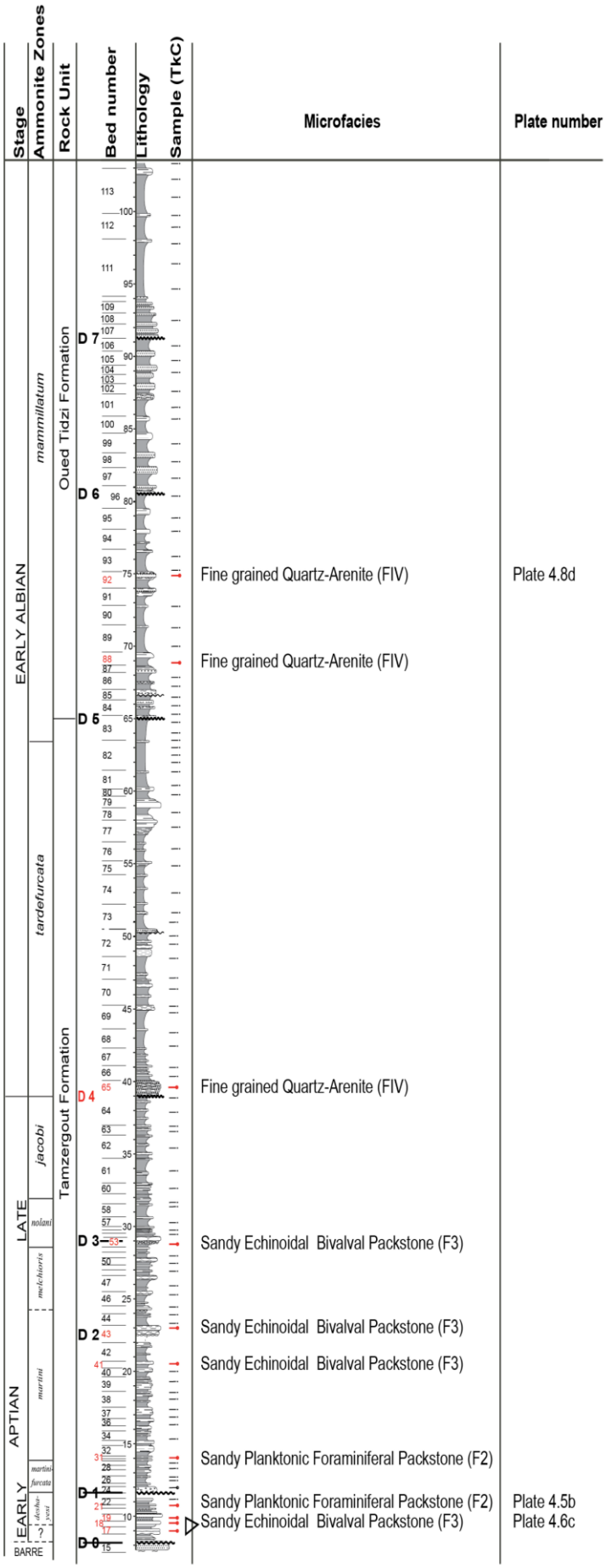

Figure 4.9: Stratigraphic succession of Tissakatine Center section showing the studied samples for microfacies

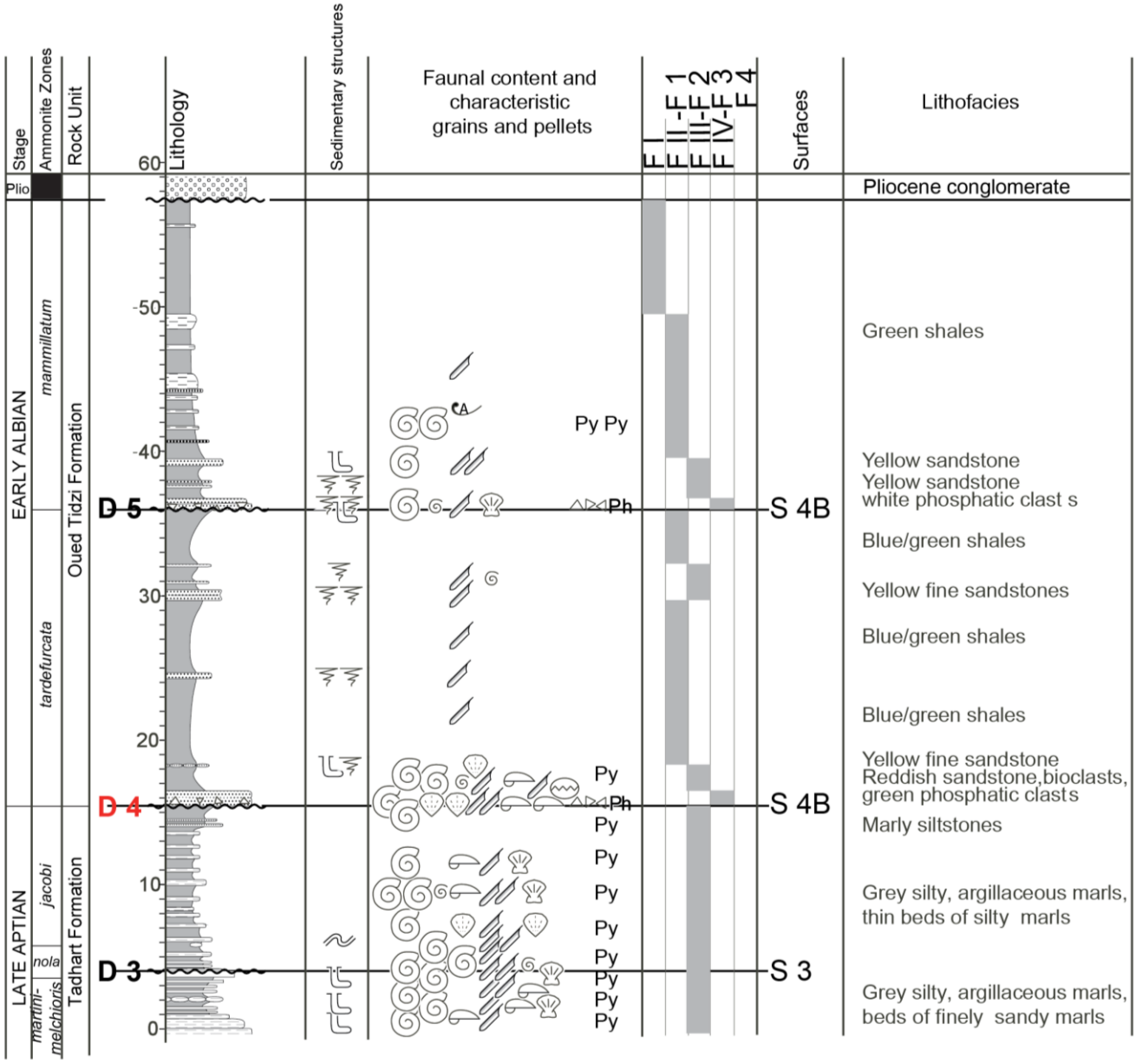

Figure 4.10: Stratigraphic succession of Taounerine, showing the biostratigraphical and sedimentological aspects.

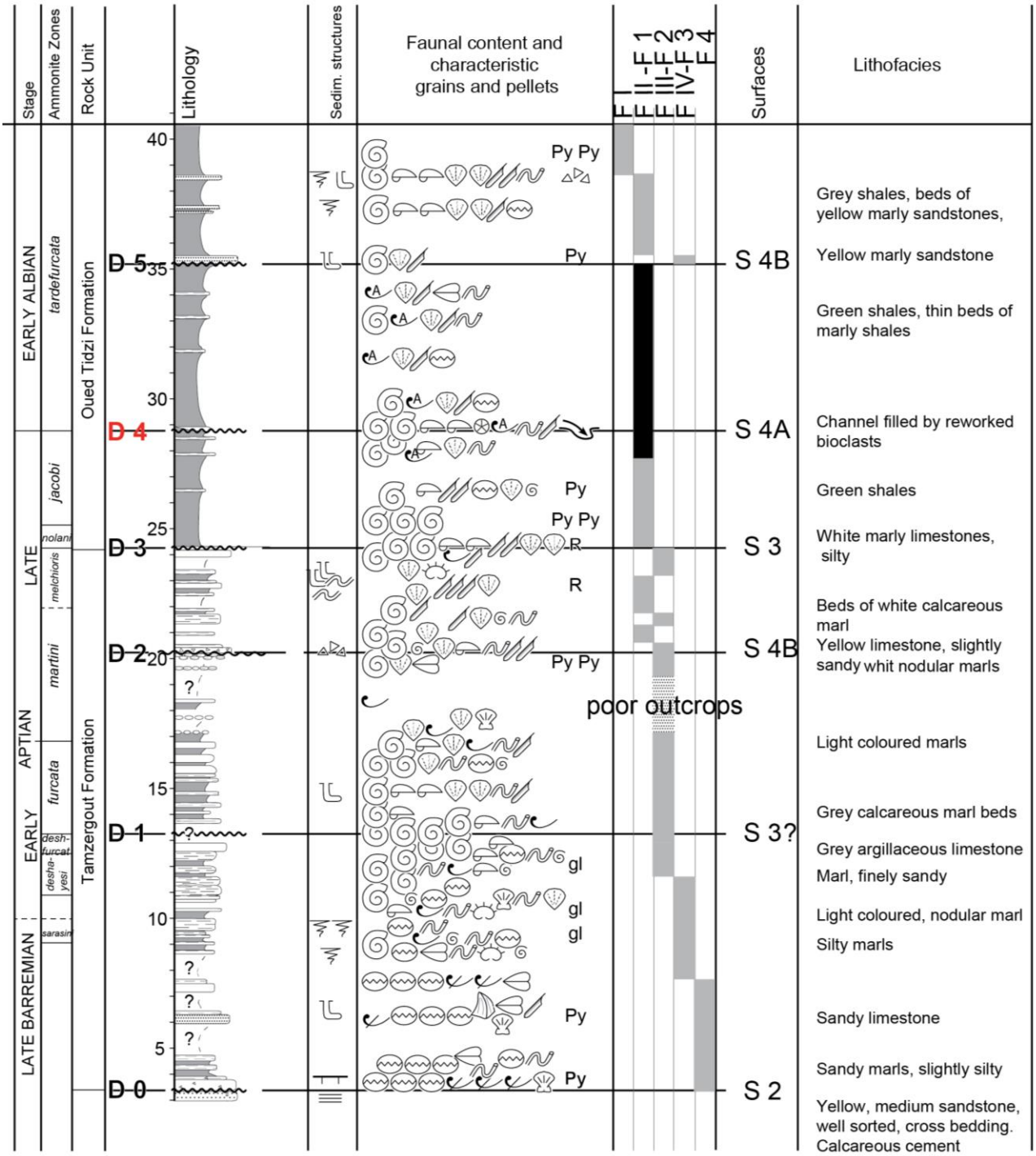

Figure 4.11: Stratigraphic succession of Ida w Shayq, showing the biostratigraphical and sedimentological aspects

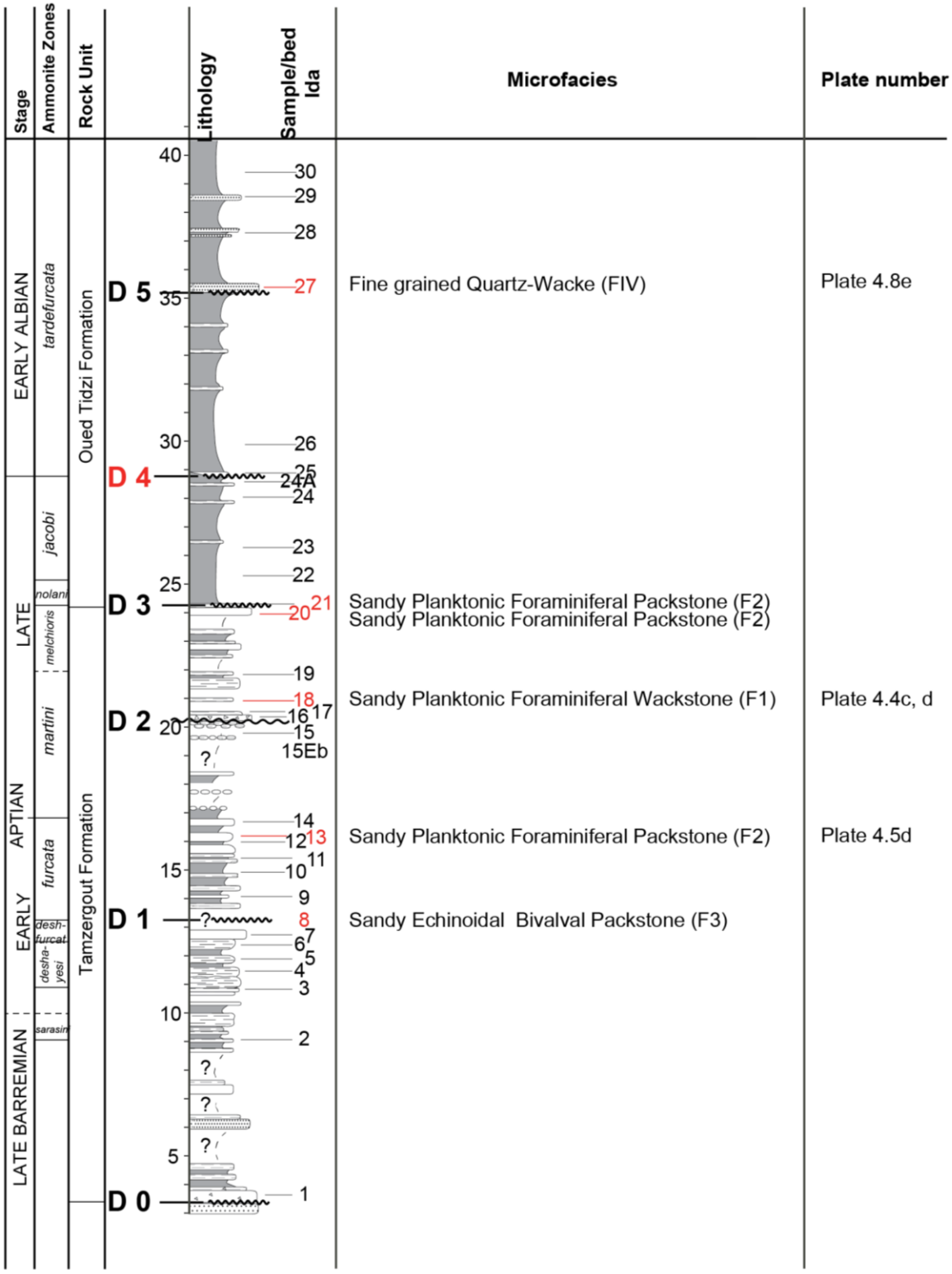

Figure 4.12: Stratigraphic succession of Ida w Shayq section showing the studied samples for microfacies

4. A. 2. Depositional surfaces

4. A.2.1. Surface 1 (S 1)

The first type of surface is usually found on top of a massive limestone bed. It is recorded at the base of the sections. It is an uneven, corroded surface, the caves of which are filled by the overlying sediment (Pl. 4.1a), or by highly glauconitic deposits. The centimeter-scale caves may penetrate in the limestone beds as much as several tens of centimeters deep. In the upper surface of the bed, the bioclasts are frequently replaced by iron oxides or iron-rich dolomite (Pl. 4.1b). Microscopically, the iron-rich dolomite is composed of dolomitized and/or oxidized bioclastic components cemented by sparite and dolomite cements (Pl. 4.1c). The core of the bioclastic components is basically filled with granular sparite and well zoned dolomite crystals, rimmed by iron oxides and recrystallized into neomorphic calcite spar (Pl. 4.1d). Some skeletal grains are completely dolomitized and/or oxidized, and appear as ghost structures. The intergranular pores are filled with tightly interlocking mosaic of idiotopic, inequigranular, zoned, ferroan dolomite crystals. They are occasionally rimmed by iron oxides. The dolomite rhombs are distributed in iron oxides and lime mud matrix and show sharp planar irregular contacts. The framework components are lumped together by the dolomitic, calcitic, ferruginous and pyritic cement. S1 surface is represented by D0-2 at Tinfoul, D0-1 at Alma, D0-1, D2 at both Anzate and Addar, D0 and partially D1 at Tissakatine east, and is not observed in the more distal sections of Ida w Shayq, Tissakatine Center and Taounerine.

Interpretation: S1 is interpreted as a karstified surface, which indicates a period of subaerial exposure. S1 is, therefore, usually interpreted as a Sequence boundary. It is only found at the base of the studied sections. The disappearance of the original depositional fabric and the presence of coarse crystalline dolomite rhombs is due to the occurrence of secondary, diagenetic dolomitization processes related to the influence of meteoric waters during emergence phases.

Plate 4.1: Depositional surface S1

a. Caves of S 1 (D1), filled by highly glauconitic deposits (red arrows). Addar section.
b. Caves of S 1 (D2). Calcite of bioclasts is replaced by iron oxides or iron-rich dolomitic (red arrow). Anzate section.
c. Thin section photomicrograph of iron-rich dolomitic bioclastic grainstone (F4), interval below D 2, unit Adr 1, Addar section, Plane Polarized Light (PPL). Bioclasts are totally replaced by iron-rich dolomite. Rare detrital quartz grains occur within a matrix of micro to meso-crystalline dolomite. Labels: bio = bioclasts; qz = quartz grains.
d. Thin section photomicrograph of iron-rich dolomitic grainstone (F4), interval below D2, unit Adr 1, Addar section, Plane Polarized Light (PPL). Bioclasts are replaced and agglutinated by mosaic, slightly zoned, euhedral to subhedral, iron-rich dolomite rhombs.

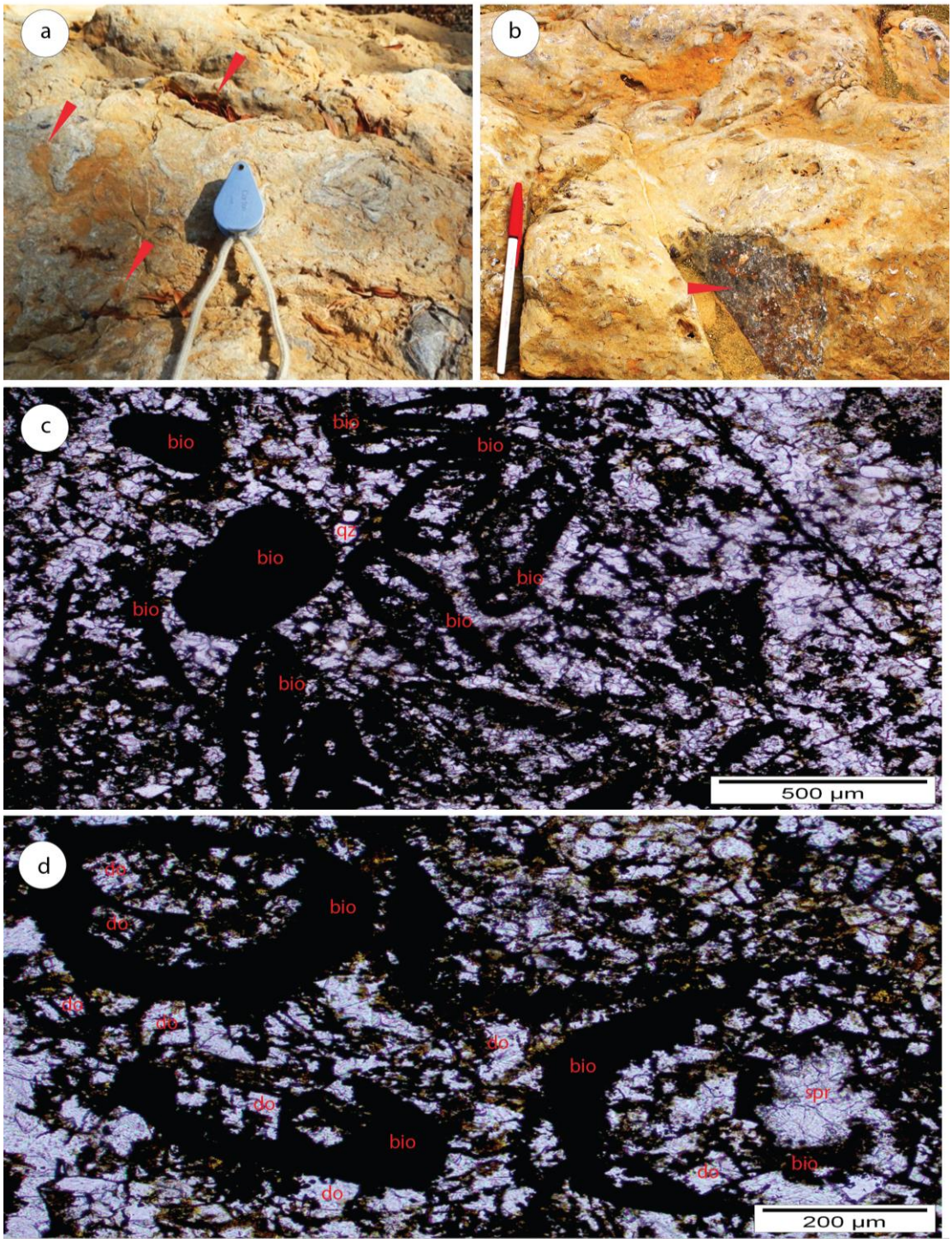

4. A.2.2. Surface 2 (S 2)

The second type of surface is made of a thin layer of highly glauconitic, sometimes phosphatic, deposit that frequently forms a 5 to 50 cm thick crust (Pl. 4.2a). It commonly contains lithoclasts, fossils and bioclasts (oysters, brachiopods, gastropods, belemnites, ammonites) of distinct nature and origin. It may fill the karstic cavities and depressions of S1 (Pl. 4.2a), or form a distinct layer. In some cases, large lithoclasts are bored. S2 occurs at the base of Ida w Shayq and Tissakatine Center sections, represented by D0, and is gradually recorded in higher levels corresponding to D1 in Tissakatine east (Pl. 4.2a).

Interpretation: S 2 is thought to represent a condensed deposit, resulting from a mainly submarine hiatus. The occurrence of varied organisms living in shallow to moderately deep environments suggests that condensation occurred during a transgressive episode. This is supported by the local presence of bored clasts, which are common in tidal environments. However, the presence of glauconite and phosphate suggests that at least part of the condensation occurred in an outer shelf environment, likely related to mineralized, deep water circulations, such as upwellings. S 2 is usually found at the base of the studied sections, or may represent a hiatus encompassing the whole sequence (Tamri section).

4. A.2.3. Surface 3 (S 3)

Surface 3 is marked by a thin, discontinuous, iron-rich crust, which covers the upper surface of marl beds. It is often associated with some small-sized lithoclasts (Pl. 4.2b), and concentrations of pelagic fauna (cephalopods, Pl. 4.2c, d). It is recorded in the Late Aptian, associated with D3 in the Addar, Tissakatine east, Taounerine and Ida w Shayq sections.

Interpretation: S 3 is interpreted as a hard ground representing a submarine hiatus, likely related to marine currents. Because the concentration of pelagic fauna is also visible in the underlying marly bed, this submarine hiatus is interpreted as the culmination of a condensation episode that was already affecting the underlying marly bed. S3 mainly characterizes the Late Aptian succession.

Plate 4.2: Depositional surfaces S2, S3, S4A and S4B

a. Highly glauconitic crust of S2, lithoclasts and bioclasts fill the karstic cavities of S1 (red arrows). D1, Tissakatine east section.
b. Small-sized lithoclasts (red arrows), characterizing S3. D1, Ida w Shayq section.
c. High concentration of cephalopods on S3. Cheloniceras beds, D1, Ida w Shayq section.
d. High concentration of cephalopods (red arrows) on S3. Nolani beds, D3, Addar section.
e. S 4A marked by high concentration of reworked fossil fragments within a shale unit. D4, Ida w Shayq section.
f. Phosphatic, bio- and litho-clasts (red arrows), characterizing S4B. D1, Tissakatine Center section.

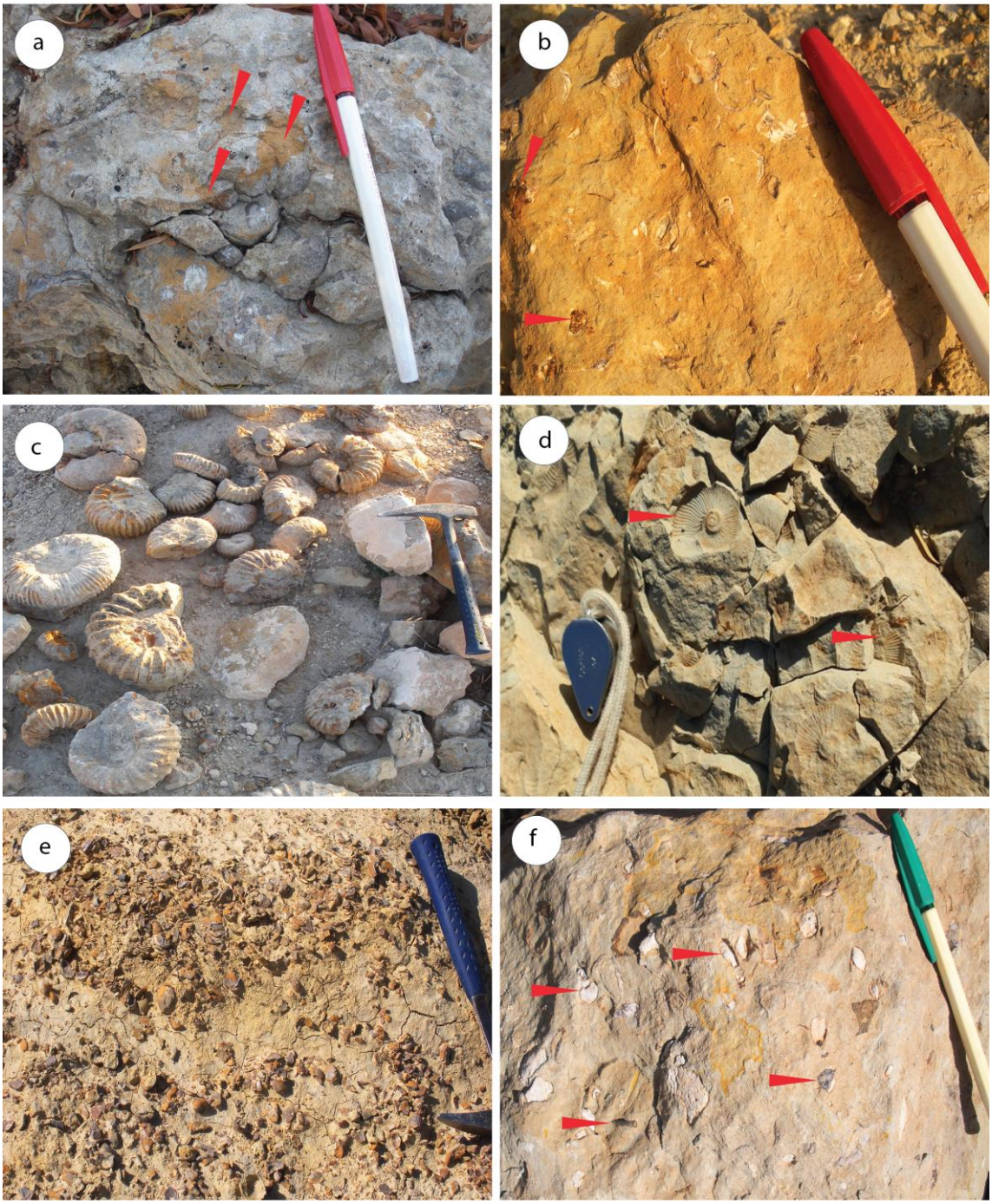

4. A.2.4. Surface 4 (S4)

Another type of surface is marked by a high concentration of belemnite rostra associated with lithoclasts, phosphatized white internal molds of fossils (commonly gastropods and ammonites; Pl. 4.2e, 4.2f; Pl. 4.3a, b) and scarce other bioclasts. These elements can be found, either as layers within shale successions (**S 4A**, only recorded in the Ida w Shayq section; Fig. 4.11), or reworked in the overlying marl or sandstone bed (**S 4B**, Pl. 4.3c, d; Figs. 4.1-4.11). In the first case, these coquinas are frequently lenticular in shape, as they overly a slightly uneven surface, and may be locally associated with fine-grained sands. In the second case, clasts, bioclasts and molds are concentrated at the base of the overlying bed, and rapidly disappear upward (Pl. 4.3c). S 4B is the most commonly observed surface. It corresponds to D4 in Tinfoul; D3, D4, D5 in both Alma and Anzate; D4, D5, D6, D7 in Addar; D2, D3, D4, D5, D6 in Tissakatine east; D1, D4, D5, D6, D7 in Tissakatine Center; D4, D5 in Taounerine, and D2, D5 in Ida w Shayq.

Interpretation: S4 is interpreted as representing a submarine hiatus, associated with erosion of the underlying marl or shale, and therefore, related to significant submarine currents. The submarine erosion removes the small-sized sedimentary particles (shale), thus bringing out their faunal and detrital content. Because the bio- and litho-clasts concentration is lenticular in shape, S4 may only be represented, in rare cases, by an abrupt lithological change, from marl or shale, to marl, limestone or sandstone, associated with an abrupt change in the faunal content, from pelagic organisms to assemblages including benthic species. This lithological change is interpreted as a S4B, within which the lens-shaped coquina is lacking. Because the reworked faunal assemblage, as well as the overlying one, are pelagic, this erosional surface is interpreted as related to relatively deep submarine currents. The frequent occurrence of phosphatic internal molds of organisms suggests that upwelling currents played a role in this erosion and allowed phosphatisation of carbonated elements during the erosional hiatus. S4 marks the latest Aptian and Early Albian succession.

Plate 4.3: Depositional surface S4

a. S4B, marked by high concentration of belemnites and lithoclasts (red arrows). D2, Ida w Shayq section.
b. Reworked bioclasts and phosphatized white internal molds of gastropods (red arrows), S 4B. D4, Tissakatine Center section.
c. Erosional surface S 4B occurring at the base of yellow sandstone beds. D4, Tissakatine Center section.
d. Reworked fossil fragment and white phosphatic clasts (red arrows), S 4B. D5, Tissakatine Center section.
e. Phosphate-rich conglomerate amalgamating S1-S4, overlying Barremian shallow-water sandy limestone at Tamri.
f. Brown phosphatic clasts (blue arrow) and glauconite (red arrow) infilling karst cavities. Tamri section.

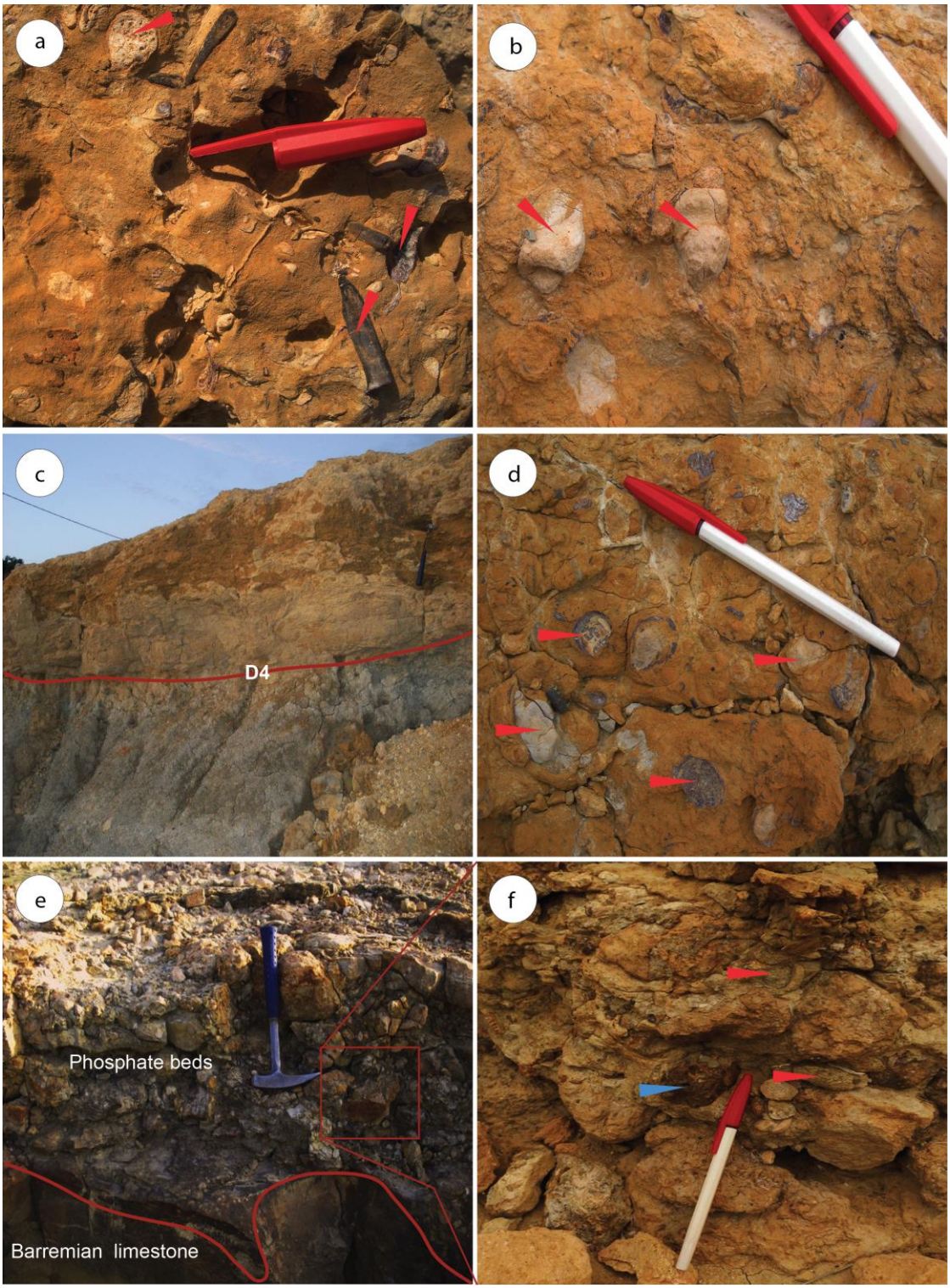

4. A.3. Facies and depositional environments of the Aptian succession

4. A.3.1. Facies 1 (F 1)

Facies 1 is made of shales or shaly marl, containing mainly belemnites and some ammonites. Sandstone or marl beds are virtually absent (less than 5% in thickness). Scarce thin-shelled bivalves, echinoderms, annelids and small sized gastropods may occur. Because of the shaly nature of the sediments, bioturbation is hardly visible. Ammonites may be pyritized. F1 is the second common facies after F2 in the Aptian successions (e.g. Pl. 4.4a, b; Figs. 4.1-4.4; 4.7; 4.8; 4.10; 4.11). F1 constitutes about 15.5% (12.5 m) of the studied succession in Addar (e.g. Pl. 4.4b); 13.5% (5 m) in Ida w Shayq; 9.5% (7 m) in Tinfoul (e.g. Pl. 4.4a, between D3 and D4); 9% (5.5 m) in Alma; 8.5% (7.5 m) in Anzate; and 0.5% (0.5 m) in Tissakatine east.

The shaly marl units have been irregularly sampled at Ida w Shayq section, and studied under the microscope. The microfacies presents a silty planktonic foraminiferal Wackestone **(**Pl. 4.4c), in which the framework components represent around 35-40% of the total rock. They consist of mainly planktonic foraminiferas, with few benthic foraminiferas (75 to 85%; Pl. 4.4d), echinoderms fragments and spines (about 15%), very small quartz grains (3%), and phosphate and glauconite pellets (2%). The planktonic foraminifera tests are mainly globular and pyritized, with few coiled and serial shape. The allochems are scattered in a micrite. Most of the bioclasts are calcitized, as echinoid fragments and foraminiferal tests. Few bioclasts are pyritized as foraminifera tests.

Interpretation: The lack or scarcity of carbonate suggests that sedimentation took place far from the euphotic zone, where photosynthesis favors the organic activity of carbonate-producing organisms (from bacteria to algae and mollusks). The strong predominance of pelagic organisms, the scarcity of benthic fauna, and the abundance of planktonic foraminiferal suggest a deposition below the euphotic zone. Therefore, facies F1 is interpreted as a pelagic deposit, in a distal outer shelf/ramp environment (Fig. 4.13).

Plate 4.4: (Facies 1)

a. Green shales (F1). Interval between D3 and D4, Tinfoul section.
b. Grey shales and marl units (F1). Interval below D3, Addar section.
c. F1: Sandy planktonic foraminiferal Wackestone. Unit Ida 18, Ida w Shayq section (PPL).
d. F1: Globular, pyritized tests of planktonic foraminiferas (dwarf hedbergellids, red arrows). Unit Ida 18, Ida w Shayq section (XPL).

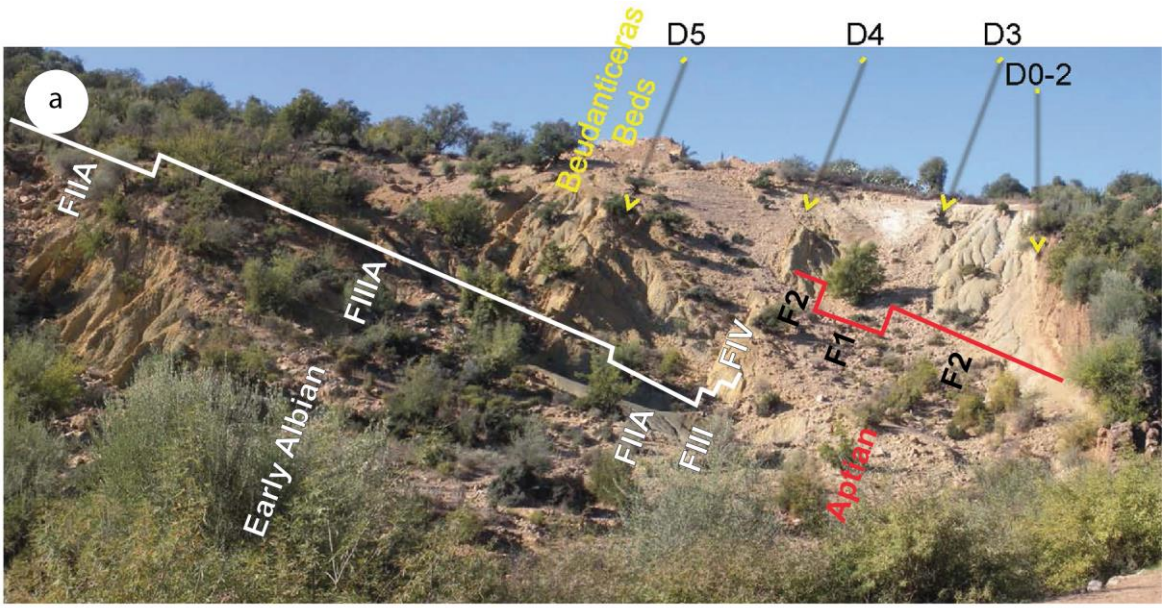

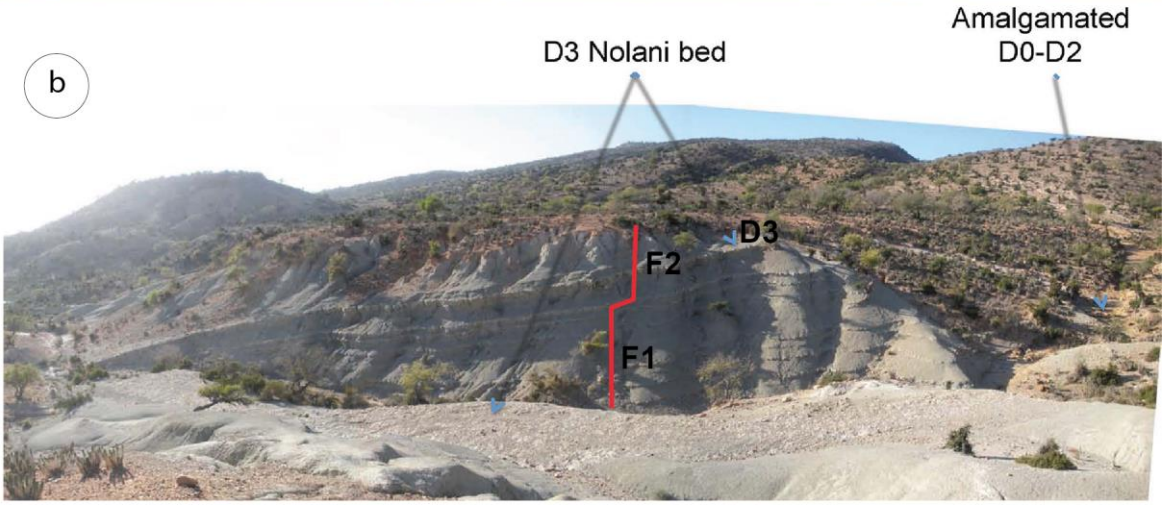

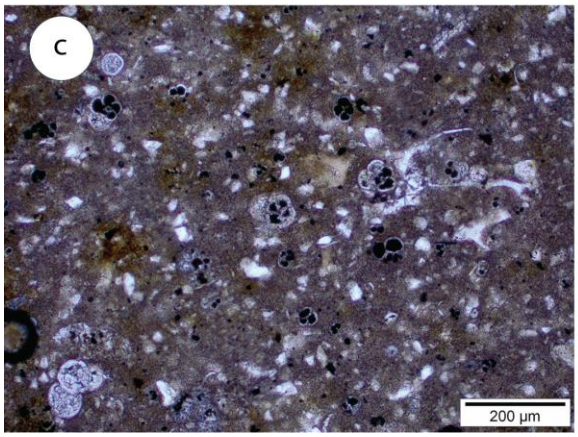

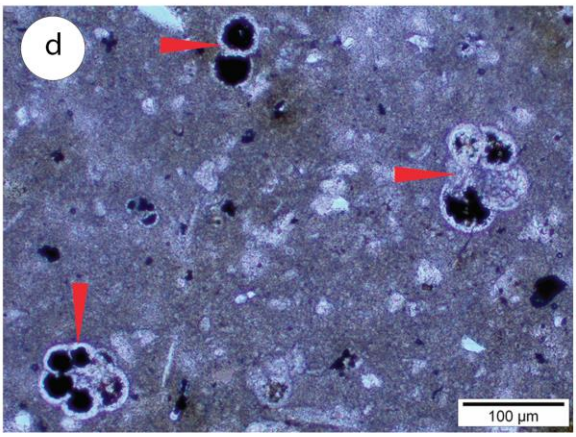

4. A.3.2. Facies 2 (F 2)

F 2 consists of shales or shaly marl, with some marly beds (about 30 % of total thickness). The faunal content is dominated by pelagic fauna (belemnites, ammonites), irregular sea urchins, brachiopods (terebratulids), echinoids and bivalves (mostly thin-shelled), among which pectinids, plicatulids and few oysters are associated with some gastropods, annelids and scarce nautiloids. Isolated corals locally occur. Bioturbations consist of track molds, small sized, curved burrows and digging traces (sediment feeders), visible in the marl beds. F2 is the most common facies, as it is recorded in all studied sections except Tamri. In Ida w Shayq, it constitutes about 29% (11 m) of the studied succession, 30% (18 m) in Alma; 12% (13 m) in Tissakatine east; 15.5% (12.5 m) in Addar; 15% (14 m) in Anzate (Pl. 4.5a); 17.5% (18 m) in Tissakatine Center; 25% (15 m) in Taounerine and 13% (10 m) in Tinfoul.

Under the microscope, F2 is mainly represented by silty planktonic foraminiferal Packstone (e.g. Tkc 31, Add 12A, Ida 13, Pl. 4.5b, c, d)**.** Allochems mainly consist of planktonic foraminiferal tests (≈ 40%), echinoid (≈ 20%) and bivalve fragments (≈ 15%), few ostracods and intraclasts (≈ 5%), quartz grains (≈ 15%), and phosphatic and glauconite pellets (≈ 5%) (Pl. 4.5c, d). The foraminiferas are small and pyritized, mainly coiled, with few serial planktonic tests of small size. The framework components are mainly pyritized. The micritic matrix fills the intragranular pores and lumps the framework components.

Interpretation: The occurrence of benthic, relatively deep water organisms (echinoids, brachiopods, plicatulids), together with planktonic fauna (cephalopods and forams) suggests a hemipelagic environment and open marine conditions. The lithological association (prevailing marl, subordinate limestone) as well as the prevalence of planktonic foraminiferas also points to an outer shelf setting. Bioturbations are dominated by sediment feeders, suggesting a proximal outer shelf/ramp environment and moderately oxygenated conditions (Fig. 4.13). Shales and marl reflect deposition from suspension with very low energy (Tucker and Wright, 1990), below storm wave base (SWB), in quiet-water conditions (Burchette and Wright, 1992).

Plate 4.5: (Facies 2)

a. Marl beds of F2. Interval between D3 and D4, Anzate section.
b. Tests of hedbergellids, planktonic foraminiferas (red arrows). Unit Tkc 31, Tissakatine Center section (XPL).
c. Echinoid fragment (yellow arrow), tests of planktonic foraminiferas (hedbergellids, red arrows). Unit Add12A, Addar section (PPL).
d. Globular tests of hedbergellid foraminiferas (red arrows), echinoid fragments (yellow arrow), and ostracod fragment (blue arrow). Unit Ida 13, Ida w Shayq section (PPL).

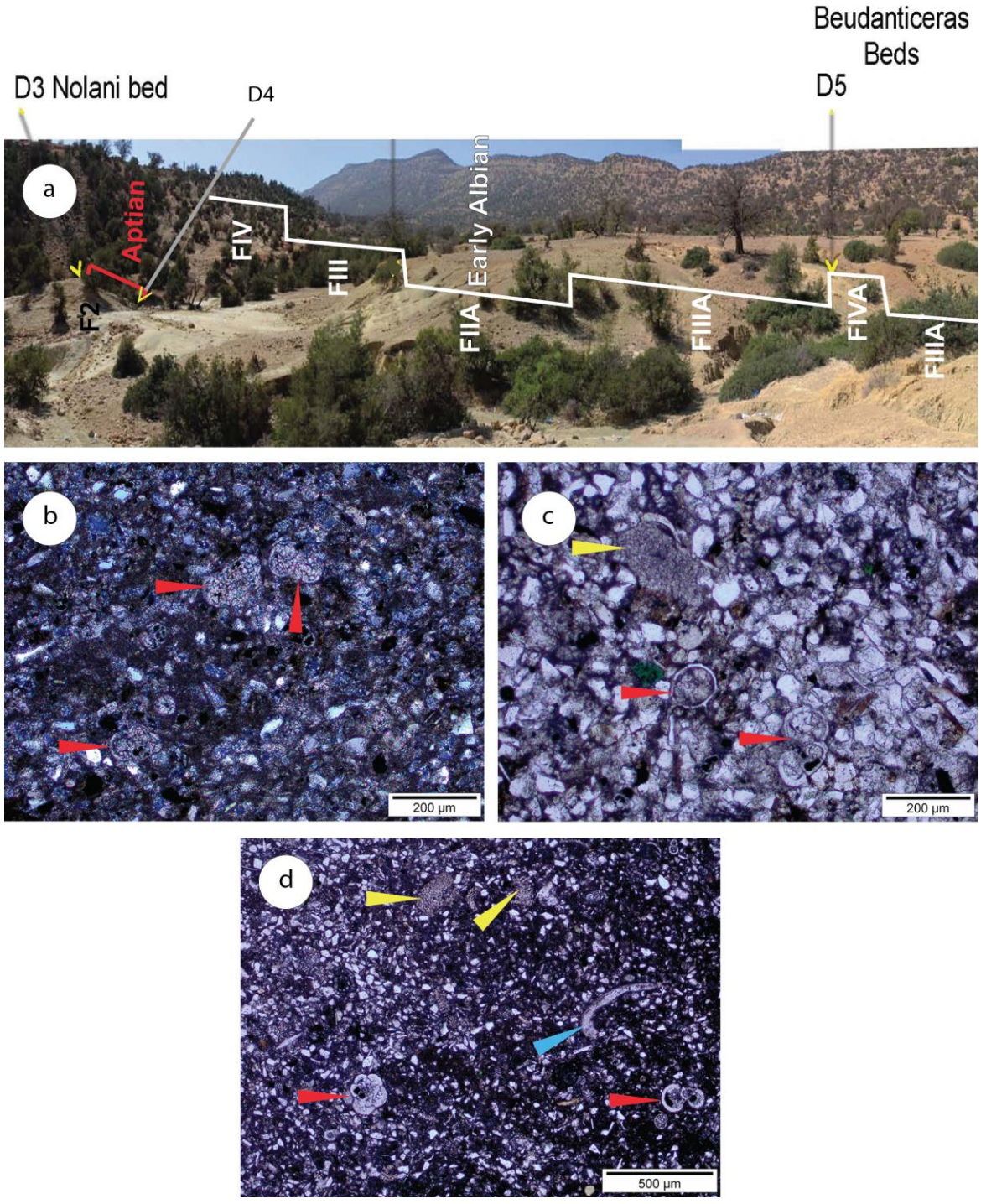

4. A.3.3. Facies 3 (F 3)

Facies 3 is made of marly limestones (about 50% of total thickness) with marly interbeds (Pl. 4.6a, b). The faunal content is dominated by benthic organisms, such as brachiopods, annelids and bivalves, among which oysters, plicatulids, pectinids and thick-shelled, large bivalves. Ammonites and belemnites frequently occur. Bioturbations dominantly consist of burrows (curved and straight) and track molds. F3 is mainly recognized in Tissakatine and Ida w Shayq sections. It constitutes 11% (10.5 m) of the succession in Tissakatine Center (e.g. Pl. 4.6a); 10.8% (4 m) in Ida w Shayq; 9% (9 m) in Tissakatine east; 5% (3 m) in Alma; and 0.5% (0.5 m) in Anzate and Addar.

The marly limestone units have been sampled between D0 and D3 at Tissakatine Center and below D1 at Ida w Shayq, and studied under the microscope. In Tissakatine Center (TKC17 and TKC18), the limestone beds are dolomitic, sandy Packstones, with echinoids and bivalves. The components are essentially crystalline calcite (60%), bivalve (≈ 15%) and echinoid fragments (≈ 10%), fine quartz grains (≈ 8%), phosphatic and glauconitic grains (≈ 4%), and arthropod fragments (≈ 3%) (Pl. 4.6c). Echinoid and bivalve fragments are partially dolomitized (Pl. 4.6c). The intergranular pores are filled with micrite and very fine crystals of calcite and patchily dolomitic cement**.**

Interpretation: The predominance of a diversified benthic fauna indicates an open marine, shallow environment, while the abundance of limestone suggest the proximity of the euphotic zone. However, the lack of algae and of very shallow organisms or features (oncolite, rudistids, corals) precludes a very shallow environment. The dominance of burrows and surficial track molds supports the interpretation of a shallow middle shelf/ramp environment (Fig. 4.13).

Plate 4.6: (Facies F3 and F4)

a. Marly limestone and grey marl beds of Facies 3. Tissakatine Center section.
b. Sandy limestone, coquina of Facies 4, covered by F3. Interval between D0 and D1, Ida w Shayq section.
c. F3: thin section photomicrograph of partially dolomitized oyster fragment (red arrow), an arthropod fragment (yellow arrow), sandy bivalval packstone. Unit Tkc18, Tissakatine Center section, (PPL).
d. F4: thin section photomicrograph of dolomitic bioclastic Packstone. Bioclasts (red arrow), dolomitic cement (yellow arrow). Unit Add 1, Addar section (XPL).

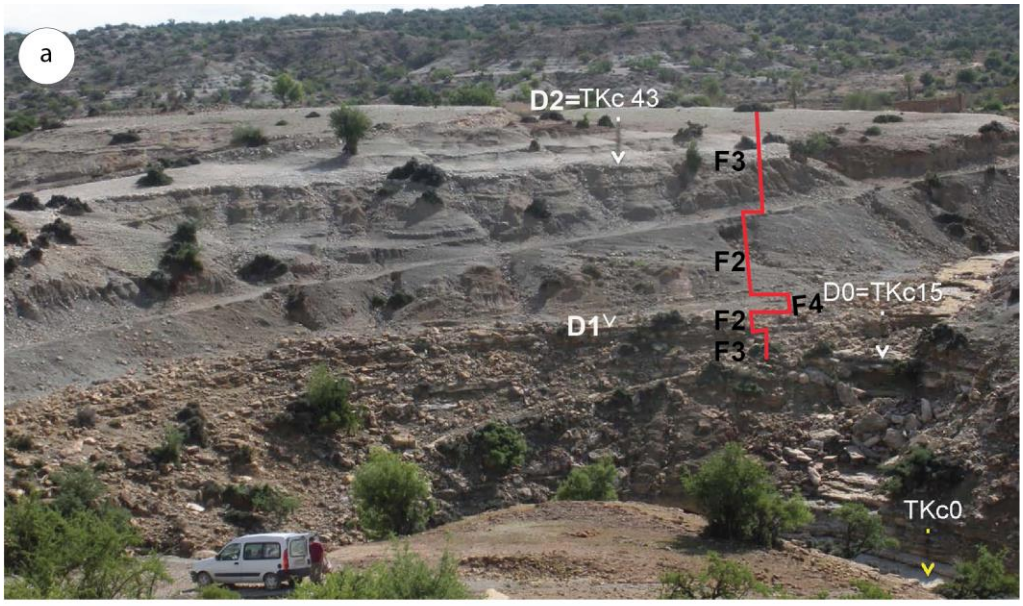

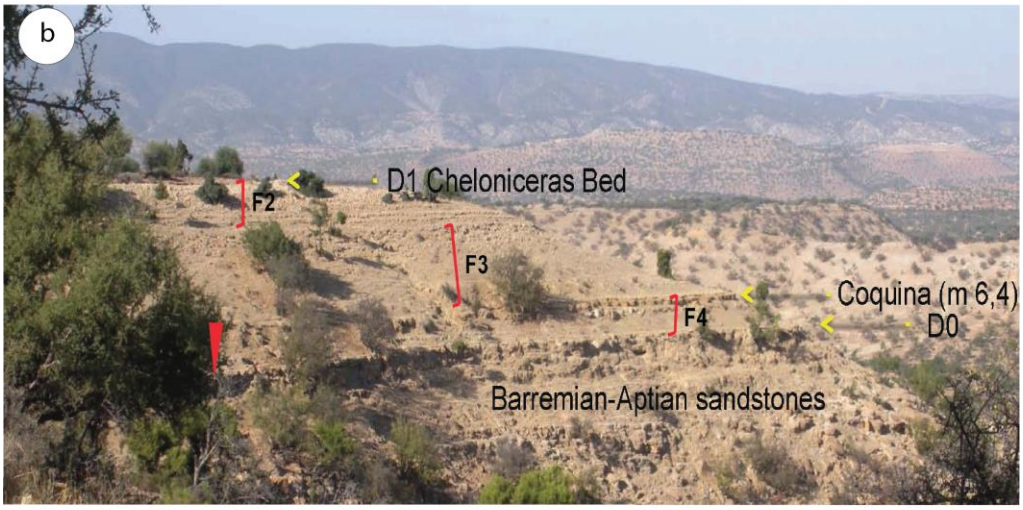

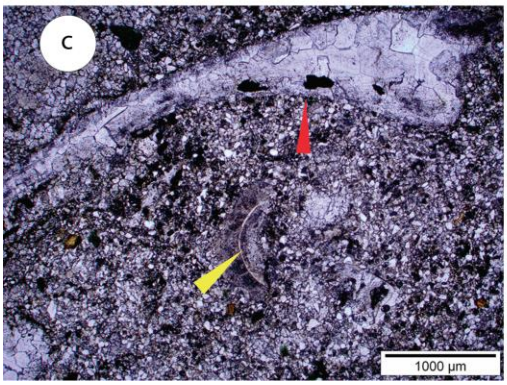

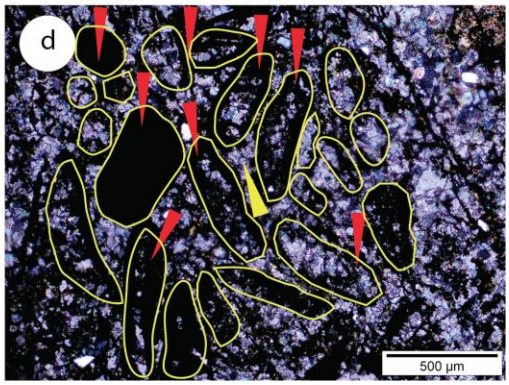

4. A.3.4. Facies 4 (F 4)

This facies is lithologically marked by thick, massive limestone beds (Pl. 4.6a, b), containing shallow marine benthic bivalves, such as abundant oysters, some trigonids and scarce rudistids. Bioclasts are common, and belemnites may occur at the top of these beds. Bioturbations are represented by burrows. The top of these beds is frequently dolomitized, karstified, topped mainly by S1. F4 is the less common facies, and is only recorded at the base of the Alma, Anzate, Addar, Tissakatine east, Tissakatine Center and Ida w Shayq sections (Figs. 4.2-4.4, 4.7-4.9, 4.11).

Microscopically, F4 is composed of sandy, dolomitic, bioclastic Packstone. The bioclastic fragments are chiefly bivalves. The intergranular pores are filled with coarse, slightly blocky mosaic crystals of dolomite cement (Pl. 4.6d). The internal structures of most skeletal grains are replaced by dolomite crystals.

Interpretation: The predominance of a shallow marine benthic fauna indicates a shallow carbonate shelf environment. Frequent evidences of emergence at the top of these deposits support this interpretation. The presence of bioclasts suggests a moderate to high energy, which is supported by the predominance of suspension feeders. F4 sediments are thus interpreted as deposited in a well oxygenated, shallow to very shallow carbonate inner shelf/ramp environment, with moderate to high energy (Fig. 4.13).

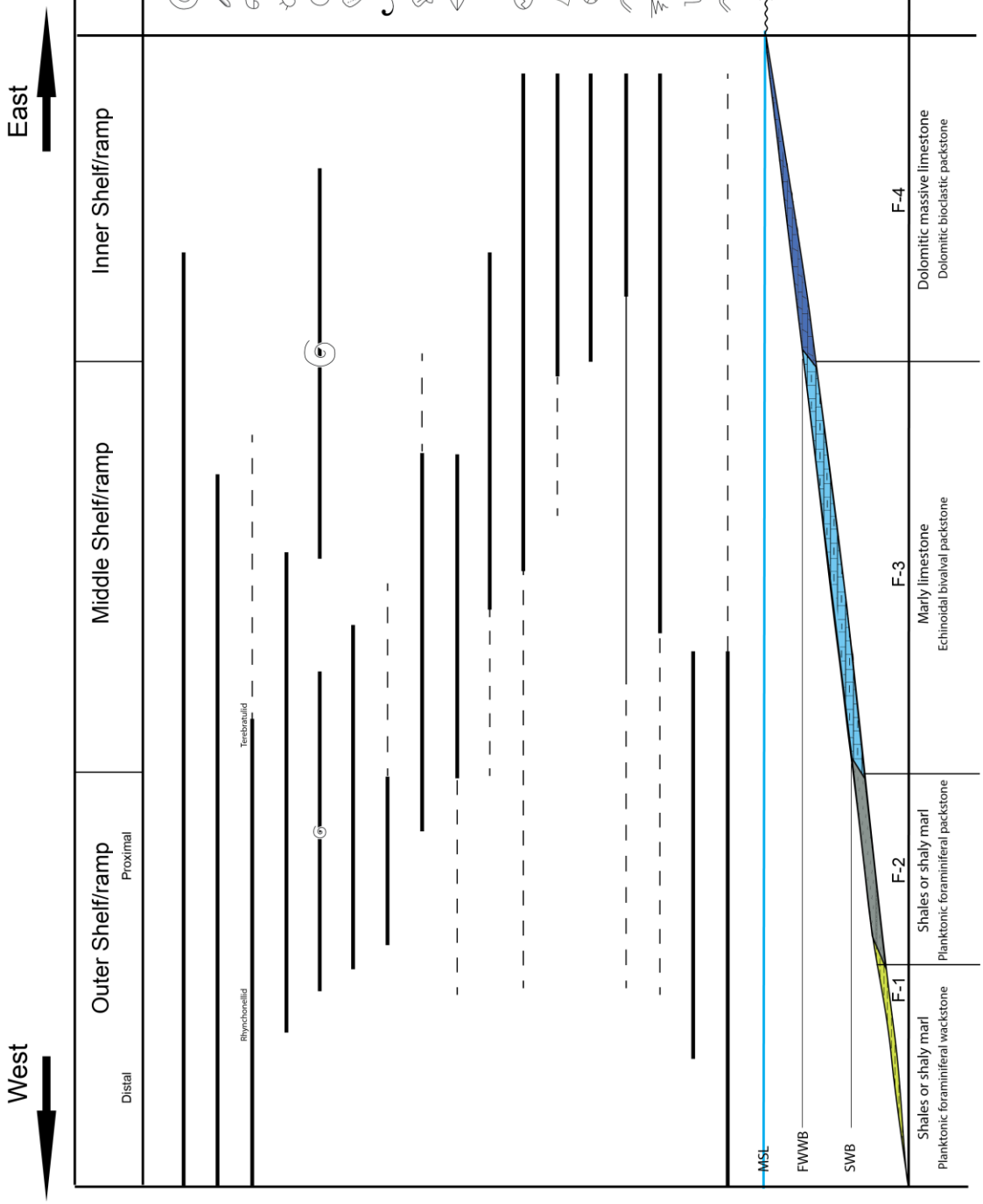

Figure 4.13: Faunal and facies distribution during the Aptian in the EAB.

4. A.4. Facies and depositional environments of Latest Aptian-Early Albian

4. A.4.1. Facies I (F I)

Facies I is made of motonous, dark-coloured, virtually azoic shales or shaly marl. Long searches on these outcrops allow to find scarce ammonites. FI is recorded above D4, consisting of 41.5% (25 m) in Alma, 18.5% (15 m) in Addar, 47% (1.8 m) in Tamri, 13% (8 m) in Taounerine and 5.5% (2 m) in Ida w Shayq sections, with average percentage up to 25% in these sections (Figs. 4.2, 4.4-4.5, 4.10-4.11).

Interpretation: The lack of sedimentary structures and of fauna makes difficult any reliable interpretations. However, since the only recovered fauna is pelagic and because this facies usually overlies the FII facies, at the top of the studied sections, it is interpreted as a pelagic, deep water marine sediment, deposited in outer shelf to basin margin environments (Fig. 4.14).

4. A.4.2. Facies II (F II)

F II is comparable to F 1 facies. It consists of silty shales or silty shaly marl, underlined by F III (Pl. 4.7a), containing mainly belemnites and some ammonites. Sandstone beds are virtually absent (less than 5 % of total thickness). Scarce thin-shelled bivalves, annelids, small sized gastropods and brachiopods (mostly rhynchonellids) may occur. Because of the shaly nature of the sediments, bioturbation cannot be seen, except in the sandstone beds, where digging tracks dominate. F II constitutes 18% of the succession (13 m) in Tinfoul, 10% (6 m) in Alma, 19% (17 m) in Anzate, 28.75% (23 m) in Addar, 29% (30 m) in Tissakatine east, 23.5% (24.5 m) in Tissakatine Center, 41.5% (25 m) in Taounerine and 8% (3 m) in Ida w Shayq, with a mean value of 20% of the rocks composing the studied sections (Figs. 4.1:4.4, 4.7:4.11).

Interpretation: The lack or scarcity of carbonate suggests that sedimentation took place far from the euphotic zone. The strong predominance of pelagic organisms and the scarcity of benthic fauna supports a deposition depth below or near the lower limit of the euphotic zone. Therefore, facies F II is interpreted as a pelagic deposit, in a distal outer shelf/ramp environment (Fig. 4.14), and is thought to be roughly equivalent to the F1 Aptian facies.

4. A.4.3. Facies III (F III)

Facies III is made of shale or shaly marl, with thin beds of sandstones or sandy marls (about 30% of the total thickness) (Pl. 4.7b). The faunal content is dominated by belemnites, ammonites and brachiopods (mostly terebratulids), associated with some gastropods and thin-shelled bivalves. Sandstone beds are devoid of current related sedimentary structures, but may be highly bioturbated. In this case, bioturbations consist of small sized curved burrows and digging traces (sediment feeders). This facies is recorded at Addar represented by 13.75% (11 m) of the total thickness, 26% (27 m) in Tissakatine east, 28% (29 m) in Tissakatine Center, and 11.5% (7 m) in Taounerine sections, with an average value of about 27% (Figs. 4.4, 4.7, 4.8, 4.10).

Interpretation: The occurrence of benthic, relatively deep water organisms (brachiopods), together with planktonic fauna (cephalopods) suggests a hemipelagic environment. The lithological association (prevailing silty marl) also points to proximal outer shelf/ramp setting (Fig. 4.14), comparable to that of Facies F 2. However, the presence of sediment feeders, even in the sandstone beds, suggests that the sea bottom waters were less oxygenated than in Facies 2.

Plate 4.7: (Facies II, III)

a. Dark green marl of facies II (FIIA) underlined by Facies FIII (FIII), interval above D7, Tissakatine Center section.

b. Facies FIIIA: varicolored dark green to yellow shale and silty marly shale intervened by few and thin beds of annelid-rich limestone and/or yellow siltstone. Interval above D5, Anzate section.

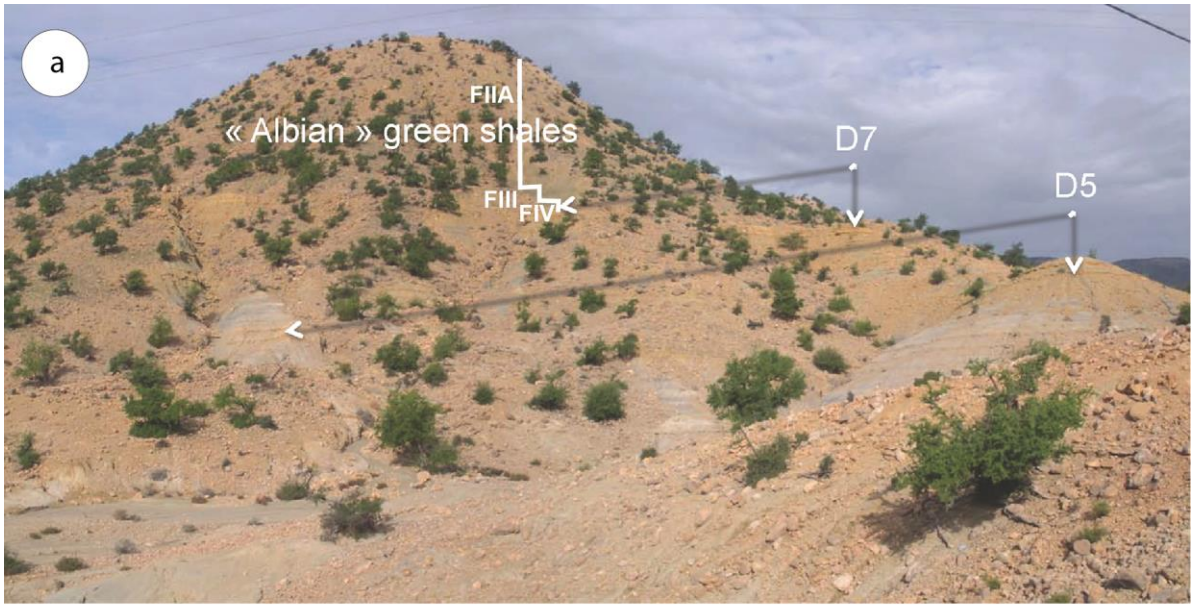

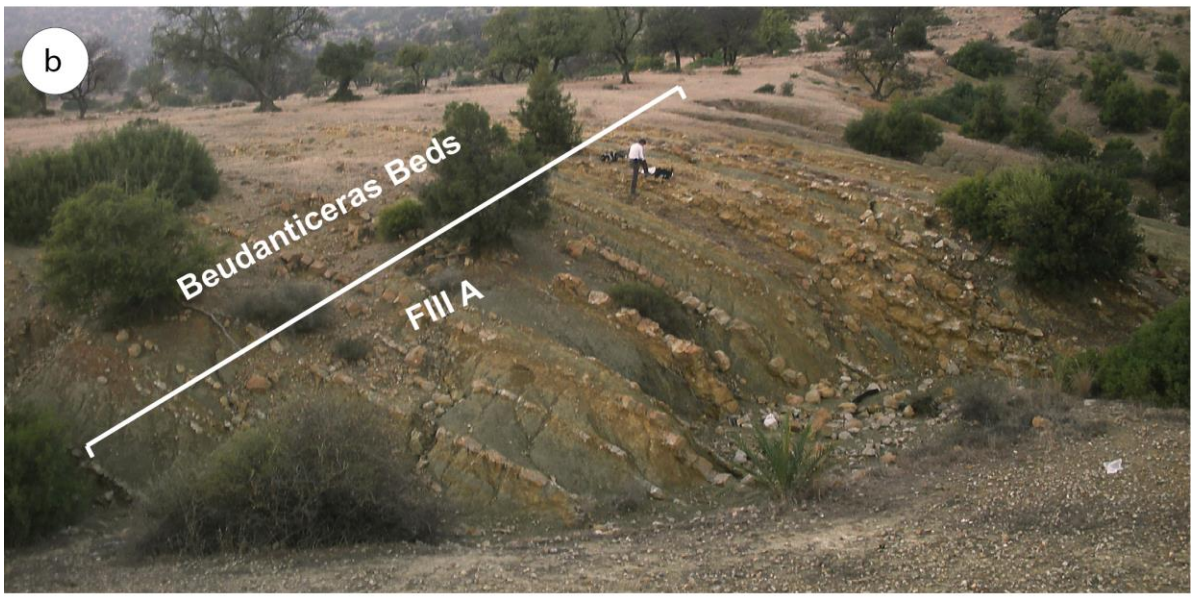

4. A.4.4. Facies IV (F IV)

F IV consists of yellow, dolomitic, well sorted sandstone beds, usually separated by silty interbeds (Pl. 4.8a, b). The faunal content is dominated by benthic organisms, such as brachiopods (mainly terebratulids) and bivalves, among which oysters, plicatulids, pectenids and bivalves are common. Ammonites frequently occur and belemnites fragments are common. Current sedimentary structures are common (ripples, cross bedding) and sometimes obscured by bioturbation. The lower part of the dolomitic sandstones is frequently rich in varied reworked elements: phosphatic fragments, internal molds of gastropods or ammonites, brachiopods, lithoclasts and belemnite rostra (Pl. 4.8c). Bioturbations consist of burrows (curved and straight), track molds and digging traces. F IV commonly overlies erosional surfaces, above described as S 4 (Pl. 4.8a-c). This facies is widely distributed in the EAB, since it is recorded almost in all sections, attaining 0.5m in Tinfoul, 1m in Alma, 4m in Anzate, 5m in Addar, 9.5m in Tissakatine east, 9m in Tissakatine Center, 1.5m in Taounerine and 0.25m in Ida w Shayq, with an total thickness of 30.75m and average percent of about 5% when considering all sections.

The sandstone beds have been sampled in the sections of Ida w Shayq (above D5) and Tissakatine Center (above D4) and were studied under the microscope (Pl. 4.8d, e). In Tissakatine Center, this facies is a glauconitic, well sorted, very fine grained, calcareous quartz-arenite (Pl. 4.8d), in which the framework components are essentially made of mono-crystalline quartz (95%), associated with few glauconitic (≈ 3%) and rare phosphatic grains (≈ 1%). Scarce bivalve fragments may occur (≈ 1%). The quartz grains are moderately sorted, very fine grained, and rounded to subrounded, showing mainly wavy and few straight extinction. The bivalve fragments are calcitic and/or dolomitized. The intergranular pores are filled with slightly blocky mosaic coarse crystals of calcite and dolomite cement of variable size**.** The framework components are lumped together by the calcite and patchily dolomitic cement. In Ida w Shayq, the sandstone is more argillaceous and can be defined as a phosphatic, pyritized, very fine grained quartz-wacke (Pl. 4.8e). The framework components are mainly made of mono-crystalline quartz (60%), reworked, rounded pyrite grains (34%), phosphatic pellets (5%) and few bivalve shell fragments (1%). The quartz grains are very fine, moderately sorted, rounded to subrounded and sometimes angular. The intergranular pores are filled with argillaceous cement**.**

Interpretation: The predominance of a diversified benthic fauna indicates an open marine environment. The occurrence of current-related structures indicates a moderate to good energy during deposition, which is supported by the good sorting of the sandstones. The abundance and diversity of bioturbations, as well as the moderate energetic conditions, support the interpretation of a middle shelf/ramp environment, above the storm wave base or close to the fear weather wave base (Fig. 4.14). When F IV deposits overly S 4 surfaces, they are interpreted as resulting from the decreasing intensity of the submarine currents responsible for the erosional surface. As these currents decrease, they allow deposition of sandstones, mixed with reworked elements, both brought out from the underlying, eroded strata.

Plate 4.8: (Facies IV)

a. F IV: Yellow calcareous sandstone. Above D4, Tissakatine Center section.
b. F IV: Yellow marly fine sandstone. Above D5, Ida w Shayq section.
c. F IV: Reworked bioclasts (red arrows), yellow marly fine sandstone, above D7, Tissakatine Center section.
d. F IV: Glauconitic, well sorted, very fine-grained quartz arenite. Unit Tkc 92, Tissakatine Center section (PPL).
e. F IV: Phosphatic, pyritized, very fine-grained, dolomitic sandstone. Unit Ida 27, Ida w Shayq section (PPL).

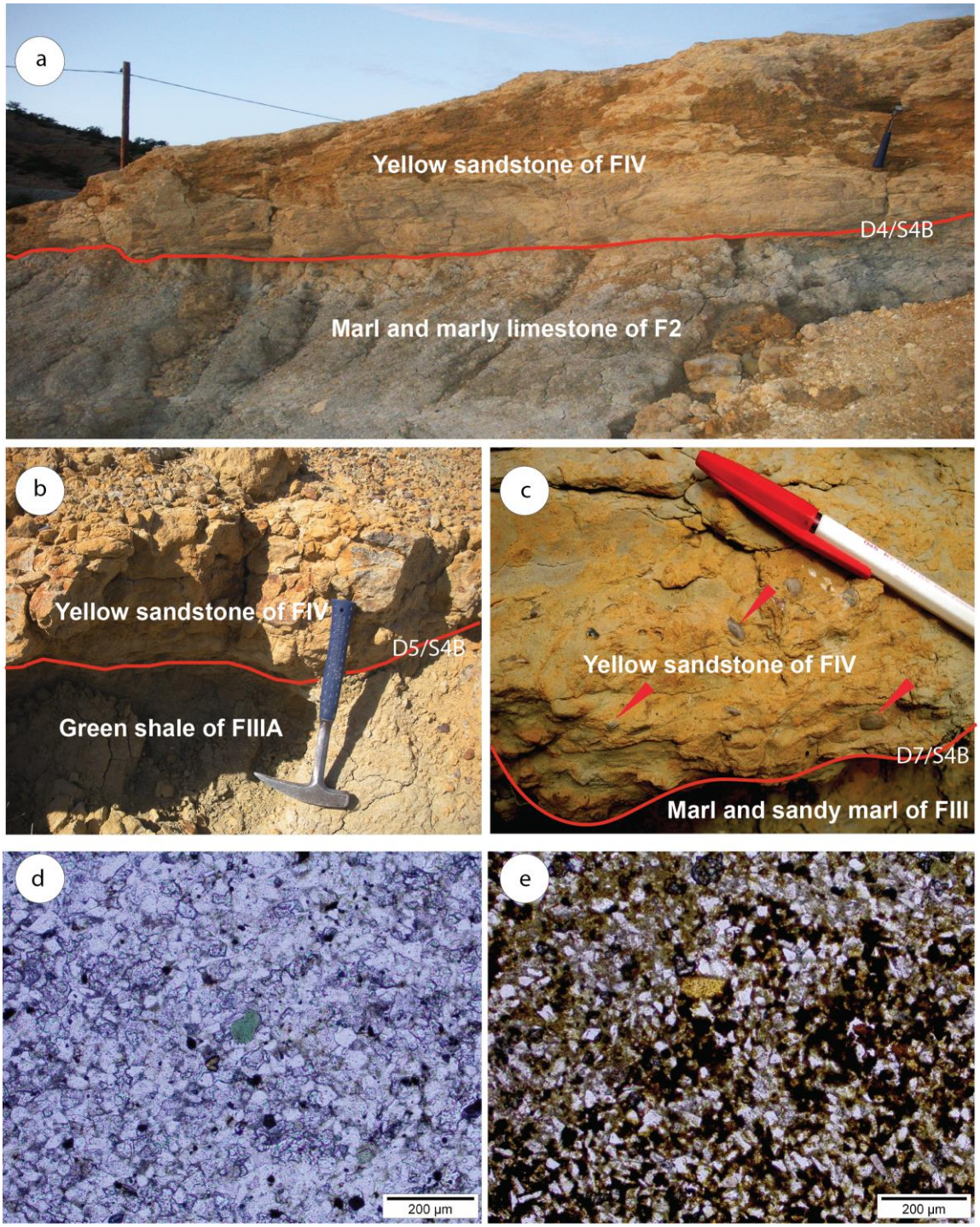

4. A.4.5. Facies A (F A)

Facies F A is characterized by a poor faunal diversity, few pelagic fauna (ammonites and belemnites), very few benthics (plicatulids), and scarce bioturbations and thalassinoids, together with the high abundance of a type of organism, usually annelids (serpulids; Pl. 4.9a) or buchidae bivalves (e.g. *Aucellina* sp., Pl. 4.9b). F A is usually associated with monotonous varicolored dark green to yellow shales or shaly marls, or with alternating marl/silty marl and marl/sandstone, with predominance of marl or silty marl (lithologies of F 1, F 2, F I, F II, F III). Pyrite grains are also observed in most sections. F A is usually observed in the upper part of the succession (above D 4).

This facies constitutes about 42% (31 m) of the thickness in the Tinfoul section; 67% (60 m) in Anzate; 35% (36 m) Tissakatine Center; 20.5% (21 m) in Tissakatine east and about 19% (7 m) in Ida w Shayq, with an average of 36.7%, when considering all mentioned sections (Figs. 4.1, 4.3, 4.7-4.8, 4.11).

Interpretation: The poor faunal diversity, as well as the predominance of organisms tolerating oxygen-depleted environments (*Aucellina* sp., e.g. Giraud et al., 2003; Reboulet et al., 2005; annelids, e.g. Hfaiedh et al., 2013) points to disaerobic conditions. The presence of pyrite grains also suggests reducing conditions. However, the occurrence of bioturbations indicates that benthic life is still possible, and therefore, that conditions are not anoxic. The scarcity of other fauna can be explained either by the high toxicity of bottom waters, or by the low biological productivity of surface water (Jansa et al., 1984). Because of the scarcity of other fauna, the deposition environment is difficult to assess precisely, and it will be interpreted based on the lithology. For this reason, disaerobic facies (F A) will be named based on their lithology, for instance F 2A or F IIA. In any case, in the studied sections, F A is restricted to outer shelf environments.

Plate 4.9: (Facies FA)

a. Facies IIIA: Annelid concentration (blue arrows). Above D5, Anzate section
b. Facies FIIIA: Concentration of *Aucelina* sp. (Oxygen depletion indicator). Just below D5, Tinfoul section.

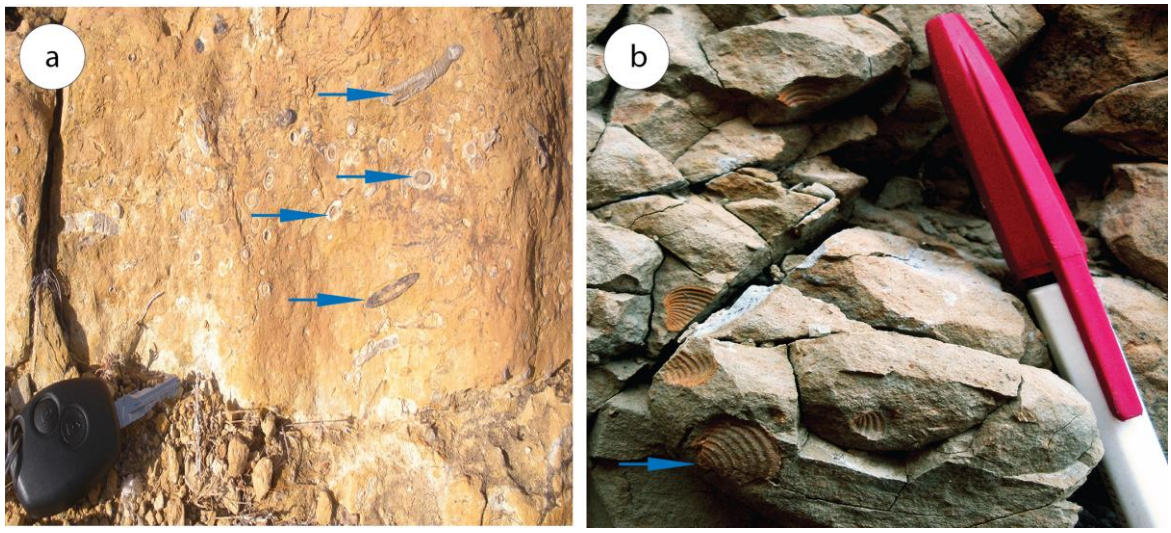

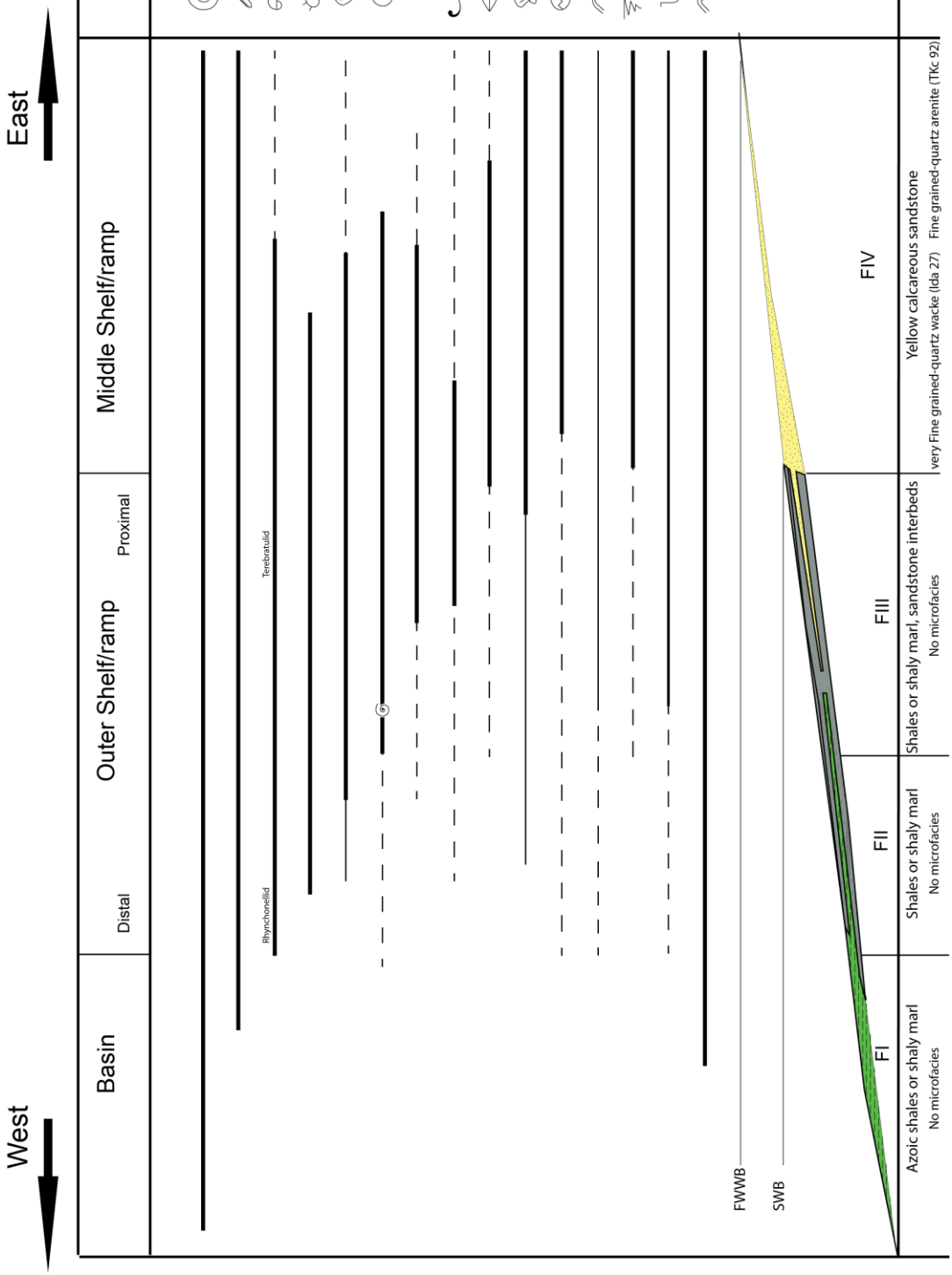

Figure 4.14: Faunal and facies distribution during the Early Albian in the EAB.

4. A.5. Early Albian environments, as compared to Aptian environments

Albian facies differ from the Aptian ones by the abundance of detrital input. As a whole, Albian sediments are marked by silty marls, shales and sandstones, while Aptian deposits comprise marls and limestones, with very few, fine grained detrital quartz. This provoked a change in the overall faunal content. As a matter of fact, pectinids and irregular sea urchins, common in the Aptian sediments, become much scarcer in the Early Albian deposits, whereas oysters and plicatulids are much more abundant in the latter. In the same way, scarce corals are present in the Aptian succession but are totally absent in the Albian series. Overall, this suggests that the Albian environment is marked by more important terrigenous supply (local occurrence of plant fragments), which provoked a change from oligotrophic to mesotrophic conditions, illustrated by the faunal change.

On the other hand, evidences of emergence periods exist in the Aptian succession (karstified surfaces), whereas they are totally lacking in the Albian succession, which is only marked by sporadic increases of the energy of deposition. This indicates that the average deposition depth appears to be higher in the Early Albian than during the Aptian. During the latter period, the deposition depth varied between 0 meters (S 1) and little below the lower limit of the photic zone (F 1), while in the Early Albian, deposition depth varied from the fair-weather wave base (F IV), to largely below the photic zone (F I). However, this qualitative assessment may be exaggerated, since the more important detrital supply during the Early Albian should have reduced the thickness of the photic zone. Therefore, we cannot rule out that F II and F III may have been deposited in environments slightly shallower that facies F 1 and F 2, respectively.

The average energy level that prevailed during deposition of the Early Albian succession was higher than during the Aptian, as illustrated by the occurrence of erosional surfaces, sandstone beds and current structures in the latter. Although upwellings were probably already present during the Aptian, since karstified surfaces are commonly infilled by glauconitic and phosphatic sediments, they may have been stronger during Early Albian times.

Finally, the F A facies are restricted to the Early (to Middle ?) Albian succession; this suggests that the EAB ramp was more oxygen-depleted at that time, than during the Aptian. Two causes may be invoked. On one hand, the O_2 depleted zone may have been too deep to reach the Moroccan ramp during the Aptian, whereas the higher deposition depth during the Early Albian allowed the O_2 depleted zone to reach and encroach the

EAB basin. On the other hand, the increasing influence of upwelling currents may have enhanced the biological activity in the outer zones of the ramp, consuming a great part available oxygen through organic life and organic matter degradation, thus favoring the extension of the O_2 depleted zone onto the EAB ramp.

Table 4.1: Facies description and depositional environments

Age	Facies (common fossils)	Lithofacies	Fossil content			Microfacies	Occurrence	Depositional environments
			Abundant	Some	Scarce			
Aptian facies	F1 (pelagic deposit)	Shales or shaly marl	Belemnite	Ammonite	Thin shelled bivalves, annelids, small gastropods	Planktonic foraminiferal wackstone	Tinfoul, Alma, Anzate, Addar, Tissakatine east, Ida w Shayq	Distal outer shelf/ramp
	F2 (hemipelagic)	Shales or shaly marl, with some marly beds	Belemnite, ammonite, irregular sea urchins, brachiopods, pectionids, plicatulids	Track molds,curved burrows, digging traces	Oysters, gastropods, annelids and nautiloids.	Planktonic foraminiferal packstone	Tinfoul, Alma, Anzate, Addar, Tissakatine east,Tissakatine center, Taounerine, Ida w Shayq	Proximal outer shelf/ramp
	F3 (benthonic)	Marly limestones with marly interbeds	Benthic organisms, brachiopods, annelids and bivalves, as oysters, plicatulids, pectinids and thick-shelled, large bivalves.	Bioturbations curved and straight burrows and track molds	Ammonites and belemnites frequently occur	Sandy bivalval packstone	Alma, Anzate, Addar,Tissakatine east, Tissakatine center, Ida w Shayq	Middle shelf/ ramp
	F4 (benthonic sessile)	Massive limestone beds	Benthic bivalves, such as abundant oysters	Trigonids	Rudistids	Bioclastic grainstone	Alma, Anzate, Addar,Tissakatine east, Tissakatine center, Ida w Shayq	Inner shelf/ramp
Early Albian facies	FI (deep pelagic)	Dark-coloured, shales or shaly marl			Ammonites	- - - - - - - - - - -	Alma, Addar,Tamri,Taounerine, Ida w Shayq	Basin to distal outer shelf
	FII (pelagic)	Silty shales or silty shaly marl	Belemnites	Ammonites	Thin-shelled bivalves, annelids and small sized gastropods may occur	- - - - - - - - - - -	Tinfoul, Alma, Anzate, Addar, Tissakatine east,Tissakatine center, Taounerine, Ida w Shayq	Distal outer shelf/ramp
	FIII (hemipelagic)	Shale or shaly marl, with thin beds of sandstones or sandy marls	Belemnites, ammonites and brachiopods	Gastropods and thin-shelled bivalves	Bioturbations in the sandstone beds, small sized curved burrows, oyster, large bivalves	- - - - - - - - - - -	Tinfoul, Anzate, Addar,Tissakatine east, Tissakatine center,Taounerine, Ida w Shayq	Proximal outer shelf/ramp
	FIV (benthonic)	Yellow, dolomitic, well to moderately sorted sandstone beds	Brachiopods, oysters, plicatulids, pectenids, bivalve and belemnite fragments.	Ammonites	Bioturbations, curved and straight burrows, track molds and digging traces	Quartz arenite, quartz-wacke	Tinfoul, Alma, Anzate, Addar, Tissakatine east,Tissakatine center, Taounerine, Ida w Shayq	Middle shelf/ ramp
Aptian/Early Albian facies	FA (characteristic fossils)	Dark green to yellow shales or shaly marls, or with alternating marl/silty marl and marl/sandstone, characterized by a poor faunal diversity	High abundance of annelids or buchidae bivalves	Ammonites and belemnites	Plicatulids, bioturbations and thalassinoids	- - - - - - - - - - -	Tinfoul, Anzate, Tissakatine east, Tissakatine center, Ida w Shayq	Restricted, outer shelf

CHAPTER FOUR

4. PALEOENVIRONMENTAL EVOLUTION IN THE EAB

PART (B): SEQUENCE STRATIGRAPHY

4. B. SEQUENCE STRATIGRAPHY

4. B.1. Sedimentary discontinuities and sequence boundaries

Eight main discontinuities have been recognized, interpreted from sedimentary processes and environments, and were correlated through the studied area. They are illustrated in Figs. 4.15 to 4.23. Five of these discontinuities have been dated.

These unconformity surfaces could be considered as sequence boundaries, which define eight sedimentary sequences, four of which are Aptian in age (Ap.1, Ap.2, Ap.3 and Ap.4), the other ones being of Albian age (Alb.1, Alb.2, Alb.3 and Alb.4) (Figs. 4.15 to 4.23). The subaerially exposed, karstified unconformity surfaces (D0, D1, and D2) are classified as type one sequence boundary (SB0, SB1, SB2). The submarine, erosional unconformity surfaces (D3, D4, D5, D6 and D7) are classified as type two sequence boundaries (SB3, SB4, SB5, SB6 and SB7).

4. B.2. Depositional sequences

The Tissakatine Center (Tkc), the most complete section, is located in the middle part of the EAB, and contains the eight depositional sequences, which can be correlated with the other studied sections. These sequences are separated by the sequence boundaries defined above. These boundaries will be described along with the sequences. Within each sequence, the vertical stacking pattern of systems tracts and stratigraphic surfaces reflects various phases of the relative sea-level fluctuations. The recognition of the systems tracts is based on: (l) identification of the different lithofacies, their faunal content and paleoenvironments, (2) analysis of facies associations which allows the definition of deepening-shallowing cycles, and (3) interpretation of their geometries and stratal stacking pattern. The systems tracts, which constitute the building blocks of these sequences, will be discussed hereunder from base to top and the studied sections are illustrated in Figs. 4.15 to 4.23.

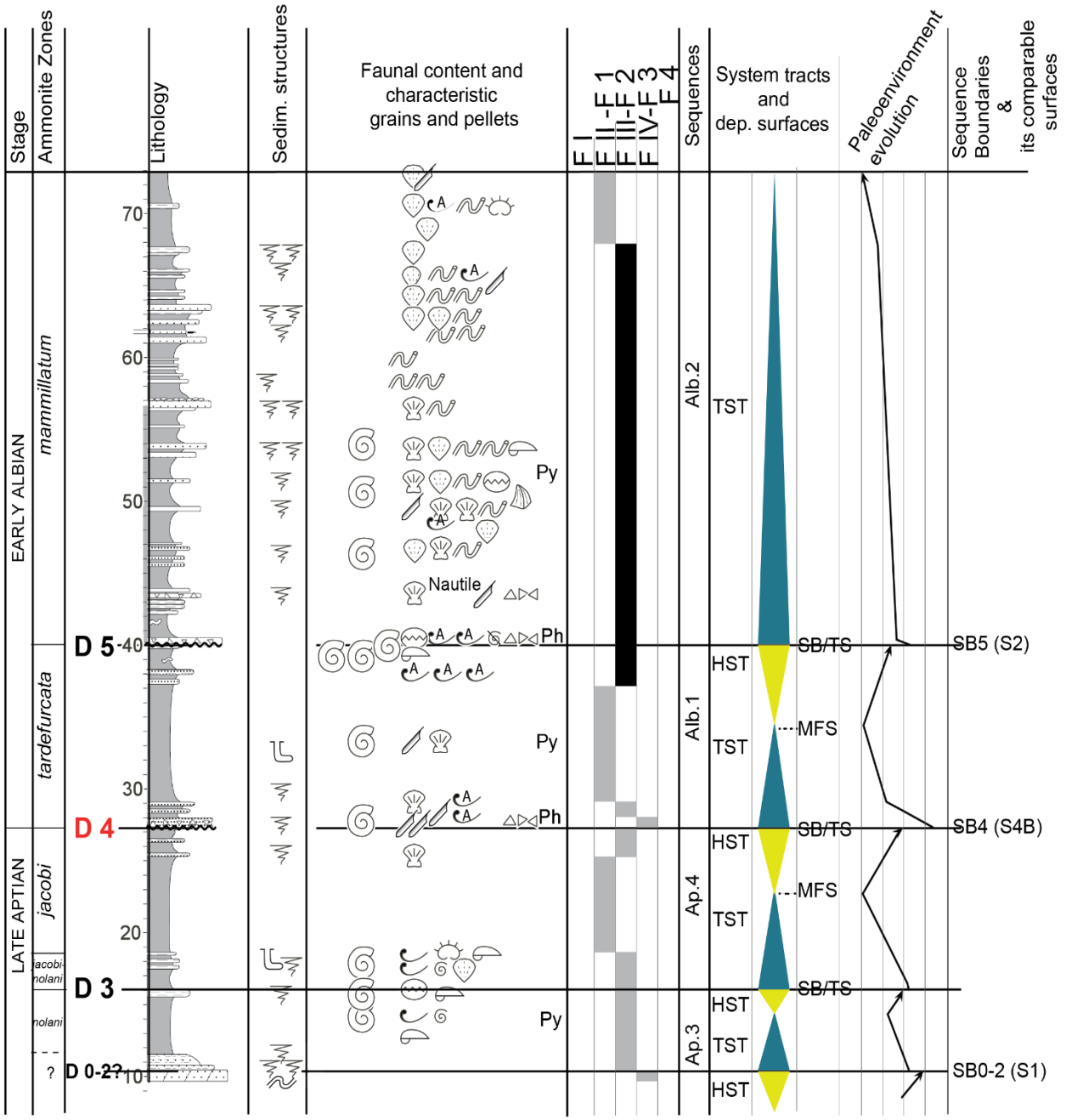

Figure 4.15: Stratigraphic changes in Tinfoul section showing the sedimentological aspects, paleoenvironments, depositional sequences, corresponding systems tracts, sequence boundaries and paleoenvironments evolution.

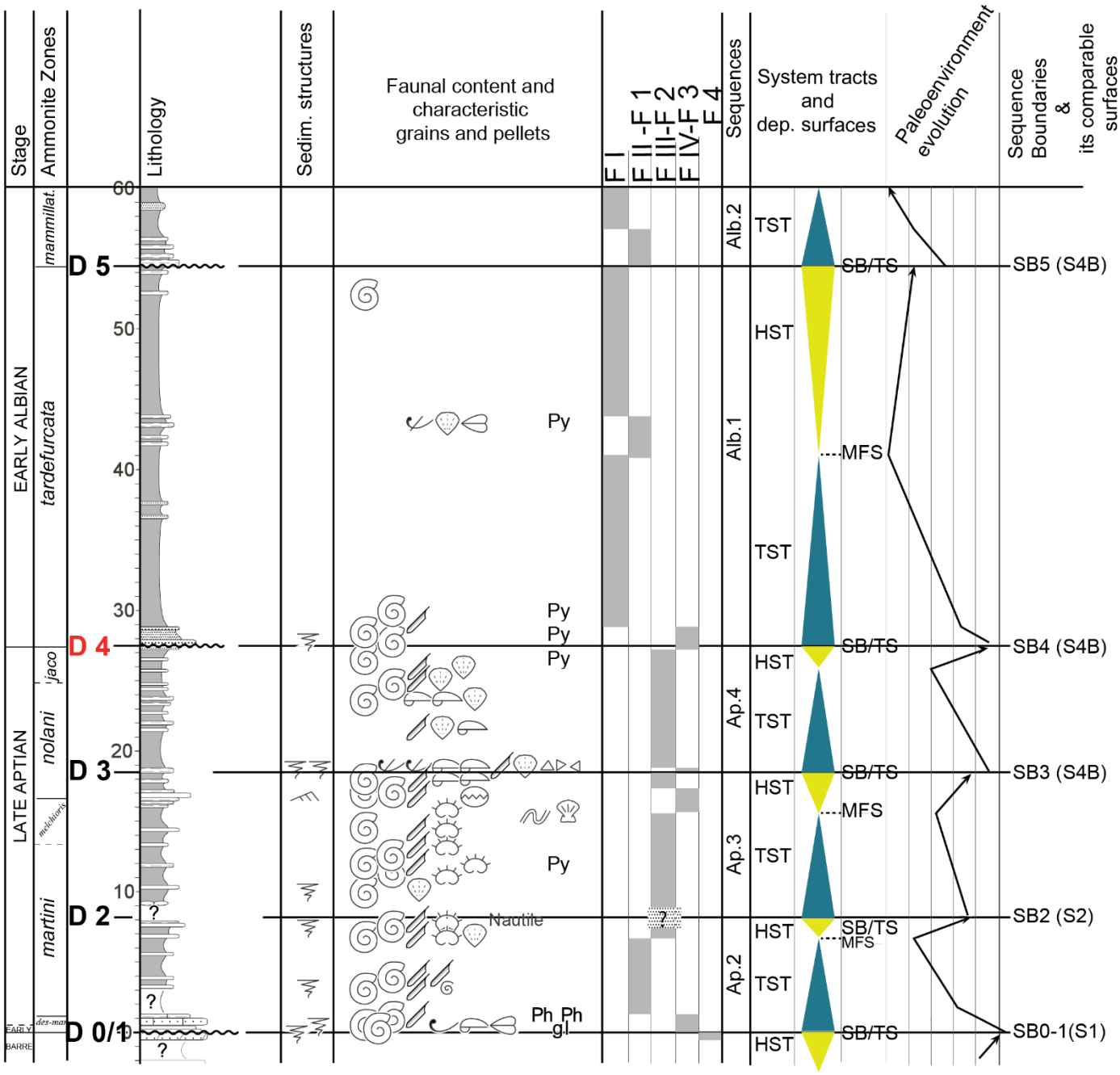

Figure 4.16: Stratigraphic changes in Alma section showing the sedimentological aspects, paleoenvironments, depositional sequences, corresponding systems tracts, sequence boundaries and paleoenvironments evolution.

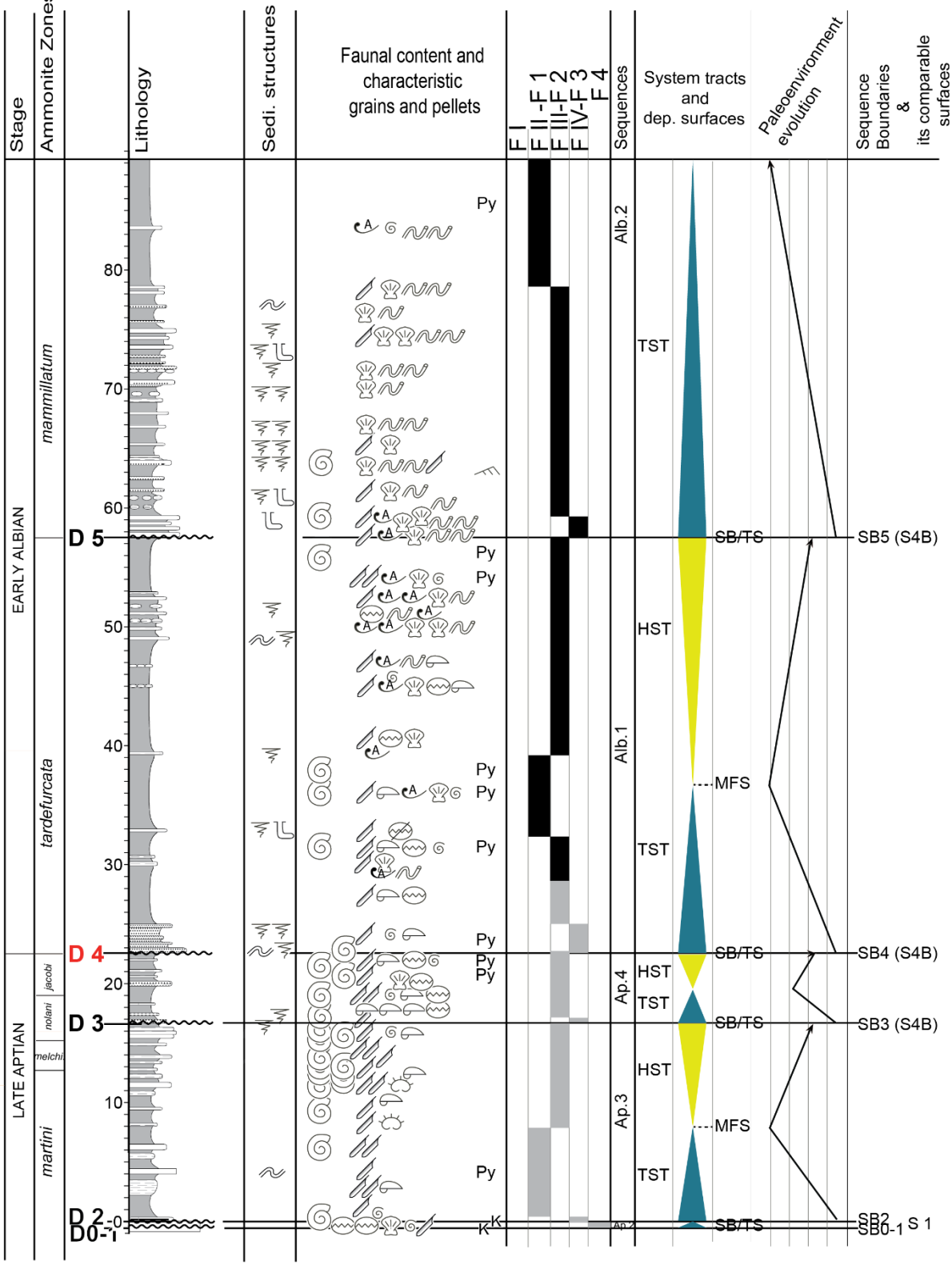

Figure 4.17: Stratigraphic changes in Anzate section showing the sedimentological aspects, paleoenvironments, depositional sequences, corresponding systems tracts, sequence boundaries and paleoenvironments evolution.

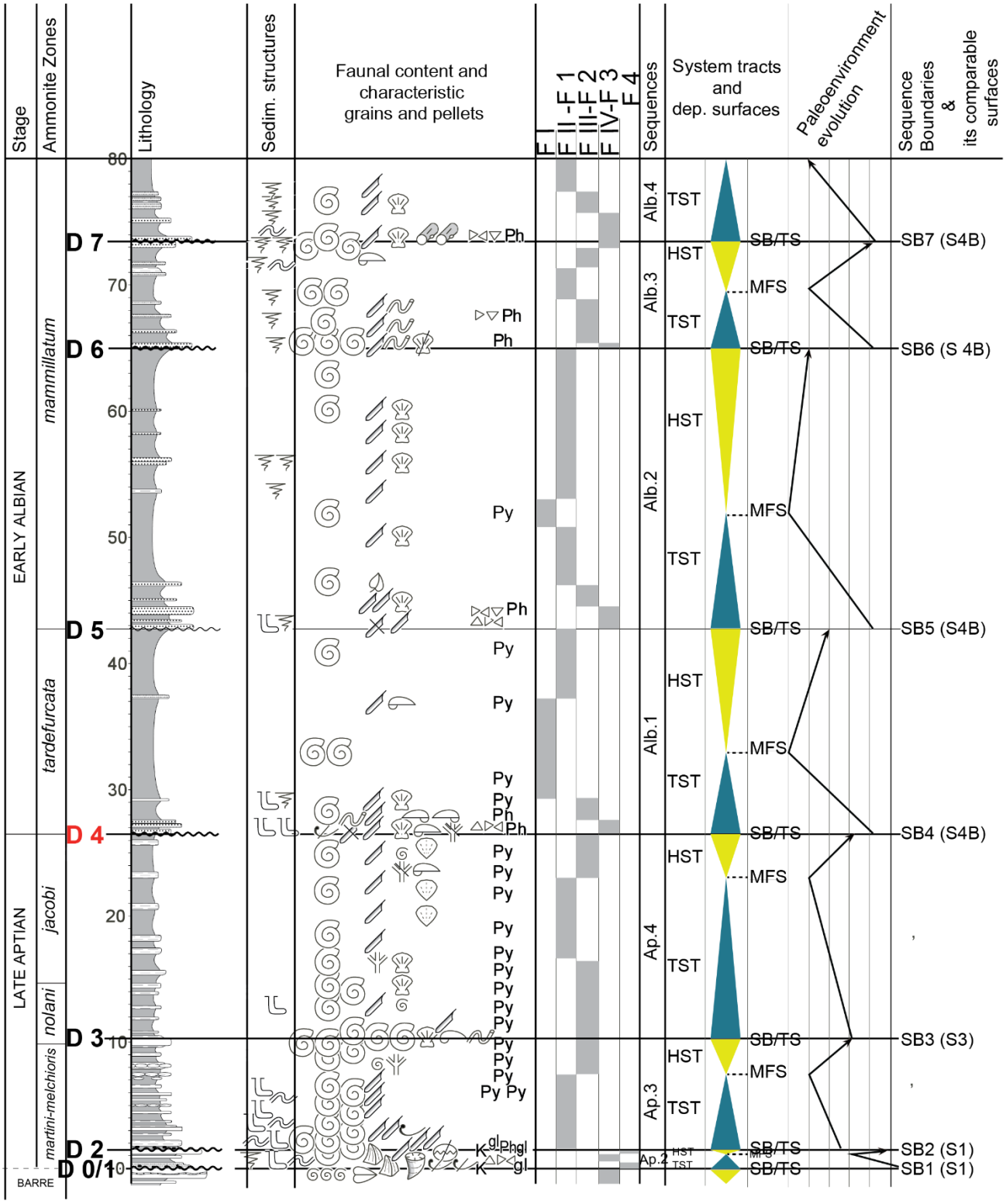

Figure 4.18: Stratigraphic changes in Addar section showing the sedimentological aspects, paleoenvironments, depositional sequences, corresponding systems tracts, sequence boundaries and paleoenvironments evolution.

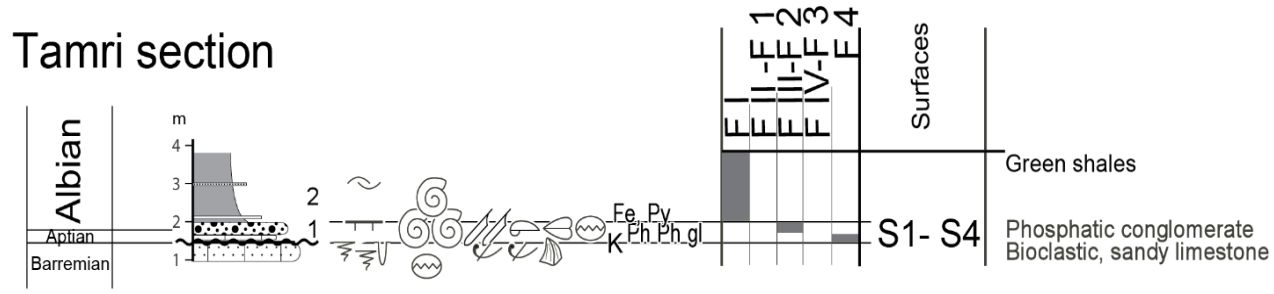

Figure 4.19: Stratigraphic changes in Tamri section showing the sedimentological aspects, paleoenvironments.

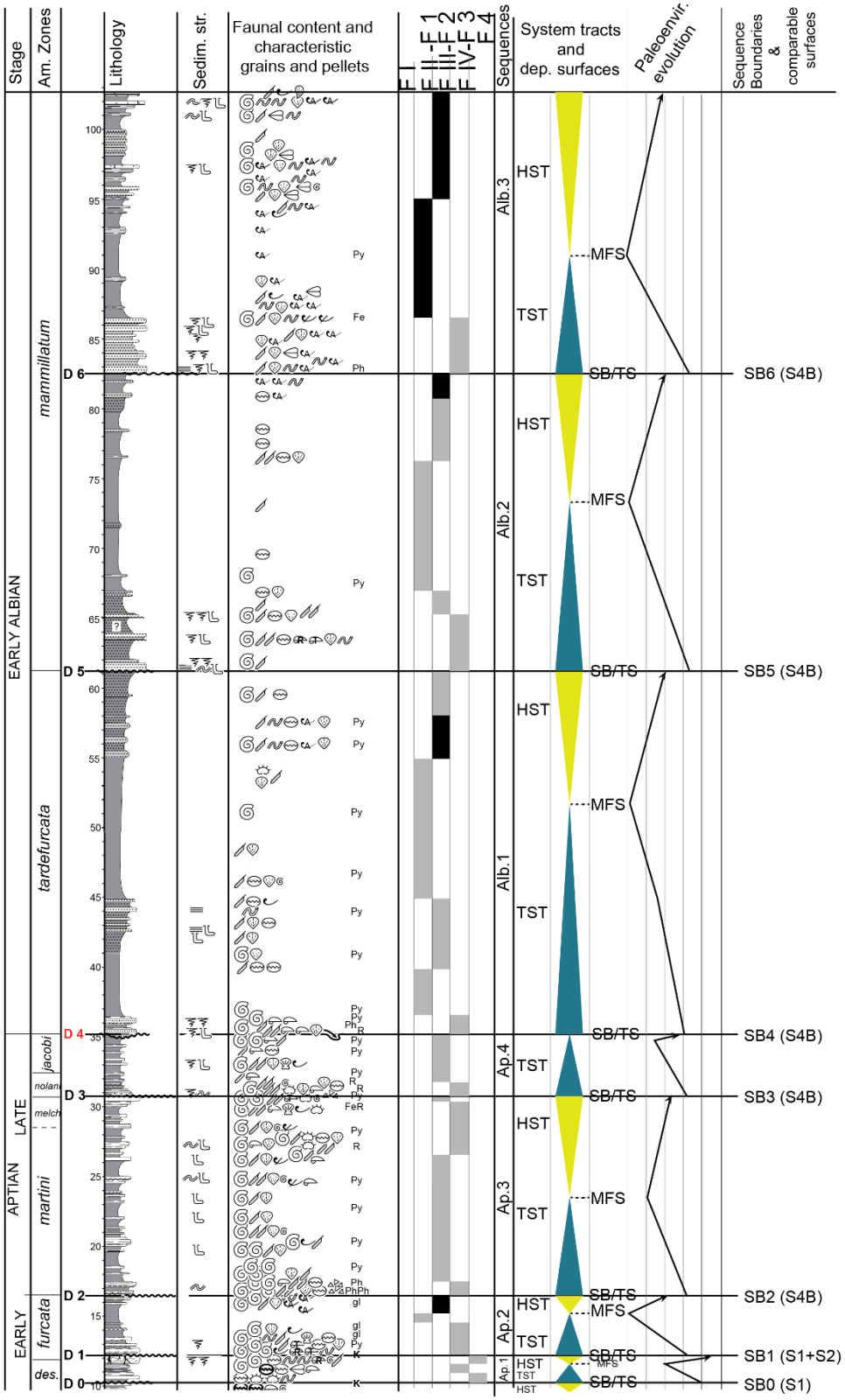

Figure 4.20: Stratigraphic changes in Tissakatine east section showing the sedimentological aspects, paleoenvironments, depositional sequences, corresponding systems tracts, sequence boundaries and paleoenvironments evolution.

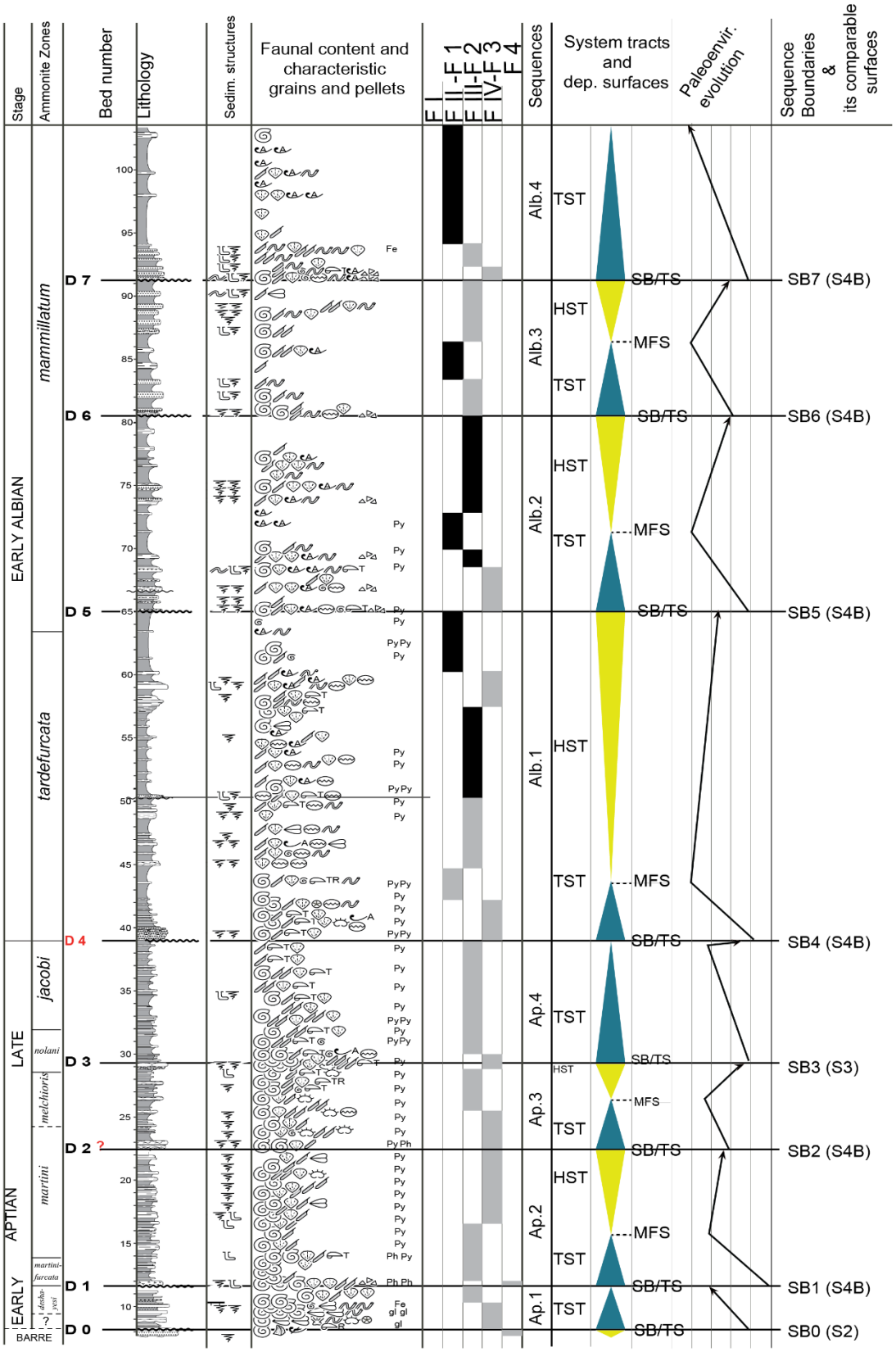

Figure 4.21: Stratigraphic changes in Tissakatine Center section showing the sedimentological aspects, paleoenvironments, depositional sequences, corresponding systems tracts, sequence boundaries and paleoenvironments evolution.

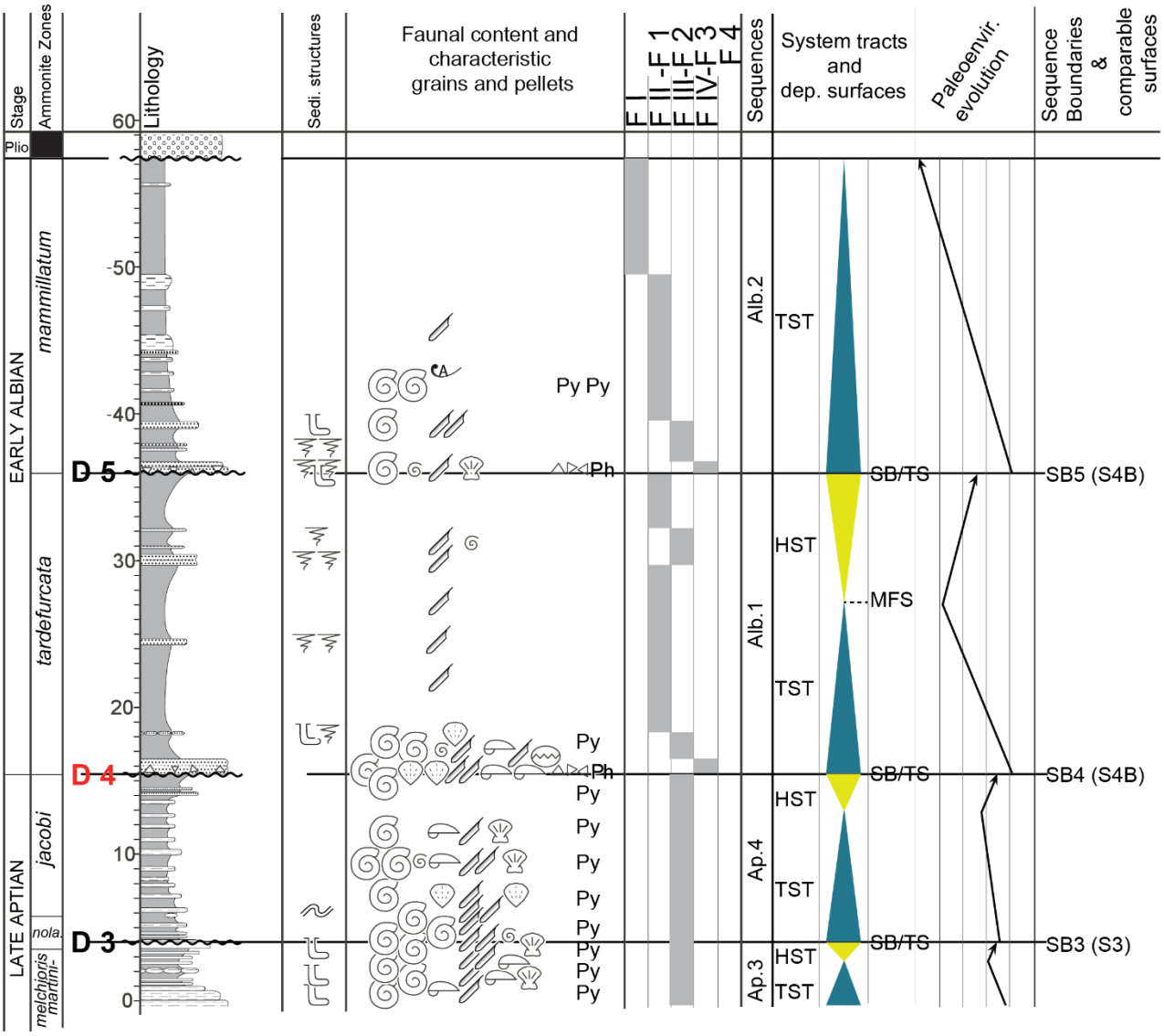

Figure 4.22: Stratigraphic changes in Taounerine section showing the sedimentological aspects, paleoenvironments, depositional sequences, corresponding systems tracts, sequence boundaries and paleoenvironments evolution.

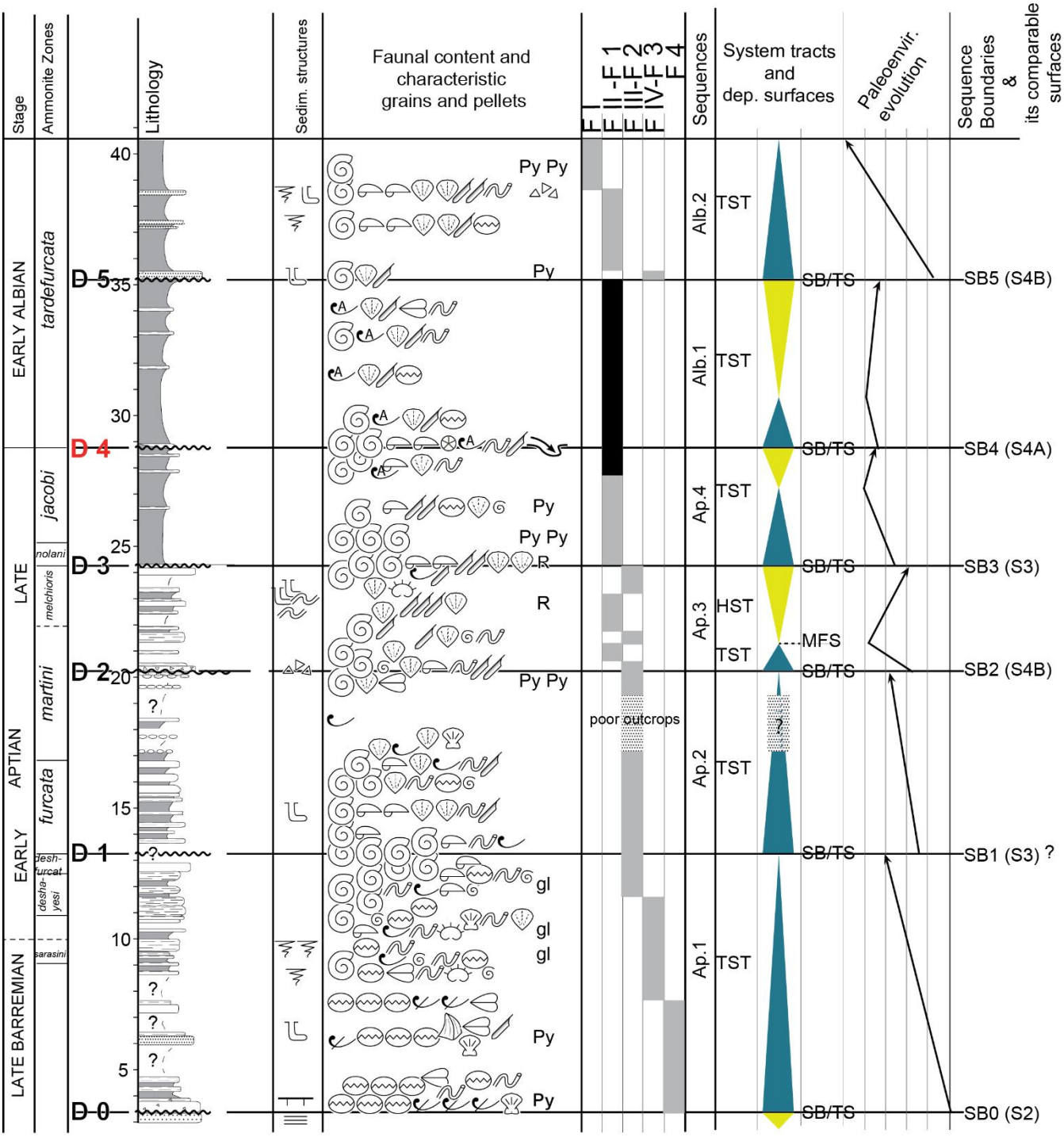

Figure 4.23: Stratigraphic changes in Ida w Shayq section showing the sedimentological aspects, paleoenvironments, depositional sequences, corresponding systems tracts, sequence boundaries and paleoenvironments evolution.

4. B.2.1. Sequence Ap.1 (Late Barremian to Early Aptian, between SB0 and SB1)

The **sequence Ap.1** is recorded in the central part of EAB, in Tissakatine east and Tissakatine Center sections, and in the northern part, in Ida w Shayq section (Figs. 4.20, 4.21, 4.23). Ap.1 is emphasized by the first sequence boundary (SB0). **SB0** is a karstified surface (S1), which indicates a period of subaerial exposure at Tissakatine east, whereas it is an erosional surface resulting from a submarine hiatus (S2) at both Ida w Shayq and Tissakatine Center sections. The lower SB and the transgressive surface (TS) are merged in Ap.1. **SB0/TS** separates the underlying Late Barremian massive, sandy limestones from the TST of Ap.1. **The transgressive system tract (TST)** develops just above the SB/TS, as retrogradational parasequences, and is 1.5m thick at Tissakatine east, 3.5m thick at Tissakatine Center, and 9.5m thick at Ida w Shayq. At Ida w Shayq, the TST is composed first of inner ramp sandy limestone, rich in oysters, evolving to middle shelf, marly limestone, associated with thick-shelled bivalves and annelids, and then to proximal outer shelf, hemipelagic, shaly marl, yielding ammonites and brachiopods. At Tissakatine Center, the TST starts with middle shelf, alternating marl and marly limestone with abundant benthic organisms (bivalves, annelids), overlain by proximal outer shelf, hemipelagic, shales and shaly marl, indicating a deepening upward trend (Fig. 4.21). At Tissakatine east, the TST is represented by inner shelf limestone and sandy limestone, with benthic bivalves such as oysters, overlain by middle shelf/ramp, marly limestone. The TST varies laterally along proximal-distal transects. From the distal section of Ida w Shayq to the proximal section of Tissakatine east, the thickness of the TST and the abundance and diversity of fossil assemblage decrease, while the sedimentary facies represent shallower marine setting. In all sections, the TST ends up with the maximum flooding surface (MFS). The **MFS** is defined at the top of the marly limestone bed, marked by the presence of ammonites, thick-shelled bivalves and brachiopods. The **Highstand system tract (HST)** is only recorded at Tissakatine east, where it is formed by a 0.5m thick, aggradational set of highly bioturbated, massive limestone beds of inner ramp setting, rich in benthic organisms and annelids. The HST is covered by SB1.

4. B.2.2. Sequence Ap.2 (Early Aptian to early Late Aptian, between SB1 and SB2)

Sequence Ap.2 is clearly defined in the northern part and central parts of the EAB, in the Ida w Shayq section (Fig. 4.23), Tissakatine Center and Tissakatine east sections (Figs. 4.20, 4.21). The Ap.2 sequence is less defined in the southern part of the basin, where it is marked by considerable thickness at Alma, with respect to very reduced thickness in the Addar and Anzate sections (Figs. 4.16-4.18). Ap.2 is underlain by SB1, which separates (1) the TST of Ap.1 and the TST of Ap.2 at Ida w Shayq and Tissakatine Center, and (2) the HST of Ap.1 and the TST of Ap.2 at Tissakatine east and Alma. The SB1 is marked, according to the sites, by an erosional surface, representing a submarine hiatus at Ida w Shayq and Tissakatine Center, and by a karstified surface in the other sections. Both the SB1and TS of AP.2 are merged, defining the base of the TST. The retrogradational parasequences of the TST at Ida w Shayq and Tissakatine Center reach 7m and 4.3m thick, respectively. They consist of hemipelagic, marly beds of proximal outer ramp setting, rich in both pelagic and benthic organisms. At Tissakatine east, the TST is made of about 3m thick, marly limestone, rich in benthic fauna of middle ramp environment. At Alma, the TST is 4m thick, and comprises white marl with pelagic organisms, of distal outer ramp setting. The TST parasequences are progressively enriched with pelagic fauna indicating a deepening upward evolution. **The maximum flooding surface (MFS) and the Highstand system tract (HST)** are observed in the Alma, Tissakatine east and Tissakatine Center sections. At Alma, the MFS is located within grey shaly marl with scarce fossils; at both Tissakatine sections it is placed at the top of a marly layer, rich in pelagic organisms (ammonites and belemnites). The **HST** is a set of parasequences evolving from aggradational to progradational at the end of the sequence. At Alma, the HST is made of a 3.5m thick series of hemipelagic shaly marl, of proximal outer shelf/ramp environment. At Tissakatine east, the HST (1.3m thick) is composed of hemipelagic shaly marl, rich in annelids and buchidae bivalves, displaying a restricted outer shelf/ramp setting. At Tissakatine Center, the 6.7m thick, HST comprises bioturbated marly limestone and grey marl, with ammonites and plicatulids, of middle shelf/ramp environment. In the HST, the pelagic faunal content is lower than in the TST and MFS, indicating a shallowing trend. This sequence is capped by SB2.

4. B.2.3. Sequence Ap.3 (Late Aptian, between SB2 and SB3)

The sequence Ap.3 is a well-developed, widely distributed sequence, which is recorded in all studied sections (Figs.4.15-4.23). Ap.3 is underlined by SB2, a karstified, subaerially exposed surface in the southern sections (Tinfoul, Anzate, and Addar). Farther North, SB2 is represented by an erosional surface, interpreted as a submarine hiatus. SB2 coincides with the TS of the Ap.3 sequence. SB2 separates the HST and/or the TST of the Ap.2 from the TST of Ap.3. At Tinfoul and Alma, the TST of AP.3 is respectively made of about 4 and 5.6 m thick, shales and shaly marl of proximal outer shelf/ramp environment. At Anzate and Addar, the TST comprises shaly marl of distal outer shelf/ramp environment, and reach 8 and 6.5m thick, respectively. Along the central transect, the TST, is 7m thick, consists of marl and marly limestone, of proximal outer shelf environment in Tissakatine east; 4m thick, marl and bioturbated marly limestone of middle shelf to proximal outer shelf setting at Tissakatine Center; 2.7m thick, argillaceous marl of proximal outer shelf setting at Taounerine. At Ida w Shayq, in the northern part of the basin, the TST is made of a 1m thick marl bed, of distal outer shelf environment. The MFS is placed where (1) the shale content is the highest, and (2) the benthic faunal content is the lowest. The MFS is enriched with pelagic and few benthic organisms in Alma; is marked by shale, rich in pelagic fossils in Anzate and Addar sections; is marked by ammonites and belemnites at Tissakatine east; overlies a shaly marl bed, poor in benthic fauna and rich in ammonites and belemnites at Tissakatine Center; and overlies a marl bed, rich in ammonites and plicatulids at Ida w Shayq. At Alma, the HST is made of 2.5m thick marly limestone and marl beds of middle shelf/ramp to proximal outer shelf setting. At Anzate and Addar, the HST is respectively made of 8.3 and 2.5m thick, marl and marly limestone, with abundant pelagic and few benthic organisms, of proximal shelf/ramp setting. It is respectively made of about 7.3 and 2.8m thick, marly limestone and marl beds, rich in benthic fossils, of middle shelf/ramp setting at Tissakatine east and Tissakatine Center sections, while it is represented by 1.5m of argillaceous marl of proximal outer shelf setting at Taounerine. In Ida w Shayq, the HST consists of 3m thick marl and marly limestone, with common belemnites and plicatulids of proximal to distal outer shelf environment.

4. B.2.4. Sequence Ap.4 (Latest Aptian, between SB3 and SB4)

The sequence Ap.4 is present in all studied sections (Figs. 4.15-4.23). Its base is defined by SB3, which is an erosional, submarine surface, marked by high concentration of belemnites and ammonites associated with lithoclasts. SB3 is interpreted as S4B at Tinfoul, Alma, Anzate and Tissakatine east; and as S3 at Addar, Tissakatine Center, Taounerine and Ida w Shayq. SB3 coincides with the TS. The TST of Ap.4 is well developed at Tinfoul, as 7m thick dark green shale, yielding scarce pelagic organisms, characterizing a proximal-distal outer shelf/ramp setting. At both Alma and Anzate sections, the TST is respectively made of about 7.3 and 3m thick, green shaly marl, marked by pelagic organisms (ammonites, belemnites) associated with brachiopods and plicatulids or oysters, of proximal outer shelf setting. At Addar, a 12.7m thick succession of shale and marl, with common pelagic fauna, reflect a proximal-distal outer shelf setting. In Tissakatine east, Tissakatine Center and Taounerine sections, the TST is respectively made of 4.5, 9.7 and 8.9m thick, marly limestone and marl beds, with hemipelagic fauna, reflecting proximal shelf/ramp setting. In the distal section of Ida w Shayq, the TST is made of green shale (3.1m) rich in pelagic organisms of distal outer shelf environment. The MFS is located at the middle part of a green shale bed at Tinfoul; at the top of an ammonite-bearing shaly marl bed at Alma; and at the top of a marl level, marked by ammonites, belemnites and pectenids at Addar. The MFS is overlain by a thin HST. The HST deposits generally consist of marly shale of proximal shelf/ramp setting, observed in the southern part of the basin (Tinfoul, 4.5m thick; Alma, 1.7m; Anzate, 3m; Addar, 3.5m). In the central part of the basin (Taounerine) it is made of 2.5m thick, marly siltstone; while in the northern part of the basin (Ida w Shayq), shale with thin beds of marly shale (1.7m) reflect a shallower depositional environment.

4. B.2.5. Sequence Alb.1 (Earliest Albian, between SB4 and SB5)

The Alb.1 sequence, of earliest Albian age, is recognized in all studied sections (Figs.4.15-4.23), and is better exposed than the other Albian sequences. The base of Alb.1 is defined by SB4, which is a S4 surface in all studied sections. SB4 is interpreted as representing a submarine hiatus associated with erosion and concentration of litho- and bio-clasts, related to significant submarine currents. SB4 coincides with the TS of Alb.1. At Tinfoul, Alma, Anzate, Addar, Taounerine, Tissakatine east and Tissakatine Center, the TST of Alb.1 is respectively,

made of about 7, 13.5, 14, 6.5, 11.5, 16.8 and 4.7m thick, yellow, marly sandstone beds of middle to proximal outer shelf/ramp environment, overlain by distal outer shelf/ramp shales. At Ida w Shayq, the TST is a 2m thick shale bed deposited in a distal outer shelf/ramp setting. The TST ends up with the MFS. The MFS is located within a shaly interval, with scarce fossils in all sections. At Tinfoul and Anzate, the overlying HST is made of 5.5 to 21m thick shales and thin beds of sandstones, with common ammonites and buchidae bivalves of restricted outer shelf/ramp environment. At Alma, 13.3m of silty, dark-colored shales were deposited a in distal outer shelf/ramp to basinal setting. At Tissakatine east about 9.5 m of yellow shale with sandstone beds, yielding a hemipelagic fauna (ammonites, belemnites, bivalves and annelids), indicate a proximal outer shelf/ramp environment. At Tissakatine Center, the HST is very thick, reaching about 21m, and is composed of two minor sequences. The first minor sequence consists of a 16m thick series of marl and bioturbated marly limestone, associated with belemnites, plicatulids, annelids, oyster, large bivalves of proximal distal environment, overlain by marly limestone, marked by buchidae bivalves, characterizing restricted outer shelf/ramp setting, and then by oyster-bearing, bioturbated sandy limestone deposited in middle shelf environment. The second minor sequence (about 5m) is composed of grey marl of distal outer shelf/ramp setting. At Taounerine, the HST is made of about 6m thick shales, with thin interbeds of sandstone of proximal outer shelf/ramp setting. At Ida w Shayq, shale and thin beds of marly shales (4.5 m) indicate a distal outer ramp setting.

4. B.2.6. Sequence Alb.2 (Early Albian, between SB5 and SB6)

The Alb.2 sequence is underlined by SB5. SB5 is a S4 surface in most studied sections, except at Tinfoul, where SB5 is defined as a S2. Both S4 and S2 are interpreted as erosional surfaces representing submarine hiatus. As usual, the SB5 is merged with the TS of Alb.2. The TST is the thickest systems tract, and is recognized in most studied sections (Figs. 4.15-4.23). At Tinfoul, the TST is made of green shales (33 m) with thin beds of sandstone deposited in a proximal outer shelf/ramp setting, which grade upward into green shales and shaly marl containing belemnites and deep water benthic fauna of distal outer shelf/ramp environment. At Alma, the TST consists of sandy marl and green shales (5.5 m) with scarce fossils, deposited in a distal outer shelf/ramp to basin environment. At Anzate, the TST is about 31.5 m thick. It starts with yellow sandstone beds of middle shelf/ramp environment, which grade upward into

shales and thin beds of bioturbated sandstone, rich in annelids and pectenids, reflecting proximal outer shelf/ramp setting, and ends up with green shales with annelids and buchidae bivalves, indicating a restricted distal outer shelf/ramp setting. At Addar, Taounerine and Ida w Shayq, the TST reaches 9.2, 21.5 and 5.5m, respectively; it evolves upward from yellow sandstone to green shales with scarce ammonites, reflecting middle shelf/ramp to outer shelf depositional setting. At Tissakatine east and Tissakatine Center, the TST is respectively made of 13.5 and 6.4 m thick, bioturbated, yellow sandstone, silty shales associated with ammonite, belemnites, plicatulids and oysters, overlain by green shales, with few pelagic and benthic fauna, indicating an evolution from middle shelf to distal outer shelf/ramp settings. The TST is capped by the MFS. At Addar, Tissakatine east and Tissakatine Center, the MFS is placed in the green shale interval, with scarce pelagic fossils. At Addar, the HST is made of 13 m thick, bioturbated, silty shales with thin beds of sandstone, overlain by green shales of proximal outer shelf/ramp setting. At Tissakatine east and Center, the HST is represented by shales with thin beds of sandstones, associated with annelids and buchidae bivalves, of restricted proximal outer shelf/ramp environment.

4. B.2.7. Sequence Alb.3 (Early Albian, between SB6 and SB7)

Alb.3 is exposed in Addar, Tissakatine east and Tissakatine Center sections (Figs. 4.18, 4.20, 4.21) and is underlined by SB6. SB6 corresponds to a S4 surface, reflecting the erosional effects of submarine currents. SB6 is merged with the TS of Alb.3. At Addar, the TST comprises 4.8m of shales and thin beds of sandstone, associated with ammonites, belemnites and annelids, overlain by green shales with scarce ammonites, expressing the evolution from proximal to outer shelf/ramp depositional environment. At Tissakatine east, it is about 8.5m thick, and consists of bioturbated, yellow sandstone associated with belemnites and bivalves of middle shelf/ramp setting, which grades upward into green shales and silty shales, with buchidae bivalves, deposited in a restricted outer shelf setting. At Tissakatine Center, the TST is made of grey marl with thin sandstone beds (6 m), deposited in a proximal outer shelf/ramp setting, overlain by grey marl, with belemnites, ammonites and buchidae bivalves of restricted, outer shelf/ramp setting. In all the studied sections, the MFS is placed within the shale interval, of distal, outer shelf/ramp environment. At Addar, Tissakatine east and Tissakatine Center, the

HST is respectively made of about 3.7, 11.5 and 5m of shales or shaly marl, with thin beds of sandstone or sandy marl, deposited in a proximal, outer shelf/ramp setting.

4. B.2.8. Sequence Alb.4 (Early Albian, lowered by SB7)

The Alb.4 sequence is recorded in Addar and Tissakatine Center (Figs. 4.18, 4.21). Its lower boundary SB7 corresponds to the TS of Alb.4. At Addar and Tissakatine Center, the TST is made of a 6.5 and 12.2m thick bed, respectively, of yellow sandstone deposited in a middle shelf/ramp setting, overlain by, shales and thin beds of sandstone of proximal outer shelf/ramp environment, and ends up with green shales or marl beds of distal outer shelf/ramp environment. In Tissakatine Center, it is marked by buchidae bivalves and annelids, reflecting restricted conditions.

Table 4.2: Depositional environments of the TST and HST, along an E-W transect in the southern part of the EAB.

Sequences	System tracts	E-W sections transect in the southern part of the EAB			
		Tinfoul	Alma	Anzate	Addar
Ap.1	TST	.....	.....	.....	.....
	HST	.....	.....	.....	.....
Ap.2	TST	.....	Mid/distal shelf	Inner shelf??	Inner/mid shelf
	HST	.....	Prox. outer shelf	.....	Mid/inner shelf
Ap.3	TST	Prox. outer shelf	Prox. outer shelf	Mid/distal outer shelf	Distal. outer shelf
	HST	.....	Mid/prox. shelf	Prox. outer shelf	Prox. outer shelf
Ap.4	TST	Pro/distal. outer sh.	Mid/prox. shelf	Mid/prox. shelf	Prox./distal outer shelf
	HST	Pro. outer shelf	Prox./mid. shelf	.....	Prox. outer shelf
Alb.1	TST	Mid/distal outer shelf	Mid shelf/basin	Mid/distal outer shelf	Mid shelf/basin
	HST	Pro. outer shelf	Distal shelf/basin	Prox. outer shelf	Distal outer shelf
Alb.2	TST	Pro/distal. outer sh.	Distal shelf/basin	Mid/distal shelf	Mid shelf/basin
	HST	.....	.....	.....	Distal shelf
Alb.3	TST	.....	.....	.....	Mid/distal shelf
	HST	.....	.....	.....	Prox./mid. shelf
Alb.4	TST	.....	.....	.....	Mid/distal shelf
	HST	.....	.....	.....	.....

Table 4.3: Depositional environments of the TST and HST, along an E-W transect, in the central and northern parts of the EAB.

Sequence	Syst. tracts	E-W transect in the central part of EAB			Northern section in EAB
		Tissakatine east	Tissakatine Center	Taounerine	Ida w Shayq
Ap.1	TST	Inner/mid shelf	Mid/prox. shelf	.....	Inner/prox. outer shelf
	HST	Inner shelf	.....	.....	.....
Ap.2	TST	Mid/distal shelf	Inner/prox. shelf	.....	Prox. outer shelf
	HST	Prox. outer shelf	Mid shelf	.....	.....
Ap.3	TST	Mid/prox. shelf	Mid/prox. shelf	??	Prox./distal. outer shelf
	HST	Mid/prox. shelf	Mid shelf	??	Pro. outer shelf
Ap.4	TST	Mid/prox. shelf	Mid/prox. shelf	Prox. outer shelf	Distal outer shelf
	HST	.....	.....	.....	Pro. outer shelf
Alb. 1	TST	Mid/distal outer shelf	Mid/distal outer shelf	Mid/distal outer shelf	distal outer shelf
	HST	Prox. outer shelf	Prox. outer shelf	Prox. outer shelf	.....
Alb. 2	TST	Mid/distal outer shelf	Mid/distal outer shelf	Mid shelf/basin	Mid shelf/basin
	HST	Prox. outer shelf	Prox. outer shelf	.....	.....
Alb. 3	TST	Mid/distal outer shelf	Prox./distal. outer shelf	.....	.....
	HST	Prox. outer shelf	Prox. outer shelf	.....	.....
Alb. 4	TST	.....	Mid/distal outer shelf	.....	.....
	HST	.....	.....	.....	.....

4. B.3. Development of carbonate platform in EAB during Aptian-Early Albian times

This study adds pieces to the reconstruction of the platform evolution of EAB, situated on the southern Tethys margin. It shows the development of the Aptian shallow-water carbonate platform, and the subsequent installation of the Early Albian outer shelf to basinal regime.

The evolution of EAB platform can be understood through correlation of the eight, time-framed Aptian-Early Albian depositional sequences. Spatial and temporal variations of each sequence can be traced along three transects, named southern, central and north-south transects (Figs. 4.24, 4.26, 4.28). These transects are illustrated by three cross-sections, showing the lateral changes in thickness for each depositional sequence (Figs. 4.25, 4.27, 4.29). These variations indicate changes related to varied external and internal parameters (e.g. climate, sea-level change, sediment accumulation, regional tectonic activity). The identification of eight, well dated depositional sequences, allow regional correlation with other basins on both the southern and northern Tethyan margins.

The stratigraphic record has been subdivided into two major transgressive cycles, based on lithology, fossil content, thickness, and recognition of major boundaries, which allow us to define two major transgressive sedimentary cycles. The first transgressive cycle is latest Barremian-Aptian in age, while, the second cycle is called the Early Albian transgressive cycle. Their boundaries reflect significant shifts in the sedimentary trends and coincide with major changes in the basin physiography, and palaeogeography. The two cycles have been interpreted as second order cycles and subdivided into eight third-order depositional sequences (Figs. 4.24, 4.26, 4.28). As the units were deposited in a platform environment, transgressive and highstand deposits make up most of the record of the third-order sequences, whereas lowstand sediments are poorly developed.

The first second-order transgressive cycle of this study corresponds to the Ap.1, Ap.2, Ap.3 and Ap.4 sequences. The second second-order transgressive cycle may correspond to Alb.1, Alb.2, Alb.3 and Alb.4.

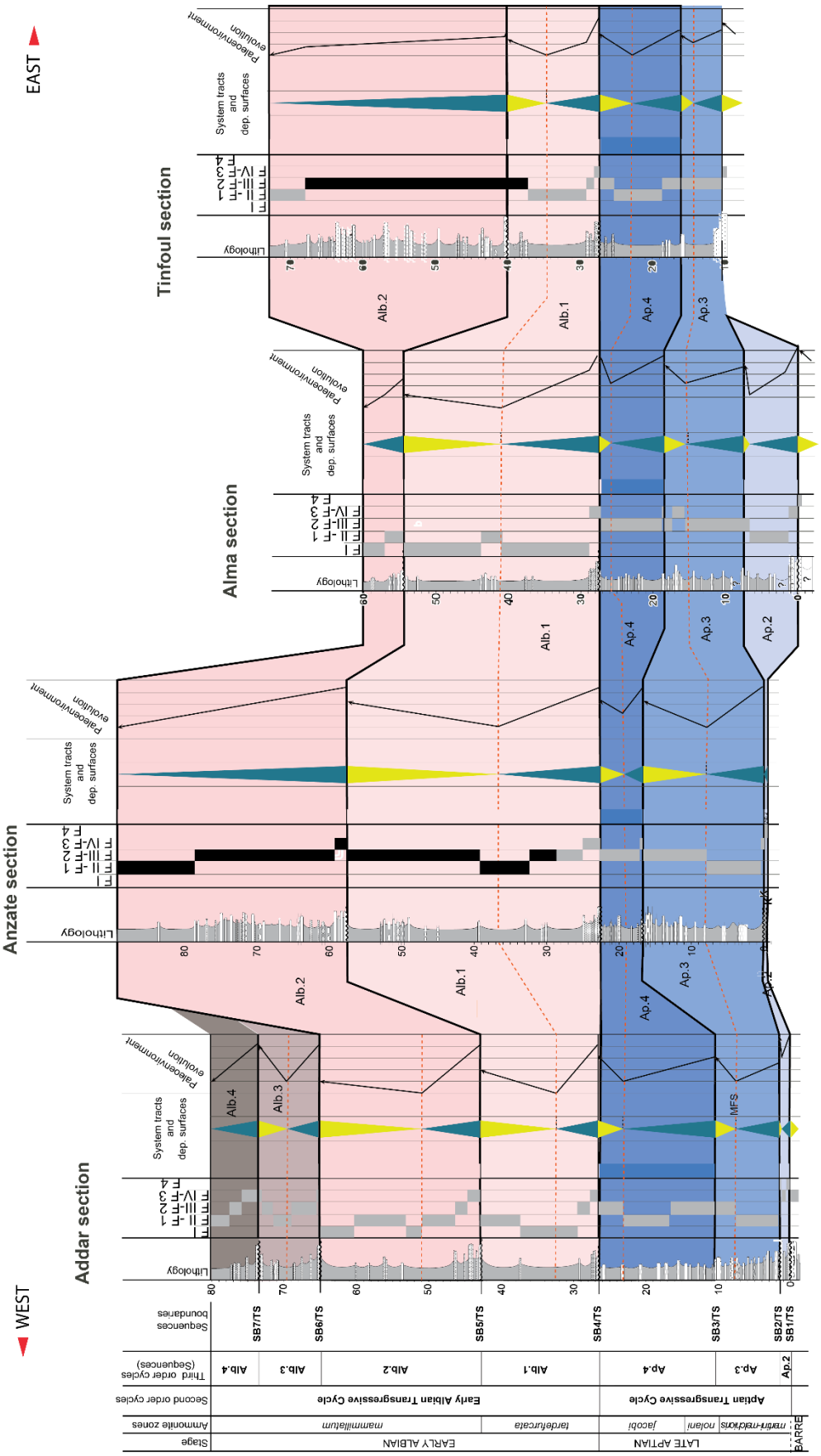

Figure 4.24: Correlation of the Aptian-Early Albian depositional sequences, along the West-East transect (Addar, Anzate, Alma, Tinfoul), in the southern part of EAB.

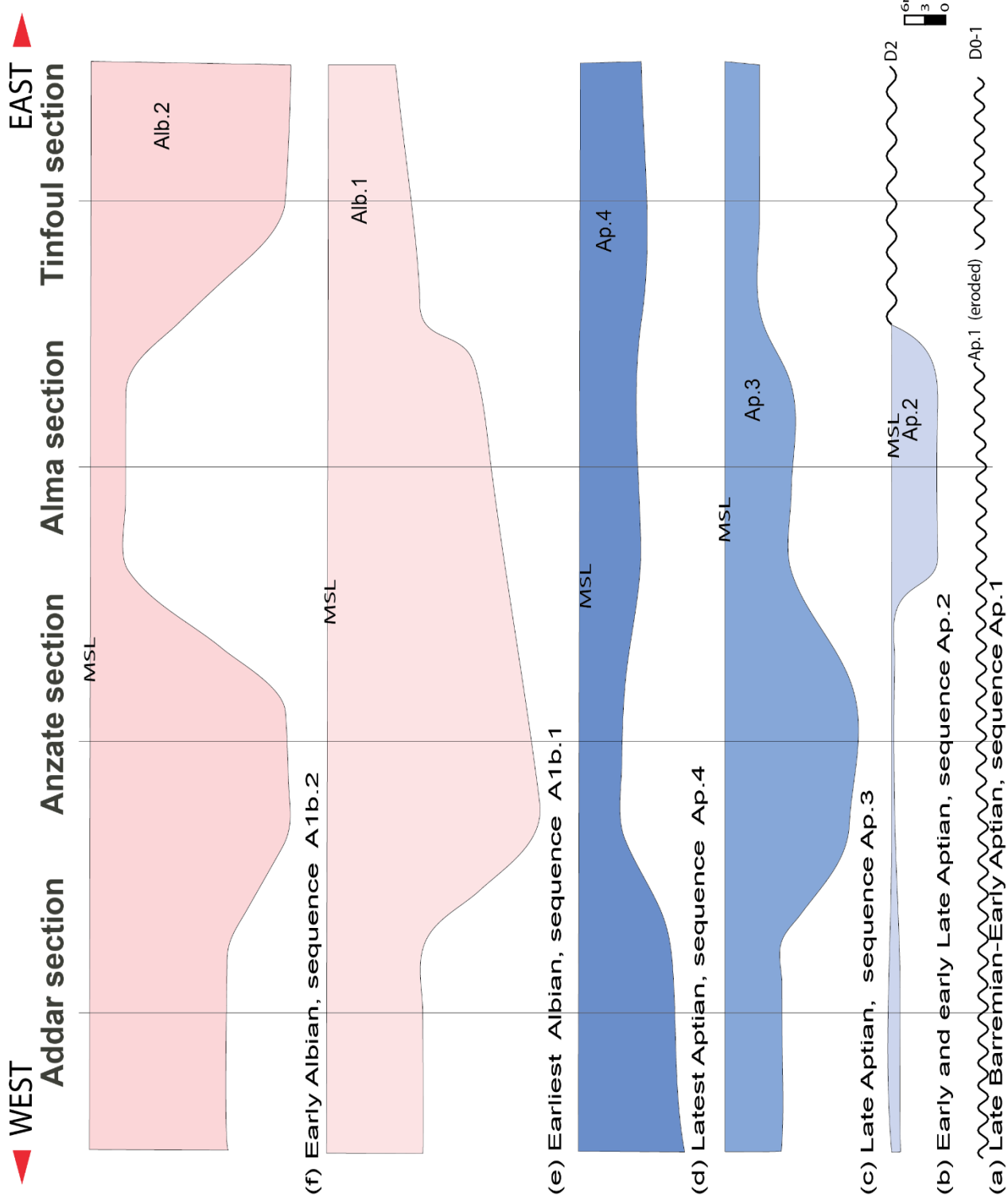

Figure 4.25: Thickness variations in the Aptian-Early Albian depositional sequences, along the West-East transect (Addar, Anzate, Alma, Tinfoul), in the southern part of EAB.

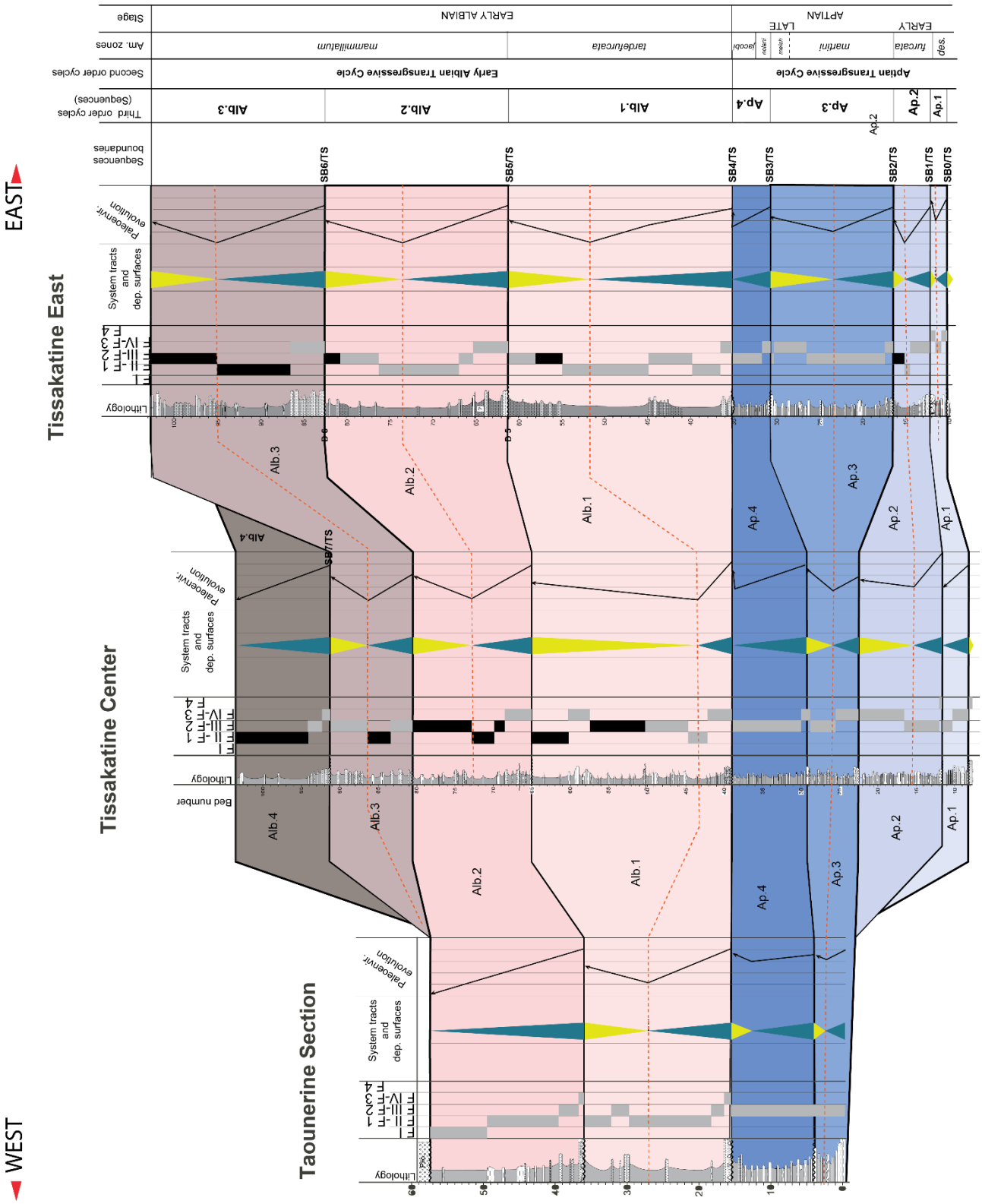

Figure 4.26: Correlation of the Aptian-Early Albian depositional sequences, along the West-East transect (Taounerine, Tissakatine Center, Tissakatine East sections), in the Central part of EAB.

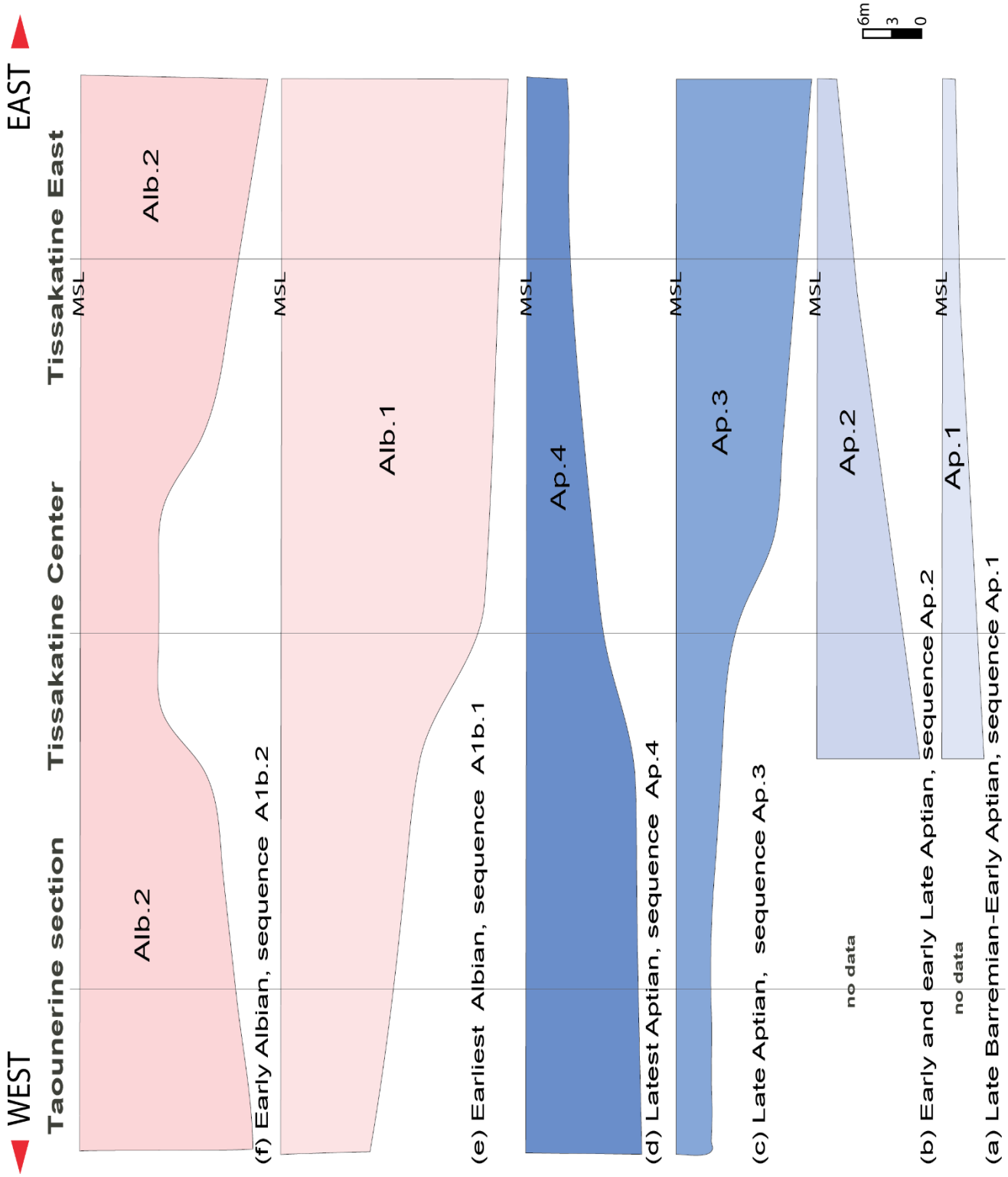

Figure 4.27: Thickness variations in the Aptian-Early Albian depositional sequences, along the West-East transect (Taounerine, Tissakatine Center, Tissakatine East sections), in the Central part of EAB.

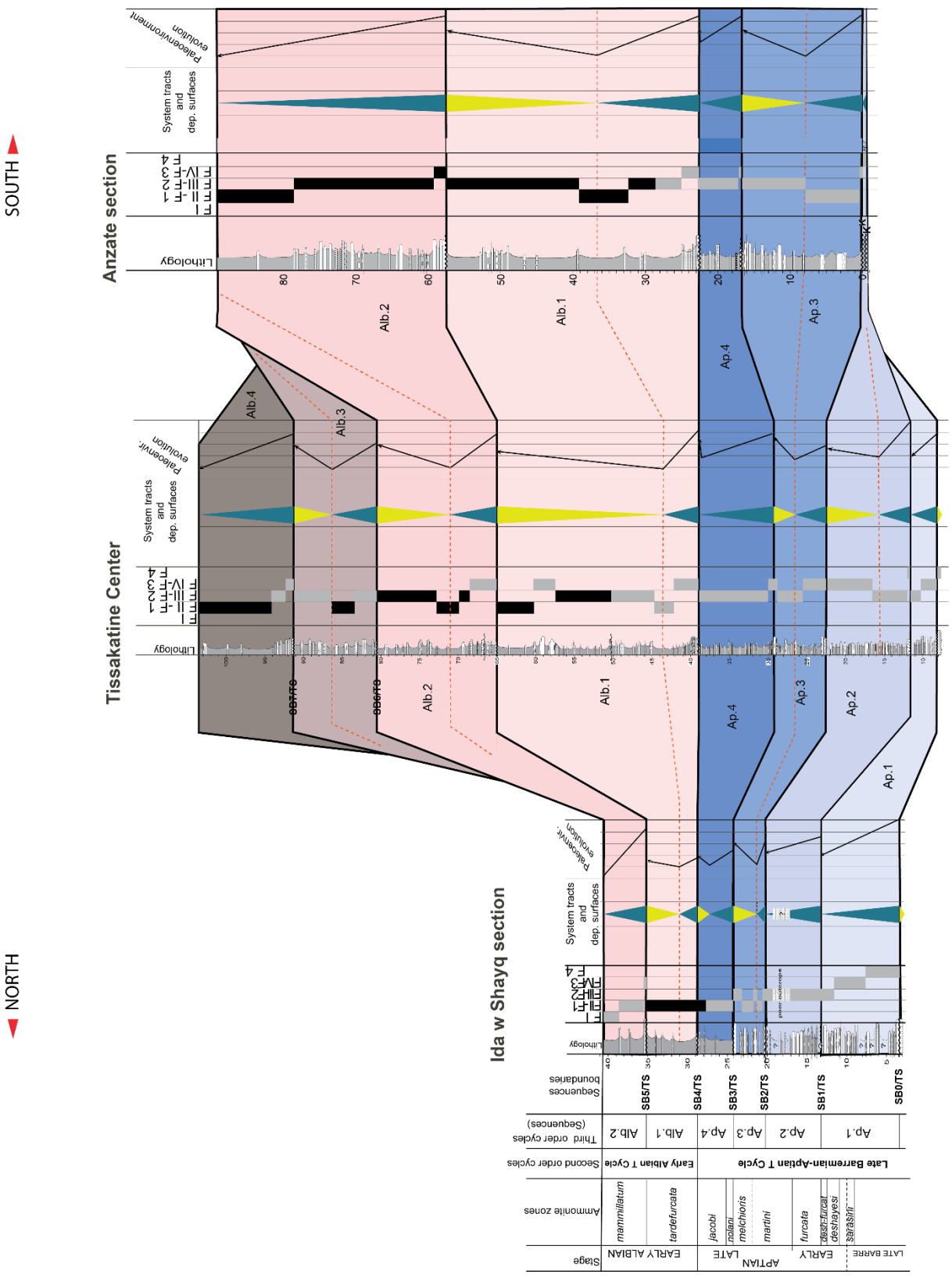

Figure 4.28: Correlation of the Aptian-Early Albian depositional sequences, along the North-South transect (Ida w Shayq, Tissakatine Center, Anzate sections), in EAB.

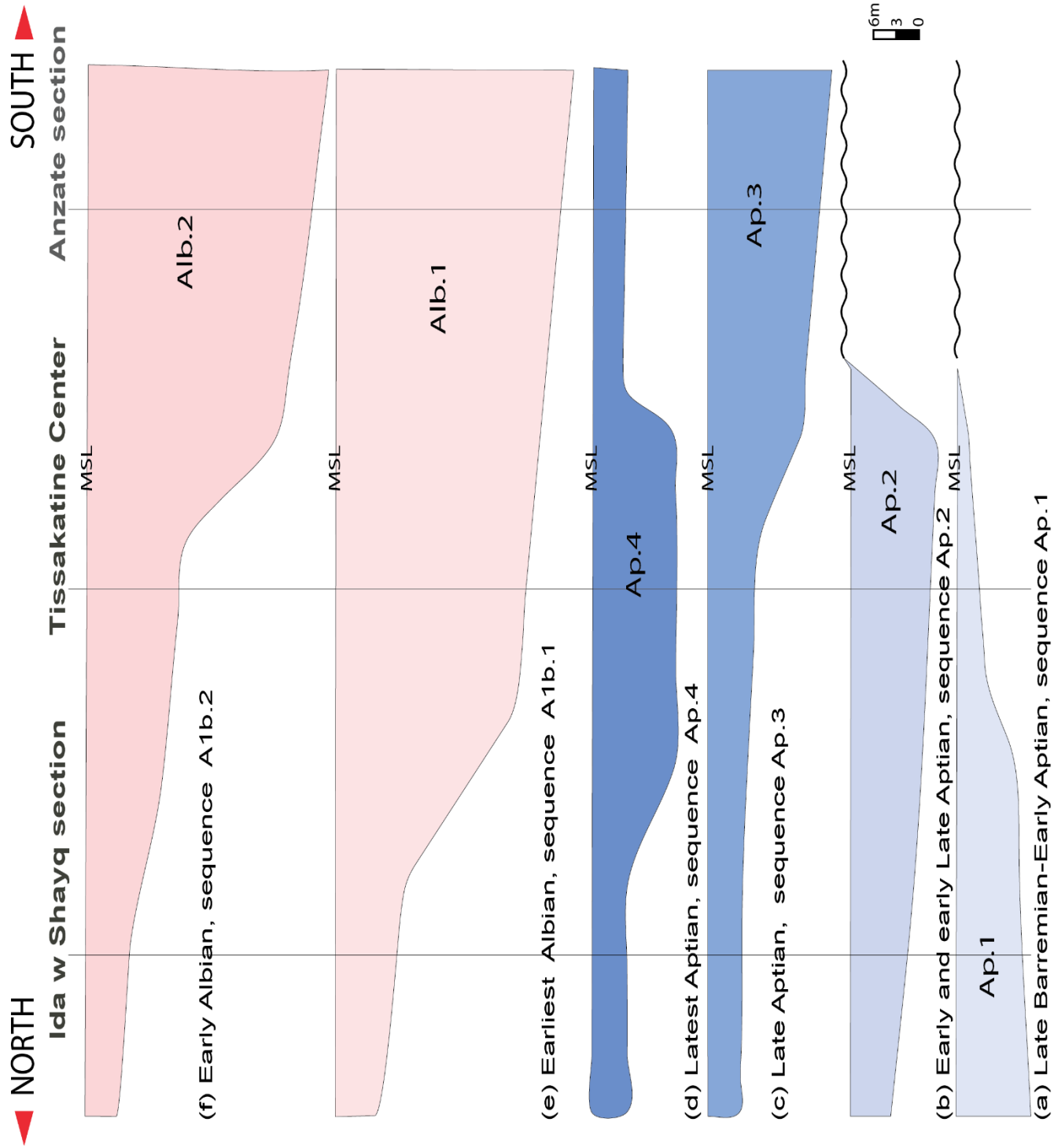

Figure 4.29: Thickness variations in the Aptian-Early Albian depositional sequences, along the North-South transect (Ida w Shayq, Tissakatine Center, Anzate sections), in EAB.

4. B.3.1. Late Barremian-Aptian Transgressive Cycle

The basal boundary of this cycle is SB0, a major karstified surface. This boundary encompasses a variable stratigraphic hiatus, the duration of which increases toward the proximal sections. Ammonites indicate that it occurred within the *sarasini* ammonite Zone of latest Barremian age in the distal section of Ida w Shayq, whereas it contains the Barremian/Aptian boundary in proximal sections. The vertical evolution of this cycle is visible in the central transect (Tissakatine sections) and along the north-south transect in the Ida w Shayq section (Figs. 4.26, 4.28). This cycle is composed of four third order sequences, and ends up with a significant sea level drop expressed by SB4, around the Aptian/Albian boundary (Figs. 4.24, 4.26, 4.28).

Sequence Ap.1 (Late Barremian and Early Aptian, *sarasini* to *deshayesi* ammonite zones)

Ap.1 is the first stage of development of the carbonate platform in the EAB, beginning with SB0. SB0 is a karstified surface in the sections located in the southern part of the EAB, reflecting subaerial exposure related to high topography; whereas it is an erosional surface, representing submarine hiatus in the central and northern parts of the EAB. In addition, the lack of sequence Ap.1 in the southern part of the EAB and its presence in the central (2 m in Tissakatine east, 3.5 m in Tissakatine Center) and northern parts of the EAB (10 m in Ida w Shayq section), indicate the presence of a topographic high in the southern part of the EAB during the Early Aptian (Fig. 4.29a). In the same way, the gradual northward increase in thickness of the Ap.1 sequence (landward-thinning wedge of sediments, filling the available accommodation space), indicates a northward dip of the platform (Fig. 4.29a). The recognition of the retrogradational TST of Ap.1 in the central and northern parts of the EAB, represented by inner to middle shelf facies, reflects deposition of Ap.1 under shallow depths during latest Barremian-earliest Aptian times.

Sequence Ap.2 (Early and early Late Aptian, *furcata* and lower part of *martini* ammonite zones)

The Ap.2 sequence starts with a karstified surface (SB1), representing subaerial exposure in the sections from the southern part of the EAB (Figs. 4.24, 4.25b). Ap.2 is very thin or is even lacking in the southern part of the basin. The presence of this sequence in the central and the northern parts (Figs. 4.26, 4.28) indicates that the southern part of the EAB was still a topographic high with no or little subsidence during deposition of Ap.2.

The lack of Ap.2 in the southern part of the EAB, and its occurrence in the central and northern parts, may indicate the presence of little syn-depositional tectonics. The variation in thickness of Ap.2 within the central and northern parts of the EAB, from 11 m at Tissakatine to 6 m at Ida w Shayq, indicates tilting of the central and northern parts toward the south, enhancing more accommodation space, with development of depocenter in the central part of the basin (Fig. 4.29b). The presence of shallow deposits (middle ramp) in the central part, and of deeper facies (outer ramp) in northern part of the basin (Ida w Shayq; Fig. 4.29), supports this interpretation.

On the other hand, facies of the Ap.2 sequence, which is composed of middle ramp to proximal outer ramp deposits, compared to the inner to middle ramp deposits of Ap.1, reflect a sea level rise from Early to early Late Aptian time.

Sequence Ap.3 (Late Aptian, upper *martini*, *melchioris* and lower *nolani* ammonite zones)

In the same way, the fact that SB2 is a karstified surface in the southern part of the EAB, and a submarine erosional surface in the central and northern parts of the basin, indicates the persistence of a little subsiding, southern high, linked to a northern depocenter (Ida w Shayq) by a northward dipping ramp before deposition of Sequence Ap.3 (Figs. 4.24-4.29).

In sequence Ap.3, the TST varies, along the southern, E-W transect of the EAB, between proximal outer shelf facies to the east (Tinfoul), and distal outer shelf facies to the west (Addar) (Fig. 4.24). Along the central transect, the TST changes from marly limestone facies, of proximal outer ramp environment in the Tissakatine sections into shales, of deeper environment at Taounerine (Fig. 4.26). Farther North, at Ida w Shayq, the TST of Ap.3 is represented by distal outer ramp/shelf environment (Fig. 4.28). The progradational HST deposits of Ap.3 vary

from middle shelf facies in the landward sections of Alma and Tissakatine east (Figs. 4.24, 4.26); to proximal, outer shelf facies in the basinward sections of Anzate, Taounerine, and Ida w Shayq (Figs. 4.24, 4.26, 4.28). The depocenter of the Ap.3 sequence is recorded in Anzate and in Tissakatine east, in the southern and central parts of the EAB. The abrupt changes of thickness of Ap.3, observed in all cross-sections in EAB, reflects the presence of local tectonics (Figs. 4.25c, 4.27c, 4.29c). However, the facies of the TST and HST of Ap.3 in the studied sections suggest a lower topographic contrast in the EAB, with respect to that present during deposition of sequences Ap.1 and Ap.2 (see Figs. 4.25, 4.27, 4.29). Finally, the TST(s) and HST(s) of Ap.3, of proximal to distal outer shelf/ramp facies, exhibit deeper depositional environments, when compared to the inner shelf/ramp and proximal outer shelf/ramp deposits of Ap.1 and Ap.2 sequences, reflecting continuous rise of sea level, and landward migration of the shoreline. Then, the sea level slightly lowered, culminating with SB3.

Sequence Ap.4 (latest Aptian, *nolani-jacobi* ammonite zones)

SB3, the lower boundary of Ap.4, is interpreted as an erosional submarine surface related to shelf submarine currents, suggesting that Ap.4 was deposited in deeper environment than the Ap.1, Ap.2 and Ap.3 sequences. This suggests that SB3 recorded a significant rise of sea level during deposition of Ap.4.

The lateral facies changes are recorded in Ap.4, along the southern, E-W transect in the EAB. There, the TST of Ap.4 varies from middle to proximal outer shelf facies toward the East (Alma and Anzate) to proximal/distal outer shelf facies to the West (Addar) (Fig. 4.24). In the central part of the basin, the TST is mainly represented by proximal outer shelf facies, while it is made of distal outer shelf deposits in the northern section of Ida w Shayq (Figs. 4. 26, 4.28), reflecting a deeper depositional environment toward the North. The HST of sequence Ap.4 is marked by proximal outer shelf facies in all studied section (Figs. 4.24, 4.26, 4.28). The variation in thickness of Ap.4 along the southern, central and north-south transects (Figs. 4.25d, 4.27d, 4.29d), reflects continuity of local tectonics in latest Aptian time.

The increase of shales and shaly marl facies of outer shelf environment, in the TST of sequence Ap.4, relatively to its equivalents of sequences Ap.1, Ap.2 and Ap.3, supports the

interpretation of a deeper depositional environment in sequence Ap.4. Consequently, it suggests a continuous sea level rise during latest Aptian time.

4. B.3.2. Early Albian Transgressive Cycle

The base of this cycle is marked by SB4, a major submarine erosional surface, which represents a drastic sea level drop at the Aptian/Albian boundary. The Early Albian succession is dominated by shale of outer shelf to basinal environment, reflecting deeper environments with respect to the Aptian ones (Fig. 4.30). This cycle consists of four relatively similar depositional sequences.

Sequence Alb.1 (earliest Albian, *tardefurcata* ammonite Zone)

The strong submarine erosion of SB4, the probable lack of the base of the *tardefurcata* ammonite Zone, and the current features in the yellow sandstone facies at the base of the Alb.1 TST, suggest a drastic sea level drop at the Aptian/Albian boundary, followed by a new transgression.

The Early Albian transgression starts with the deposition of Alb.1. Along the southern part of the EAB, the depositional environments of the TST vary from outer shelf to basinal (Fig. 4.24). They show distal outer shelf facies in the central part of EAB (Tissakatine-Taounerine; Fig. 4.26); and restricted distal outer shelf facies in the Ida w Shayq section (Fig. 4. 28). Then, the aggradational HST of sequence Alb.1, vary in the southern part of the basin, from proximal to distal outer shelf facies, from east to west (Fig. 4.24). Moreover, Tissakatine and Taounerine are marked by proximal outer shelf facies (Fig. 4.26), while Ida w Shayq exhibits distal outer shelf/ramp facies in the northern part of the basin (Fig. 4. 28).

Finally, after drastic drop at the Aptian/Albian boundary, the Alb.1 sequence presents deeper environments than their counterparts of sequence Ap.4, reflecting a second phase of sea level rise. This suggests an extension and enlargement of the EAB, and a probable onlap of the Early Albian deposits along the E-W and N-S transects.

Sequence Alb.2 (Early Albian, *mammillatum* ammonite Zone)

As in all Albian sequences in EAB, the sequence Alb.2 starts with the submarine erosional surface SB5, associated with strong submarine currents, reflecting a stratigraphic hiatus; it is followed by the TST, which shows distal outer shelf facies in the eastern sections (Tinfoul, Anzate) and basinal facies in the western and northern sections (Addar, Taounerine, Ida w Shayq; Figs. 4.24, 4.26, 4.28). Then, the HST of Alb.2 is represented by proximal outer shelf facies in the Tissakatine sections.

The Early Albian sequences Alb.3 and Alb.4, are only defined in the Addar and Tissakatine sections (Figs. 4.24, 4.26, 4.28). They are dated as within the *mammillatum* ammonite Zone. These sequences resemble the Alb.1 and Alb.2 sequences, reflecting the similar depositional environments and comparable conditions.

4. B.4. Factors controlling sedimentation during Aptian-Albian times in EAB

The drastic change in facies, from carbonate dominated in Aptian, to shale dominated in Early Albian, the abrupt change from small thicknesses during the Aptian, to large thicknesses in the Early Albian ones, as well as, the change of depocenters in space and time from the northern part of the basin in the Early and Late Aptian to the southern part in the Late Aptian-Early Albian (Fig. 4.31), reflect a major change in the external and internal factors controlling the sedimentation processes. Aptian successions are marked by deposits of reduced thickness, carbonate dominated facies of shallow marine environment, reflecting little accommodation space and slow sea level rise, supported by the occurrence of periods of subaerial exposure during Early Aptian time. Conversely, Early Albian times are marked by thicker sediment accumulation, detrital dominated facies, deeper marine environments indicating creation of accommodation space and rapid sea level rise. This inflection in sedimentation is documented when comparing the facies forming the TSTs and HSTs of both Ap.4 and Alb.1 in the EAB (Figs. 4.24: 4.29). This is probably related to a sea level rise during the Early Albian, supported by development of deeper, oxygen depleted, pelagic deposits, of basinal setting. The spatial variation of thickness and the migration of the depocenters through Aptian-Early Albian times could be due to salt tectonics occurring in subsurface. As a matter of fact, Hafid (2000, 2006)

and Tari and Jabour (2013) described active salt diapirs in subsurface, offshore of the EAB (Fig. 4.32). In the same way, Bertotti and Gouiza (2012) recognized syn-sedimentary deformations associated with salt diapirs in outcrops, north of the study area (Fig. 4.32). Therefore, we suspect that salt tectonics played a role in the migration of the depocenters, although we did not recognize any syn-sedimentary faults, nor outcrops of salt diapirs in the study area.

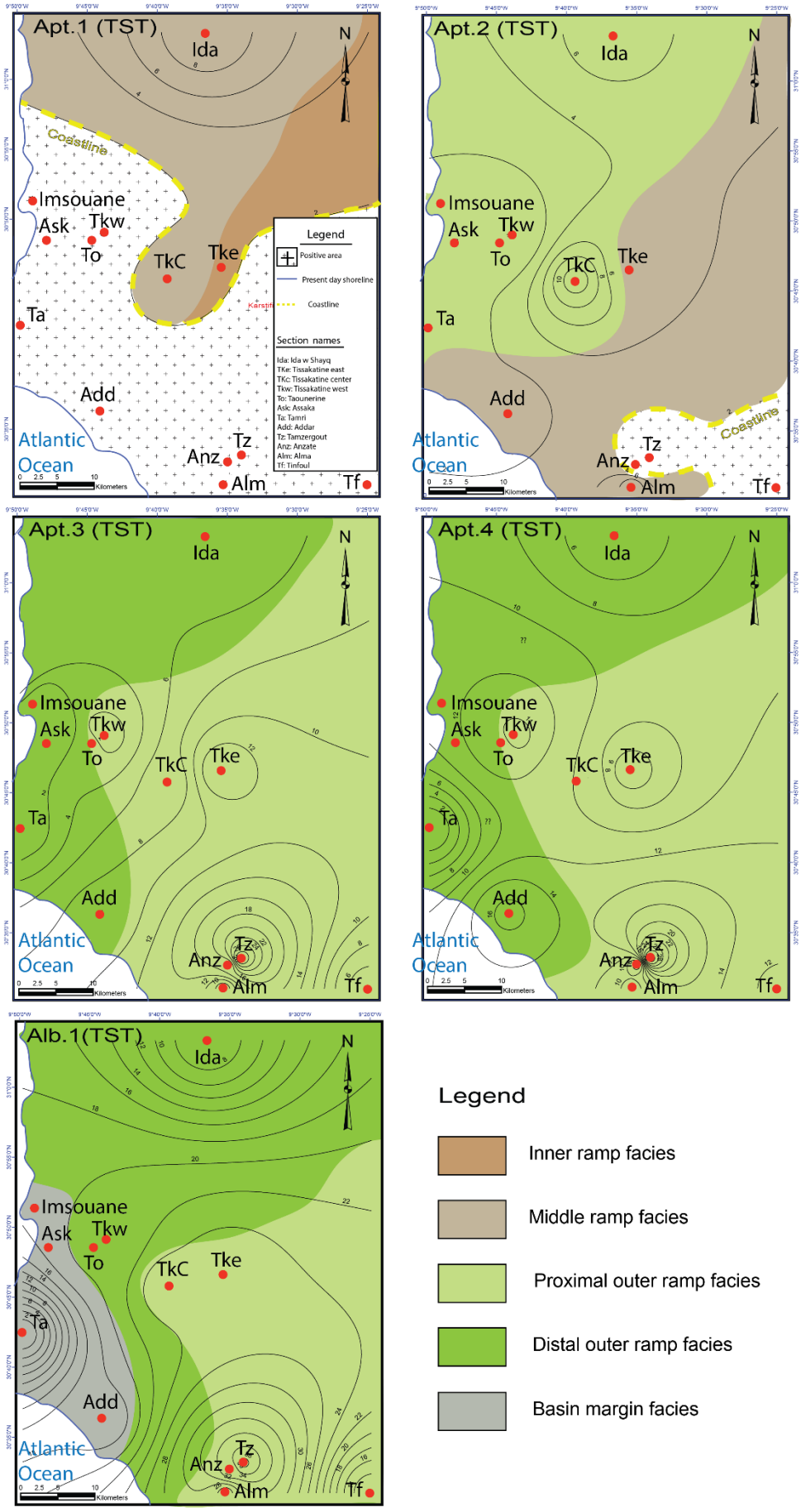

Figure 4.30: Facies maps of the TST(s) of Aptian and Earliest Albian depositional sequences showing the deepening upward trend and the continuous sea level rise through Late Aptian and Early Albian times.

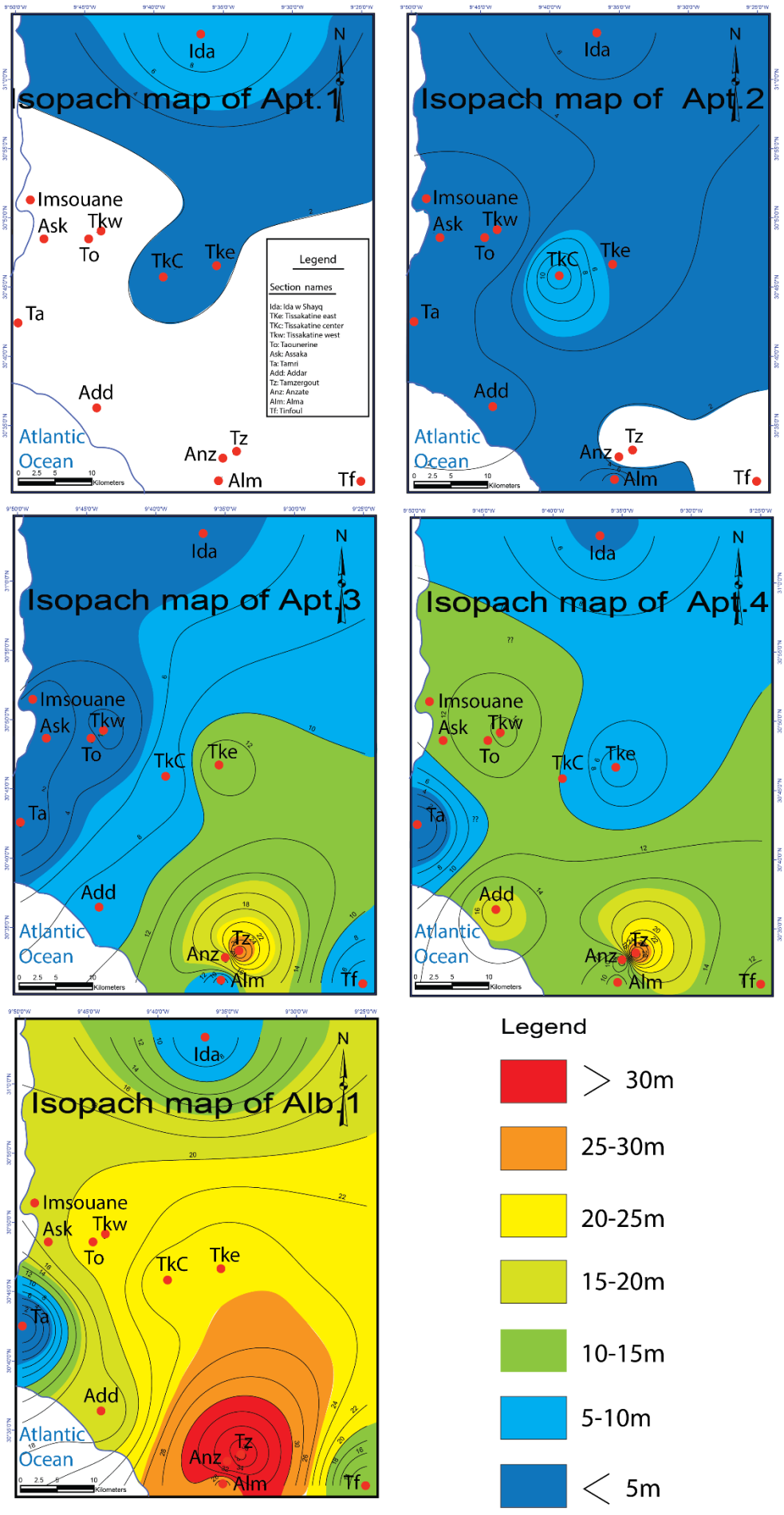

Figure 4.31: Isopach maps of the Aptian and Earliest Albian sequences showing the migration of the depocenters from the northern part of the basin in the Aptian to the southern part in Early Albian times.

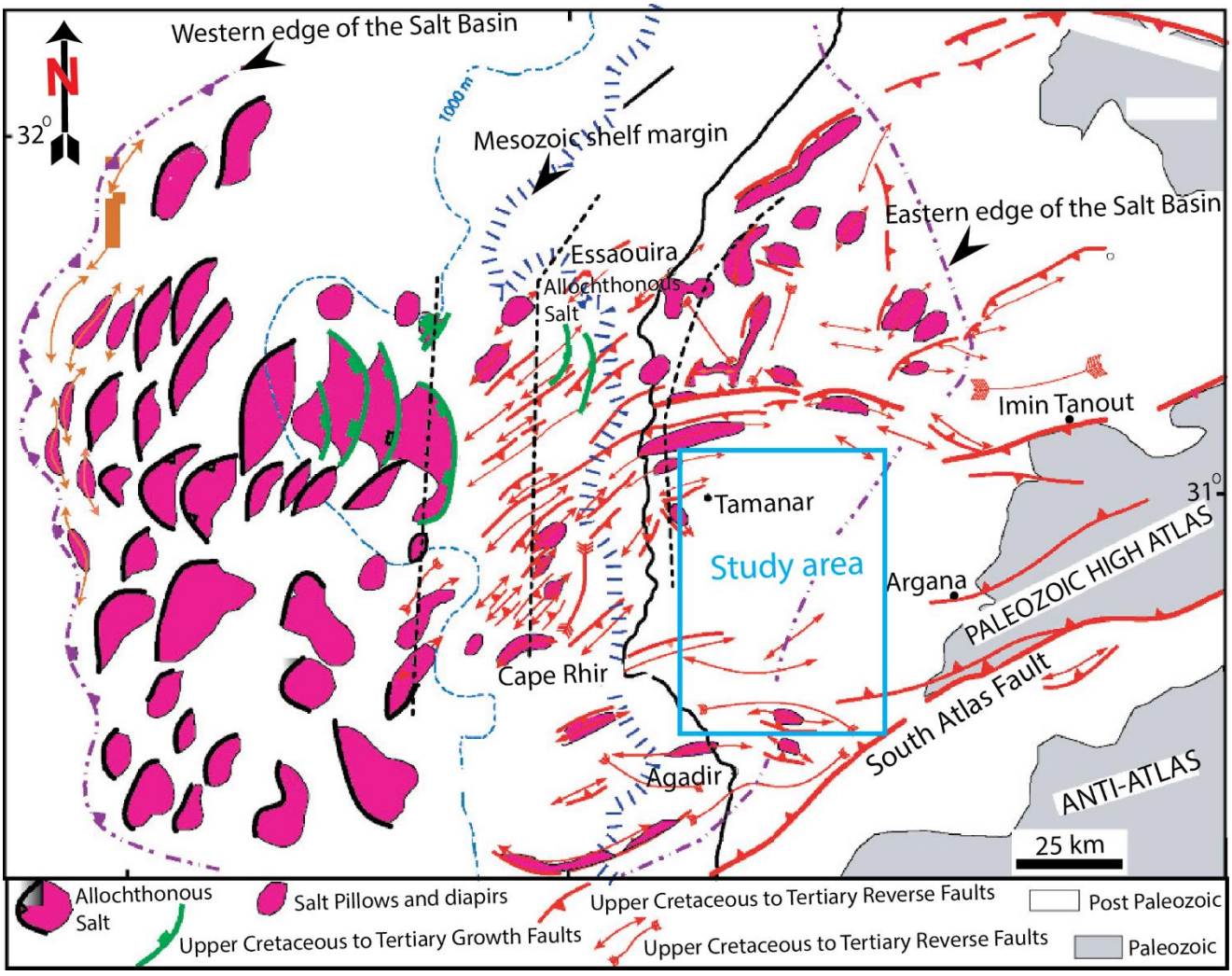

Figure 4.32: Shows the occurrence of salts diapirs in and around the EAB: offshore (west of the study area in subsurface) and onshore (outcrops north of the study area).

CHAPTER FOUR

4. PALEOENVIRONMENTAL EVOLUTION IN THE EAB

PART (C): CALCIUM CARBONATE CONTENT AND CALCAREOUS NANNOFOSSILS

4. C. CALCIUM CARBONATE CONTENT AND CALCAREOUS NANNOFOSSILS

4. C.1. Methodology

The calcium carbonate content was measured in 139 samples of the four sections, and determined using the carbonate bomb technique (Müller and Gastner 1971), which measures CO_2 pressure during a hydrochloric acid attack. For the calculation of the calcium carbonate percent, see Appendix A in Peybernes et al. (2013).

Samples for nannofossil studies were prepared using the random settling technique of Geisen et al. (1999), a method adapted from Beaufort (1991) allowing the calculation of absolute abundances (number of specimens per gram of rock). Nannofossils were observed using light polarizing microscope, at 1560 X magnification. In the richest samples, 500 specimens were generally counted in a variable number of fields of view. In the poorest samples, 150 to 300 specimens were counted following different longitudinal transverses. All nannofossils with at least more than half of the specimen preserved have been counted. The taxonomic frameworks of Perch-Nielsen (1985) and Burnett et al. (*in* Bown, 1998) were followed. Both absolute and relative abundances of each species were also calculated for each sample. In these calculations, *Nannoconus* spp. are excluded from the total sum of nannofossils because of their uncertain biological affinity (Aubry et al., 2005). Species richness, Shannon Diversity Index and evenness (defined by Shannon and Weaver, 1949) have been also calculated. *Nannoconus* are excluded from these calculations as explained before. The calcareous nannofossil preservation was evaluated following the classes defined by Roth (1983). Countings are given in Appendix A.

4. C.2. Results

Along the north-south transect, the preservation of calcareous nannofossils varies from poor to good in the Tissakatine Center and Ida w Shayq sections (Figs. 4.33, 4.34). The means of nannofossil total absolute abundance (4.3 x 10^8), species richness (26), diversity (3) and evenness (0.7) are higher in Tissakatine Center than in the Ida w Shayq section (3.5 x 10^8, 25, 2.7, and 0.58, respectively). However, in the Early Albian, upper part of the sections (above D4), the means of species richness (32), diversity (3.5) and evenness (0.7) are higher in Ida w Shayq than in Tissakatine Center (27, 3.25, and 0.68, respectively), while the mean of nannofossil total absolute abundance is comparable (3.4 x 10^8) in both sections.

Along the east-west transect, the preservation of calcareous nannofossils varies from poor to good in the Anzate and Tinfoul sections (Figs. 4.35, 4.36). The means of nannofossil total absolute abundance, species richness, diversity and evenness are higher (1.8×10^8, 31.1, 3.8, and 0.74) in Anzate than in Tinfoul (1.3×10^8, 29, 3.3, and 0.68).

The nannofossil total assemblages for all sections are composed of 93 species (selected taxa, composing of the marker species are illustrated in Plates 4.10 and 4.11). Fourteen species or group of species represent about 90 % of the total assemblage and display important abundance fluctuations (Figs. 4.37, 4.38, 4.39, 4.40). Some taxa exhibiting similar morphology or same ecological preferences have been grouped. The *Biscutum* spp. group includes *B. constans* and *B. ellipticum*, since they belong to the same morphological continuum as mentioned by Bornemann and Mutterlose (2006). The *Cretarhabdus* group includes all species of the genera *Cretarhabdus* and *Retecapsa* (Roth and Krumbach, 1986; Watkins, 1989; Street and Bown, 2000). *Rhagodiscus* spp. includes *R. achlyostaurion* and *R. asper*, which present the same paleoecological affinities (Crux, 1991; Eleson and Bralower, 2005). *Seribiscutum* spp. includes *S. gaultensis* and *S. primitivum* (Mutterlose, 1992b). *Watznaueria barnesiae* and *W. fossacincta* are lumped together because they are believed to represent end-members of a morphological continuum (Lees et al., 2004, 2006; Bornemann and Mutterlose, 2006). *Staurolithites* spp. includes all species of the genus *Staurolithites* (Eleson and Bralower, 2005). All zeugrhabdotids (including *Z. erectus*) with major axis smaller than 5 µm are combined under small *Zeugrhabdotus* spp. (Erba et al., 1992). The other species that contribute significantly to the assemblage are *Discorhabdus rotatorius, Hayesites irregularis, Lithraphidites carniolensis, Repagulum parvidentatum, Watznaueria communis,* and *Zeugrhabdotus diplogrammus.* Nannoconids are grouped into *Nannoconus* spp.

Plate 4.10: Selected nannofossil taxa

Family Chiastozygaceae Rood et al., 1973 emend. Varol & Girgis, 1994.

1, *Staurolithites gausorhethium* (Hill, 1976) Varol & Girgis, 1994, XPL, TF 14, Early Albian.

2, *Staurolithites mutterlosei* Crux, 1989, XPL, ANZ 4, Early Albian.

3, *Staurolithites siesseri* Bown in Kennedy et al., 2000, XPL, TF 7, Late Aptian.

4, 5, *Tranolithus gabalus* Stover, 1966. 4, XPL, ANZ 4, Early Albian; 5, as 4, TF 2.

6-8, *Zeugrhabdotus bicrescenticus* (Stover, 1966) Burnett in Gale et al., 1996. 6, XPL, ANZ 4, Early Albian; 7, as 6, TF 2, Late Aptian;7, TF7, Late Aptian; 8 as 7, TF 24, Early Albian.

9, *Zeugrhabdotus diplogrammus* (Deflandre, in Deflandre & Fert, 1954) Burnett, in Gale et al., 1996, XPL, TF6, Late Aptian.

10, 11, *Zeugrhabdotus embergeri* (Noël, 1958) Perch-Nielsen, 1984. 10, XPL, ANZ 1, Early Albian; 11, as 10, TF 7, Late Aptian.

12, *Zeugrhabdotus noeliae* Rood et al., 1971, XPL, ANZ 4, Early Albian.

13, *Zeugrhabdotus scutula* (Bergen, 1994) Rutledge and Bown, 1996, XPL, TF 7.

14, *Zeugrhabdotus streetiae* Bown in Kennedy et al. 2000, XPL, ANZ 1, Early Albian.

15, *Zeugrhabdotus trivectis* Bergen, 1994, XPL, TF 10, Early Albian.

16, 17, *Zeugrhabdotus xenotus* (Stover, 1966) Burnett in Gale et al., 1996.16, XPL, ANZ 4, Early Albian;17, as 16, TF 2, Late Aptian.

Family Eiffellithaceae Reinhardt, 1965.

18-20, *Helicolithus trabeculatus* (Gorka, 1957) Verbeek, 1977. 18, XPL, ANZ 1; 19, as 18, ANZ 4; 20 as 18, ANZ 4, Early Albian.

21, *Eiffelithus hancockii* Burnett, 1998, XPL, TF2, Late Aptian.

Family Rhagodiscaceae Hay, 1977.

22, 23, *Percivalia fenestrata* (Worsley, 1971) Wise, 1983. 22, XPL, TF 2. ; 23, as 22, TF 12, Early Albian.

24, *Rhagodiscus achylostaurion* (Hill, 1976) Doeven, 1983, XPL, TF 7, Late Aptian.

25, *Rhagodiscus angustus* (Stradner, 1963) Reinhardt, 1971, XPL, ANZ 4, Early Albian.

26-28, *Rhagodiscus asper* (Stradner, 1963) Reinhardt, 1967. 26, XPL, ANZ 4, Early Albian; 27, as 26, TF 2; 28 as 26, TF4, Late Aptian.

29, *Rhagodiscus gallagheri* Rutledge & Bown, 1996, XPL, TF 16, Early Albian.

Family Stephanolithiaceae Black, 1968.

30, *Cylindratus nudus* Bukry, 1969, XPL, TF 12, Early Albian.

31, *Stoverius achylosus* (Stover, 1966) Perch-Nielsen, 1986, XPL, ANZ 4, Early Albian.

Family Arkhangelskiellaceae Bukry, 1969 emend. Bown & Hampton, in Bown & Young, 1997.

32, *Broinsonia signata* (Noël, 1969) Noël, 1970, XPL, TF4, Late Aptian.

33, *Broinsonia stenostaurion* Hill, 1976, XPL, TF10, Early Albian.

Family Biscutaceae Black, 1971a.

34, 35, *Biscutum ellipticum* (Gorka, 1957) Grün in Grün and Allemann, 1975. 34, XPL, ANZ 4. ; 35, as 34, ANZ 4, Early Albian.

36, 37, *Discorhabdus rotatorius* (Bukry, 1969) Thierstein, 1973. 36, XPL, TF 2. ; 37, as 36, TF 14, Early Albian.

38, *Seribiscutum gaultensis* Mutterlose, 1992, XPL, ANZ 4, Early Albian.

39, *Seribiscutum primi*tivum (Thierstein, 1974) Filewicz et al., in Wise and Wind, 1977, XPL, TF 2, Late Aptian.

Family Cretarhabdaceae Thierstein, 1973.

40, *Cretarhabdus striatus* (Stradner, 1963) Black, 1973, XPL, TF 2, Late Aptian.

41, 42, *Flabellites oblongus* (Bukry, 1969) Crux, in Crux et al. (1982). 41, XPL, ANZ 4. ; 42, as 41, TF 10, all specimens Early Albian.

The bar scale that illustrated below each image is 2 μm. The bar scale may vary from image to image during the enlargement process. Specimen orientation reflects the original position on the microscope stage.

Plate 4.10: Selected nannofossil taxa

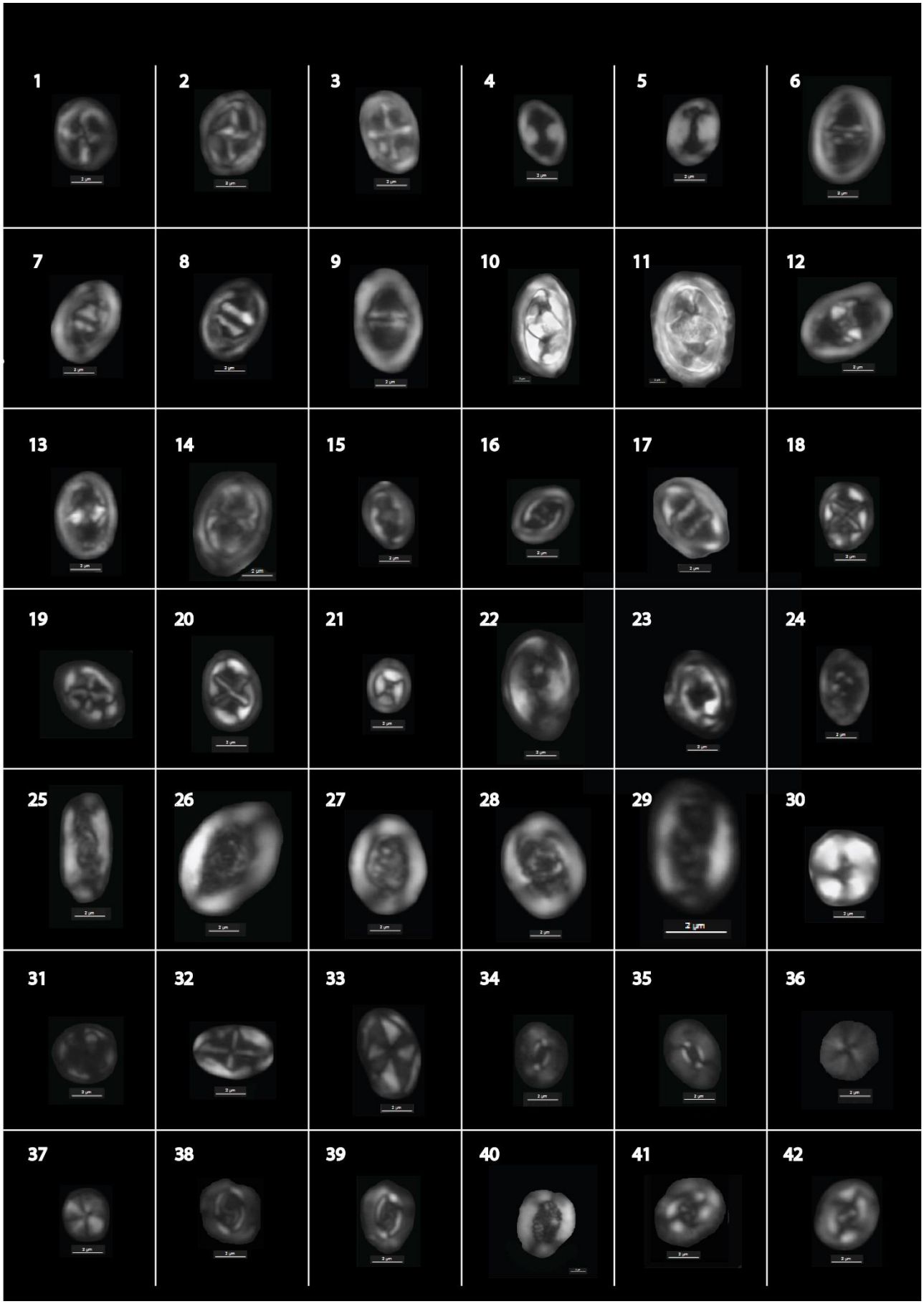

Plate 4.11: Selected nannofossil taxa

Family Cretarhabdaceae Thierstein, 1973.

1, *Helenea chiasta* Worsley, 1971, XPL, ANZ 1, Early Albian.

2, *Repagulum parvidentatum* (Deflandre and Fert, 1954) Forchheimer, 1972, XPL, ANZ 4, Early Albian.

Family Prediscosphaeraceae Rood et al., 1971.

3–6, *Prediscosphaera columnata* (Stover, 1966) Perch-Nielsen, 1984. 3, 4, circular form, XPL, ANZ4, Early Albian; 5, as 3, 4, TF7; 6, subcircular, XPL, TF 7, Late Aptian.

7, 8, *Prediscosphaera spinosa* (Bramlette & Martini, 1964) Gartner, 1968. 7, XPL, ANZ 4, Early Albian; 8, as 7, TF2, Late Aptian.

Family Tubodiscaceae Bown and Rutledge in Bown and Young, 1997.

9, *Tubodiscus burnettiae* Bown in Kennedy et al., 2000, XPL, TF 8, Late Aptian.

Family Watznaueriaceae Rood et al., 1971.

10, *Cyclagelosphaera reinhardtii* (Perch-Nielsen, 1968) Romein, 1977, XPL, TF 11, Early Albian.

11, *Watznaueria barnesiae* (Black in Black and Barnes, 1959) Perch-Nielsen, 1968, XPL, ANZ 1, Early Albian.

12, 13, *Watznaueria communis* Reinhardt, 1964. 12, XPL, ANZ 4, Early Albian; 13, as 12, TF4, Late Aptian.

14, *Watznaueria ovata* Bukry, 1969, XPL, TF 7, Late Aptian.

Holococcoliths: Family Calyptrosphaeraceae Boudreaux & Hay, 1969.

15, *Orastrum partitum* Varol in Al-Rifaiy et al. 1990, XPL, TF 12, Early Albian.

16, 17, *Orastrum perspicuum* Varol in Al-Rifaiy et al. 1990. 16, XPL, TF 7; 17, as 16, TF12, all specimens Early Albian.

Nannoliths: Family Braarudosphaeraceae Deflandre, 1947.

18, *Braarudosphaera hockwoldensis* Black, 1973, XPL, ANZ 1, Early Albian.

19, *Micrantholithus hoschulzii* (Reinhardt, 1966) Thierstein, 1971; PPL, IDM 19, Early Albian.

Family Microrhabdulaceae Deflandre, 1963.

20, *Lithraphidites carniolensis* Deflandre, 1963, XPL, ANZ 4, Early Albian.

Family Nannoconaceae Deflandre, 1959.

21, *Nannoconus circularis* Deres and Achéritéguy, 1980, PPL, IDM 9, Early Aptian.

22, 23, *Nannoconus quadriangulus apertus* Deflandre & Deflandre-Rigaud 1962. 22, XPL, TF 11; 23 as 22, TF12, all specimens Early Albian.

24, *Nannoconus quadriangulus quadriangulus* Deflandre & Deflandre-Rigaud, 1962, XPL, TF 11, Early Albian.

25, *Nannoconus truitti rectangularis* Deres and Achéritéguy, 1980, XPL, TF 11, Early Albian.

26, *Nannoconus truitti truitti* Brönnimann, 1955, XPL, TF 11, Early Albian.

27, *Nannoconus vocontiensis* Deres & Ache´rite´guy, 1980, PPL, IDM 9, Early Aptian.

28, *Nannoconus wassallii* Brönnimann, 1955, PPL, IDM 11, Early Aptian.

Family Polycyclolithaceae Forchheimer, 1972.

29-31, *Eprolithus floralis* (Stradner, 1962) Stover, 1966. 29, XPL, ANZ 1; 30, as 29, TF10; 31, as 29, XPL, TF 16, all specimens Early Albian.

32, *Radiolithus planus* Stover, 1966, XPL, TF 16, Early Albian.

33, *Assipetra infracretacea* (Thierstein, 1973) Roth, 1973, XPL, TF 4, Late Aptian.

34, 35, *Rucinolithus terebrodentarius* (Applegate et al. in Covington and Wise, 1987), Rutledge and Bergen in Bergen, 1994, youngii Tremolada and Erba, 2002, emend, 34, XPL, TF 20, Early Albian; 35, PPL, IDM 13, Late Aptian.

36-39, *Hayesites albiensis* Manivit, 1971. 36, XPL, ANZ1; 37, XPL, ANZ 4; 38. PPL, ANZ 4; 39 as 36, 37, TF16, all specimens Early Albian.

40-42, *Hayesites irregularis* (Thierstein in Roth and Thierstein, 1972) Applegate, et al., in Covington and Wise, 1987). 40, regular-rayed specimen but >6 rays, XPL, ANZ1, Early Albian; 41, relatively regular ray distribution, 7 rays, XPL,TF 2, Late Aptian; 42, irregularly developed rays, 8 rays, XPL, TF 4, Late Aptian.

Plate 4.11: Selected nannofossil taxa

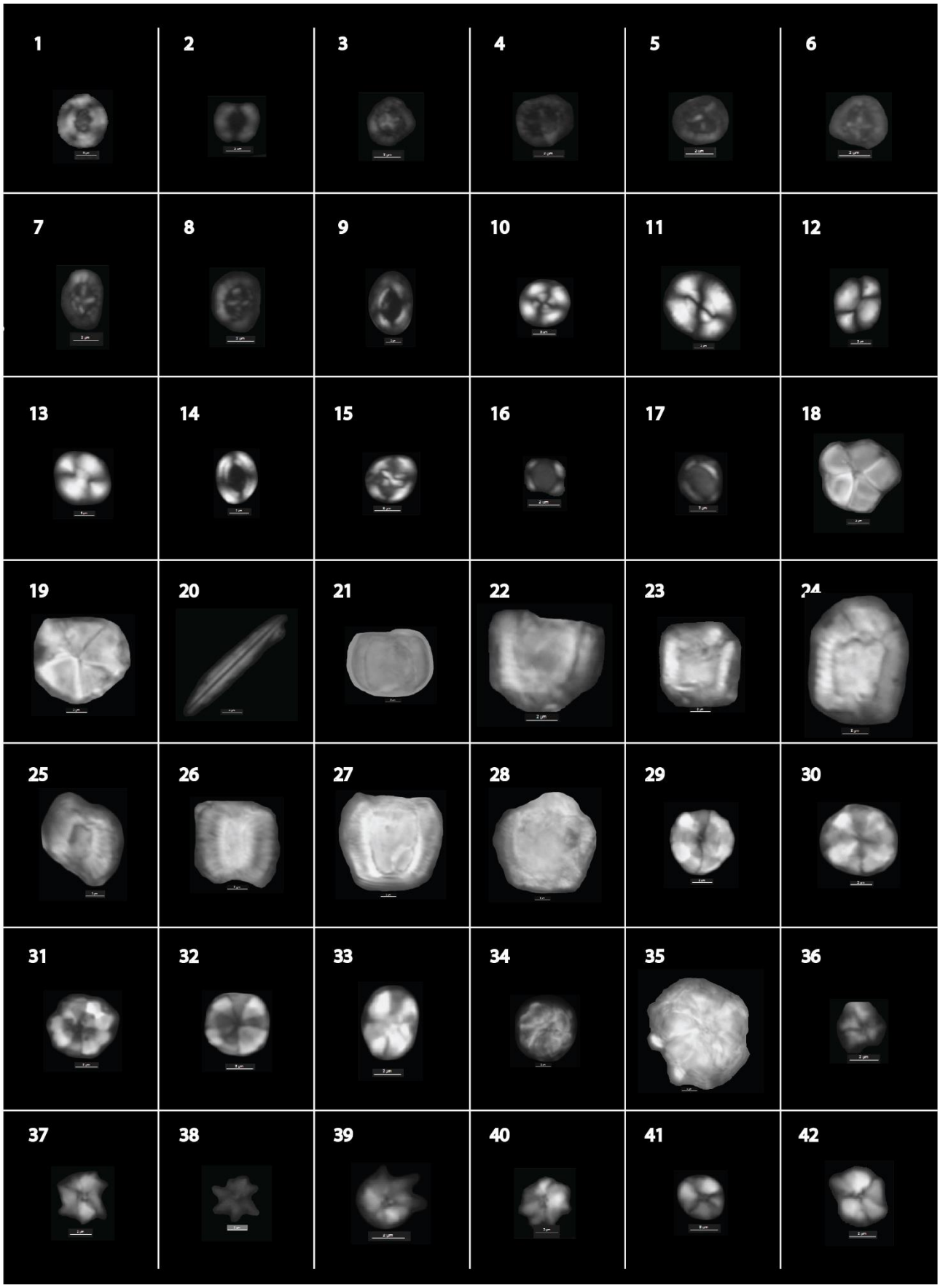

4. C.2.1. The Ida w Shayq section

The carbonate content was measured in thirty-six samples. It varies from 13 to 89% with an average of 53.8% during Aptian-Early Albian times (Fig. 4.33). Highest values are recorded in the Aptian, up to the sedimentary discontinuity D3. Above D3, the calcium carbonate sharply decreases and stays constant before to reach a minimum value above D5; then it slightly increases at the top of the succession.

Nannofossil analysis was carried out in the same samples selected for both geochemistry and calcium carbonate content. The preservation varies from poor to good (Fig. 4.33). Five samples display well-preserved nannofossils with slight etching and overgrowth (categories E1 and O1), located in the upper part of the section, above D3. Seventeen samples display moderately etched and overgrown nannofossils (categories E2 and O2), positioned in the upper two-thirds of the section. Fourteen samples show moderately to strongly both etched and overgrown nannofossils (categories E2 or E3 and O3), mostly distributed in the lower part of the section. The nannofossil total absolute abundance ranges from 7.8×10^6 to 1.6×10^9 specimens per gram of sediments (Fig. 4.33). In the lower part of the Ida w Shayq section, until above D1, the nannofossil total absolute abundance is very low and corresponds to badly preserved samples. Higher values with respect to the base and the uppermost part of the succession are reached in the interval from below D2 up to D4 (Fig. 4.33). Species richness is comprised between 2 and 40 (Fig. 4.33). The Shannon index and evenness range from 0.22 to 4.14, and 0.126 to 0.97, respectively. The species richness, Shannon index and evenness are generally higher in the shale rich upper part of the section (above D3), than in the carbonate rich lower part, where poorly preserved samples are observed (Fig. 4.33).

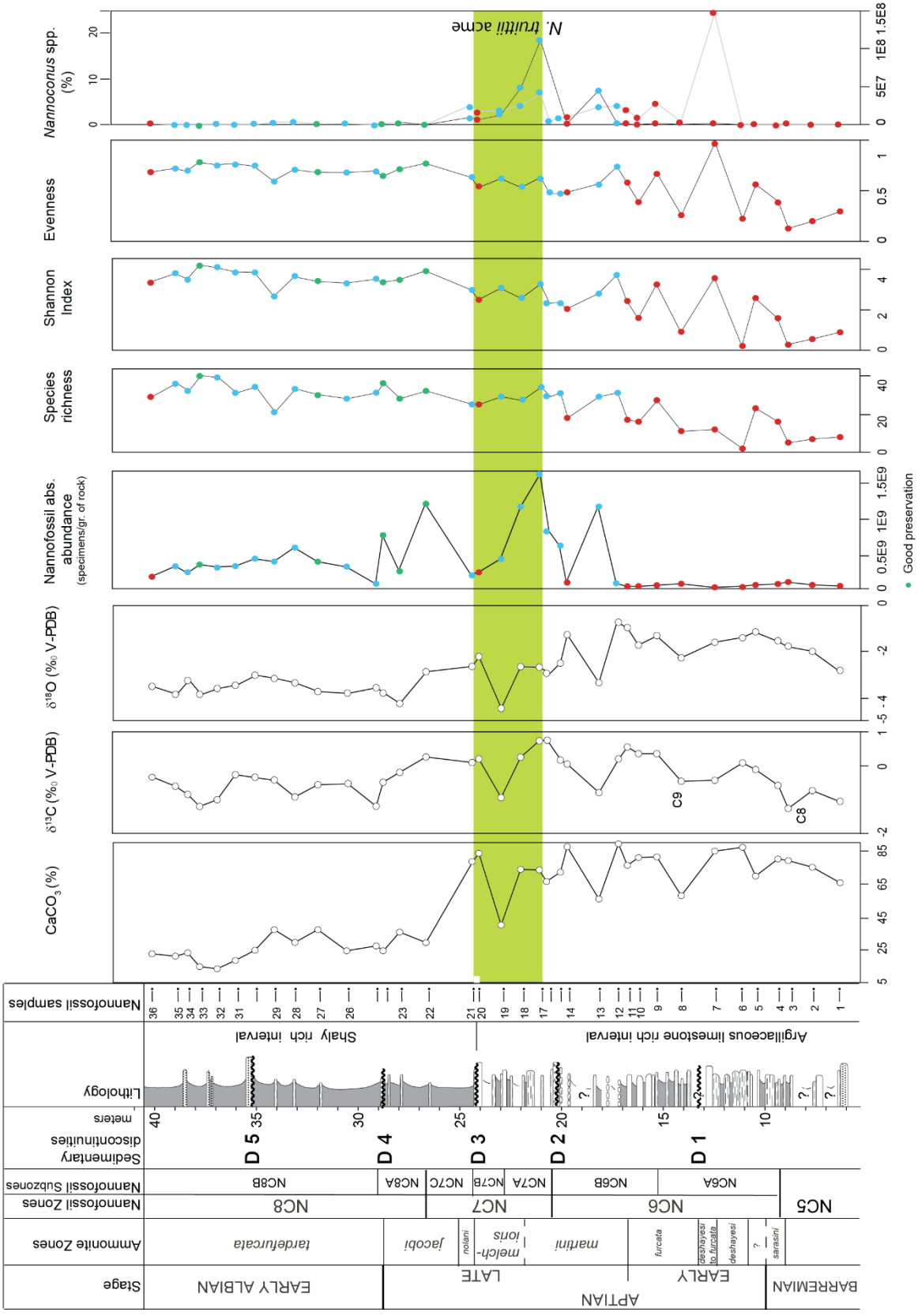

Figure 4.33: Biostratigraphy and stratigraphic changes in calcium carbonate content, carbon & oxygen-isotopes, calcareous nannofossil total absolute abundance, species richness, Shannon Index, evenness and macrofossil abundance and diversity for the Ida w Shayq section. Position of samples is indicated by a small line.

The absolute abundances for all taxa generally follow the same trend as the total absolute abundance (Fig. 4.34), with lowest values in the lower part of the section (above D1), and highest values between D3 and D4, in the latest Aptian. The absolute abundance trend for *Repagulum parvidentatum* is different from the other taxa with high values above D3 up to the top of the succession (Fig. 4.34). Low absolute abundances, recorded for all the taxa in the lower part of the section, are clearly related to the poor preservation of nannofossils.

Watznaueria (barnesiae + fossacincta) is the dominant group with percentages varying from 21.6 to 96.7%, with an average value of 54%. The relative abundance of *Watznaueria (barnesiae + fossacincta)* is significantly higher in the lower part of the succession (within the carbonate rich interval located below D3, of Aptian stage), than in the upper part (shale rich succession of latest Aptian-Early Albian age; Fig. 4.34). Above D3, the relative abundance of *Watznaueria* (*barnesiae + fossacincta*) is more or less constant. *W. communis* is the second species in terms of relative abundance. Its percentage varies from 2.6 to 22.6% with an average value of 8.7%, and it is relatively constant through the entire section (Fig. 4.34), although highest percentages are observed below D1 and around D5. The small *Zeugrhabdotus* spp. is the third most abundant group; its percentage fluctuates from 0 to 22.5%, with a mean value of 7.6%; percentages are higher in the upper shaly part, than in the lower, carbonate rich part of the succession (Fig. 4.34). The relative abundance of *L. carniolensis* fluctuates from 0 to 10.6%, with a mean value of 4.9%. Highest values are recorded in the lower and middle parts of the succession (Fig. 4.34). The relative abundance of *Z. diplogrammus* fluctuates from 0 to 9.5%, with an average value of 4%; its highest percentage is observed in the topmost part of the section, above D5. It is well represented in the middle and upper parts of the section, above D2, and is abundant in both shale- and carbonate-rich, intervals (Fig. 4.34). The relative abundance of *Rhagodiscus* spp. varies from 0 to 7.9% with a mean value of 2.5%. *Rhagodiscus* spp. presents higher percentages in the middle part of the succession (from below D2 up to D4; Fig. 4.34). The relative abundance of *D. rotatorius* varies from 0 to 7% with a mean value of 2.3%, and is higher in the upper shaly interval than in the lower part of the succession (Fig. 4.34). The relative abundance of *Nannoconus* spp. varies from 0 to 24.4%, with a mean value around 2% (see Appendix). The highest value is documented below D1, within the carbonate rich interval, and percentages remain very low above D3 (Fig. 4.34). The relative abundance of *Staurolithites* spp. fluctuates from 0 to 5.2%, with a mean value of 1.9%. Only small

fluctuations are recorded, with a maximum value above D4 (Fig. 4.34). The relative abundances of *Seribiscutum* spp. and *R. parvidentatum* vary from 0 to 5.9%, and from 0 to 5%, with mean values of 1.3% and 1.2%, respectively. Higher values are observed in the upper, shaly part of the section, above D3, with respect to the lower part, and maximum is reached in the uppermost part of the series (Fig. 4.34). The relative abundance of *Cretarhabdus* spp. fluctuates from 0 to 3.2%, with a mean value of 1.1%. It records a maximum just below D1 and a significant decrease between D4 and D5 (Fig. 4.34). The relative abundance of *Biscutum* spp. varies from 0 to 2.9% with an average of 1%. *Biscutum* spp. are more abundant in the middle and uppermost parts of the section (Fig. 4.34).

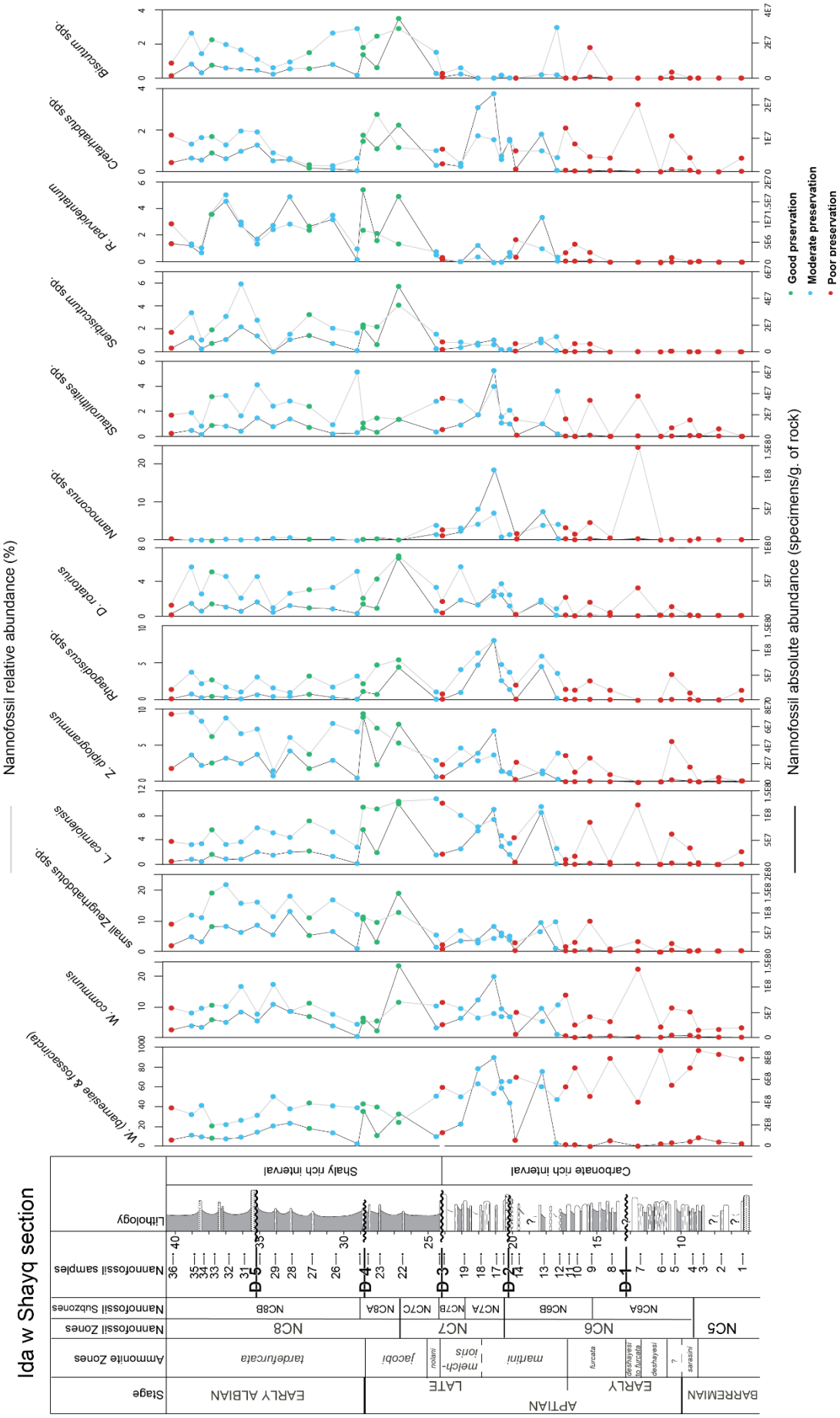

Figure 4.34: Absolute and relative abundances of selected calcareous nannofossil taxa for the Ida w Shayq section.

4. C.2.2. The Tissakatine Center section

The carbonate content varies from 3.6 to 84% with an average at 29.7% during the Aptian-Early Albian (Fig. 4.35). The calcium carbonate content is higher in the lower part of the section (Aptian) with respect to the rest of the succession (Early Albian). The highest value is recorded below D4. Then, it sharply decreases in the latest Aptian until a slight recovery before D5. Then, it decreases, reaching a minimum value just above D6, and slightly increases in the uppermost part of the section.

Among the fifty-four samples of the Tissakatine Center section, one is barren of nannofossils and two contain very rare nannofossils (Fig. 4.35). The preservation fluctuates all along the succession (Fig. 4.35). Seven samples display well-preserved nannofossils with slight etching and overgrowth (categories E1 and O1), 29 samples display moderately etched and overgrown nannofossils (categories E2 and O2) and 15 samples show moderately to strongly etched and strongly overgrown nannofossils (categories E2 or E3 and O3).

The nannofossil total absolute abundance ranges from 2.6 x 10^5 to 1.3 x 10^9 specimens per gram of sediments and decreases upward through Albian times (Fig. 4.35).

The species richness is comprised between 3 and 38. It does not present strong fluctuations through the succession and no clear trend can be recognized. The lowest values usually correspond to poorly preserved nannofossil samples (Fig. 4.35). The Shannon index and evenness range from 1.73 to 4.14, and from 0.40 to 0.82, respectively, and present trends comparable to the species richness (Fig. 4.35).

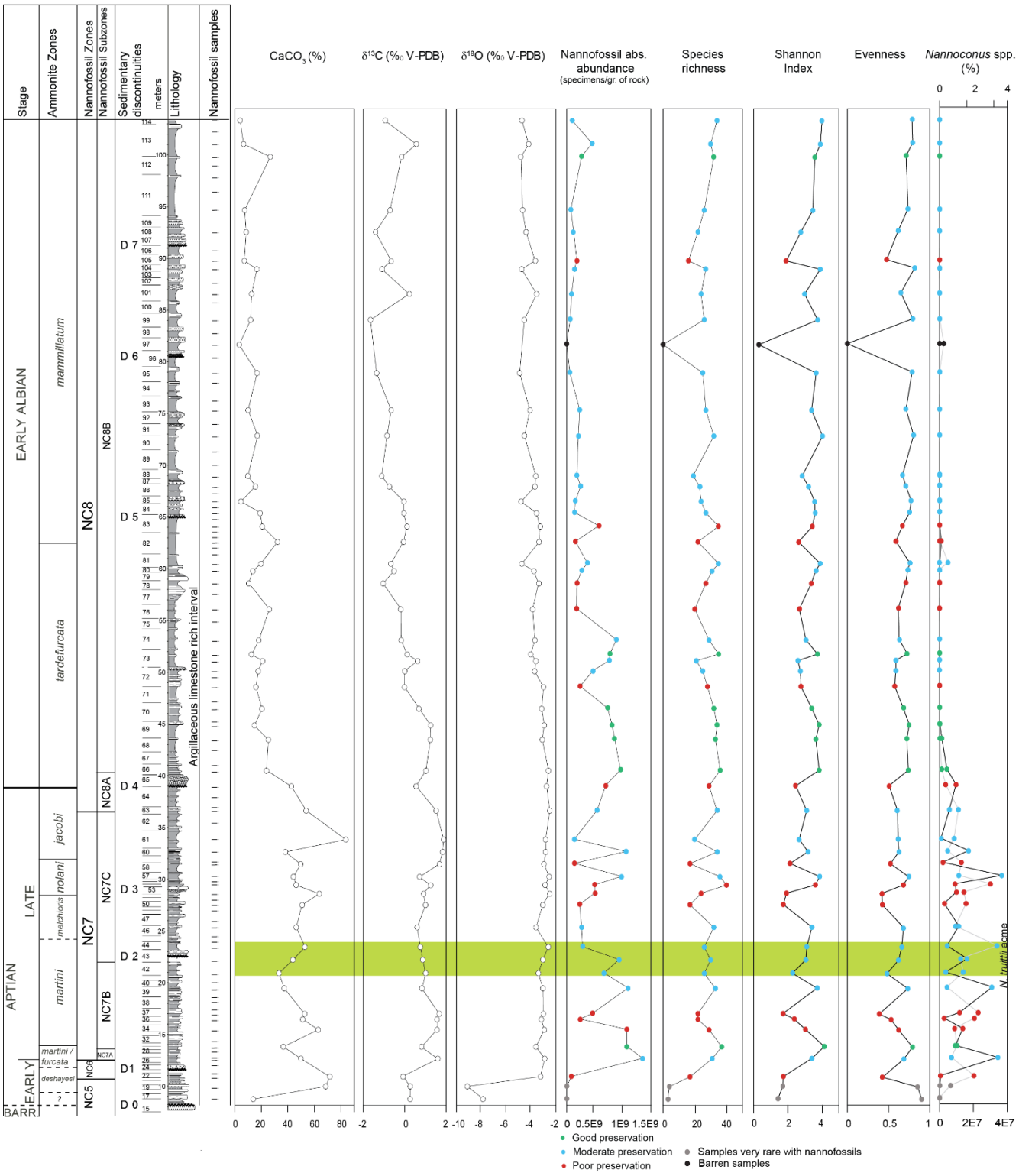

Figure 4.35: Biostratigraphy and stratigraphic changes in calcium carbonate content, carbon & oxygen-isotopes, calcareous nannofossil total absolute abundance, species richness, Shannon Index, evenness and macrofossil abundance and diversity for the Tissakatine Center section. Position of samples is indicated by a small line.

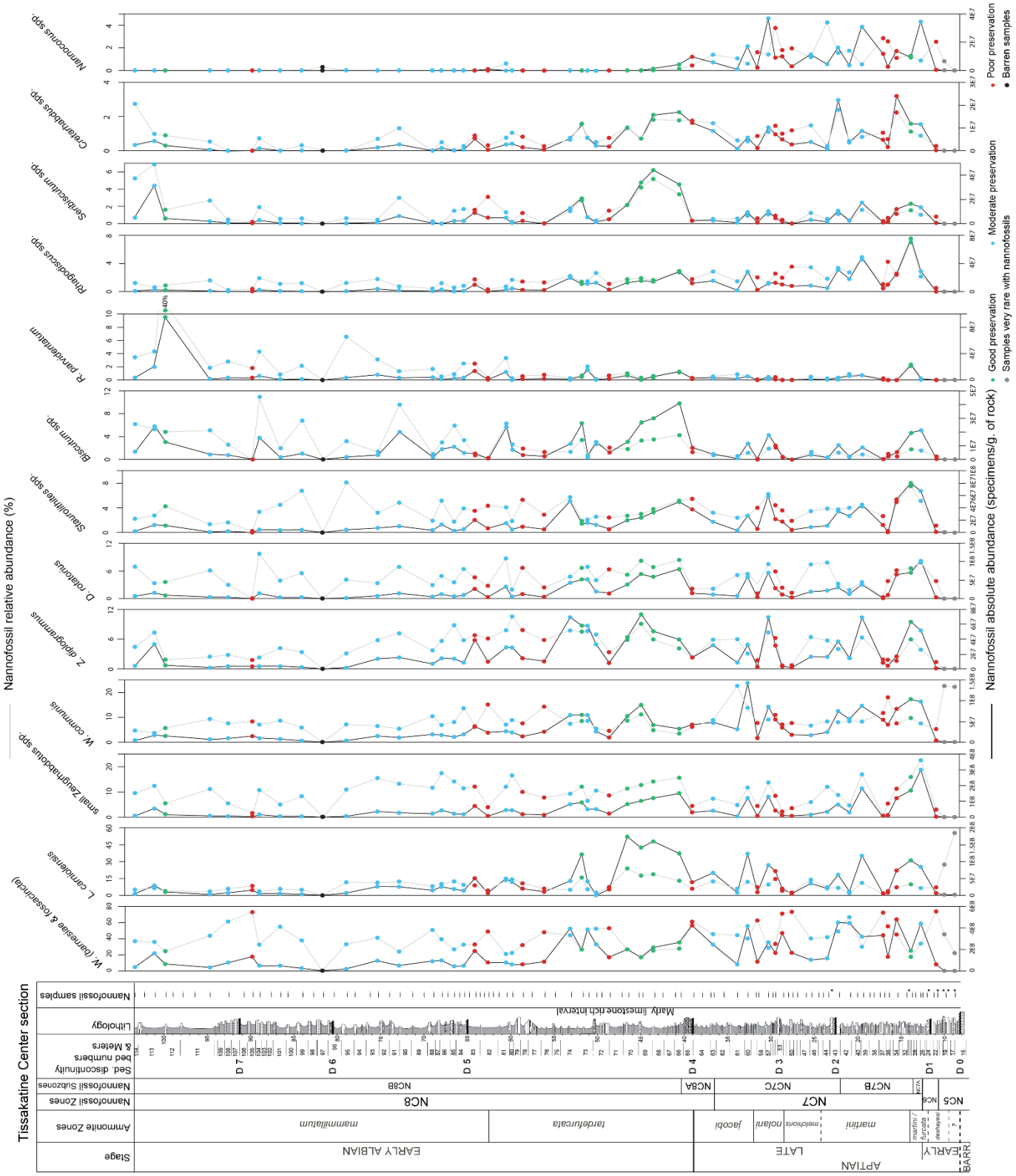

Figure 4.36: Absolute and relative abundances of selected calcareous nannofossil taxa for Tissakatine Center section.

The absolute abundance trends of the different taxa (Fig. 4.36) decrease upward with a short recovery in the uppermost part of the section, and follow those of the nannofossil total abundance (Fig. 4.36). The maximum absolute abundance for *Watznaueria* (*barnesiae* + *fossacincta*), small *Zeugrhabdotus* spp., *D. rotatorius*, *Rhagodiscus* spp., *R. parvidentatum*, *Staurolithites* spp. and *Cretarhabdus* spp. is observed between D1 and D2, whereas it is recorded above D3 for *W. communis* and *Nannoconus* spp., and above D4 for *L. carniolensis*, *Biscutum* spp., *Seribiscutum* spp. and *Z. diplogrammus*.

The relative abundance of *Watznaueria* (*barnesiae* + *fossacincta*) shows a rather constant trend through Aptian-Albian time (Fig. 4.36). *W.* (*barnesiae* + *fossacincta)* is the most abundant group, with percentages varying from 17 to 73.8%, with an average value of 41.3%. The highest values are recorded in the basal part of the section, and below D7. *L. carniolensis* is the second most abundant group. Its relative abundance fluctuates from 1 to 23.9 %, with a mean value of 9.6 %; the highest percentages are documented in the middle part of the section, between D3 and D5, with a maximum above D4 (Fig. 4.36). The small *Zeugrhabdotus* spp. are the third most abundant group after *L. carniolensis*. Their relative abundance varies from 0 to 22.6 %, with a mean value of 9.2 %. Higher percentages are observed in the basal part from D1 to below D2, and in the middle part of the succession between D4 and D6, with respect to the rest of the succession (Fig. 4.36). The relative abundance of *W. communis* fluctuates from 3.4 to 22.5%, with a mean value of 8.9 %, and highest values are observed between D3 and D4 (Fig. 4.36). The trend of relative abundance of *Z. diplogrammus* differs from those of the other taxa**; it** fluctuates from 0.6 to 10.6 %, with an average value of 4.6 %, and highest values are observed in the middle part of the section, between D3 and D6 (Fig. 4.36). The relative abundance of *D. rotatorius* fluctuates from 0 to 9.8 %, with a mean value of 4.6%. The highest percentages are recorded in the middle part of the section, from D4 to below D7 (Fig. 4.36). The relative abundance of *Staurolithites* spp. fluctuates from 0.2 to 8.1 %, with a mean value of 3.4 %. It does not show any significant variations through the section, and maximum value is documented below D6 (Fig. 4.36). The relative abundance of *Biscutum* spp. varies from 0 to 11%, with a mean value of 2.3 %. The highest percentages are recorded in the middle part of the section, from D4 to below D7. The relative abundance of small *Zeugrhabdotus* spp., *D. rotatorius* and *Biscutum* spp. have similar trends through the entire succession (Fig. 4.36). The relative abundance of *R. parvidentatum* is low in Aptian time, and generally increases upward through

Albian time (Fig. 4.36). It shows a trend comparable to that of its absolute abundance. Its relative abundance fluctuates from 0 to 35.7% with a mean value of 1.8%. The relative abundance of *Rhagodiscus* spp. generally decreases upward, varying from 0.2 to 7% (mean value: 1.8%); the highest value is observed just above D1 (Fig. 4.36). The relative abundance of *Seribiscutum* spp. fluctuates from 0 to 6.9%, with a mean value of 1.3%; it is maximum between D4 and D5 and in the uppermost part of the section, above D7 (Fig. 4.36). The relative abundance of *Cretarhabdus* spp. ranges from 0 to 2.4% with a mean value of 0.9%. The highest percentages are recorded in the lower part of the section (Fig. 4.36). The relative abundance of *Nannoconus* spp. fluctuates from 0 to 4.3%, with a mean value of 0.7%. It remains very low above D4 (Fig. 4.36).

4. C.2.3. The Anzate section

The carbonate content varies from 7.4 to 53% with an average of 24.6% during the Early Albian (Fig. 4.37). The calcium carbonate generally decreases toward the top of the succession, through Albian time (Fig. 4.37).

Among the twenty-three samples, two are barren of nannofossils and four contain very rare, poorly preserved nannofossils (Fig. 4.37). The preservation varies throughout the section. Six samples display well preserved nannofossils with slight etching and overgrowth (categories E1 and O1). Eleven samples display moderately etched and overgrown nannofossils (categories E2 and O2). The nannofossil total absolute abundance ranges from 2.1 x 10^7 to 1.2 x 10^9 specimens per gram of sediments (Fig. 4.37). Species richness is comprised between 2 and 52 (Fig. 4.37)

The absolute abundances for all taxa (Fig. 4.38) generally follow the same trend as the total absolute abundance, decreasing upward in the Early Albian with sometimes a short recovery above D5 (Fig. 4.38).

The relative abundances of *W.* (*barnesiae* + *fossacincta*) and *W. communis* (Fig. 4.38) are more or less constant through Albian time. *W.* (*barnesiae* + *fossacincta)* is the dominant group in the nannofossil assemblages with percentage ranging from 14 to 41% and an average value of 30.1%; the highest values are recorded above D5 within the alternating shale-sandstone interval. *W. communis* is relatively less common in this section, and its percentage fluctuates from 2.8 to 15%, with a mean value of 6.8%; higher percentage are observed above D5 within the intercalated shale-sandstone interval. The relative abundances of small *Zeugrhabdotus* spp., *D. rotatorius, L. carniolensis,*

Rhagodiscus spp., *Zeugrhabdotus diplogrammus*, *H. irregularis* and *Nannoconus* spp. (Fig. 4.38) decrease upward through Albian time. Small *Zeugrhabdotus* spp. is the second abundant group after *W. barnesiae*; its percentage fluctuates from 6.3 to 17.6% (mean value: 8.4%), and presents a maximum in the lower part of the succession. The relative abundance of *D. rotatorius* varies between 2.8 and 9.9%, with an average value of 4.4%; it is more abundant in both the lower and upper parts of the section. The relative abundance of *L. carniolensis* fluctuates from 0 to 6.8%, with a mean value of 3.8%; both relative and absolute abundances present the same pattern. The relative abundance of *L. carniolensis* reaches highest values in the interval just above D5. Percentages of *Rhagodiscus* spp. and *Zeugrhabdotus diplogrammus* vary from 1.3 to 9% and from 0 to 8%, with mean values of 3% and 2.2%, respectively. The relative abundance of *Rhagodiscus* spp. is higher in the interval located below D5 with respect to the top. *Z. diplogrammus* presents higher percentages in the middle part of the succession (45 - 70 meters) with respect to the base and the top. *Cretarhabdus* spp., *H. irregularis* and *Nannoconus* spp. percentages range from 0 to 10.5, from 0 to 4.8%, and from 0 to 1.5%, with mean values of 1.8, 1.2 and 0.8%, respectively. The highest values for *Cretarhabdus* spp. are observed above D5, within the shale-sandstone interval; while high abundances of *H. irregularis* are recorded just above D5. Higher percentages are observed in the lower and middle parts of the section, with respect to the upper part, for both *Cretarhabdus* spp. and *H. irregularis*. The relative abundance of *Nannoconus* remains low, with only higher values around D5. Three species or group of species present higher percentages in the upper part of the succession than in the lower part: *Biscutum* spp., *R. parvidentatum* and *Seribiscutum* spp. (Fig. 4.38), which generally increase upward, with maximum percentages above D5 within both the shale-sandstone and marly intervals. Their relative abundances fluctuate from 1.8 to 15.8%, 1.4 to 24% and 0 to 6.9%, with mean values of 3.9%, 6.4% and 2.3%, respectively.

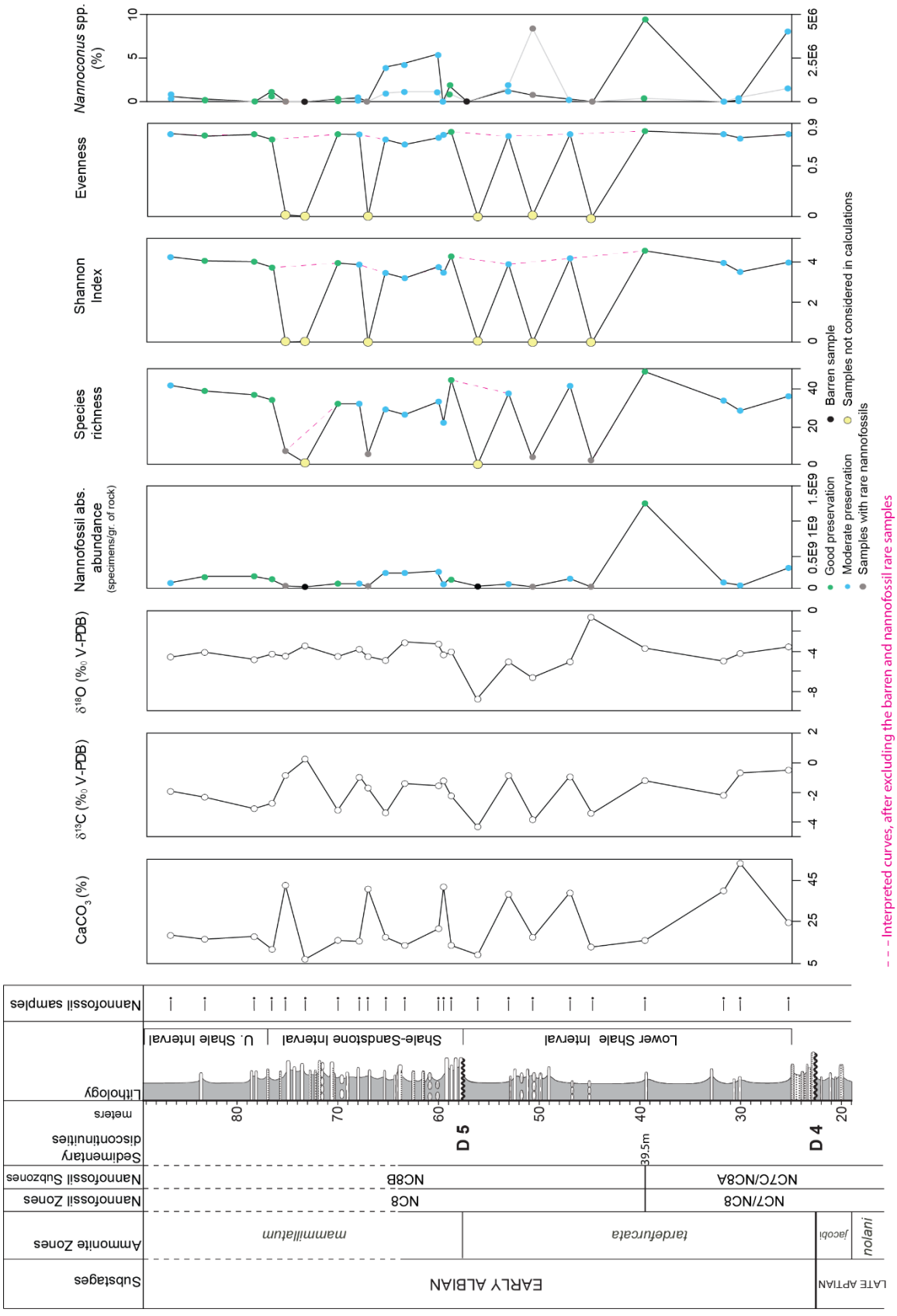

Figure 4.37: Biostratigraphy and stratigraphic changes in calcium carbonate content, carbon & oxygen-isotopes, calcareous nannofossil total absolute abundance, species richness, Shannon Index, evenness and macrofossil abundance and diversity for the Anzate section. Position of samples is indicated by a small line.

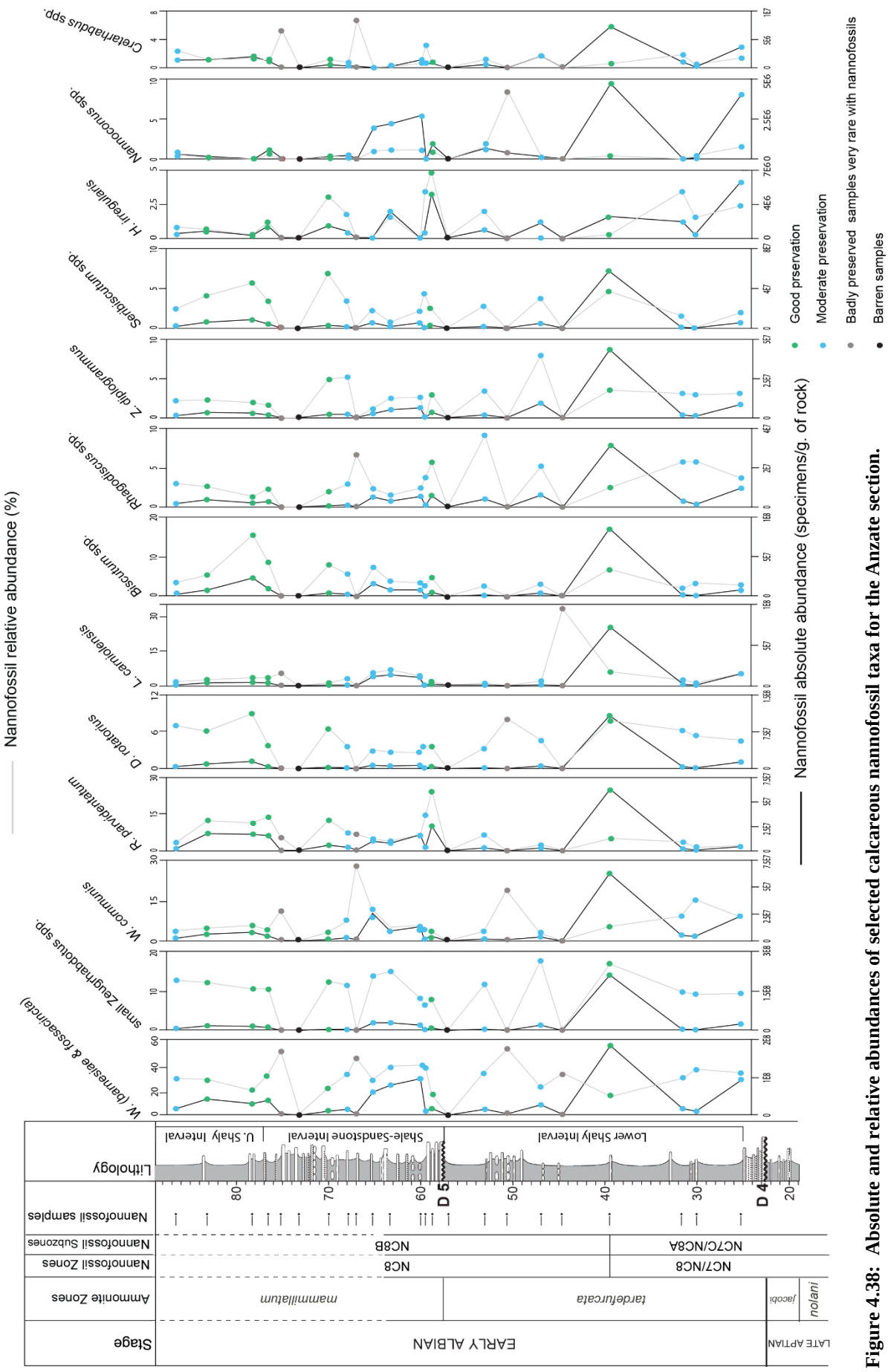

Figure 4.38: Absolute and relative abundances of selected calcareous nannofossil taxa for the Anzate section.

4. C.2.4. The Tinfoul section

In Tinfoul, the carbonate content varies from 11.4 to 38.7%, with an average of 22.6% (Fig. 4.39). It is maximum at the base of the section, remains relatively constant until the earliest Albian, and then decreases in the upper part of the section (Fig. 4.39).

The calcareous nannofossil preservation fluctuates all along the succession (Fig. 4.39). Three samples display well-preserved nannofossils with slight etching and overgrowth (categories E1 and O1), 16 samples display moderately etched and overgrown nannofossils (categories E2 and O2) and 7 samples show moderately to strongly etched and strongly overgrown nannofossils (categories E2 or E3 and O3).

The nannofossil total absolute abundance ranges from 2.2 x 10^7 to 7.5 x 10^8 specimens per gram of sediments, and decreases upward through Albian time (Fig. 4.39). The species richness is comprised between 16 and 40, and is generally higher in the interval located between 20 and 50 meters, if one excepts a maximum at the base. The lowest values generally correspond to poorly preserved nannofossil samples (Fig. 4.39). The Shannon index and evenness range from 2 to 4.17 and from 0.467 to 0.828, respectively, and present the same trend as the species richness (Fig. 4.39).

The absolute abundances trends of the different taxa decrease upward (Fig. 4.40), following those of the nannofossil total absolute abundance (Fig. 4.39). Maximum absolute abundances for *W. communis, L. carniolensis, D. rotatorius, Rhagodiscus* spp., *Seribiscutum* spp., *Biscutum* spp. and *R. parvidentatum* are recorded at 13.5 m. For *Watznaueria* (*barnesiae* + *fossacincta*), *Z. diplogrammus* and *Cretarhabdus* spp., maximum is observed just below D4. For small *Zeugrhabdotus* spp., it is recorded above D4, and just below D5 for *Nannoconus* spp.

The relative abundances of *Watznaueria* (*barnesiae* + *fossacincta*) and *W. communis* (Fig. 4.40) roughly increase in the upper part of the succession (within the shale-sandstone interval located above D5). *W. barnesiae* shows high percentages along the entire succession, while *W. communis* presents high percentages in the shale-sandstone interval. Percentages vary from 18.7 to 63.5% and 6 to 30.5%, with average values of 41.2% and 13%, respectively. The relative abundance of *H. irregularis* fluctuates from 0 to 7.4%, with an average value of 1.5%, and with highest value recorded around 60 meters, within the shale-sandstone interval. The relative abundances of *Lithraphidites carniolensis, Rhagodiscus* spp., *Zeugrhabdotus diplogrammus, Cretarhabdus* spp. and *Nannoconus* spp. (Fig. 4.40) generally decrease upward, and

trends of both relative and absolute abundances are relatively similar. The percentages of *L. carniolensis* fluctuate from 0.6 to 14%, with a mean value of 5.6% and maximum is recorded in the uppermost part of the section. The relative abundance of *Rhagodiscus* spp. varies from 0.6 to 12.2%, with a mean value of 2.8%, and the highest value is recorded just below D3. The percentages of *Z. diplogrammus* fluctuate from 0 to 8.7%, with an average value of 2.6%. Highest percentage is observed just above D5. *Cretarhabdus* spp. fluctuates from 0 to 1.7%, with mean value 0.7%, and highest value below D4. *Nannoconus* spp. varies from 0 to 5.5%, with mean value 0.5%, and highest value between D4 and D5.

The relative abundances of small *Zeugrhabdotus* spp., *D. rotatorius*, *Seribiscutum* spp., *Biscutum* spp. and *R. parvidentatum* fluctuate, and present trends relatively similar to their absolute abundances (Fig. 4.40). Their highest values are observed around D5. The relative abundances of abovementioned taxa are inversely proportional with that of *Watznaueria barnesiae*.

Next to the *Watznaueria* spp., the Small *Zeugrhabdotus* spp. represents the second most abundant species (0 to 19.9%, average value of 9.1%). The highest abundance is recorded in the middle part of the section, from the base of D4 to just above D5. In general, the abundance of Small *Zeugrhabdotus* spp. in the upper part of the section is much higher with respect to the lowermost part. *D. rotatorius* vary from 0.9 to 15.2%, with mean value of 5.6%, and its highest value is observed just above D5. *Seribiscutum* spp. ranges from 0 to 5% with the mean value of 1.9%. Indeed, it is relatively high all over the succession, with the maximum values just above D4, although lower values for *Seribiscutum* spp. are recorded between ≈ 50 and 60 meters. The relative abundance of *Biscutum* spp. vary from 0 to 4.4%, with a mean value of 1.8%. The middle part of the section, around D5, presents the higher values for *Biscutum* spp.. Moreover, an exceptional high value of *Biscutum* spp. is recorded at the base of the studied section, below D3 (4.2%). *R. parvidentatum* values oscillate from 0 to 4.9% with the mean value of 1.2%. The higher values are observed in the upper two-thirds of the section (from D4 upward). Conversely, the relative abundance of *R. parvidentatum* is minimum in the lowermost part of the section, just below D4.

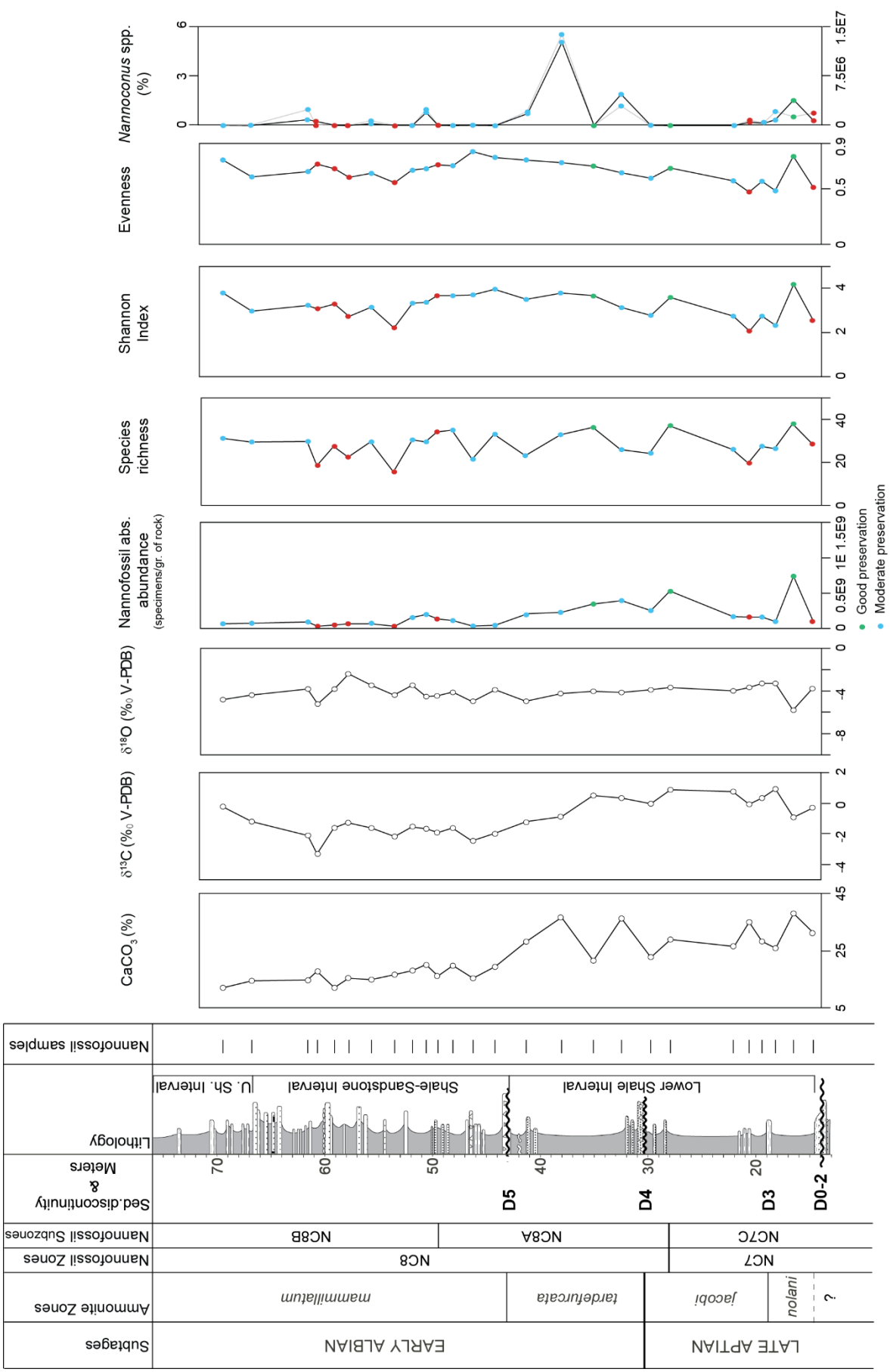

Figure 4.39: Biostratigraphy and stratigraphic changes in calcium carbonate content, carbon & oxygen-isotopes, calcareous nannofossil total absolute abundance, species richness, Shannon Index, evenness and macrofossil abundance and diversity for the Tinfoul section. Position of samples is indicated by a small line.

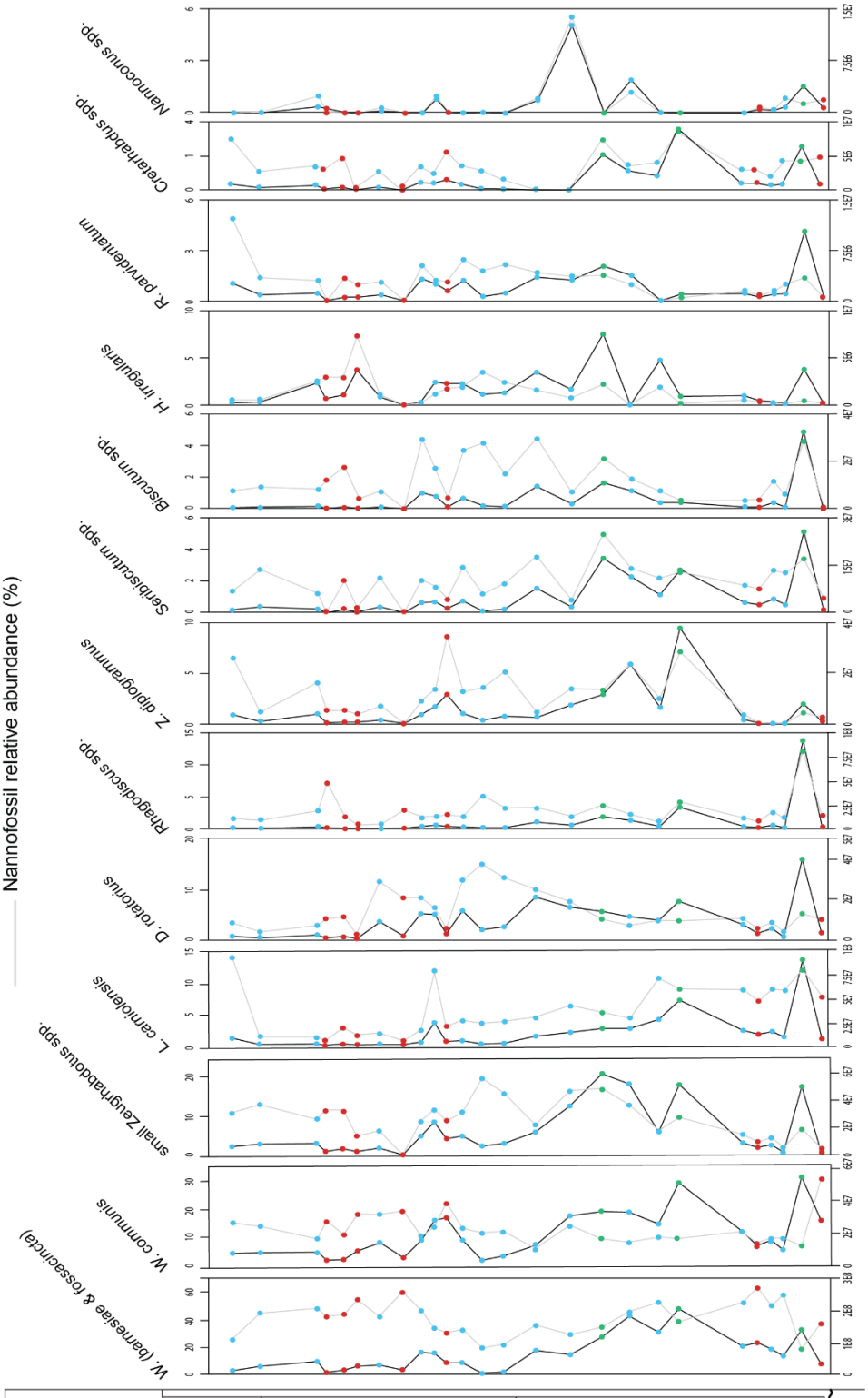

Figure 4.40: Absolute and relative abundances of selected calcareous nannofossil taxa for the Tinfoul section.

4. C.3. Interpretation

4. C.3.1. Preservation

In all studied sections, samples with moderate preservation (E2-O2), poor preservation (E2-O3/E3-O3) and good preservation (E1-O1), represent 53.5%, 31 % and 15.5% of the total number of samples, respectively. The preservation state can control nannofossil assemblages (absolute abundance, species richness, and relative abundance of both dissolution resistant and delicate species). We will consider the relative abundance of *Watznaueria barnesiae* and of delicate taxa encountered in this study. *W. barnesiae* is considered as the most dissolution-resistant taxon (Table 4.4). Delicate taxa are susceptible-dissolution taxa such as *Biscutum* spp., *D. rotatorius* and small *Zeugrhabdotus* spp. (Table 4.4).

In the studied sections the highest values of nannofossil total absolute abundances and species richness are recorded in well preserved samples, in the middle part of the section (between D2 and D4) at Ida w Shayq (Fig. 4.33), in the basal argillaceous limestone interval (below D5) at Tissakatine Center (Fig. 4.35), and in the lower shale interval (below D5) in both the Anzate and Tinfoul sections (Figs. 4.37, 4.39). The lowest values are observed in moderately to poorly preserved samples, in the argillaceous interval at Ida w Shayq and Tissakatine Center (Figs. 4.33, 4.37), and in the shale-sandstone interval at Anzate and Tinfoul (Figs. 4.37, 4.39).

W. barnesiae is the most common species in the studied sections. The mean relative abundance of *W. barnesiae* in Ida w Shayq, Tissakatine Center, Anzate and Tinfoul sections reaches 53%, 41.3%, 30.1% and 41.2%, respectively. Roth and Krumbach (1986) considered that assemblages containing more than 40 % of *W. barnesiae* are heavily altered by diagenesis leading to a decrease in nannofossil species richness. Williams and Bralower (1995) indicated that the nannofossil assemblages are strongly affected by diagenesis when the percentage of *W. barnesiae* is higher than 70%, and that lower percentages are largely controlled by environmental factors rather than by preservational effects. Values equal and/or higher than 40% of *W. barnesiae* are recorded in moderately to well preserved samples from different paleolatitudinal and paleoenvironmental settings (platform or epicontinental basin *versus* hemipelagic or pelagic) through Aptian-Albian times (see Table 4.5).

Table 4.4: Dissolution susceptibility of selected nannofossil taxa encountered in this study

Dissolution susceptibility of selected nannofossil taxa encountered in this study.
1 - Hill (1975); 2 - Thierstein (1980); 3 - Roth and Bowdler (1981); 4 - Roth and Krumbach (1986);
5 - Roth (1981) 6 - Mutterlose and wise, (1990); 7 - Thierstein and Roth (1991); 8 - Bornemann and Mutterlose (2006)

Taxa	Susceptibility to dissolution
B. constans =*B. ellipticum*	dissolution-susceptible[1,2,3,4,7,8] moderately dissolution-susceptible[5]
D. rotatorius	dissolution-susceptible[2]
Z. erectus	dissolution-susceptible[1,4,5]
small *Zeugrhabdotus* (with major axis ≤ 5 μm)	dissolution-susceptible[1,8]
Zeugrhabdotus spp.	dissolution-susceptible[4,6,7]
W. barnesiae	dissolution-resistant[1,2,3,4,5,6,7,8]

Table 4.5: High relative abundances of *W. barnesiae* are recorded in moderately to well preserved samples in carbonate platform and hemipelagic-pelagic sequences.

Environment	Locality	*W. barnesiae* (%)	Age	Reference
Carbonate platform	1) EAB, Morocco	Average value up to 43%	Aptian-Albian	Peybernes et al. (2013)
	2) Tinfoul and Tissakatine sections, EAB	up to 41%	Aptian-Albian	this study
	3) Ida W Shayq section, EAB	up to 53%	Aptian-Albian	this study
Pelagic-hemipelagic carbonate	3) Sites 802,ODP, Western Pacific Ocean	up to 56%	Aptian-Albian	Erba (1992)
	4) Gault Clay Formation,S. England	up to 25%	Albian	Erba et al (1992)
	5) Vocotian Basin, SE France; Mazagan Plateau,NW Africa	up to 35%	Aptian-Albian	Herrle (2002)
	6) Cismon and Piobbico cores (Tethys) and DSDP Site 463 (Pacific Ocean).	more than 40%	Aptian	Bottini et al. (2015)
	7) Piobbico core, central Italy	Mean 55%	Albian	Tiraboschi et al (2009)

* Erba (1992) and Erba et al (1992) consider the increasing in the *Watznaueria* abundances reflect primary environmental factors.
Abbreviations: EAB:Essaouira-Agadir Basin; Av.:Average.

Tiraboschi et al (2009) and Bottini et al. (2015); believe that the relatively high percentages of *W. barnesiae* in the studied sections preserve a primary signal.;

The highest percentages of *W. barnesiae* are recorded in poorly preserved samples in the four sections (Figs. 4.34, 4.36, 4.38, 4.40). On the contrary, poor preservation will decrease the relative abundance of delicate taxa. The lowest percentages of delicate taxa are observed in poorly preserved samples from the four studied sections (Figs. 4.33, 4.36, 4.38, 4.40).

These data show that nannofossil assemblages are affected by diagenesis in the poorly preserved samples from the four studied sections. These samples must be considered with caution, and we decided not to take into account samples with strongly etched and overgrown nannofossils (E3-O3) for paleoecological interpretations.

In the following paragraphs, we have added data from the reference section of Addar (described in Peybernes et al., 2013) because it is located in the more distal position on the southern east-west transect.

4. C.3.2. Carbonate production variations during the Aptian-Early Albian interval in the EAB

In the carbonate platform of the EAB, carbonate production may come either from pelagic, or from benthic fauna. Then, carbonate production is estimated from the calcium carbonate content, nannofossil total absolute abundance, and semi-quantitative abundance of benthic faunal content.

The carbonate production in the EAB is lower in the Early Albian with respect to the Aptian. This is shown by 1) a decrease in the carbonate content starting approximately around D4 (Figs. 4.33, 4.35, 4.37, 4.39), 2) a progressive decrease in the nannofossil total absolute abundances (**NTAA**) through the Aptian-Early Albian interval, except for the Ida w Shayq section, which shows a sharp decrease at the Aptian/Albian boundary (Figs. 4.33, 4.35, 4.37, 4.39), and 3) the decrease in both absolute and relative abundances of the larger nannofossil calcifier (*Nannoconus;* Figs. 4.33, 4.35, 4.37, 4.39).

We have compared the spatial variations of the carbonate production between the different sections for two different time periods: 1) Aptian (below D4); and 2) Early Albian (above D4), based on the abrupt change in the carbonate content occurring around D4. We have made different maps of the carbonate production taking into account mean calcium carbonate content, mean nannofossil total absolute abundance (strongly etched and overgrowth samples are excluded) and mean faunal benthic content.

The maps show that below D4, the mean of $CaCO_3$ content increases toward the western section of Addar and is maximum toward the northern section of Ida w Shayq (Fig. 4.41a). The mean NTAA reaches a maximum at Addar, is lower and comparable in both Tissakatine Center and Ida w Shayq, and is minimum in Tinfoul (Fig. 4.41c). The mean faunal benthic content increases both along the E-W transect toward Anzate and Addar, and along the N-S transect, reaching highest values at Tissakatine Center (Fig. 4.42a). So, in the Aptian (below D4), the mean calcium carbonate content, as well as the mean NTAA and benthic faunal content increase toward more distal sections of Addar and Ida w Shayq (Fig. 4.41a, c; Fig.4.42a). The carbonate production is then

higher in the distal sections than in the proximal section (Fig. 4.41a). The higher mean nannofossil abundance and benthic faunal content toward the distal sections support the significant role of both pelagic and benthic organisms contribution in the carbonate production. On the other hand, the decrease in carbonate content toward the proximal section of Tinfoul could result from a more abundant clastic supply, which dilutes the carbonate content, and reduces the euphotic zone, hindering the pelagic and benthic life (Figs. 4.41c, 4.42a).

Above D4, a maximum mean $CaCO_3$ content is recorded in both the Anzate and Ida w Shayq sections (Fig. 4.41b). The mean NTAA increases both along the E-W transect, and along the N-S transect. Highest NTAA and high mean faunal benthic content are recorded in Tissakatine Center (Figs. 4.41d and 4.42b**).** So, in the Early Albian, the carbonate production is geographically controlled in the EAB; in the distal sections of Addar and Ida w Shayq, the calcareous nannofossils were the main contributors for the carbonate fraction. In the eastern section of Anzate, the carbonate production chiefly derived from benthic organisms, whereas in Tissakatine Center, the carbonates are produced both by nannofossils and benthic organisms.

In the studied sections, there is no significant correlation between calcium carbonate content and nannofossil total abundance (Fig. 4.43a-c). However, relationships between these two variables are more positive for the more distal sections (Ida w Shayq and Tissakatine Center) than for the more proximal section (Anzate), showing that the contribution of the pelagic part (nannofossils) to the total carbonate increases in the distal part of the platform. This is confirmed by the results obtained in Addar (most distal section), where a positive correlation is observed between the calcium carbonate content and the nannofossil absolute abundance (Fig. 4.43d), with high $r = 0.6$ and $P < 0.05$ supporting the role of nannofossils as carbonate producer in this distal parts of the basin. There, the low benthic faunal content suggests that deep, aphotic conditions hindered the development of benthic communities (Fig. 4.42b).

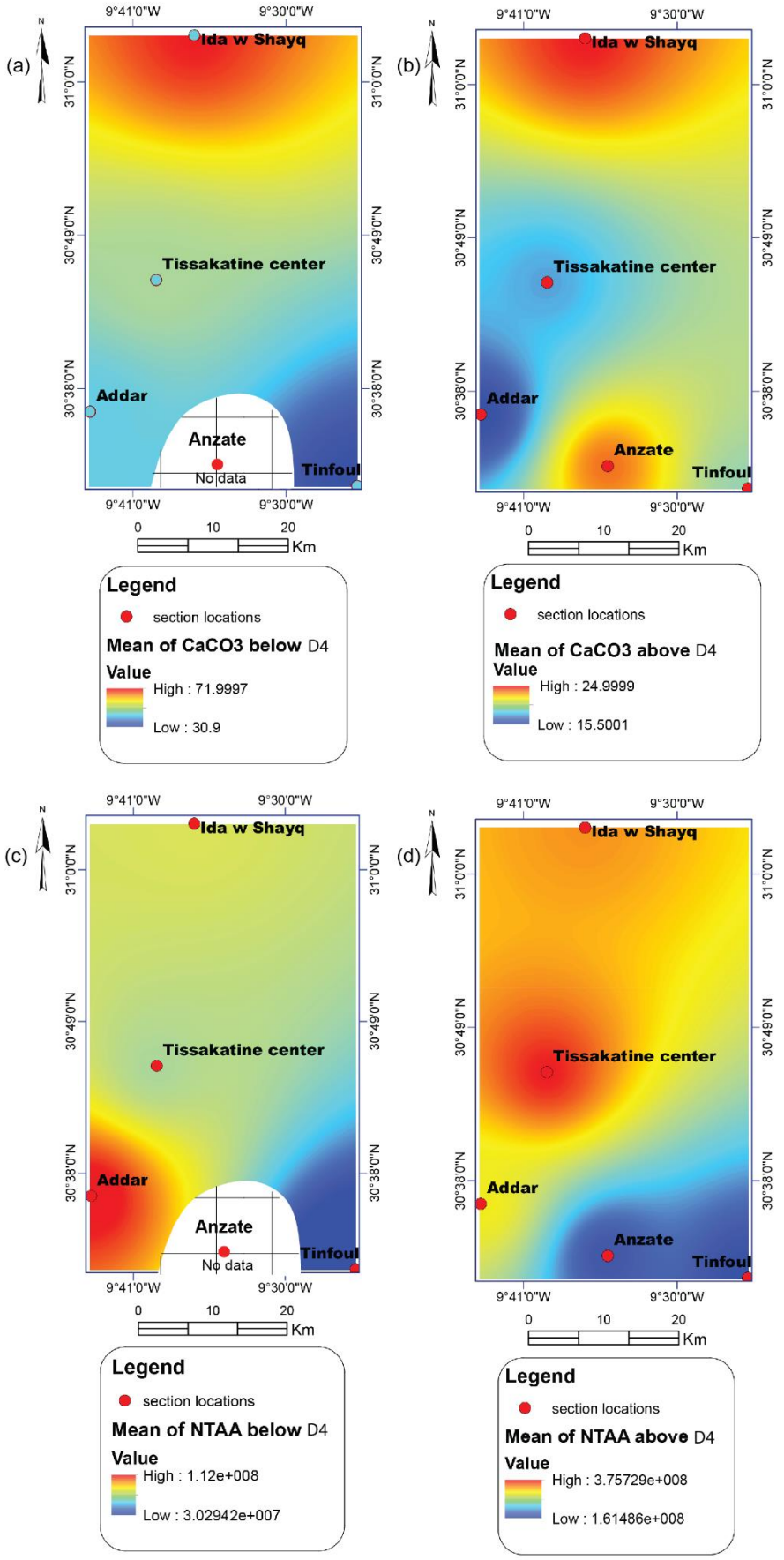

Figure 4.41: Show the spatial and temporal changes in the mean calcium carbonate content and nannofossil total absolute abundance in Essaouira-Agadir Basin; in two time intervals, Aptian Stage below (D4) and in Early Albian Substage (Above D4). Abbreviations: NTAA, Nannofossil total absolute abundances

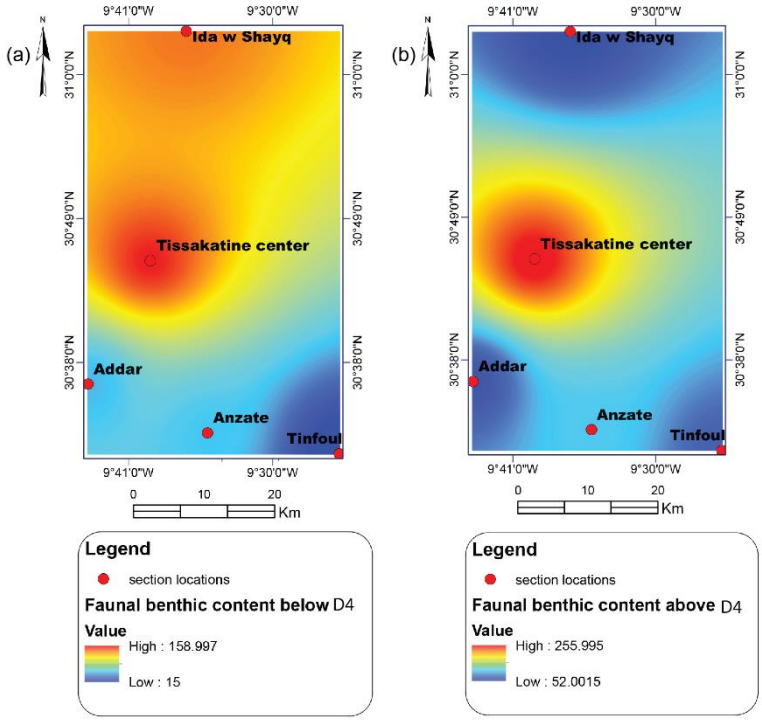

Figure 4.42: Show the spatial and temporal changes in semi-quantitative analysis of faunal benthic content in Essaouira-Agadir Basin; in two time intervals, Aptian stage below (D4) and in Early Albian substage (Above D4).

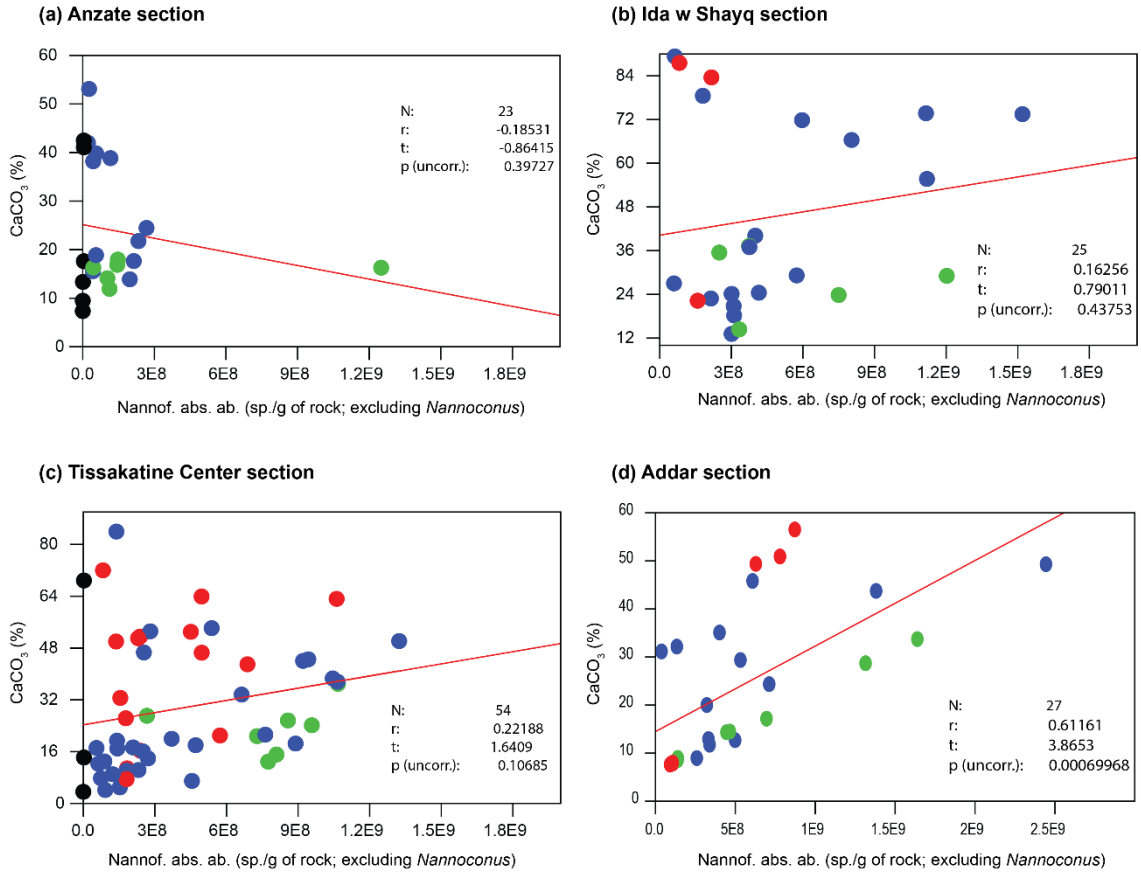

Figure 4.43: Bivariate plots between carbonate content and nannofossil absolute abundance showing a negative correlation for (a) the Anzate section and positive correlation for sections of (b) Ida w Shayq, (c) Tissakatine center and (d) Addar. Abbreviations: r, coefficient of correlation; p, probability; N, number of measurements.

4. C.3.3. Calcareous nannofossil primary productivity during Aptian-Early Albian times

The calcareous nannofossil primary productivity is estimated based on both nannofossil total absolute abundance and the relative abundance of the following taxa: *Biscutum* spp., *D. rotatorius*, *L. carniolensis* and small *Zeugrhabdotus* spp., which are considered as meso-eutrophic indicators (Table 4.6). Both curves of NTAA and of meso-eutrophic taxa relative abundance have been drawn for each section, following east-west and north-south transects (Figs. 4.44, 4.45).

The relative abundance of meso-eutrophic taxa = SUM (RA of *Biscutum* spp.+ RA of *D. rotatorius* + RA of *L. carniolensis* + RA of small *Zeugrhabdotus* spp.).

Abbreviations: RA = Relative Abundance.

The stratigraphic evolution of these two parameters shows opposite long-term trends (Figs. 4.44, 4.45). The nannofossil total absolute abundance decreases from the Aptian to the Early Albian, whereas the relative abundance of meso-eutrophic taxa increases in the earliest Albian.

The nannofossil total absolute abundance depends on primary productivity, preservation and sedimentation rate. The preservation effect has already been discussed above. The sedimentation rate varies from the Aptian to Early Albian for all the sections. The Aptian lower parts of the sections are more condensed than the Early Albian upper parts, and the change occurs around D4 (Figs. 4.44, 4.45). So the decrease in nannofossil total absolute abundance recorded in all sections may be due to an increase in the sedimentation rate rather than to a decrease of calcareous nannofossil primary productivity. So, we used only the relative abundances of meso-eutrophic taxa to discuss the changes in calcareous nannofossil primary productivity.

In all the sections, the calcareous nannofossil primary productivity increases in the interval comprised between D3 and D5 (except in Anzate, because of the lack of data for this time interval). After this increase, the calcareous nannofossil primary productivity remains high until the end of the lower part of the *mammillatum* Zone (around D6, in Tissakatine and Addar). Above D6, it slightly decreases.

We will discuss now the spatial evolution of the calcareous nannofossil primary productivity following the two transects.

Along the east-west transect (Tinfoul, Anzate and Addar sections; Fig. 4.44), the relative abundance of meso-eutrophic taxa is higher in the distal section of Addar than in the proximal section of Tinfoul, during the Late Aptian, while during the Early Albian, the percentages of meso-eutrophic taxa are roughly comparable between the different sections. At Tinfoul, the amount of meso-eutrophic taxa increases above D3 until the onset of the shale-sandstone sedimentary interval, above D5 (Fig. 4.44). This sedimentary interval, which is well developed at Tinfoul, is much thinner toward the west, representing only 5 meters at Addar (Fig. 4.44). It was deposited during low sea-level. At Tinfoul, which is in a proximal position, the lowering of sea level reduces the distance to the continent and consequently increases the input of siliciclastic and associated nutrients in this zone. This could explain the increase in calcareous nannofossil productivity recorded in this proximal section.

Along the south-north transect (Anzate, Tissakatine Center and Ida w Shayq sections; Fig. 4.45), at this moment we cannot see any spatial changes for the relative abundance of meso-eutrophic taxa from south to north. In the studied sections, the relative abundance of meso-eutrophic taxa is higher in the Early Albian, from D4 to above D5 and/or below D6, when compared with the lower abundances in the Aptian and in the section above D6. A small decrease recorded around D5 in Anzate is much reduced toward the distal section of Ida w Shayq. For both Ida w Shayq and Tissakatine Center, the more distal sections on this transect, highest abundance of meso-eutrophic taxa are observed during sea level rises. Increasing nutrient conditions may be due to enhanced upwelling activity during periods of high sea level.

Table 4.6: Paleoecological significance of selected nannofossil taxa

Taxa	Fertility of surface waters	Ecological strategy	Paleoceanography
B. constans	eutrophic[1,2,3,4,5,6,7,8,9,35,43] meso-eutrophic[19]	low diversified assemblages[8] eurytopic[39]	cool surface waters[9,43] mid-low latitude[9] upwelling[1,2,3,4,5,8,35] shelf surface waters[9,10] low diversified assemblages[8] restricted sea assemblages[1] more abundant carbonate-rich lithologies[6] cosmopolitan[9,45]
*B. ellipticum**	eutrophic[2,11] meso-eutrophic[16]	r-selected[8,12,13,14]	cool surface waters[2,11,15,46] high latitude[12] upwelling[2,11] lower salinity[2,11]
Biscutum spp.**	mesotrophic[17]		shelf surface waters[2]
D. rotatorius	meso-eutrophic[4,11,13,15,32,46]	eurytopic[39]	
L. carniolensis	mesotrophic[4,13]	eurytopic[39]	
Staurolithites spp.	meso-eutrophic[19]		
R. parvidentatum			high latitude [9,13,15,21,40,41,42,43,46]
Seribiscutum primitivum *Seribiscutum gaultensis* *Seribiscutum* spp.		stenotopic[38]	high latitude [3,9,16,21,38,39,41,42, 44,45] high latitude [39] high latitude [15,46]
C. conicus		K-selected[14]	
C. striatus		K-selected[14]	
Cretarhabdus spp.	oligotrophic[8,11,18,19,20]		warm waters[18,19]
Nannoconus spp.	oligotrophic[8,32,33]	r-selected[9]	low latitude[2,3,9,37] warm waters[8,9,34,43,44] neritic[1,2,3,9,42,46]
R. asper			low latitude[3,36,16] warm waters[4,8,9,13,21,34,35,42,46] cosmopolitan[45]
R. achlyostaurion	oligotrophic[19,20]	K-selected[14]	low latitude[21,22] warm waters[20,22]
H. irregularis			low latitude[21] warm waters[42]
W. barnesiae	oligotrophic[3,5,6,12,15,19,46] mesotrophic[23]	eurytopic[10,24,25] r-selected[12,14,23] first blooming during the early spring[27]	oceanic setting[2] cosmopolitan[26,45] low latitude[12] not highest latitude[12,28,29,30,31]
Z. erectus	eutrophic[1,2,3,4,5,6,7,9,11,15,35,46] more eutrophic than B. constans[13]	r-selected[13,14,23] low diversified assemblages[8]	upwelling[1,2,3,4,5,35] mid-low latitude[9] cool surface waters[9] more abundant in darker lithologies[5] more abundant in marls[8] shelf surface waters[8]
small *Zeugrhabdotus* (with major axis ≤ 5 mm)	eutrophic[6,13]		
Zeugrhabdotus spp.*	eutrophic[1,43]		upwelling[1,8] restricted sea assemblages[1]
Zeugrhabdotus spp.**	eutrophic[10]		shelf surface waters[9,10] cosmopolitan[9]

*_B. ellipticum_ is considered as a morphotype of B. constans (Bornemann and Mutterlose, 2006)
**_Biscutum_ spp.: _B. constans_ (abundant), B. ellipticum (common) (Linnert and Mutterlose, 2010)
*_Zeugrhabdotus_ spp. (e.g. _erectus, elegans and diplogrammus_; Roth, 1981)
**_Zeugrhabdotus_ spp. (e.g. _erectus, elegans and noeliae_; Street and Bown, 2000)
Zeugrhabdotus erectus more eutrophic than _B. constans_ (Erba,1992)
B. constans increases in abundance before _Z. erectus_ (Roth1981, Erba, 1992)

[1]Roth (1981); [2]Roth and Bowlder (1981); [3]Roth and Krumbach (1986); [4]Premoli Silvá et al. (1989); [5]Roth (1989); [6]Watkins (1989); [7]Williams and Bralower (1995);[8]Mutterlose and Kessels (2000); [9]Street and Bown (2000); [10]Noël et al. (1987); [11]Giraud et al. (2003); [12]Thierstein (1981); [13]Erba et al. (1992); [14]Lees (2002); [15]Herrle et al. (2003); [16]Mutterlose (1992b); [17]Linnert and Mutterlose (2010); [18]Mutterlose (1996); [19]Eleson and Bralower (2005); [20]Eshet and Almogi-Labin (1996); [21]Crux (1991); [22]Linnert and Mutterlose (2008); [23]Pittet and Mattioli (2002); [24]Mutterlose (1991); [25]Lees et al. (2005); [26]da Gama (2000); [27]Thomsen (1989); [28]Wind (1979); [29]Shafik (1990); [30]Huber and Watkins (1992); [31]Watkins et al. (1996); [32]Coccioni et al., (1992); [33]Erba (1994); [34]Mutterlose (1989); [35]Erba (1992); [36]Erba (1987); [37]Thierstein (1974); [38]Mutterlose (1992a); [39]Mutterlose (1992c); [40]Ruckheim et al. (2006); [41]Wise (1988); [42] Bown (2005); [43]Mutterlose et al. (2003); [44] Bown and Mutterlose in Baumgartner et al. (1992); [45] Mutterlose and Wise (1990); [46]Herrle(2002).

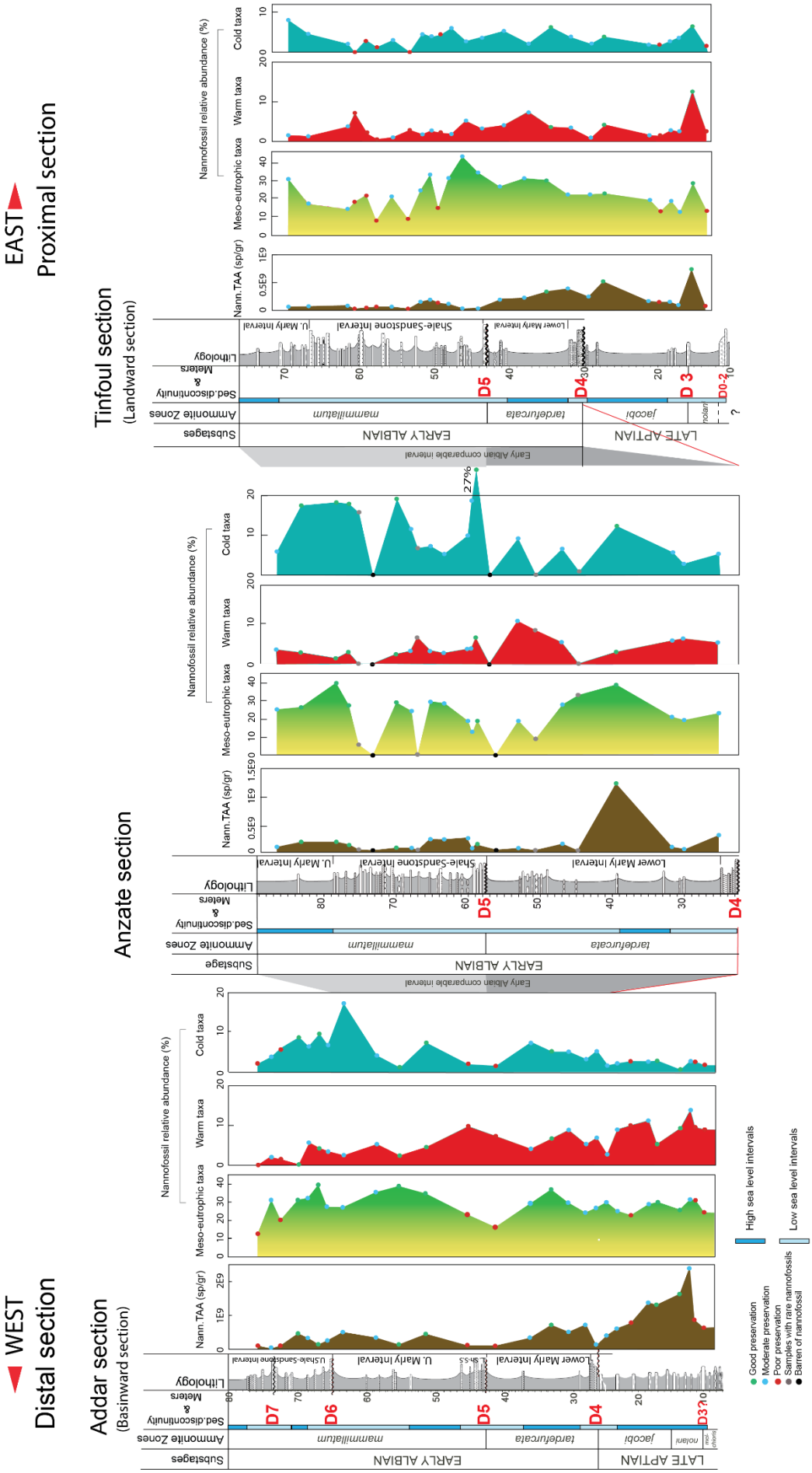

Figure 4.44: Stratigraphic changes in nannofossil total absolute abundance, relative abundance of meso-eutrophic taxa (small *Zeugrhabdotus* spp., *Biscutum* spp., *D. rotatorius* and *L. carniolensis*), relative abundance of cold taxa (*R. parvidentatum*, *Seribiscutum* spp., *Crucibiscutum* spp. and *Rhagodiscus angustus*), and two groups of warm taxa (*Nannoconus* spp. and *Rhagodiscus* spp.), along the East-West transect with respect to sea level change through Late Aptian-Early Albian time. Abbreviations; Nann.TAA (sp/gr): Nannofossil Total Absolute Abundance (specimens/gram).

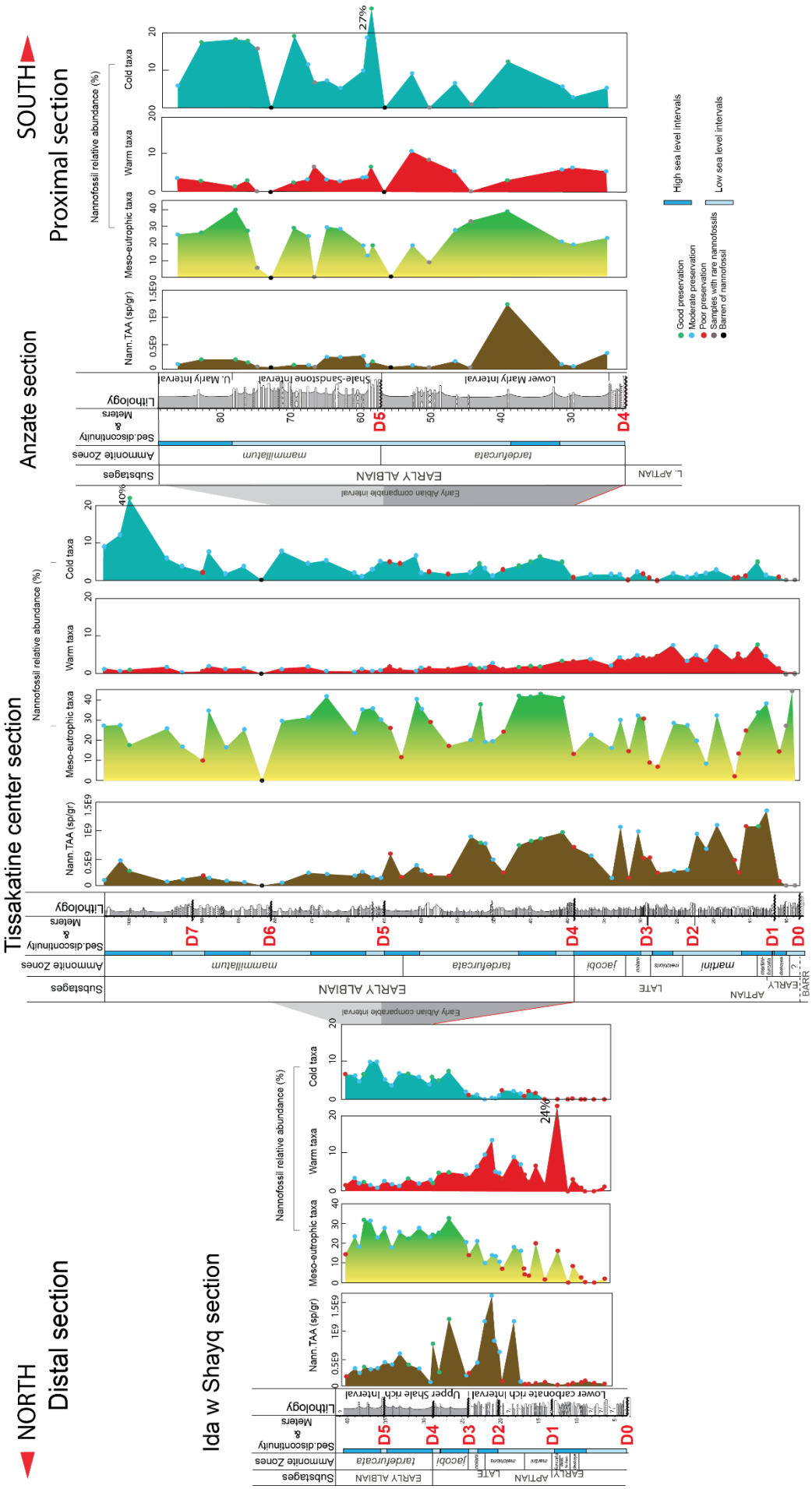

Figure 4.45: Stratigraphic changes in nannofossil total absolute abundance, relative abundance of meso-eutrophic taxa (small *Zeugrhabdotus* spp., *Biscutum* spp., *D. rotatorius* and *L. carniolensis*), relative abundance of cold taxa (*R. parvidentatum*, *Seribiscutum spp.*, *Crucibiscutum* spp. and *Rhagodiscus angustus*), and two groups of warm taxa (*Nannoconus* spp. and *Rhagodiscus* spp.), in North-South transect with respect to sea level change through Aptian-Early Albian time. Abbreviations; Nann.TAA (p/gr): Nannofossil Total Absolute Abundance (specimens/gram).

4. C.3.4. Sea-surface temperature changes during Late Aptian-Early Albian times

In this study, changes in sea-surface temperature have been estimated considering six nannofossil taxa or group of taxa with sea-surface temperature affinities: four cold surface-water indicators (*Crucibiscutum* spp., *R. parvidentatum*, *Rhagodiscus angustus* and *Seribiscutum* spp.) and two groups of warm surface-water conditions (*Nannoconus* spp. and *Rhagodiscus* spp. (Table 4.6).

The relative abundance of cold taxa = SUM (RA of *Crucibiscutum* spp.+ RA of *R. parvidentatum* + RA of *Rhagodiscus angustus* + RA of *Seribiscutum* spp.).

The relative abundance of warm taxa = SUM (RA of *Nannoconus* spp. + RA of *Rhagodiscus* spp.).

Abbreviations: RA: Relative Abundance

In all studied sections, the relative abundance of cold taxa increases from the Late Aptian to Early Albian, with no spatial changes (except in Anzate, which presents higher percentages with respect to the other sections; Figs. 4.44, 4.45). Conversely, the warm taxa show a decrease upward (Figs. 4.44, 4.45), reflecting cooling upward through Early Albian time.

4. C.3.5. Paleoecological affinities proposed or confirmed for some calcareous nannofossil taxa

In order to better describe the relationships between the relative abundance of different calcareous nannofossil species or group of species, a principal component analysis (PCA) was performed with the software STATVIEW. One hundred and forty five samples were selected from the four sections studied in this work and from the reference section of Addar (Peybernes et al., 2013). Poorly preserved samples (categories E3-O3) were removed from this analysis. We used all species, or group of species, representing more than 1% of the total assemblage. Since some species or groups present low relative abundance compared to the others, the percentages were normalized following an angular transformation, or arcsine transformation (Sokal and Rohlf, 1995). The angular transformation allows the normalization of the lowest and the highest percentages (<5% or >95%). The results of the PCA did not allow to identify new relationships between the different species or group of species, with respect to those already shown by the raw data (stratigraphic changes of the relative abundances). Consequently, results of the PCA are not presented in this work.

Species or group of species exhibiting spatial abundance changes

Both the relative and absolute abundances of *Nannoconus* spp. and *Staurolithites* spp. increase toward distal sections. Conversely, abundances of *Hayesites irregularis* increase toward the proximal sections.

Even though the percentages of *Nannoconus* spp. are low in all sections, there are some differences along the proximal-distal transect. The proximal section of Tinfoul (Fig. 4.40) is characterized by lower *Nannoconus* spp. percentages than in the more distal sections of Ida w Shayq, Tissakatine Center (Figs. 4.34, 4.36) and Addar (see, Fig. 6, in Peybernes et al., 2013 for Addar). We did not take into account Anzate, since only the Early Albian has been studied in this section, and *Nannoconus* spp. are rare in the Early Albian. *Nannoconus* spp. has been considered as a deep dweller (Table 4.6). In distal environments, the photic zone is deeper than in proximal ones, leading deep dweller to develop. The increase in the relative abundance of *Nannoconus* spp. from Tinfoul to more distal sections may be due to an increasing depth of the photic zone. However, in all sections, *Nannoconus* spp. are more or less restricted to the Late Aptian, carbonate rich lower part, corresponding also to lower fertility in surface waters and warmer conditions, with respect to the Early Albian, upper parts of the sections.

Staurolithites spp. is frequent in the distal sections of Ida w Shayq, Tissakatine Center and Addar (Figs 4.34, 4.36, 4.46), whereas it is rare in Anzate and Tinfoul (see countings in Appendix A), probably reflecting a preference for deeper, distal settings. Meso-eutrophic affinities have been proposed for *Staurolithites* spp. (Table 4.6), which are not confirmed by this study, since *Staurolithites* spp. do not present any significant temporal variations through the Aptian-Early Albian interval. This study suggests that *Staurolithites* spp. may be interpreted as an oceanic taxon.

Hayesites irregularis is frequent in both the Tinfoul and Anzate sections (Figs. 4.38-4.40), whereas it is rare in the other distal sections (see countings in Appendix A for Ida w Shayq and Tissakatine Center; Fig. 4.46 for Addar), and it does not present any temporal variation. *H. irregularis* was interpreted as low latitude species, a tropical taxa and/or a warm-water species (Table 4.6). This study shows that *H. irregularis* can be interpreted as a coastal taxon.

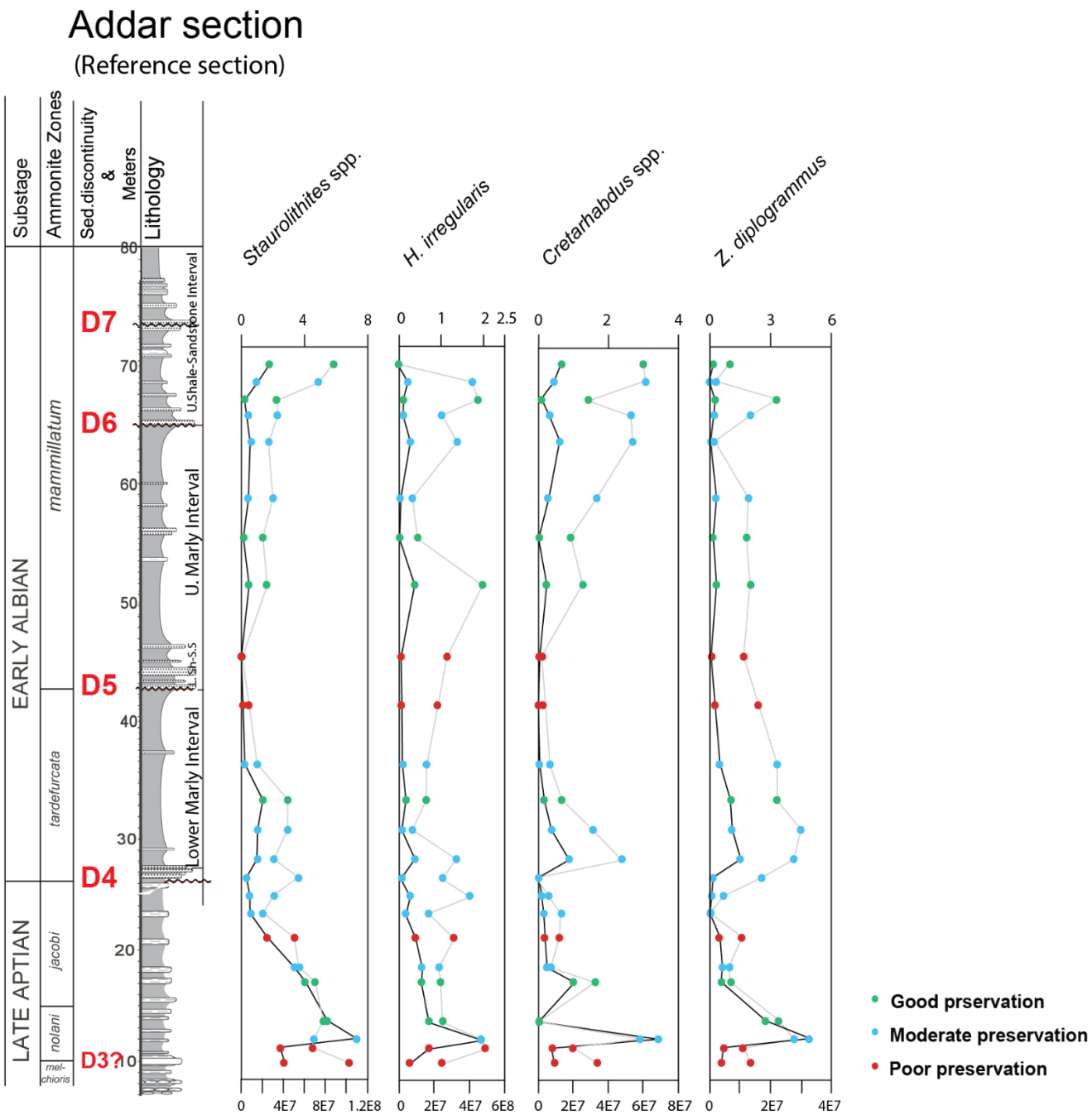

Figure 4.46: Stratigraphic changes for some calcareous nannofossil taxa proposed or confirmed to some paleoecological affinities in Addar section not have been figured in Peybernes., 2013: such as *Staurolithites* spp., *Hayesites irregularis, Cretarhabdus* spp. and *Zeugrhabdotus diplogrammus*

Species or group of species exhibiting no spatial and/or temporal abundance changes

Watznaueria communis is one of the most common species in all studied sections (Figs. 4.34, 4.36, 4.38, 4.40; see Peybernes et al., 2013 for Addar; Fig. 6); in which, *W. communis* has an opposite trend with counterparts in another studied section of Tamzergout (Fig. 7). It does not show any clear spatial and temporal trends among sections involved in this study and sections studied in Peybernes et al. (2013). It can be considered as a cosmopolitan species, as already proposed by some authors for the group of *Watznaueria* spp. (Bown, 2005; Vulc, 2008).

Cretarhabdus spp. is frequent in both proximal (Tinfoul, Fig. 4.40; rare in Anzate; Fig. 4.38) and distal sections (Ida w Shayq, Tissakatine Center, Addar, Figs 4.34, 4.36, 4.43), without spatial and temporal changes in the studied interval. Previous workers interpreted *Cretarhabdus* spp. as an oligotrophic or warm taxon (Table 4.6). Such paleoecological affinities for *Cretarhabdus* spp. are not confirmed by this study.

Zeugrhabdotus diplogrammus is common/frequent in all studied sections (Figs. 4.34, 4.36, 4.38, 4.40) and in the reference section of Addar (Fig. 4.46), and does not present any clear spatial and temporal variation. The previous interpretation for *Z. diplogrammus* as a warm taxon (Herrle, 2002; Herrle et al., 2003; Bottini et al., 2015) is not confirmed by this study.

CHAPTER FIVE

DISCUSSION AND CONCLUSIONS

CHAPTER FIVE
DISCUSSION AND CONCLUSIONS

5.1. SEDIMENTARY GAPS MAY CONTROL BIOSTRATIGRAPHY

Several sedimentary gaps (hiatuses) are contained within the discontinuity surfaces of the Aptian-Early Albian succession. These discontinuities comprise subaerial-karstified, and submarine-erosional surfaces. The subaerial-karstified surfaces occur in the lower part of the successions (Early Aptian-early Late Aptian) and are named D0, D1 and D2. The submarine-erosional surfaces are located in the upper part of the succession (Late Aptian-Early Albian), and are named D3, D4, D5, D6 and D7. These discontinuity surfaces enclose variable time gaps, probably longer in the karstified surfaces with respect to the submarine-erosional ones. In addition, the duration of these time gaps varies along the proximal-distal transects (east-west and north-south; Figs. 5.1, 5.2).

During the Early Aptian-early Late Aptian interval, along the east-west transect the D0, D1, D2 discontinuity surfaces are amalgamated as D0-2 in the more proximal section of Tinfoul, reflecting successive subaerial exposures, accompanied by erosion and/or dissolution of the underlying deposits. This time gap is probably shorter westward in the distal section of Addar, because only D0 and D1 are amalgamated. Northward in the EAB, the duration of these hiatuses becomes shorter, and some ammonite zones are identified, representing small submarine hiatuses at Tissakatine Center, Tissakatine east and Ida w Shayq (Fig. 5.1d).

The Late Aptian unconformity (D3) is interpreted as a hard ground, condensation episode, representing a submarine hiatus, likely related to marine currents (S3) in the western part of the EAB at Addar and Tissakatine Center. In the eastern part of the EAB, at Tissakatine east and Ida w Shayq, D3 is a submarine hiatus, associated with erosion of the underlying sediments, related to significant submarine currents (S4); it removes some previously deposited sediments, reflecting an increasing eastward duration of the hiatus (Fig. 5.2a).

The **Early Albian unconformities** D4, D5, D6, and D7 are mainly represented by submarine erosional surface (S4), probably reflecting a considerable time gap in all sections, particularly in the more proximal sections as Tissakatine east, in which the sedimentary facies overlying S4 is shallower than its counterparts of the distal sections (Fig. 5.2b).

The better understanding of the nature and of the lateral change of sedimentary discontinuities as well as their time gaps (by determining the decreasing and increasing direction of the time gap) in the Aptian-Early Albian succession of the EAB could explain several facts. (1) The lack and/or poor identification of some Early Aptian ammonite zones, particularly in the more proximal sections (e.g. Tinfoul), which are associated with long time gaps. (2) The sedimentary gaps and submarine erosions included within D4 and D5, which occur in the Late Aptian-Early Albian succession, may suggest the lack of part of both the *jacobi* and *tardefurcata* ammonite zones.

These missing parts of the ammonite zones correspond to similar absence of parts of the nannofossil zones and of the carbon isotope record in the same sections. (3) The laterally variable duration of time gaps, along the proximal-distal transects, as well as the absence of variable sedimentary intervals could explain the weak correlation of relative abundances of both cold-warm and meso-eutrophic nannofossil taxa between the studied sections.

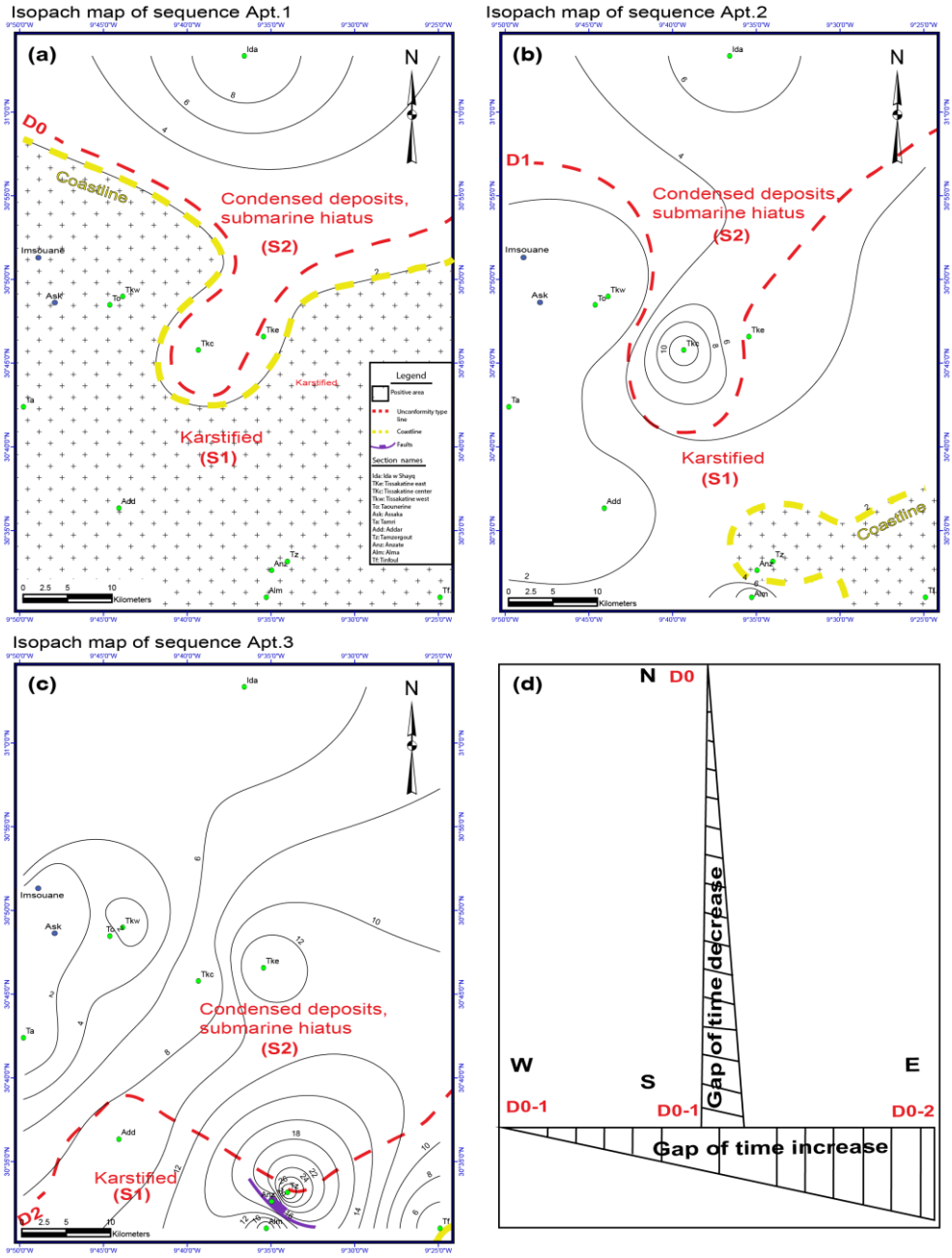

Figure 5.1: Boundary limiting the distribution of both the subaerial- erosional surface (S1) and the submarine-erosional surface (S2) (red line), the position of coastline (yellow line) as well as the isopach maps of the Early-Late Aptian depositional sequences a) Ap.1, b) Ap.2, c) Ap.3., and d) W-E increase and S-N decreasing gap of time for the same surfaces (D0-D2).

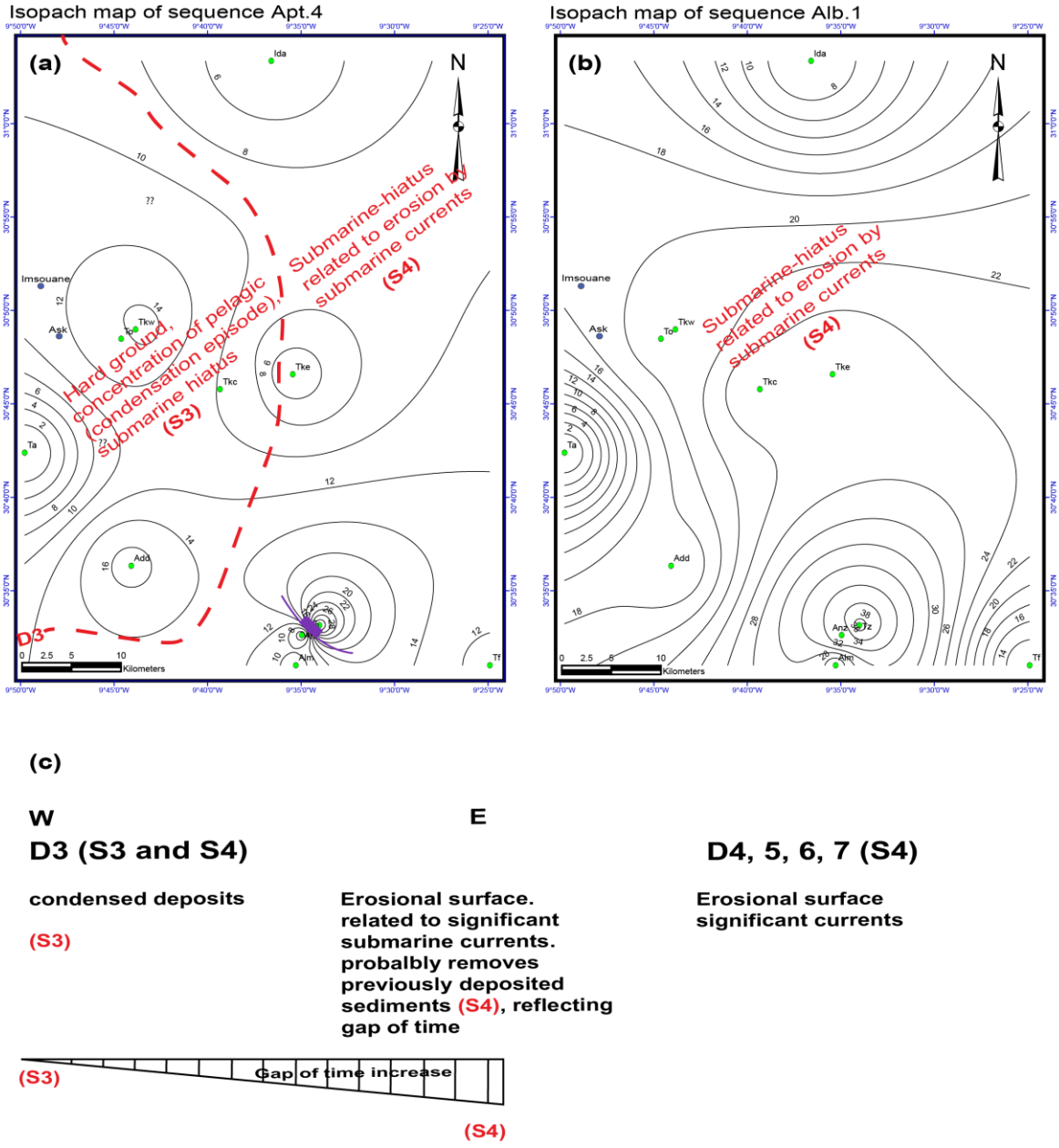

Figure 5.2:

a) Boundary limiting the distribution of the submarine hiatus, related to condensation episode (S3) and the submarine hiatus, related to erosion by submarine currents (S4) (red line), as well as the Isopach maps of the latest Aptian depositional sequence (Ap.4),

b) The wide extension of the submarine hiatus, related to erosion by submarine currents (S4) during all Early Albian depositional sequences (Alb.1, Alb.2, Alb. 3, and Alb.4.), and

c) W-E increasing gap of time between S3 and S4 during the latest Aptian.

5.2. BIOSTRATIGRAPHY

5.2.1. Ammonite biostratigraphy

Our analysis of the distribution of the ammonite species identified in the Aptian-Albian series of the EAB allowed E. Robert to establish a detailed faunal succession. Our succession can be easily correlated with the Standard Mediterranean Zonation proposed by the IUGS Lower Cretaceous Ammonite Working Group ("Kilian Group"; Reboulet et al., 2011; 2014). We were able to correlate the ammonite succession with the four Late Aptian standard zones and with the first two zones of the Lower Albian. The Early Aptian and basal Late Aptian zones have also been identified, although with much less accuracy because of condensed sedimentation and temporal hiatuses (Robert, *in* Peybernes et al., 2013). Various new species and/or genus have been recognized in the ammonite faunas of the EAB (Robert, *in* Peybernes et al., 2013). However, because the purpose of this section is to present our stratigraphic framework, these endemic species are not mentioned in the text (Robert, *in* Peybernes et al., 2013). In addition, the Upper Barremian *Martelites sarasini* Zone has been recorded in the Ida w Shayq section, and also occurs in the Upper Barremian of Eastern Europe (Hoedemaeker et al., 1993).

The Aptian-Early Albian ammonite succession of the EAB could be correlated with that of both southern and northern Tethyan margins (Fig. 5.3), especially with the faunas collected from SE France, marked by its famous abundance and good preservation, and considered as the base of the lower Cretaceous zonation (Hoedemaeker et al., 1993).

The Early Aptian in the EAB, is represented by the *Deshayesites deshayesi* and *Dufrenoyia furcata* ammonite zones, which could be correlated with the *deshayesi* Zone of Tunisia (Memmi, 1981), with the *matheroni-deshayesi* Zone in Gabal abu Ruqum (North Sinai), with the *deshayesi* Zone of Gabal Risan Aneiza, north Sinai (Egypt) defined by Hamama and Gabir (2001), and with the *matheroni* Zone of Gabal Lagama, north Sinai (Aly and Abdel Gawad, 2001). In the northern Tethyan margin, the ammonite zones are represented by the *Deshayesites deshayesi* and *Tropaeum bowerbanki* in the Vocontian Basin, SE France (Bréhéret, 1997, Moullade et al., 1998; Kennedy et al., 2000), *D. oglanlensis, D. weissi*, *D. deshayesi* and *D. Furcata* in the Cassis-La Bédoule area, SE France (Ropolo et al., 2008), and by *D. oglanlensis*, *D. forbesi (*equal to *weissi)*, *D. deshayesi* and *D. furcata* in the Maestrat Basin, E Spain (Garcia et al., 2014).

Late Aptian times are represented by the *Epicheloniceras martini*, *Parahoplites melchioris, Acanthohoplites nolani* and *Hypacanthoplites jacobi* ammonite zones in the EAB. In Tunisia, Memmi (1981) defined three Late Aptian ammonite zones; 1) *Aconeceras nisus* (correlatable to *martini* and *melchioris* zones), 2) *Diadochoceras subnodosocostatum* (comparable to *nolani* Zone), and 3) *jacobi* ammonite Zone. In North Sinai, Egypt, Aly and Abdel Gawad (2001) defined three ammonite zones: *martinoides* (comparable to *martini* ammonite Zone), *nolani* and *jacobi*. In the Vocontian Basin, SE France, many authors as Bréhéret (1997); Moullade et al. (1998) and Kennedy et al. (2000), defined four ammonite zones; *martinoides* (equal to *martini* in the EAB), *Parahoplites nutfieldensis* (equivalent to *melchioris*), *nolani* and *jacobi*. In the Cassis-La Bédoule

area, SE France, Ropolo et al. (2008) defined two ammonite zones; *martini* and *melchioris*. In the Maestrat Basin, E Spain, Garcia et al., (2014) defined three Zones; *martini*, *melchioris* and *nolani*.

The **Early Albian** *Leymeriella tardefurcata* and *Douvilleiceras mammillatum* ammonite zones in the EAB, allow correlations with Tunisia (Memmi, 1981; Latil, *in* Chihaoui et al., 2010; Latil, 2011), North Sinai, Egypt (Aly and Abdel Gawad, 2001), the Vocontian Basin of SE France (Bréhéret, 1997; Moullade et al., 1998; Kennedy et al., 2000), or the Maestrat Basin, E Spain (Garcia et al., 2014). Therefore the ammonite zonation is easily recognized and applicable in both sides of the Tethyan margins and it could be used as the building stone for the biostratigraphic framework in the EAB.

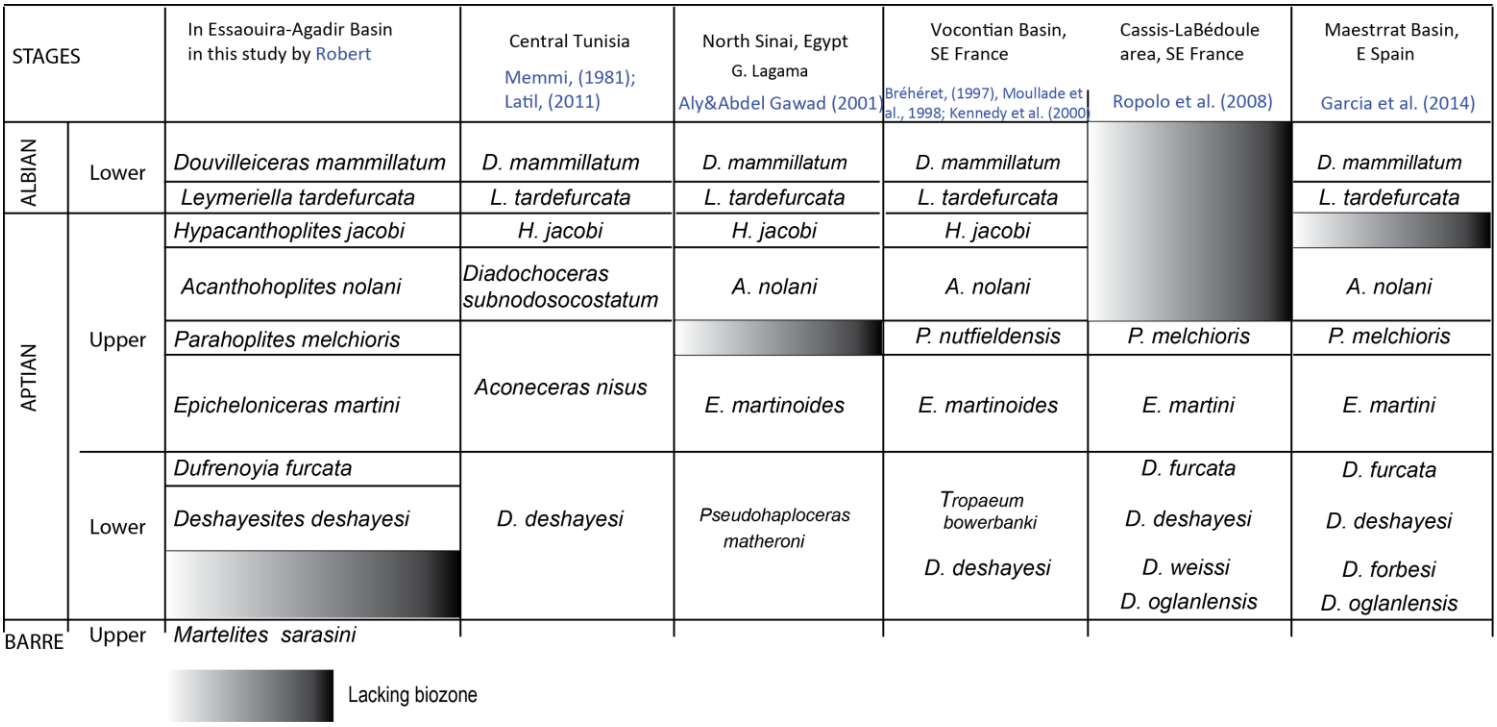

Figure 5.3: Correlation of the ammonite zones along both southern and northern margins of the Tethyan Ocean.

5.2.2. The Aptian-Early Albian calcareous nannofossil biostratigraphy in the Moroccan sections in comparison with the Vocontian Basin, SE France

The presented calcareous nannofossil zonation of the Aptian-Early Albian succession of the EAB, is the first attempt to develop a calcareous nannofossils biostratigraphic zonation in Morocco, and therefore, provides an excellent opportunity to correlate the nannofossil zones with adjacent sections and basins of the Tethyan realm. In this study, we consider the Tissakatine Center section as the most complete section for the Aptian-Early Albian nannofossil zones, which allows comparison with similar studies in other basins (Fig. 3.11).

The Aptian-Early Albian interval has been recovered in both DSDP sites 370 and 545. The DSDP site 370 is located in the deep basin off the Atlantic coast of Morocco, very close to the base of the Moroccan continental slope. The Aptian-Early Albian interval is characterized by hemipelagic, nannofossil-bearing clays and marls alternating with fine to coarse siliciclastic deposits, showing the proximity of the Atlas Mountains. The DSDP Site 545 is close to the DSDP Site 370, located on the Mazagan Escarpment and corresponds to a shallower environment (upper part of the slope) with respect to the DSDP Site 370 (Fig. 1.10). The studied time interval is represented by light green nannofossil claystones. Both DSDP sites represent deeper environments with respect to the Essaouira-Agadir Basin for the studied time interval. For both sites, a revision of the nannofossil biostratigraphy has been made by Bralower et al. (1993), and we used these data for comparison with our study of the EAB. The FO of *Eprolithus floralis* (marking the base of NC7) is recorded close to the Early/Late Aptian Boundary, and the FO *Hayesites albiensis* (marking the top of NC8A) is recorded in the earliest Albian in both the EAB (Tissakatine Center section) and DSDP Site 370 with respect to earlier FO of *H. albiensis* in latest Aptian in DSDP site 545 (Bralower et al., 1993). The comparison of both Moroccan DSDP sites with the land sections of the EAB reveals that the nannofossil biostratigraphic resolution is higher in the upper bathyal environment of the DSDP Site 545 and in the shallow environment of the Essaouira-Agadir Basin, with respect to the deeper environment of the DSDP Site 370. The lower biostratigraphic resolution observed in the DSDP Site 370, as well as the younger FO of *H. albiensis* in DSDP site 370 and the EAB, could be due to the occurrence of many siliciclastic sandstone levels within the successions in both DSDP site 370 and in the EAB, reflecting less favorable conditions to the preservation of rare taxa such as marker species, with respect to nannofossil claystones recovered in the DSDP Site 545 (Bralower et al., 1993).

More recently, Herrle (2002), Herrle and Mutterlose (2003) have established an Aptian-Albian nannofossil biostratigraphy in the Vocontian Basin (SE France; northern Tethyan margin). Their study shows that the FO of both *Eprolithus floralis* and *Hayesites albiensis* are recorded earlier, in the Early Aptian and latest Aptian respectively, in the Vocontian Basin with respect to the EAB. This diachronism in the FO of both *Eprolithus floralis* and *Hayesites albiensis*, could be interpreted in terms of preservation and regional differences in paleoenvironmental conditions. The poorly to moderately preserved nannofossil assemblages encountered in the Moroccan sections could be explained by the dominance of siliciclastic sediments, which are less favorable for a good preservation of nannofossils with respect to more carbonate sediments, and/or due to the important

burial (up to 1800m) of the Aptian-Albian successions in the EAB; Daoudi et al., 2010), could explain the younger occurrences of both taxa in the EAB. *E. floralis* is described as a species common in high-latitudes by Roth and Krumbach (1986). Therefore, the shorter migration to reach Europe with respect to Africa, may reflect the earlier the FO of this species in the Vocontian Basin with respect to the EAB.

5.3. SEDIMENTARY CYCLES AND SEQUENCE STRATIGRAPHY IN THE EAB DURING APTIAN-EARLY ALBIAN TIMES

The lithology, fossil content, thickness of the Aptian-Early Albian succession of the EAB, as well as the recognition of major boundaries, allow us to define two major sedimentary cycles. The Late Barremian-Aptian transgressive cycle, and the Early Albian transgressive cycle (Figs. 4.24, 4.26, 4.28).

Late Barremian-Aptian Transgressive Cycle. It is bounded by two major boundaries. It is floored by SB0 and topped by (SB4), and encloses four depositional sequences, named Ap.1, Ap.2, Ap.3 and Ap.4, and discussed below:

The Ap.1 sequence, underlined by SB1, corresponds to the upper part of sequence Ba-Ap.1 (based by ravinement surface) and lower part of sequence Ap.2 (based by hard surface) of Witam (1998) (Fig. 5.4).

In this study, the lower sequence boundary (SB0, Latest Barremian, *sarasini* ammonite Zone) of sequence Ap.1 corresponds to the KBa5 (126.4), of Latest Barremian age in Haq et al. (2014). Its upper boundary (SB1, Early Aptian, located between the *deshayesi* and *furcata* ammonite zones), is located just below KAP2 (latest Early Aptian, *furcata* ammonite Zone, in Haq et al., 2014). In addition, the KAP1 (125.6), of earliest Aptian age, which is located within the *forbesi* ammonite Zone is not recognized in the EAB. The *forbesi* ammonite Zone is not defined in the EAB. In the EAB therefore, either KAP1 does not exist, or it is eroded and/or amalgamated with KBa5.

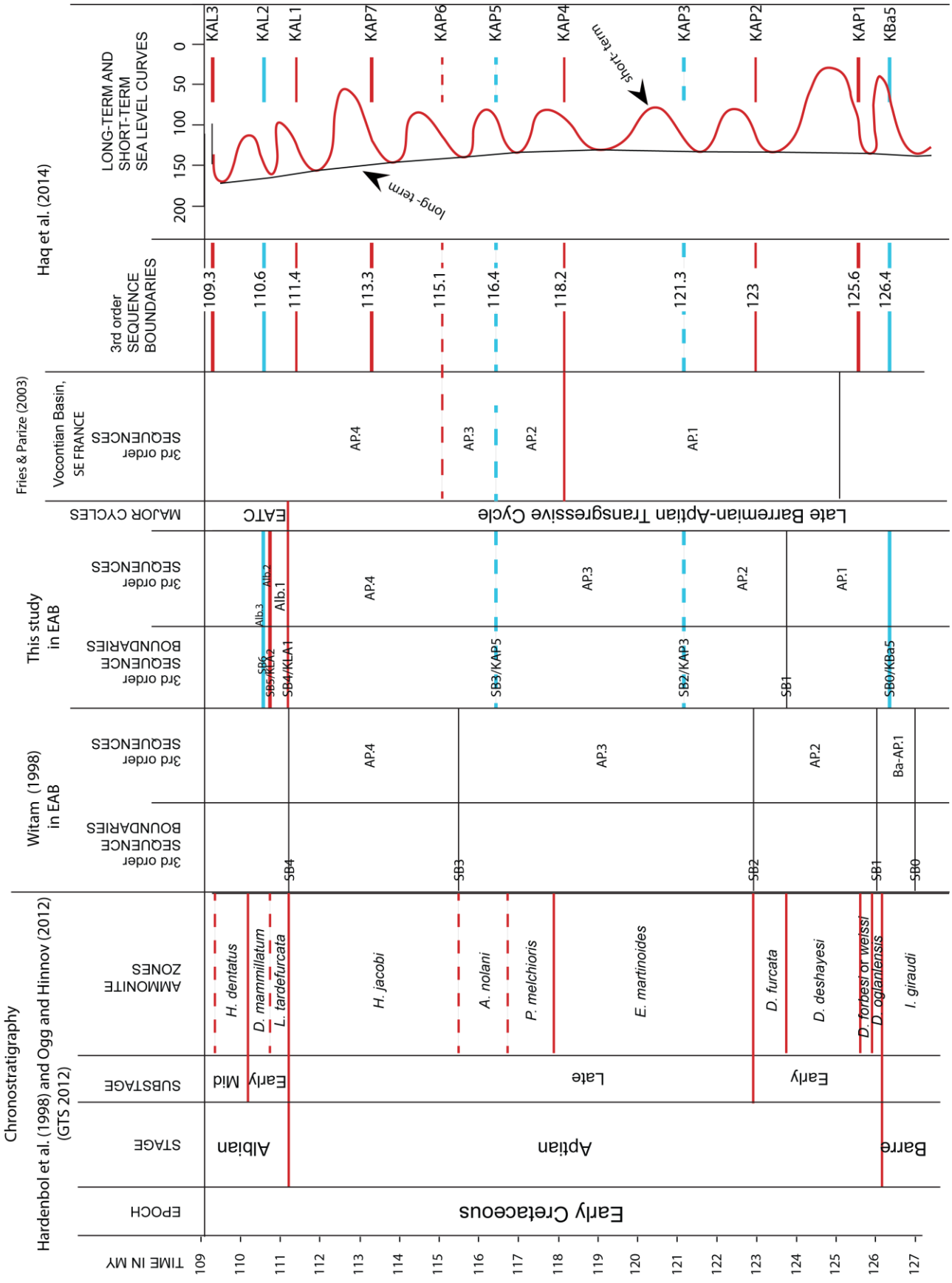

Figure 5.4: Chronostratigraphic chart compare the sequence boundaries and depositional sequences in EAB during the Aptian-Early Albian time, with Vocontian Basin, SE France and Global sea level curve of Haq et al. (2014). Abbreviations: EATC, Early

The sequence Ap.2 is comparable to the upper part of Ap.2-lower part of Ap.3 of Witam (1998) (Fig. 5.4). The upper sequence boundary (SB2), mostly occurred within the *martini* ammonite Zone, and coincides with KAP3 (121.3 my) of Haq et al. (2014) (Fig. 5.4).

The sequence Ap.3 is correlated to the middle part of Ap.3 of Witam (1998) (Fig. 5.4). The upper sequence boundary (SB3) of Ap.3, is placed at the boundary between *melchioris* and *nolani* ammonite zones, in some studied sections. However, in the Alma, Anzate, Taounerine and Tissakatine Center sections, it occurred in the lower part of the *nolani* ammonite Zone, as KAP5 (116.4 my) of Haq et al. (2014) (Fig. 5.4). KAP4 (118.2 my), is not recognized in the EAB.

The sequence Ap.4 is equal to the uppermost part of Ap.3 and to Ap.4 of Witam (1998) (Fig. 5.4). In the EAB, its upper sequence boundary (SB4) is approximately placed at the top of the *jacobi* ammonite Zone, just above KAL1 (111.4 my), placed at the uppermost part of the *jacobi* ammonite Zone by Haq et al. (2014) (Fig. 5.4). Both KAP6 and KAP7 that occur at the base and in the middle part of the *jacobi* ammonite Zone, respectively, are not recognized in the EAB.

Early Albian Transgressive Cycle. This cycle is underlined by SB4, and consists of four deepening upward sequences, named Alb.1, Alb.2, Alb.3 and Alb.4. Compared to the Aptian sequences, they are marked by an increase in the detrital content, and by higher thicknesses, indicating a higher accommodation space and a sea level rise (Figs. 4.24, 4.26, 4.28).

No sequence stratigraphy work has been done before this study for the Early Albian in the EAB. The upper sequence boundary (SB5) of sequence Alb.1 is placed between the *tardefurcata* and *mammillatum* ammonite zones, and is located just below KAL2 (110.6 my), which is placed in lower *mammillatum* ammonite Zone in Haq et al. (2014).

All Early Albian sequences (Alb.2, Alb.3 and Alb.4) are located within the *mammillatum* ammonite Zone. SB6, the upper boundary of Alb.2, is located in the lower part of the *mammillatum* ammonite Zone. Therefore, SB6 could be correlated with KAL2. The upper boundary of Alb.3, SB7, is also placed within the *mammillatum* ammonite Zone. KAL3, dated at 109.3 my by Haq et al. (2014), is placed in the middle Albian *Hoplites dentatus* ammonite Zone, which is not recorded in the EAB (Fig. 5.4).

The four Early Albian sequences Alb.1, Alb.2, Alb.3 and Alb.4, about 75 m thick in the Tissakatine sections (Fig. 4.26), represent the *tardefurcata* and *mammillatum* ammonite zones, approximately located between KAL1 (111.4 my) and KAL2 (110.6 my), a total time duration about 1 my (Fig. 5.4). This reflects a high sedimentation rate, associated with a large accommodation space during the Early Albian.

Witam (1998) made the sequence stratigraphy for the Aptian succession in the EAB. Witam performed his study on many different sections; some of these sections correspond to our studied sections like Addar; some other sections are very close to our, as Tamzergout and Assaka, whereas other sections were studied far from our sections. The sequences defined by Witam (1998), observed in all sections, are composed of LST, TST, HST, bounded by two SBs. Conversely, in our study, some Aptian sequences are lacking in some sections (like Ap.1 and Ap.2 in the southern part of the basin), the LST is not recognized in all sequences, and the MFS and HST are missing in some sequences. Moreover, there are important differences in the thicknesses observed by Witam and those measured in this study. The thickness of our Tamri section is about 50 cm thick, while the Assaka section in Witam's study is about 35 m thick. Finally, the sequence boundaries found by Witam are poorly correlated to the boundaries of our study (Fig. 5.4). In our study (1) the sequence boundaries (SBs) are well defined in the field, are dated by ammonite and classified into subaerial and submarine surfaces, and allow a good understanding of the nature of the stratigraphic gaps, and (2) the system tracts and depositional surfaces (TS and MFS), are precisely defined through well constrained depositional environments interpreted from an analysis of sedimentary facies.

5.3.1 Aptian-Albian sedimentation and sea level changes in the EAB

According to Haq and Qahtani (2005), that regional cyclicity mimics global cyclicity during a discrete time interval, indicates that eustasy was the dominant control on sedimentary patterns. Conversely, little or no correspondence between regional and global patterns suggest prevailing tectonic and other regional factors.

In the EAB, during the Aptian-Early Albian time, there is a good agreement of four sequence boundaries (SB0, SB2, SB3 and SB6), with the eustatic sequence boundaries KBa5 (126.4 my), KAP3 (121.3 my), KAP5 (116.4 my) and KAL2 (110.6 my) of Haq et al. (2014), respectively. KAP1, KAP2, KAP4, KAP6, KAP7 and KAL1 are poorly defined in the EAB (Fig. 5.4). From the field observations, there are no clear evidences on occurrence of both subsidence and tectonics. Consequently, the later sequence boundaries could be amalgamated with the previous ones, due to the presence of several gaps. Therefore, these sequences could be directly related to the third-order cycles of the eustatic chart, suggesting that eustasy was more important than regional and/or local tectonics, and was the an important factor controlling factor on the EAB carbonate platform architecture. However, the subsidence history for the EAB, have been studied by Bouatmani et al. (2007), suggesting low subsidence in the Aptian, followed by higher subsidence during Albian time. Therefore, the relative sea-level changes recorded by the EAB (Fig. 5.4), may have been also controlled by mild, local tectonic activity during Aptian-Albian times (see Figs. 4.25, 4.27, 4.29).

5.4. FACTORS CONTROLLING THE CARBONATE PRODUCTION DURING THE APTIAN-EARLY ALBIAN TIME

The carbonate production in the EAB, is higher in the Aptian than during the Early Albian. The Aptian carbonate-rich succession is composed mainly of marls and marly limestones. The Early Albian succession consists of shales intervened by thin beds of fine sandstones and siltstones. The carbonate production in the EAB, during the Aptian-Early Albian time is temporally controlled by environmental factors, such as relative sea level changes, and paleogeography-bathymetry and siliciclastic input.

Environnemental Factors

Carbonate production records environnemental conditions. The climate and nature of the carbonate-producing biota are probably the most important factors (Lees, 1975; Schlager et al., 1987; Philip, 2003; Raspini, 2012). The Aptian period was a warm spell followed by a peak of cooling in latest Aptian-Early Albian times (Herrle and Mutterlose 2003; Mutterlose et al., 2009), which played an important role in the carbonate production in the EAB. Carbonate production prevails in warm conditions (Philip, 2003). The Aptian carbonate platform of the EAB is characterized by more abundant warm surface-water nannofossil taxa with respect to the Early Albian.

Conversely, the Early Albian successions shows a significant change in the calcareous nannofossil community, represented by an increase in cold surface-water nannofossil taxa. This significant changes likely reflects changes in environmental conditions, triggered by fluctuations in sea-surface temperatures.

The Aptian succession is characterized by shallower marine organisms, as oysters, thick shelled bivalves, brachiopods, gastropods and echinoderms, while the Albian deposits are marked by deeper pelagic fauna such as ammonites and belemnites, and organisms restricted to dysoxic conditions (Buchidae bivalves and annelids). These significant changes in the biotic communities likely reflect a eustatic sea level rise, which stressed the platform biota, reflecting a deepening phase.

Both benthic organisms and calcareous nannofossils are the main carbonate producers in the EAB, during the Aptian-Albian, such as in many basins on both Tethyan margins.

In the EAB, Aptian times present high abundances of both benthic organisms and calcareous nannofossils, including nannoconids, which are considered as the biggest and more calcified nannofossils during Late Aptian, in the interval known as the "*Nannoconus truittii* Acme" described by Mutterlose (1989), and constitute the major component of the carbonate fraction produced by nannofossils, as observed in the Tethyan and Boreal realms (Mutterlose, 1989; Erba, 1994; Herrle and Mutterlose, 2003). Therefore, the high carbonate content in Aptian times (mean $CaCO_3$ content ≈ 48%), with respect to Albian (mean $CaCO_3$ value ≈ 20.5 %) could be attributed

to higher abundances of both benthic organisms and calcareous nannofossils with respect to the Early Albian.

Latest Aptian and Early Albian times are marked in the EAB by a relative decrease in calcareous nannofossils abundances, with particular sharp decrease in *Nannoconus* abundances, in the North Sea (Rückheim et al., 2006a, b), North Germany (Mutterlose et al., 2003), Italy (Erba, 1994; Cobianchi et al., 1997), the Vocontian Basin (Herrle and Mutterlose, 2003), and the Atlantic, Pacific and Antarctic oceans (Wise, 1983; Mutterlose and Wise, 1990; Herrle, 2002; Mutterlose et al., 2009), reflecting cool conditions and a decrease in carbonate production during Late Aptian-Early Albian times (Herrle and Mutterlose, 2003; Mutterlose et al., 2009; Peybernes et al., 2013).

Relative sea level changes

Relative sea-level changes include the contributions of both subsidence and eustasy to the space available for sediments accumulation (e.g. Watts and Steckler, 1979; Posamentier et al., 1988; Vail et al., 1991). Relative sea level rises are due to subsidence or eustatic sea level rise. Conversely, relative sea level falls are due to tectonic uplift or eustatic sea level fall (Jervey, 1988).

In the EAB, the TSTs and HSTs of the Aptian sequences are deposited under shallow depths of inner to middle shelf settings, reflecting increasing or decreasing accommodation space, respectively, while the emergence karstified surfaces (SBs) are representing periods of negative accommodation space. The Aptian/Albian Boundary is mainly represented by an erosional submarine surface (SB4), associated with thin beds sandstone, deposited in middle ramp setting, reflecting a drastic drop in sea level. The Aptian-Albian sea level drop recorded in the EAB is comparable to similar falling stage on the global sea level curve of Haq et al. (1987, 2014) and Hardenbol et al. (1998). During the Early Albian, the TSTs and the HSTs of the Early Albian sequences are deposited in deeper, outer shelf to basinal environments (Fig. 4.30). This, as well as the absence of emergence surfaces, suggests rapid sea level rise, possibly associated with rapid subsidence rate during the Albian. In addition, the presence of salt diapirs in subsurface may explain the spatial change in thickness of the Albian depositional sequences (see Figs. 4.25, 4.27, 4.29, 4.32). As a matter of fact, higher subsidence during Albian time in the EAB is suggested by Bouatmani et al. (2007), and local tectonic activity is documented by Witam (1998).

The depositional sequences are subdivided into two transgressive facies cycles; latest Barremian-Aptian transgressive facies cycle and Early Albian transgressive facies cycle, reflecting long-term sea level rise. Therefore, the Aptian-Early Albian sedimentary facies building up the carbonate platform in the EAB, is controlled by eustacy.

However, during the Aptian-Early Albian, the EAB is considered as a relatively stable basin, developed on a passive margin, partially controlled by subsidence and local tectonics. Nevertheless, Aptian-Albian times are characterized by the opening of the Equatorial Atlantic Ocean, initiating local tectonics in some basins. So, some Aptian and/or Albian basins are tectonically controlled especially on the southern margin of the Tethys, for example in Tunisia

(Jaillard et al., 2013; Marco et al., 2014), Egypt and Israel (Bachmann et al., 2010), and the Arabian Peninsula (Van Buchem et al., 2010). Along the northern Tethyan margin, tectonically controlled basins have been recorded in Portugal (Dinis et al., 2002), Spain (Fernandez-Mendiola and Garcia-Mondejar, 1988, 2013; Rosales, 1999; Castro et al., 2008), Italy (Ruberti et al., 2013; Basilone et al., 2016), Turkey (Masse et al., 2009), and Iran (Mansouri-Daneshvar et al., 2015).

In the EAB, the Aptian-Albian successions may be divided into two different depositional cycles. The Aptian cycle is characterized by carbonate dominated sediments, deposited under shallow marine water, between the inner and middle ramp setting. The Early Albian cycle is marked by shale and sandstone dominated sediments, deposited in deeper environments, between the outer ramp and basinal settings. The carbonate production increases during the Aptian in shallow water depths during relative slow rise and/or highstand of sea level (e.g. Philip, 2003; Chihaoui et al., 2010; Raspini, 2011), whereas it decreases during Early Albian time and is associated with a relatively rapid sea level rise. During sea level rise, carbonate platforms are sometimes not able to keep up, leading to slowdown of the carbonate production (Gômez-Pérez, 1997; Raspini, 2011). So, the carbonate production in the EAB seems to be controlled by changes in relative sea level. In case of sea level fall or stabilization (HST), the carbonate production increases, as during the Aptian. Conversely, in case of sea level rise, as during the Early Albian interval, the carbonate production decreases.

Paleogeography, bathymetry and siliciclastic input

According to paleogeographic maps for the Aptian–Albian North Atlantic region (Trabucho-Alexandre et al., 2011; Fig.1.3), the EAB was located approximately at 15° N latitude, in the arid belt of Chumakov et al. (1995) and Voigt (1996).

Little accommodation space in the EAB and low sea level during Aptian time, gave way to shallow basins and suggests low rate of sedimentation (Jervey, 1988). During Aptian time, the position of EAB in the arid belt, associated with shallow depth, low sedimentation rate and little siliciclastic input, led to the development of a large photic zone and warm conditions in the marine realm, favorable for carbonate production.

During Early Albian time, sea level rise and siliciclastic input in the EAB, allowed the development of deeper basins and deposition of thick successions. This reduced the thickness of the photic zone, and consequently led to the decrease of carbonate production.

In Summary, the carbonate production during Aptian stage is favored by the presence of warm conditions, slow rising or/standing up of relative sea level, and by the presence of shallow basin, without or with little terrigenous input.

5.5. CALCAREOUS NANNOFOSSIL PRIMARY PRODUCTIVITY DURING THE APTIAN-EARLY ALBIAN TIME

High resolution reconstruction of nannofossil primary productivity and surface water temperature has been made for selected Aptian-Early Albian intervals, such as the DSDP site 545 (Mazagan Plateau), the Vocontian Basin (SE France) (Herrle, 2003; Herrle et al., 2003b, 2010), in Piobbico core (Umbria-Marche Basin, Central Italy) (Tiraboschi et al., 2009; Bottini et al. (2015); and for the DSDP site 463 in Pacific Ocean (Bottini et al. (2015). However, these studies are difficult to correlate with the studied sections in the EAB, due to the occurrence of several sedimentary gaps with variable duration, and to the existence of condensed successions characterizing the Aptian-Albian time. Therefore, the objectives of this study are to document Aptian-Early Albian long-term trends in surface water fertility and temperature in the EAB.

In the EAB, the calcareous nannofossil primary productivity is higher in Early Albian time than in the Aptian. In such a ramp-shaped platform, nutrients may come either from coastal upwellings, or from continental terrigenous influx. During high sea level, most of nutrient likely come from upwelling currents, while during low sea level, most nutrient are likely provided by the continental input.

In the EAB, the change in eustatic sea level during Aptian-Early Albian times could be easily recognized in the more proximal sections than in the distal ones (Figs. 4.24, 4.26, 4.28). The proximal sections reflect a slow rise and/or standing up of sea level during the Aptian, interrupted by a short drastic drop at the Aptian/Albian Boundary. It is followed by an important sea level rise during the Early Albian, suggesting an upward increase of nutrient input from upwelling current through Early Albian time. In the more distal sections, as in Ida w Shayq, the relative sea level is relatively fluctuated, always reflecting deeper environments, with reduced hiatuses between depositional sequences (Figs. 4.26, 4.28), and high abundance of meso-eutrophic taxa at Ida w Shayq section (Fig. 4.45), suggesting a stable rise of sea level during Latest Aptian-Early Albian times, with stronger upwelling currents.

In the EAB, the Latest Aptian-Early Albian interval is marked by a high relative abundance of nannofossil upwelling indicators such as *Biscutum* spp. and *Zeugrhabdotus* spp. (Figs. 4.44, 4.45, Table 4.6), and by the presence of phosphatic clasts due to submarine currents, above the Aptian/Albian Boundary in most studied sections, with special concentration recorded in the more distal section of Tamri (Fig. 4.6). The presence of upwellings along the Moroccan margin (Mazagan Plateau) was suggested by Leckie (1984), based on the high abundance of radiolarians, the high benthic/planktonic foraminifera ratio, and the high abundance of fish debris. In northern Tunisia (Fadhel et al., 2011; 2014), the influence of upwellings was inferred from the abundance of radiolarian and calcispheres. Upwelling zones are documented parallel to southern Tethys margin, during the Aptian-Albian (Trabucho-Alexandre et al., 2011; Fig. 1.3). In addition to, a regional study performed by Mutterlose et al. (2009). This study is mainly concentrated on both low and high palaeolatitude areas, including BGS Borehole 81/40 (North Sea Basin); Vöhrum section (North Germany); a composite section in Vocontian Basin (SE France); DSDP Site 545

(Mazagan Plateau, off-shore Morocco); ODP Site 766 (off-shore northwest Australia); DSDP Site 511 (off-shore southern Argentina); ODP Hole 693A (Land of East Antarctica). This Aptian-Albian upwelling areas is documented by a bloom of high fertility siliceous organisms; 1) diatoms in North Germany (Georgi, 1976; Benda, 1982), East Antarctica (Gersonde and Harwood, 1990; Harwood and Gersonde, 1990), Australia (Gersonde and Harwood, 1990) and Mazagan Plateau (Leckie et al., 2002), and 2) silicoflagellates in East Antarctica (McCartney et al., 1990) and Mazagan Plateau (Leckie et al., 2002), reflecting widespread extension of upwelling current, controlling nutrient input, increased fertility and primary productivity. In the EAB, the highest calcareous nannofossil primary productivity is associated with the high sea level period during Latest Aptian-Early Albian times in Ida w Shayq section. This conclusion supporting the significant role of upwelling in more distal sections during rising of sea level, as recorded in Blake Nose, western North Atlantic (Browning and Watkins, 2008); Umbria-Marche Basin, Central Italy (Tiraboschi et al., 2009), and in areas studied by Mutterlose et al. (2009).

During the Early Albian, the mean relative abundance of the mesotrophic taxa was higher on the Mazagan Plateau (~ 45%) than in the EAB (~24.5%), reflecting that the nannofossil productivity is lower in the EAB than on the Mazagan Plateau. This indicates that the Mazagan Plateau was located deeper, within the main upwelling area, while the EAB was located on the margin of upwelling area.

The co-occurrence of higher calcareous primary productivity and cooler surface water temperature during Late Aptian-Early Albian time in the EAB, could reflect the role of upwelling inducing cold-water rich in nutrients (Roth and Bowdler, 1981; Roth and Krumbach, 1986; Föllmi et al., 2006). On the Atlantic margin off Morocco (Site 545), marked by water circulation due to connection between the North and South Atlantic Ocean basins by late Aptian time (Mutterlose et al., 2009), the cooling may have caused increased water circulation and high surface water fertility (Mutterlose et al., 2009).

The comparison between the southern and the northern Tethyan margins shows that the nannofossil productivity is higher in the Vocontian Basin with respect to both the Mazagan Plateau and the EAB during the Late Aptian-Early Albian interval (Peybernès et al., 2013). The Vocontian Basin is located near the boundary between the tropical-equatorial hot arid belt and the northern mid-latitude in the warm humid climatic belts (Chumakov et al., 1995; Voigt, 1996; Figs. 1.2; 1.3), and more nutrients are associated with runoff. Moreover, Herrle (2002) and Herrle et al. (2003) showed that the Vocontian Basin was submitted to a monsoon climate-type during the Early Albian. More recently, Trabucho-Alexandre et al. (2011), in a study focused on the Early Albian in western Tethys, located both the Moroccan margin and the Vocontian Basin within the tropical-equatorial, hot arid belt of Chumakov et al. (1995), proposed that the enhanced primary productivity during-the Early Albian OAE1b was controlled by upwelling currents, thus reducing the role played by river nutrient input, and proposing that rivers are playing an important role in sites located at high latitudes in the humid temperate climate zone, while aeolian nutrient input dominated at lower latitudes within the arid climate belt.

The clay mineral assemblages from different low to mid palaeolatitudes, including the Algarve Basin, SW Portugal (Heimhofer et al., 2008), the EAB (SW Morocco; Daoudi and Deconinck, 1994; Daoudi et al., 2010) and the Vocontian Basin (SE France; Bréhéret, 1997), show very similar patterns with high abundances of illite, indicating high physical weathering rates in the source areas, associated with arid climate in both the northern and southern margins of the Tethys. Consequently, with respect to the northern margin, both in neritic (Heldt et al., 2010) and pelagic realms on the southern Tethyan margin the trophic conditions in sea surface water were probably lower. That is most likely due to more arid climatic conditions to the South (Peybernès et al., 2013).

5.6. SEA-SURFACE TEMPERATURE CHANGES DURING APTIAN-EARLY ALBIAN TIMES

The Aptian-Albian transition has been identified as a period of significant climate cooling. Evidences for this cooling episode mainly proceed from high-latitude records and are supported by lithological, geochemical and paleontological proxies (Peybernés et al., 2013). Decreasing surface water temperatures are indicated by a first global decline of Tethyan nannoconids in the Late Aptian at both high and low latitudes, associated with increasing nannofossil boreal taxa in low latitudes during the Late Aptian to Early Albian period (Herrle and Mutterlose, 2003; Mutterlose et al., 2009).

This cooling episode, is **either** defined in the Late Aptian, such as in the North Sea Basin (Mutterlose et al., 2009); in Site 545, Mazagan Plateau, Atlantic Ocean (McAnena et al., 2013)**,** in Cismon and Piobbico cores, Italy, (Bottini et al., 2015), and in DSDP Site 463, Pacific Ocean (Bottini et al., 2015), **Or** identified in Late Aptian-Early Albian time, such as in the Vocontian Basin (Bown in Kennedy et al., 2000; Herrle and Mutterlose, 2003; Mutterlose et al., 2009), in the North Sea Basin (Bown et al., 1998; Jeremiah, 2001; Rückheim et al., 2006a), in Northwest Germany Basin (Bornemann and Mutterlose ,in Mutterlose et al., 2003; Mutterlose et al., 2009), in the Weddell Sea, East Antarctica (Mutterlose and Wise, 1990; Mutterlose, 1992; Mutterlose et al., 2009), in DSDP Site 511, Falkland Plateau, Southern Argentina (Mutterlose et al., 2009), in ODP Hole 766A, Exmouth Plateau, northwest Australia (Mutterlose et al., 2009), in DSDP Site 545 Mazagan Plateau (Mutterlose et al., 2009), and in EAB, Southern Morocco (Peybernés et al., 2013).

In the EAB, the Late Aptian-Early Albian period is characterized by an increase in the relative abundance of cold nannofossil taxa, associated with a general rise in sea-level. The higher relative abundance of cold-water taxa in the Tethyan realm during the Late Aptian-Early Albian with respect to the Early Aptian indicates migration of cosmopolitan biota from high-latitude sites close to the poles of both hemispheres into the Tethyan realm (Heimhofer et al., 2008). Where, the Equatorial Atlantic Seaway between Africa and South America came into existence only in the Late Aptian-Albian allowing for an exchange of biota, and may reflect the occurrence of glacial climatic event (Mutterlose et al., 2009). A rise of sea floor spreading rate and rapid volcanic

eruptions accompanied by a higher sea level, and transgression during the Early Albian (Haq et al., 1987, 2014) allowed the connection between northwestern Europe and the Tethyan region. Conversely, the warm water taxa present low abundances in the EAB during the Early Albian, as also observed in the North Sea and in North Germany (Jeremiah, 2001; Rückheim et al., 2006a, b). The Late Aptian-Early Albian cooling event is supported by a decline of Tethyan taxa and by a subsequent expansion of species of high latitudinal affinities, and by several other evidences, exposed below:

1. Sedimentological observations evidenced ice rafted dropstones and glendonites in Upper Aptian sediments from Arctic Canada, Australia (Kemper, 1978; Frakes et al., 1995), Spain (Rodríguez-López et al., 2016), and glendonite beds in the upper Aptian to lower Albian deposits, in the High Arctic of Canada (Sverdrup Basin, Kemper, 1987; Herrle et al., 2015).

2. Stable isotope studies of benthic foraminifera at DSDP site 511 (Fassell and Bralower, 1999), at ODP site 1049 on the Blake Nose Plateau (Huber et al., 2003), of latest Aptian low surface temperature deduced from planktonic foraminifera (Huber et al., 2003) and belemnites (Ditchfield et al., 1994; Pirrie et al., 1995, 2004) from Antarctica, Australia and Argentina indicate cool climatic conditions during the Early Albian in the shelf seas around the Gondwana margin. Erbacher et al. (2001) attributed the Early Albian positive oxygen isotope values of both benthonic and planktonic foraminifera to either cool temperatures and/or high salinities. The Aptian-Albian cooling event is recorded in Songliao Basin, northeast China, based on oxygen isotope data from ostracods (Wang et al., 2013).

3. Paleontological evidences, such as the abundance of cool taxa from fossil plants (Francis and Poole, 2002), pollens (Heimhofer et al., 2008), calcareous nannofossils (Mutterlose et al., 2009) support a cooling event in Aptian-Albian times. Moreover, extinction of the rudist bivalves in the Late Aptian would result from a climatic cooling of Aptian seawater, in the Arabian platform (e.g. Strohmenger et al., 2010), Qatar (Raven et al., 2010) and Iran (Mansouri-Daneshvar et al., 2015).

4. On the basis of TEX_{86} paleo-temperature proxy, McAnena et al. (2013) documented cold snaps of Late Aptian age in Site 545, Mazagan Plateau, associated with a decrease in both planktonic foraminifera and nannoconids abundances, as well as in the Cantabrian Basin in Spain (Millán et al., 2014).

Decreasing surface water temperatures are indicated by a first global decline of Tethyan nannoconids in the Late Aptian at both high and low latitudes, which is associated with increasing nannofossil boreal taxa, indicating migration toward low latitudes during the latest Aptian to earliest Albian period (Herrle and Mutterlose, 2003; Rückheim et al., 2006; Mutterlose et al., 2009; Peybernes et al., 2013). Erba et al. (2015) attributed the extinction in the Late Aptian of most nannoconids and of many nannoplankton and planktonic foraminiferal taxa, in the Kerguelen Plateau, located in Indian Ocean, to the prevalence of cold surface waters.

In the EAB, the warm surface water taxa (*Nannoconus* spp.) sharply decreased during the latest Aptian, and this species becomes rare during the Early Albian (see also Peybernes et al., 2013). The decrease in *Nannoconus* abundances and the increase of relative abundance of surface water

cold taxa at the Aptian-Albian transition could result from cooling climatic conditions at low latitudes.

The information provided by cold surface-water taxa abundances, indicates a decrease of sea surface temperature in the EAB through the Late Aptian-Early Albian, allowing migration of the nannoflora from high (polar realm, latitude between 30 and 60) to low (tropical to subtropical, latitudes between 0 and 30) latitudes**.** Our study shows that the cooling episode identified at the Aptian-Albian transition is recorded in the EAB and coincided with 1) a decline in the calcium carbonate content and in the total nannofossil abundances, and 2) an increase in the relative abundances of nannofossil cold taxa, which are consistent with cooler climatic conditions. In addition, the cooling conditions in the EAB are enhanced by cold water circulation related to the connection with the South Atlantic Ocean and by upwelling currents favored by the elevation of sea level, associated with the complete opening and expansion of Atlantic Ocean.

5.7. FUNCTIONING OF THE CARBONATE PLATFORM IN THE EAB, DURING THE APTIAN-EARLY ALBIAN TIME

The little change in facies between the Aptian sequences, the similarity of facies between Early Albian sequences, and, conversely, the significant difference between both Aptian and Albian sequences, reflect distinct sedimentation and paleoecological conditions for each stage. Analyzing at least, one Aptian and one Albian depositional sequence, is enough to explain what was going on in both stages in the EAB.

The Aptian time in the EAB (Figs. 5.5, 5.7), was a period characterized by thin deposits which indicates both little (small) accommodation space and low sedimentation rates; dominance of carbonate suggests slow sea level rise. Few terrigenous input allows the clarity of water, and the development of a large photic zone, which is favorable for both planktonic and benthic organisms. The shallow depths, the location of EAB in the arid belt, and the high abundance of *Nannoconus* spp., reflect prevalence of warm and oligotrophic conditions. The shallow water conditions, as well as the presence of many emergence episode, reflecting subaerial exposure during the Early Aptian time, could explain the lack of the Oceanic anoxic event 1a (OAE1a) in the EAB.

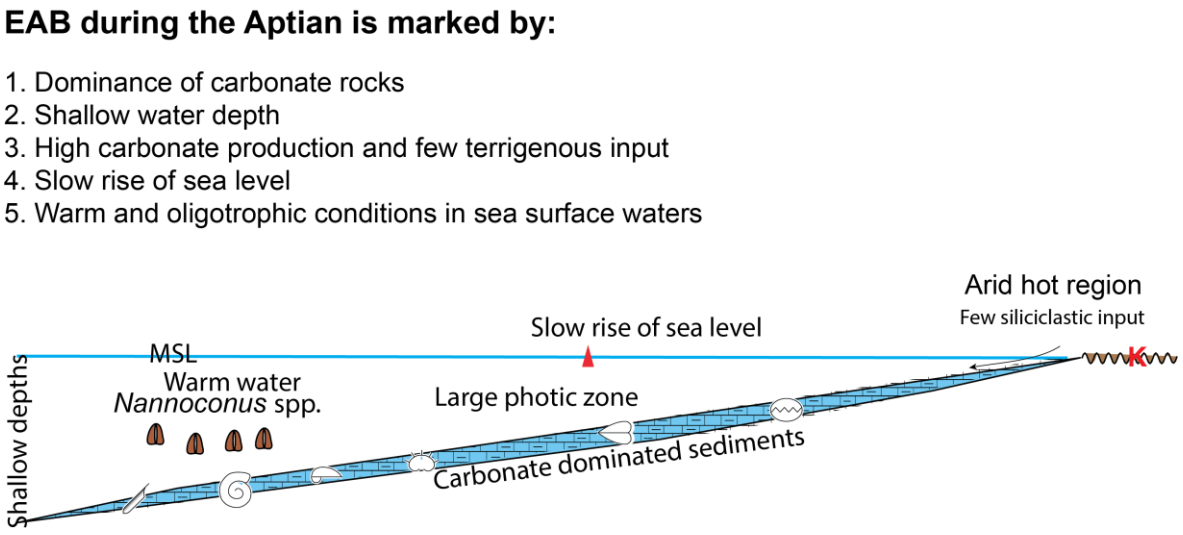

Figure 5.5: Depositional model showing the functioning mechanism of the EAB carbonate platform during Aptian time. Slow sea level rise and hot and arid climate induced low detrital input, low sedimentation rate, shallow environments, high carbonate production and decrease of primary productivity.

The Early Albian time in the EAB (Figs. 5.6, 5.7) was a period characterized by rapid rise of sea level, possible mild local tectonic activity and large accommodation space. This allowed the accumulation of thick sediments characterized by high siliciclastic input. All these conditions reduce the development of the photic zone, leading to the decrease of the abundance of both planktonic (big carbonate producers such as nannoconids) and benthic organisms and then to the decrease of carbonate production. Moreover, rapid rise of sea level in late Early Albian, enhanced deposition under deep marine environments, and favored deposition of dysoxic sediments. The increasing influence of upwelling currents may have enhanced the biological activity in the outer zones of the ramp, consuming a great part available oxygen through organic life and organic matter degradation, thus favoring the extension of the O_2 depleted zone onto the EAB ramp.

Both the co-occurrence of upwelling related to sea level rise, and the increase of detrital input (thin sandstone beds) during low sea level periods, support the increase in nannofossil primary productivity (increasing relative abundance of meso-eutrophic taxa) during the Early Albian in the EAB.

Higher relative abundance of cold surface water nannofossil taxa in the EAB during the Early Albian with respect to the Aptian, reflects the decrease of sea surface temperature, due to a global cooling event. The cooling conditions in the EAB, are partially enhanced by cold deep water circulation, associated with upwelling currents.

The absence of Oceanic Anoxic event 1b (OAE1b) in earliest Albian deposits in the EAB, could partly result from the prevalence of siliciclastic input and high sedimentation rate, which dilute the concentration of organic matter in this interval.

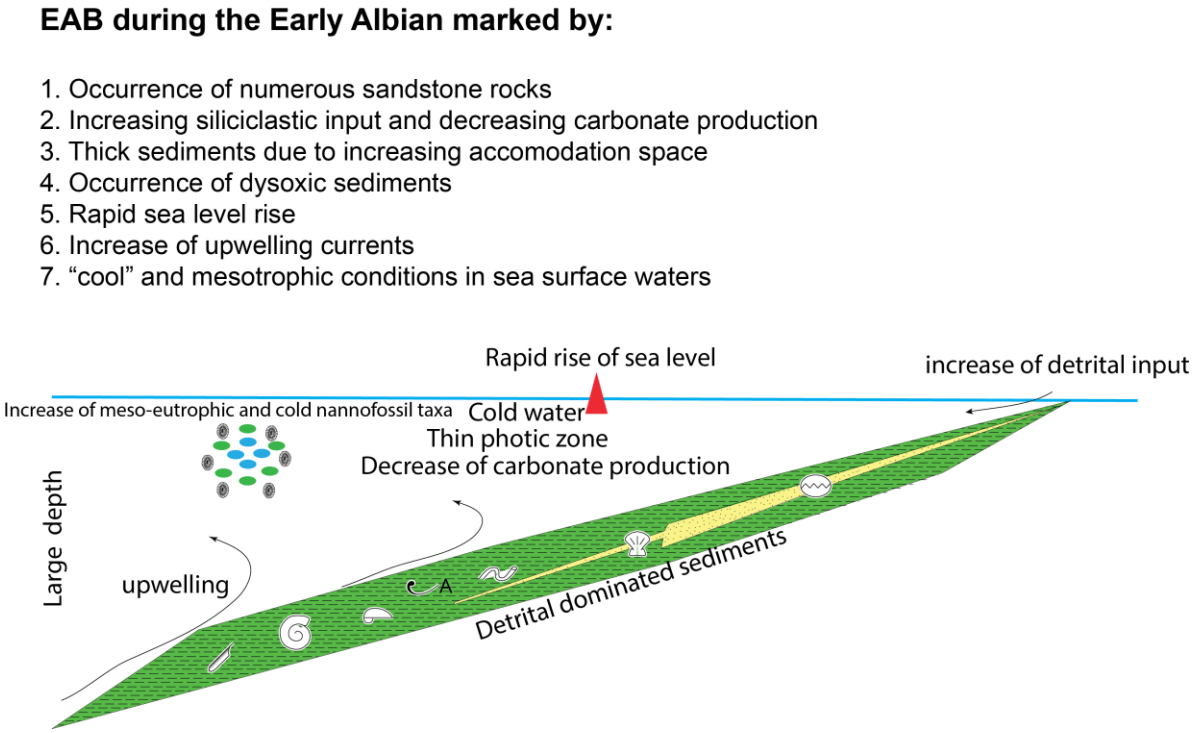

Figure 5.6: Depositional model showing the functioning mechanism of EAB carbonate platform during Early Albian time. Rapid sea level rise and cool, probably more humid climate induced high sedimentation rate, deeper marine environments, low carbonate production, and increased primary productivity.

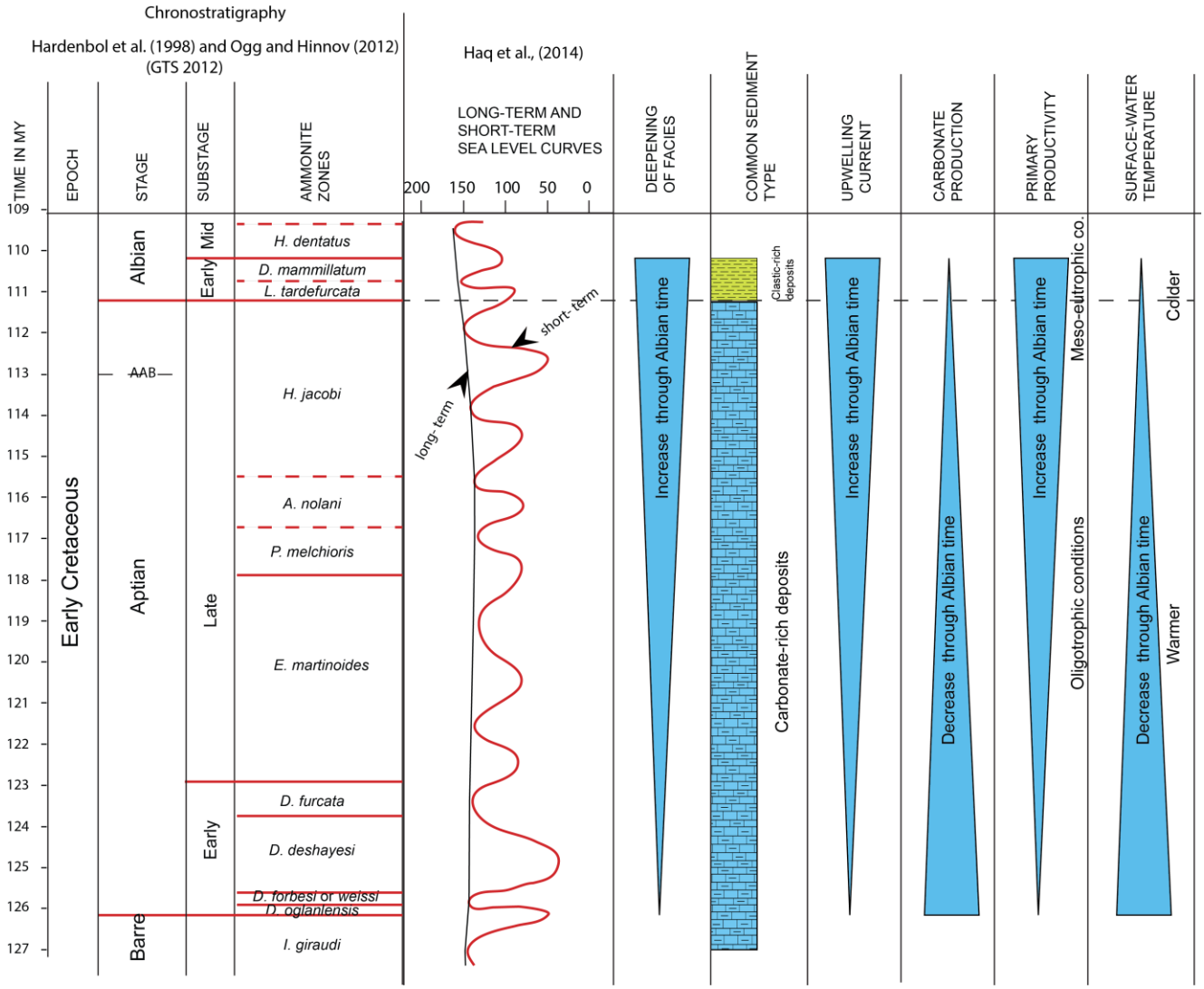

Figure 5.7: Summarized changes in facies development, common type of sediments, upwelling currents, carbonate production, primary productivity and surface water temperature during Aptian-Early Albian times in the EAB.

5.8. CONCLUSIONS

The results of this study could be summarized in the following points:

1. The time framework of the Aptian-Albian sediments in the Essaouira-Agadir Basin is established based on the integration of high-resolution biostratigraphy (ammonites and calcareous nannofossil biozonations), identification of sedimentary discontinuities and depositional sequences, and chemo-stratigraphy based on stable carbon isotopes. Regarding the stage and substage boundaries, and the age of global biological events, we will mention the following points:

- The Barremian/Aptian Boundary is approximately defined in the Ida w Shayq section based on ammonites; it is placed between *Kutatissites* sp. and *Pseudocrioceras* sp. (latest Barremian), and *Cheloniceras* sp. (Early Aptian).
- The Early/Late Aptian Boundary is defined by the FO of *Eprolithus floralis*, at Tissakatine Center, and by the first maximum value of carbon isotope (B), at both Ida w Shayq and Tissakatine Center.
- The Late Aptian *Nannoconus truittii* acme has been recognized in both Ida w Shayq and Tissakatine Center.
- The Aptian/Albian Boundary is determined by the identification of ammonite species marking the base of the *Leymeriella tardefurcata* ammonite Zone (*Puzosia quenstedti*, *Neosilesites palmensis*, in Ida w Shayq; *Hypacanthoplites* cf. *roberti*, in Tissakatine Center), supported by the FO of both *Prediscosphaera columnata* and *Hayesites albiensis* nannofossil taxa around D4, and by the decrease of carbon isotope values in all studied sections.

2. The facies and depositional environments of the Aptian-Early Albian rocks are identified based on their lithology, biogenic sedimentary structures, fossil content and microfacies. Then, we identified (1) four types of surfaces (S1, karstified surface; S2, submarine hiatus, related to upwellings; S3, submarine hiatus, related to marine currents, and S4, submarine hiatus related to significant submarine currents), (2) four major sedimentary facies in the Aptian (F1, interpreted as a pelagic deposit, in a distal outer ramp environment; F2, a hemipelagic deposits of proximal outer ramp environment; F3, marly limestones, of middle ramp environment; F4, massive limestone, of inner ramp environment), and (3) four Early Albian sedimentary facies (F I, pelagic deposit of outer ramp to basin margin environments; F II, pelagic deposit of distal outer ramp environment; F III, hemipelagic deposits of proximal outer ramp; F IV, yellow sandstone, of a

middle ramp environment). These facies reflect deposition in adjacent and gradational paleoenvironments.

3. The Aptian-Early Albian stratigraphic interval of the EAB, has been subdivided into two second order transgressive facies cycles, floored by two major erosional surfaces. The latest Barremian-Aptian transgressive facies cycle, is underlined by a major karstified-erosional surface (SB0). The Early Albian transgressive facies cycle, overlies a major submarine-erosional surface (SB4). The first cycle consists of four third-order depositional sequences (Ap.1, latest Barremian-Early Aptian; Ap.2, Early Aptian to early Late Aptian; Ap.3, Late Aptian and Ap.4, latest Aptian). The second cycle also contains four depositional sequences (Alb.1, earliest Albian, and Alb.2, Alb.3, Alb.4, of Early Albian age). The depositional sequences are defined by sequence boundaries, named SB0, SB1, SB2, SB3, SB4, SB5, SB6 and SB7. The vertical change of both TSTs and HSTs in the depositional sequences indicates a deepening upward trend related to sea level rise. The thicknesses of the Early Albian sequences are about 75 m in Tissakatine sections, the time duration of both *Leymeriella tardefurcata* and *Douvilleiceras mammillatum* ammonite zones are around 1 My (GST 2012). Therefore, the sedimentation rate is high during the Early Albian, reflecting development of the accommodation space.

- The depositional sequences and sequence boundaries of EAB, present good correspondence with the third-order cycles of the eustatic chart and global patterns of Haq et al. (2014, Fig. 5.4), suggesting that eustacy was more important than regional or local tectonics as a control on the EAB carbonate platform architecture.

4. Along the north-south transect, the preservation of calcareous nannofossils varies from poor to good in both the Tissakatine Center and Ida w Shayq sections. The means of nannofossil total absolute abundance (4.3×10^8), species richness (26), diversity (3) and evenness (0.7) are higher in the Tissakatine Center section with respect to the Ida w Shayq section (3.5×10^8, 25, 2.7, and 0.58, respectively). However, in the upper part of the sections (above D4, Early Albian), the means of species richness (32), diversity (3.5) and evenness (0.7) are higher in the Ida w Shayq section, with respect to the Tissakatine Center section (27, 3.25, and 0.68, respectively), while the means of nannofossil total absolute abundance are comparable (3.4×10^8) in both sections.

- Along the east-west transect, the preservation of calcareous nannofossils varies from poor to good in both the Anzate and Tinfoul sections. The means of nannofossil total absolute abundance,

species richness, diversity and evenness are higher (1.8×10^8, 31.1, 3.8, and 0.74) in Anzate with respect to Tinfoul (1.3×10^8, 29, 3.3, and 0.68).

- The nannofossil total assemblage for all sections is composed of 93 species. Fourteen species or group of species represent about 90 % of the total assemblage and display important abundance fluctuations; the *Biscutum* spp. includes *B. constans* and *B. ellipticum*, *Cretarhabdus* includes all species of the genera *Cretarhabdus* and *Retecapsa*. *Nannoconus* spp., *Rhagodiscus* spp. includes *R. achlyostaurion* and *R. asper, Seribiscutum* spp. includes *S. gaultensis* and *S. primitivum, Watznaueria barnesiae* and *W. fossacincta* are lumped together, *Staurolithites* spp., small *Zeugrhabdotus* spp., *Discorhabdus rotatorius, Hayesites irregularis, Lithraphidites carniolensis, Repagulum parvidentatum, Watznaueria communis,* and *Zeugrhabdotus diplogrammus.*

- Both relative and absolute abundances of *Nannoconus* spp. and *Staurolithites* spp. increase toward distal sections, probably reflecting a preference for deeper, distal settings. Conversely, abundances of *Hayesites irregularis* increase toward the proximal sections, and may, therefore, be interpreted as a coastal taxon.

5. The carbonate production in the EAB, is higher in the Aptian than during the Early Albian, due to warm conditions, and/or slow rise of sea level, shallow depth of the basin, and little detrital influx (arid conditions).

6. The nannofossil total absolute abundance decreases from the Aptian to the Early Albian, due to increasing in the sedimentation rate.

7. The nutrient input, fertility and calcareous nannofossil primary productivity are higher in the Early Albian with respect to the Aptian, and are mainly controlled by rising sea level and upwelling currents.

8. The Latest Aptian-Early Albian period is characterized by high abundances of cold taxa, accompanied by a general rise in sea-level, migration of cosmopolitan biota from Boreal realm into the Tethyan realm, which may reflect the occurrence of a glacial climatic event.

CHAPTER SIX

REFERENCES

REFERENCES

Aguado, R., Castro, J. M., Company, M. and De Gea, G. A. (1999). Aptian bio-events - an integrated biostratigraphic analysis of the Almadich Formation, Inner Prebetic Domain, SE Spain. *Cretaceous Research*, **20**(6), 663-683.

Aguado, R., de Gea, G. A., Castro, J. M., O'Dogherty, L., Quijano, M. L., Naafs, B.D.A. and Pancost, R. D. (2014). Late Barremian-early Aptian dark facies of the Subbetic (Betic Cordillera, southern Spain): Calcareous nannofossil quantitative analyses, chemostratigraphy and palaeoceanographic reconstructions. *Palaeogeography, Paleoclimatology, Paleoecology*, **395**, 198-221.

Algouti, A., Algouti, A. and Taj-Eddine, K. (1999). Le Sénonien du Haut Atlas occidental, Maroc: sédimentologie, analyse séquentielle et paléogéographie. *Journal of African Earth Sciences*, **29**, 643-658.

Allan, J. R. and Matthews, R. K. (1982). Isotope signatures associated with early meteoric diagenesis. *Sedimentology*, **29**(6), 797-817.

Aly, M.F. and Abdel-Gawad, G.I. (2001). Early Cretaceous ammonites of Gebel Lagama, north Sinai, Egypt. *Palaeontographica Abteilung* (A) **262**, 25-52.

Ambroggi, R. (1963). Etude géologique du versant méridional du Haut-Atlas occidental et de la plaine de Souss. *Notes et Mémoires du Service géologique du Maroc*, **157**, 1-321.

Ando, A., Kaiho, K., Kawahata, H. and Kakegawa, T. (2008). Timing and magnitude of early Aptian extreme warming: unraveling primary $\delta^{18}O$ variation in indurated pelagic carbonates at Deep Sea Drilling Project Site 463, central Pacific Ocean. *Palaeogeography, Paleoclimatology, Paleoecology*, **260**(3), 463-476.

Ando, A., Kakegawa, T., Takashima, R. and Saito, T. (2002). New perspective on Aptian carbon isotope stratigraphy: data from $\delta^{13}C$ records of terrestrial organic matter. *Geology*, **30**(3), 227-230.

Andreu, B. (1989). Le Crétacé moyen de la transversale Agadir-Nador (Maroc): précisions stratigraphiques et sédimentologiques. *Cretaceous Research*, **10**, 49-80.

Andreu, B. (1991). Les ostracodes du Crétacé moyen (Barrémien à Turonien) le long d'une transversale Agadir-Nador. *Act. Lab. Ceol. Sed. Paléo*., Univ. Paul Sabatier, Toulouse, série 2, vol. **14**, 2 tomes, 765 pages.

Andreu, B. (1992). Associations d'ostracodes et paléoécologie du Crétacé (Barrémien a Turonien) le long d'une transversale Agadir-Nador (Maroc). *Palaeogeography, Paleoclimatology, Paleoecology*, **99**, 291-319.

Andreu, B. (1992). Distribution stratigraphique des ostracodes du Barrémien au Turonien, le long d'une transversale Agadir-Nador (Maroc). *Géologie Méditerranéenne*, **19**, 165-187.

Arboleya, M. L., Teixell, A., Charroud, M. and Julivert, M. (2004). A structural transect through the High and Middle Atlas of Morocco. *Journal of African Earth Sciences*, **39**(3), 319-327.

Arnaud, H., Arnaud-Vanneau, A., Bulot, L.G., Beck, C., MacSotay, O., Stephan, J. and Vivas, V. (2000). Le Crétacé inférieur du Venezuela oriental: stratigraphie séquentielle des carbonates sur la transversale Casanay-Maturin (Etats de Anzoátegui, Monagas et Sucre). *Géologie Alpine*, **76**, 3-81.

Arnaud-Vanneau, A. and Arnaud, H. (1990). Hauterivian to Lower Aptian carbonate shelf sedimentation and sequence stratigraphy in the Jura and northern Subalpine chains (southeastern France and Swiss Jura). In: Tucker, M.E., Wilson, J.L., Crevello, P.D., Sarg, J.R., Read, J.F. (Eds.), *Carbonate Platforms: Facies, Sequences and Evolution*. Blackwell Scientific Publications, IAS Special Publication, 203-233.

Arthur, M. A. and Natland J. (1979). Carbonaceous sediments in the North and South Atlantic: The role of salinity in stable stratification of Early Cretaceous basins. Deep drilling results in the Atlantic Ocean: continental margins and paleoenvironment, 375-401.

Arthur, M. A. and Premoli Silva, I. (1982). Development of widespread organic carbon-rich strata in the Mediterranean Tethys. *Nature and origin of Cretaceous carbon-rich facies*. Academic Press, London: 7-54.

Arthur, M. A., Schlanger, S. T. and Jenkyns, H. C. (1987). The Cenomanian-Turonian Oceanic Anoxic Event II. Palaeoceanographic controls on organic matter production and preservation. *Geological Society Special Publications*, **26**(1), 401-420.

Arthur, M.A., Brumsack, H.J., Jenkyns, H. C. and Schlanger, S.O. (1990). Stratigraphy, geochemistry and paleoceanography of organic carbon-rich Cretaceous sequences. In: Ginsburg, R.N. and Beaudoin, B. (eds.), *Cretaceous Resources, Events and Rhythms*, Vol. 304C, 75-119.

Arthur, M.A., Dean, W.E. and Schlanger, S.O. (1985). Variations in the global carbon cycle during the Cretaceous related to climate, volcanism, and changes in atmospheric C02. In: Sundquist, E.T.S. and Broecker, W.S. (eds.), The Carbon Cycle and Atmospheric C02: Natural Variations Archean to the present, Vol. 32, pp. 504- 529. Geophysical Monograph, Washington D.C.

Askri, H., Belmecheri, A., Benrabah, B., Boudjema, A., Boumendjel, K., Daoudi, M., Drid, M., Ghalem, T., Docca, A.M., Ghandriche, H. and Ghomari, A. (1995). Geology of Algeria. In Well Evaluation Conference Algeria (1-93).

Aubry, M. P., Bord, D., Beaufort, L., Kahn, A. and Boyd, S. (2005). Trends in size changes in the coccolithophorids, calcareous nannoplankton, during the Mesozoic: a pilot study. *Micropaleontology*, **51**(4), 309-318.

Auzende J. M., Von Rad. U., Ruellan E. and CYAMAZ group. (1984). Outline and results of the CYAMAZ cruise (Mazagan Escarpment. West Morocco). in: submersible Cyana studies of the Mazagan Escarpment (Moroccan continental margin), CYAMAZ cruise 1982, edited by J. M. Auzende and U. Von Rad, *Oceanologica Acta*, nº sp., 5-58.

Auzende J. M., Monti S. and Ruellan E. (1984). Multibeam echosounding bathymetry of El Jadida Plateau and Escarpment, Mazagan, west Morocco, in: *initial Report of Deep Sea Drilling Project*, edited by K. Hinz, E. L. Winterer et al., Vol **79**, Washington, US Government Printing Office, 365-367.

Auzende, J. M., Ceuleneer, G., Cornen, G., Juteau, T., Lagabrielle, Y., Lensch, G., Mevel, C., Nicolas, A., Prichard, H., Ribeiro, A. and Ruellan, E., (1984). Intraoceanic tectonism on the Gorringe Bank: observations by submersible. *Geological Society, Special Publications*, **13**(1), 113-120.

Bachmann, M. and Hirsch, F. (2006). Lower Cretaceous carbonate platform of the eastern Levant (Galilee and the Golan Heights): stratigraphy and second-order sea-level change. *Cretaceous Research*, **27**(4), 487-512.

Bachmann, M. and Willems, H. (1996). High-frequency cycles in the Upper Aptian carbonates of the Organyi basin, NE Spain. *Geologische Rundschau*, **85**, 586-605.

Bachmann, M., Kuss, J. and Lehmann, J. (2010). Controls and evolution of facies patterns in the Upper Barremian–Albian Levant Platform in North Sinai and North Israel. *Geological Society, Special Publications*, **341**(1), 99-131.

Bailey, T. R., Rosenthal, Y., McArthur, J. M., Van De Schootbrugge, B. and Thirlwall, M. F. (2003). Paleoceanographic changes of the Late Pliensbachian-Early Toarcian interval: a possible link to the genesis of an Oceanic Anoxic Event. *Earth and Planetary Science Letters*, **212**(3), 307-320.

Barash, M. (2008). Evolution of the Mesozoic oceanic biota: Response to abiotic factors. Oceanology 48(4), 538-553.

Barker, C. E., Pawlewicz, M. and Cobabe, E. A. (2001). Deposition of sedimentary organic matter in black shale facies indicated by the geochemistry and petrography of high-resolution samples, Blake Nose, western North Atlantic. *Geological Society, Special Publications*, **183**(1), 49-72.

Barragan-Manzo, R. and Diaz-Otero, C. (2004). Analisis de microfacies y datos micropaleontológicos de la transición Barremiano-Aptiano en la Sierra de Rosario, Durango, Mexico. *Revista Mexicana de Ciencias Geologicas*, **21**, 247-259.

Barrier, J. (1977a). Nannofossiles calcaires des marnes de l'Aptien inferieur type: Bedoulien de Cassis-La Bedoule (Bouches-du-Rhone). *Bulletin du Museum National d'Histoire Naturelle*, **437** (59), 1-67.

Barrier, J. (1977b). Nannofossiles calcaires du Gargasien stratotypique. *Bulletin du Museum National d'Histoire Naturelle*, **485** (62), 172-227.

Barron, E. J. (1983). A warm, equable Cretaceous: the nature of the problem. *Earth-Science Reviews*, **19**(4), 305-338.

Barron, E. J. and W. H. Peterson (1990). Mid-Cretaceous ocean circulation: Results from model sensitivity studies. *Paleoceanography*, **5**(3), 319-337.

Barron, E. J. and W. M. Washington (1985). Warm Cretaceous climates: Warm Cretaceous climates: high atmospheric C02 asa plausible mechanism. In: Sundquist, E.T. & Broecker, W.S. (eds.), *The Carbon Cycle and Atmospheric C02 : Natural variations Archean to Present*, **32**, 546-553. Geophysical Monograph.

Barron, E. J., Fawcett, P. J., Peterson, W. H., Pollard, D. and Thompson, S. L. (1995). A simulation of Mid-Cretaceous climate. *Paleoceanography*,**10**(5), 953-962.

Basilone, L., Morticelli, M. G. and Lena, G. (2010). Mesozoic tectonics and volcanism of Tethyan rifted continental margins in western Sicily. *Sedimentary Geology*, **226**(1), 54-70.

Baudin, F. (1995). Depositional controls on Mesozoic source rocks in the Tethys. In : Paleogeography, Paleoclimate, and source rock, Huc, A., edi, 191-211. *AAPG*, Oklahoma, U.S.A.

Baudin, F., Fiet, N., Coccioni, R. and Galeotti, S. (1998). Organic matter characterisation of the Selli Level (Umbria-Marche Basin, central Italy). *Cretaceous Research*, **19**(6), 701-714.

Baumgartner, P. O., Bown, P., Marcoux, J., Mutterlose, J., Kaminski, M. A., Haig, D. and McMinn, A. (1992). Early Cretaceous biogeographic and oceanographic synthesis of Leg 123 (off Northwestern Australia). In: *Proceedings of the Ocean Drilling Program: Scientific Results*, Vol. **123**, 739-758.

Beaufort, L. (1991). Adaptation of the random settling method for quantitative studies of calcareous nannofossils. *Micropaleontology*, **37**, 415-418.

Beerling, D. and Royer, D. (2002). Fossil plants as indicators of the Phanerozoic global carbon cycle. *Annual review of earth and planetary sciences*, **30**(1), 527-556.

Behrens, M. and Siehl, L. A. (1982). Sedimentation in the Atlas Gulf I: Lower Cretaceous clastics. In : Geology of the Northwest African continental margin, Von Rad, U., Hinz, K., Sarntheim, M. and Seibold, E., eds, 427-439. Springer-Verlag, New York.

Behrens, M., Krumsiek, K., Meyer, D. E., Schäfer, A., Siehl, A., Stets, J., Thein, J. and Wurster, P. (1978). Sedimentations abläufe im Atlas-Golf (Kreide Küstenbecken Marokko). *Geologische Rundschau*, **67**(2), 424-453.

Bellanca, A., Erba, E., Neri, R., Silva, I. P., Sprovieri, M., Tremolada, F. and Verga, D. (2002). Palaeoceanographic significance of the Tethyan 'Livello Selli' (Early Aptian) from the Hybla Formation, northwestern Sicily: biostratigraphy and high-resolution chemostratigraphic records. *Palaeogeography, Palaeoclimatology, Palaeoecology*, **185**(1), 175-196.

Benda, L. (1982). Die Diatomeen des späten Apt in Nordwestdeutschland. *Geologisches Jahrbuch*, (A), 65, 405-411.

Berger, A., Imbrie, J., Hays, J., Kukla , G. and Saltzman, B. (1984). Milankovitch and climate. Reidel, Dortrecht. 2, 895 p.

Berner, R. A., Lasaga, A. C. and Garrels, R. M. (1983). The carbonate-silicate geochemical cycle and its effect on atmospheric carbon dioxide over the past 100 million years. *American Journal of Science*, **283**(7), 641-683.

Bertotti, G. and Gouiza, M. (2012). Post-rift vertical movements and horizontal deformations in the eastern margin of the Central Atlantic: The Middle Jurassic to Early Cretaceous evolution of Morocco. *International Journal of Earth Sciences* DOI 10.1007/s00531-012-0773-4.

Better, I. (1988). *Etude palynologique dans le Crétacé inferieur du Bassin d'Agadir (Maroc)*. Doctorat de l'Université Claude Bernard, Lyon.

Biju-Duval, B., Dercourt, J. and Le Pichon, X. (1977). From the Tethys ocean to the Mediterranean seas: a plate tectonic model of the evolution of the western Alpine system. Histoire structurale des bassins méditerranéens, 143.

Binks, R. M. and Fairhead, J. D. (1992). A plate tectonic setting for Mesozoic rifts of West and Central Africa. *Tectonophysics*, **213**(1-2), 141-151.

Bischoff, G. and Mutterlose, J. (1998). Calcareous nannofossils of the Barremian/Aptian boundary interval in NW Europe: biostratigraphic and palecologic implications of a high resolution study. *Cretaceous Research*, **19**, 635-661.

Bodin, S., Fröhlich, S., Boutib, L., Lahsini, S. and Redfern, J. (2011). Early Toarcian Source-Rock Potential In The Central High Atlas Basin (Central Morocco): Regional Distribution And Depositional Model. *Journal of Petroleum Geology*, **34**(4), 345-363.

Bodin, S., Mattioli, E., Fröhlich, S., Marshall, J. D., Boutib, L., Lahsini, S. and Redfern, J. (2010). Toarcian carbon isotope shifts and nutrient changes from the Northern margin of Gondwana (High Atlas, Morocco, Jurassic): palaeoenvironmental implications. *Palaeogeography, Palaeoclimatology, Palaeoecology*, **297**(2), 377-390.

Bodin, S., Petitpierre, L., Wood, J., Elkanouni, I. and Redfern, J. (2010). Timing of early to mid-cretaceous tectonic phases along North Africa: New insights from the Jeffara escarpment (Libya–Tunisia). *Journal of African Earth Sciences*, **58**(3), 489-506.

Bornemann, A. and Mutterlose, J. (2006). Size analyses of the coccolith species Biscutum constans and Watznaueria barnesiae from the Late Albian Niveau Breistroffer(SE France): taxonomic and palaeoecological implications. *Geobios*, **39**(5), 599-615.

Bornemann, A., Aschwer, U. and Mutterlose, J. (2003). The impact of calcareous nannofossils on the pelagic carbonate accumulation across the Jurassic-Cretaceous boundary. *Palaeogeography, Palaeoclimatology, Palaeoecology*, **199**(3), 187-228.

Bottini, C., Cohen, A. S., Erba, E., Jenkyns, H. C. and Coe, A. L. (2012). Osmium-isotope evidence for volcanism, weathering, and ocean mixing during the early Aptian OAE 1a. *Geology*, **40**(7), 583-586.

Bottini, C., Erba, E., Tiraboschi, D., Jenkyns, H. C., Schouten, S. and Sinninghe Damsté, J. S. (2015). Climate variability and ocean fertility during the Aptian Stage. *Climate of the Past*, **11**(3), 383-402.

Bottini, C., Erba, E., Tiraboschi, D., Jenkyns, H. C., Schouten, S. and Damsté, J. S. (2014). Climate variability and relationship with ocean fertility during the Aptian Stage. *Climate of the Past* Discussions, **10**, 689-738.

Bouatmani, R., Chakor Alimi, A. and Medina, F. (2007). Subsidence, évolution thermique et maturation des hydrocarbures dans le bassin d'Essaouira (Maroc): apport de la modélisation. *Bulletin de l'Institut Scientifique Rabat*, **29**, 15-36.

Bourgeoini, Y. (1994). *Etude micropaléontologique et biostratigraphique de l'Aptien et de l'Albien du bassin d'Essaouira. Haut Atlas occidental, Maroc*. Mémoire de doctorat de l'Université de Tunis, 274 p.

Bourgeoini, Y., Ben Haj Ali, N., Razgallah, S. andTajeddine, K. (2002). Etude biostratigraphique du Crétacé inférieur (Barrémien supérieur-Albien) du Haut Atlas occidental (Maroc). *Estudios Geologicos*, **58**, 105-112.

Bown, P. R. (1998). *Calcareous nannofossil biostratigraphy*. Chapman and Hall; Kluwer Academic, 315 pp.

Bown, P. R. (2005). Calcareous nannoplankton evolution: a tale of two oceans. *Micropaleontology*, **51**(4), 299-308.

Bown, P. R. (2005). Early to mid-Cretaceous calcareous nannoplankton from the northwest Pacific Ocean, Leg 198, Shatsky Rise. In: *Proceedings of the Ocean Drilling Program: Scientific Results*, Vol. **198**, 1-82.

Bown, P. R. (2005). Selective calcareous nannoplankton survivorship at the Cretaceous-Tertiary boundary. *Geology*, **33**(8), 653-656.

Bown, P. R., Lees, J. A. and Young, J. R. (2004). Calcareous nannoplankton evolution and diversity through time. In: Coccolithophores, 481-508. Springer, Berlin Heidelberg.

Bracene, R., Patriat, M., Ellouz, N. and Gaulier, J. M. (2003). Subsidence history in basins of northern Algeria. *Sedimentary Geology*, **156**(1), 213-239.

Bralower, T. J. and Thierstein, H. R. (1984). Low productivity and slow deep-water circulation in mid-Cretaceous oceans. *Geology*, **12**(10), 614-618.

Bralower, T. J., Arthur, M. A., Leckie, R. M., Sliter, W. V., Allard, D. J. and Schlanger, S. O. (1994). Timing and paleoceanography of oceanic dysoxia/anoxia in the Late Barremian to Early Aptian (Early Cretaceous). *Palaios*, **9,** 335-369.

Bralower, T. J., CoBabe, E., Clement, B., Sliter, W. V., Osburn, C. L. and Longoria, J. (1999). The record of global change in mid-Cretaceous (Barremian-Albian) sections from the Sierra Madre, northeastern Mexico. *The Journal of Foraminiferal Research*, **29**(4), 418-437.

Bralower, T. J., Fullagar, P. D., Paull, C. K., Dwyer, G. S. and Leckie, R. M. (1997). Mid-Cretaceous strontium-isotope stratigraphy of deep-sea sections.*Geological Society of America Bulletin*, **109**(11), 1421-1442.

Bralower, T. J., Monechi, S. and Thierstein, H. R. (1989). Calcareous nannofossil zonation of the Jurassic-Cretaceous boundary interval and correlation with the geomagnetic polarity timescale. *Marine Micropaleontology*, **14**(1), 153-235.

Bralower, T. J., Sliter, W. V., Arthur, M. A., Leckie, R. M., Allard, D. and Schlanger, S. O. (1993). Dysoxic/anoxic episodes in the Aptian-Albian (Early Cretaceous). The Mesozoic Pacific: geology, tectonics, and volcanism,**77**, 5-37. American Geophysical Union Monograph.

Bralower, T.J. (1992). Aptian-Albian calcareous nannofossil biostratigraphy of ODP Site 763, and the correlation between high and low latitude zonations. In: Duncan, R.A., Rea, D.K., Kidd, R.B., von Rad, U. and Weisse!, J.K. (eds.), *Synthesis of Results from Scientific Drilling in the Indian Ocean*, **70**, 245-252. Geophysical Monograph.

Bralower, T.J. and Thierstein, H.R. (1984). Low productivity and slow deep-water circulation in mid-Cretaceous oceans. *Geology*, **12**, 614-618.

Bralower, T.J., Leckie, R.M., Sliter, W.V. and Thierstein, H.R. (1995). An integrated Cretaceous microfossil biostratigraphy. *Society of Economic Palaeontologists and Mineralogists, Special Publications*, **50**, 65-79.

Brass, G. W., Southam, J. R. and Peterson, W. H. (1982). Warm saline bottom water in the ancient ocean. *Nature*, **296**, 620-623

Bréhéret, J. G. (1988). Episodes de sédimentation riche en matière organique dans les marnes bleues d'âge aptien et albien de la partie pélagique du bassin vocontien. *Bulletin de la Société Géologique de France*, **4**(2), 349-356.

Bréhéret, J. G. (1997). L'Aptien et l'Albien de la Fosse vocontienne (des bordures au bassin). Evolution de la sédimentation et enseignements sur les événements anoxiques. *Société Géologique du Nord, Publication*, **25**, 614 pp.

Bréhéret, J. G., Caron, M. and Delamette, M. (1986). Niveaux riches en matiére organique dans l'Albien vocontien; quelques caractéres du paléoenvironnement; essai d'interprétation génétique. *Documents du Bureau des Recherches Géologiques et Miniéres*, **110**, 141–191.

Bréhéret, J.G. (1997). L'Aptien et L'Albien de Ia Fosse vocontienne (bordures au bassin): Evolution de Ia sedimentation et enseignements sur les evenements anoxiques. *Publications de Ia Société Géologique du Nord*, 25, 614 pp.

Brives, A. (1905). Contribution à l'étude géologique de l'Atlas marocain. *Bulletin de la Société géologique de France*, **5**, 379-398.

Brives, A. (1905). Les terrains crétacés dans le Maroc occidental. *Bull. Soc. Géol. de France*, **5**, 905 pp.

Browning, E. L. and Watkins, D. K. (2008). Elevated primary productivity of calcareous nannoplankton associated with ocean anoxic event 1b during the Aptian/Albian transition (Early Cretaceous). *Paleoceanography*, **23**(2).

Bucur, I. (1988). Les paléoenvironnements mésozoïques de la zone de Resita-Moldova Noua et leur succession en temps. *Evolution and Adaptation*, **3**, 103-109.

Burchette, T. P. and Wright, V. P. (1992). Carbonate ramp depositional systems. *Sedimentary Geology*, **79**, 3-57.

Burla, S., Heimhofer, U., Hochuli, P. A., Weissert, H. and Skelton, P. (2008). Changes in sedimentary patterns of coastal and deep-sea successions from the North Atlantic (Portugal) linked to Early Cretaceous environmental change. *Palaeogeography, Palaeoclimatology, Palaeoecology*, **257**(1), 38-57.

Butt, A. (1981). Depositional environments of the Upper Cretaceous rocks in the northern part of the Eastern Alps. Cushman Found. *Foraminiferal Research, Special Publication*, **20**, 1-121.

Butt, A. (1982). Micropaleontological bathymetry of the Cretaceous of western Morocco. *Palaeogeography, Palaeoclimatology, Palaeoecology*, **37**(2), 235-275.

Butt, A., Stets, J. and Wurster, P. (1984). Micropaleontological and sedimentological aspects of High Atlas Cretaceous onshore sediments (Atlas-Gulf, Morocco). *Initial Reports of the Deep Sea Drilling Project*, **79**, 923-934.

Calvert, S. and Pedersen, T. (1992). Organic carbon accumulation and preservation in marine sediments: how important is anoxia. *Organic matter: productivity, accumulation, and preservation in recent and ancient sediments, Columbia University Press, New York*, 533, 231-263.

Canerot, J., Cugny, P., Peybernès, B., Rahhali, I., Rey, J. and Thieuloy, J. P. (1986). Comparative study of the Lower and Mid-Cretaceous sequences on different Maghrebian shelves and basins-their place in the evolution of the North African Atlantic and Neotethysian margins. *Palaeogeography, Palaeoclimatology, Palaeoecology*, **55**(2), 213-232.

Caron, M. (1985). *Cretaceous planktonic formanifera. In: Planktic stratigraphy* (Bolli, H. M., Sanders, 1. B., et Peris-Nielson, K., edits.). Cambridge Earth Sciences, 17-86.

Carras, N. (1995). *La piattaforma carbonatica del Parnasso durante il Giurassico superiore-Cretacico inferiore.* PhD thesis, University of Athens, 232 pp.

Casey, R. (1961). The stratigraphical palaeontology of the Lower Greensand. *Palaeontographical Society*, **3**(4), 487-621.

Casey, R. (1962). A monograph of the Ammonoidea of the Lower Greensand, Part IV. *Palaeontographical Society*, 217-288.

Casey, R. (1965). A monograph of the Ammonoidea of the Lower Greensand, Pt. 6. *Palaeontographical Society*, monograph 118, 399-546.

Castro, J. M., De Gea, G. A., Ruiz-Ortiz, P. A. and Nieto, L. M. (2008). Development of carbonate platforms on an extensional (rifted) margin: the Valanginian-Albian record of the Prebetic of Alicante (SE Spain). *Cretaceous Research*, **29(**5), 848-860.

Chihaoui, A., Jaillard, E., Latil, J. L., Zghal, I., Susperregui, A. S., Touir, J. and Ouali, J. (2010). Stratigraphy of the Hameima and lower Fahdene Formations in the Tadjerouine area (Northern Tunisia). *Journal of African Earth Sciences*, **58**(2), 387-399.

Choubert, G. and Faure-Muret, A. (1962). Evolution du domaine atlasique marocain depuis les temps paleozoıques. *Société géologique de France*. **1**, 447-527.

Chumakov, N.M., Zharkov, M.A., Herman, A.B., Doludenko, M.P., Kalandadze, N.N., Lebedev, E.L., Ponomarenko, A.G. and Rautian, A.S. (1995). Climatic zones in the middle of the Cretaceous Period. *Stratigraphy and Geological Correlation*, , **3**, 241-260.

Clarke, L. J. and Jenkyns, H. C. (1999). New oxygen isotope evidence for long-term Cretaceous climatic change in the Southern Hemisphere. *Geology*, **27**(8), 699-702.

Cobianchi, M., Luciani, V. and Bosellini, A. (1997). Early Cretaceous nannofossils and planktonic foraminifera from northern Gargano (Apulia, southern Italy). *Cretaceous Research*, **18**, 249-293.

Cobianchi, M., Luciani, V. and Menegatti, A. (1999). The Selli Level of the Gargano Promontory, Apulia, southern Italy: foraminiferal and calcareous nannofossi data. *Cretaceous Research,* **20**, 255-69.

Coccioni, R., Erba, E. and Premoli-Silva, I. (1992). Barremian-Aptian calcareous plankton biostratigraphy from the Gorgo Cerbara section (Marche, central Italy) and implications for plankton evolution. *Cretaceous Research*, **13**, 517-537.

Coccioni, R., Luciani, V. and Marsili, A. (2006). Cretaceous oceanic anoxic events and radially elongated chambered planktonic foraminifera: paleoecological and paleoceanographic implications. *Palaeogeography, Palaeoclimatology, Palaeoecology*, **235**(1), 66-92.

Coccioni, R., Nesci, O., Tramontana, C.F., Wezel, C.F. and Moretti, E. (1987). Descrizione di un livello guida ‘‘Radiolaritico-Bituminoso-Ittiolitico’’ alla base delle Mattinata Formation nell’Appennino Umbro-Marchigiano. *Bollettino della Societa` Geologica Italiana*, **106**, 183-192.

Coffin, M. F., Duncan, R. A., Eldholm, O., Fitton, J. G., Frey, F. A., Larse, H. C., Mahoney, J. J., Saunders, A. D., Schlich, R. and Wallace, P. J. (2006). Large igneous provinces and scientific ocean drilling. Status quo and a look ahead, Oceanography, **19**, 150-160.

Colombié, C., Lécuyer, C. and Strasser, A. (2011). Carbon-and oxygen-isotope records of palaeoenvironmental and carbonate production changes in shallow-marine carbonates (Kimmeridgian, Swiss Jura). *Geological Magazine*, **148**(01), 133-153.

Company, M., Saandoval, J., Tavera, J.M., Aoutem, M. and Ettachfini, M. (2008). Barremian ammonite faunas from the western High Atlas, Morocco: biostratigraphy and palaeobiogeography. *Cretaceous Research*, **29**, 9-26.

Courtillot, V.E. and Renne, P.R. (2003). On the ages of flood basalt events. *Comptes Rendus Geoscience* **335**, 113-140.

Coward, M. and Ries, A. (2003). Tectonic development of North African basins. *Geological Society, Special Publications*, **207**(1), 61-83.

Crux, J. A. (1991). Albian calcareous nannofossils from the Gault Clay of Munday’s Hill (Bedfordshire, England). *Journal of Micropalaeontology*, **10**(2), 203-221.

Császár, G. (2002). Urgon formations in Hungary. *Geologica Hungarica - Series Geologica*, **25**, 1-209.

Császár, G., Szinger, B. and Piros, O. (2013). From continental platform towards rifting of the Tisza Unit in the Late Triassic to Early Cretaceous. *Geologica Carpathica*, **64**(4), 279-290.

D’Argenio, B., Ferreri, V. and Ruberti, D., (1987). Cyclic versus episodic deposition in a carbonate platform sequence, Lower Cretaceous of Matese Mountains, Southern Apennines. *Memorie della Società Geologica Italiana*, **40**, 375-382.

da Gama, R. (2000). *Calcareous nannoplankton palaeoecology from the Cenomanian-Turonian of Tarfaya, Morocco*. Unpublished MSc thesis, University College London, 60 pp.

Daoudi, L. O. (2010). Comparative influence of burial depth on the clay mineral assemblage of the Agadir-Essaouira basin (western High Atlas, Morocco). *Clay Minerals*, **45**, 453-467.

Daoudi, L. O. and Deconinck, J. F. (1994). Contrôles paléogéographique et diagénétique des successions sédimentaires argileuses du Bassin Atlasique au Crétacé (Haut-Atlas Occidental, Maroc). *Journal of African Earth Sciences*, **18**(2), 123-134.

D'Argenio, B. (2004). A multidisciplinary approach to global correlation and geochronology. The Cretaceous shallow-water carbonates of southern Apennines, Italy. in: Cyclostratigraphy; approaches and cases histories, edited by: D’Argenio, B., Fischer, A. G., Premoli Silva, I., Weissert, H., and Ferreri, V., SEPM (Society for Sedimentary Geology), Special Publication No. 81, 103-122.

Davison, I. (2005). Central Atlantic margin basins of North West Africa: geology and hydrocarbon potential (Morocco to Guinea). *Journal of African Earth Sciences*, **43**(1), 254-274.

Delamette, M. (1988). Relation between the condensed Albian deposits of the Helvetic domain and the oceanic current-influenced continental margin of the northern Tethys. *Bulletin de la Société Géologique de France*, **4**(5), 739-745.

Delamette, M., Caron, M. and Bréhéret, J. G. (1986). Essai d’interprétation génétique des facies euxeniques de l’Eo-Albien du

bassin vocontien (SE France). *Comptes Rendus Hebdomadaires des Séances de l'Académie des Sciences, Paris*, **302**, 1085-1090.

Deres, F. and Achéritéguy, J. (1980). Biostratigraphie des nannoconides. *Bulletin des Centres de Recherches Exploration-Production Elf-Aquitaine*, **4**(1), 1-53.

Dinis, J., Rey, J. and de Graciansky, P. C. (2002). Le Bassin lusitanien (Portugal) à l'Aptien supérieur–Albien: organisation séquentielle, proposition de corrélations, évolution. *Comptes Rendus Geoscience*, **334**(10), 757-764.

Ditchfield, P. W., Marshall, J. D. and Pirrie, D. (1994). High latitude palaeotemperature variation: New data from the Thithonian to Eocene of James Ross Island, Antarctica. *Palaeogeography, Palaeoclimatology, Palaeoecology*, **107**(1-2), 79-101.

Donnadieu, Y., Dromart, G., Godd´eris, Y., Puc´eat, E., Brigaud, B., Dera, G., Dumas, C., and Olivier, N. (2011). A mechanism for brief glacial episodes in the Mesozoic greenhouse, *Paleoceanography*, **26**, PA3212.

Dot, J. A. M., Baamonde, J. M., Reyes, D. and Whilchy, R. (2015). The Cogollo Group and the oceanic anoxic events 1a and 1b, Maracaibo basin, Venezuela. *Brazilian Journal of Geology*, **45**, 41-61.

Douvillé, H. (1916). Les terrains secondaires dans le massif du Moghara à l'est de l'isthme de Suez, d'après les explorations de M. Couyat-Barthoux: Paléontologie. Première et deuxième parties. Gauthier-Villars.

Dubourdieu, G. G. (1956). Étude géologique de la région de l'Ouenza:(confins Algéro-Tunisiens). 1. Texte. *Service de la Carte Géologique de l'Algérie*.

Duffaud, F., Brun, L. and Plauchut, B. (1966). Le bassin du Sud-Ouest marocain. In: Reyre, D. (Ed.), Bassins sédimentaires du Littoral africain, 1ère partie. Frimin Didot Publications, Paris, 5-12.

Dutour, Y. (2005). *Biostratigraphie, évolution et renouvellements des ammonites de l'Aptien supérieur (Gargasien) du bassin vocontien (Sud-Est de la France)*. Doctoral dissertation, Université Claude Bernard-Lyon 1.

Einsele, G. and Wiedmann, J. (1982). Turonian Black Shales in the Moroccan Coastal Basins: First Upwelling in the Atlantic Ocean?, *In* von Rad, U, Hinz, K., Sarnthein, M., Seibold, E. (Eds), *Geology of the Northwest African Continental Margin:* Berlin (Springer-Verlag), pp. 396-414.

El-Araby, A. (1999). Facies analysis and sequence stratigraphy of the Late Aptian-Albian Risan Aneiza Formation in northern Sinai, Egypt. *Egyptian Journal of Geology*, **34**(2), 151-181.

Eleson, J. W. and Bralower, T. J. (2005). Evidence of changes in surface water temperature and productivity at the Cenomanian/Turonian Boundary. *Micropaleontology*, **51**(4), 319-332.

Elkhazri, A., Abdallah, H., Razgallah, S., Moullade, M. and Kuhnt, W. (2013). Carbon-isotope and microfaunal stratigraphy bounding the Lower Aptian Oceanic Anoxic Event 1a in northeastern Tunisia. *Cretaceous Research*, **39**, 133-148.

Elkhazri, A., Razgallah, S., Abdallah, H. and Ben Haj Ali, N. (2009). L'événement anoxique «OAE 1a» Barrémo-Aptien en Tunisie nordorientale: Intérêt des foraminifères. *Revue de Paléobiologie*, **28**(1), 93-130.

Ellero, A., Ottria, G., Malusa, M. G., and Ouanaimi, H. (2012). Structural Geological Analysis of the High Atlas (Morocco): Evidences of a Transpressional Fold-Thrust Belt. *Tectonics - Recent Advances*, 229-258. DOI: 10.5772/50071.

Emery, K. and Uchupi., E. (1984). *The Geology of the Atlantic Ocean*. Springer, New York.

Erba, E. (1987). Mid-Cretaceous cyclic pelagic facies from the Umbrian-Marchean Basin: What do calcareous nannofossils suggest ? *Int. Nannofossil Assoc. Newsletters*. **9**, 52-53.

Erba, E. (1988). Aptian-Albian calcareous nannofossil biostratigraphy of the Scisti a Fucoidi at Piobbico (Central Italy). *Rivista Italiana de Paleontologia e Stratigrafia*, **94** (2), 249-284.

Erba, E. (1992). Calcareous nannofossil distribution in pelagic rhythmic sediments (Aptian-Albian Piobbico core, central Italy). *Rivista Italiana di Paleontologia e Stratigrafia*, **97**, 455-484.

Erba, E. (1994). Nannofossils and superplumes: the early Aptian nannoconid crisis. *Paleoceanography*, **9**(3), 483-501.

Erba, E. (1996). The Aptian stage. *Bulletin de l'Institut Royal des Sciences Naturelles de Belgique*, **66**, 31-43.

Erba, E. (2004). Calcareous nannofossils and Mesozoic oceanic anoxic events. *Marine Micropaleontology*, **52**(1), 85-106.

Erba, E. and Tremolada, F. (2004). Nannofossil carbonate fluxes during the Early Cretaceous: phytoplankton response to nutrification episodes, atmospheric CO_2, and anoxia. *Paleoceanography*, **19**(1), 1-18.

Erba, E., Bottini, C., Weissert, H. J. and Keller, C. E. (2010). Calcareous nannoplankton response to surface-water acidification around Oceanic Anoxic Event 1a. *Science*, **329**(5990), 428-432.

Erba, E., Castradori, D., Guasti, G. and Ripepe, M. (1992). Calcareous nannofossils and Milankovitch cycles: the example of the Albian Gault Clay Formation (southern England). *Palaeogeography, Palaeoclimatology, Palaeoecology*, **93**(1-2), 47-69.

Erba, E., Coccioni, R. and Premoli Silva, I. (1989). The Scisti a Fuccoidi in the Umbria-Marche area: The Apecchiese road sections. In: Cresta, S., Monechi, S. and Parisi, G. (eds.), MesozoicCenozoic stratigraphy in the Umbria-Marche area, Vol. **39**, pp. 146-164. Ministero dell' Ambiente Servizio Geologico D'ltalia, Roma. *Memorie descriptive della Carta Geologica D 'Italia*.

Erba, E., Duncan, R. A., Bottini, C., Tiraboschi, D., Weissert, H., Jenkyns, H. C. and Malinverno, A. (2015). Environmental consequences of Ontong Java Plateau and Kerguelen Plateau volcanism. *Geological Society of America Special Papers*, **511**, SPE511-15.

Erba, E., Premoli Silva, I. and Watkins, D. (1995). Cretaceous calcareous plankton biostratigraphy of sites 872 through 879 (ODP Leg 144). In: Haggerty, J.A., et al. (Eds.), *Proc. ODP Sci. Results*, vol. **144**, pp. 157-169.

Erbacher, J. and Thurow, J. (1997). Influence of oceanic anoxic events on the evolution of mid Cretaceous radiolaria in the North Atlantic and western Tethys. Marine Micropaleontology, **30**, 139-158.

Erbacher, J., Hemleben, C., Huber, B. T. and Markey, M. (1999). Correlating environmental changes during early Albian oceanic anoxic event 1B using benthic foraminiferal paleoecology. *Marine Micropaleontology*, **38**(1), 7-28.

Erbacher, J., Huber, B. T., Norris, R. D. and Markey, M. (2001). Increased thermohaline stratification as a possible cause for an ocean anoxic event in the Cretaceous period. *Nature*, **409**(6818), 325-327.

Erbacher, J., Thurow, J. and Littke, R. (1996). Evolution patterns of radiolaria and organic matter variations: a new approach to identify sea-level changes in mid-Cretaceous pelagic environments. *Geology*, **24**(6), 499-502.

Eshet, Y. and Almogi-Labin, A. (1996). Calcareous nannofossils as paleoproductivity indicators in Upper Cretaceous organic-rich sequences in Israel. *Marine Micropaleontology*, **29**, 37-61.

Essafraoui, B., Ferry, S., Groshény, D., Içame, N., El Aouli, H., Masrour, M., Bulot, L. G., Yves G. and Aoutem, M. (2015). Sequence stratigraphic architecture of marine to fluvial deposits across a passive margin (Cenomanian, Atlantic margin, Morocco, Agadir transect). *Carnets de Geologie-Notebooks on Geology*.

Ettachfini, E. M., Souhel, A., Andreu, B. and Caron, M. (2005). La limite Cénomanien-Turonien dans le Haut Atlas central, Maroc. *Geobios*, **38**(1), 57-68.

Fadhel, M. B., Layeb, M., Hedfi, A. and Youssef, M. B. (2011). Albian oceanic anoxic events in northern Tunisia: Biostratigraphic and geochemical insights. *Cretaceous Research*, **32**(6), 685-699.

Fadhel, M. B., Zouaghi, T., Amri, A. and Youssef, M. B. (2014). Radiolarian and planktic foraminifera biostratigraphy of the early Albian organic rich beds of Fahdene Formation, Northern Tunisia. *Journal of African Earth Science*, **25**(1), 45-63.

FassellL, M. L. and Bralower, T. J. (1999). Warm, equable mid-Cretaceous: Stable isotope evidence. *Geological Society of America Special Papers*, **332**, 121-142.

Fernández-Mendiola, P. A. and García-Mondéjar, J. (1989). Evolution of a Mid-Cretaceous carbonate platform, Gorbea (northern Spain). *Sedimentary geology*, **64**(1-3), 111-126.

Fernández-Mendiola, P. A., Malo, J. P. and García-Mondéjar, J. (2015). Facies analysis and correlation in an Albian carbonate platform (Cuchía quarry, Cantabria, Spain). *Geogaceta*, **57**, 99-102.

Fernández-Mendiola, P. A., Mendicoa, J., Hernandez, S., Owen, H. G. and García-Mondéjar, J. (2013). A facies model for an Early Aptian carbonate platform (Zamaia, Spain). *Facies, **59**(3), 529-558.*

Flügel, E. (2004). Diagenesis, Porosity, and Dolomitization. In: *Microfacies of Carbonate Rocks*, 267-338. Springer, Berlin Heidelberg.

Föllmi, K. B. (2012). Early Cretaceous life, climate and anoxia. *Cretaceous Research*, **35**, 230-257.

Föllmi, K. B. (1986). *Die Garschella-und Seewer Kalk-Formation (Aptian-Santonian) im Voralberger Helvetikum und Ultrahelvetikum*, Diss. Naturwiss. ETH Zürich, Nr. 8100.

Follmi, K. B. (1989). Evolution of the mid-Cretaceous triad: platform carbonates, phosphatic sediments, and pelagic carbonates along the northern Tethys margin. *Lecture Notes in Earth Sciences*, **23**, Springer Verlag, Berlin.

Föllmi, K. B. (2008). A synchronous, middle Early Aptian age for the demise of the Helvetic Urgonian platform related to the unfolding oceanic anoxic event 1a (Selli event). *Revue de Paléobiologie*, **27**(2), 461-468.

Föllmi, K. B. and Gainon, F. (2008). Demise of the northern Tethyan Urgonian carbonate platform and subsequent transition towards pelagic conditions: the sedimentary record of the Col de la Plaine Morte area, central Switzerland. *Sedimentary Geology*, **205**(3), 142-159.

Föllmi, K. B., Godet, A., Bodin, S. and Linder, P. (2006). Interactions between environmental change and shallow water carbonate buildup along the northern Tethyan margin and their impact on the Early Cretaceous carbon isotope record. *Paleoceanography*, **21**(4), 1-16. doi:10.1029/2006PA001313.

Föllmi, K.B., Bodin, S., Godet, A., Linder, P. and van de Schootbrugge, B. (2007). Unlocking paleo-environmental interaction from Early Cretaceous shelf sediments in the Helvetic Alps: stratigraphy is the key! *Swiss Journal of Geosciences*, **100**, 349-369.

Ford, D. and Golonka, J. (2003). Phanerozoic paleogeography, paleoenvironment and lithofacies maps of the circum-Atlantic margins. Marine and Petroleum *Geology*, **20**(3), 249-285.

Forster, A., Schouten, S., Baas, M. and Damsté, J. S. S. (2007). Mid-Cretaceous (Albian-Santonian) sea surface temperature record of the tropical Atlantic Ocean. *Geology*, **35**(10), 919-922.

Frakes, L. A. and Francis, J. E. (1988). A guide to Phanerozoic, cold polar climates from high-latitude ice rafting in the Cretaceous. *Nature*, **333**, 547-549.

Frakes, L. A., Alley, N. F. and Deynoux, M. (1995). Early Cretaceous ice rafting and climate zonation in Australia. *International Geology Review*, **37**, 567-583.

Francis, J. E. and Frakes, L. A. (1993). Cretaceous climates, In: V.P. Wright (Editor), Sedimentology Review, 17-30, Blackwell Scientific Publications, Oxford.

Francis, J. E. and Poole, I. (2002). Cretaceous and early Tertiary climates of Antarctica: evidence from fossil wood. *Palaeogeography, Palaeoclimatology, Palaeoecology*, **182**(1), 47-64.

Friedrich, O., Nishi, H., Pross, J., Schmiedl, G. and Hemleben, C. (2005). Millennial-to centennial-scale interruptions of the Oceanic Anoxic Event 1b (Early Albian, mid-Cretaceous) inferred from benthic foraminiferal repopulation events. *Palaios*, **20**(1), 64-77.

Frizon de Lamotte, D., Fourdan, B., Leleu, S., Leparmentier, F. and Clarens, P. (2015). Style of rifting and the stages of Pangea breakup. *Tectonics*, **34**(5), 1009-1029.

Frizon de Lamotte, D., Leturmy, P., Missenard, Y., Khomsi, S., Ruiz, G., Saddiqi, O., Guillocheau, F. and Michard, A. (2009). Mesozoic and Cenozoic vertical movements in the Atlas system (Algeria, Morocco, Tunisia): an overview. *Tectonophysics*, **475**(1), 9-28.

Frizon de Lamotte, D., Saint Bezar, B., Bracène, R. and Mercier, E. (2000). The two main steps of the Atlas building and geodynamics of the western Mediterranean. *Tectonics*, **19**(4), 740-761.

Frizon de Lamotte, D., Zizi, M., Missenard, Y., Hafid, M., El Azzouzi, M., Maury, R. A., Taki Z., Benammi M. and Michard, A. (2008). The atlas system. In: *Continental evolution: the geology of Morocco*, 133-202. Springer, Berlin Heidelberg.

Funk, H., Föllmi, K.B. and Mohr, H. (1993). Evolution of the Tithonian-Aptian carbonate platform along the northern Tethyan margin, eastern Helvetic Alps. In: Simo, J.A.T., Scott, R.W., Masse, J.P. (Eds.), *Cretaceous carbonate platforms*. United States, Tulsa, 387-407.

Galeotti, S., Sprovieri, M., Coccioni, R., Bellanca, A. and Neri, R. (2003). Orbitally modulated black shale deposition in the upper Albian Amadeus Segment (Central Italy): a multi-proxy reconstruction. *Palaeogeography, Palaeoclimatology, Palaeoecology*, **190**, 441-458.

Garcia, R., Moreno-Bedmar, J. A., Bover-Arnal, T., Salas, R., Latil, J. L., Martín-Martín, J. D., Gomez-Rivas, E., Bulot, L.G., Delanoy, G., Martínez, R. and Grauges, A. (2014). Lower Cretaceous (Hauterivian-Albian) ammonite biostratigraphy in the Maestrat Basin (E Spain). *Journal of Iberian Geology*, **40**(1), 99.

García-Mondéjar, J. and Fernández-Mendiola, P. (1989). Evolución plataforma/cuenca en el Albiense de Lunada y Soba (Burgos y Cantabria). Secuencias, asociaciones de sistemas sedimentarios (systems tracts) y cambios del nivel del mar. *XII Congr. Esp. Sedimentol., Libro-Guía Excursiones Geol.*, Excursión No. I. Dep. Estratigr., Geodin. Paleontol.(Univ. País Vasco), and Div. Invest. Recursos (Ente Vasco de la Energía), Leioa-Bilbao, 7-43.

Geisen, M., Bollmann, J., Herrle, J. O., Mutterlose, J. and Young, J. R. (1999). Calibration of the random settling technique for calculation of absolute abundances of calcareous nannoplankton. *Micropaleontology*,45, 437-442.

Gentil, L. (1905). Observations géologiques dans le sud marocain. *Bulletin de la Société géologique de France*, **5**, 521-523.

Georgi, K. H. (1976). Mikrofaunistisch-lithologische Untersuchungen der Hilssandstein-Region (Apt/Alb) im Raum Salzgitter-Goslar. *Mitteilungen aus dem Geologischen Institut der technischen Universität Hannover*, **13**, 5-112.

Gersonde, R. and Harwood, D. M. (1990). Lower Cretaceous diatoms from ODP LEG 113 Site 693 (Weddell Sea). Part 1: Vegetative cells. In: Barker, P.F. and Kennett, J.P. (Eds.): *Proceedings of the Ocean Drilling Program, Scientific Results*, **113**, 365-402.

Giese, P. and Jacobshagen, V. (1992). Inversion tectonics of intracontinental ranges: High and Middle Atlas, Morocco. *Geologische Rundschau*, **81**(1), 249-259.

Giraud, F., Olivero, D., Baudin, F., Reboulet, S., Pittet, B. and Proux, O. (2003). Minor changes in surface water fertility across the Oceanic Anoxic Event 1d (latest Albian, SE France) evidenced by calcareous nannofossils. *International Journal of Earth Sciences*, **92**, 267-284.

Godet, A., Durlet, C., Spangenberg, J. E. and Föllmi, K. B. (2016). Estimating the impact of early diagenesis on isotope records in shallow-marine carbonates: A case study from the Urgonian Platform in western Swiss Jura. *Palaeogeography, Palaeoclimatology, Palaeoecology*, **454**, 125-138.

Godet, A., Föllmi, K.B., Bodin, S., de Kaenel, E., Matera, V. and Adatte, T. (2010). Stratigraphic, sedimentological and palaeoenvironmental constraints on the rise of the Urgonian platform in the western Swiss Jura. *Sedimentology*, **57**, 1088-1125.

Godet, A., Hfaiedh, R., Arnaud-Vanneau, A., Zghal, I., Arnaud, H. and Ouali, J. (2014). Aptian palaeoclimates and identification of an OAE1a equivalent in shallow marine environments of the southern Tethyan margin: Evidence from Southern Tunisia (Bir Oum Ali section, Northern Chott Chain). *Cretaceous Research*, **48**, 110-129.

Gómez Pérez, I. (1997). Contransting shallowing versus deepening upward cycles and their position in a carbonate ramp (Lower Cretaceous, Gorbea, Bizkaia). *Geogaceta*, **22**, 77-80.

Gouiza, M. (2011). *Mesozoic source-to-sink systems in NW Africa: Geology of vertical movements during the birth and growth of the Moroccan rifted margin*. Wörmann: Vrije Universiteit.150 pp.

Gradstein, F. M., Agterberg, F. P., Ogg, J. G., Hardenbol, J., Veen, P., Thierry, J. and Huang, Z. (1994). A Mesozoic time scale. *Journal of Geophysical Research, Solid Earth*, **99**(B12), 24051-24074.

Gradstein, F. M., Ogg, J. G., Schmitz, M. and Ogg, G. (Eds.). (2012). *The geologic time scale 2012*, 2-volume set. Elsevier.

Grafe , K. U. and Wiedmann, J. (1993). Sequence stratigraphy in the Upper Cretaceous of the Bascu-Cantabrian Basin (northern Spain). *Geologische Rundschau*, **82** (2), 327-361.

Granot, R. and Dyment, J. (2015). The Cretaceous opening of the South Atlantic Ocean. *Earth and Planetary Science Letters*, **414**, 156-163.

Graziano, R. (2000). The Aptian-Albian of the Apulia Carbonate Platform (Gargano Promontory, southern Italy): evidence of palaeoceanographic and tectonic controls on the stratigraphic architecture of the platform margin. *Cretaceous Research*, **21**(1), 107-126.

Graziano, R. (2013). Sedimentology, biostratigraphy and event stratigraphy of the Early Aptian oceanic anoxic event (OAE1A) in the Apulia Carbonate Platform margin-Ionian basin system (Gargano promontory, southern Italy). *Cretaceous Research*, **39**, 78-111.

Graziano, R. and Raspini, A. (2015). Long-and short-term hydroclimatic variabilities in the Aptian Tethys: Clues from the orbital chronostratigraphy of evaporite-rich beds in the Apennine carbonate platform (Mt. Faito, southern Italy). *Palaeogeography, Palaeoclimatology, Palaeoecology*, **418**, 319-343.

Gréselle, B. and Pittet, B. (2005). Fringing carbonate platforms at the Arabian Plate margin in northern Oman during the Late Aptian-Middle Albian: evidence for high-amplitude sea-level changes. *Sedimentary Geology*, **175**(1), 367-390.

Grőtsch, J., Billing, I. and Vahrenkamp, V. (1998). Carbon-isotope stratigraphy in shallow-water carbonates: implications for Cretaceous black-shale deposition. *Sedimentology*, **45**, 623-634.

Guiraud, R. and Maurin, J. (1992). Early Cretaceous rifts of Western and Central Africa: an overview. *Tectonophysics*, **213**(1-2), 153-168.

Guiraud, R., Bosworth, W., Thierry, J. and Delplanque, A. (2005). Phanerozoic geological evolution of Northern and Central Africa: an overview. *Journal of African Earth Sciences*, **43**(1), 83-143.

Hafid, M. (2000). Triassic–early Liassic extensional systems and their Tertiary inversion, Essaouira Basin (Morocco). *Marine and Petroleum Geology*, **17**(3), 409-429.

Hafid, M. (2006). Styles structuraux du Haut Atlas de Cap Tafelney et de la partie septentrionale du Haut Atlas occidental: tectonique salifere et relation entre l'Atlas et l'Atlantique. *Notes et mémoires du Service géologique*, **465**, 172.

Hafid, M., Salem, A. A. and Bally, A. W. (2000). The western termination of the Jebilet-High Atlas system (Offshore Essaouira Basin, Morocco). Marine and Petroleum *Geology*, **17**(3), 431-443.

Hafid, M., Tari, G., Bouhadioui, D., El Moussaid, I., Echarfaoui, H., Salem, A. A., Nahim, M. and Dakki, M. (2008). Atlantic basins. In : *The Geology of Morocco*, 303-329. Springer Berlin Heidelberg.

Hallam, A. (1975). Evolutionary size increase and longevity in Jurassic bivalves and ammonites. *Nature*, **258**, 493-496.

Hallam, A. (1984). Continental humid and arid zones during the Jurassic and Cretaceous. *Palaeogeography, Palaeoclimatology, Palaeoecology*, **47**(3), 195-223.

Hallock, P. (1988). The role of nutrient availability in bioerosion: consequences to carbonate buildups. *Palaeogeography, Palaeoclimatology, Palaeoecology*, **63**(1), 275-291.

Hallock, P. and Schlager, W. (1986). Nutrient excess and the demise of coral reefs and carbonate platforms. *Palaios*, **1**, 389-398.

Hamama, H. and Gabir, M. (2001). Lower Cretaceous (Barremian-Albian) ammonites of Gabal Risan Aneiza, north Sinai, Egypt. In: *Proceedings of the 2nd International Conference on the Geology of Africa*, Assiut, 421-444.

Handford, C. R. and Loucks, R. G. (1993). Carbonate Depositional Sequences and Systems Tracts. Responses of Carbonate Platforms to Relative Sea-Level Changes, Chapter 1, 3-41.

Haq, B. U. (2014). Cretaceous eustasy revisited. *Global and Planetary Change*, **113**, 44-58.

Haq, B.U. and Al-Qahtani, A.M. (2005). Phanerozoic cycles of sea-level change on the Arabian Platform. *GeoArabia*, **10**, 127-160.

Haq, B.U., Hardenbol, J. and Vail, P.R. (1987). Chronology of fluctuating sea levels since the Triassic. *Science*, **235**, 1156–1167.

Hardenbol, J., Thierry, J., Farley, M.B., Jacquin, T., Graciansky, P.C. and de Vail, P.R., (1998). Mesozoic and Cenozoic sequence chronostratigraphic framework in European basins. In: Graciansky, P.-C., de Hardenbol, J., Jacquin, T., Vail, P.R. (Eds.), Mesozoic and Cenozoic Sequence Stratigraphy of European Basins. *SEPM Special Publication*, **60**, 3-13.

Harland, M., Francis, J. E., Brentnall, S. J. and Beerling, D. J. (2007). Cretaceous (Albian–Aptian) conifer wood from Northern Hemisphere high latitudes: forest composition and palaeoclimate. *Review of Palaeobotany and Palynology*, **143**(3), 167-196.

Hart, M.B., Amedro, F. and Owen, H.G. (1996). The Albian Stage and Substage boundaries. *Bulletin de l'Institut Royal des Sciences Naturelles de Belgique, Sciences de la Terre*, **66** (Supplement), 45-56.

Hay, W. W. (2008). Evolving ideas about the Cretaceous climate and ocean circulation. *Cretaceous Research*, **29**(5), 725-753.

Hay, W. W., DeConto, R. M., Wold, C. N., Wilson, K. M. and Voigt, S. (1999). Alternative global Cretaceous paleogeography. *Geological Society of America Special Papers*, **332**, 1-47.

Hays, J. D. and Pitman, W. C. (1973). Lithospheric plate motion, sea level changes and climatic and ecological consequences. *Nature*, **246**(5427), 18-22.

Heimhofer, U., Adatte, T., Hochuli, P. A., Burla, S. and Weissert, H. (2008). Coastal sediments from the Algarve: low-latitude climate archive for the Aptian-Albian. *International Journal of Earth Sciences*, **97**(4), 785-797.

Heldt, M., Bachmann, M. and Lehmann, J. (2008). Microfacies, biostratigraphy, and geochemistry of the hemipelagic Barremian–Aptian in north-central Tunisia: Influence of the OAE 1a on the southern Tethys margin. *Palaeogeography, Palaeoclimatology, Palaeoecology*, **261**(3), 246-260.

Heldt, M., Bachmann, M., Lehmann, J., Kuss, J., Thielemann, J., Negra, H. and Bey, S. (2008). Absence of a global marine biocalcification crisis during the late Early Aptian Oceanic Anoxic Event 1a. Palaeoenvironmental evolution of the Tunisian carbonate platform margin. Response to global oceanographic and climatic changes (Barremian-Aptian), *Geology*, 4-45.

Heldt, M., Lehmann, J., Bachmann, M., Negra, H. and Kuss, J. (2010). Increased terrigenous influx but no drowning: palaeoenvironmental evolution of the Tunisian carbonate platform margin during the Late Aptian. *Sedimentology*, **57**(2), 695-719.

Herrle, J. O. (2002). Mid-Cretaceous paleoceanographic and paleoclimatologic implications on black shale formation of the Vocontian Basin and Atlantic. Evidence from calcareous nannofossils and stable isotopes. *Institut und Museum für Geologie und Paläontologie der Universität Tübingen*, **27**, 114 pp.

Herrle, J. O. (2003). Reconstructing nutricline dynamics of mid-Cretaceous oceans: evidence from calcareous nannofossils from the Niveau Paquier black shale (SE France). *Marine Micropaleontology*, **47**(3), 307-321.

Herrle, J. O. and Mutterlose, J. (2003). Calcareous nannofossils from the Aptian–Lower Albian of southeast France: palaeoecological and biostratigraphic implications. *Cretaceous Research*, **24**(1), 1-22.

Herrle, J. O., Kössler, P. and Bollmann, J. (2010). Palaeoceanographic differences of early Late Aptian black shale events in the Vocontian Basin (SE France). *Palaeogeography, Palaeoclimatology, Palaeoecology*, **297**(2), 367-376.

Herrle, J. O., Kößler, P., Friedrich, O., Erlenkeuser, H. and Hemleben, C. (2004). High-resolution carbon isotope records of the Aptian to Lower Albian from SE France and the Mazagan Plateau (DSDP Site 545): a stratigraphic tool for paleoceanographic and paleobiologic reconstruction. *Earth and Planetary Science Letters*, **218**(1), 149-161.

Herrle, J. O., Pross, J., Friedrich, O. and Hemleben, C. (2003b). Short-term environmental changes in the Cretaceous Tethyan Ocean: micropalaeontological evidence from the Early Albian Oceanic Anoxic Event 1b. *Terra Nova*, **15**(1), 14-19.

Herrle, J. O., Pross, J., Friedrich, O., Kößler, P. and Hemleben, C. (2003a). Forcing mechanisms for mid-Cretaceous black shale formation: evidence from the Upper Aptian and Lower Albian of the Vocontian Basin (SE France). *Palaeogeography, Palaeoclimatology, Palaeoecology*, **190**, 399-426.

Herrle, J. O., Schröder-Adams, C. J., Davis, W., Pugh, A. T., Galloway, J. M. and Fath, J. (2015). Mid-Cretaceous High Arctic stratigraphy, climate, and oceanic anoxic events. *Geology*, **43**(5), 403-406.

Hfaiedh, R., Vanneau, A. A., Godet, A., Arnaud, H., Zghal, I., Ouali, J., Latil, J. and Jallali, H. (2013). Biostratigraphy, palaeoenvironments and sequence stratigraphy of the Aptian sedimentary succession at Jebel Bir Oum Ali (Northern Chain of Chotts, South Tunisia): Comparison with contemporaneous Tethyan series. *Cretaceous Research*, **46**, 177-207.

Hill, M.E. (1975). Selective dissolution of mid-Cretaceous (Cenomanian) calcareous nannofossils. *Micropaleontology*, **21**, 227-235.

Hillgartner, H. (1998). Discontinuity surfaces on a shallow marine carbonate platform (Berrasian, Valarginian, France and Switzerland). *Journal Sedimentary Research*, **68** (2), 1093-1108.

Hinnov, L.A. and Hilgen, F.J. (2012). Cyclostratigraphy and Astrochronology. In: Gradstein, F.M., Ogg, J.G., Schmitz, M., Ogg, G. (Eds.), *The Geologic Timescale 2012*, 10.1016/B978-0-444-59425-9.00004-4 Elsevier, Amsterdam, 63-83.

Hinz, K., Winterer, E.L., Baumgartner, P.O., Bradshaw, M.J., Channell, J.E.T., Jaffrezo, M., Jansa, L.F., Leckie, R.M., Moore, J.N., Rullko¨ tter, J., Schaftenaar, C.H., Steiger, T.H., Vuchev, V.T. and Wiegard, G.E. (1984). Site 545. In: *Initial Reports of the Deep Sea Drilling Project*, Eds: K. Hinz, E.L. Winterer, P.O. Baumgartner, M.J. Bradshaw, J.E.T. Channell, M. Jaffrezo, L.F. Jansa, R.M. Leckie, J.N. Moore, J. Rullkötter, C.H. Schaftenaar, T.H. Steiger, V.T. Vuchev and G.E. Wiegard, Vol. **79**. 81-177, U.S. Govt. Printing Office, Washington DC.

Hoedemaeker, Ph.J., Company, M., Aguirre-Urreta, M.B., Avram, E., Bogdanova, T.N., Bujtor, L., Bulot, L., Cecca, F., Delanoy, G., Ettachffini, M., Memmi, L., Owen, H. G., Rawson, P.F., Sandoval, J., Tavera, J.M., Thieuloy, J.-P., Tovbina, S.Z. and Vašíček, Z. (1993). Ammonite zonation for the Lower Cretaceous of the Mediterranean region; basis for the stratigraphic correlations within IGCP-Project 262. *Revista Española de Paleontología*, **8**, 117-120.

Hofmann, P., Stüsser, I., Wagner, T., Schouten, S. and Damsté, J. S. S. (2008). Climate-ocean coupling off North-West Africa during the Lower Albian: the oceanic anoxic event 1b. *Palaeogeography, Palaeoclimatology, Palaeoecology*, **262**(3), 157-165.

Holbourn, A. and Kuhnt, W. (2001). No extinctions during oceanic anoxic event 1b: The Aptian-Albian benthic foraminiferal record of ODP Leg 171. *Geological Society, Special Publications*, **183**(1), 73-92.

Holbourn, A., Kuhnt, W. and Erbacher, J. (2001). Benthic foraminifers from Lower Albian black shales (Site 1049, ODP Leg 171): evidence for a non uniformitarian record. *The Journal of Foraminiferal Research*, **31**(1), 60-74.

Hong, S.K. and Lee, Y.I. (2012). Evaluation of atmospheric carbon dioxide concentrations during the Cretaceous. *Earth Planetary Science Letters*, **327**, 23-28, doi:10.1016/j.epsl.2012.01.014.

Hosseinpour, M., Williams, S., Seton, M., Barnett-Moore, N. and Müller, R. D. (2016). Tectonic evolution of Western Tethys from Jurassic to present day: coupling geological and geophysical data with seismic tomography models. *International Geology Review*, 1-30, DOI: 10.1080/00206814.2016.1183146.

Hu, G., Hu, W., Cao, J., Yao, S., Liu, W. and Zhou, Z. (2014). Fluctuation of organic carbon isotopes of the Lower Cretaceous in coastal southeastern China: Terrestrial response to the Oceanic Anoxic Events (OAE1b). *Palaeogeography, Palaeoclimatology, Palaeoecology*, **399**, 352-362.

Hu, X., Jansa, L. and Sarti, M. (2005). Mid-Cretaceous oceanic red beds in the Umbria-Marche Basin, central Italy: Constraints on paleoceanography and paleoclimate. *Palaeogeography, Palaeoclimatology, Palaeoecology*, **233**, 163-186.

Hu, X., Zhao, K., Yilmaz, I. O. and Li, Y. (2012). Stratigraphic transition and palaeoenvironmental changes from the Aptian oceanic anoxic event 1a (OAE1a) to the oceanic red bed 1 (ORB1) in the Yenicesihlar section, central Turkey. *Cretaceous Research*, **38**, 40-51.

Huang, Y., Yang, G., Wang, C. and Wu, H. (2012). The stabilisation of the long-term Cretaceous greenhouse climate: Contribution from the semi-periodical burial of phosphorus in the ocean, Cretaceous Research, 38, 7-15.

Huber, B. T. and Leckie, R. M. (2011). Planktic foraminiferal species turnover across deep-sea Aptian/Albian boundary sections. *The Journal of Foraminiferal Research*, **41**(1), 53-95.

Huber, B. T., Hodell, D. A. and Hamilton, C. P. (1995). Middle–Late Cretaceous climate of the southern high latitudes: stable isotopic evidence for minimal equator-to-pole thermal gradients. *Geological Society of America Bulletin*, **107**(10), 1164-1191.

Huber, B. T., Leckie, R. M., Norris, R. D., Bralower, T. J. and CoBabe, E. (1999). Foraminiferal assemblage and stable isotopic change across the Cenomanian-Turonian boundary in the subtropical North Atlantic. *The Journal of Foraminiferal Research*, **29**(4), 392-417.

Huber, B. T., Norris, R. D. and MacLeod, K. G. (2002). Deep-sea paleotemperature record of extreme warmth during the Cretaceous. *Geology*, **30**(2), 123-126.

Huber, B. T., Price, N. A. and Macleod, K. G. (2003). Planktic Foraminiferal Turnover and Stable Isotope Stratigraphy across OAE1B in the Subtropical North Atlantic. *Eos Transactions AGU*, **84** (46), 42C-03.

Huber, B.T. and Watkins, D.K. (1992). Biogeography of Campanian-Maastrichtian calcareous plankton in the region of the Southern Ocean: paleogeographic and paleoclimatic implications. The Antarctic paleoenvironment: a perspective on global change. *Antarctic Research Series*, **56**, 31-60.

Huck, S., Heimhofer, U. and Immenhauser, A. (2012). Early Aptian algal bloom in a neritic proto–North Atlantic setting: Harbinger of global change related to OAE1a?. *Geological Society of America Bulletin*, **124**(11-12), 1810-1825.

Huck, S., Heimhofer, U., Immenhauser, A. and Weissert, H. (2013). Carbon-isotope stratigraphy of Early Cretaceous (Urgonian) shoal-water deposits: Diachronous changes in carbonate-platform production in the north-western Tethys. *Sedimentary Geology*, **290**, 157-174.

Huck, S., Heimhofer, U., Rameil, N., Bodin, S. and Immenhauser, A. (2011). Strontium and carbon-isotope chronostratigraphy of Barremian–Aptian shoal-water carbonates: Northern Tethyan platform drowning predates OAE 1a. *Earth and Planetary Science Letters*, **304**(3), 547-558.

Huck, S., Rameil, N., Korbar, T., Heimhofer, U., Wieczorek, T. D. and Immenhauser, A. (2010). Latitudinally different responses of Tethyan shoal-water carbonate systems to the Early Aptian oceanic anoxic event (OAE1a). *Sedimentology*, **57**(7), 1585-1614.

Hunt, D. and Tucker, M. E. (1993). The Middle Cretaceous Urgonian platform of Southeastern France, Chapter 32, *in*: Simo, J.A.T., Scott, R.W., Masse, J.P., eds., Cretaceous Carbonate Platforms, *AAPG Memoir*, 56, 409-453.

Husinec, A., Harman, C.A., Regan, S.P., Mosher, D.A., Sweeney, R.J. and Read, J.F. (2012). Sequence development infl uenced by intermittent cooling events in the Cretaceous Aptian greenhouse, Adriatic platform, Croatia. *AAPG Bulletin*, **96**, 2215-2244.

Immenhauser, A., Hillgärtner, H. and Van Bentum, E. (2005). Microbial-foraminiferal episodes in the Early Aptian of the southern Tethyan margin: ecological significance and possible relation to oceanic anoxic event 1a. *Sedimentology*, **52**(1), 77-99.

Immenhauser, A., Hillgartner, H., Sattler, U., Bertotti, G., Schoepfer, P., Homewood, P., Vahrenkamp, V., Steuber, T., Masse, J.P. and Droste, H. (2004). Barremian-lower Aptian Qishn Formation, Haushi-Huqf area, Oman: a new outcrop analogue for the Kharaib/Shu'aiba reservoirs. *Geoarabia*, **9** (1), 153-194.

Jahren, A. H. (2002). The biogeochemical consequences of the mid-Cretaceous superplume, J. Geodyn., 34, 177-191.

Jaillard, E., Dumont, T., Ouali, J., Bouillin, J. P., Chihaoui, A., Latil, J. L., Arnaud, H., Arnaud-Vanneau, A., and Zghal, I. (2013). The Albian tectonic crisis in Central Tunisia: Nature and chronology of the deformations. *Journal of African Earth Sciences*, **85**, 75-86.

James, N. P. (1997). The cool-water carbonate depositional realm. In: James, N.P., Clarke, J.A.D. (Eds.), Cool-Water Carbonates. *Soc. Econ. Paleontol. Mineral. Spec. Publ.*, **56**, 1-20.

Jansa, L. F. and Wiedmann, J. (1982). Mesozoic-Cenozoic development of the eastern North American and northwest African continental margins: a comparison. In *Geology of the Northwest African continental margin*, 215-269. Springer, Berlin

Heidelberg.

Jansa, L. F., Steiger, T.H. and Bradshaw, M. (1984). Mesozoic carbonate deposition on the outer continental margin off Morocco. In: Hinz, K. and Winterer, E.L. (eds.), *Initial Reports ofthe Deep Ocean Drilling Project*, **79**, 857-891. U.S. Govt Printing Office, Washington DC.

Jati, M., Grosheny, D., Ferry, S., Masrour, M., Aoutem, M., Icame, N., Gauthier-Lafaye, F. and Desmares, D. (2010). The Cenomanian–Turonian boundary event on the Moroccan Atlantic margin (Agadir basin): Stable isotope and sequence stratigraphy. *Palaeogeography, Palaeoclimatology, Palaeoecology*, **296**(1), 151-164.

Jenkyns, H. C. (1980). Cretaceous anoxic events: from continents to oceans. Journal of the Geological Society, 137(2), 171-188.

Jenkyns, H. C. (1995). Carbon-isotope stratigraphy and paleoceanographic significance of the Lower Cretaceous shallow-water carbonates of Resolution Guyot, Mid-Pacific Mountains. In: *Proceedings of the Ocean Drilling Program, Scientific Results*, **143**, 99-104, Texas.

Jenkyns, H. C. (1996). Relative sea-level change and carbon isotopes: data from the Upper Jurassic (Oxfordian) of central and southern Europe. *Terra Nova*, **8**, 75-85.

Jenkyns, H. C. (1999). Mesozoic anoxic events and palaeoclimate. *Zentralblatt für Geologie und Paläontologie* 1997, 943-949.

Jenkyns, H. C. (2003). Evidence for rapid climate change in the Mesozoic–Palaeogene greenhouse world. *Philosophical Transactions of the Royal Society of London A: Mathematical, Physical and Engineering Sciences*, **361**(1810), 1885-1916.

Jenkyns, H. C. (2010). Geochemistry of oceanic anoxic events. *Geochemistry, Geophysics, Geosystems*, **11**(3), Q03004, doi:10.1029/2009GC002788.

Jenkyns, H. C. and Clayton, C. J. (1986). Black shales and carbon isotopes from the Tethyan Lower Jurassic, *Sedimentology*, **33**, 87-106.

Jenkyns, H. C. and P. A. Wilson (1999). Stratigraphy, paleoceanography, and evolution of Cretaceous Pacific guyots: relics from a greenhouse Earth. *American Journal of Science*, **299**(5), 341-392.

Jeremiah, J. (2001). A Lower Cretaceous nannofossil zonation for the North Sea Basin. *Journal of Micropalaeontology*, **20**(1), 45-80.

Jervey, M. T. (1988). Quantitative geological modeling of siliciclastic rock sequences and their seismic expression, in: C. K. WiIgus, B. S. Hastings, C. G. St. C. Kendall, H. W. Posarnentier, C. A. Ross, and J. C. Van Wagoner, eds., Sea Level Changes: An Integrated Approach. *SEPM Special Publication*, **42**, 4749.

Joly, B. (2000). Les Juraphyllitidae, Phylloceratidae, Neophylloceratidae (Phylloceratacеae, Phylloceratina, Ammonoidea) de France au Jurassique et au Crétacé. *Géobios, Mémoire Spécial*, **23**, and *Mémoire de la Société Géologique de France*, **174**, 202 pp.

Joly, B. and Delamette, M. (2008). Les Phylloceratoidea (Ammonoidea) aptiens et albiens du bassin vocontien (Sud-Est de la France). *Carnets de Géologie/Notebooks on Geology, Université de Rennes*, Mémoire 2008/04 (CG2008_M04) : 60 pp.

Jones, C. E. and Jenkyns, H. C. (2001). Seawater strontium isotopes, oceanic anoxic events, and seafloor hydrothermal activity in the Jurassic and Cretaceous. *American Journal of Science*, **301**(2), 112-149.

Keller, C. E., Hochuli, P. A., Weissert, H., Bernasconi, S. M., Giorgioni, M. and Garcia, T. I. (2011). A volcanically induced climate warming and floral change preceded the onset of OAE1a (Early Cretaceous). *Palaeogeography, Palaeoclimatology, Palaeoecology*, **305**(1), 43-49.

Keller, G. (2008). Cretaceous climate, volcanism, impacts, and biotic effects. *Cretaceous Research*, **29**(5), 754-771.

Kemp, D.B., Coe, A.L. and Cohen, A.S., L.S. (2005). Astronomical pacing of methane release in the Early Jurassic period. *Nature* 437, 396-399.

Kemper, E. (1987). Das Klima der Kreide-Zeit. *Geologisches Jahrbuch*, **96**, 185 pp.

Kemper, E. and Zimmerle, W. (1978). Die anoxischen Sedimente der präoberaptischen Unterkreide NW-Deutschlands und ihr paläogeographischer Rahmen. *Geologisches Jahrbuch A*, **45**, 3-41.

Kennedy, W. J., Gale, A. S., Bown, P. R., Caron, M., Davey, R. J., Gröcke, D. and Wray, D. S. (2000). Integrated stratigraphy across the Aptian-Albian boundary in the Marnes Bleues, at the Col de Pre-Guittard, Arnayon (Drome), and at Tartonne (Alpes-de-Haute-Provence), France: A candidate global boundary stratotype section and boundary point for the base of the Albian stage. *Cretaceous Research*, **21**(5), 591-720.

Kennedy, W. J., Gale, A. S., Huber, B. T., Petrizzo, M. R., Bown, P., Barchetta, A. and Jenkyns, H. C. (2014). Integrated stratigraphy across the Aptian/Albian boundary at Col de Pré-Guittard (southeast France): A candidate global boundary stratotype section. *Cretaceous Research*, **51**, 248-259.

Keupp, H. and Mutterlose, J. (1994). Calcareous phytoplankton from the Barremian/Aptian boundary interval in NW Germany. *Cretaceous Research*, **15**(6), 739-763.

Kiessling, W. (2002). Radiolarian diversity patterns in the latest Jurassic–earliest Cretaceous. *Palaeogeography, Palaeoclimatology, Palaeoecology*, **187**(1), 179-206.

Kiessling, W., Flügel, E. and Golonka, J. (1999). Paleoreef maps: evaluation of a comprehensive database on Phanerozoic reefs. *AAPG Bulletin*, **83**(10), 1552-1587.

Kiessling, W., Flügel, E. and Golonka, J. A. N. (2003). Patterns of Phanerozoic carbonate platform sedimentation. *Lethaia*, **36**(3), 195-225.

Kilian, W. and Gentil, L. (1907). Sur les terrains crétacés de l'Atlas Occidental marocain. *Comptes rendus sommaire de l'Académie des Sciences de Paris*, **144**, 49-51.

Kilian, W. and Gentil, L. (1906). Découverte de deux horizons crétacés remarquables au Maroc. *Comptes rendus sommaire de l'Académie des Sciences de Paris*, **142**, 603-605.

Kochhann, K. G., Koutsoukos, E. A. and Fauth, G. (2014). Aptian–Albian benthic foraminifera from DSDP Site 364 (offshore Angola): A paleoenvironmental and paleobiogeographic appraisal. *Cretaceous Research*, **48**, 1-11.

Kochhann, K. G., Koutsoukos, E. A., Fauth, G. and Sial, A. N. (2013). Aptian-Albian Planktic Foraminifera From Dsdp Site 364 (offshore Angola): Biostratigraphy, Paleoecology and Paleoceanographic Significance. *The Journal of Foraminiferal Research*, **43**(4), 443-463.

Korte, C., Hesselbo, S. P., Jenkyns, H. C., Rickaby, R. E. and Spötl, C. (2009). Palaeoenvironmental significance of carbon- and oxygen-isotope stratigraphy of marine Triassic-Jurassic boundary sections in SW Britain. *Journal of the Geological Society*, **166**(3), 431-445.

Kuhnt, W., Holbourn, A. and Moullade, M. (2011). Transient global cooling at the onset of early Aptian oceanic anoxic event (OAE) 1a. *Geology*, **39**(4), 323-326.

Kump, L. R., Brantley, S. L. and Arthur, M. A. (2000). Chemical weathering, atmospheric CO2, and climate. Annual Review of Earth and Planetary Sciences, 28(1), 611-667.

Kuypers, M. M., Blokker, P., Erbacher, J., Kinkel, H., Pancost, R. D., Schouten, S. and Damsté, J. S. S. (2001). Massive expansion of marine archaea during a mid-Cretaceous oceanic anoxic event. *Science*, **293**(5527), 92-95.

Kuypers, M. M., Blokker, P., Hopmans, E. C., Kinkel, H., Pancost, R. D., Schouten, S. and Damste, J. S. S. (2002). Archaeal remains dominate marine organic matter from the early Albian oceanic anoxic event 1b. *Palaeogeography, Palaeoclimatology, Palaeoecology*, **185**(1), 211-234.

Kuypers, M. M., van Breugel, Y., Schouten, S., Erba, E. and Damsté, J. S. S. (2004). N2-fixing cyanobacteria supplied nutrient N for Cretaceous oceanic anoxic events. *Geology*, **32**(10), 853-856.

Lancelot Y. and Winterer E.L. (1980). Evolution of the Moroccan Oceanic Basin and adjacent continental margin: a synthesis. In: Y. Lancelot and E.L. Winterer, Editors, *Init. Repts DSDP*, **50**, U.S. Govt Printing Office, Washington, 801-821.

Larson, R. (1991a). Latest pulse of Earth: Evidence for a mid-Cretaceous superplume. *Geology*, **19**(6), 547-550.

Larson, R. L. (1991b). Geological consequences of superplumes. *Geology*, **19**(10), 963-966.

Larson, R. L. and E. Erba (1999). Onset of the mid-Cretaceous greenhouse in the Barremian-Aptian: Igneous events and the biological, sedimentary, and geochemical responses. *Paleoceanography*, **14**(6), 663-678.

Latil, J. L. (2011). Early Albian ammonites from Central Tunisia and adjacent areas of Algeria. *Revue de Paléobiologie*, **30**(1), 321-429.

Latil, J. L. and Aly, M. F. (2012). Knemiceras gracile DOUVILLÉ, 1916: a misunderstood Early Albian ammonite from north Sinai (Egypt), and considerations on the genus Platiknemiceras Bataller, 1954. *Revue de Paléobiologie*, **31**(1), 159-170.

Latil, J.-L., in Chihaoui, A., Jaillard, E., Latil, J.-L., Zghal, I., Susperregi, A.-S., Touir, J. and Ouali, J. (2010). Stratigraphy of the Hameima and lower Fahdene Formations in the Tadjerouine area (Northern Tunisia). *Journal of African Earth Sciences*, **58**, 387-399.

Laville, E. and Piqué, A. (1992). Jurassic penetrative deformation and Cenozoic uplift in the central High Atlas (Morocco): a tectonic model. Structural and orogenic inversions. *Geologische Rundschau*, **81**(1), 157-170.

Le Roy, P. and Piqué, A. (2001). Triassic–Liassic Western Moroccan synrift basins in relation to the Central Atlantic opening. Marine geology, 172(3), 359-381.

Le Roy, P., Guillocheau, F., Piqué, A. and Morabet, A. M. (1998). Subsidence of the Atlantic Moroccan margin during the Mesozoic. *Canadian Journal of Earth Sciences*, **35**(4), 476-493.

Leckie, R. (1984). Mid-Cretaceous Planktonic Formaminiferal Biostratigraphy Off Central Morocco, Deep-Sea Drilling Project Leg-79, Site-545 and Site-547. *Initial Reports of the Deep Sea Drilling Project*, **79**, 579-620.

Leckie, R. M. (1989). An oceanographic model for the early evolutionary history of planktonic foraminifera. *Palaeogeography, Palaeoclimatology, Palaeoecology*, **73**, 107- 138.

Leckie, R. M., Bralower, T. J. and Cashman, R. (2002). Oceanic anoxic events and plankton evolution: Biotic response to tectonic forcing during the mid-Cretaceous. *Paleoceanography*, **17**(3), 1-29. 1041, doi:10.1029/2001PA000623.

Leckie, R.M. (1984). Mid-Cretaceous planktonic foraminiferal biostratigraphy off Central Morocco, Deep Sea Drilling Project Leg 79, Sites 545 and 54 7. In: Hinz, K. and Winterer E.L. (eds.), *Initial Reports of the Deep Sea Drilling Project*, **79**, 579-620. U.S. Govt Printing Office, Washington D.C.

Lees, A. (1975). Possible influence of salinity and temperature on modern she1f carbonate sedimentation: *Marine Geology*, **19**, 159-198.

Lees, J. A. (2002). Calcareous nannofossil biogeography illustrates palaeoclimate change in the Late Cretaceous Indian Ocean. *Cretaceous Research*, **23**, 537-634.

Lees, J. A., Bown, P. R. and Mattioli, E. (2005). Problems with proxies? Cautionary tales of calcareous nannofossil paleoenvironmental indicators. *Micropaleontology*, **51**(4), 333-343.

Lees, J. A., Bown, P. R. and Young, J. R. (2006). Photic zone palaeoenvironments of the Kimmeridge Clay Formation (Upper Jurassic, UK) suggested by calcareous nannoplankton palaeoecology. *Palaeogeography, Palaeoclimatology, Palaeoecology*, **235**(1), 110-134.

Lees, J. A., Bown, P. R., Young, J. R. and Riding, J. B. (2004). Evidence for annual records of phytoplankton productivity in the Kimmeridge Clay Formation coccolith stone bands (Upper Jurassic, Dorset, UK). *Marine Micropaleontology*, **52**(1), 29-49.

Lehmann, C., Osleger, D. A., Montañez, I. P., Sliter, W., Vanneau, A. A. and Banner, J. (1999). Evolution of Cupido and Coahuila carbonate platforms, early Cretaceous, northeastern Mexico. *Geological Society of America Bulletin*, **111**(7), 1010-1029.

Lemoine, P. (1905). In: Mission dans le Maroc occidental, Automne 1904. *Rapport.* Comité du Maroc (Paris), 223 pp.

Li, X., Bralower, T. J., Montañez, I. P., Osleger, D. A., Arthur, M. A., Bice, D. M., Herbert, T.D., Erba, E. and Silva, I.P. (2008). Toward an orbital chronology for the early Aptian oceanic anoxic event (OAE1a,~ 120 Ma). *Earth and Planetary Science Letters*, **271**(1), 88-100.

Li, X., Wei, Y., Li, Y. and Zhang, C. (2016). Carbon isotope records of the early Albian oceanic anoxic event (OAE) 1b from eastern Tethys (southern Tibet, China). *Cretaceous Research*, **62**, 109-121.

Linnert, C. and Mutterlose, J. (2008). Kalkige Nannofossilien des Untercampans (Oberkreide) von Buldern (Stadt Dülmen; NRW). *Geologie Paläontologie, Westfalen*, **71**, 77-101.

Linnert, C., Mutterlose, J. and Erbacher, J. (2010). Calcareous nannofossils of the Cenomanian/ Turonian boundary interval from the Boreal Realm (Wunstorf, northwest Germany). *Marine Micropaleontology*, **74**, 38-58.

Lorenz, J. C. (1988). Synthesis of Late Paleozoic and Triassic redbed sedimentation in Morocco. In: *The Atlas System of Morocco*, 139-168. Springer Berlin Heidelberg.

Lorenzen, J., Kuhnt, W., Holbourn, A., Flögel, S., Moullade, M. and Tronchetti, G. (2013). A new sediment core from the Bedoulian (Lower Aptian) stratotype at Roquefort-La Bédoule, SE France. *Cretaceous Research*, **39**, 6-16.

Luciani, V., Cobianchi, M. and Jenkyns, H. C. (2001). Biotic and geochemical response to anoxic events: the Aptian pelagic succession of the Gargano Promontory (southern Italy). *Geological Magazine*, **138**(03), 277-298.

Luciani, V., Cobianchi, M. and Jenkyns, H. C. (2004). Albian high-resolution biostratigraphy and isotope stratigraphy: The Coppa della Nuvola pelagic succession of the Gargano Promontory (Southern Italy). *Eclogae Geologicae Helvetiae*, **97**(1), 77-92.

Luciani, V., Cobianchi, M. and Lupi, C. (2006). Regional record of a global oceanic anoxic event: OAE1a on the Apulia Platform margin, Gargano Promontory, southern Italy. *Cretaceous Research*, **27**(6), 754-772.

Mahanipour, A., Mutterlose, J., Kani, A. L. and Adabi, M. H. (2011). Palaeoecology and biostratigraphy of early Cretaceous (Aptian) calcareous nannofossils and the δ 13 C carb isotope record from NE Iran. *Cretaceous Research*, **32**(3), 331-356.

Malinverno, A., Erba, E. and Herbert, T. D. (2010). Orbital tuning as an inverse problem: Chronology of the early Aptian oceanic anoxic event 1a (Selli Level) in the Cismon APTICORE. *Paleoceanography*, **25**(2), PA2203, doi:10.1029/2009PA001769.

Malkoč, M., Mutterlose, J. and Pauly, S. (2010). Timing of the Early Aptian δ13C excursion in the Boreal Realm. *Newsletters on Stratigraphy*, **43**(3), 251-273.

Mansouri-Daneshvar, P., Moussavi-Harami, R., Mahboubi, A., Gharaie, M. H. M. and Feizie, A. (2015). Sequence stratigraphy of the petroliferous Dariyan Formation (Aptian) in Qeshm Island and offshore (southern Iran). *Petroleum Science*, **12**(2), **232-251.**

Manspeizer, W. (1982). Triassic-Liassic basins and climate of the Atlantic passive margins. *Geologische Rundschau*, **71**(3), 895-917.

Manzo, R. B. and Otero, C. D. (2004). Análisis de microfacies y datos micropaleontológicos de la transición Barremiano-Aptiano en la Sierra del Rosario, Durango, México. *Revista mexicana de ciencias geológicas*, **21**(2), 247-259.

Marco, I., Dhahri, F., Haji, T. and Boukadi, N. (2014). Aptian-Albian transition in Central Tunisia: Tectonosedimentary and paleogeographic records. *Journal of Earth Science*, **25**(5), 787-798.

Marshall, J. D. (1992). Climatic and oceanographic isotopic signals from the carbonate rock record and their preservation. *Geological Magazine*, **129**(02), 143-160.

Masrour, M., Aoutem, M. and Atrops, F. (2004). The echinoid faunas of the Lower Cretaceous of the Atlantic High Atlas region (Morocco); systematic revision and biostratigraphical results. *Geobios*, **37**(5), 595-617.

Masse, J. P. (2003). Integrated stratigraphy of the Lower Aptian and applications to carbonate platforms: a state of the art. In: *North African Cretaceous carbonate platform systems* (203-214). Springer, Netherlands.

Masse, J. P., Tüysüz, O., Fenerci-Masse, M., Özer, S. and Sari, B. (2009). Stratigraphic organisation, spatial distribution, palaeoenvironmental reconstruction, and demise of Lower Cretaceous (Barremian-lower Aptian) carbonate platforms of the Western Pontides (Black Sea region, Turkey). *Cretaceous Research*, **30**(5), 1170-1180.

Masse, J.-P. (1976). *Les calcaires urgoniens de Provence (Valanginien-Aptien inférieur). Stratigraphie, paléontologie, les paléoenvironnements et leur évolution*. PhD thesis, University of Aix-Marseille II, 445 pp.

Masse, J.-P. (1989). Relations entre modifications biologiques et phénomènes géologiques sur les plates-formes carbonatées du domaine périméditerranéen au passage Bédoulien-Gargasien. In: Cotillon, P. (Ed.), Les Événements de la Partie Moyenne de la Crétacé (Aptien à Turonien). Geobios, Mémoire Spéciale, 11, 279-294.

Masse, J.-P., Fenerci-Masse, M. (2011). Drowning discontinuities and stratigraphic correlation in platform carbonates. The late Barremian-early Aptian record of southeast France. *Cretaceous Research*, **32**, 659-684.

Mattauer, M., Tapponnier, P. and Proust, F. (1977). Sur les mécanismes de formation des chaînes intracontinentales; l'exemple des chaînes atlasiques du Maroc. *Bulletin de la Société géologique de France*, **7**(3), 521-526.

Mattioli, E. and Pittet, B. (2002). Contribution of calcareous nannoplankton to carbonate deposition: a new approach applied to the Lower Jurassic of central Italy. *Marine Micropaleontology*, **45**(2), 175-190.

Mattis, A. F. (1977). Nonmarine Triassic sedimentation, Central High Atlas Mountains, Morocco. *Journal of Sedimentary Research*, 47**(**1), 107-119.

Maurer, F., Van Buchem, F. S., Eberli, G. P., Pierson, B. J., Raven, M. J., Larsen, P. H., Al-Husseini, M.I. and Vincent, B. (2013). Late Aptian long-lived glacio-eustatic lowstand recorded on the Arabian Plate. *Terra Nova*, **25**(2), 87-94.

Maury R.C., Charrière A., Taki Z., Benammi M. and Michard A. (2008). The Atlas System, in : The Geology of Morocco, eds A. Michard, O. Saddiqi, A. Chalouan, A. Frizon de Lamotte, **116**, 133-202, Springer, Berlin Heidelberg.

McAnena, A., Flögel, S., Hofmann, P., Herrle, J. O., Griesand, A., Pross, J., Talbot, H. M., Rethemeyer, J., Wallmann, K. and Wagner, T. (2013). Atlantic cooling associated with a marine biotic crisis during the mid-Cretaceous period. *Nature Geoscience*, **6**(7), 558-561.

McCartney, K.,Wise, S. W. jr and Harwood, D. M. (1990). Enigmatic Lower Albian silicoflagellates from ODP Site 693: Progenitors of the order silicoflagellata? - In: Barker, P. F. and Kennett, J. P. (Eds.): *Proceedings of the Ocean Drilling Program, Scientific Results*, **113**, 427-442.

Medina, F. (1994). *Evolution structurale du Haut-Atlas Occidental et des régions voisines du Trias a l'actuel. Dans le cadre de l'ouverture de l'Atlantique central et la collision Afrique–Europe*. Unpublished Doctorate, Doctorat de 3ème Cycle, Univ. Mohammed V, Rabat, Morocco, 271 pp.

Medina, F. (1995). Syn- and post-rift evolution of the El Jadida–Agadir Basin (Morocco): Constraints for the rifting models of the Central Atlantic. *Canadian Journal of Science*, **32**, 1273-1291.

Méhay, S., Keller, C. E., Bernasconi, S. M., Weissert, H., Erba, E., Bottini, C. and Hochuli, P. A. (2009). A volcanic CO2 pulse triggered the Cretaceous Oceanic Anoxic Event 1a and a biocalcification crisis. *Geology*, **37**(9), 819-822.

Mehdi, K., Griboulard, R. and Bobier, C. (2004). Rôle de l'halocinèse dans l'évolution du bassin d'Essaouira (Sud-Ouest marocain). *Comptes Rendus Géoscience*, **336**, 587-595.

Memmi, L. (1981). Biostratigraphie du Crétacé inferieur de la Tunisie nord-orientale. *Bull. Soc. Geol. France*, **23** (2),175-183.

Menegatti, A. P., Weissert, H., Brown, R. S., Tyson, R. V., Farrimond, P., Strasser, A. and Caron, M. (1998). High-resolution $\delta^{13}C$ stratigraphy through the Early Aptian Livello Selli of the Alpine tethys. *Paleoceanography*, **13**(5), 530-545.

Millán, M. I., Weissert, H. J. and López-Horgue, M. A. (2014). Expression of the late Aptian cold snaps and the OAE1b in a highly subsiding carbonate platform (Aralar, northern Spain). ***Palaeogeography, Palaeoclimatology, Palaeoecology*, 411, 167-179.**

Millán, M. I., Weissert, H. J., Fernández-Mendiola, P. A. and García-Mondéjar, J. (2009). Impact of Early Aptian carbon cycle perturbations on evolution of a marine shelf system in the Basque-Cantabrian Basin (Aralar, N Spain). *Earth and Planetary Science Letters*, **287**(3), 392-401.

Millán, M. I., Weissert, H. J., Owen, H., Fernández-Mendiola, P. A. and García-Mondéjar, J. (2011). The Madotz Urgonian platform (Aralar, northern Spain): Paleoecological changes in response to Early Aptian global environmental events. *Palaeogeography, Palaeoclimatology, Palaeoecology*, **312**(1), 167-180.

Moore, C. H. (2001). Carbonate Reservoirs: Porosity, Evolution and Diagenesis in a Sequence Stratigraphic Framework. *Development in Sedimentology*, Elsevier, 55, 444 pp.

Moreno-Bedmar, J.A., Company, M., Bover-Arnal, T., Salas, R., Delanoy, G., Maurrasse, F.J.-M.R., Grauges, A. and Martínez, R. (2010a). Lower Aptian ammonite biostratigraphy in the Maestrat Basin (Eastern Iberian Chain, Eastern Spain). A Tethyan transgressive record enhanced by synrift subsidence. *Geologica Acta*, **8**, 3, 281-299.

Moret, L. and Mahmoud, I. G. (1953). Nouvelles observations stratigraphiques et paléontologiques sur l'Albien du massif du Moghara (Sinai-Egypte). *Travaux du Laboratoire de Ggologie de Grenoble*, **31**, 269-274.

Moss, S. J. and Tucker, M. E. (1996). Dolomitization associated with transgressive surfaces - a mid-Cretaceous example. *Sedimentary Geology*, **107**(1), 11-20.

Moulin, M., Aslanian, D. and Unternehr, P. (2010). A new starting point for the South and Equatorial Atlantic Ocean. *Earth-Science Reviews*, **98**(1), 1-37.

Moullade M., Kuhnt W., Bergen J.A., Masse J.-P. and Tronchetti G. (1998). Correlation of biostratigraphic and stable isotope events in the Aptian historical stratotype of La Bédoule (southeast France). *Comptes Rendus de l'Académie des Sciences Paris, Sciences de la Terre et des Planètes*, (IIa), **327**(10), 693-698.

Moullade, M., Mascle, J., Benkhelil, J., Cousin, M. and Tricart, P. (1993). Occurrence of marine mid-Cretaceous sediments along the Guinean slope (Equamarge II cruise): their significance for the evolution of the central Atlantic African margin. *Marine geology*, **110**(1-2), 63-72.

Mouty, M. and Saint-Marc, P. (1982). Le Crétacé moyen du massif alaouite (NW Syrie). *Cahiers de Micropaléontologie*, **3**, 55-69.

Müller, G. and Gastner, M. (1971). The'Karbonat-Bombe', a simple device for the determination of carbonate content in sediment, soils, and other materials. *Neues Jahrbuch für Mineralogie-Monatshefte*, **10**, 466-469.

Müller, R. D., Seton, M., Zahirovic, S., Williams, S. E., Matthews, K. J., Wright, N. M., Shephard, G.E., Maloney, K., Barnett-Moore, N., Hosseinpour, M. and Bower, D. J. (2016). Ocean basin evolution and global-scale plate reorganization events since Pangea breakup. *Annual Review of Earth and Planetary Sciences*, **44**(1), 107-138.

Murphy, M. A. (1967). Aptian-cenomanian members of the ammonite genus Tetragonites. Joly, B. and Delamette, M. (2008). Les Phylloceratoidea (Ammonoidea) aptiens et albiens du bassin vocontien (Sud-Est de la France). *Carnets de Géologie/Notebooks on Geology*, Mémoire, **4**.

Mutterlose, J. (1989). Temperature-controlled migration of calcareous nannofloras in the north- west European Aptian. In: Crux, J.A. and van Heck, S.E. (eds.), *Proceedings of the International Nannofossil Association Conference*, 122-142. Ellis Horwood, Chichester.

Mutterlose, J. (1991). Das Verteilungs- und Migrations-Muster des kalkigen Nannoplanktons in der Unterkreide Valangin-Apt NW-Deutschland. *Palaeontographica*, **B 221**, 27-152.

Mutterlose, J. (1992a). Biostratigraphy and palaeobiogeography of Early Cretaceous calcareous nannofossils. *Cretaceous Research*, **13**(2), 167-189.

Mutterlose, J. (1992b). Lower Cretaceous nannofossil biostratigraphy off northwestern Australia (Leg 123). In Gradstein, F.M., Ludden, J.N., et al., *Proc. ODP, Sci. Results*, **123**, 343-368.

Mutterlose, J. (1992c). Migration and evolution patterns of floras and faunas in marine Early Cretaceous sediments of NW Europe. *Palaeogeography, Palaeoclimatology, Palaeoecology*, **94**(1), 261-282.

Mutterlose, J. (1996). Calcareous nannofossil palaeoceanography of the Early Cretaceous of NW Europe. *Mitteilungen aus dem Geologischen Staatsinstitut in Hamburg*, **77**, 291-313.

Mutterlose, J. and Böckel, B. (1998). The Barremian–Aptian interval in NW Germany: a review. *Cretaceous Research*, **19**(5), 539-568.

Mutterlose, J. and Wise, S. W. (1990). Lower Cretaceous nannofossil biostratigraphy of ODP Leg 113 Holes 692B and 693A, continental slope off East Antarctica, Weddell Sea. In Barker, P. F., Kennett, J. P., et al., *Proc. ODP, Sci. Results*, **113**, 325-351.

Mutterlose, J., and Kessels, K. (2000). Early Cretaceous calcareous nannofossils from high latitudes: implications for palaeobiogeography and palaeoclimate. *Palaeogeography, Palaeoclimatology, Palaeoecology*, **160**, 347-372.

Mutterlose, J., Bornemann, A. and Herrle, J. O. (2005). Mesozoic calcareous nannofossils - state of the art. *Paläontologische Zeitschrift*, **79**(1), 113-133.

Mutterlose, J., Bornemann, A. and Herrle, J.O. (2009). The Aptian - Albian cold snap: Evidence for mid Cretaceous icehouse interludes. *Neues Jahrbuch für Geologie und Paläontologie - Abhandlungen*, **252**, 217-225.

Mutterlose, J., Bornemann, A., Luppold, F. W., Owen, H. G., Ruffell, A., Weiss, W. and Wray, D. (2003). The Vöhrum section (northwest Germany) and the Aptian/Albian boundary. *Cretaceous Research*, **24**(3), 203-252.

Mutterlose, J., Bottini, C., Schouten, S. and Damsté, J. S. S. (2014). High sea-surface temperatures during the early Aptian Oceanic Anoxic Event 1a in the Boreal Realm. *Geology*, **42**(5), 439-442.

Mutterlose, J., Brumsack, H., Flögel, S., Hay, W., Klein, C., Langrock, U., Lipinski, M., Ricken, W., Söding, E., Stein, R. and Swientek, O. (2003). The Greenland-Norwegian Seaway: A key area for understanding Late Jurassic to Early Cretaceous paleoenvironments. *Paleoceanography*, **18**(1), 1-10.

Najarro, M., Rosales, I., Moreno-Bedmar, J. A., de Gea, G. A., Barrón, E., Company, M. and Delanoy, G. (2011). High-resolution chemo-and biostratigraphic records of the Early Aptian oceanic anoxic event in Cantabria (N Spain): Palaeoceanographic and palaeoclimatic implications. *Palaeogeography, Palaeoclimatology, Palaeoecology*, **299**(1), 137-158.

Neagu, T. (1986). BarremianeLower Aptian Miliolid Fauna in Southern Dobrogea. *Revista Espanola de Micropaleontologia*, **18**, 313-348.

Nikolov, T. (1969). On the age of the urgonian sediments in the fore-balkan. *Bulletin of the Geological Institute, Series Stratigraphy and Lithology*, **18**, 73-82.

Norris, R. D. and Wilson, P. A. (1998). Low-latitude sea-surface temperatures for the mid-Cretaceous and the evolution of planktic foraminifera. *Geology*, **26**(9), 823-826.

North, F.K. (1985). Episodes of source-sediment deposition. *Journal of Petroleum Geology*, **2**, 199-218.

Nouidar, M. and Chellaï, E.H. (2001). Facies and sequence stratigraphy of a Late Barremian wave-dominated deltaic deposit, Agadir Basin, Morocco. *Sedimentary Geology*, **150**, 375-384.

Nouidar, M. and Chellaï, E.H. (2002). Facies and sequence stratigraphy of an estuarine incised-valley fill: Lower Aptian Bouzergoun Formation, Agadir Basin, Morocco. *Cretaceous Research*, **22**, 93-104.

Ouwehand, P.J. (1987). Die Garschella-Formation (Helvetischer Gault, Aptian–Cenomanian) der Churfirsten-Alvier Region (Ostschweiz). *Mitteillungen aus dem geologischen Institut der ETH und der Universität Zürich, Neue Folge*, **275**, 296 pp.

Owen, H.G. (1979). Ammonite zonal stratigraphy in the Albian of North Germany and its setting in the hoplitinid faunal province. In: Wiedmann, J. (Ed.). Aspekte der Kreide Europas. *IUGS Series A*, **6**, 563-588.

Owen, H.G. (2002). The base of the Albian Stage determined by ammonites and the North German succession; comments on recent proposals. *Cretaceous Research*, **23**, 1-13.

Pancost, R. D., Crawford, N., Magness, S., Turner, A., Jenkyns, H. C. and Maxwell, J. R. (2004). Further evidence for the development of photic-zone euxinic conditions during Mesozoic oceanic anoxic events. *Journal of the Geological Society*, **161**(3), 353-364.

Parrish, J. T. and Curtis, R. L. (1982). Atmospheric circulation, upwelling, and organic-rich rocks in the Mesozoic and Cenozoic eras. *Palaeogeography, Palaeoclimatology, Palaeoecology*, **40**(1), 31-66.

Parrish, J. T., Ziegler, A. M. and Scotese, C. R. (1982). Rainfall patterns and the distribution of coals and evaporites in the Mesozoic and Cenozoic. *Palaeogeography, Palaeoclimatology, Palaeoecology*, **40**(1), 67-101.

Perch-Nielsen, K. (1979). Calcareous nannofossils in Cretaceous/Tertiary boundary sections in Denmark. In: *Proceedings, Cretaceous/Tertiary Boundary Event Symposium, Copenhagen*, **1**, 120-6.

Perch-Nielsen, K. (1985). Mesozoic Calcareous nannofossils. In: H. M. Bolli, J. B. Saunders and K. Perch-Nielsen (Editors), *Plankton stratigraphy*, Cambridge University Press, Cambridge, 329 426.

Pérez-Díaz, L. and Eagles, G. (2014). Constraining South Atlantic growth with seafloor spreading data. *Tectonics*, **33**(9), 1848-1873.

Pervinquière, L. (1907). *Etudes de paléontologie tunisienne*, Vol. **1**. FR de Rudeval.

Petrizzo, M. R., Huber, B. T., Gale, A. S., Barchetta, A. and Jenkyns, H. C. (2012). Abrupt planktic foraminiferal turnover across the Niveau Kilian at Col de Pré-Guittard (Vocontian Basin, southeast France): new criteria for defining the Aptian/Albian boundary. *Newsletters on Stratigraphy*, **45**(1), 55-74.

Petrizzo, M.R., Huber, B.T., Gale, A.S., Barchetta, A. and Jenkyns, H.C. (2013). Erratum to Abrupt planktic foraminiferal turnover across the Niveau Kilian at Col de Pré-Guittard (Vocontian Basin, southeast France): new criteria for defining the Aptian/Albian boundary. *Newsletters on Stratigraphy*, **46**, 93.

Peybernès, B. (1976). *Le Jurassique et le Crétacé inférieur des Pyrénées francoespagnoles entre la Garonne et la Méditerranée*. PhD thesis, University Paul Sabatier, Toulouse, 459 pp.

Peybernès, B. (1979). L'Urgonien de Hongrie. *Geobios Mémoire Spécial*, **3**, 231-243.

Peybernès, B., Conrad, M.A. and Cugny, P. (1979). Contribution à l'étude biostratigraphique, micropaléontologique et paléontologique des calcaires urgoniens du Barrémo-bédoulien bulgare (Prébalkan et plate-forme moésienne). *Revue de Micropaléontologie*, **21**, 181-199.

Peybernes, C., Giraud, F., Jaillard, E., Robert, E., Masrour, M., Aoutem, M. and Içame, N. (2013). Stratigraphic framework and calcareous nannofossil productivity of the Essaouira-Agadir Basin (Morocco) during the Aptian-Early Albian: Comparison with the north-Tethyan margin. *Cretaceous Research*, **39**, 149-169.

Philip, J. (2003). Peri-Tethyan neritic carbonate areas: distribution through time and driving factors. *Palaeogeography, Palaeoclimatology, Palaeoecology*, **196**(1), 19-37.

Pictet, A., Delanoy, G., Adatte, T., Spangenberg, J. E., Baudouin, C., Boselli, P., Kindler, P. and Föllmi, K. B. (2015). Three successive phases of platform demise during the early Aptian and their association with the oceanic anoxic Selli episode (Ardèche, France). *Palaeogeography, Palaeoclimatology, Palaeoecology*, **418**, 101-125.

Piqué, A., Tricart, P., Guiraud, R., Laville, E., Bouaziz, S., Amrhar, M. and Ouali, R. A. (2002). The Mesozoic-Cenozoic Atlas belt (North Africa): an overview. *Geodinamica Acta*, **15**(3), 185-208.

Pirrie, D., Doyle, P., Marshall, J. D. and Ellis, G. (1995). Cool Cretaceous climates: new data from the Albian of Western Australia. *Journal of the Geological Society*, **152**(5), 739-742.

Pirrie, D., Marshall, J. D., Doyle, P. and Riccardi, A. C. (2004). Cool early Albian climates; new data from Argentina. *Cretaceous Research*, **25**(1), 27-33.

Pittet, B. and Mattioli, E. (2002). The carbonate signal and calcareous nannofossil distribution in an Upper Jurassic section (Balingen-Tieringen, Late Oxfordian, southern Germany). *Palaeogeography, Palaeoclimatology, Palaeoecology*, **179**, 71-96.

Pittet, B., Van Buchem, F. S., Hillgärtner, H., Razin, P., Grötsch, J. and Droste, H. (2002). Ecological succession, palaeoenvironmental change, and depositional sequences of Barremian-Aptian shallow-water carbonates in northern Oman. *Sedimentology*, **49**(3), 555-581.

Pletsch, T., Chamley, H., Daoudi, L., Deconinck, J. F. and Charroud, M. (1996). Palaeogeographic controls on palygorskite occurrence in mid-Cretaceous sediments of Morocco and adjacent basins. *Clay Minerals*, **31**(3), 403-416.

Pletsch, T., Erbacher, J., Holbourn, A. E. L., Kuhnt, W., Moullade, M., Oboh-Ikuenobede, F. E., Söding, E. and Wagner, T. (2001). Cretaceous separation of Africa and South America: the view from the West African margin (ODP Leg 159). *Journal of South American Earth Sciences*, **14**(2), 147-174.

Posamentier, H. W. and Vail, P. R. (1988). Eustatic controls on clastic deposition 11-sequence and systems tract models, in C. K. Wilgus, B. S. Hastings, C. G. St. C. Kendall, H. W. Posamentier, C. A. Ross, and J. C. Van Wagoner, eds., Sea Level Changes: An Integrated Approach. *Society Economic Palaeontologists Mineralogists, Special Publication*, **42**, 125-154.

Posamentier, H.W., Jervey, M.T. and Vail, P.R., (1988). Eustatic controls on clastic deposition I-conceptual framework. In: Wilgus, C.K., Hastings, B.S., Kendall, C.G.St.C., Posamentier, H., Ross, C.A., Van Wagoner, J. (Eds.), Sea-level Changes: An Integrated Approach. *Society Economic Palaeontologists Mineralogists, Special Publication*, **42**, 109-204.

Poulsen, C. J., Gendaszek, A. S. and Jacob, R. L. (2003). Did the rifting of the Atlantic Ocean cause the Cretaceous thermal maximum ?. *Geology*, **31**(2), 115-118.

Premoli Silva, I. (2010). Annual Report 2010 of the International Subcommission on Cretaceous Stratigraphy. Available at. http://www2.mnhn.fr/hdt203/info/iscs.

Premoli Silva, I. and Sliter, W. V. (1995). Cretaceous planktonic foraminiferal biostratigraphy and evolutionary trends from the Bottaccione section, Gubbio (Italy). *Palaeontographia Italica*, **82**, 1-89.

Premoli Silva, I. and Sliter, W. V. (1999). Cretaceous paleoceanography: evidence from planktonic foraminiferal evolution. *Geological Society of America Special Paper*, **332**, 301-28.

Premoli Silva, I., Erba, E. and Tornaghi, M. (1989a). Paleoenvironmental signals and changes in surface fertility in Mid Cretaceous Corg-Rich pelagic facies of the Fucoid Marls (Central Italy). *Geobios*, **22**, 225-236.

Premoli Silva, I., Erba, E., Salvini, G., Locatelli, C. and Verga, D. (1999). Biotic changes in Cretaceous oceanic anoxic events of the Tethys. *Journal of Foraminiferal Research*, **29**, 352-70.

Premoli Silva, I., Ripepe, M. and Tornaghi, M. (1989b). Planktonic foraminiferal distributions record productivity cycles: evidence from the AptianeAlbian Piobbico core (central Italy). *Terra Nova*, **1**, 443-448.

Price, G. D. (2003). New constraints upon isotope variation during the early Cretaceous (Barremian-Cenomanian) from the Pacific Ocean. *Geological Magazine*, **140**(05), 513-522.

Pucéat, E., Lécuyer, C., Sheppard, S. M., Dromart, G., Reboulet, S. and Grandjean, P. (2003). Thermal evolution of Cretaceous Tethyan marine waters inferred from oxygen isotope composition of fish tooth enamels. *Paleoceanography*, **18**(2), 1029. doi:10.1029/2002PA000823.

Rabinowitz, P. D. and LaBrecque, J. (1979). The Mesozoic South Atlantic Ocean and evolution of its continental margins. J*ournal of Geophysical Research, Solid Earth*, **84**(B11), 5973-6002.

Raspini, A. (1998). Microfacies analysis of shallow water carbonates and evidence of hierarchically organized cycles: Aptian of Monte Tobenna, southern Apennines, Italy. *Cretaceous Research*, **19**(2), 197-223.

Raspini, A. (2011). Shallow water carbonate platforms (Late Aptian, Southern Apennines) in the context of supraregional to global changes. *Solid Earth Discuss*, **3**, 901-942.

Raspini, A. (2012). Shallow water carbonate platforms (Late Aptian-Early Albian, Southern Apennines) in the context of supraregional to global changes: re-appraisal of palaeoecological events as reflectors of carbonate factory response. *Solid Earth*, **3**(2), 225-249.

Raven, M. J., Van Buchem, F. S. P., Larsen, P. H., Surlyk, F., Steinhardt, H., Cross, D., Klem, N. and Emang, M. (2010). Late Aptian incised valleys and siliciclastic infill at the top of the Shu'aiba Formation (Block 5, offshore Qatar). Barremian-Aptian stratigraphy and hydrocarbon habitat of the eastern Arabian Plate. *GeoArabia Special Publication*, **4**(2), 469-502.

Read, J. F. (1985). Carbonate platform facies models. *AAPG Bulletin*, **69**(1), 1-21.

Reboulet, S., Giraud, F. and Proux, O. (2005). Ammonoid abundance variations related to changes in trophic conditions across the Oceanic Anoxic Event 1d (Latest Albian, SE France). *Palaios*, **20**(2), 121-141.

Reboulet, S., Klein, J., Barragán, R., Company, M., González-Arreola, C., Lukeneder, A., Raisossadat, S.N., Sandoval, J., Szives, O., Tavera, J.M., and Vašíček, Z. (2009). Report on the 3rd international meeting of the IUGS lower Cretaceous ammonite working group, the Kilian Group. *Cretaceous Research*, **30**(2), 496-502.

Reboulet, S., Rawson, P. F., Moreno-Bedmar, J. A., Aguirre-Urreta, M. B., Barragán, R., Bogomolov, Y., Company, M., González-Arreola, C., Stoyanova, V.I., Lukeneder, A. and Matrion, B. (2011). Report on the 4th international meeting of the IUGS Lower Cretaceous ammonite working group, the Kilian Group. *Cretaceous Research*, **32**(6), 786-793.

Reboulet, S., Szives, O., Aguirre-Urreta, B., Barragán, R., Company, M., Idakieva, V., Ivanov, M., Kakabadze, M.V., Moreno-Bedmar, J.A., Sandoval, J. and Baraboshkin, E.J. (2014). Report on the 5th International Meeting of the IUGS Lower Cretaceous ammonite working group, the Kilian group. *Cretaceous Research*, **50**, 126-137.

Révész, K. M. and Landwehr, J. M. (2001). δ13C and δ18O isotopic composition of CaCO3 measured by continuous flow isotope ratio mass spectrometry: statistical evaluation and verification by application to Devils Hole core DH-11 calcite. *Rapid Communications in Mass Spectrometry*, **16**(22), 2102-2114.

Rey, J. (1972). *Recherches géologiques sur le Crétacé inférieur de l'Estremadura (Portugal)*. PhD thesis, University Paul Sabatier Toulouse, 529 p.

Rey, J., Canerot, J., Peybernès, B. and Taj-Eddine, J. P. (1988). Lithostratigraphy, biostratigraphy and sedimentary dynamics of the Lower Cretaceous deposits in the northern side of western High Atlas (Morocco). *Cretaceous Research*, **9**, 141-158.

Rey, J., Canérot, J., Peybernès, B., Taj-Eddine, K. and Thieuloy, J. P. (1986 a). le Crétacé inférieur sur le versant. nord du Haut Atlas (régions d'Imi N'Tanout et d'Amizmiz): Données biosratigraphiques et évolution sédimentaire. Revue Fac. Sci. Manakech, Sect. Sci. de la terre, Numéro special, **2**. PICG Nº 183

Rey, J., Canérot, J., Peybernès, B., Taj-Eddine, K. and Thieuloy, J. P. (1988). Lithostratigraphy, biostratigraphy and sedimentary dynamics of the Lower Cretaceous deposits on the northern side of the western High Atlas (Morocco). *Cretaceous Research*, **9**(2), 141-158.

Rey, J., Canérot, J., Peybernès, B., Taj-Eddine, K., Rahhali, i. and Thieuloy, J. P. (1986 b). Le Crétacé inférieur de la région d'Essaouira: données biostratigraphiques et évolutions sédimentaires. *Revue Fac. Sci. Marrakech, Sect. Sci. de la Terre*, Numéro spécial, **2**. PICG-UNESCO, nº 183.

Robert, E., B. Peybernès and L.G. Bulot (2001). Caractérisation d'une nouvelle sous-Zone d'ammonites au passage Aptien-Albien dans les «Marnes noires à Hypacanthoplites» des Pyrénées espagnoles. *Geobios*, **34**(1), 53-62.

Robinson, S. A., Williams, T. and Bown, P. R. (2004). Fluctuations in biosiliceous production and the generation of Early Cretaceous oceanic anoxic events in the Pacific Ocean (Shatsky Rise, Ocean Drilling Program Leg 198). *Paleoceanography*, **19**(4), 4024.

Roch, E. (1930). *Etudes géologiques dans la région méridionale du Maroc occidental*, (9), Protat frères, imprimeurs.

Roch, E. (1930). Histoire stratigraphique du Maroc. *Notes et Mémoires du Service géologique du Maroc*, **80**, 440 pp.

Rodríguez-López, J. P., Liesa, C. L., Pardo, G., Meléndez, N., Soria, A. R. and Skilling, I. (2016). Glacial dropstones in the western Tethys during the late Aptian–early Albian cold snap: Palaeoclimate and palaeogeographic implications for the mid-Cretaceous. *Palaeogeography, Palaeoclimatology, Palaeoecology*, **452**, 11-27.

Ropolo P., Gonnet R. & Conte G. (1999). The *Pseudocrioceras* interval and adjacent beds at La Bédoule (SE France): implications to highest Barremian/lowest Aptian biostratigraphy. *In*: Rawson P.F. & Hoedemaeker P.J. (eds.), Proceedings 4th International Workshop Cephalopod Team (IGCP-Project 362)- *Scripta Geologica*, Leiden, Special Issue **3**, 159-213.

Ropolo, P., Conte, G., Moullade, M., Tronchetti, G. and Gonnet, R. (2008). The Douvilleiceratidae (Ammonoidea) of the Lower Aptian historical stratotype area at Cassis-La Bédoule (SE France). *Carnets de Géologie/Notebooks on Geology*, Memoir, **3**.

Rosales, I. (1999). Controls on carbonate-platform evolution on active fault blocks: the Lower Cretaceous Castro Urdiales platform (Aptian-Albian, northern Spain). *Journal of Sedimentary Research*, **69**(2), 447-465.

Rossi A. (l992). *Le Crétacé inférieur de I'anticlinal d'lda Ou Zemzem (Atlas Atlantique, Maroc). Stratigraphie séquentielle et évolution godynamique*. Thése de 3ème cycle. Univ. Cadi. Ayyad. Fac. Sci. Marrakech.

Roth, P. H. (1978). Cretaceous nannoplankton biostratigraphy and oceanography of the northwestern Atlantic Ocean. In: Benson, W.E. and Sheridan, R.E. et al. (eds.), *Initial Reports of the Deep Sea Drilling Project*, **44**, 731-759. Govt Printing Office, Washington, D.C.

Roth, P. H. (1981). Mid-Cretaceous calcareous nannoplankton from the Central Pacific: Implications for paleoceanography. *Initial Reports of the DSDP*, **62**, 471-489.

Roth, P. H. (1983). Jurassic and Lower Cretaceous calcareous nannofossils in the western North Atlantic (Site 534): biostratigraphy, preservation, and some observations on biogeography and palaeoceanography. In: Sheridan, R.E. and Gradstein, F.M. (eds.), *Initial Reports Deep Sea Drilling Project*, **76**, 587-621. US Govt Printing Office, Washington DC.

Roth, P. H. (1989). Ocean circulation and calcareous nannoplankton evolution during the jurassic and Cretaceous, *Palaeogeography, Palaeoclimatology, Palaeoecology*, **74**, 111-126.

Roth, P. H. and Bowdler, J.L. (1981). Middle Cretaceous calcareous nannoplankton biogeography and oceanography of the Atlantic Ocean. *Soc. Econ. Paleontol. Mineral. Special Publication*, **32**, 517-- 546.

Roth, P. H. and Krumbach, K. R. (1986). Middle Cretaceous calcareous nannofossil biogeography and preservation in the Atlantic and Indian Oceans: implications for paleoceanography. *Marine Micropaleontology*, **10**(1), 235-266.

Roth, P. H. and Thierstein, H.R. (1972). Calcareous Nannoplankton: Leg 14 of the Deep Sea Drilling Project. In: Hayes, D.E. (eds.), *Initial Reports of the Deep Sea Drilling Project*, **14**, 421-485. U.S. Govt Printing Office, Washington D.C.

Ruberti, D., Bravi, S., Carannante, G., Vigorito, M. and Simone, L. (2013). Decline and recovery of the Aptian carbonate factory in the southern Apennine carbonate shelves (southern Italy): climatic/oceanographic vs. local tectonic controls. *Cretaceous Research*, **39**, 112-132.

Rückheim, S., Bornemann, A. and Mutterlose, J. (2006a). Integrated stratigraphy of an Early Cretaceous (Barremian-Early Albian) North Sea borehole (BGS 81/40). *Cretaceous Research*, **27**, 447- 463.

Rückheim, S., Bornemann, A. and Mutterlose, J. (2006b). Planktic foraminifera from the mid-Cretaceous (Barremian-EarlyAlbian) of theNorth Sea Basin: Palaeoecological and palaeoceanographic implications. *Marine Micropalaeontology*, **58**, 83-102.

Ruellan, E., Auzende, J. M. and Dostmann, H. (1985). Structure and evolution of the Mazagan (El Jadida) plateau and escarpment

off central Morocco. *Oceanologica Acta*, Special issue, 59-72.

Saadi, M. (1982). Schema structural du Maroc. Notes et Me´moires du Service Géologique du Maroc, 278B.

Sabatino, N., Coccioni, R., Manta, D. S., Baudin, F., Vallefuoco, M., Traina, A. and Sprovieri, M. (2015). High-resolution chemostratigraphy of the late Aptian-early Albian oceanic anoxic event (OAE 1b) from the Poggio le Guaine section (Umbria–Marche Basin, central Italy). *Palaeogeography, Palaeoclimatology, Palaeoecology*, **426**, 319-333.

Saint-Marc, P. (1970). Contribution à la connaissance du Crétacé basal au Liban. Revue de Micropaléontologie, 12, 224-233.

Savin, S. M. (1977). The history of the Earth's surface temperature during the past 100 million years. *Annual review of earth and planetary sciences*, **5**, 319-355.

Schaer, J. P. (1987). Evolution and structure of the High Atlas of Morocco. In J.-P. Schaer and J. Rodgers (Eds.), *The anatomy of mountain ranges*, 107-128. Princeton University Press.

Schaer, J. P. (1988). Deformation of igneous dikes in and around the Tichka granite, high Atlas-Morocco. In: *The Atlas System of Morocco*, 129-138. Springer ,Berlin Heidelberg.

Schlager, W. (1981). The paradox of drowned reefs and carbonate platforms. *Geological Society of America Bulletin*, **92**(4), 197-211.

Schlager, W. and Camber, O. (1986). Submarine slope angles, drowning unconformities, and self-erosion of limestone escarpments. *Geology*, **14**(9), 762-765.

Schlanger, S.O. and Jenkyns, H.C. (1976). Cretaceous anoxic events: causes and consequences. *Geologie en Mijnbouw*, **55**, 179-184.

Schlanger, S.O., Arthur, M.A., Jenkyns, H.C. and Scholle, P.A. (1987). The Cenomanian-Turonian oceanic anoxic event: I. Stratigraphy and distribution of organic carbon-rich beds and the marine d13C excursion. In: Brooks, J., Fleet, J.A. (Eds.), Marine Petroleum Source Rocks. *Geological Society of London Special Publication*, **26**, 371-399.

Schröder-Adams, C. J., Herrle, J. O., Embry, A. F., Haggart, J. W., Galloway, J. M., Pugh, A. T. and Harwood, D. M. (2014). Aptian to Santonian foraminiferal biostratigraphy and paleoenvironmental change in the Sverdrup Basin as revealed at Glacier Fiord, Axel Heiberg Island, Canadian Arctic Archipelago. *Palaeogeography, Palaeoclimatology, Palaeoecology*, **413**, 81-100.

Schwizer, N. (1984). *Die Tristel-Formation Vergleichende Untesuchung in Graubünde, Liechtenstein, Vorarlberg und Bayern*. University of Bern, 185 pp.

Scotese, C.R. (2013). Paleomap Project. www.scotese.com (last accessed 16.01.2013).

Sellwood, B. W. (1986). Shallow marine carbonate environment. In: Reading Ed., *Sedimentary environments and facies*, 283-342. Blackwell Scientific publication.

Sellwood, B. W., Price, G. D. and Valdest, P. J. (1994). Cooler estimates of Cretaceous temperatures. *Nature*, **370**, 453-455.

Seton, M., Gaina, C., Müller, R. D. and Heine, C. (2009). Mid-Cretaceous seafloor spreading pulse: Fact or fiction ?. *Geology*, **37**(8), 687-690.

Shafik, S. (1990). Late Cretaceous nannofossil biostratigraphy and biogeography of the Australian western margin. *Bureau of Mineral Resources, Geology and Geophysics Report*, **295**, 1-164.

Shannon, C. E. and Weaver, W. (1949). The Mathematical Theory of Communication. University of Illinois Press. Urbana, 104-107.

Simo, J. A.T., Scott, R.W. and Masse, J.-P. (1993). Cretaceous Carbonate Platforms: An Overview. In: Simo, J.A.T., Scott, R.W., Masse, J.-P., 1993, (eds), Cretaceous Carbonate Platforms, *AAPG Mem.*, **56**, 1-14.

Skelton, P.W. (2003). *The Cretaceous World*. The Open University, Cambridge University Press, Cambridge, 360 pp.

Snow, L. J., Duncan, R. A. and Bralower, T. J. (2005). Trace element abundances in the Rock Canyon Anticline, Pueblo, Colorado, marine sedimentary section and their relationship to Caribbean plateau construction and oxygen anoxic event 2. *Paleoceanography*, **20**(3), PA3005. http://dx.doi.org/10.1029/2004PA001093.

Sokal, R. R. and Rohlf, F. J. (1995). The arcsine transformation. *Biometry*, 419-422.

Stanley, S. M. (2006). Influence of seawater chemistry on biomineralization throughout Phanerozoic time: Paleontological and experimental evidence. *Palaeogeography, Palaeoclimatology, Palaeoecology*, **232**(2), 214-236.

Stein, M., Föllmi, K. B., Westermann, S., Godet, A., Adatte, T., Matera, V., Fleitmann, D. and Berner, Z. (2011). Progressive palaeoenvironmental change during the Late Barremian–Early Aptian as prelude to Oceanic Anoxic Event 1a: evidence from the Gorgo a Cerbara section (Umbria-Marche basin, central Italy). *Palaeogeography, Palaeoclimatology, Palaeoecology*, **302**(3), 396-406.

Stets, J. and Wurster, P. (1982). Atlas and Atlantic-structural relations. In: *Geology of the Northwest African continental margin*, 69-85. Springer**.**

Stoll, H. M. and Schrag, D. P. (2000). High-resolution stable isotope records from the Upper Cretaceous rocks of Italy and Spain: Glacial episodes in a greenhouse planet ?. *Geological Society of America Bulletin*, **112**(2), 308-319.

Strasser, A., Pittet, B., Hillgartner, H. and Pasquier, J. (1999). Depositional sequences in shallow carbonate-dominated sedimentary systems: concepts for a high-resolution analysis. *Sedimentary Geology*, **128**, 201-221.

Street, C. and Bown, P. R. (2000). Palaeobiogeography of early Cretaceous (Berriasian–Barremian) calcareous nannoplankton. *Marine Micropaleontology*, **39**(1), 265-291.

Strohmenger, C. J., Steuber, T., Ghani, A., Barwick, D. G., Al-Mazrooei, S. H. A. and Al-Zaabi, N. O. (2010). Sedimentology and chemostratigraphy of the Hawar and Shu'aiba depositional sequences, Abu Dhabi, United Arab Emirates. Barremian-Aptian stratigraphy and hydrocarbon habitat of the eastern Arabian Plate. *GeoArabia Special Publication*, **4**, 341-365.

Summerhayes, C. (1983). Sedimentation of organic matter in upwelling regimes. In : *Coastal Upwelling. Its Sediment Record*, Plenum Press New York, 29-72.

Summerhayes, C. P. (1981). Organic facies of middle Cretaceous black shales in deep North Atlantic. *AAPG Bulletin*, **65**(11), 2364-2380.

Taj-Eddine, K. (1991). *Le Jurassique terminal et le Crétacé basal dans l'Atlas atlantique (Maroc): Biostratigraphie, sédimentologie, stratigraphie séquentielle et géodynamique*. Unpublished State Doctorate, Doctorat de 3éme Cycle, Univ. Cadi Ayyad, Marrakech/Morocco, 285 p.

Taj-Eddine, K. (1992). Le Jurassique terminal et le Crétacé basal dans l'Atlas atlantique (Maroc) : biostratigraphie, sédimentologie, stratigraphie séquentielle et géodynamique. *Strata*, **16**, 285 pp.

Taj-Eddine, K., Rey, J., Aoutem,M., Ettachfini, M., Hoedemaeker, P., (1990). Les couches de passage du Jurassique au Crétacé dans la région d'Agadir (Maroc): nouveaux éléments de datation et séquences de dépôt. *Revue de Paléobiologie*, **9**, 113-120.

Takashima, R., Nishi, H., Huber, B. T. and Leckie, R. M. (2006). Greenhouse. *Oceanography*, **19**(4), 64.

Takashima, R., Sano, S. I., Iba, Y. and Nishi, H. (2007). The first Pacific record of the Late Aptian warming event. *Journal of the Geological Society*, **164**(2), 333-339.

Tarduno, J. A., Brinkman, D. B., Renne, P. R., Cottrell, R. D., Scher, H. and Castillo, P. (1998). Evidence for extreme climatic warmth from Late Cretaceous Arctic vertebrates. *Science*, **282**(5397), 2241-2243.

Tari, G. and Jabour, H. (2013). Salt Tectonics along the Atlantic Margin of Morocco in: *Conjugate Divergent Margins, Geological Society, London, Special Publications*, **v.369**.

Tari, G., Molnar, J., Ashton, P. and Hedley, R. (2000). Salt tectonics in the Atlantic margin of Morocco. The Leading Edge, 1074-1078.

Tejada, M. L. G., Suzuki, K., Kuroda, J., Coccioni, R., Mahoney, J. J., Ohkouchi, N., Sakamoto, N. and Tatsumi, Y. (2009). Ontong Java Plateau eruption as a trigger for the early Aptian oceanic anoxic event. *Geology*, **37**(9), 855-858.

Thielemann, J. (2006). *Veränderungen der Levantischen Karbonatplattform in der Mittleren Kreide unter besonderer Beru¨cksichtigung des OAE-1a am Beispiel des Gebel Raghawi, Nordsinai, Agypten*. Diploma thesis, Univ. Bremen, 91 pp.

Thierstein, H. R. (1971). Tentative Lower Cretaceous nannoplankton zonation. *Eclog. Geol. Helvet.*, **64**, 459-488.

Thierstein, H. R. (1973). Lower Cretaceous calcareous nannoplankton biostratigraphy. *Abhandl. Geologisch. Bundesan.*, **29**, 1-52.

Thierstein, H. R. (1974). Calcareous nannoplankton - Leg 26, Deep Sea Drilling Project. *Initial Reports of the Deep Sea Drilling Project*, **26**, 619-667.

Thierstein, H. R. (1980). Selective dissolution of Late Cretaceous and earliest Tertiary calcareous nannofossils; experimental evidence. *Cretaceous Research*, **1**, 165-176.

Thomsen, E. (1989). Seasonal variation in boreal Early Cretaceous calcareous nannofossils. *Marine Micropaleontology*, **15**, 123-152.

Tiraboschi, D., Erba, E. and Jenkyns, H. C. (2009). Origin of rhythmic Albian black shales (Piobbico core, central Italy): Calcareous nannofossil quantitative and statistical analyses and paleoceanographic reconstructions. *Paleoceanography*, **24**(2),1-21.

Tomás, S., Löser, H. and Salas, R. (2008). Low-light and nutrient-rich coral assemblages in an Upper Aptian carbonate platform of the southern Maestrat Basin (Iberian Chain, eastern Spain). *Cretaceous Research*, **29**(3), 509-534.

Torsvik, T. H., Rousse, S., Labails, C. and Smethurst, M. A. (2009). A new scheme for the opening of the South Atlantic Ocean and the dissection of an Aptian salt basin. *Geophysical Journal International*, **177**(3), 1315-1333.

Trabucho-Alexandre, J. T., van Gilst, R. I., Rodríguez-López, J. P. and De Boer, P. L. (2011). The sedimentary expression of oceanic anoxic event 1b in the North Atlantic. *Sedimentology*, **58**(5), 1217-1246.

Trabucho-Alexandre, J., Negri, A. and de Boer, P. L. (2011). Early Turonian pelagic sedimentation at Moria (Umbria-Marche, Italy): Primary and diagenetic controls on lithological oscillations. *Palaeogeography, Palaeoclimatology, Palaeoecology*, **311**(3), 200-214.

Tremolada, F. and Erba, E. (2002). Morphometric analyses of Aptian Assipetra infracretacea and Rucinolithus terebrodentarius nannoliths: implications for taxonomy, biostratigraphy and paleoceanography. Marine Micropaleontology, 44(1), 77-92.

Tribovillard, N.-P. and Gorin, G. E. (1991). Organic facies of the early Albian Niveau Paquier, a key black shales horizon of the Marnes Bleues formation in the Vocontian Trough (Subalpine Ranges, SE France). *Palaeogeography, Palaeoclimatology, Palaeoecology*, **85**(3), 227-237.

Tsikos, H., Jenkyns, H.C., Walsworth-Bell, B., Petrizzo, M.R., Forster, A., Kolonic, S., Erba, E., Premoli Silva, I., Baas, M., Wagner, T. and Sinninghe Damsté, J.S. (2004). Carbon-isotope stratigraphy recorded by the Cenomanian-Turonian oceanic anoxic event: correlation and implications based on three key localities. *Geological Society London, Special Publication*, **161**, 711-719.

Tsikos, H., Karakitsios, V., Van Breugel, Y. V. O. N. N. E., Walsworth-Bell, B. N., Bombardiere, L., Petrizzo, M. R., Damsté Js, Schouten, S., Erba, E., Silva, p., Farrimond, P. (2004). Organic-carbon deposition in the Cretaceous of the Ionian Basin, NW Greece: the Paquier Event (OAE 1b) revisited. *Geological Magazine*, **141**(04), 401-416.

Tucker, M. and Wright, V. P. (1990). *Carbonate sedimentology*. Blackwell, Oxford. 482 pp.

Uchupi, E. (1989). The tectonic style of the Atlantic Mesozoic rift system. Journal of African Earth Sciences (and the Middle East) 8(2), 143-164.

Vail, P. R., Audemard, F., Bowman, S. A., Eisner, P.N. and Perez-Cruz, C. (1991). The stratigraphic signatures of tectonics, eustasy and sedimentology - an overview. In: Einsele, G., Ricken, W. and Seilacher, A. (eds), *Cycles and Events in Stratigraphy*, 617-659. Springer, Berlin, Heidelberg.

Van Breugel, Y., Schouten, S., Tsikos, H., Erba, E., Price, G. D. and Sinninghe Damsté, J. S. (2007). Synchronous negative carbon isotope shifts in marine and terrestrial biomarkers at the onset of the early Aptian oceanic anoxic event 1a: Evidence for the release of 13C-depleted carbon into the atmosphere. *Paleoceanography*, **22**(1), PA1210, doi:10.1029/2006PA00134.1.

Van Buchem, F. S., Baghbani, D., Bulot, L. G., Caron, M., Gaumet, F., Hosseini, A., Keyvani F, Schroeder R., Swennen R., Vedrenne V., Vincent B. and Vincent., B. (2010). Barremian-Lower Albian sequence stratigraphy of southwest Iran (Gadvan, Dariyan and Kazhdumi formations) and its comparison with Oman, Qatar and the United Arab Emirates. *GeoArabia Special Publication*, **4**(2), 503-548.

Velic, I. (2007). Stratigraphy and Paleobiogeography of Mesozoic Benthic Foraminifera of the Karst Dinarides (SE Europe). *Geologica Croatica*, **60**, 1-114.

Velic, I., Tisljar, J. and Sokac, B. (1987). The variability of thickness of the Barremian, Aptian and Albian carbonates as a consequence of changing depositional environments and emersion in western Istria (Croatia, Yugoslavia). *Memorie della Società Geologica Italiana*, **40**, 209-218.

Vila, J.M. (1980). *La chaîne alpine d'Algérie Orientale et des confins Algéro-Tunisiens*. PhD thesis, University Pierre et Marie Curie, Paris VI, 663 pp.

Vilas, L., Masse, J. P. and Arias, C. (1995). Orbitolina episodes in carbonate platform evolution: the early Aptian model from SE Spain. *Palaeogeography, Palaeoclimatology, Palaeoecology*, **119**(1), 35-45.

Voigt, S. (1996). Paläobiobiogeographie oberkretatzische Inoceramen und Rudisten: Ozeanographische und klimatologische Konsequenzen einer neuen Paläobiogeographie. *Münchner Geowissenschaftliche Abhandlungen*, (A) **31**, 10l pp.

Voigt, S. (1996). Paläobiogeographie oberkretazischer Inoceramen und klimatologische Konsequenzen einer neuen Paläogeographie. *Münchner Geowissenschaftliche Abhandlungen A, Geologie/Paläontologie*, **31**, 5-102.

Vulc, A. M. (2008). Lower Cretaceous calcareous nannofossils from the Southern Apuseni Mountains, Romania. *Studia UBB Geologia*, **53**(2), 5-11.

Wagner, T. and Pletsch, T. (1999). Tectono-sedimentary controls on Cretaceous black shale deposition along the opening Equatorial Atlantic Gateway (ODP Leg 159). *Geological Society, Special Publications*, **153**, 241-265.

Wagner, T., Herrle, J. O., Damsté, J. S. S., Schouten, S., Stüsser, I. and Hofmann, P. (2008). Rapid warming and salinity changes of Cretaceous surface waters in the subtropical North Atlantic. *Geology*, **36**(3), 203-206.

Wagner, T., Wallmann, K., Herrle, J. O., Hofmann, P. and Stuesser, I. (2007). Consequences of moderate∼ 25,000 yr lasting emission of light CO 2 into the mid-Cretaceous ocean. *Earth and Planetary Science Letters*, **259**(1), 200-211.

Wang, C., Feng, Z., Zhang, L., Huang, Y., Cao, K., Wang, P. and Zhao, B. (2013). Cretaceous paleogeography and paleoclimate and the setting of SKI borehole sites in Songliao Basin, northeast China. *Palaeogeography, Palaeoclimatology, Palaeoecology*, **385**, 17-30.

Warme, J., (1988). Jurassic carbonate facies of the central and eastern High Atlas rift, Morocco. In: Jacobshagen, V. (Ed.), *The Atlas System of Morocco*. Springer Verlag, Berlin, 169-199.

Watkins, D. K. (1989). Nannoplankton productivity fluctuations and rhythmically-bedded pelagic carbonates of the Greenhorn Limestone (Upper Cretaceous). *Palaeogeography, Paleoclimatology, Paleoecology*, **74**(1), 75-86.

Watkins, D.K., Wise, S.W., Pospichal, J.J. and Crux, J. (1996). Upper Cretaceous calcareous nannofossil biostratigraphy and paleoceanography of the Southern Ocean. In: Moguilevsky, A. and Whatley, R., Eds., *Microfossils and oceanic environments*. University of Wales, Aberystwyth Press, 355-381.

Watts, A. B. and Steckler, M. S. (1979). Subsidence and eustasy at the continental margin of eastern North America. Deep Drilling Results in the Atlantic Ocean: Continental Margins and Paleoenvironment, 218-234.

Weissert, H. (1989). C-isotope stratigraphy, a monitor of paleoenvironmental change: a case study from the Early Cretaceous. *Surveys in Geophysics*, **10**(1), 1-61.

Weissert, H. and Breheret, J. (1991). A carbonate carbon-isotope record from Aptian-Albian sediments of the Vocontian Trough (SE France). *Bulletin de Ia Société Geologique de France*, **162** (6), 1133-1140.

Weissert, H. and Erba, E. (2004). Volcanism, CO2 and palaeoclimate: a Late Jurassic–Early Cretaceous carbon and oxygen isotope record. *Journal of the Geological Society*, **161**(4), 695-702.

Weissert, H. and Lini, A. (1991). Ice age interludes during the time of Cretaceous greenhouse climate. In: Muller, D.W., Mckenzie, J.A. & Weissert, H. (eds.), *Controversies in modern geology*, *Evolution of geological theories in sedimentology,earth history and tectonics*, 173-191.

Weissert, H., Lini, A., Föllmi, K. B. and Kuhn, O. (1998). Correlation of Early Cretaceous carbon isotope stratigraphy and platform drowning events: a possible link ?. *Palaeogeography, Palaeoclimatology, Palaeoecology*, **137**(3), 189-203.

Whalen, M. T., Day, J., Eberli, G. P., and Homewood, P.W. (2002). Microbial carbonates as indicators of environmental change and biotic crises in carbonate systems: examples from the Late Devonian, Alberta basin, Canada, *Palaeogeography, Palaeoclimatology, Palaeoecology*, **181**, 127-151.

Wiedmann, J., Butt, A. and Einsele, G. (1978). Vergleich von marokkanischen Kreide-Küstenaufschlüssen und Tiefseebohrungen (DSDP): stratigraphie, paläoenvironment und subsidenz an einem passiven kontinentalrand. *Geologische Rundschau*, **67**(2), 454-508.

Wiedmann, J., Butt, A. and Einsele, G. (1982). Cretaceous stratigraphy, environment, and subsidence history at the Moroccan continental margin. In : *Geology of the Northwest African continental margin*, 366-395. Springer, Berlin-Heidelberg.

Wiegand, G. E. (1984). Calcareous nannofossils from the north-west African margin, Deep Sea Drilling Project Leg 79. In: Hinz, K., Winterer, E. L. et al. (Eds.), *Initial Reports of the Deep Sea Drilling Program*, **79**, 563-578.

Williams, J. R. and Bralower, T. J. (1995). Nannofossil assemblages, fine fraction stable isotopes, and the paleoceanography of the Valanginian-Barremian (early Cretaceous) North Sea Basin. *Paleoceanography*, **10**(4), 815-839.

Wilmsen, M. (2000). Evolution and demise of a mid-Cretaceous carbonate shelf: the Altamira Limestones (Cenomanian) of northern Cantabria (Spain). *Sedimentary Geology*, **133**(3), 195-226.

Wilmsen, M., Fürsich, F. T. and Majidifard, M. R. (2013). The Shah Kuh Formation, a latest Barremian–Early Aptian carbonate platform of Central Iran (Khur area, Yazd Block). *Cretaceous Research*, **39**, 183-194.

Wilson, J. L. (1975). *Carbonate facies in geologic history*. Springer-Verlag, New York, 471 pp.

Wilson, P. A. and Norris, R. D. (2001). Warm tropical ocean surface and global anoxia during the mid-Cretaceous period. *Nature*, **412**(6845), 425-429.

Wind, F. H. (1979). Maestrichtian-Campanian nannofloral provinces of the southern Atlantic and Indian Oceans. In : Deep drilling results in the Atlantic Ocean: continental margins and paleoenvironment, ed. by Talwani, M., Hay, W. W. and Ryan, W. B. F., *Maurice Ewing Series* **3**, 123-137. AGU, Washington DC).

Wise, S.W. (1983). Mesozoic and Cenozoic calcareous nannofossils recovered by Deep Sea Drilling Project Leg 71 in the Falkland Plateau Region, Southwest Atlantic Ocean. In: W.J. Ludwig, V.A. Krasheninnikov and others, *Initial Reports of the Deep Sea Drilling Project*, **71**, 481-550, U.S. Govt Printing Office, Washington D.C.

Wise, S.W. (1988). Mesozoic-Cenozoic history of calcareous nannofossils in the region of the Southern Ocean. *Palaeogeography, Palaeoclimatology, Palaeoecology*, **67**, 157-179.

Wissler, L., Funk, H. and Weissert, H. (2003). Response of Early Cretaceous carbonate platforms to changes in atmospheric carbon dioxide levels. *Palaeogeography, Palaeoclimatology, Palaeoecology*, **200**(1), 187-205.

Witam, O. (1998). Le Barrémien-Aptien de l'Atlas Atlantique (Maroc): lithostratigraphie, biostratigraphie, sédimentologie, stratigraphie séquentielle, géodynamique et paléontologie, *Strata*, **30**, 1-421. Université Paul Sabatier, Toulouse.

Witam, O., Rey, J., Aajour, M. and Marguiez, J. F. (1993). Nouvelles données biostratigraphiques et séquentielles sur la série Barrémienne et Aptienne du bassin d'Agadir (Maroc). *Revue de Paléobiologie*, **12**, 193-202.

Wortmann, U. G., Herrle, J. O. and Weissert, H. (2004). Altered carbon cycling and coupled changes in Early Cretaceous weathering patterns: evidence from integrated carbon isotope and sandstone records of the western Tethys. *Earth and Planetary Science Letters*, **220**(1), 69-82.

Yamamoto, K., Ishibashi, M., Takayanagi, H., Asahara, Y., Sato, T., Nishi, H. and Iryu, Y. (2013). Early Aptian paleoenvironmental evolution of the Bab Basin at the southern Neo-Tethys margin: Response to global carbon-cycle perturbations across Ocean Anoxic Event 1a. *Geochemistry, Geophysics, Geosystems*, **14**(4), 1104-1130.

Yilmaz, I.Ö., Altiner, D., (2007). Cyclostratigraphy and sequence boundaries of inner platform mixed carbonate-siliciclastic successions (BarremianeAptian) (Zonguldak, NW Turkey). *Journal of Asian Earth Sciences*, **30**, 253-270.

Ziegler, A., Eshel, G., Rees, P. M., Rothfus, T., Rowley, D. and Sunderlin, D. (2003). Tracing the tropics across land and sea: Permian to present. *Lethaia*, **36**(3), 227-254.

Zühlke, R., Bouaouda, M. S., Ouajhain, B., Bechstädt, T. and Leinfelder, R. (2004). Quantitative Meso-/Cenozoic development of the eastern central Atlantic continental shelf, western High Atlas, Morocco. *Marine and Petroleum Geology*, **21**(2), 225-276.

APPENDIX 1 : Countings of Ida W Shayq section, Continued

Samples	*Assipetra infracretacea*	*Axopodorhabdus* sp.	*Biscutum constans*	*Biscutum ellipticum*	*Braarudosphaera holckwoldensis*	*Broinsonia stenostaurion*	*Bukrylithus ambiguus*	*Chiastozygus litterarius*	*Conusphaera rothi*	*Corollithion achylosum*	*Cretarhabdus conicus*	*Diazomatolithus lehmanii*	*Discorhabdus rotatorius*	*Eiffelithus striatus*	*Eprolithus floralis*	*Flabellites oblongus*	*Grantarhabdus coronadventis*	*Hayesites albiensis*	*Hayesites irregularis*	*Helenea chiasta*	*Lithraphidites carniolensis*	*Loxolithus armilla*	*Manivitella pemmatoidea*	*Microrhabdulus* sp.	*Nannoconus* sp.	*Nannoconus circularis*	*Nannoconus fragilis*	*Nannoconus globulus*	*N. steinmanni steinmanni*	*Nannoconus truitti truitti*	*Nannoconus vocontiensis*	*Nannoconus wassallii*	*Orastrum perspicuum*	*Percivalia fenestrata*	*Placozygus fibuliformis*	*Polypodorhabdus madingleyensis*	*Prediscosphaera columnata*	*Radiolithus planus*	*Repagulum parvidentatum*	*Retecapsa crenulata*	*Retecapsa surirella*
IDM1	0	0	0	0	0	0	0	0	0	0	1	0	0	0	0	0	0	0	0	1	3	0	0	0	0	0	0	0	0	0	0	0	0	0	0	0	0	0	0	0
IDM2	0	0	0	0	0	0	0	0	0	0	0	0	0	0	0	0	0	0	0	0	0	0	0	0	1	0	0	1	0	0	0	0	0	0	0	0	0	0	0	0
IDM3	0	0	0	0	0	0	0	0	2	0	0	0	0	0	0	0	0	0	0	0	1	0	0	0	0	0	0	0	0	6	0	0	0	0	0	0	0	0	0	0
IDM4	0	0	0	0	0	0	0	0	2	0	2	0	0	0	0	0	0	0	1	0	8	0	0	1	0	0	0	0	0	2	0	0	1	0	2	0	0	0	0	0
IDM5	0	0	0	1	0	0	0	0	6	0	3	0	3	0	0	0	0	0	0	2	14	0	1	0	0	1	0	0	0	0	0	0	2	0	3	0	0	1	1	0
IDM6	0	0	0	0	0	0	0	0	0	0	0	0	0	0	0	0	0	0	0	0	0	0	0	0	0	1	0	0	0	0	0	0	0	0	0	0	0	0	0	0
IDM7	0	0	0	0	0	0	0	0	1	0	1	0	1	0	0	0	0	0	2	0	3	0	0	0	3	7	0	1	0	1	3	0	0	0	0	0	0	0	0	0
IDM8	1	0	0	0	0	0	0	0	0	0	2	0	1	0	0	0	0	0	0	0	1	0	0	0	2	2	0	2	0	1	0	0	0	0	0	0	0	0	0	0
IDM9	3	0	3	2	0	0	0	0	6	3	2	0	4	0	0	0	0	0	4	0	19	0	0	0	2	0	0	2	0	1	25	0	0	4	0	0	0	0	2	0	0
IDM10	1	0	0	0	0	0	0	0	0	0	2	0	0	0	0	0	0	0	0	0	2	0	0	0	3	10	0	0	0	2	15	0	0	1	0	0	0	0	2	0	0
IDM11	0	0	0	0	0	0	0	1	0	0	3	0	3	0	0	0	0	0	0	0	1	0	0	0	1	3	0	0	0	2	30	2	0	0	0	1	0	0	1	0	0
IDM12	1	0	7	2	1	0	0	0	0	0	2	1	2	0	0	0	0	0	2	0	8	1	0	1	2	8	0	0	0	3	14	1	0	0	0	0	0	0	1	0	0
IDM13	0	0	0	1	0	0	0	0	0	0	5	0	9	1	0	0	0	0	0	2	47	1	1	0	0	6	0	0	0	4	12	0	0	0	0	7	0	0	5	0	0
IDM14	0	0	0	0	0	0	0	0	0	0	3	0	0	0	0	0	0	0	0	1	13	0	0	0	0	0	0	0	0	3	0	0	0	0	0	2	0	0	5	0	0
IDM15	0	0	0	0	0	1	2	0	0	0	8	0	12	0	0	1	0	0	1	4	17	0	0	0	0	6	0	0	0	5	0	0	0	1	0	1	0	0	2	0	0
IDM16	0	0	0	1	0	1	0	0	0	0	3	0	19	0	1	1	0	0	8	1	24	0	0	0	0	6	0	0	0	10	0	0	1	1	0	0	0	0	0	0	0
IDM17	0	0	0	0	0	0	0	0	0	0	8	0	12	0	0	0	0	0	3	3	38	0	1	0	1	0	0	2	0	32	3	0	0	0	0	0	0	0	0	0	0
IDM18	0	0	0	0	0	0	0	0	0	0	9	0	7	0	0	1	0	0	3	2	32	0	0	0	1	0	0	0	0	22	0	0	0	0	0	0	0	0	2	0	0
IDM19	0	0	0	3	0	0	0	0	0	0	2	0	28	0	0	1	0	0	4	1	40	0	0	0	1	0	0	0	0	15	0	0	1	0	0	0	0	0	0	0	0
IDM20	0	0	1	0	0	0	0	0	0	0	4	0	6	0	0	3	0	0	3	1	36	0	0	0	0	0	0	0	0	11	0	0	1	0	0	0	0	0	1	0	0
IDM21	0	0	6	0	0	0	0	0	0	0	4	0	13	0	0	0	0	0	2	5	42	0	0	0	0	0	0	0	0	16	0	0	1	0	0	1	0	0	3	0	0
IDM22	0	0	13	2	0	0	0	2	0	0	6	0	36	0	0	1	0	0	0	3	53	0	1	0	0	0	0	0	0	0	0	0	3	2	0	6	2	0	7	0	0
IDM23	0	1	0	8	0	0	0	0	0	0	9	0	14	0	1	0	0	0	5	1	30	1	1	0	1	0	0	0	0	1	0	0	0	0	0	4	1	0	7	0	0
IDM24	0	1	1	9	0	0	0	0	0	1	8	0	11	0	2	0	0	0	5	2	51	1	1	0	0	0	0	0	0	1	0	0	0	1	0	1	1	0	13	0	0
IDM25	0	1	9	0	0	0	0	0	0	0	2	1	16	0	1	0	1	1	1	2	9	1	2	1	0	0	0	0	0	0	0	0	0	1	0	0	1	0	3	0	0
IDM26	0	2	1	8	0	0	0	1	0	1	1	0	11	0	1	0	0	0	0	2	18	1	0	0	0	0	0	0	0	1	0	0	0	1	0	2	0	0	12	0	0
IDM27	0	0	0	5	0	0	0	0	0	0	1	0	10	0	1	2	0	0	2	3	24	0	0	2	0	0	0	0	0	1	0	0	0	0	0	2	0	1	8	0	0
IDM28	0	0	3	0	0	0	0	0	0	0	2	0	8	0	0	0	0	0	2	3	14	0	1	0	1	0	0	0	0	1	0	0	0	1	0	2	1	2	9	0	0
IDM29	0	0	2	0	0	0	0	1	0	0	3	0	3	0	0	0	0	0	4	0	17	0	0	0	0	0	0	0	0	2	0	0	0	0	0	0	0	1	8	0	0
IDM30	0	0	0	4	0	0	0	2	0	0	7	0	17	0	1	1	0	0	2	3	22	0	0	2	0	0	0	0	0	0	0	0	0	2	0	5	1	0	5	0	0
IDM31	0	0	0	5	0	1	0	0	0	0	6	0	6	0	0	2	0	0	1	2	11	0	1	0	0	0	0	0	0	0	0	0	0	3	0	5	0	0	9	0	0
IDM32	0	0	1	8	0	0	0	1	0	1	4	0	21	0	0	2	0	0	6	1	15	1	0	0	0	0	0	0	0	0	0	0	0	0	1	4	1	0	23	0	1
IDM33	0	0	1	11	0	0	1	0	0	0	7	0	27	0	0	1	0	0	4	3	30	2	1	5	0	0	0	0	0	0	0	0	0	2	0	6	0	1	19	0	1
IDM34	0	0	0	7	0	0	0	0	0	0	8	0	12	0	1	2	0	0	4	2	17	0	1	0	0	0	0	0	0	0	0	0	0	2	0	4	0	0	5	0	0
IDM35	0	1	4	10	0	0	0	0	0	0	7	0	30	0	0	3	0	0	4	1	17	0	0	0	0	0	0	0	0	0	0	0	0	2	0	2	1	0	7	0	0
IDM36	0	0	0	3	0	0	0	1		0	6	0	4	0	0	0	0	0	0	1	13	1	0	0	0	0	0	0	0	1	0	0	0	0	0	1	0	0	10	0	0

APPENDIX 1 : Countings of Ida w Shayq section

Samples	*Rhagodiscus achylostaurion*	*Rhagodiscus angustus*	*Rhagodiscus asper*	*Rhagodiscus gallagheri*	*Rhagodiscus splendens*	*Rotelapillus laffittei*	*Rucinolithus terebrodentarius*	*Seribiscutum gaultensis*	*Seribiscutum primitivum*	*Staurolithites* sp.	*Staurolithites aenigma*	*Staurolithites angustus*	*Staurolithites flavus*	*Staurolithites aausorhethium*	*Staurolithites imbricatus*	*Staurolithites mitcheneri*	*Staurolithites mutterlosei*	*Staurolithites siesseri*	*Staurolithites stradneri*	*Tranolithus gabalus*	*Tranolithus minimus*	*Tubodiscus burnettiae*	*Watznaueria barnesiae*	*Watznaueria biporta*	*Watznaueria britannica*	*Watznaueria communis*	*Watznaueria fossacincta*	*Watznaueria manivitiae*	*Watznaueria ovata*	*Zeugrhabdotus bicrescenticus*	*Zeugrhabdotus diplogrammus*	*Zeugrhabdotus elegans*	*Zeugrhabdotus embergeri*	*Zeugrhabdotus erectus*	*Zeugrhabdotus scutula*	*Zeugrhabdotus streetiae*	*Zeugrhabdotus trivectis*	*Zeugrhabdotus xenotus*	small *Zeugrhabdotus* < 5µm	*Zeugrhabdotus* sp.	Unidentified forms
IDM1	0	0	2	0	0	0	0	0	0	0	0	0	0	0	0	0	0	0	0	0	0	0	133	1	1	5	2	0	0	0	0	0	0	0	0	0	0	0	0	2	2
IDM2	0	0	0	0	0	0	0	0	0	0	0	0	0	0	0	0	0	0	1	0	1	0	152	2	0	5	2	0	0	0	1	0	0	0	0	0	0	0	0	0	2
IDM3	0	0	0	0	0	0	0	0	0	0	0	0	0	0	0	0	0	0	0	0	0	0	295	1	0	8	2	0	0	0	0	0	0	0	0	0	0	0	0	0	0
IDM4	1	0	2	1	0	0	0	0	0	2	0	0	0	2	0	0	0	0	0	1	0	0	230	1	0	26	11	0	1	0	6	0	0	0	0	0	0	1	0	1	2
IDM5	1	0	9	1	0	0	0	0	0	1	0	0	0	1	0	0	0	0	0	1	0	0	167	2	0	28	11	0	2	0	16	0	0	2	0	0	1	1	5	6	6
IDM6	0	0	0	0	0	0	0	0	0	0	0	0	0	0	0	0	0	0	0	0	0	0	162	0	0	6	0	0	0	0	0	0	0	0	0	0	0	0	0	0	0
IDM7	0	0	0	0	0	0	0	0	0	0	0	0	0	1	0	0	0	0	0	0	0	0	13	0	0	7	1	0	0	0	0	0	0	1	0	0	0	1	0	0	0
IDM8	1	0	3	1	0	0	0	0	0	0	0	0	0	0	0	0	0	0	0	0	0	0	264	0	0	16	4	0	0	0	3	0	0	2	0	0	0	1	0	1	3
IDM9	0	1	7	3	0	0	0	0	2	5	2	0	0	1	0	0	0	0	0	4	0	0	138	0	1	19	1	0	1	3	9	0	1	7	0	0	0	1	20	2	9
IDM10	0	0	2	1	0	1	0	0	1	0	0	0	0	0	0	0	0	0	0	0	0	0	117	1	0	6	2	0	0	0	2	0	1	3	0	0	0	0	1	1	4
IDM11	0	0	2	2	0	0	2	0	0	1	1	0	0	0	0	0	0	0	0	0	0	0	84	0	0	20	2	0	3	1	5	0	1	0	0	0	0	0	2	4	7
IDM12	1	0	10	3	0	3	1	0	4	5	0	0	0	3	0	0	0	1	2	0	0	1	124	0	1	33	18	0	2	0	12	0	3	8	0	0	4	5	21	8	4
IDM13	1	1	29	3	0	0	0	0	4	3	1	0	0	1	0	0	0	0	0	1	0	0	285	1	1	26	18	3	0	1	5	0	1	9	0	0	0	1	24	1	3
IDM14	0	0	6	1	0	0	0	0	2	3	0	0	0	1	0	0	0	0	0	1	1	0	210	0	0	25	0	1	0	0	8	0	0	4	1	0	0	2	4	5	1
IDM15	5	2	14	1	0	1	0	0	1	4	2	0	0	0	0	0	0	1	4	2	2	0	336	1	0	36	3	0	0	0	7	0	1	8	0	0	1	2	17	1	13
IDM16	5	1	20	1	0	0	1	0	1	2	1	0	0	1	0	0	0	2	2	1	1	0	334	0	0	36	1	1	0	0	7	1	0	12	0	0	0	3	13	3	6
IDM17	8	0	33	0	0	2	0	0	3	5	6	0	0	2	1	0	1	3	3	1	1	1	273	2	1	41	2	0	1	0	19	2	3	14	2	0	2	5	8	2	7
IDM18	8	0	25	0	0	2	0	0	3	1	5	0	0	0	0	0	0	2	1	1	1	0	330	2	0	35	0	0	0	1	15	1	2	6	0	0	1	4	7	5	8
IDM19	4	2	16	0	0	0	0	1	3	4	3	0	0	3	0	0	1	3	0	1	2	0	250	1	0	48	2	1	0	0	23	0	1	8	0	0	0	5	26	4	6
IDM20	1	0	2	0	0	0	0	0	3	1	4	0	0	3	0	0	1	2	0	1	0	0	214	0	0	42	1	0	0	1	9	0	3	2	1	0	0	0	6	2	7
IDM21	1	0	3	0	0	2	0	0	6	4	4	0	0	3	0	0	0	0	0	1	0	0	201	0	0	42	0	0	0	1	11	0	0	6	1	0	0	5	15	2	9
IDM22	11	10	17	0	0	4	0	0	21	3	3	0	0	1	0	0	0	0	0	2	0	2	126	0	0	61	3	0	0	2	27	0	1	24	1	0	1	2	41	11	7
IDM23	7	1	8	0	1	0	0	0	7	1	1	0	0	2	0	0	0	1	0	2	0	1	129	0	0	18	1	0	0	0	24	0	0	9	0	0	0	1	22	3	6
IDM24	7	5	5	0	0	2	0	0	13	2	1	0	0	2	0	0	1	0	0	2	0	1	234	0	0	28	1	0	1	1	51	2	4	26	1	0	0	6	35	4	4
IDM25	4	3	6	0	0	2	0	0	5	9	5	0	0	2	0	0	0	0	0	1	0	1	120	0	0	14	1	0	2	0	21	0	0	15	1	0	0	2	22	6	16
IDM26	4	1	2	0	0	1	0	0	7	0	0	0	0	3	0	0	0	0	0	0	1	0	134	0	0	26	6	0	0	1	27	0	1	12	0	0	0	0	45	4	4
IDM27	8	4	3	0	0	1	0	0	11	1	0	0	0	5	0	0	0	1	1	1	0	0	143	0	0	38	3	0	0	1	13	0	1	17	0	0	0	0	20	4	1
IDM28	0	7	3	0	0	3	0	1	4	3	0	0	1	2	0	0	1	1	2	0	0	1	116	0	0	28	3	0	1	0	19	0	1	15	1	0	0	5	42	7	3
IDM29	2	3	3	0	0	1	0	0	0	4	0	0	0	1	0	0	0	1	2	0	0	0	165	0	0	58	0	0	1	0	5	0	0	7	1	0	0	0	30	2	5
IDM30	5	3	6	0	0	1	0	0	10	3	4	2	0	5	0	0	1	1	1	0	2	0	110	0	0	29	4	1	1	0	26	0	1	9	0	1	0	3	49	6	6
IDM31	0	3	3	0	0	2	0	0	18	2	1	1	0	1	0	0	1	0	0	2	1	1	74	0	0	51	6	4	0	0	20	0	2	19	0	0	0	1	28	6	5
IDM32	3	8	5	0	0	3	0	0	14	6	1	1	0	4	0	1	1	1	1	0	2	0	98	0	0	48	8	2	0	1	40	1	0	37	1	1	0	2	62	15	2
IDM33	7	7	7	0	0	4	0	0	10	6	0	1	0	4	0	0	0	4	3	4	0	4	110	0	0	57	5	1	1	1	33	0	1	35	2	0	2	7	66	19	9
IDM34	5	10	6	0	0	3	0	0	5	3	1	0	0	0	0	0	0	0	0	2	1	4	190	0	0	47	10	1	3	0	40	0	2	23	1	0	4	4	30	16	11
IDM35	4	8	16	0	0	0	0	0	18	1	1	0	1	4	0	0	0	2	2	2	0	2	167	0	0	43	3	1	4	6	50	1	1	23	2	0	1	3	40	20	14
IDM36	2	6	3	0	0	6	0	1	5	2	2	0	0	2	0	0	0	0	0	3	0	2	132	0	0	34	3	0	2	3	32	0	0	12	0	0	1	6	18	9	21

APPENDIX 2 : Countings of Tissakatine Center section, Continued

Sample	*Assipetra infracretacea*	*Axopodorhabdus* sp.	*Biscutum constans*	*Biscutum ellipticum*	*Braarudosphaera*	*Bukrylithus ambiguus*	*Chiastozygus litterarius*	*Corollithion achylosum*	*Cretarhabdus striatus*	*Cretarhabdus conicus*	*Crucibiscutum salebrosum*	*Discorhabdus rotatorius*	*Eiffelithus hancockii*	*Eiffelithus striatus*	*Eprolithus floralis*	*Flabellites oblongus*	*Grantarhabdus coronadventis*	*Hayesites albiensis*	*Hayesites irregularis*	*Helenea chiasta*	*Lithraphidites carniolensis*	*Loxolithus armilla*	*Manivitella pemmatoïdea*	*Microanth0lithus hoschulzii*	*Nannoconus* sp.	*Nannoconus elongatus*	*Nannoconus quadriangulus*	*Nannoconus truitti truitti*	*Orastrum partitum*	*Orastrum perspicuum*	*Owenia dispar*	*Percivalia fenestrata*	*Placozygus fibuliformis*
TC16	0	0	0	0	0	0	0	0	0	0	0	0	0	0	0	0	0	0	0	0	10	0	0	0	0	0	0	0	0	0	0	0	0
TC 19	0	0	0	0	0	0	0	0	0	0	0	0	0	0	0	0	0	0	0	0	6	0	0	0	0	0	0	0	0	0	0	0	0
TC 21	0	0	2	0	0	0	0	0	0	1	0	14	0	0	0	1	0	0	2	0	26	0	0	0	0	0	0	3	0	0	0	0	0
TC 26	1	2	2	9	1	0	0	0	0	6	0	54	0	0	1	0	0	0	14	4	44	0	0	1	10	0	0	8	0	0	0	1	0
TC 29	0	1	5	3	0	0	2	0	0	5	0	30	0	1	0	2	0	0	4	7	44	0	0	0	4	0	0	0	0	0	1	4	0
TC 34	0	1	2	1	0	0	0	0	0	12	0	38	0	0	0	3	0	0	7	4	43	0	0	0	7	0	0	0	0	0	0	4	0
TC 36 ibc	0	0	3	1	0	0	0	0	0	3	0	17	0	0	0	0	0	0	2	0	15	0	0	0	3	0	0	0	0	0	0	1	0
TC 37 ibc	0	1	0	0	0	0	1	0	0	4	0	1	0	0	1	1	0	0	0	0	4	0	0	0	10	0	0	0	0	0	0	0	0
TC 39a bc	0	2	4	1	0	0	0	0	0	4	2	22	0	0	1	0	0	0	2	0	68	0	0	2	18	0	0	0	0	0	0	5	0
TC 42 ibc	0	0	1	1	0	0	3	0	0	3	0	10	0	0	0	0	0	0	2	6	9	0	0	0	3	0	0	0	0	0	0	1	0
TC 43	1	0	1	6	0	1	0	0	0	15	0	20	0	0	0	0	0	0	6	2	41	0	0	0	0	0	0	11	0	6	0	3	0
TC44a	1	0	1	1	0	0	0	0	0	1	0	30	0	0	0	1	0	0	3	3	27	0	0	3	0	0	0	16	0	5	0	4	0
TC 46 bc	0	0	2	3	0	0	2	0	0	5	0	30	0	0	1	2	0	0	2	2	56	0	0	2	16	1	0	0	0	0	0	3	0
TC 50 ibc	0	0	0	0	0	0	0	0	0	5	0	5	0	0	0	0	0	0	5	1	9	0	0	0	5	0	0	0	0	0	0	0	0
TC 52 bc	0	0	0	2	0	0	0	0	0	5	0	12	0	0	0	0	0	0	1	0	20	0	0	0	10	0	0	0	0	0	0	0	0
TC 54 ibc	0	0	6	5	0	0	0	0	0	8	0	32	0	1	0	1	0	0		1	79	0	0	1	6	2	0	0	1	0	0	1	0
TC 57 ibc	0	0	3	9	0	0	1	0	0	7	0	48	0	0	0	0	1	0	9	11	61	0	0	1	25	0	0	0	0	0	0	2	0
TC 58	0	0	0	0	0	0	0	0	0	3	0	11	0	0	0	2	0	0	1	2	25	0	0	0	5	0	0	0	0	0	0	0	0
TC 60 a	0	0	2	4	0	0	1	0	0	3	0	31	0	0	0	0	0	0	3	1	65	0	1	1	7	0	1	0	0	0	0	0	0
TC 61 ibc	0	0	0	2	0	0	0	0	0	2	0	17	0	0	0	0	0	0	0	0	19	0	0	0	1	0	0	0	0	0	0	0	0
TC 63 ibc	0	0	2	2	0	0	0	0	0	9	0	12	0	0	0	0	0	0	0	6	69	0	0	1	6	0	0	0	1	0	0	0	0
TC 64b ibc	0	0	0	7	0	0	2	0	1	9	0	12	0	0	0	0	0	0	0	4	32	0	1	0	8	0	0	0	0	0	0	1	0
TC 66a	0	4	2	27	0	0	0	0	0	10	0	57	3	0	1	0	0	1	7	4	88	0	1	4	3	0	0	0	0	0	0	1	0
TC 68b ibc	0	5	11	12	0	1	1	0	0	11	1	45	0	0	0	0	0	1	6	3	123	0	0	0	1	0	0	0	0	0	0	0	0
TC 69 ibc	0	7	6	13	0	0	0	1	0	4	0	47	0	0	1	0	0	0	7	3	100	1	3	0	0	0	0	0	0	0	0	0	0
TC 70 ibc	0	2	4	9	0	0	1	0	0	10	0	38	0	0	0	0	0	0	8	3	175	0	1	0	0	0	0	0	0	0	0	2	0
TC 71b ibc	0	0	0	11	0	0	0	0	0	3	0	34	0	0	0	1	0	0	4	5	39	0	2	1	0	0	0	0	0	0	0	0	0
TC 72b ibc	0	1	1	15	0	0	1	0	0	3	0	24	0	0	0	0	0	0	5	4	14	0	2	0	0	0	0	0	0	0	0	0	0
TC 73a ibc	0	1	0	2	0	0	1	0	0	4	0	37	0	0	0	0	0	0	1	0	29	0	0	0	0	0	0	0	0	0	0	0	0
TC 73b ibc	0	2	8	16	0	0	1	1	0	11	0	47	0	1	0	3	0	0	4	8	111	0	2	0	0	0	0	0	0	0	0	0	0
TC 74 ibc	0	1	2	6	0	0	1	0	0	4	0	30	0	0	0	0	0	0	2	7	30	1	1	0	0	0	0	0	0	0	0	0	0
TC 76 ibc	0	0	0	5	0	0	0	0	0	1	0	9	0	0	0	0	0	0	1	2	22	0	0	0	0	0	0	0	0	0	0	0	0
TC 78 ibc	0	1	1	8	0	0	0	0	0	4	0	33	0	0	0	0	0	0	2	5	52	0	2	0	0	0	0	0	0	0	0	0	0
TC 80 ibc	0	0	2	10	0	0	0	0	0	5	0	9	0	0	0	2	0	0	1	6	69	0	1	0	0	0	0	0	0	0	0	0	0
TC 81 ibc	0	0	3	31	0	0	3	0	0	4	0	47	0	0	2	1	0	0	2	8	72	0	0	1	0	0	0	0	0	0	0	3	1
TC 82b ibc	0	0	0	1	0	0	0	0	0	1	0	9	0	0	0	0	0	0	2	3	14	0	0	0	2	0	0	0	0	0	0	0	0
TC 83a ibc	0	0	1	3	0	0	1	0	0	5	0	26	0	1	1	0	0	0	3	7	50	0	0	0	0	0	0	0	0	0	0	0	0
TC 84a ibc	0	0	1	11	0	0	0	0	0	1	0	23	0	0	0	1	0	0	1	2	33	0	0	0	0	0	0	0	0	0	0	1	0
TC 85 ibc	0	0	5	15	0	0	0	0	0	0	0	12	0	0	2	0	0	0	2	3	42	0	0	0	0	0	0	0	0	0	0	0	0
TC 86b ibc	0	2	2	10	0	0	0	0	0	2	0	20	0	0	0	0	0	0	4	0	41	0	0	0	0	0	0	0	0	0	0	1	0
TC 88 ibc	0	0	0	4	0	0	0	0	0	0	0	12	0	0	0	0	0	0	2	4	33	0	1	0	0	0	0	0	0	0	0	1	0
TC 90 bc	0	1	14	37	0	0	0	0	0	7	0	37	0	0	1	1	0	0	7	3	65	0	1	0	0	0	0	0	0	0	0	1	0
TC 93a ibc	0	2	0	6	0	0	0	0	0	3	0	15	0	0	0	0	0	0	2	2	50	0	1	0	0	0	0	0	0	0	0	1	0
TC 95 ibc	0	0	0	10	0	0	1	0	0	0	0	13	0	1	0	1	0	0	1	2	37	0	0	0	0	0	0	0	0	0	0	0	0
TC 97 ibc	0	0	0	0	0	0	0	0	0	0	0	0	0	0	0	0	0	0	0	0	0	0	0	0	0	0	0	0	0	0	0	0	0
TC 99 ibc	0	1	4	18	0	0	0	0	0	1	0	18	0	0	0	3	0	0	4	1	16	0	0	1	0	0	0	0	0	0	0	0	0
TC 101 ibc	0	1	1	6	0	0	0	0	0	0	0	14	0	0	0	0	0	0	2	5	20	0	0	1	0	0	0	0	0	0	0	0	0
103 ibc	0	1	15	31	0	0	0	0	0	2	0	41	0	0	0	0	0	0	3	4	14	0	0	0	0	0	0	0	0	0	0	2	0
105 ibc	0	0	0	0	0	0	0	0	0	0	0	0	0	0	0	0	0	0	2	1	42	0	0	0	0	0	0	0	0	0	0	0	0
108 ibc	0	0	2	9	0	0	0	0	0	0	0	13	0	0	1	0	0	0	2	1	25	0	2	0	0	0	0	0	0	0	0	1	0
111a ibc	0	0	4	15	0	1	0	1	0	2	0	23	0	0	0	0	0	0	1	1	13	1	1	0	0	0	0	0	0	0	0	0	0
112 bc	0	1	6	21	0	0	0	0	0	5	0	20	0	0	0	1	0	0	2	2	21	1	1	1	0	0	0	0	0	0	0	0	0
TC 113 ibc	0	0	13	20	0	0	0	2	0	6	0	21	0	0	2	0	0	0	1	9	40	2	2	0	0	0	0	0	0	0	0	0	0
TC 114 ibc	0	0	6	19	0	1	0	1	0	6	0	28	0	1	0	0	0	0	3	2	20	0	0	1	0	0	0	0	0	0	0	2	0

APPENDIX 2 : Countings of Tissakatine Center section

Sample	*Polypodorhabdus madingleyensis*	*Prediscosphaera columnata*	*Repagulum parvidentatum*	*Retecapsa surirella*	*Rhagodiscus achylostaurion*	*Rhagodiscus angustus*	*Rhagodiscus asper*	*Rotelapillus laffittei*	*Rucinolithus terebrodentarius*	*Seribiscutum gaultensis*	*Seribiscutum primitivum*	*Scapholithus fossilis*	*Staurolithites* sp.	*Staurolithites aeniama*	*Staurolithites mitcheneri*	*Tubodiscus burnettiae*	*Watznaueria barnesiae*	*Watznaueria biporta*	*Watznaueria britannica*	*Watznaueria communis*	*Watznaueria fossacincta*	*Watznaueria manivitiae*	*Watznaueria ovata*	*Zeugrhabdotus bicrescenticus*	*Zeugrhabdotus diplogrammus*	*Zeugrhabdotus elegans*	*Zeugrhabdotus embergeri*	*Zeugrhabdotus erectus*	*Zeugrhabdotus scutula*	*Zeugrhabdotus trivectis*	*Zeugrhabdotus xenotus*	small *Zeugrhabdotus* < 5µm	Unidentified forms
TC16	0	0	0	0	0	0	0	0	0	0	0	0	0	0	0	0	4	0	0	4	0	0	0	0	0	0	0	0	0	0	0	0	0
TC 19	0	0	0	0	0	0	0	0	0	0	0	0	0	0	0	0	10	0	1	5	0	0	0	0	0	0	0	0	0	0	0	0	0
TC 21	0	0	0	0	0	0	2	0	0	0	3	0	3	0	0	0	270	1	0	19	1	0	0	5	0	0	3	0	0	1	8	1
TC 26	0	0	1	0	0	1	13	2	1	0	7	0	16	7	0	0	229	0	0	51	1	0	1	0	27	0	3	21	0	0	2	135	10
TC 29	2	0	10	0	0	5	26	0	0	0	7	0	14	3	1	0	77	1	0	44	2	0	2	1	27	0	1	26	1	0	5	46	14
TC 34	1	0	0	2	0	0	13	1	0	0	7	0	14	7	0	0	280	0	0	47	0	0	1	0	10	0	2	16	0	0	2	54	28
TC 36 ibc	0	0	0	0	0	0	17	1	0	0	3	0	3	4	0	0	245	0	0	80	2	1	1	0	8	0	0	2	0	0	1	22	11
TC 37 ibc	0	0	1	0	0	0	3	1	0	0	1	0	2	4	0	0	279	0	0	45	0	0	2	0	7	0	0	0	0	0	2	3	7
TC 39a bc	4	0	4	1	0	1	22	0	0	0	10	0	9	11	0	1	180	2	0	51	4	0	4	0	40	0	0	22	2	0	4	83	15
TC 42 ibc	1	0	5	0	0	3	10	0	0	0	2	0	12	4	0	0	361	1	0	46	5	0	0	0	12	0	0	4	0	0	0	21	4
TC 43	0	0	2	0	5	0	16	1	1	0	7	0	10	3	0	0	303	4	0	50	1	0	1	0	25	0	1	10	0	0	1	45	15
TC44a	0	0	1	0	0	0	7	1	1	0	2	0	9	4	0	0	160	0	0	33	0	1	0	0	22	0	0	6	2	0	4	40	11
TC 46 bc	0	0	2	1	3	0	11	0	0	0	5	0	7	6	0	0	160	0	0	27	1	0	1	0	26	0	0	6	0	0	1	18	10
TC 50 ibc	0	0	0	0	1	0	14	0	0	0	0	0	6	1	0	0	309	0	0	32	0	1	0	0	3	0	1	3	0	0	0	12	7
TC 52 bc	0	0	0	0	1	1	9	0	0	0	2	0	13	2	0	0	354	2	0	36	3	0	0	1	3	0	1	1	0	0	0	10	15
TC 54 ibc	0	0	2	0	2	2	12	2	0	0	5	0	10	8	0	0	182	1	0	60	2	4	0	0	34	2	2	13	0	0	2	33	6
TC 57 ibc	1	0	3	0	1	4	7	1	0	0	7	0	13	2	0	0	181	2	0	58	0	0	0	1	47	0	2	19	0	0	6	69	13
TC 58	0	0	0	0	0	0	7	0	0	0	2	0	9	1	0	0	219	0	0	27	0	0	0	0	6	0	0	1	0	0	1	14	12
TC 60 a	0	0	3	0	3	0	12	2	0	0	5	1	6	6	0	0	219	0	0	75	2	1	0	0	17	1	0	19	1	0	4	45	8
TC 61 ibc	0	0	3	0	0	0	5	0	0	0	2	0	3	3	0	0	148	0	0	75	0	0	3	0	20	0	0	11	0	0	0	5	6
TC 63 ibc	2	1	3	0	4	2	12	3	0	0	3	0	10	3	0	0	253	1	0	50	2	2	1	0	33	0	0	13	2	0	4	29	10
TC 64b ibc	1	0	1	0	4	1	6	0	0	0	2	0	17	3	0	0	348	0	0	35	1	0	0	1	13	1	1	3	0	0	2	22	18
TC 66a	2	0	9	2	9	1	11	2	0	0	23	0	16	6	0	0	184	0	0	23	4	0	1	0	28	0	1	46	0	0	7	60	4
TC 68b ibc	1	1	4	1	6	2	5	2	0	0	34	1	11	1	0	0	163	0	0	32	4	0	0	0	39	2	0	31	0	0	6	62	6
TC 69 ibc	0	1	1	0	6	3	5	3	0	0	24	0	12	0	0	1	91	1	0	64	6	0	0	1	52	5	2	33	0	0	9	40	2
TC 70 ibc	2	0	7	0	2	5	11	2	0	0	16	1	11	1	0	0	195	0	0	64	1	0	2	0	43	2	1	29	0	0	3	54	7
TC 71b ibc	0	0	4	1	2	3	4	3	0	0	8	0	8	2	0	1	282	0	0	25	1	0	0	0	18	1	1	10	0	0	0	36	12
TC 72b ibc	0	0	1	0	6	4	10	5	0	0	2	0	12	2	0	0	312	0	0	33	4	0	0	1	42	0	0	14	0	0	0	50	17
TC 73a ibc	0	0	11	0	4	2	4	1	0	0	4	0	9	1	0	0	276	0	0	46	0	0	0	1	41	0	0	7	0	0	0	28	14
TC 73b ibc	0	0	5	0	5	7	5	3	0	0	19	0	3	1	0	2	180	0	0	60	4	0	2	3	53	5	4	27	0	0	9	58	4
TC 74 ibc	1	0	1	0	9	3	5	2	0	0	9	0	19	3	0	1	275	2	0	46	2	0	0	0	49	0	0	6	0	0	2	52	19
TC 76 ibc	0	0	3	0	3	3	2	0	0	0	0	0	6	0	0	0	180	0	0	54	1	1	0	0	22	0	0	4	2	0	3	25	14
TC 78 ibc	1	1	3	0	2	2	5	4	0	0	6	0	17	3	0	0	153	0	0	37	5	0	0	0	38	0	1	9	0	0	6	40	27
TC 80 ibc	4	1	1	0	3	7	5	1	0	0	1	0	3	0	0	0	102	0	0	42	3	1	0	1	50	4	1	30	2	0	6	48	14
TC 81 ibc	0	1	18	0	4	10	0	2	0	0	7	0	9	5	0	1	111	0	0	38	2	0	0	1	42	3	2	11	0	0	5	54	9
TC 82b ibc	1	0	1	0	1	3	0	0	0	0	10	0	8	2	0	0	157	0	0	49	1	0	0	0	20	1	0	6	0	0	1	7	18
TC 83a ibc	1	0	14	0	6	5	4	1	0	0	9	0	11	2	1	0	182	1	0	37	5	1	3	4	39	1	0	15	0	0	0	54	51
TC 84a ibc	1	1	9	0	3	3	0	0	0	0	6	0	8	1	0	1	112	0	0	49	5	0	0	2	21	0	0	10	0	0	3	31	3
TC 85 ibc	2	0	3	0	2	1	0	0	0	1	4	0	5	0	0	1	87	0	0	28	4	0	0	1	30	4	0	6	0	0	0	42	17
TC 86b ibc	1	0	2	0	3	2	2	0	0	0	0	0	15	2	0	0	160	1	0	28	0	0	0	0	23	0	0	12	0	0	1	59	5
TC 88 ibc	0	0	7	0	2	0	0	4	0	0	1	0	5	0	0	0	206	0	0	43	3	0	0	0	15	0	0	8	0	0	1	40	9
TC 90 bc	2	0	7	0	2	5	2	2	0	0	16	0	13	4	0	0	128	0	0	29	0	2	3	0	39	0	1	14	0	1	3	56	9
TC 93a ibc	0	1	14	0	7	4	1	1	0	0	2	0	8	0	0	0	180	0	0	29	3	0	2	0	26	1	2	19	0	0	1	50	5
TC 95 ibc	0	0	21	0	3	2	1	3	0	0	2	0	16	1	0	0	105	0	0	23	1	0	0	0	10	0	0	6	0	0	0	29	11
TC 97 ibc	0	0	0	0	0	0	0	0	0	0	0	0	0	0	0	0	0	0	0	0	0	0	0	0	0	0	0	0	0	0	0	0	0
TC 99 ibc	1	0	7	0	4	3	0	5	0	0	2	0	14	0	0	0	123	0	0	19	0	0	2	0	11	0	1	5	0	0	7	22	14
TC 101 ibc	0	1	3	0	3	1	1	3	0	0	2	0	7	1	0	0	194	0	0	31	2	0	1	0	15	1	0	3	0	0	1	15	11
103 ibc	4	0	18	1	4	6	4	0	0	0	8	0	6	2	0	0	135	0	0	30	0	0	0	0	10	0	2	5	0	1	2	40	12
105 ibc	1	1	9	0	2	1	0	0	0	0	1	0	0	0	0	0	368	0	0	42	0	0	2	0	9	0	1	3	0	0	0	5	7
108 ibc	1	0	12	0	1	2	0	0	0	0	2	0	5	1	0	0	262	0	0	32	0	0	1	0	12	0	2	4	0	0	0	19	3
111a ibc	3	0	7	0	4	5	2	3	0	0	10	0	3	0	0	0	163	0	0	35	1	0	0	0	9	0	0	4	0	0	1	38	13
112 bc	0	1	200	0	3	2	2	2	0	0	9	1	11	7	0	0	135	0	0	32	1	0	1	1	10	0	1	4	0	0	3	27	9
TC 113 ibc	5	1	27	0	2	6	2	2	0	1	42	0	6	3	0	0	224	0	0	23	0	1	2	0	46	1	0	35	0	1	0	43	16
TC 114 ibc	1	0	14	5	4	1	1	2	0	2	19	0	4	0	0	1	147	0	0	19	1	1	0	1	18	0	1	6	0	0	4	32	12

APPENDIX 3 : Countings of Anzate section, Continued

Sample	*Axopodorhabdus* sp.	*Biscutum constans*	*Biscutum ellipticum*	*Braarudosphaera*	*Broinsonia signata*	*Broinsonia stenostaurion*	*Bukrylithus ambiguus*	*Chiastozygus litterarius*	*Corollithion achylosum*	*Cretarhabdus* sp.	*Cretarhabdus conicus*	*Cribrosphaerella ehrenbergii*	*Crucibiscutum hayi*	*Crucibiscutum salebrosum*	*Cyclagelosphaera margerelii*	*Diazomatolithus lehmanii*	*Discorhabdus rotatorius*	*Eiffelithus hancockii*	*Eiffelithus striatus*	*Eprolithus floralis*	*Flabellites oblongus*	*Grantarhabdus coronadventis*	*Haquius circumradiatus*	*Hayesites* cf *albiensis*	*Hayesites irregularis*	*Helenea chiasta*	*Helicolithus trabeculatus*	*Lithraphidites* sp.	*Lithraphidites carniolensis*	*Loxolithus armilla*	*Manivitella pemmatoïdea*	*Microrhabdulus* sp.	*Nannoconus* sp.	*Nannoconus* cf. *abundans*	*Nannoconus fragilis*	*Nannoconus truitti truitti*	*Orastrum partitum*	*Owenia dispar*	*Percivalia fenestrata*	*Perrisocylus taylorae ?*	*Polypodorhabdus*	*Prediscosphaera* sp?	*Prediscosphaera columnata*
ANZ 1	3	0	15	0	0	0	3	0	0	4	3	0	2	0	0	1	27	0	0	8	6	0	0	0	12	1	0	0	27	1	0	0	5	2	1	0	0	0	0	3	0	0
ANZ 2	0	6	1	0	1	1	0	4	0	0	1	0	1	0	0	0	12	1	0	0	0	0	0	0	3	1	0	0	2	0	0	0	1	0	0	0	0	0	1	0	0	0
ANZ 3	0	4	2	0	0	0	0	0	0	0	5	0	1	0	0	1	23	0	0	0	1	0	0	0	11	0	0	0	8	1	0	0	0	0	0	0	0	0	3	0	1	0	0
ANZ 4	1	4	32	0	0	0	2	0	3	0	3	0	2	0	1	2	45	0	1	2	1	0	0	1	1	2	0	0	30	11	1	2	2	0	0	0	0	1	2	0	10	0	1
ANZ 5	0	0	0	0	0	0	0	0	0	0	0	0	0	0	0	0	0	0	0	0	0	0	0	0	0	0	0	0	1	0	0	0	0	0	0	0	0	0	0	0	0	0	0
ANZ 6	2	7	8	0	0	0	0	1	2	0	7	0	0	0	0	0	26	0	1	0	0	0	1	0	7	1	2	2	8	0	0	0	1	0	0	0	0	0	4	0	9	0	0
ANZ 7	0	0	0	0	0	0	0	0	0	0	0	0	0	0	0	0	1	0	0	0	0	0	0	0	0	0	0	0	0	0	0	0	1	0	0	0	0	0	0	0	0	0	0
ANZ 8	0	5	3	0	0	0	0	1	0	0	3	0	0	0	0	0	12	0	0	0	1	0	0	0	6	1	0	0	3	1	0	1	5	0	0	0	1	0	3	0	0	0	0
ANZ 9	0	0	0	0	0	0	0	0	0	0	0	0	0	0	0	0	0	0	0	0	0	0	0	0	0	0	0	0	0	0	0	0	0	0	0	0	0	0	0	0	0	0	0
ANZ 10	1	21	6	0	0	0	1	0	2	0	2	0	0	0	0	0	22	0	0	1	2	1	0	0	27	0	0	0	10	4	0	4	5	0	0	0	1	0	10	0	5	0	0
ANZ 11	0	3	1	0	0	0	0	1	0	0	4	0	0	0	0	0	6	0	1	0	0	0	0	0	5		0	0	0	0	0	0	0	0	0	0	0	0	0	0	2	0	0
ANZ 12	0	1	16	0	0	0	0	0	1	0	3	0	1	0	0	0	14	0	0	1	3	0	0	0	0	2	0	0	21	8	0	1	0	0	0	6	0	0	0	0	11	0	0
ANZ 13	1	6	14	0	0	0	0	0	0	0	0	3	0	0	0	0	16	0	0	1	0	0	0	0	8	1	0	0	36	4	0	0	4	0	0	2	0	0	0	0	2	0	0
ANZ 14	0	10	28	0	0	0	0	0	0	0	0	0	0	0	0	0	17	0	0	0	2	0	0	0	0	1	0	0	27	4	0	0	5	0	0	0	0	0	0	0	2	1	0
ANZ 15	0	0	0	0	0	0	0	0	0	0	1	0	0	0	0	0	0	0	0	0	0	0	0	0	0	0	0	0	0	0	0	0	0	0	0	0	0	0	1	0	0	0	0
ANZ 16	0	14	9	0	0	0	0	1	2	0	3	0	0	0	0	1	16	0	1	0	0	0	0	0	7	0	0	0	12	2	0	0	1	0	0	0	0	0	4	0	1	0	1
ANZ 17	0	32	9	1	0	0	2	0	0	0	4	0	0	1	0	0	36	0	0	0	0	0	0	0	15	1	0	0	6	5	0	1	2	0	0	0	0	0	6	0	1	0	0
ANZ 18	0	0	0	0	0	0	0	0	0	0	0	0	0	0	0	0	0	0	0	0	0	0	0	0	0	0	0	0	0	0	0	0	0	0	0	0	0	0	0	0	0	0	0
ANZ 19	0	0	0	0	0	0	0	0	0	0	0	0	0	0	0	0	0	0	0	0	0	0	0	0	0	0	0	0	1	0	0	0	0	0	0	0	0	0	0	0	0	0	0
ANZ 20	0	43	2	2	0	0	0	0	0	0	4	0	0	0	0	0	23	0	1	2	0	0	0	0	6	1	0	0	17	0	1	0	3	0	0	0	1	0	2	0	1	0	0
ANZ 21	2	72	11	1	0	0	1	1	1	0	5	0	0	0	0	0	52	0	1	0	0	0	0	0	1	0	0	0	18	3	0	2	0	0	0	0	0	0	3	1	3	0	1
ANZ 22	0	24	5	0	0	0	0	0	0	0	4	0	0	0	0	0	36	0	0	1	2	1	0	0	3	2	0	0	13	1	0	0	1	0	0	0	3	0	3	0	1	0	0
ANZ 23	1	6	7	1	0	0	0	0	2	0	4	0	0	0	0	0	28	0	0	2	0	1	0	0	3	1	0	0	6	0	1	2	2	0	0	0	1	0	6	2	5	0	0

APPENDIX 3 : Countings of Anzate section

Sample	*Prediscosphaera spinosa*	*Repagulum parvidentatum*	*Retecapsa angustiforata*	*Retecapsa crenulata*	*Retecapsa surirella*	*Rhagodiscus achylostaurion*	*Rhagodiscus angustus*	*Rhagodiscus asper*	*Rhagodiscus splendens*	*Rotelapillus laffittei*	*Seribiscutum gaultensis*	*Seribiscutum primitivum*	*Scapholithus fossilis*	*Staurolithites* sp.	*Staurolithites aeniqma*	*Staurolithites gausorhethium*	*Staurolithites imbricatus*	*Staurolithites mitcheneri*	*Staurolithites mutterlosei*	*Staurolithites siesseri*	*Staurolithites stradneri*	*Tetralithus aothicus?*	*Tranolithus gabalus*	*Tranolithus minimus*	*Tubodiscus burnettiae*	*Watznaueria barnesiae*	*Watznaueria biporta*	*Watznaueria britannica*	*Watznaueria communis*	*Watznaueria fossacincta*	*Watznaueria manivitiae*	*Watznaueria ovata*	*Zeugrhabdotus bicrescenticus*	*Zeugrhabdotus diplogrammus*	*Zeugrhabdotus elegans*	*Zeugrhabdotus embergeri*	*Zeugrhabdotus erectus*	*Zeugrhabdotus noeliae*	*Zeugrhabdotus scutula*	*Zeugrhabdotus streetiae*	*Zeugrhabdotus trivectis*	*Zeugrhabdotus xenotus*	small *Zeugrhabdotus* < 5µm
ANZ 1	0	8	0	0	0	6	7	13	0	6	10	0	0	1	2	0	0	1	0	0	1	0	0	2	7	163	2	0	44	14	0	4	3	16	0	0	7	0	0	0	6	7	41
ANZ 2	0	3	0	0	0	4	1	8	1	0	0	0	0	2	1	1	0	0	0	0	0	0	2	2	0	76	0	0	31	3	0	0	0	6	0	0	3	0	1	0	0	0	16
ANZ 3	0	12	0	0	1	8	0	11	0	0	0	5	0	2	1	1	0	0	0	0	0	0	4	11	0	91	3	2	29	6	0	0	3	10	0	1	6	1	1	0	1	7	26
ANZ 4	0	26	0	0	0	1	12	12	0	6	21	3	0	2	5	2	0	0	0	0	1	0	5	2	4	71	1	0	26	5	1	1	1	18	1	0	22	0	5	2	2	2	65
ANZ 5	0	0	0	0	0	0	0	0	0	0	0	0	0	0	0	0	0	0	0	0	0	0	0	0	0	1	0	0	0	0	0	0	0	0	0	0	0	0	0	0	0	0	0
ANZ 6	1	13	0	0	2	3	2	23	0	0	0	19	0	4	1	1	0	0	0	0	1	0	1	2	0	113	1	1	14	1	0	0	11	40	0	1	17	0	1	1	2	21	72
ANZ 7	0	0	0	0	0	0	0	0	0	0	0	0	0	0	0	0	0	0	0	0	0	0	0	0	0	6	0	0	2	0	0	0	0	0	0	0	0	0	0	0	0	0	0
ANZ 8	0	20	0	0	1	9	1	20	0	0	0	9	0	1	1	1	1	0	0	1	0	0	1	3	0	107	1	0	11	4	0	1	3	11	1	2	6	0	0	0	0	3	31
ANZ 9	0	0	0	0	0	0	0	0	0	0	0	0	0	0	0	0	0	0	0	0	0	0	0	0	0	0	0	0	0	0	0	0	0	0	0	0	0	0	0	0	0	0	0
ANZ 10	0	137	0	0	2	21	1	11	0	1	0	14	1	7	1	4	0	0	1	1	2	0	4	1	1	90	0	0	21	2	0	0	4	17	8	3	4	0	1	0	8	9	40
ANZ 11	0	23	0	0	1	2	0	4	0	0	0	7	0	1	0	0	0	0	0	1	0	0	1	1	0	60	0	0	7	2	0	0	2	0	0	0	1	0	0	0	0	4	9
ANZ 12	0	33	0	0	0	4	9	8	0	3	6	5	0	0	0	0	0	0	0	1	1	0	0	0	0	198	0	1	28	9	2	0	4	13	0	2	6	0	0	3	1	20	35
ANZ 13	0	20	0	0	1	4	4	4	0	0	0	4	0	2	3	1	0	0	0	1	0	1	0	0	0	208	0	0	25	3	0	1	3	13	0	0	6	0	0	0	0	0	72
ANZ 14	0	24	0	0	0	6	2	6	0	2	3	9	1	0	1	0	0	0	0	1	0	0	0	1	0	140	1	0	61	4	1	0	1	6	0	0	5	0	0	0	1	3	66
ANZ 15	0	1	0	0	0	1	0	0	0	0	0	0	0	0	0	0	0	0	0	0	0	0	0	0	0	7	0	0	4	0	0	0	0	0	0	0	0	0	0	0	0	0	0
ANZ 16	0	30	0	0	0	4	5	8	0	2	2	12	0	0	0	0	0	0	0	1	1	0	1	0	0	136	0	0	29	1	0	0	0	21	6	1	17	0	5	0	5	4	30
ANZ 17	0	64	0	0	2	2	4	8	0	0	4	31	0	1	0	1	0	0	0	1	0	0	1	0	0	113	0	0	15	1	1	1	5	25	0	3	10	0	0	0	6	2	53
ANZ 18	0	0	0	0	0	0	0	0	0	0	0	0	0	0	0	0	0	0	0	0	0	0	0	0	0	0	0	0	0	0	0	0	0	0	0	0	0	0	0	0	0	0	0
ANZ 19	0	1	0	0	1	0	2	0	0	0	0	0	0	0	1	0	0	0	0	0	0	0	0	0	0	10	0	0	2	0	0	0	0	0	0	0	0	0	0	0	0	0	0
ANZ 20	0	72	0	0	1	5	6	7	0	0	2	16	0	6	0	1	0	0	0	0	0	0	3	1	0	170	0	0	21	2	1	0	2	8	5	4	11	0	1	0	3	3	43
ANZ 21	0	59	0	0	2	3	12	4	0	2	4	26	0	1	0	1	0	0	0	2	0	0	2	0	2	104	0	0	28	0	0	0	2	10	1	3	8	1	1	0	0	3	47
ANZ 22	0	66	0	0	2	6	13	8	0	4	4	18	0	3	2	0	0	0	0	3	0	0	5	0	0	153	0	0	24	4	0	1	3	12	1	5	15	1	1	0	7	5	49
ANZ 23	0	12	1	2	2	5	8	6	0	0	2	7	0	8	3	3	0	0	0	8	2	0	2	1	0	110	0	0	14	2	1	2	1	8	0	0	9	0	0	0	2	13	38

APPENDIX 4 : Countings of Tinfoul section, Continued

Sample	*Axopodorhabdus* sp.	*Biscutum constans*	*Biscutum ellipticum*	*Braarudosphaera*	*Broinsonia signata ?*	*Broinsonia stenostaurion*	*Bukrylithus ambiguus*	*Calculites* sp.	*Chiastozygus litterarius*	*Corollithion achylosum*	*Cretarhabdus conicus*	*Cretarhbdus striatus*	*Cribrosphaerella erhenbergii*	*Crucibiscutum hayi*	*Cyclagelosphaera reinhardtii*	*Discorhabdus rotatorius*	*Dodekapodorhabdus noelia?*	*Eiffelithus striatus*	*Eprolithus floralis*	*Farhania varolii*	*Flabellites oblongus*	*Hayesites* cf *albiensis*	*Hayesites irregularis*	*Helenea chiasta*	*Helicolithus trabeculatus*	*Lapidaecassis mariae*	*Lithraphidites carniolensis*	*Lithraphidites quadratus*	*Loxolithus armilla*	*Manivitella pemmatoïdea*	*Microrhabdulus* sp.	*Nannoconus* sp.	*Nannoconus elongatus*	*Nannoconus quadriangulus*	*Nannoconus truitti truitti*	*Orastrum perspicuum*	*Percivalia fenestrata*	*Perrisocylus taylorae ?*	*Pickelhaube* cf *furtiva?*	*Polypodorhabdus*	*Prediscosphaera columnata*	*Prediscosphaera spinosa*
TF 1	2	0	1	0	0	0	1	0	1	0	3	0	0	1	0	21	0	0	1	0	1	0	1	0	0	0	41	0	3	0	0	2	0	1	1	3	0	2	0	0	0	0
TF 2	0	7	18	0	0	0	1	0	4	0	3	0	0	3	0	31	0	0	0	1	4	0	3	0	0	1	71	0	9	0	13	2	0	0	1	0	7	0	0	10	0	3
TF 3	0	1	4	0	0	0	0	0	0	0	5	0	0	1	0	9	0	0	0	0	1	0	1	0	0	0	53	0	6	0	0	5	0	0	0	0	3	0	0	6	0	4
TF 4	0	0	9	0	0	0	0	0	0	0	2	0	0	0	0	18	0	0	1	0	1	0	1	0	0	0	47	0	8	1	1	1	0	0	0	1	0	0	0	2	0	2
TF 5	0	0	2	0	0	0	0	0	0	0	0	0	0	0	0	7	0	0	0	0	0	0	1	1	0	0	24	0	3	0	1	1	0	0	0	0	0	0	0	0	0	1
TF 6	1	0	2	0	0	0	0	0	0	0	0	0	0	0	0	15	0	0	0	0	3	0	2	3	0	0	31	0	2	0	0	0	0	0	0	1	0	0	0	0	0	0
TF 7	0	2	1	0	0	0	0	0	0	0	10	0	0	1	0	21	0	0	1	0	0	0	1	2	0	0	53	0	0	0	1	0	0	0	0	0	3	2	0	0	1	3
TF 8	0	0	4	0	0	0	0	0	0	0	3	0	0	0	0	14	0	0	0	0	0	0	7	2	0	0	40	0	0	0	0	0	0	0	0	0	0	0	0	1	0	0
TF 9	0	0	8	0	0	0	0	0	0	0	1	0	0	0	0	12	0	0	0	0	4	0	0	3	0	0	19	0	0	0	1	2	1	0	2	0	2	1	0	0	0	1
TF 10	2	6	11	0	0	0	0	0	1	0	4	0	0	0	0	22	0	0	0	0	6	0	12	4	0	0	28	0	0	0	0	0	0	0	0	0	1	0	1	2	0	0
TF 11	0	1	4	2	0	3	0	0	0	3	0	0	0	0	1	37	2	0	0	0	6	0	4	2	0	0	31	0	1	0	0	10	0	0	19	3	2	0	0	0	0	0
TF 12	0	5	11	1	0	0	0	2	0	0	0	0	0	0	0	36	0	0	0	0	0	0	6	0	0	0	16	0	0	0	0	0	0	0	3	24	0	0	0	0	0	0
TF 13	0	5	2	1	0	0	0	0	0	0	1	0	0	0	0	40	0	0	6	0	1	0	8	1	0	0	12	0	1	0	0	0	0	0	0	0	1	2	0	2	0	0
TF 14	0	2	5	0	0	0	0	0	0	0	1	0	0	0	0	26	0	0	1	0	2	0	6	1	0	0	6	0	4	0	0	0	0	0	0	0	0	0	0	1	1	0
TF 15	3	12	3	0	1	0	0	0	0	0	3	0	1	0	0	49	0	1	1	0	1	0	8	2	1	0	16	0	0	1	0	0	0	0	0	0	0	0	0	5	0	0
TF 16	0	1	2	0	0	0	0	0	0	1	3	0	0	0	0	10	0	0	2	0	0	1	8	1	0	0	13	0	6	0	0	0	0	0	0	0	1	0	0	2	1	0
TF 17	0	3	8	0	0	0	0	0	0	0	2	0	0	0	0	26	0	0	1	0	4	0	5	2	0	0	50	1	1	0	0	0	0	0	4	0	0	0	0	1	0	0
TF 18	2	6	13	0	0	0	0	0	0	0	3	0	0	0	0	36	1	0	0	0	2	0	1	1	0	0	10	0	0	0	0	0	0	0	0	0	0	0	0	2	1	0
TF 19	0	0	0	1	0	0	0	0	0	0	0	0	0	0	0	14	0	0	3	0	0	0	0	3	0	0	1	0	0	0	0	0	0	0	0	0	0	0	0	1	0	0
TF 20	0	2	2	0	0	0	0	0	0	1	2	0	0	0	0	42	0	0	2	0	1	1	4	4	0	0	7	0	1	0	0	0	0	0	1	0	0	0	0	2	0	0
TF 21	0	0	2	0	0	0	0	0	0	0	0	0	0	0	0	3	0	0	0	0	0	0	24	1	0	0	5	0	1	0	0	0	0	0	0	0	0	0	0	0	0	0
TF 22	0	5	3	0	0	1	0	0	0	1	3	0	0	0	0	14	0	0	0	0	4	0	9	0	0	0	8	0	0	0	0	0	0	0	0	0	0	0	0	1	1	0
TF 23	0	1	2	0	0	0	0	0	0	1	1	0	0	0	0	7	0	0	0	0	2	0	5	0	0	0	1	0	4	0	0	0	0	0	0	0	0	0	0	3	0	0
TF 24	1	0	5	0	0	0	0	0	0	0	3	0	0	0	0	11	0	3	0	0	5	1	11	1	0	0	5	0	0	0	0	0	0	0	4	0	1	0	0	3	1	0
TF 25	1	1	4	0	0	0	0	0	0	0	2	0	0	0	0	5	0	1	0	0	1	0	2	1	0	0	5	0	1	0	0	0	0	0	0	0	0	0	0	1	0	0
TF 26	1	2	2	0	0	0	0	0	0	1	5	1	0	0	0	12	0	0	0	0	0	0	2	1	0	0	52	0	1	0	0	0	0	0	0	0	1	0	0	1	0	0

APPENDIX 4 : Countings of Tinfoul section

Sample	*Radiolithus planus*	*Repagulum parvidentatum*	*Retecapsa crenulata*	*Retecapsa surirella*	*Rhagodiscus achylostaurion*	*Rhagodiscus angustus*	*Rhagodiscus asper*	*Rhagodiscus splendens*	*Rotelapillus crenulatus*	*Rotelapillus laffittei*	*Seribiscutum gaultensis*	*Seribiscutum primitivum*	*Staurolithites* sp.	*Staurolithites aenigma*	*Staurolithites angustus*	*Staurolithites gausorhethium*	*Staurolithites imbricatus*	*Staurolithites mutterlosei*	*Staurolithites siesseri*	*Staurolithites stradneri*	*Tetralithus gothicus?*	*Tranolithus gabalus*	*Tranolithus minimus*	*Tubodiscus burnetiae*	*Watznaueria barnesiae*	*Watznaueria biporta*	*Watznaueria britannica*	*Watznaueria communis*	*Watznaueria fossacincta*	*Watznaueria manivitiae*	*Watznaueria ovata*	*Zeugrhabdotus bicrescenticus*	*Zeugrhabdotus diplogrammus*	*Zeugrhabdotus elegans*	*Zeuarhabdotus emberaeri*	*Zeugrhabdotus erectus*	*Zeuarhabdotus scutula*	*Zeugrhabdotus streetiae*	*Zeugrhabdotus trivectis*	*Zeugrhabdotus xenotus*	small *Zeugrhabdotus* < 5µm	*Zeugrhabdotus* sp.	Unidentified forms
TF 1	1	1	0	1	2	4	8	0	0	3	0	5	0	0	0	1	0	0	0	0	0	0	3	0	198	0	1	162	5	0	0	0	3	0	1	3	0	0	0	0	5	1	41
TF 2	0	8	0	1	33	9	39	0	0	12	1	19	0	0	0	3	0	0	0	1	0	5	0	2	101	1	0	42	9	1	0	0	6	1	4	19	0	1	0	0	20	23	36
TF 3	1	6	0	0	0	1	10	0	0	5	0	15	1	0	0	1	0	0	0	2	0	0	0	1	354	0	0	59	0	1	0	0	0	0	1	6	0	0	0	1	6	4	33
TF 4	0	3	0	0	1	0	13	0	0	2	1	13	0	0	0	0	0	0	0	0	0	1	0	0	251	0	0	51	14	1	4	2	0	0	0	13	0	1	0	0	11	12	34
TF 5	0	1	1	0	2	0	2	0	0	0	1	4	0	0	0	0	0	0	0	0	0	0	0	2	208	0	0	26	6	1	0	1	0	0	0	6	0	0	0	0	5	7	24
TF 6	0	2	0	1	2	0	4	0	0	0	2	4	1	0	0	0	0	0	0	0	2	0	0	1	178	1	1	42	5	0	0	3	3	0	1	14	0	0	0	0	4	8	9
TF 7	0	1	0	0	8	7	17	0	0	5	0	15	6	1	0	1	2	0	0	2	0	0	2	1	218	2	1	56	11	0	2	6	42	1	2	23	0	0	4	7	34	7	3
TF 8	0	0	0	0	2	0	2	0	0	0	2	6	1	0	0	1	0	0	0	1	0	1	1	1	192	3	1	37	3	0	0	6	9	0	1	14	0	0	0	2	10	0	2
TF 9	0	4	0	1	4	2	6	0	0	1	0	12	2	0	0	3	0	0	0	0	0	0	1	0	191	0	0	35	5	0	2	4	25	0	0	34	0	0	0	2	21	2	18
TF 10	0	8	0	2	1	2	19	0	2	0	1	26	1	0	0	3	0	0	1	1	0	1	0	1	178	3	0	52	10	0	1	0	18	0	1	38	0	0	1	4	55	3	7
TF 11	0	7	0	0	1	2	9	0	0	0	0	4	4	0	0	2	0	0	0	0	0	1	3	1	138	0	0	70	8	1	2	0	17	1	0	15	0	0	1	1	67	12	24
TF 12	0	6	0	0	4	1	8	1	0	0	3	10	3	0	0	2	3	0	0	0	0	2	1	0	122	0	0	22	10	0	0	0	4	0	0	4	0	0	0	1	24	10	20
TF 13	0	7	0	0	5	0	6	0	0	2	2	4	0	0	0	1	0	0	0	2	0	3	0	0	58	0	1	40	14	0	1	0	17	1	1	12	2	0	0	1	40	16	9
TF 14	0	3	0	0	5	0	4	0	0	0	0	2	0	0	0	1	0	0	0	0	0	1	0	0	32	0	0	20	2	0	0	0	6	0	0	6	0	0	0	0	28	5	1
TF 15	2	10	0	0	4	4	4	0	0	0	3	9	0	0	0	2	1	0	0	1	0	1	0	0	129	0	0	54	8	0	1	2	13	0	2	8	0	0	0	2	38	3	4
TF 16	1	5	0	1	4	12	6	0	1	0	0	4	3	0	0	1	0	0	3	0	0	0	2	0	120	0	0	100	16	0	4	1	39	3	2	18	2	0	0	4	22	18	5
TF 17	0	5	0	0	4	3	4	1	0	3	0	7	0	0	0	0	0	0	0	1	0	1	0	1	134	0	0	57	7	1	0	0	14	0	1	5	2	0	0	0	44	3	14
TF 18	1	9	0	0	2	4	6	0	0	1	0	9	0	0	1	0	0	1	0	0	2	3	0	1	172	1	0	45	32	0	4	0	10	0	0	5	1	0	0	2	34	5	7
TF 19	1	0	0	0	2	0	3	0	0	1	0	0	1	0	0	0	0	0	0	0	0	0	0	0	94	1	0	33	9	0	2	0	0	0	0	0	0	0	0	0	0	0	1
TF 20	0	4	0	0	0	0	3	0	0	3	0	8	1	0	0	0	2	0	0	0	1	1	0	0	139	1	0	67	15	0	3	0	6	0	0	5	1	0	1	1	18	5	7
TF 21	1	3	0	0	1	0	1	0	0	0	0	1	1	0	0	0	0	0	0	0	0	1	0	1	120	2	1	59	57	0	3	0	3	0	0	3	0	0	0	0	12	2	14
TF 22	0	4	0	0	2	0	4	0	0	0	0	6	3	0	1	1	0	1	0	0	1	1	0	0	115	0	0	33	19	0	2	0	4	0	1	5	1	0	0	0	30	4	16
TF 23	0	0	0	0	6	0	6	0	0	0	0	0	1	0	0	0	0	0	0	0	0	0	0	0	65	0	0	26	5	0	0	0	2	0	1	2	0	0	0	0	17	4	4
TF 24	1	5	0	0	6	0	6	0	0	1	0	5	5	0	0	4	0	0	0	1	0	0	1	1	189	0	0	40	14	1	0	2	17	0	0	7	0	0	1	2	32	8	17
TF 25	0	5	0	0	1	3	4	0	0	1	0	10	2	0	0	0	0	0	0	0	1	2	0	1	153	1	0	51	14	0	3	0	4	0	1	17	1	0	0	0	31	11	26
TF 26	0	18	0	0	2	8	4	0	0	0	0	5	0	1	0	0	0	0	3	0	0	0	0	0	72	0	0	56	24	0	4	1	24	0	2	15	1	1	0	6	25	9	7